INTERACTION OF REEDS, HYDRAULICS AND RIVER MORPHOLOGY

CS James • AL Birkhead • AA Jordanova
KA Kotschy • CR Nicolson • MJ Makoa

WRC Report No. 856/1/01

Water Research Commission

Disclaimer

This report emanates from a project financed by the Water Research Commission (WRC) and is approved for publication. Approval does not signify that the contents necessarily reflect the views and policies of the WRC or the members of the project steering committee, nor does mention of trade names or commercial products constitute endorsement or recommendation for use.

Vrywaring

Hierdie verslag spruit voort uit 'n navorsingsprojek wat deur die Waternavorsingskommissie (WNK) gefinansier is en goedgekeur is vir publikasie. Goedkeuring beteken nie noodwendig dat die inhoud die siening en beleid van die WNK of die lede van die projek-loodskomitee weerspieël nie, of dat melding van handelsname of -ware deur die WNK vir gebruik goedgekeur of aanbeveel word nie.

INTERACTION OF REEDS, HYDRAULICS AND RIVER MORPHOLOGY

by

C S JAMES, A L BIRKHEAD, A A JORDANOVA,
K A KOTSCHY, C R NICOLSON AND M J MAKOA

Centre for Water in the Environment
University of the Witwatersrand
Private Bag 3
Wits 2050
Johannesburg
South Africa

Report to the Water Research Commission on the Project
"Interaction of Reed Distribution, Hydraulics and
Geomorphology in Semi-Arid Rivers"

Project Leader: C S James

WRC Report No: 856/1/01
ISBN No: 1 86845 731 1

February 2002

EXECUTIVE SUMMARY

1 BACKGROUND AND MOTIVATION

Environmental management of rivers requires understanding and prediction of the processes linking management actions to biological response. This involves firstly relating the discharge (or flow rate) in a river to management decisions concerning upstream land use and water resources development, and secondly relating this managed discharge to biological response. The relationship between discharge and biological response necessarily involves the local hydraulic conditions, manifest by flow depth, velocity and boundary shear stress. The ability to describe the hydraulic conditions in a river is therefore crucial to effective management.

In a river, the local hydraulics, channel form (or morphology), and instream vegetation constitute a mutually dependent trinity, and no one entity can be meaningfully considered independently of the other two. The project aimed at developing a better understanding and description of this mutual dependence for the purpose of increasing the effectiveness of river management.

Reeds are the vegetation type focussed on in this study because of their widespread presence in South African rivers, the relative simplicity presented by their common occurrence in monospecific stands, and the existing evidence of their important influence on morphological change and ecological functioning. Heritage et al (1997) have shown that the interaction between reeds and sediment is an important process in morphological change in rivers of the Kruger National Park. The occurrence of reeds is highly dynamic, ecologically important (Carter and Rogers, 1989) and a major contributor to transpiration loss (Birkhead et al, 1997). The influence of reeds on hydraulics also has relevance to engineering applications, including flood analysis and channel stabilization.

2 OBJECTIVES

The statement of objectives as specified in the contract is as follows:

> The overall aim of this project is to develop the knowledge and ability to model reedbed dynamics and the associated morphological change and hydraulic effects in semi-arid rivers.
>
> This requires investigation of the characteristics of reedbed dynamics, hydraulics and sedimentation that influence their mutual interaction, and the formulation of a model to describe this interaction. The following specific objectives (with equal priority) are defined therefor:
>
> **Reedbed Dynamics**
>
> 1. Document historical rates and extents of reedbed expansion and contraction in the Sabie and Letaba Rivers within the Kruger National Park, and correlate these with sedimentation patterns and flow regimes.

2. Describe the phenology and propogation modes of relevant reed species.

3. Determine the local hydraulic conditions and sedimentation states conducive to reedbed establishment, maintenance, expansion and contraction.

4. Describe the reed life history characteristics that influence hydraulics and sedimentation, and how they might be affected by disturbance.

Hydraulics

1. Determine the flow resistance of a reedbed and how it is influenced by reed life history characteristics and water stage. Propose an appropriate method for quantifying reedbed resistance.

2. Determine the effect on overall resistance in a channel of the distribution pattern of reed cover, and propose a method for predicting overall resistance in a channel with a mixture of surface types.

3. Describe the variation of ecologically relevant and sediment-related hydraulic conditions in a partially reeded river reach, and propose methods for their prediction.

Sedimentation

1. Determine the effectiveness of a reedbed in trapping coarse and fine sediment, and the influence on trapping of reedbed distribution pattern, flow condition and reed life history characteristics.

2. Determine the stabilising effect of reeds on a sediment deposit and the conditions required for sediment remobilisation.

Modelling

1. Construct a rule-based model to describe the reedbed dynamics and associated morphological change.

2. Define modelling rules using the results obtained from the reedbed dynamics, hydraulic and sedimentation investigations.

3. Verify the model using observations from the Sabie and Letaba Rivers.

4. Apply the model to generate responses to different management scenarios.

For budgetary reasons it was agreed at the first Steering Committee meeting to modify the specific objectives, and particularly to reduce the scope of the biological and modelling objectives. No new research would be undertaken into the phenology and propagation modes of reeds and the project would rely on existing biological knowledge. The modelling objectives were reduced to the first two items listed above, and the intention would be to produce a conceptual framework rather than a complete model.

3 MAJOR RESULTS AND CONCLUSIONS

3.1 REEDS IN SEMI-ARID RIVERS

The occurrence of reeds in the Letaba and Sabie Rivers in the Kruger National Park was studied and documented (Chapter 3). The characteristics of the *Phragmites mauritianus* species, its habitat and distribution within the macro-channel have been described. The hydraulically relevant characteristics of stems and their seasonal changes, and reedbeds have been determined through field measurement. Observations of sediment movement around reedbeds and the effects of flows on them have been documented and interpreted. This work makes a significant contribution in guiding the study and modelling of hydraulic and sedimentation processes.

3.2 BASIC RESISTANCE DUE TO REEDS

An experimental programme was carried out to investigate the influence of reed characteristics on the basic flow resistance of a reedbed (Chapter 4). Tests on stems represented by rigid rods were carried out in two different flumes, one with a rigid bed and one with a mobile bed, to quantify the influence on resistance of stem density and shape under different hydraulic conditions determined by bed slope and discharge. Tests were also done using rods with different cross-sectional shapes.

The results show that resistance, expressed in terms of Manning's n, increases with stem density. The velocity is uniform with depth for emergent flow conditions and within the stem region for submerged flow. Small differences in stem shape have little influence on resistance, especially at mild channel slopes. However, real stems have foliage which enhances their drag characteristics. The drag coefficients of some natural reed and bulrush stems were therefore measured with different amounts of foliage intact. The results show that foliage on natural stems increases the drag coefficient considerably. The drag coefficient values also depend on Reynolds number at higher values than indicated for cylinders on standard curves.

The experimental results also showed that Manning's n varies significantly with flow depth. This confirms that this type of equation, which was developed for situations where flow is controlled by boundary shear, is not appropriate where the dominant resistance arises from stem drag. An alternative equation form has therefore been proposed (Chapter 5). This predicts the flow velocity, V, as being independent of depth, according to

$$V = \frac{1}{F}\sqrt{S} \qquad 1$$

with

$$F = \frac{1}{\sqrt{\frac{2g}{C_D N d}\left(1 - \frac{N\pi d^2}{4}\right)}} \qquad 2$$

in which S is the channel slope, g is gravitational acceleration, C_D is the stem drag coefficient, N is the number of stems per square metre, and d is the stem diameter. For shallow flows or sparse stems the influence of bed roughness can be accounted for by replacing the coefficient F with F_f, given by

$$F_f = \frac{1}{\sqrt{\left(\frac{1 - \frac{N\pi d^2}{4}}{\frac{f}{8} + \frac{1}{2} C_D N y d}\right) gy}} \qquad 3$$

in which f is the Darcy-Weisbach friction factor for the bed, and y is the flow depth. The bed resistance term can also be expressed n terms of Manning's n, i.e.

$$\frac{f}{8} = \frac{gn^2}{y^{1/3}} \qquad 4$$

These equations reproduced the experimental results well without calibration. They also reproduced stage-discharge data for crops of wheat grown in a flume (Turner and Chanmeesri, 1984) and bulrushes grown in a flume (Waterways Experiment Station, 1994) satisfactorily if calibrated by adjusting C_D. The values of C_D required to ensure good prediction were consistent with those measured for natural reed and bulrush stems. Sensitivity analysis showed that the term $(1 - N\pi d^2/4)$, representing the volume occupied by stems, can be ignored with negligible error. A comparative analysis suggested that the more complex form of resistance coefficient, F_f, need only be used for conditions where the value of Ny is less than about 50.

Development of a more rigorous computational model (REEDFLO) for predicting the hydraulic characteristics associated with flow through reed beds is described in Chapter 6. The model has modest data requirements, including discharge, channel bed slope, effective bed roughness, stem density and diameter, and drag coefficient values for the specific vegetation type. The model, which is based on force balance principles, accounts for both bed roughness and vegetational resistance due to flexible stems, and is applicable for both emergent and submerged conditions. The force applied to the vegetation is described using the well known drag force function, which requires the estimation of an effective drag force coefficient. The complex velocity field arising within flow through vegetation is described using the velocity defect principle. This allows an effective drag coefficient, based on the average flow velocity through the vegetation, to be

determined. The drag coefficient depends on the cross-sectional shape of the submerged vegetation and may be adjusted to account for leaves, litter on the bed, as well as different types of vegetation.

REEDFLO uses numerical techniques to obtain solutions to the finite-difference equations describing the balance of applied and resisting forces acting on the flow system. The model predicts, as a function of the data requirements described previously, the flow depth, vertical distribution of average velocity and shear stress, shear stress applied to the channel bed, the force resisted by the reeds and the effective height of flexible stems, the effective drag coefficient based on the average velocity through the reeds, and the effective channel boundary resistance (e.g. Manning's n or the friction factor, f). Flow through the vegetated region is modelled using the eddy-viscosity function, and flow above the reeds is described using the mixing length approximation. Measured data from emergent and submerged flume experiments were used to calibrate empirical coefficients in the resistance model. The flow depths predicted by the resistance model show excellent agreement with other experimental data collected for reedbed sedimentation under emergent conditions. Additional data are required for confirmation of the resistance model for submerged conditions.

As this model is highly computational and not appropriate for routine application, it was used hypothetically to develop a simpler formulation (Chapter 7). A sensitivity analysis was carried out to identify bed slope, stem diameter, stem spacing and drag coefficient as the most important factors determining flow resistance through stems. The general form of equation (1) was accepted and the model applied over a wide range of conditions to quantify F. A regression of the input variables used produced the following equation for F.

$$F = 1.885\left(\frac{a}{D}\right)^{-0.653}\left(\frac{D}{y}\right)^{0.071} C_D{}^{0.483} \qquad 5$$

In equation (5) a is stem spacing and D is stem diameter. Equation (1) with F given by equation (5) was also tested against the experimental data and the data of Turner and Chanmeesri (1984) and the Waterways Experiment Station (1994) and produced good predictions.

3.3 HYDRAULICS OF PARTIALLY REEDED CHANNELS

In river corridors, reeds commonly occur in strips along the channel banks or in strips or patches within the active channel. Laboratory tests were carried out to examine the effect of reedbed distribution on overall channel resistance (Chapter 8). Two cases were investigated: longitudinal strip patterns and discrete patch patterns.

All the longitudinal strips collectively covered 50% of the channel area, but with a variety of widths and positions. The results show that resistance increases with the number of stem-water interfaces, i.e. the more the strips were subdivided the greater was the resistance. The overall value of Manning's n increased by a factor of about 1.8 when the pattern was changed from two

thick bank strips to four thin strips distributed across the channel. In all cases Manning's n varied significantly with flow depth, indicating a dominance of stem drag resistance over bed friction. The strips decreased the average clear channel velocity considerably, but resulted in a wider range of velocities across the section, with significant retardation adjacent to the strip edges. The variation of velocity with discharge was reduced considerably, however. Detailed measurement of the transverse velocity profiles showed that velocity increased rapidly away from the strip edges, and that the width of this transition zone was not greatly affected by the width of the vegetation strip. However, the mid-channel velocity beyond the zone of rapid variation appeared to depend on the strip width, suggesting that the influence of vegetation is more extensive than originally thought.

A method for predicting the conveyance of channels with strips of reeds, including the common case of strips along the banks has been proposed (Chapter 9). The total discharge can be determined as the sum of vegetation and clear channel zone discharges calculated separately. The clear channel zone discharges can be calculated using Manning's equation with an effective value of n determined by the composite roughness equations of Horton (1933),

$$n_e = \left(\frac{\sum_{i=1}^{N} \left(P_i n_i^{3/2} \right)}{P} \right)^{2/3} \qquad 6$$

or Einstein and Banks (1950),

$$n_e = \left(\frac{\sum_{i=1}^{N} \left(P_i n_i^{2} \right)}{P} \right)^{1/2} \qquad 7$$

in which n_e is the effective value, P is wetted perimeter, the subscript i denotes the subdvision value, and N is the number of subdvisions. This procedure requires knowledge of an n value for the stem surface, which was determined for the experimental cases, but still requires assessment in the field.

The discharge within the reeded zones can be calculated using equation (1) with a resistance coefficient that accounts for the momentum transferred across the stem-water interface given by

$$F_s = \frac{1}{\sqrt{\frac{2\left(g + \frac{n_w^{\,2} V_s^{\,2}}{R_w^{\,1/3} L_g S} \right)}{C_D N d}}} \qquad 8$$

in which n_s is Manning's n for the stem surface, V_c is the average clear channel velocity, R_s is the hydraulic radius associated with the stem surface in the clear channel, and L_R is the width of the reeded zone. (An alternative form in terms of the f value for the stem surface is also given).

The influence of discrete reedbed patch distribution on resistance was tested using 15 different patch patterns. It was found that resistance is strongly influenced by the distribution pattern as well as the overall areal coverage. As expected, resistance increased consistently with increasing areal coverage, and for a similar distribution pattern Manning's n varied linearly with the proportion of channel occupied by reedbed. However, for any particular value of coverage, the resistance also varied significantly with overall distribution pattern of the patches, the size and shape of the patches, and the degree of fragmentation as reflected by patch discontinuity and the length of stem-clear water interface. As for the strip patterns, there was evidence that Manning's n varies significantly with depth where there is a strong stem drag contribution to overall resistance; this was clearly apparent for all cases where areal coverage exceeded about 25%. A method for predicting conveyance for channels with this kind of reedbed distribution has not yet been developed.

3.4 SEDIMENTATION IN REEDBEDS

The influence of vegetation on sedimentary processes is largely a consequence of the modification by vegetation of the hydraulic parameters that determine the movement of sediment. Understanding of the hydraulics through and around vegetation is still not sufficient for the sedimentary responses to be predicted, however, and elucidation of sediment/vegetation interaction still requires direct investigation.

The morphology of the kind of rivers this project considers is determined by accumulations of sediment that moves predominantly as bed load. A quantitative relationship between bed load rate, hydraulics and vegetation characteristics is fundamental to predicting morphological change that is influenced by vegetation, and laboratory experiments have been carried out to develop such a relationship (Chapter 10). The experiments were conducted in a flume in which an array of artificial stems had been installed. Sediment and water were supplied at the upstream end of the flume and continued until an equilibrium slope had established; the relationship between slope, flow depth, discharge, sediment discharge and stem characteristics could then be defined for the equilibrium condition. Two series of experiments were performed: in the first series the water discharge was kept constant and the sediment supply rate was varied, and in the second series the sediment supply rate was kept constant and the water discharge was varied. The data from the first series were used to calibrate a du Boys type equation for bed load, resulting in

$$q_s = 0.017\left(\tau_b - \tau_c\right)^{1.047} \qquad 9$$

in which q_s is the unit width bed load rate in kg/s/m, τ_b is the bed shear stress and τ_c is the critical bed shear stress at incipient motion. The bed shear stress is calculated from a force balance of the downslope weight component of the water, the bed shear force and the total stem drag. The critical shear stress can be determined from the Shields diagram. Equation (9) was tested against

the data for the second series of experiments (using a τ_c value inferred from the first series) and predicted the five cases with an average absolute error of 7.2%.

The sediment trapping effect of reedbeds was investigated in a more qualitative way. Experiments were conducted to examine the transfer of bed load from the clear channel zone into longitudinal vegetation strips, and the erosion of sediment deposited within the strips. It was found that the rate of transfer into the strips increases with discharge, implying that most deposition would be expected during flood conditions. An equilibrium state of sediment storage exists, related to discharge magnitude, and deposition rate decreases with time as this state is approached. Similar trends were observed for erosion of sediment from the strips. Experiments on the formation of lee bars associated with vegetation patches showed the size and extent of deposition to depend on flow condition as well as patch size and shape. The bar deposits were shown to be active, representing a dynamic equilibrium of erosion and deposition, indicating that relic bars reflect both sediment supply and hydraulics conditions during their formation.

3.5 MODELLING MORPHOLOGICAL CHANGE IN REEDED RIVERS

The integration of vegetative, hydraulic and sedimentary processes in determining river morphology can only be described reliably for prediction purposes through simulation modelling. It is our contention that conventional computational river modelling is inappropriate for predicting morphological change in semi-arid, bedrock-controlled, vegetated rivers. These rivers have highly variable and complex geometries, complex hydraulics, sediment movement regimes that are often supply limited and episodic, and strong vegetation influences, all of which militate against description by partial differential equations. Most existing models also apply process descriptions derived from small scale observations, which may not be representative at the natural river scales relevant to management. As an alternative, a qualitative, rule-based approach has been proposed, in which system state is defined in terms of low resolution descriptions and processes are described by logical rule statements rather than differential equation solutions (Chapter 11).

A prototype model has been presented and applied to demonstrate the facility of this approach in describing sediment/vegetation interactions and reedbed dynamics in morphological evolution and response to changing hydrology. The model is based on a sediment budget for a series of cells with different sediment storage and conveyance characteristics. Sediment transport capacity is described by pre-determined relationships between channel reach type and flow event description. Sediment storage is permitted on the river bed or in bars and experience-based rules allocate incoming sediment to these locations, depending on the growth state of reedbeds. Because most sediment movement is episodic, the hydrograph is represented by discrete event categories (e.g. the rise and fall of small, medium and large floods). The dynamics of reedbeds is described by considering the reeds to be in one of four growth states, and allowing the state to change in accordance with rules accounting for seasonal and annual sequences of flow events. Reedbed/sediment interaction is reflected in the influence of reedbed state on sediment transport capacity, reduction of erosion of alluvial bars, and enhancement of sediment deposition on bars. All of these influences can easily be incorporated into the model structure by specification of appropriate rules.

The model has been applied to illustrate the approach. Applications show how the development of bars in a river reach can be simulated, how reedbed dynamics can be described, and how their effect on bar development can be accounted for. Although rudimentary, the model shows how realistic behaviour can be simulated with even a simple set of rules. It is shown how vegetation can have a profound effect on sediment dynamics and morphological change for long distances downstream, as well as in the reaches they occupy.

This work has shown that accounting for vegetation is imperative in predicting river response, and that the rule-based approach is suitable for doing this. The modelling framework is sound and the inability to apply it realistically at present is due to lack of understanding of the processes in formulating rules, rather than deficiencies in the model structure.

4 ATTAINMENT OF OBJECTIVES

The project achieved the modified objectives, as listed in Section 2 above, as follows.

4.1 REEDBED DYNAMICS

- Existing knowledge relating to historical rates and extents of reedbed expansion and contraction was used, as documented by Carter and Rogers (1995) and Kotschy et al, (2000).

- The relationship between water table levels and reedbed expansion has been described, but the influence of sediment states has not been established. No detailed information relating to reedbed maintenance, expansion and contraction processes has been documented, but useful knowledge about reedbed dynamics, lifespan and persistence has been gained.

- Data on stem characteristics that influence hydraulics and sedimentation was collected and documented. These include stem diameters, heights, number of branches, and densities, as well as descriptions of how they change with time over a season, including some disturbance effects. Preliminary indications of reedbed response to flow conditions have been provided.

4.2 HYDRAULICS

- The influence of some reed characteristics on flow resistance was established by experiments on artificial stems. The detailed model (REEDFLO) enables effects of all stem characteristics to be assessed. Drag coefficient measurements enable the results to be extended to real reeds. An appropriate equation has been proposed for quantifying resistance, and merely requires additional real stem drag coefficient data to be practically useful. This equation provides a realistic alternative to the traditional equations, such as Manning's, which are not

applicable where stem drag dominates over bed friction

- The effect on overall resistance of reed cover distribution pattern has been clearly demonstrated and a method for calculating conveyance in channels with strip resistance has been proposed. This requires some field data for practical application, but is potentially valuable for situations not adequately provided for at present. The characteristics of discrete patches that influence resistance have been identified, but a prediction technique still needs to be developed.

- Variations of depth with discharge and in-channel variations of velocity and bed shear stress were measured for a variety of conditions. The results can be used qualitatively for practical applications, but detailed prediction models were not developed.

4.3 SEDIMENTATION

- Experiments were undertaken to show qualitatively the influence of reedbed distribution pattern on sediment trapping and morphological development. However, only limited conditions were tested and in insufficient detail to account for all reed life history characteristics.

- An equation for bed load transport rate through reed stems was developed, which can be applied to establish the conditions for sediment remobilization and the stabilizing effect through reduction of applied bed shear. Only one sediment size and stem spacing was used in the experiments, however, and this work needs extension.

4.4 MODELLING

- A modelling framework was developed to describe reedbed dynamics and associated morphological change, and this was shown by hypothetical application to be sound and useful. This preliminary modelling has yielded useful understanding of how a river would respond to different managed flow regimes.

- The rules used in the model application were defined from experience, including that gained through the above investigations. However, these investigations proceeded in parallel with model development and many results were not available at the time the model was compiled. Realistic rules for practical application can be formulated using some of the results, but additional laboratory and field work is necessary.

5 RECOMMENDATIONS FOR FURTHER RESEARCH

This project addressed a wide range of issues that are important in themselves, as well as through their interaction. Because the integration of the different aspects was of primary importance, the scope of the project was too wide for the individual aspects to be investigated in great depth. However, many important questions emerged from the study and which deserve greater attention.

5.1 REEDBED DYNAMICS

The relationships between flow and reedbeds presented in Fig. 3.10 are hypothetical and need to be tested. This could be done through detailed monitoring of water levels and changes within reedbeds over a longer time period than done within this study.

The conditions required for establishment of new reedbeds, both from clonal fragments and from seed need to be reliably determined. The required conditions and mechanism of reedbed removal during floods need to be observed and described.

The effect of clay on reed growth and reedbed persistence should be investigated.

5.2 HYDRAULICS

The resistance equation proposed for flow through emergent stems requires specification of drag coefficient values. In this study values were measured for a few natural stems only, and the equation's potential for general use depends on a reliable documentation of typical values for reeds and other species. This requires further laboratory measurements.

The method proposed for estimating the conveyance of channels with longitudinal strip reedbeds requires specification of effective resistance coefficient values for the clear channel side surfaces formed by the stems. This would need detailed field measurements in channels with reeded banks.

The project produced a limited description of the influence of vegetation boundaries on the transverse distributions of velocity and bed shear stress. The influence appears to be extensive and is important for ecological and sedimentation purposes. More detailed laboratory and modelling work is required.

A method is necessary for describing the resistance effect of large, discrete roughness elements, including in-channel reedbeds, alluvial bars and bedrock features. This requires a major investigation including laboratory, field and analytical work.

5.3 SEDIMENTATION

The bed load equation presented is based on experiments with one grain size and one stem

arrangement only. The equation needs to be tested on more extensive data, and generalized if necessary.

The interaction between reedbeds and sediment dynamics needs to be more thoroughly investigated. This requires field work, laboratory work and modelling.

5.4 MODELLING

The model development in this project has established a promising framework. Although more reliable process description has higher priority, further model development would be useful to develop improved logic algorithms, incorporate GIS techniques and generally ensure that appropriate computation methods are identified and utilized.

ACKNOWLEDGEMENTS

The research presented in this report was undertaken as a project funded by the Water Research Commission, whose support is gratefully acknowledged. The Steering Committee responsible for this project consisted of the following persons:

Mr D S van der Merwe	Water Research Commission (Chairman)
Dr S A Mitchell	Water Research Commission
Mr W van Greuning	Water Research Commission (Secretary)
Miss U Wium	Water Research Commission (Secretary)
Mr R van der Merwe	Water Research Commission (Secretary)
Professor J U Grobbelaar	University of the Orange Free State
Professor T S McCarthy	University of the Witwatersrand
Professor A Rooseboom	University of Stellenbosch
Professor K M Rowntree	Rhodes University
Mr W Uys	Agricultural Research Council - IAE
Professor S J van Vuuren	University of Pretoria

The support and understanding of the chairman in managing the project, and the contributions of members of this committee through useful comments and suggestions are greatly appreciated

In addition to the authors, other individuals made valuable contributions to this study. The Centre for Water in the Environment provided continual support, particularly through the efforts of Professor Kevin Rogers. Mrs Wendy Midgley, as always, was invaluable in the administration and financial control of the project. James Mackenzie and Alan van Coller advised on botanical aspects of the project. John Ogony Odiyo assisted with the basic resistance laboratory experiments. The experiments on vegetation strip resistance and part of the analysis of the results were undertaken by Moeti Makoa as his 6-month MSc(Eng) research project, with support from NMDS, Lesotho. The experimental work on the transverse velocity distribution dependence on strip thickness was done by Richard Sharpe and Fareed Nagdi as their undergraduate investigational project in the Department of Civil Engineering, University of the Witwatersrand. Warren Brusse carried out the experiments on sediment deposition in and around vegetation patches as his undergraduate investigational project. The reed and bulrush stem drag coefficients and the resistance characteristics of square stems were measured by Matthew Wolstenholme. Some of the discrete patch resistance experiments were carried out by Sam Mokatsanyane. Chapter 11 is derived from the PhD studies of Craig Nicolson, which were carried out in parallel with this project as a complementary study, with bursary funding from the Foundation for Research Development. Chapter 3 is derived from the MSc studies of Karen Kotschy, also undertaken as a complementary study with bursary funding from the Foundation for Research Development. These contributions are all greatly appreciated.

CONTENTS

LIST OF TABLES

LIST OF FIGURES

LIST OF SYMBOLS AND ABBREVIATIONS

a	Bed area occupied by stems [L^2]
a	Coefficient in resistance law
a	Coefficient in vegetation resistance equation
a	Factor in resistance equation for channel with bars
a	Proportionality factor between bed shear stress and average velocity
a	Stem spacing [L]
a	Longitudinal stem spacing [L]
a_f	Factor associated with riffles in resistance equation for channel with bars
a_x	Longitudinal cylinder spacing [L]
a_z	Transverse cylinder spacing [L]
A	Area of bed [L^2]
A	Coefficient of u_{j-1} in force balance equation
A	Cross-sectional flow area [L^2]
A	Cross-sectional area of stem [L^2]
A	Integration constant in velocity distribution
A	Momentum-absorbing area of vegetation [L^2]
A	Projected stem area [L^2]
A_{bed}	Net area of bed over which shear stress acts [L^2]
A_i	Projected area of ith stem [L^2]
A_p	Area of stems projected in flow direction [L^2]
A_r	Integration constant in velocity distribution for smooth bed
b	Coefficient in resistance law
b	Exponent of slope in vegetation resistance equation
b	Exponent in du Boys type bed load equation
b	Channel width [L]
b	Stem spacing [L]
b	Lateral distance between stems [L]
b_m	Width of flood plain vegetation contributing to main channel resistance [L]
B	Damping factor
B	Coefficient of u_j in force balance equation
c	Coefficient in resistance law
c	Exponent of y in vegetation resistance equation
c_f	Friction coefficient
c_j	Cross-sectional shape factor for stems of species j
c_T	Dimensionless slip velocity at flood plain/main channel interface
C	Chézy resistance coefficient [$L^{1/2}T^{-1}$]
C	Coefficient of u_{j+1} in force balance equation
C_d	Drag coefficient
C_{de}	Effective drag coefficient
C_{dm}	Mean drag coefficient (using mean velocity) for ith cylinder in row
C_{dn}	Drag coefficient of nth stem
C_{ds}	Drag coefficient for single element within stand
C_D	Drag coefficient
C_{De}	Effective drag coefficient
C_{Dj}	Drag coefficient for stems of species j

d Average flow depth [L]
d Rod/stem diameter [L]
d' Average depth accounting for varied ground topography [L]
d_f Flow depth [L]
d_i Local flow depth for subsection i [L]
d_m Maximum flow depth [L]
d_p Cylinder diameter [L]
d_p Particle diameter [L]
d_r Average flow depth over riffles [L]
d_{50} Median grain size [L]
D Channel depth [L]
D Stem diameter [L]
D Stem density [L^{-2}]
D Constant term in force balance equation
D_b Roughness height for bar form resistance [L]
D_g Roughness height for grain resistance [L]
D_i Grain size for which i% of mixture is smaller [L]
D_i Drag force on ith stem [MLT^{-2}]
D_f Roughness height for channel bed [L]
D_l Roughness height for left bank [L]
D_r Roughness height for right bank [L]
D_s Mass of deposited sediment per unit area [ML^{-2}]
D_t Roughness height for reach, including pools and riffles [L]
e Modulus of elasticity of stem [$ML^{-1}T^{-2}$]
E Modulus of elasticity of plant (Young's modulus) [$ML^{-1}T^{-2}$]
E_s Mass of entrapped sediment per unit area [ML^{-2}]
f Darcy-Weisbach friction factor
f_b Darcy-Weisbach friction factor associated with bed roughness
f_c Equivalent Darcy-Weisbach friction factor for composite channel
f_f Darcy-Weisbach friction factor for flume
f_r Darcy-Weisbach friction factor over riffles
f_s Basic Darcy-Weisbach friction factor for boundary surface
f_v Vegetation component of Darcy-Weisbach friction factor
f_w Darcy-Weisbach friction factor for sidewalls
f_w Darcy-Weisbach friction factor for stem-water interface
f_1 Darcy-Weisbach friction factor for part 1 of conduit
f_2 Darcy-Weisbach friction factor for part 2 of conduit
F Resistance coefficient for vegetation
F_A Force applied by weight of water to unit bed area [$ML^{-1}T^{-2}$]
F_{bed} Shear force exerted by bed [MLT^{-2}]
F_B Resisting force of unit bed area [$ML^{-1}T^{-2}$]
F_D Drag force [MLT^{-2}]
F_f Resistance coefficient for vegetation, including bed resistance
F_r Froude number
F_s Resistance coefficient for stem zone, including interface shear
F_V Resistance force of vegetation per unit plan area [$ML^{-1}T^{-2}$]

F_w	Shear force exerted by stem-water interfaces [MLT^{-2}]
Fr	Froude number
Fr_d	Froude number based on stem diameter
Fx	Drag force per unit plan area of reed stand [$ML^{-1}T^{-2}$]
g	Gravitational acceleration [LT^{-2}]
G	Roughness coefficient in vegetation resistance equation
h	Flow depth [L]
h	Average plant height [L]
he	Effective height of reed stems [L]
i	Cell number
i	Subsection indicator
i	Second moment of area of stem cross section [L^4]
I	Cross-sectional second moment of area of plant [L^4]
ICM	Integrated Catchment Management
j	Plant species indicator
J	Plant flexural rigidity = EI [ML^3T^{-2}]
k	Apparent/effective roughness size [L]
k	Constant in du Boys type bed load equation
k_{bi}	Equivalent roughness for friction for subsection i [L]
k_{ci}	Equivalent roughness for friction, local losses and vegetation drag for subsection i [L]
k_i	Equivalent roughness for friction only for subsection i [L]
k_s	Nikuradse roughness size [L]
k_s^+	Shear Reynolds number
k_{se}	Equivalent hydraulic roughness for composite channel [L]
k_{si}	Hydraulic roughness for subsection i [L]
k_{sw}	Effective roughness of walls [L]
k_{s1}	Hydraulic roughness for part 1 of conduit [L]
k_{s2}	Hydraulic roughness for part 2 of conduit [L]
k_t	Imaginary roughness height for floodplain/main channel interface [L]
K	Coefficient in vegetation resistance equation
K	Channel conveyance [L^3T^{-1}]
K_i	Conveyance for ith subsection [L^3T^{-1}]
l	Mixing length [L]
l^+	Dimensionless mixing length
l_e	Effective wake length [L]
l_0	Mixing length at effective height of reeds [L]
L	Length of channel [L]
L	Length of flow element [L]
L	Length of vegetation [L]
L_R	Width of stem zone [L]
L_v	Effective length of vegetative filter [L]
m	Relative stem density
m	Number of stems in longitudinal direction
m	Exponent of flow depth in vegetation resistance equation
m	Exponent in du Boys type equation
mei	Flexural rigidity of vegetation per unit area [ML^3T^{-2}]

n Manning resistance coefficient [$TL^{-1/3}$]
n Number of stems in unit width flow element [L^{-1}]
n Number of stems in lateral direction
n Number of cells
n Number of sediment layers in du Boys model
n_b Basic value of n, excluding vegetation influence [$TL^{-1/3}$]
n_c *Equivalent Manning coefficient in compositely rough channel* [$TL^{-1/3}$]
n_i Manning coefficient for ith subsection [$TL^{-1/3}$]
n_w Manning coefficient for stem-water interface [$TL^{-1/3}$]
n_1 Number of rods across section in first of alternating rows
n_2 Number of rods across section in second of alternating rows
N Number of stems in given bed area [L^{-2}]
N Number of subsections in composite channel
N_{ij} Number of stems of species j in subsection i
N_1 Number of rods per unit channel length in first of alternating rows [L^{-1}]
N_2 Number of rods per unit channel length in second of alternating rows [L^{-1}]
p_b Proportion of sediment deposition allocated to bars
p_e Proportion of sediment erosion allocated to bars
p_1 Proportion of wetted perimeter with roughness k_{s1}
p_2 Proportion of wetted perimeter with roughness k_{s2}
P Wetted perimeter [L]
P Circumference of stem [L]
P' Effective total wetted perimeter [L]
P_b Wetted perimeter for bed [L]
P_i Wetted perimeter for ith subsection [L]
P_i Total sediment transport potential for cell i
P_l Wetted perimeter of left bank [L]
P_l' Effective wetted perimeter of left bank [L]
P_r Wetted perimeter of right bank [L]
P_r' Effective wetted perimeter of right bank [L]
P_w Wetted perimeter for sidewalls [L]
q Number of vegetation species
q Unit width discharge [L^2T^{-1}]
q_s Unit width sediment transport rate [$ML^{-1}T^{-1}$]
q_{sd} Sediment load downstream of sediment wedge [$ML^{-1}T^{-1}$]
q_{se} Equilibrium sediment load per unit width [$ML^{-1}T^{-1}$]
q_{si} Incoming sediment load [$ML^{-1}T^{-1}$]
q_{so} Outflowing sediment load [$ML^{-1}T^{-1}$]
Q Discharge [L^3T^{-1}]
Q_i Sediment entering cell i [L^3T^{-1}]
Q_s Sediment supply from catchment [L^3T^{-1}]
Q_s Total bed load transport rate [MT^{-1}]
R Hydraulic radius [L]
R Fraction of sediment retained in vegetation
R_b Hydraulic radius for bed zone [L]
R_f Hydraulic radius for flume [L]

R_s Spacing hydraulic radius [L]
R_w Hydraulic radius for sidewall zone [L]
R' Effective hydraulic radius [L]
Re Reynolds number
Re_b Reynolds number for bed zone
Re_d Stem Reynolds number
Re_f Reynolds number for flume
Re_w Reynolds number for sidewall zone
Re_* Shear Reynolds number
R_i Hydraulic radius for *i*th subsection [L]
R_v Equivalent hydraulic radius for vegetated channel [L]
R_v Percent of sediment retained in vegetation
s Spread of wake [L]
s_e Effective wake spread [L]
S Energy gradient
S Channel gradient
S Average water surface slope
S_b Energy slope component associated with bar resistance
S_c Channel slope
S_d Sedimentation deposition factor
S_f Energy gradient
S_g Energy slope component associated with grain roughness
S_o Bed slope
S_r Average water surface slope over riffles
S_t Total energy slope
T_e Sediment trapping efficiency
u Local velocity [LT^{-1}]
u Average (root mean square) velocity [LT^{-1}]
u' Longitudinal turbulent velocity fluctuation [LT^{-1}]
u_a Approach velocity [LT^{-1}]
$u_{a\infty}$ Asymptotic approach velocity to stem [LT^{-1}]
u_d Flow velocity defect [LT^{-1}]
u_{max} Maximum velocity defect [LT^{-1}]
u_{reed} Average velocity in reed zone [LT^{-1}]
u_* Shear velocity [LT^{-1}]
u^+ Dimensionless local velocity (u/u_*)
u_j^* Velocity at node j from previous iteration [LT^{-1}]
U Average free stream velocity [LT^{-1}]
U Depth-averaged velocity [LT^{-1}]
U_c Mean velocity through stems based on channel flow area [LT^{-1}]
U_{ai} Average approach velocity to *i*th cylinder [LT^{-1}]
U_w Depth-averaged velocity for sidewall zone [LT^{-1}]
U_∞ Reference free stream velocity [LT^{-1}]
UDL Equivalent uniformly distributed load on stem [MT^{-2}]
v Depth-averaged velocity [LT^{-1}]
v_{fp} Velocity over flood plain not influenced by main channel [LT^{-1}]

v_s	Sediment velocity increment between layers in du Boys model [LT^{-1}]
V	Cross-section averaged flow velocity [LT^{-1}]
V	Depth-averaged flow velocity [LT^{-1}]
$V_{approach}$	Approach velocity to single stem [LT^{-1}]
V_{avg}	Average velocity in reed stand [LT^{-1}]
V_c	Velocity in clear channel [LT^{-1}]
V_{cell}	Volume of flow element [L^3]
V_l	Local approach velocity [LT^{-1}]
V_r	Velocity ratio
V_s	Sediment particle settling velocity [LT^{-1}]
$V_{0.2}$	Velocity at 0.2 times depth from bed [LT^{-1}]
$V_{0.4}$	Velocity at 0.4 times depth from bed [LT^{-1}]
$V_{0.8}$	Velocity at 0.8 times depth from bed [LT^{-1}]
$w(z/y)$	Wake function
w'	Vertical turbulent velocity fluctuation [LT^{-1}]
W	Average channel width [L]
W	Downflow weight component of flow element [MLT^{-2}]
W	Flow width [L]
W_r	Average channel width over riffles [L]
x	Correction factor for wall roughness in velocity distribution
x	Distance from upstream obstruction [L]
x	Longitudinal direction
x	Direction across channel
x_N	Wake length [L]
y	Flow depth [L]
y	Elevation above bed [L]
y	Lateral direction
y	Lateral distance relative to obstruction [L]
y^*	Depth ratio
y_b	Perpendicular distance from channel bed to point of highest velocity [L]
y_d	Flow depth downstream of local obstruction [L]
y_l	Perpendicular distance from left bank to point of highest velocity [L]
y_o	Flow depth [L]
y_r	Perpendicular distance from right bank to point of highest velocity [L]
y_u	Flow depth upstream of local obstruction [L]
z	Flow depth [L]
z	Height above bed [L]
z	Transverse distance across channel [L]
z	Vertical direction
z_w	Wake width [L]
z^*	Dimensionless elevation above bed (yu_*/ν)
z_0	Distance from bed of zero velocity [L]
Z_r	Ratio of flow depth to stem diameter
α	Exponent of S in vegetation resistance equation
α	Slope of channel
α	Empirical correction factor in shear stress relationship

αC_D	Effective drag coefficient for rods
β	Exponent of depth in vegetation resistance equation
β	Exponent of depth in vegetation resistance equation for density and topography variation
β_1	Blockage factor for first of alternating rows of rods
β_2	Blockage factor for second of alternating rows of rods
γ	Unit weight of water [$ML^{-2}T^{-2}$]
γ_s	Unit weight of sediment [$ML^{-2}T^{-2}$]
Γ	Van Driest damping function
δ	Theoretical bed level for zero velocity [L]
δ	Height of viscous sublayer [L]
δ_j	Stem diameter for species *j* [L]
δ_2	Horizontal displacement of bent stem [L]
ΔC	Differential drag force coefficient
ΔC_D	Drag coefficient term for gravitational force
Δl_i	Length of channel considered [L]
ε	Thickness of sediment layers in du Boys model [L]
ζ	Local energy loss coefficient
θ	Channel slope
θ_i	Transverse inclination of wetted perimeter of subsection *i*
θ_l	Transverse slope angle of left bank
θ_r	Transverse slope angle of right bank
κ	Von Karman constant
λ	Stem density parameter [L^{-2}]
ν	Kinematic viscosity [L^2T^{-1}]
ξ	Dimensionless distance from bed
Π	Coles wake strength parameter
ρ	Density of water [ML^{-3}]
ρ_s	Density of sediment [ML^{-3}]
τ	Shear stress in turbulent flow [$ML^{-1}T^{-2}$]
τ	Mean boundary shear stress [$ML^{-1}T^{-2}$]
τ_b	Bed shear stress [$ML^{-1}T^{-2}$]
τ_c	Critical bed shear stress at incipient motion [$ML^{-1}T^{-2}$]
τ_0	Bed shear stress [$ML^{-1}T^{-2}$]
τ_{stem}	Bed shear stress equivalent of stem drag [$ML^{-1}T^{-2}$]
τ_s	Component of resistance per unit bed area representing stem drag [$ML^{-1}T^{-2}$]
τ_v	Viscous shear from bed [$ML^{-1}T^{-2}$]
τ_w	Shear stress on stem-water interface [$ML^{-1}T^{-2}$]
τ_w	Shear force per unit area on boundary [$ML^{-1}T^{-2}$]
τ_B	Bed shear stress [$ML^{-1}T^{-2}$]
ϕ	Einstein bed load transport factor
ϕ_*	Einstein bed load transport factor
χ	Roughness parameter [L]
χ	Du Boys sediment coefficient [$M^{-1}L^{-1}T^3$]
χ'	Du Boys sediment coefficient for median grain size [$M^{-1}L^{-1}T^3$]
ψ	Shear intensity parameter
$\forall$	Horizontal bed area covered by vegetation x flow depth [L^3]

Chapter 1

INTRODUCTION

Environmental management of rivers requires understanding and prediction of the processes linking management actions and biological response. The flow of water in a river is the fundamental and pivotal variable in this linkage (Poff et al, 1997; Walker et al, 1995) because it is the prime manifestation of human impact (and hence management actions) on rivers, as well as the basic driver of instream physical and biological processes. As a product of human action, it is controllable, or manageable, to a high degree; it is the variable that needs to be specified for the "ecological reserve", and what can be imposed on a river reach by controlled reservoir releases. With regard to biological response, flow of water is the basic determinant of habitat in aquatic systems. In this context, the flow is best expressed quantitatively as the discharge (or flow rate) and defined in terms of its magnitude and all of the temporal dimensions describing its frequency, duration, timing and rate of change (Poff et al, 1997).

The influence of management options on river discharge arises through the modification of natural hydrological processes in the contributing catchments by land use and water resources development, properly as guided by Integrated Catchment Management (ICM) procedures (Fig. 1.1). The hydrological processes and the effects of such modifications can be described fairly reliably by application of hydrological models, and the effects of management actions on discharge are therefore predictable for practical purposes.

The causative linkage between discharge and biological response is more complicated, mainly because biota do not respond directly to discharge, but through local hydraulic variables, such as flow depth, velocity, boundary shear and area of inundation - each with the same dimensions as discharge (i.e. magnitude, frequency, duration, timing and rate of change) (Fig. 1.1). In South African conditions, and for natural systems generally, these cannot be controlled directly in the same way as can discharge. Because of this, it is necessary to understand how the hydraulic variables are related to discharge, so that management of discharge produces the desired local hydraulics defining habitat. Hydraulic analysis is therefore a crucially important part of environmental river management.

The local hydraulic conditions in a river are determined by the discharge, together with the form of the channel, and strongly influenced by instream vegetation. The form (or morphology) of the river channel is determined by the discharge, the sediment supply from the catchment (Q_s) (which is another catchment input influenced by management), the local geology, instream vegetation, and the local hydraulics. The occurrence of vegetation is determined by the habitat defined by the local hydraulics and the channel morphology. There is therefore a strong interactive, mutual feedback relationship between vegetation, hydraulics and channel morphology in river function (Fig. 1.1). Elucidation of this relationship is the underlying purpose of the project presented in this report.

Reedbeds are common features in South African rivers, and attention is focussed on this vegetation type. Research on rivers in the Kruger National Park has shown that the interaction of reeds with sediment is an important process in fluvial change (Heritage et al, 1997), and that the occurrence of reeds is highly dynamic and tends to increase, with important consequences for

both morphological change and consumptive use of water (Carter and Rogers, 1989). Reedbeds have also been shown to play an important role in the establishment of woody riparian vegetation along the Sabie River (Carter, 1995). Prediction of reedbed dynamics is therefore important in management considerations and this requires development of a modelling strategy that can incorporate the influence of managed flow regimes, and which accounts for the three-way dependence of reeds, hydraulics and morphology outlined above.

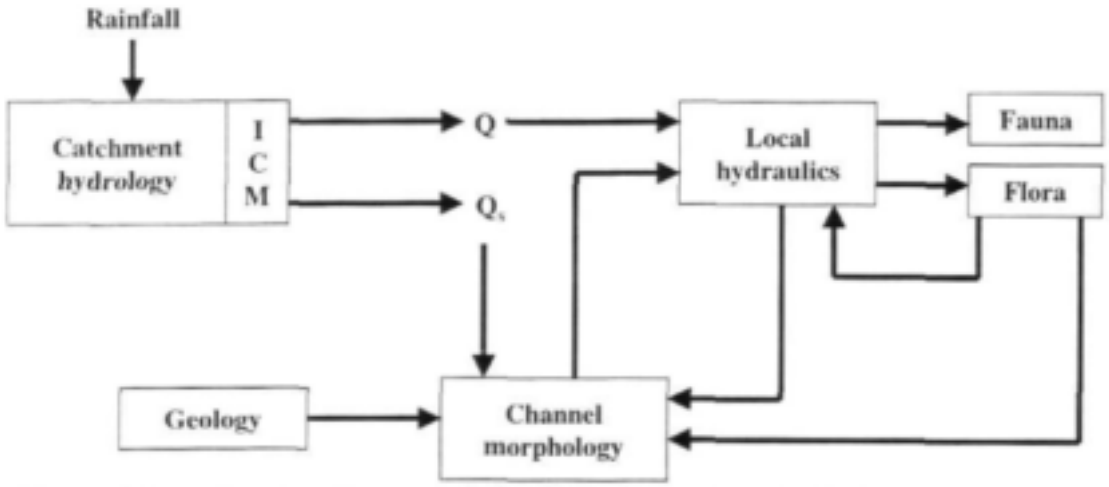

Figure 1.1 Functional structure of a river system, showing linkages between management actions and biotic response, and the interdependence of hydraulics, vegetation and channel morphology (after James, 1998)

The role of reeds in determining hydraulic characteristics needs to be accounted for in predicting reedbed dynamics, but also has other important applications. In extensively reeded wetlands and in partially reeded rivers, the resistance to flow imposed by the reeds determines flood levels and velocities. The ability to quantify reed resistance is therefore essential in engineering applications as well as for environmental management.

In the light of this background, the objectives of the research programme were originally proposed as follows.

> The overall aim of this project is to develop the knowledge and ability to model reedbed dynamics and the associated morphological change and hydraulic effects in semi-arid rivers.
>
> This requires investigation of the characteristics of reedbed dynamics, hydraulics and sedimentation that influence their mutual interaction, and the formulation of a model to describe this interaction. The following specific objectives (with equal priority) are defined therefor:

Reedbed Dynamics

1. Document historical rates and extents of reedbed expansion and contraction in the Sabie and Letaba Rivers within the Kruger National Park, and correlate these with sedimentation patterns and flow regimes.

2. Describe the phenology and propogation modes of relevant reed species.

3. Determine the local hydraulic conditions and sedimentation states conducive to reedbed establishment, maintenance, expansion and contraction.

4. Describe the reed life history characteristics that influence hydraulics and sedimentation, and how they might be affected by disturbance.

Hydraulics

1. Determine the flow resistance of a reedbed and how it is influenced by reed life history characteristics and water stage. Propose an appropriate method for quantifying reedbed resistance.

2. Determine the effect on overall resistance in a channel of the distribution pattern of reed cover, and propose a method for predicting overall resistance in a channel with a mixture of surface types.

3. Describe the variation of ecologically relevant and sediment-related hydraulic conditions in a partially reeded river reach, and propose methods for their prediction.

Sedimentation

1. Determine the effectiveness of a reedbed in trapping coarse and fine sediment, and the influence on trapping of reedbed distribution pattern, flow condition and reed life history characteristics.

2. Determine the stabilising effect of reeds on a sediment deposit and the conditions required for sediment remobilisation.

Modelling

1. Construct a rule-based model to describe the reedbed dynamics and associated morphological change.

2. Define modelling rules using the results obtained from the reebed dynamics,

hydraulic and sedimentation investigations.

3. Verify the model using observations from the Sabie and Letaba Rivers.

4. Apply the model to generate responses to different management scenarios.

In view of a limited budget it was agreed at the first Steering Committee meeting that the specific objectives would be modified. In particular, the biological and modelling objectives were reduced in scope. No new research would be undertaken into the phenology and propagation modes of reeds and the project would rely on existing biological knowledge. The modelling objectives were reduced to the first two items listed above, and the intention would be to produce a conceptual framework rather than a complete model. It was understood, however, that other research projects being undertaken by the Centre for Water in the Environment could contribute in these areas.

The objectives have been addressed by undertaking field work in the Kruger National Park, laboratory investigations in the Hydraulics Laboratory in the School of Civil and Environmental Engineering at the University of the Witwatersrand, data analysis, theoretical development and computer modelling.

The report is structured to present findings in the areas defined by the major specific objectives outlined above, preceded by a general literature survey (Chapter 2). Findings related to **Reedbed Dynamics** are presented in Chapter 3. The **Hydraulics** investigations are covered in Chapters 4 to 9. Chapter 4 describes the experimental work undertaken on the basic resistance effects of reed stems under submerged and emergent conditions. In Chapter 5, a theoretical development is presented of an appropriate equation form for emergent vegetation, and this is tested and confirmed using the data obtained from the experiments and from the literature. This analysis does not account for all effects and a more complete model of flow through stems was developed, as described in Chapter 6. Although providing a rigorous description of vegetation resistance, this model is too computationally intensive for routine application, and was applied hypothetically to develop a simple formulation accounting for the main influences (Chapter 7). In Chapter 8 the experiments undertaken to determine the effects of reedbed distribution on overall resistance are described, and a proposed method for predicting overall resistance in a channel with bank or mid-channel strips of emergent vegetation is presented in Chapter 9. Chapter 10 deals with **Sedimentation** aspects and presents the experimental and analytical work carried out to develop the ability to predict bed load transport rates through reed stems, as well as some more qualitative experiments and interpretations of sediment deposition patterns associated with vegetation. Chapter 11 addresses the **Modelling** objectives, and presents a modelling framework that enables the interaction between hydraulics, sediment movement and reedbed dynamics to be simulated. Chapter 12 summarizes the major conclusions of the project, attainment of the objectives, and recommendations for further work.

Chapter 2

LITERATURE SURVEY

2.1 INTRODUCTION

The interaction of processes underlying reedbed dynamics and morphological change in rivers is poorly understood at present, and little directly applicable information is available in the literature. However, many of the relevant hydraulic and sedimentary processes have been studied in great detail in different contexts or in isolation. This literature survey was undertaken to identify and review the disparate topics that might be appropriately integrated to develop understanding of the interaction and feedback between reeds, hydraulics and sedimentation.

The survey begins with a general review of evidence for the influence of vegetation on river morphology, both in terms of overall channel dimensions and morphological unit characteristics. Attention is then focussed on the processes underlying channel change. Morphological change is a consequence of sediment movement, which is driven by the local hydraulic conditions, i.e. the flow velocity, flow depth and bed shear stress. These conditions are, to a large degree, reflections of the resistance to flow of the river, and this is strongly influenced by the presence of reeds. The ways in which flow resistance is described and how the effects of reeds on basic resistance can be accounted for are therefore explored. Reeds do not usually cover river channels completely, and flow in the clear channel areas between reedbeds is just as significant for sedimentary processes as that amongst the stems. Techniques for describing the net effect of composite roughness in a channel are therefore potentially useful for predicting resistance in partially reeded rivers, and these are reviewed. The interaction between sediment and vegetation depends on the prevailing hydraulic conditions, as influenced by the vegetation. This interaction has been studied both by laboratory experimentation and in the field, and relevant observations are reported.

2.2 INFLUENCE OF VEGETATION ON RIVER MORPHOLOGY

The direct link between vegetation and fluvial systems in dryland rivers has been recognised for some time (e.g. by Graf, 1988). Although the role of vegetation in defining channel morphology has been neglected because of difficulties in its quantification (Hickin, 1984, Thomas and Tsoar, 1991), there is growing awareness of its importance as a geomorphic agent (Viles, 1988; Thornes, 1991). A comprehensive review of the influence of vegetation on river morphology is presented by Nicolson (1999), and is summarized here.

The influence of vegetation on the form of river channels can be demonstrated in two different ways, firstly through the "regime" characteristics of stable vegetated and unvegetated channels, and secondly by the response of channels subjected to sudden temporal changes in vegetation. The influences are manifest in both characteristic channel dimensions and in the nature of sedimentary features.

The effect of vegetation on river dimensions can be established by comparing the hydraulic geometry relationships of channels with different vegetation characteristics. Charlton et al (1978)

compared the relationships between channel width and bankfull discharge for gravel-bed rivers in Britain with both grassy and tree-lined banks. They found that channels with grassy banks were 30% wider than the overall average and channels with tree-lined banks were 30% narrower than the overall average. Andrews (1984) analysed the relationships between dimensionless width, depth and bankfull discharge on 20 gravel-bed rivers in Colorado. He classified the degree of bank vegetation as being either *thick* or *thin* and found that the dimensionless width of channels (W/d_{50}, where W is the channel width and d_{50} is the median bed sediment grain size) was approximately 25% lower for channels with thick vegetation than for those with thin vegetation. Thorne et al (1988) used a "rational regime" approach to predict values of width, depth and slope for known values of discharge, sediment load, bed material size and bank slope. They found that prediction was significantly improved by accounting for bank vegetation. They defined four categories of bank vegetation in terms of percentage tree and shrub cover. Separating their data into these categories rather than treating them together, improved the success rate for predicting width within 15% of measured values from 47% to 77%, and the success rate for predicting depth within 15% from 63% to 73%. These studies all show that vegetated channels are narrower and deeper than unvegetated ones. Rowntree (1991) measured channel widths and depths at 10 sites on the Bell River in the Eastern Cape, South Africa, and ranked the degree of bank vegetation for each site. Her data showed a clear trend of decreasing width-depth ratio with increasing vegetation density, supporting the indications of the regime studies of Charlton et al (1978), Andrews (1984) and Thorne et al (1988).

Studies of river form change through time resulting from vegetation change has also confirmed the influence of vegetation on channel morphology. In one particular case Clifton (1989) estimated that over a 50-year period the growth of grasses, sedges and willow thicket on formerly denuded banks resulted in a 94% decrease in cross-sectional area. Williams (1978) documented a substantial reduction in channel width on the North Platte and Platte Rivers in Nebraska during the twentieth century - over a period of just over 100 years the width had reduced in places by as much as 80%. Eschner et al (1983) attributed this change on the Platte River to encroaching bank vegetation, which was itself a result of the reduced flow regime established in the 1930s by river regulation and irrigation diversions. Graf (1978) observed average reductions in channel width of 27% associated with the upstream invasion of the Green River in Colorado by tamarisk (*Tamarix chinensis*) at the rate of approximately 20 km per year. This evidence for vegetation influence has not gone unchallenged, however: Everitt (1979) has suggested that Graf's (1978) observations may represent a vegetation response to channel change, rather than the other way round; Hickin (1984) has pointed out that long term evidence is difficult to interpret because vegetative change has accompanied other environmental changes in climate, hydrology and sediment supply, and the attribution of causation may be impossible. Nevertheless, these observations support the findings from the "regime" studies, and it is safe to conclude that encroachment of vegetation is accompanied by a decrease in the form ratio of a river.

Overall channel dimensions are not the only way to describe a river. An alternative is description of the channel as an assemblage of morphological units such as the bed, alluvial bars, channel shelf, pools, riffles and floodplain. The influence of vegetation on river form can be described through the influences on these units.

Changes in the channel bed are caused by erosion and deposition of sediment, which is influenced

by vegetation through modification of flow resistance and erosive force. Watts and Watts (1990) described the formation of a silt mound downstream of a clump of vegetation as a result of the alteration of erosive force and velocity distribution by the vegetation. The role of vegetation in the formation and dynamics of alluvial bars is considerable. Nanson (1981) has suggested that scroll bars along rivers in British Columbia and Alberta initially develop around trees and logs, and Hickin (1984) has described the importance of vegetative debris in the growth and accretion of bars. Dietz (1952) explained the formation of "fosse and ridge" topography, with a line of willow (*Salix longifola, S. caroliniana and S. nigra*) trees growing on an elevated longitudinal ridge flanked by an eroded fosse (or furrow) on either side, as a result of deposition of seeds along a receding flood line along a bar. The seeds germinated and seedlings established after the flood, which induced erosion and deposition during subsequent events. This observation is particularly pertinent as reeds in the rivers of the Kruger National Park commonly grow in extended longitudinal strips and establish a similar topography. Vegetation also has a strong influence on the development of channel shelf features. Hadley (1961) studied the growth of tamarisk (*Tamarisk pentandra*) on the channel shelf in the Oraibi Wash in northeastern Arizona, and concluded that the sediment deposition induced would eventually force all flood waters over the banks and on to the floodplain. Graf (1978) found that the increased resistance associated with tamarisk on a channel shelf had induced sufficient deposition to raise the shelf by up to 2.5 m.

These examples give evidence of the influence of vegetation on the form of sedimentary features through alteration of the erosive forces acting on a sedimentary surface (and hence stabilization of the deposit and increase of its resistance to erosion) and stimulation of further deposition of sediment. The effect is to produce generally narrower, deeper channel dimensions, modified patterns of deposition and erosion along the channel bed, and increased heights of alluvial bars and channel shelves.

Because channel form is the result of fluvial processes occurring over periods of time, the effect of vegetation on morphology must be a result of its modification of the formative processes. In order to develop models of change, understanding the influence of vegetation on process is of great importance. The influence of vegetation on sedimentation may be addressed directly, as discussed in section 2.5, or indirectly through first accounting for its effect on the hydraulics and then relating the modified hydraulics to sediment dynamics. The indirect approach requires first and foremost an understanding of the effect of vegetation on flow resistance, which is reviewed in sections 2.3 and 2.4.

2.3 BASIC RESISTANCE DUE TO REEDS

The relationship between flow velocity and the physical characteristics of a river is normally described by one of the following familiar resistance equations.

Chézy:

$$V = C\sqrt{RS} \qquad 2.1$$

Here V is the average velocity over the flow section, R is the hydraulic radius ($= A/P$ where A is the cross-sectional flow area and P is the wetted perimeter) S is the energy gradient (equal to the

bed gradient for uniform flow), and C is the Chézy resistance coefficient.

Manning:

The Chézy coefficient C has been found to vary with the hydraulic radius according to

$$C = \frac{R^{1/6}}{n} \qquad 2.2$$

Incorporating this into equation (2.1) gives the Manning equation

$$V = \frac{1}{n} R^{2/3} S^{1/2} \qquad 2.3$$

in which n is the Manning resistance coefficient.

Darcy-Weisbach:

$$V = \sqrt{\frac{8g}{f}} \sqrt{RS} \qquad 2.4$$

Here g is gravitational acceleration and f is the friction factor.

Equations (2.1), (2.3) and (2.4) are clearly similar in form and are interchangeable in practice, with obvious relationships between C, n and f. By convention, different equations are used in different circumstances and the appropriate coefficients estimated in different ways.

In regular channels, particularly constructed canals, the resistance to flow arises almost entirely from boundary friction. The resistance coefficient or friction factor can then be related to the size of roughness elements on the bed, usually represented by the Nikuradse roughness k_s, and the Reynolds Number. Values of k_s are tabulated for various surfaces and used to determine f or C from the Moody diagram (with the Reynolds Number defined as $Re = 4RV/\nu$ (ν is kinematic viscosity) and the relative roughness defined as $4R/k_s$). For laminar flow the friction factor depends on Re only, and not on the surface roughness, according to

$$f = \frac{8g}{C^2} = \frac{64}{Re} \qquad 2.5$$

For turbulent flow the relationship between f, C, Re and relative roughness is commonly expressed by the following equations.

For hydraulically rough flow :

$$\frac{1}{\sqrt{f}} = \frac{C}{\sqrt{8g}} = c\log\left(a\frac{R}{k_s}\right) \qquad 2.6$$

For hydraulically smooth flow :

$$\frac{1}{\sqrt{f}} = \frac{C}{\sqrt{8g}} = c\log\left(Re\frac{\sqrt{f}}{b}\right) \qquad 2.7$$

For transitional flow :

$$\frac{1}{\sqrt{f}} = \frac{C}{\sqrt{8g}} = -c\log\left(\frac{k_s}{aR} + \frac{b}{Re\sqrt{f}}\right) \qquad 2.8$$

The ASCE Task Force on Friction Factors in Open Channels (1963) have presented values of the coefficients a, b and c derived from various data sets for rigid boundary channels. The value of c does not vary greatly for regular, prismatic channels and $c = 2$ is recommended by Ackers (1958) as a standard value. The value of a depends on the value of c selected and $a = 12$ is representative for regular channels with sand scale roughness. The value of b depends on the value of c and the shape of the cross section, with $b = 2.51$ being a typical value.

The type of flow, and hence the appropriate equation can be determined from the value of the Shear Reynolds Number, defined as

$$Re_* = \frac{u_* k_s}{\nu} \qquad 2.9$$

in which u_* is the shear velocity of the flow, given by

$$u_* = \sqrt{\frac{\tau_o}{\rho}} \qquad 2.10$$

with τ_o being the bed shear stress and ρ the density of water.

The commonly accepted criteria for defining the flow conditions are

$$\begin{aligned} Re_* &> 70 && \textit{hydraulically rough} \\ 5 < Re_* &< 70 && \textit{transitional} \\ Re_* &< 5 && \textit{hydraulically smooth} \end{aligned} \qquad 2.11$$

Manning's n can be related to k_s by Strickler's relationship:

$$n = \frac{k_s^{1/6}}{7.7\, g^{1/2}} \qquad 2.12$$

It should be noted that Manning's equation and all the recommendations for estimating values of n neglect consideration of the effect of Re. It is therefore valid only for hydraulically rough turbulent flow.

In natural rivers the resistance to flow arises not only from boundary friction, but also from various other energy loss mechanisms associated with form resistance, channel irregularity, channel curvature and drag induced by objects in the flow, including vegetation. The non-friction contributions to resistance are obviously not accounted for by k_s and the above equations. The influence of form resistance associated with alluvial bed forms has been fairly reliably and objectively quantified, but most other effects - which can have overriding importance - have thus far eluded satisfactory description. The Manning equation has become the most popular resistance equation for natural rivers, with n providing a lumped resistance coefficient to account for all energy loss influences. Estimation of n for complex natural channels defies rational assessment and values are selected largely on the basis of qualitative information and "judgement". The most reliable approach in current practice is probably that of matching the problem channel characteristics with photographs of channels for which values of n have been obtained from field stage-discharge measurements, such as provided by Barnes (1967).

The influence of in-channel and riparian vegetation on flow resistance can be significant and has been widely investigated (Dawson and Charlton, 1988). The hydraulic effects of vegetation are attributed by Starosolszky (1983) to three causes, viz. reduction of the flow area, increased roughness, and the generation of additional turbulence by oscillatory movement. Attention here will be focussed on the work pertaining to reeds or other emergent species or emergent conditions from which insight into the effect of reeds can be obtained.

In keeping with the tradition of accounting for a variety of resistance effects through Manning's n, many recommendations have been proposed for the adjustment of a basic value associated with the channel substrate to account for the various contributions of non-friction energy losses, including those associated with emergent vegetation. These are widely used, notwithstanding the highly questionable assumption that the different effects can be treated independently and superposed.

The Soil Conservation Service (1963) proposed a method for determining an overall value of n by assuming a basic value for a straight, regular channel in the required material and then adding correction factors to account for vegetation, channel irregularity, obstructions, and channel alignment. Recommended adjustment values are provided, corresponding to qualitative descriptions of the channel characteristics. This method is presented by French (1985). The recommendations for vegetation adjustment include emergent vegetation along the channel banks, but not reeds specifically. The maximum recommended augmentation of the basic n value attributable to vegetation is 0.100.

Hall and Freeman (1994) carried out tests in a 1.2 m wide, 150 m long flume to determine values of Manning's n for flow through soft stem bulrush (*Scirpus validus*) at different growth stages and densities. They measured values ranging from 0.27 for a stem density of 400 stems per square metre (with average stem diameter = 7.0 mm) up to 0.7 for a stem density of 800 stems per square metre (with average stem diameter = 7.6 mm). They also found the n value to decrease with increasing flow velocity.

Starosolszky (1983) presents information on the resistance of reeds measured in a 1.0 m wide flume. The reed stem diameter was 4.6 mm and tests were conducted with emergent reeds as well as harvested stubble for which the stem height was less than the water depth. For the emergent condition with a stem density of 220 per m^2 the data lead to the following relationship for the friction factor.

$$f = 7.83*10^{-6} Re^{1.161} \qquad 2.13$$

Using the same data, Gáspár (1983) presents graphical relationships for the Chézy C for the same conditions, as well as a diagram to determine C for reed stands with any density, stem diameter and flow depth. Some notation on this diagram is ambiguous, however.

Nnaji and Wu (1973) adopted the form of the relationship for C used by Sayre and Albertson (1961) and Keulegan (1938):

$$\frac{V}{u_*} = \frac{C}{\sqrt{g}} = \frac{1}{\kappa} ln \frac{R}{\chi} \qquad 2.14$$

in which κ is the von Karman constant and χ is a roughness parameter purported to account for all characteristics of roughness elements. Nnaji and Wu proposed that χ for cylindrical elements is given by

$$\chi = 0.36 \lambda^{1.47}$$
$$\lambda = N \frac{A_p}{A} \qquad 2.15$$

in which N is the number of cylindrical elements in a given area of bed, A_p is the area of the elements projected in the direction of flow, and A is the area of bed under consideration.

Various attempts have been made to account for the contribution of emergent vegetation to overall resistance by quantifying the drag force on the stems, and thereby expressing the friction factor or resistance coefficient in terms of a drag coefficient. The drag force on a stem, F_D, may be calculated as

$$F_D = C_D A \frac{1}{2} \rho V^2 \qquad 2.16$$

in which C_D is the drag coefficient for the stem (of the order of 1.0) and A is the projected area of the stem. The sum of drag forces on a group of stems can be expressed as an equivalent boundary shear stress (τ_{0veg}) by dividing by the bed area occupied by the stems (a), i.e.

$$\tau_{0veg} = \frac{\sum F_D}{a} = C_D \frac{\sum A_i}{a} \frac{1}{2} \rho V^2 \qquad 2.17$$

in which A_i is the projected area of the ith plant in the upstream direction. Since the friction factor can be defined (by rearranging equation (2.4)) as

$$f = 8\left(\frac{u_*^2}{V^2}\right) = 8\left(\frac{\tau_0 / \rho}{V^2}\right) \qquad 2.18$$

the vegetation component can be expressed in terms of the drag coefficient, i.e.

$$f_v = 4C_D\left(\frac{\sum A_i}{a}\right) \qquad 2.19$$

By analysing the forces on a control volume including rigid, emergent vegetation under steady, uniform flow conditions, Petryk and Bosmajian (1975) derived an expression for the total Manning's n, i.e.

$$n = n_b\sqrt{1 + \frac{C_D \sum A_i}{2gAL}\left(\frac{1}{n_b}\right)^2 R^{4/3}} \qquad 2.20$$

in which n_b is the Manning n value excluding the influence of vegetation, A is the cross-sectional area of the flow, and L is the length of channel under consideration.

Christensen (1996) approximated equation (2.6) (with $c = 2$ and $a = 14.9$) as the power function

$$\frac{1}{\sqrt{f}} = 2.97\left(\frac{R}{k}\right)^{1/6} \qquad 2.21$$

and showed that Manning's n is related to apparent roughness, k, by

$$\frac{n}{k^{1/6}} = 0.0380 \qquad 2.22$$

in SI units. He used the term "apparent roughness" because the values of k corresponding to measured values of n are unrealistic if interpreted in the original sense of k_s. For example, a value of $n = 0.225$ measured in a vegetated watercourse implies through equation (2.22) a k value of 43000 m. Christensen assumed that the total energy loss over a reach of uniform flow in a channel containing different species of rigid, emergent vegetation comprises friction, local losses associated with irregularities in the flow path and losses associated with drag on the vegetation elements. By considering equilibrium of forces acting on a control volume and projected on the bed, and using the Darcy-Weisbach equation with f defined by equation (2.21) to represent the appropriate energy gradients, he derived the following expression for the equivalent roughness for a subsection i of a cross-section accounting for friction, local losses and vegetation drag.

$$k_{e,i} = k_{h,i}\left[1 - \frac{1}{\cos\theta_i}\sum_{j=1}^{j=q} N_{j,i} c_j \delta_j^2 + \frac{35.3 d_i^{4/3}(\cos\theta_i)^{1/3}}{k_{h,i}^{1/3}}\sum_{j=1}^{j=q} N_{j,i}\delta_j C_{D,j}\right]^3 \qquad 2.23$$

with $k_{h,i}$ given by

$$k_{h,i} = k_i\left[1 + 35.3\frac{(d_i\cos\theta_i)^{4/3}}{k_i^{1/3}}\frac{\sum\zeta}{\Delta l_i}\right]^3 \qquad 2.24$$

In equations (2.23) and (2.24) $k_{e,i}$ is the equivalent roughness for subsection i accounting for friction, local losses and vegetation drag, $k_{h,i}$ is the equivalent roughness accounting for friction and local losses, k_i is the equivalent roughness accounting for friction only, θ_i is the transverse inclination of the wetted perimeter of subsection i, j represents one of q vegetation species , $N_{j,i}$ is the number of stems of species j in subsection i, c_j is the cross-sectional shape factor for stems of species j (= $\pi/4$ for circular cylinder), δ_j is the stem diameter for species j, d_i is the local flow depth for subsection i, C_{Dj} is the drag coefficient for species j stems (= 1.0), $\Sigma\zeta$ is the sum of local energy loss coefficients (applied to the velocity head), and Δl_i is the length of channel under consideration. Once a value for $k_{e,i}$ has been determined, this can be used to calculate the corresponding value of n using equation (2.22). (It must be noted that local losses associated with channel irregularities may be influenced by the presence of vegetation (Liu, 1997) and can not always be treated independently as the above procedure suggests).

Klaassen and van der Zwaard (1974) proposed a method for estimating C for flow through fruit trees, based on 1:10 scale model studies. C is estimated as a function of C_D, the projected plant area, the value of C in the absence of trees and a velocity coefficient based on a logarithmic vertical distribution of velocity. Values of C_D were determined from the model studies and the mean value of 1.5 was proposed for prototype application although the data show clear trends with density, pattern and Re, with significantly higher values for Re < ~5000.

Ackers (1991) proposed the following expression for the overall resistance of a rod-roughened surface with the rods arranged in a regular, staggered formation of alternating rows.

$$f = 4\alpha C_D(\beta_1 N_1 + \beta_2 N_2)dz / P + (\beta_1 + \beta_2) f_s / 2 \qquad 2.25$$

In this equation f_s is the basic friction factor for the boundary surface, d is the rod diameter, z is the flow depth, P is the wetted perimeter, N_1 and N_2 are the numbers of rods per unit channel length for the two alternating rows, αC_D is the effective drag coefficient for the rods, and β_1 and β_2 account for the blockage effects of the alternate rows of rods. The blockage coefficients are given by

$$\beta_1 = \left(1 - \frac{n_1 z d}{A}\right)^{-2} \qquad 2.26$$

and

$$\beta_2 = \left(1 - \frac{n_2 z d}{A}\right)^{-2} \qquad 2.27$$

in which n_1 and n_2 are the numbers of rods across the section in the alternating rows, and A is the cross-sectional area of the section. The effective drag coefficient is given by

$$\alpha C_D = 1.184 - 0.277 Z_* + \sqrt{0.529 Z_* - 0.843} \qquad 2.28$$

for $1.75 < Z_* < 6.6$, otherwise

$$\alpha C_D = 0.95 \qquad 2.29$$

for which $Z_* = z/d$.

In most cases where formulations for Manning's n or friction factor incorporate the drag coefficient (C_D), a value of C_D of about 1.0 is recommended, corresponding to the case of a single, isolated cylinder in turbulent flow. Li and Shen (1973) confirm a value of 1.2, based on experimental measurements, provided that the wave drag is small, no aeration takes place behind the cylinder, and the cylinder Reynolds number is greater than about 8×10^3, but still within the subcritical regime before laminar separation of the boundary layer occurs. This value also applies to a cylinder within a group of cylinders if the local approach velocity is used in the drag equation. The local approach velocity is different from the mean velocity based on the channel flow area, however, because of the velocity defect associated with wake formation from each cylinder. The mean drag coefficient (to be used with the mean velocity in the drag equation) for the i^{th} cylinder in a row is given by

$$C_{Dmi} = \frac{V_i^2}{V^2} C_D \qquad 2.30$$

in which V_i is the local approach velocity and V is the mean velocity (based on channel flow area). Li and Shen (1973) used Petryk's (1969) linear superposition of velocity defect model to determine the variation of local drag coefficient in two basic cylinder distribution patterns, viz. "parallel" where the cylinders in any row are located directly downstream from those in the preceding row, and "staggered" where the cylinders in any row are located downstream of the gap between the cylinders in the preceding row. This value tends to a constant asymptotic value in a field of cylinders, which can be used as an effective drag coefficient (C_{D_c}) for a large group. Li and Shen's predicted variations of asymptotic mean drag coefficient values with cylinder spacing for these patterns (with equal longitudinal and transverse cylinder spacing) are reproduced in Fig. 2.1.

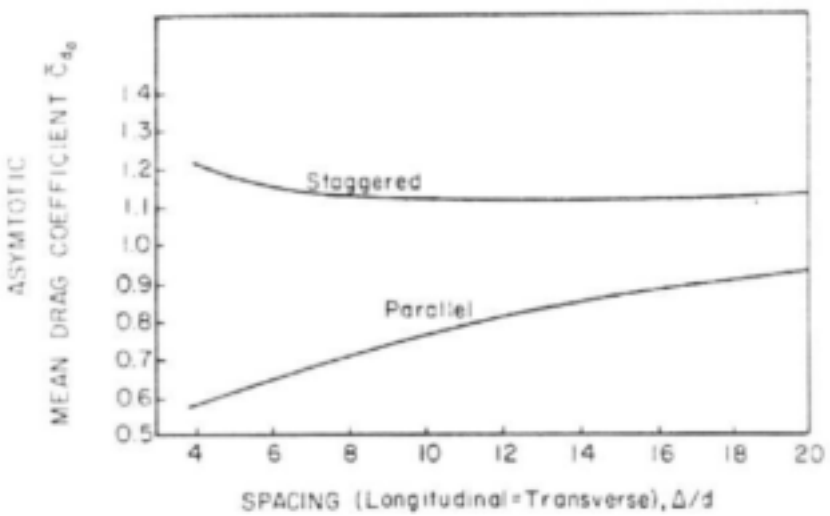

Figure 2.1 Asymptotic mean drag coefficient for staggered and parallel cylinder arrangements (Li and Shen, 1973)

Lindner (1982) extended Li and Shen's (1973) work (see Pasche and Rouvé, 1985) and proposed that the effective drag coefficient for a large group of cylindrical rods can be estimated as

$$C_{D_c} = \left(1 + 1.9 \frac{d_p}{a_z} C_D\right) V_r^2 + \Delta C_D \qquad 2.31$$

The first term in equation (2.31) accounts for the narrowing effect of neighbouring cylinders and the second term (ΔC_D) accounts for the resistance due to gravitational force. In this equation d_p is the cylinder diameter, a_z is the transverse cylinder spacing, C_D is the value for a single cylinder in two-dimensional flow (as given in standard texts), and V_r is a velocity ratio given by

$$V_r^2 = 0.923\left(\frac{x_N}{a_x}\right)^{-0.374} + 0.61\left(\frac{z_N}{a_z}\right)^{1.33} \qquad 2.32$$

in which a_x is the longitudinal cylinder spacing. The wake length, x_N, is given by

$$0.03 = 0.90\left(\frac{x_N}{C_D d_p}\right)^{-0.70}\left(\frac{1}{1+\frac{8x_N S}{V^2/2}}\right)^{1.5} \qquad 2.33$$

The wake width is given by

$$\frac{2z_n}{C_{De} d_p} = 0.48\left(\frac{x_N}{C_D d_p}\right)^{0.59} \qquad 2.34$$

The second term in equation (2.31), accounting for the resistance due to gravitational force, is given by

$$\Delta C_D + \frac{2}{Fr^2}(1 - y^*) \qquad 2.35$$

in which Fr is the Froude number and y^* is a depth ratio obtained from

$$\frac{V}{\sqrt{gh}} = \sqrt{\frac{y^*(y^{*2}-1)}{2\left(y^* - \frac{a_z}{a_z - d_p}\right)}} \qquad 2.36$$

in which h is the flow depth.

Pasche and Rouvé (1985) proposed calculating the flow velocity through emergent vegetation using the Darcy-Weisbach equation with

$$f = f_b + f_v \qquad 2.37$$

in which f_b is the friction factor associated with the bed roughness and f_v is the friction factor associated with the vegetation, as given by

$$f_v = \frac{4hd_p}{a_x a_z} C_{De} \qquad 2.38$$

with C_{De} quantified by Lindner's (1982) method (equations (2.31) to (2.36)).

Based on the investigations by Lindner (1982) and Kaiser (1984), Nuding (1994) also used equation (2.38) to determine f_v, with C_{De} normally having a value of 1.0, but ranging from 0.6 to 2.5 depending on the form of the vegetation elements. He recommends values of the ratio $d_p/(a_x a_z)$ between 0.1 m^{-1} for light and 3.0 m^{-1} for dense vegetation.

Fathi-Maghadam and Kouwen (1997) found that the resistance coefficient is affected significantly by the flexibility of plants because bending causes streamlining, which decreases the drag coefficient and reduces the momentum absorbing area. The resistance coefficient also varies with flow depth because foliage is nonuniform vertically and hence the momentum absorbing area changes with relative submergence of the vegetation. They used dimensional analysis to establish the following functional relationship for subcritical, turbulent flow in channels with nonsubmerged, tall, dense vegetation.

$$C_D\left(\frac{A}{\forall}\right)h = fn\left(\frac{\rho V^2 y_n^4}{J}\right) \qquad 2.39$$

In equation (2.39) $\forall = ay_n$, a is the horizontal bed area covered by vegetation, y_n is the flow depth, A is the momentum absorbing area, h is the average plant height, and J is the flexural rigidity of the plant. J is the product EI, where E is the modulus of elasticity and I is the cross-sectional second moment of area of the plant. The momentum absorbing area is greater than the projected area because the foliage behind the frontal areas also absorbs momentum, and should therefore be determined on a volumetric basis. Equation (2.39) defines the friction factor through equation (2.19) and hence Manning's n can be determined. Fathi-Maghadam and Kouwen (1997) quantified equation (2.39) by conducting experiments on pine and cedar saplings and hence determined values of Manning's n for a range of relative flow depths (similar results could be obtained from experiments with reeds). They conclude that, for emergent conditions for vegetation with a linear relationship between momentum absorbing area and depth of submergence, Manning's n increases in proportion to the square root of flow depth. The variation of n with depth is caused by the variation of submerged momentum absorbing area, so the density of vegetation is the dominant factor.

Kutija and Hong (1996) accounted for bending in determining the effective height of reeds when evaluating the drag force. They calculated the deflection of the reed stem using cantilever beam theory under a vertically varying drag force, reed diameter and reed stiffness. This calculation requires iteration as the effective height is reduced by bending, which in turn reduces the drag force.

The approaches presented thus far are based on the conventional open-channel resistance equations (Manning, Chézy and Darcy-Weisbach) with the relevant coefficients determined directly from experimental results or through estimation of the drag coefficient for the vegetation elements. The use of the open-channel equations has been criticized because they really apply to situations where flow is controlled by bottom drag and not vegetation element drag (Kadlec, 1990). The Manning equation and the equations for f (and hence C) in hydraulically rough and transitional flow exhibit a variation of resistance with flow depth, reflecting the logarithmic distribution of velocity away from the boundary. In vegetated flows the distribution is more nearly uniform and the equations and coefficients do not apply in the same way. For example, Manning's n is not approximately constant with depth as for an unvegetated channel, but has been shown to vary strongly with the product VR. Although relationships between n and VR have been determined, this approach is not satisfactory, apart from the undesirability of an equation for velocity including a coefficient which itself depends on velocity. Major criticisms (Smith et al, 1990) are that the same value of VR may be obtained from different pairs of values of V and R for which the flow condition and resistance characteristics are clearly different, and that the n-VR relationship is not independent of slope. Kadlec (1990) also points out that wetland flows are often in the transition region between laminar and turbulent flow, for which Manning's equation does not apply, even in unvegetated channels.

Turner and Chanmeesri (1984) and Smith et al (1990) suggested a more general form of resistance equation, viz

$$q = aS^b y^c \qquad 2.40$$

in which q is the unit width discharge, y is the flow depth and a, b and c are empirically fitted parameters. They determined values for a, b and c for four different crop species under emergent conditions with good correlation, but cautioned that the high variability of these parameters between different crop types and flow conditions makes it essential to determine appropriate values experimentally for each situation.

Kadlec (1990) recommends a similar equation for overland flow in wetlands with emergent vegetation, which he expresses as

$$q = Kd^{\beta}S^{\alpha} = V_a d'^{\beta} \qquad 2.41$$

in which d is the average depth, V_a is the average superficial velocity and d' is the average depth of free water which accounts for spatially varied ground topography. The value of β reflects both the vertical variation in vegetation density and the bed topography and is typically in the range $2 \le \beta \le 4$. The value of α is 1.0 if the stem Reynolds number is in the laminar range and 0.5 if it is in the turbulent range. K needs to be determined from field data.

An alternative approach to using a resistance equation with the resistance coefficient determined through vegetation characteristics is to simulate the resistance phenomena directly. This approach was used by Thompson and Roberson (1976). They developed a model of the vertical velocity

distribution through emergent and submerged vegetation (represented by cylindrical elements), allowing for bending. The velocity profile through the full depth was described as a composite of three zones, viz. a viscous sublayer close to the channel bed, a zone between the viscous sublayer and the tops of the stems, and the zone above the vegetation for the submerged condition. They assumed that the total resistance per unit bed area (τ_o) comprised components of viscous shear stress from the bed (τ_s) and a component representing the stem drag (τ_r), i.e.

$$\tau_s + \tau_r = \tau_o \qquad 2.42$$

The separation of total resistance into bed and stem components, as suggested by equation (2.42) is particularly important for sediment interaction descriptions, as it is the bed component (τ_s) that drives bed load. Reliable quantification of equation (2.42) therefore needs to be confirmed.

2.4 RESISTANCE IN PARTIALLY REEDED CHANNELS

The distribution of reeds in semi-arid rivers is generally not uniform over the whole cross section, and depends on the occurrence of alluvium and the local hydraulic regime. Reed beds colonize alluvial dominated areas and their abundance is closely related to water level. In the Sabie River the maximum abundance of *Phragmites mauritianus* occurs between 0 and 1.25 m above the 1.5 m^3/s stage level, with 75% of reeds occurring between 0 and 1.50 m above this level (Mackenzie et al, 1997). The reed beds thus colonize alluvial locations, such as lateral and mid-channel bars, subjected to perennial or seasonal flooding to about the 1.05 year return period. By contrast, growth of *Phragmites australis* is most vigorous where the water table is just above the ground level (Ostendorp, 1991). These habitat preferences mean that stands of reeds will become established only in certain locations in a river reach, resulting in a nonuniform distribution of hydraulic roughness.

Determining the conveyance of a river channel to define a stage-discharge relationship or calculate the average flow velocity requires estimation of the overall resistance. Because the resistance to flow through reeds is significantly greater than through unvegetated areas, a procedure must be established for obtaining a representative friction factor or resistance coefficient for the whole channel, accounting for the effects of all the surfaces present.

Several approaches have been proposed for estimating an equivalent value of Manning's n for a channel with a number of different surface roughnesses across a section. For the following formulations the channel cross section is divided into N subsections, each with a wetted perimeter (P_i) which does not include the interfaces with adjacent subsections, and with a known local value of the resistance coefficient, n_i.

Horton (1933) assumed that the velocities in the subsections are all equal to the average velocity for the whole cross section. This assumption leads to the following expression for the equivalent, overall, value of Manning's n:

$$n_e = \left(\frac{\sum_{i=1}^{N} \left(P_i n_i^{3/2} \right)}{P} \right) \qquad 2.43$$

in which n_e is the equivalent value and P is the total wetted perimeter. The assumption of equal velocities in all subsections is rarely valid, as different local depths and roughnesses will give rise to different local velocities.

Einstein and Banks (1950) assumed that the total boundary shear force for the whole cross section is the sum of the subsection shear forces. The equivalent value of Manning's n is then given by

$$n_e = \left(\frac{\sum_{i=1}^{N} \left(P_i n_i^{2} \right)}{P} \right)^{1/2} \qquad 2.44$$

By assuming the total discharge for the whole cross section to be the sum of the subsection discharges, calculated separately, Lotter (1933) formulated the following expression for the equivalent resistance coefficient:

$$n_e = \frac{P R^{5/3}}{\sum_{i=1}^{N} \frac{P_i R_i^{5/3}}{n_i}} \qquad 2.45$$

in which R_i is the hydraulic radius of the ith subsection.

Colebatch (1941) assumed local flow conditions to be associated with flow area rather than wetted perimeter, and proposed that the equivalent resistance coefficient is given by

$$n_e = \left(\frac{\sum_{i=1}^{N} \left(A_i n_i^{3/2} \right)}{A} \right)^{2/3} \qquad 2.46$$

Krishnamurthy and Christensen (1972) derived expressions for the equivalent hydraulic roughness and Manning's n for shallow cross sections by adding together the subsection discharges. Each subsection discharge is calculated from the logarithmic vertical velocity distribution, using the velocity at $0.368d_i$ above the bed to represent the average velocity, where d_i is the local flow depth. The equivalent hydraulic roughness is given by

$$ln\, k_{se} = \frac{\sum_{i=1}^{N} P_i d_i^{3/2} ln\ k_{si}}{\sum_{i=1}^{N} P_i d_i^{3/2}} \qquad 2.47$$

and through the knowledge that $n \propto k_s^{1/6}$, the equivalent Manning's n is given by

$$ln\, n_e = \frac{\sum_{i=1}^{N} P_i d_i^{3/2}\, ln\, n_i}{\sum_{i=1}^{N} P_i d_i^{3/2}} \qquad 2.48$$

Krishnamurthy and Christensen recommend use of equivalent k rather than equivalent n because the differences between local k_s values will be greater than differences between local n values, and because it is usually more accurate to estimate local k_s than local n. For wide channels where the bank influence is negligible these relationships become

$$ln\, k_{se} = \frac{\sum_{i=1}^{N} P_i\, ln\, k_{si}}{P} \qquad 2.49$$

and

$$ln\ n_e = \frac{\sum_{i=1}^{N} P_i ln\ n_i}{P} \qquad 2.50$$

In an assessment of the different formulae using data from the Mississippi River, Krishnamurthy and Christensen (1972) found their formula for n_e to agree more closely with measured values than those of Horton (1933), Lotter (1933) and Einstein and Banks (1950). However, Motayed and Krishnamurthy (1980) also assessed the performance of these four equations at 36 natural

cross sections where Manning's equation was considered applicable, and found Lotter's (1933) formula (equation (2.45)) to predict composite roughness with the least error.

Equivalent hydraulic roughnesses or resistance coefficients can also be determined as weighted averages of subsection values. For example, Fisher (1993) reports that values of k_s and f from design charts can be weighted by wetted perimeter to obtain equivalent values. The equivalent hydraulic roughness for a surface with two characteristic roughness values is therefore

$$k_{se} = p_1 k_{s1} + p_2 k_{s2} \qquad 2.51$$

in which p_1 and p_2 are the proportions of the total perimeter occupied by surfaces with roughnesses k_{s1} and k_{s2} respectively. Similarly, the effective friction factor is given by

$$f_e = p_1 f_1 + p_2 f_2 \qquad 2.52$$

This approach is recommended where the difference in roughness is not too great ($0.05 < k_{s1}/k_{s2} < 20$) and the areas occupied by the surfaces are similar ($0.33 < p_1/p_2 < 3.0$). The first of these conditions is unlikely to be met in partially reeded channel reaches. Equations (2.51) and (2.52) were originally proposed for pipes and their applicability to channels is apparently not established.

Each of these expressions will give a different value for n_e. The most reliable in any particular case will be the value produced by the expression whose underlying assumption is most closely approximated by the actual situation. The assumption in all that the interface between adjacent subsections can be neglected in the wetted perimeter is poor in almost all cases as there will be shear stresses on these interfaces wherever the velocity distribution is not uniform.

Rather than evaluating an equivalent resistance coefficient for a section, the total discharge or conveyance (K) is often calculated directly by dividing the cross section into elements with constant roughness, performing the calculations for each element independently, and then adding them. The conveyance in terms of Manning's equation is defined as

$$K = \frac{1}{n} A R^{2/3} \qquad 2.53$$

The total conveyance for a channel with m subdivisions is then given by

$$K = \sum_{i=1}^{m} K_i \qquad 2.54$$

in which the subscript i denotes the subdivision value.

Garbrecht and Brown (1991) present an exposé of the consequences of this subsection summation approach. They showed that this approach always leads to overestimation of the total conveyance because of the introduction of a lateral velocity gradient, neglect of lateral shear between elements, and the computation of the nonlinear conveyance as a linear summation of components. They assessed the degree of overestimation for various simple concave channels with uniform roughness under one-dimensional, uniform, steady flow conditions. The degree of overestimation depends on the section shape and increases with the number of section elements specified. For rectangular and trapezoidal sections with width to depth ratios (W/D) greater than 20 the overestimation of conveyance may be expected to be less than 5%, but increases substantially for narrower channels. Subdivision should be avoided for channels with $W/D < 10$.

Probably the most effective approach to account for the nonuniform velocity distribution and lateral momentum transfer across a section in estimating conveyance is through turbulence modelling. Wark (1993) and Wark et al (1991) have proposed the Lateral Distribution Method for describing the distribution of flow within a channel. Although this method was developed for application to compound channels, it is also suitable for simple channels with composite roughness. The method involves the numerical solution of the two-dimensional shallow water equations, derived for steady, uniform flow in a channel with a laterally horizontal water surface by integration of the general three-dimensional turbulence equations. Solution of the model for every case would be tedious, but some general results could be obtained by hypothetical applications. Application requires specification of the channel geometry, bed roughness and lateral eddy viscosity in each sub-section of the channel.

Fisher (1993) carried out a series of experiments to determine the overall resistance characteristics of a channel with different patterns of roughness elements. The bed of a 25 m long, 0.9 m wide flume was roughened with 10 mm gravel laid in the patterns shown in Fig. 2.2. A range of discharges were passed through the flume and the values of Manning's n and k_s calculated from the measured discharge and depth. The k_s value was calculated from the Colebrook-White formula in the form

$$V = -\sqrt{32gRS}\log\left(\frac{k_s}{14.8R} + \frac{1.255\nu}{R\sqrt{32gRS}}\right) \qquad 2.55$$

The measured values of n, together with those calculated using the methods of Lotter (1933), Horton (1933), Einstein and Banks (1950) and Krishnamurthy and Christensen (1972) are plotted against % roughness cover for one discharge in Fig. 2.3. Measured values of k_s are plotted together with values calculated from design charts and equation (2.51) are plotted against % roughness cover for the same discharge in Fig. 2.4. These results show that the effective resistance depends strongly on the pattern of roughness as well as on the percentage cover.

One special case of composite roughness that has received detailed attention is that where the channel bed and banks, or side walls, have different roughnesses.

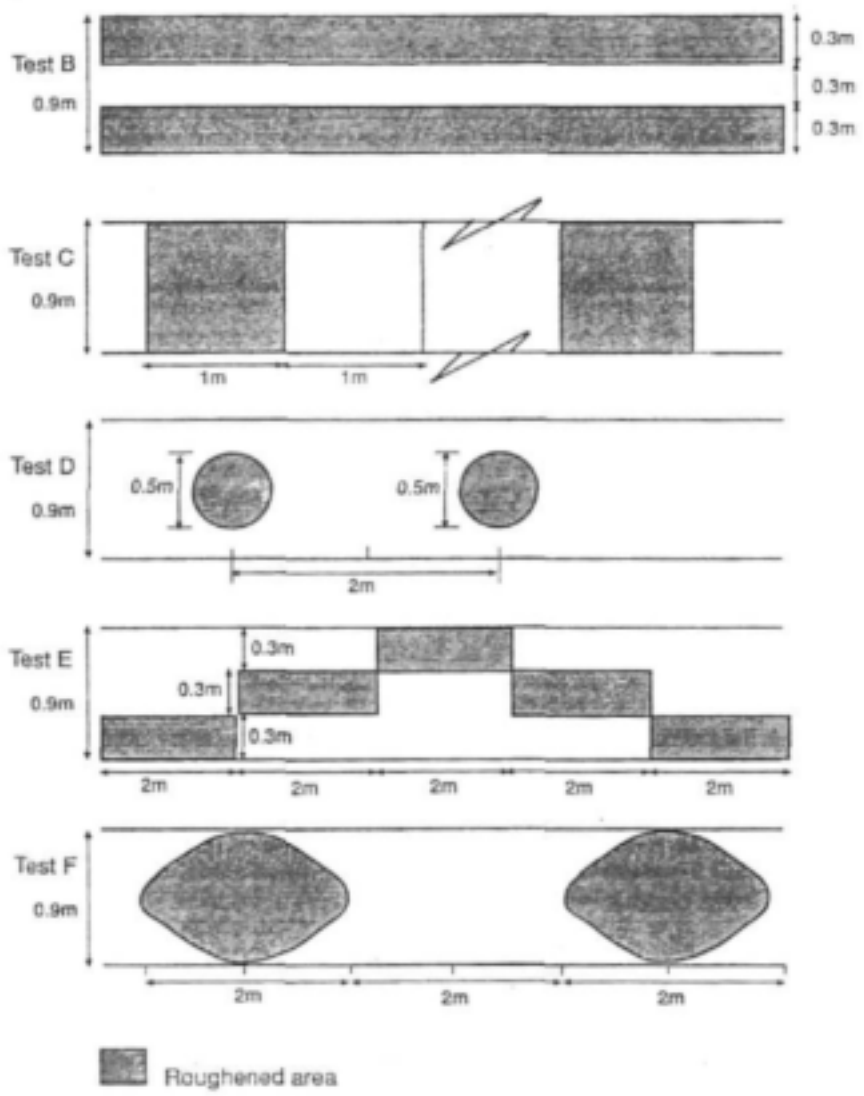

Figure 2.2 Layout of bed roughness used by Fisher (1973)

Vanoni and Brooks (1957) proposed a method for determining the average shear stress on a channel bed from overall flow characteristics, primarily for analysing laboratory experiment results. In this method it is assumed that the cross section can be divided by planes on which there is no shear into portions in which the flow is resisted by the bed and side walls independently (Fig. 2.5).

It is further assumed that the average flow velocities and the energy gradients in the different subareas are identical. Under these assumptions the ratio R/f is the same for each sub area and the total area and so a value for the side walls can be determined from measurements of f and R taken for the whole cross section. The friction factor for the walls, f_w, can then be obtained from a graphical relationship between f_w and R/f provided by Vanoni and Brooks (1957) for the case of smooth side walls. The assumption of equal velocities and energy gradients and the geometrical condition that the total area is the sum of the subareas leads to the following relationship between the friction factors for the bed (f_b), the side walls and the whole cross section (f).

$$f_b = f + \frac{2y}{b}\left(f - f_w\right) \qquad 2.56$$

in which y is the flow depth and b is the channel width

The friction factor for the bed can thus be derived and a value for the hydraulic radius associated with the bed obtained by applying the Darcy-Weisbach equation.

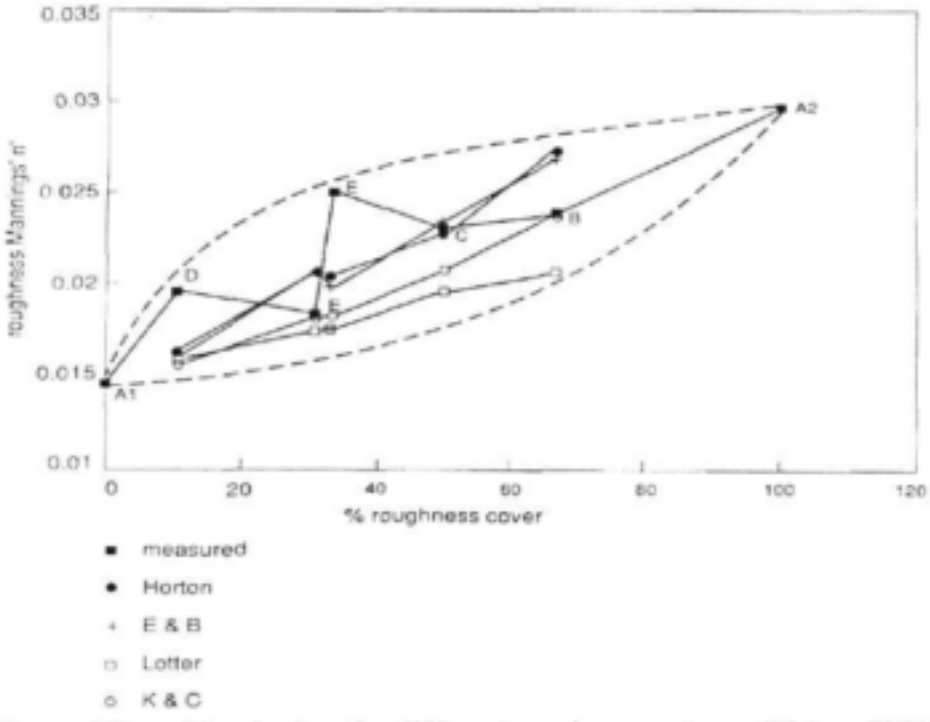

Figure 2.3 Manning's n for different roughness patterns (Fisher, 1993)

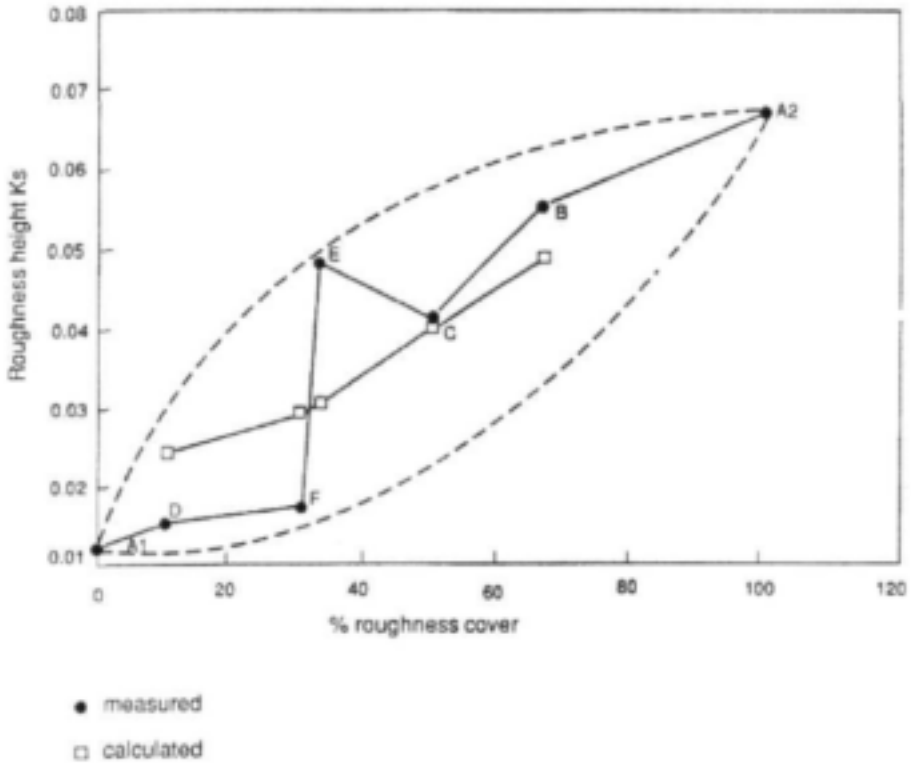

Figure 2.4 Roughness heights for different roughness patterns (Fisher,1993)

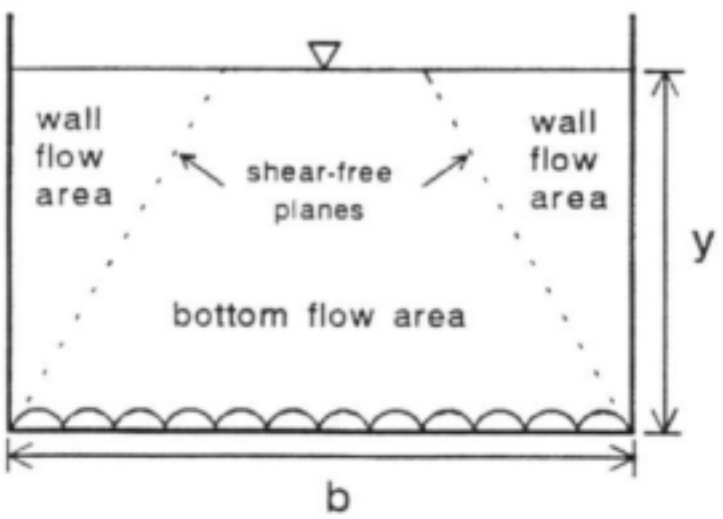

Figure 2.5 Subdivision of flow area into subareas resisted by bed and banks

Brownlie (1981) modified this procedure to allow for rough side walls by incorporating an iterative use of the Moody diagram in place of the smooth wall function provided by Vanoni and Brooks (1957). The ratio R/f is calculated as before and a straight line plotted on the Moody diagram with an intercept at $f = 0.01$ of $0.01R/f$ and a slope of 1 in log units. The desired values of f_w and R_w lie on this line and are found by trial. The values for the bed are then obtained from

$$Pf = P_b f_b + P_w f_w \qquad 2.57$$

and the equality of the ratios R/f for the subareas and total area.

Hey (1979) pursued the idea of dividing the cross section into portions resisted by the bed and banks in order to evaluate the total flow resistance in a channel with different roughnesses on the bed and banks. He defined the positions of the division planes as the locus of points where the velocities on the logarithmic profiles relative to the bed and banks are equal (Fig. 2.6). These planes may be located by defining the points of maximum velocity on them as

$$\frac{y_l}{y_b} = \frac{D_l}{D_b} \qquad 2.58$$

and

$$\frac{y_r}{y_b} = \frac{D_r}{D_b} \qquad 2.59$$

in which y_l, y_r and y_b are the perpendicular distances from the left bank, right bank and bed to the points of maximum velocity respectively, and D_l, D_r and D_b are the roughness heights of the left and right banks and the bed.

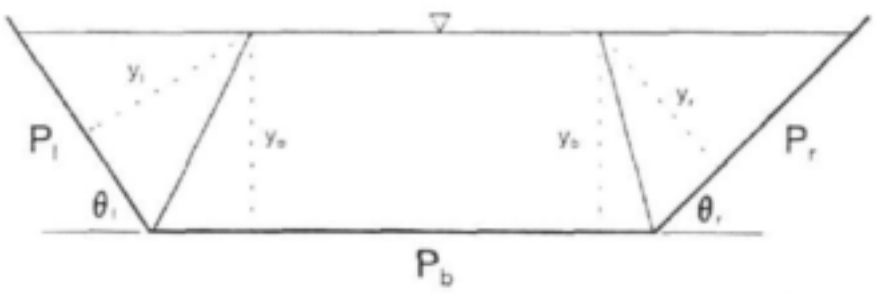

Figure 2.6 Cross section subdivision by Hey (1979)

The subdivision shown in Fig. 2.6 enables the hydraulic radius to be determined for each portion of the cross section, and hence its friction factor from equation (2.6) with k_s defined by the appropriate roughness height. To evaluate the flow resistance of the cross section as a whole, Hey (1979) standardized the roughness heights of the banks to that of the bed by transforming the cross section to its equivalent plane surface. The effective wetted perimeters for the left and right banks are then given by

$$P_l' = \frac{y_l}{\sin\theta_l} \qquad 2.60$$

and

$$P_r' = \frac{y_r}{\sin\theta_r} \qquad 2.61$$

in which θ_l and θ_r are the inclinations of the left and right banks respectively. The total effective wetted perimeter is then

$$P' = P_b + P_l' + P_r' \qquad 2.62$$

in which P_b is the wetted perimeter of the bed, and the effective hydraulic radius is

$$R' = \frac{A}{P'} \qquad 2.63$$

where A is the total cross-sectional area. The effective friction factor can then be found from equation (2.6) using D_b as the roughness height and R' as the hydraulic radius. The average flow velocity is then as given by the Darcy-Weisbach equation (equation (2.4)) using R' as the hydraulic radius.

When using equation (2.4) to determine f, Hey (1979) recommends a value for c of 2.03. The value of a depends on the cross-sectional geometry and varies between 11.1 (for infinitely wide channels) and 13.46 (the value for pipes). Hey found a unique relationship between a and the ratio of hydraulic radius to the perpendicular distance from the boundary to the point of maximum velocity (y), as presented in Fig. 2.7. This relationship can be used to define a when using the actual or effective values of hydraulic radius and the corresponding values of y.

Masterman and Thorne (1992, 1994) applied Hey's (1979) method of channel subdivision to calculate the resistance of channels with vegetated banks. Knowledge of the roughness heights for the bed and banks enables the friction factor values to be determined from equation (2.6) and the subdivision mean flow velocities to be calculated from the Darcy-Weisbach equation

(equation (2.4)). The subdivision discharges can then be calculated as products of mean velocity and area, and the total discharge by addition of the subdivision values. The effective roughness height for the bed can be determined from the size of the bed material (such as done by Hey (1979)). For submerged bank vegetation, Masterman and Thorne (1992, 1994) recommend the results presented by Kouwen et al (1969), Kouwen and Li (1980) and Kouwen (1988). These authors showed the effective roughness height for flexible, submerged vegetation to depend on the vegetation stiffness and the strength of flow over it, according to

$$k = 0.14h\left(\frac{\left(\frac{mei}{\tau}\right)^{0.25}}{h}\right)^{1.59} \qquad 2.64$$

in which h is the vegetation height, τ is the mean boundary shear stress and mei is a composite parameter representing the flexural rigidity of the vegetation per unit area (in Nm^2). In this parameter m is the relative stem density, e is the modulus of elasticity (Pa) and i is the second moment of area of the stem cross section (m^4); the product ei is therefore the stem flexural rigidity (Nm^2). The value of k determined by equation (2.64) can be used to represent the roughness height in equation (2.6).

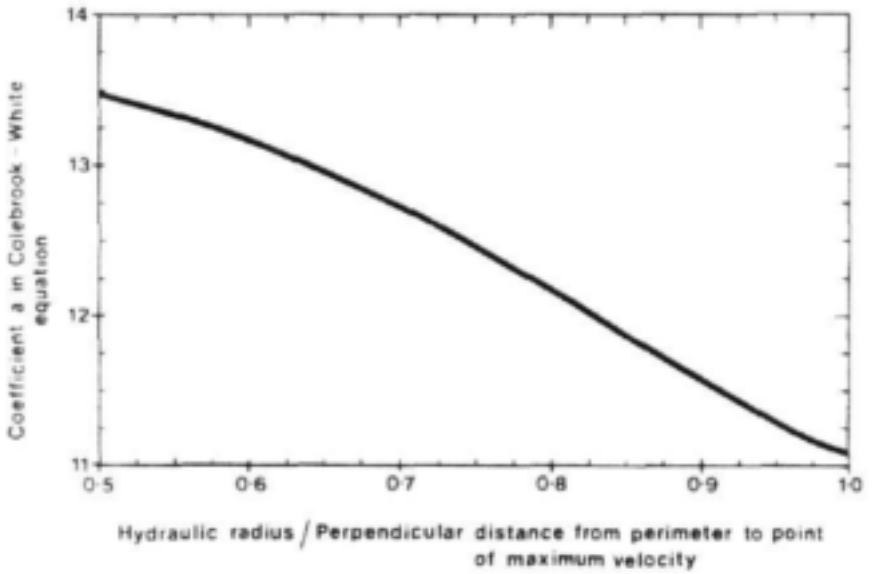

Figure 2.7 Variation of coefficient a in equation (2.6) with channel geometry (Hey, 1979

Equation (2.64) shows the effective roughness height for vegetation to depend on the boundary shear stress, which is different on the channel bed and banks. Flintham and Carling (1988) developed a method for distributing boundary shear stress over the bed and banks. This depends,

however, on the effective roughness values of each subarea, and an iterative solution is therefore necessary.

Masterman and Thorne (1994) incorporated emergent, non-flexible vegetation into the analysis by using results for the wake velocity in emergent vegetation developed from the model of Li and Shen (1973) by Thompson and Roberson (1976). These give the wake velocities for staggered and parallel vegetation arrangements as functions of the spacings and diameters of the vegetation elements.

Darby and Thorne (1996) refined the analysis of flow in channels with bank vegetation by applying the lateral distribution model proposed by Wark (1993) to compute the distribution of boundary shear.

Pasche and Rouvé (1985) accounted for bank vegetation by describing the lateral velocity distribution rather than defining zones within which velocity could be assumed constant. Although their study was for a compound channel with vegetated flood plains, their approach would be equally valid for strips of vegetation on the banks of simple channels. Lateral velocity distributions are computed independently for four distinct zones across the flow section: flood plain flow not influenced by the main channel flow, flood plain flow influenced by the main channel, main channel flow influenced by the flood plain flow and main channel flow not influenced by the flood plain flow.

The velocity in the region of flood plain flow not influenced by the main channel is determined by vegetation resistance and described by equations (2.31) to (2.38) as already presented.

The flow in the main channel influenced by the flood plain flow is assumed by Pasche and Rouvé (1985) to be controlled by the interface between the flood plain and the main channel acting hydrodynamically as a wall. The lateral velocity distribution within this zone can then be described by a logarithmic law,

$$\frac{v(z)}{v_*} = \frac{1}{k} ln\left(\frac{z}{k_T}\right) + c_T \qquad 2.65$$

in which $v(z)$ is the depth-averaged velocity at a distance z from the imaginary wall representing the interface between the main channel and the flood plain roughness, k_T is an imaginary roughness height associated with the flood plain roughness, and c_T represents the dimensionless slip velocity at the imaginary wall. This relationship can be integrated to obtain a resistance law and friction factor for this region. Pasche and Rouvé assumed (and subsequently demonstrated experimentally) that only a certain width b_m of flood plain vegetation contributes to the resistance in this region.

In the region of flood plain flow influenced by the main channel, Pasche and Rouvé assumed the stepwise absorption of the apparent shear stress on the interface by the roughness elements to be approximated by a parabolic function. This leads to a velocity distribution described by

$$v(z) = \Delta v_{fi}\left(1 - \frac{z}{b_m}\right)^3 + v_{fi} \qquad 2.66$$

in which v_{fi} is the velocity in the flood plain region not influenced by the main channel flow. The momentum balance in this flow region leads to a set of equations for determining the width b_m.

For uninfluenced flow in the main channel Pasche and Rouvé calibrated the Colebrook-White equation for the friction factor, using their experimental results.

Pasche and Rouvé (1985) carried out experiments for a range of flows, flood plain geometries and roughness densities and found their theoretical velocity distribution to be confirmed well. They also confirmed that the friction factor for flow in the main channel influenced by the flood plain flow is hardly influenced by the width of the vegetation zone.

The resistance afforded by vegetation in a channel depends not only on its areal extent and density, but also on its spatial distribution. Trissler and Stevens (1994) investigated the influence of spatial pattern by carrying out experiments with fully penetrating rod roughness elements in a 0.38 m wide flume. They arranged the rods in strips with the same density and total width along both sides of the channel, along one side of the channel and down the centre of the channel. Compared with the value for a strip along one side only, the value of Manning's n was 31% greater for the central strip and 22% greater for half-width strips on both sides. In addition, they modified the side strips to present wavy borders to the main flow and found this to increase the value of Manning's n by 16% for such a strip on one side of the channel and to decrease Manning's n by 18% for strips on both sides.

It would appear that reeds increase the overall resistance in a channel by imposing greater local resistance in the portions of the cross-sectional area they occupy, and by imposing an additional effective roughness to adjacent clear channel zones. There is evidence that extensive, longitudinal reedbeds may also influence overall resistance by modifying the flow structure and hence apparently unrelated energy mechanisms. James et al (2001), for example, have shown that marginal vegetation can reduce separation and spill resistance and in some cases actually reduce overall resistance.

Reeds occur in rivers not only in extensive beds along the banks or across the channel, but also in relatively small, isolated beds on bars or small islands or in association with bedrock outcrops. In these situations the resistance may prove to be better described by considering the reed patches as large scale roughness elements rather than contributors to composite roughness in the conventional sense. This would be analogous to the treatment of alluvial bed forms where the contributions of skin friction and form resistance are accounted for explicitly.

Some research has been carried out on resistance of unvegetated gravel bars, which may be suitable for extension to reed-covered sand bars. Hey (1988) formulated a procedure for estimating the resistance of gravel bars in pool-riffle morphologies. He assumes that the total effective roughness height (D_r) for a reach including pools and riffles is the sum of roughness

heights associated with grain resistance (D_g) and bar form resistance (D_b), i.e.

$$D_t = D_g + D_b \tag{2.67}$$

The effective friction factor is obtained from a Keulegan-type relationship in terms of D_t,

$$\frac{1}{\sqrt{f}} = 2.03 \log\left(\frac{ad}{D_t}\right) \tag{2.68}$$

in which d is the average flow depth over the reach including pools and riffles, a is given by

$$a = 11.1\left(\frac{R}{d_m}\right)^{-0.314} \tag{2.69}$$

in which d_m is the maximum flow depth, and D_t is the total roughness height given by

$$D_t = a d \left(\frac{D_g}{a_r d_r}\right)^{(f_r/f)^{1/2}} \tag{2.70}$$

in which the subscript r denotes values over riffles. The grain roughness height is related to the bed material size by

$$D_g = 3.5 D_{84} \tag{2.71}$$

in which D_{84} is the grain size for which 84% of the sediment is smaller.

The ratio of friction factors for the riffles and over the reach is given by

$$\frac{f_r}{f} = \frac{d_r^3 W_r^2 S_r}{d^3 W^2 S} \tag{2.72}$$

in which W is the average channel width and S is the average water surface slope.

The velocity can then be determined from the Darcy-Weisbach equation.

Parker and Peterson (1980) and Prestegaard (1983) divided the total energy slope (S_t) into grain (S_g) and bar-influenced (S_b) components, i.e.

$$S_t = S_g + S_b \qquad 2.73$$

Using measured values of d/D_{84} for the grain slope in a Keulegan-type equation, Prestegaard (1983) proposed that the grain component is given by

$$S_g = Fr^2 \left(6.25 + 5.75 \log \frac{d}{D_{84}} \right)^2 \qquad 2.74$$

in which Fr is the Froude number, given by

$$Fr^2 = \frac{V}{gd} \qquad 2.75$$

Prestegaard (1983) assessed the grain and bar components on data from 12 reaches of rivers with high width-depth ratios, low sinuosity and with well-developed pool-riffle sequences and found that bar resistance accounted for between 50% and 70% of the total resistance. In some cases the contribution from bars was exaggerated as it included energy losses associated with large-scale turbulence around individual boulders.

2.5 SEDIMENT VEGETATION INTERACTION

A complex feedback interaction takes place between river flow, the occurrence of vegetation and the channel morphology. Suitable habitats for aquatic macrophyte species are determined by flow and substrate characteristics, but the flow characteristics are themselves influenced by the occurrence of the plants through their resistance effects and the substrate is a consequence of the deposition of sediment, which is also influenced by the plants. Relationships between channel morphological characteristics and the occurrence of vegetation have been reviewed in section 2.2. This section focuses on the physical processes underlying these relationships, which entail the stabilization of sand bodies and the inducement of sediment deposition by vegetation.

The stabilization of cohesionless sand bodies by vegetation results at least partly from its modification of the flow field, and particularly the reduction in boundary shear through the absorption of momentum. The inducement of deposition in vegetated areas results from the

influence of the reduced boundary shear on the capacity for bed load transport and the effects of changes in turbulence structure on suspended load.

Tollner et al (1982) investigated the influence of vegetation on steady state sediment transport capacity relationships for the purpose of predicting sediment deposition in vegetated areas. Rather than describing the partitioning of resistance between stem drag and bed shear, they postulated an analogy between flow at a depth d through a bed of stems with a spacing of b and flow through a deep, narrow channel with the same flow depth and a width equal to b. The boundary shear stress can then be calculated as

$$\tau_o = \rho g R_s S \qquad 2.76$$

in which R_s is the equivalent hydraulic radius, given by

$$R_s = \frac{b\,d}{b + 2\,d} \qquad 2.77$$

Tollner et al (1982) carried out an experimental investigation of the sediment transport capacity through a medium of cylindrical rods, using a range of discharges, rod spacings, sediment particle sizes and sediment input concentrations. They found good agreement between measured rates of bed load, suspended load and total load and values predicted by the methods of Einstein (1942) and Graf (1971) if the bed shear was calculated using equation (2.76). They also found good agreement with Neill's (1967) incipient motion criterion with the hydraulic radius defined by equation (2.77). These results were confirmed for natural grasses by comparing predicted movement of sediment with measured values.

Abt et al. (1994) carried out laboratory experiments to assess the effect of submerged vegetation on deposition of sediment in a channel. The experiments were conducted in an 18 m long trapezoidal channel with a base width of 2.1 m and slope of 0.004. The channel had a sinuosity of 1.05 and included one wave length. Sediment with a median grain size of 0.09 mm was injected at the head of the reach and collected from vegetation patches located in the straight crossover section and both the insides and outsides of the two bends. Three vegetation types were used, all Kentucky bluegrass, but cut to different blade lengths (0.5, 3.0 and 8 inches). It was concluded that sediment deposition was enhanced by the grass but became significantly less as the blade length increased.

Valuable contributions to understanding of sediment/vegetation interactions have been made by Tsujimoto and his co-workers at Kanazawa University in Japan (e.g. Tsujimoto and Shimizu, 1994; Tsujimoto et al., 1991; Tsujimoto and Kitamura, 1994).

Tsujimoto and Kitamura (1996) described the interaction between the growth of riparian vegetation (including *Phragmites japonica*) and channel degradation downstream of dams. The reduction of flood flows allows encroachment of vegetation towards the middle of the channel during the extended base flow periods. During periods of higher flow, the channel resistance is increased by the vegetation and flow is concentrated in the central part of the channel, causing

accelerated degradation. By assuming rotational degradation, Tsujimoto and Kitamura were able to simulate the interaction of degradation and vegetation encroachment over a cycle of flood and base flow sequences. The rotational degradation model is based on an incremental adjustment of channel slope from the current value towards the equilibrium value defined by the bed shear stress imposed by the current flood event. This approach is very much in line with that envisaged for the reed-channel morphology model to be proposed by this project in that it is not based on high resolution sediment dynamic modelling, but rather operates at realistic scales and resolution levels.

Tsujimoto et al. (1996) described the interaction between the expansion of an isolated patch of vegetation and the deposition of sediment which it induces. They observed that deposition of suspended sediment in the lee of willow (*Salix gilgianna*) bushes in a gravel-bed stream provided suitable substrate for expansion of the bushes. Using artificial vegetation they experimentally simulated the growth of a vegetation patch and found that the area of sediment deposition decreased as the vegetation patch became longer. This behaviour was attributed to the flow velocity field induced by the vegetation: for a very short vegetation zone the velocity decreased to a minimum on the downstream side whereas for a longer zone the minimum velocity occurred within the vegetation and the velocity increased in the lee zone, inhibiting deposition. These observations were reproduced by application of a two-dimensional (depth-averaged) k-ε turbulence model to describe the velocity field through and around the vegetation. Flow characteristics generated by this model were used in a two-dimensional suspended sediment transport model to describe the patterns of sediment deposition associated with the vegetation, which agreed well with the experimental results. By allowing vegetation to cover the deposition zone during the low flow after a flood, the expansion of vegetation could be simulated for a sequence of river flows including repeated flood events. These experimental observations and simulations explain why isolated patches of vegetation increase in length to a definite limit only.

Field studies also indicate interaction between vegetation and sediment in bar development. Hickin(1984) reported that gravel-bed and sand-bed rivers often have stranded and partly buried trees and logs associated with mid-channel bars. The log or tree is typically at the head of the bar with a trail of sand and gravel deposited in its wake. Hickin (1984) pointed out, however, that accumulated vegetation in these features can also be a result, rather than a cause of bar formation. Similar features observed in the Sabie River, Kruger National Park, after the devastating floods of February, 2000, were however clearly a result of deposition in the lee of vegetation or vegetative debris. Even where vegetation does not influence the origin and location of mid-channel bars, it certainly does influence growth and development of bars on which it becomes established. This applies both to mid-channel bars (Hickin, 1984) and to lateral bars (Hadley, 1961; Graf, 1978). The sediment trapping effect on bars has been observed in several environments: Hadley (1961) found that up to 0.15 m of sediment was deposited in a two-year period on vegetated lateral bars on the Oriabi Wash in northeastern Arizona, and Hickin (1984) reported that the mid-channel bars with the highest elevation in the Squamish River (British Columbia) were those with vegetation growing in the sedimentary deposits. During a four-year investigation on the Sabie River, van Niekerk and Heritage (1993) also observed stabilization of mid-channel bars by reeds (*Phragmites mauritianus*).

The processes by which river channel width changes have been studied intensively by Thorne and

his colleagues at the University of Nottingham (e.g. Thorne, 1978, 1982, 1990). Bank retreat occurs by both progressive erosion and mass failure, which both depend on soil cohesion and the presence of vegetation. Erosion near banks is reduced by vegetation through the reduction of local velocity and bed shear stress, and the damping of turbulence (turbulence damping reduces the range, and hence the highest magnitudes of instantaneous velocity and shear stress). The soil erodibility is also reduced by the binding effect of roots and rhizomes. A study by Smith (1976) showed that the erodibility of alluvium in the banks of the Kicking Horse River in British Columbia varied inversely and exponentially with root density. A subsequent study by Hickin and Nanson (1984) confirmed that river banks which are particularly well bound by roots can offer far greater resistance to lateral erosion than simple unvegetated banks of alluvium. Bank stability against mass failure is enhanced by vegetation because the roots improve drainage and hence reduce pore pressures during rapid drawdown. Vegetation also acts to reinforce the soil by taking tension and hence redistributing stresses through the soil; Waldron (1977) found that the shear strength of soil can be increased by 100% and more by root reinforcing.

Bank accretion occurs when a bank is stable and sediment supply exceeds sediment transport downstream. Vegetation enhances this process by stabilizing the basal area and increasing roughness, hence reducing flow velocity and increasing deposition of both bed load and wash load. Harvey and Watson (1986) noted that bank advance by berm building in streams in Mississippi was greatly enhanced by the establishment of willows that induced wash-load deposition.

2.6 GENERAL APPROACH AND METHODOLOGY

This literature review has confirmed that, while the role of vegetation in influencing river hydraulics, sediment dynamics and hence channel morphology is widely recognised, there is currently insufficient knowledge and understanding of the processes involved to enable prediction of vegetated channel response to altered flow regimes. Very little is known about the hydraulic characteristics and growth behaviour of *Phragmites* reeds, possibly the most important vegetation type in semi-arid rivers. The effect of vegetation on flow resistance has been studied quite extensively, but most formulations are in terms of Manning's n, which is not ideal because of its variation with flow depth; a more rational equation recognising the dominant effect of stem drag resistance would be preferable. No reliable methods exist for predicting conveyance in partially vegetated channels, especially with reeds or other emergent vegetation types. Very little research has been done on the interaction between vegetation and sediment; there are no reliable relationships describing sediment transport in vegetated channels, and influences of vegetation patches on adjacent erosion and deposition processes have been investigated only in very particular situations. There appear to be no existing models which account effectively for vegetation influences in prediction of river morphology changes in response to modified hydrology.

The approach followed in carrying out this project was to address these important issues separately, using appropriate field, laboratory and analytical methods, and with due cognizance of their mutual dependence and the requirement for their ultimate integration. Much of the laboratory investigation ideally requires corroboration and extension through field work, but this

was not possible within the ambit of the project.

The hydraulically relevant characteristics of reeds (*Phragmites mauritianus*) were determined through field studies in the Kruger National Park. This established appropriate ranges of relevant parameter values for inclusion in the resistance investigations.

The basic resistance phenomenon of flow through reed stems was studied by laboratory investigation and theoretical analysis. Laboratory tests were carried out to enable the influences of fundamental variables to be described, and to provide data for confirming theoretically based resistance formulations (additional data from the literature were also used for this purpose). The theoretical analyses were done to establish an appropriate form of resistance equation, and to provide a detailed description of the phenomenon to enable generalization of the equation.

The influence of reedbed distribution on channel conveyance was demonstrated and quantified by laboratory investigation, and a method for predicting conveyance in rivers with extensive, longitudinal strip reedbeds was developed analytically.

The interaction between sediment and reedbeds was investigated experimentally under idealized laboratory conditions. This was necessary because of the primitive state of knowledge of the fundamental processes involved and the inability to undertake meaningful field investigation. Analysis of the data enabled bed load transport through reed stems to be quantified, and some sedimentation patterns to be described.

An approach to modelling the influence of vegetation in morphological change in rivers was developed using information from the literature and, where possible, guided by the findings of the other components of the project.

Chapter 3

REEDS IN SEMI-ARID RIVERS

3.1 INTRODUCTION

The effect of reeds on flow and sediment deposition is determined both by the morphology of the individual reed stems and properties of the whole reedbed.

The most important stem characteristic required for calculating drag forces on reed stems is the diameter. Characteristics such as stem height, flexibility and distribution of leaves and branches are also of interest when considering the effect of flow depth on the resistance due to reeds. The resistance coefficient will vary with flow depth because bending of stems causes streamlining, which reduces the drag coefficient. The momentum absorbing area also changes with relative submergence of the vegetation, because foliage is non-uniformly distributed vertically. Reedbed characteristics such as stem density, reedbed shape and size, and the roughness of the boundary will also affect the total resistance provided by a reedbed. In addition, the distribution of reedbeds at the reach scale is important for determining conveyance in partially reeded rivers. (Fisher (1993) showed that effective resistance depends strongly on both the pattern of roughness and the percentage cover).

The data presented in this chapter were gathered during field work in the Letaba and Sabie Rivers in the Kruger National Park. These rivers may be considered typical examples of semi-arid rivers.

The chapter presents realistic ranges of hydraulically relevant stem and reedbed characteristics for reeds in these rivers, including stem diameter, height and number of branches, as well as real distribution pattern characteristics in the field. Hypotheses are also developed about the effect of flow on reedbeds and changes in reedbeds over time, which can eventually be used in the development of rules for modelling morphological change in these rivers.

3.1.1 Species Description

The genus *Phragmites* contains three species, two of which are indigenous to southern Africa. While *Phragmites australis* is distributed throughout southern Africa, *Phragmites mauritianus* occurs only in the northern provinces of South Africa and northwards into tropical Africa (Gibbs Russell et al., 1990). The results presented in this chapter refer to *Phragmites mauritianus*, as it is this species which is present in the rivers of the Kruger National Park (KNP).

Phragmites mauritianus differs from *P. australis* primarily in above-ground characteristics. The two species are separated taxonomically by the shape of the leaf tips, the attachment of the leaf bases and the length of the glumes (Gibbs Russell et al., 1990). These characteristics are not expected to have a large influence on the resistance provided by the stems, except that *P. australis* stems will provide slightly more resistance in winter because the old leaf sheaths remain on the culm, unlike *P. mauritianus* where they do not.

P. mauritianus is common and locally dominant on the macro-channel floor of the Kruger National Park rivers, where it either forms monospecific stands or occurs in combination with various shrub species. It is the key species for one of the six riparian vegetation community types defined by van Coller (1993) for the Sabie River.

P. mauritianus is a perennial, rhizomatous grass with tall (to 5m), robust culms (Fig. 3.1). The leaves are up to 300mm long and 30mm wide, with sharp, rigid tips. The leaves are deciduous at the base of the leaf sheath, so that old culms are left bare. Lateral branches may be produced, especially when the main stem has been damaged, but these are usually of a much smaller diameter.

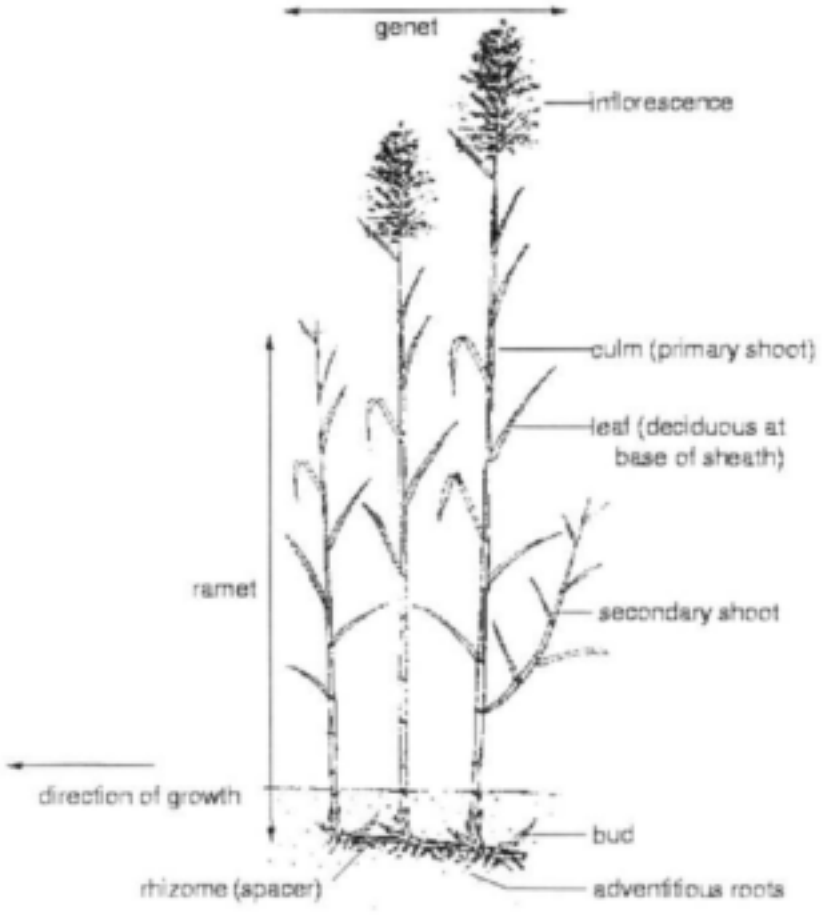

Figure 3.1 Morphology of *Phragmites mauritianus*

The shoots are connected below ground by an extensive network of rhizomes, which can extend to a depth of 2 m (Kotschy, 2001). Both horizontal and vertical rhizomes are present (Fig. 3.2). Several layers of horizontal rhizomes are present beneath mature reedbeds. Vertical rhizomes arise from buds on the horizontal ones, and it is the vertical rhizomes which give rise to the

shoots. Stolons may also be produced. These differ from rhizomes in that they have a smaller diameter, are photosynthetic and grow along the surface instead of below ground.

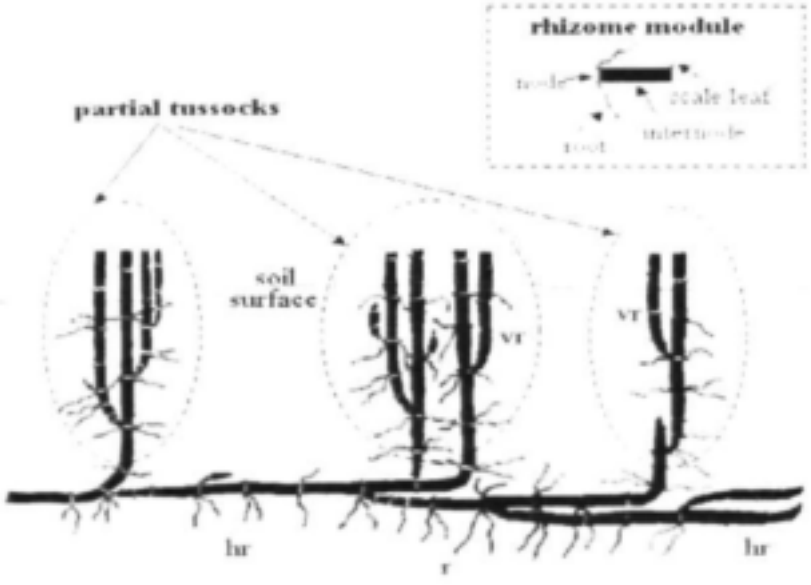

Figure 3.2 Rhizome architecture in *Phragmites mauritianus*

Phragmites mauritianus is a clonal plant with the capacity for vigorous lateral spread by the repeated production of new shoots along its rhizomes. Such growth is known as vegetative or clonal growth. The shoots so produced are all genetically identical and are known as ramets. The group of ramets produced from a single seed is referred to as a genet or clone (Fig. 3.1). The ramets belonging to a particular genet do not necessarily remain physically connected. The establishment of fragments of a clone in new locations is thought to be an important mechanism for reed establishment in the Kruger National Park rivers.

Phragmites mauritianus is also able to reproduce sexually. Flowering occurs from January to June (Gibbs Russell et al., 1990), although inflorescences may persist on the plants for longer. Both fruit and seeds are small and dispersed primarily by wind.

3.1.2 Habitat

Phragmites mauritianus is characteristic of riverbanks or flood plains with well-drained, sandy soils and permanently or frequently flowing water. In this respect it differs from *P. australis*, which is most commonly found in backwater swamps or other places with restricted drainage, and on organically rich or clayey sand (Thompson, 1985; Gordon-Gray and Ward, 1971). *P. australis* has, however, been shown to grow on any substrate where it is not moisture limited (Ostendorp,

1991). Gordon-Gray and Ward (1971) noted that in places where the distribution of the two species overlaps, *P. mauritianus* tends to occupy microsites with better drainage. These differences suggest that *P. mauritianus* has a lower tolerance of the anaerobic conditions associated with flooding.

In the rivers of the KNP, *P. mauritianus* reedbeds occur at low elevations on the macro-channel floor, where they are exposed to perennial or seasonal flooding. Van Coller *et al.* (1997) calculated that in the Sabie River 75% of reedbeds are exposed to perennial flow or seasonal floods with a 1 to 1.05-year return period. Reeds in these rivers are also closely associated with sedimentary geomorphic features. They are associated with alluvial bars rather than with bedrock or bedrock-dominated bars, and are more frequent in alluvial-dominated channels than in bedrock-dominated channels (van Coller and Rogers, 1996; van Coller et al, 1997).

3.2 DISTRIBUTION OF REEDBEDS WITHIN THE MACRO-CHANNEL

Reedbeds are commonly found along channel margins, but are not restricted to these areas. They may also be found in small patches within channels and in areas away from active channels where sediment is available (Fig. 3.3). The distribution pattern of reeds in these rivers is complicated by the fact that the active channels may change their courses periodically. Reedbeds frequently mark the position of old active channels.

The proportion of the macro-channel area covered by reeds in the Kruger National Park rivers varies between 10% and 50%, with considerable variation in both space and time (Carter and Rogers, 1995). For example, reed cover in the Letaba River in 1965 ranged between 15% and 50%, depending on factors such as geology, topographic position and valley width. The mean reed cover in this river decreased dramatically with time, from 46.7% in 1965 to 13.6% in 1977, and has remained low since then. The decrease is thought to be due to the combined effects of large floods in 1977 and a subsequent drought period (Kotschy et al, 2000). Reedbeds in the Letaba River are dynamic elements of the landscape - only 13% of reedbeds persisted throughout the 8-year period between 1988 and 1996 (Kotschy et al, 2000).

3.3 REED STEM CHARACTERISTICS RELEVANT TO RESISTANCE

Reed stem attribute data are available from three independent studies carried out in the rivers of the Kruger National Park (Table 3.1).

Study 1 was carried out on the Sabie and Sand Rivers, near Skukuza, in late September to mid-December 1988. Reedbeds were subjectively sampled to cover a range of variation in density and maturity. Quadrats of 0.5 m x 0.5 m were randomly placed within reedbeds (A. Carter, unpublished data). Study 2 was done on the Sabie River in September 1990. Transects consisting of 5 m x 2.5 m contiguous quadrats were used to sample the reeds. Zero values, i.e. where reeds were absent on the transect, were not included in the calculations (A. van Coller, unpublished data). Study 3 was carried out on the Letaba River, between Engelhardt and Mingerhout Dams, between September 1998 and early June 1999. Quadrats of 0.5 m x 0.5 m were randomly placed

within the densest part of reedbeds (characteristics of stems at reedbed edges and in newly colonised areas surrounding reedbeds were also collected but are not shown here) (K. Kotschy, unpublished data).

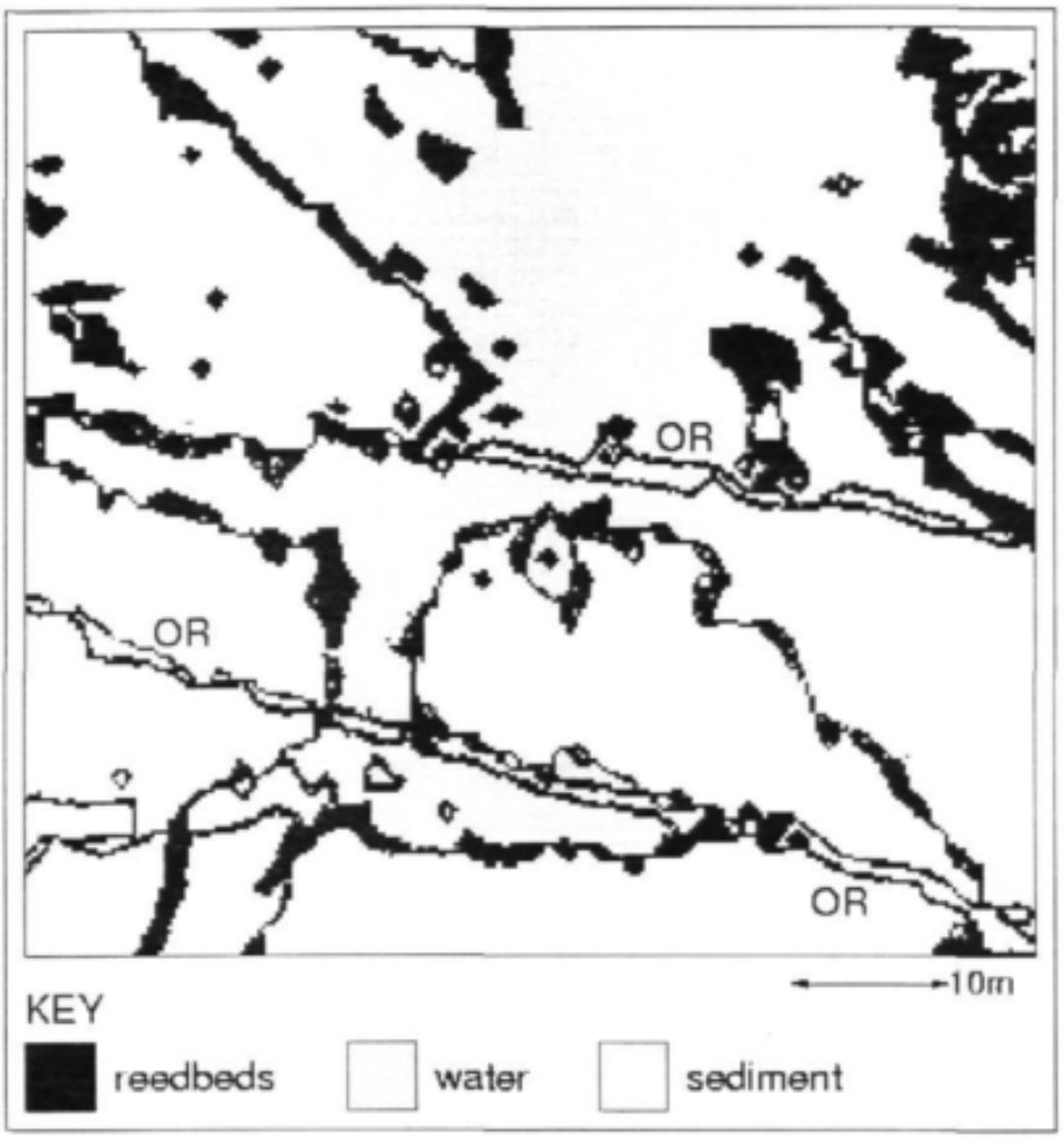

Figure 3.3 Map of typical rhizome distribution in Letaba River, digitized from areal photographs

Table 3.1 Stem attribute data collected in three independent studies on the Sabie, Sand and Letaba Rivers. Details of the sampling methods, locations and dates of the three studies are given in the text.

Study	Measure	Basal diameter (mm)	Stem height (m)	No. of branches per stem	Primary branch length (m)	Degree of branching
1	Mean±SE	6.1±0.08	0.64±0.015	3.21±0.085[a]	0.2± 0.013	1.81±0.038
	Range	6.0-16.5	0.01-3.14	0-20	0-1.32	0-6
2	Mean±SE	11.0±0.1	1.82±0.04[b]	---	---	---
	Range	1.0-40.0	0.3-3.0	---	---	---
3	Mean±SE	9.0±0.12	1.71±0.02	12.01± 0.53[c]	---	---
	Range	3.0-22.0	0.35-3.7	0-87	---	---

[a] only primary branches were counted
[b] this reflects mean maximum stem height per quadrat
[c] total number of branches of all orders

In *Phragmites australis*, stem diameter is closely correlated with other stem characteristics such as height, mean growth rate, and the beginning and length of the growth period within one growing season (Ostendorp, 1991). Although such relationships have not been formally investigated in *P. mauritianus*, preliminary calculations have shown little evidence of a correlation between stem diameter and height (A.J. Carter, pers. comm.). This is probably due mainly to differences in climate and habitat between the reed populations studied and not to genetic differences between the two species (see Section 3.1.1).

A reedbed, at any particular point in time, consists of a range of stems of different sizes. Shoots at reedbed edges are, on average, thinner and shorter than those in the centre. Shoots on the outer edges of reedbeds in the Letaba River had a mean diameter of 6 mm and a height of 0.9 m (Kotschy, 2001). Stem branches seem to be produced in response to damage to the main stem. This could be caused by browsing, trampling or flood damage. Stems that are heavily browsed tend to have many branches, especially near the damaged tip, but branching has also been observed in stems that have not been browsed or broken (K. Kotschy, field observation).

3.3.1 Seasonal Changes in Stem Characteristics

Seasonal changes in stem characteristics need to be understood if the interaction between reeds and flow is to be modelled effectively.

The effect of season on the mean stem diameter, height and number of branches in reedbeds was investigated by Kotschy (2001). Reedbeds were sampled at two different dates, September 1998

and May/June 1999. These dates were chosen as they represent the end of the dry season and the end of the wet season respectively. In the subtropical climate of the KNP, seasons are much less distinct than in temperate regions, and temperature triggers are unlikely to be important for the growth of *Phragmites mauritianus*. The transition between wet and dry seasons is likely to have a greater effect on growth.

Significant differences were observed in stem diameter, height and number of branches between the two sampling dates (Table 3.2).

Table 3.2 **Changes in reed stem characteristics between the beginning and end of the wet season, September 1998 to May/June 1999. Data are given as mean±SE. Quadrats were placed along transects extending from within reedbeds, across their boundaries and into areas of adjacent sediment being colonised by reeds. These are referred to as "reedbed", "edge" and "outside" quadrats respectively. The significance of the differences between dates was assessed using a crossed ANOVA with quadrat location, sampling date and site as factors. All p-values are significant at the 0.1% level.**

Stem characteristic	Quadrat	Before wet season	After wet season	p-value for effect of date
Diameter (mm)	Reedbed	9.3±0.16	8.7±0.18	$<2.2 \times 10^{-16}$
	Edge	8.4±0.18	5.6±0.17	
	Outside	8.0±0.17	4.4±0.12	
Height (m)	Reedbed	1.72±0.03	1.69±0.04	$<2.2 \times 10^{-16}$
	Edge	1.47±0.03	1.12±0.04	
	Outside	1.24±0.03	0.65±0.02	
No. of branches per stem	Reedbed	8.92±0.5	16.23±1.01	1.085×10^{-6}
	Edge	5.63±0.41	5.82±0.53	
	Outside	3.63±0.28	2.18±0.25	

On average, stems were significantly thinner and shorter after the wet season than they had been at its beginning. From examining the changes in each type of quadrat, it is clear that the reduction in stem diameter and height occurred mainly in the "edge" and "outside" quadrats, and that the mean stem size in the centre of the reedbeds remained much the same. An analysis of the frequency distribution of stem size classes at the two dates shows that the decrease in mean diameter and height was due to an increase in the number of small shoots present (Fig. 3.4). As

the stem density (in all quadrats) did not differ significantly between the two dates, the increase in number of small shoots must have been accompanied by a decrease in the number of larger shoots.

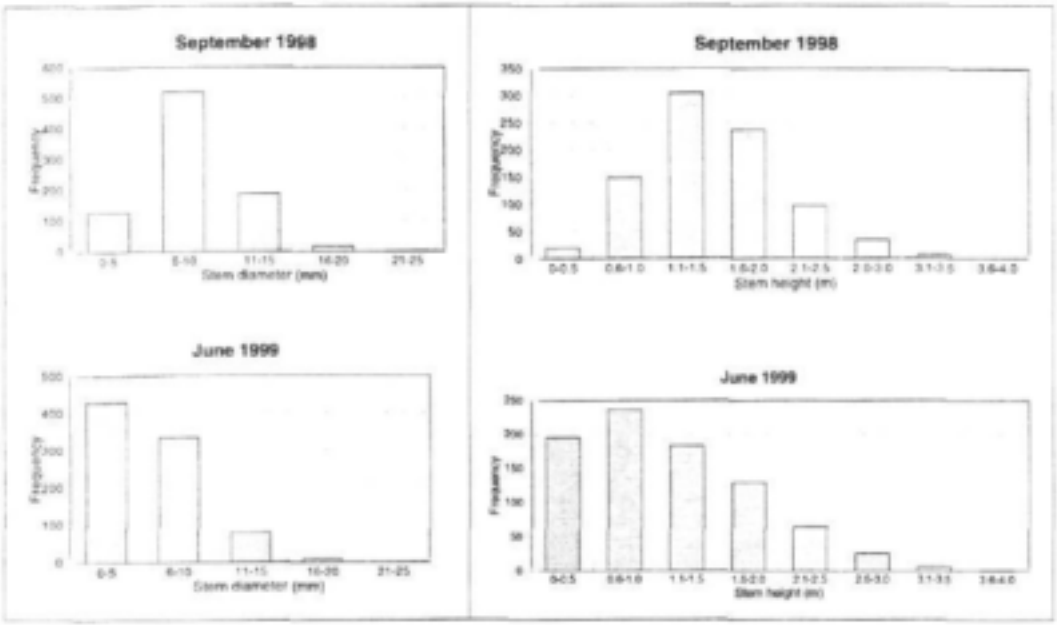

Figure 3.4 Frequency distributions of stem diameter and height in reedbeds from Letaba River in September 1998 and May/June 1999 (before and after the wet season)

These changes in the distribution of stem sizes suggest that larger (and presumably older) shoots were removed or died during the wet season, and that new shoots were produced to replace them. This occurred primarily at the edges of reedbeds, where the stem density was much lower. Although the reedbeds in this section of the Letaba were inundated for most of the wet season

(from November to the end of May), the fact that larger stems in the centre of reedbeds were not affected suggests that the shoots did not die as a result of the anoxic conditions associated with inundation. The most likely explanation of their fate, based on observations made in the field in June 1999, is that they were physically damaged by the flow, being broken, flattened and/or buried by sediment. Stems damaged in this way are able to resprout rapidly from the nodes, giving rise to new vertical shoots. Shoots at the edges of reedbeds would be most susceptible to this sort of damage as flow velocities are higher here than in the denser part of the reedbed.

In the centres of reedbeds, the only stem characteristic that differed significantly between the two dates was the number of branches per stem. After the wet season, the number of branches present on stems in the "reedbed" quadrats was almost double what it had been before the wet season. This is most likely a response of the plant to bending of its stems; it is unlikely to reflect the

effects of browsing by herbivores because the reedbeds were inaccessible for most of the period due to high water levels. The mean height of stems within reedbeds also did not decrease (Table 3.2), suggesting that browsing or breakage of stems by floodwaters was insignificant.

Ostendorp (1991) developed a simple model which makes it possible to estimate the height of individual stems of *Phragmites australis* at any time during the growing season. This is possible because the growth characteristics of this species in temperate regions are rather simple. Shoots are strictly annual. Natality and mortality are triggered by temperature changes. The growth rate of an individual stem is a linear function of time, and the period of growth depends on the basal diameter of the stem (but is generally about 3 months).

In the subtropical climate of the KNP, the seasons are much less distinct. The growth period is much longer, potentially all year depending on the availability of water. Unlike in temperate regions, *Phragmites* shoots generally remain green during winter. Kotschy (2001) recorded the occurrence of active buds on the rhizomes as well as young shoots at the end of winter (September 1998), suggesting that new stems had been produced and growth had occurred during the winter. Individual shoots of *P. mauritianus* appear to persist over several years, possibly 2 or 3, although no data are available to confirm this. These factors, together with the variable flow regime and disturbance by flooding, make the growth of *P. mauritianus* much less deterministic than that of *P. australis*.

3.4 REEDBED CHARACTERISTICS RELEVANT TO RESISTANCE

3.4.1 Density

A wide range of stem densities have been measured in reedbeds in the Kruger National Park (Table 3.3).

Table 3.3 Reedbed density data (stems/m^2) collected in three independent studies on the Sabie, Sand and Letaba Rivers. Details of the sampling methods, locations and dates of the three studies are given in the text (Section 3.3).

Study 1	Mean±SE	244.4±19.44
	Range	124-400
Study 2	Mean±SE	112±3.13
	Range	11-467
Study 3	Mean±SE	118.4±17.65
	Range	20-384

Stems tend not to be uniformly spaced within the reedbed. Rather, the stems arising from a single vertical rhizome (Fig. 3.2) form clumps of up to 10 stems. In *Phragmites australis* these "partial

tussocks" persist for 3 to 6 years, with new stems arising from buds on the vertical rhizome each spring (Haslam, 1969).

3.4.2 Shape

Phragmites reedbeds in the rivers of the KNP have a characteristic appearance when viewed from the air (Fig. 3.5). They appear as linear strips oriented parallel to the direction of flow. This striated pattern is particularly evident in reedbeds close to the active channels and those in the path of flow. Reedbeds which are less frequently inundated, such as those near the macro-channel banks, are criss-crossed by animal paths but are otherwise more uniform. This, together with the fact that *Phragmites* reedbeds in lakes and marshes do not show such linear striations, suggests that the striated pattern results from the effects of flow on the reedbeds.

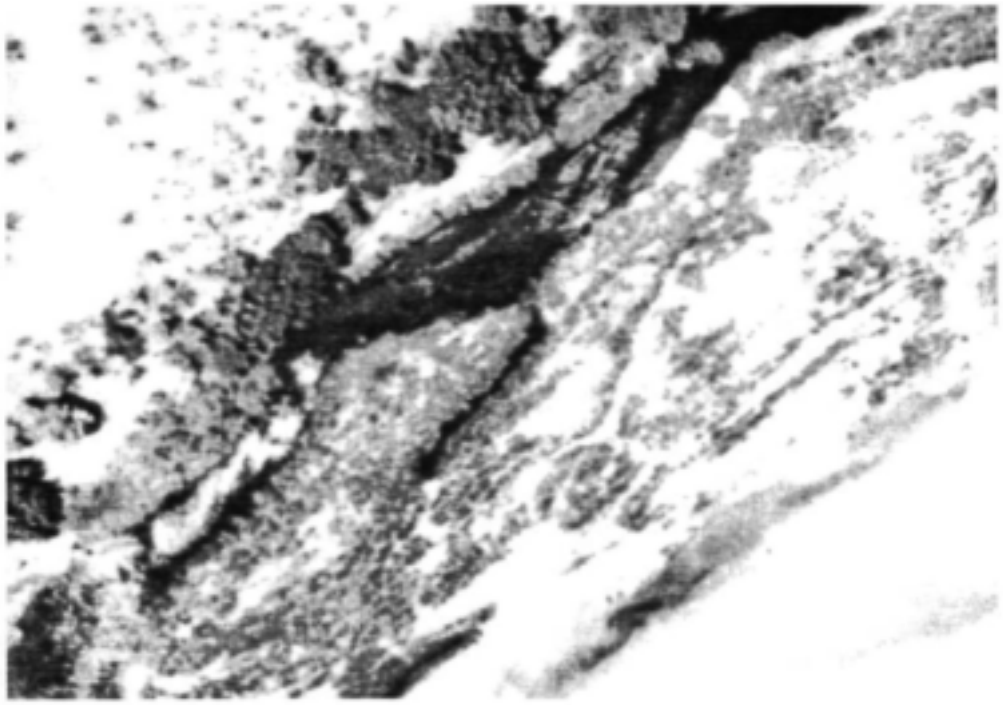

Figure 3.5 Aerial view of *Phragmites mauritianus* reedbeds in the Letaba River, showing the characteristically striated appearance of reedbeds near the active channel

The striated appearance of reedbeds in these rivers is due, at least in part, to a phenomenon described by Ashton (1987). Reed rhizomes near the sediment surface are displaced during floods and left trailing downstream. Resprouting of shoots from these rhizomes results in the edge of the reedbed becoming more clearly defined, as well as in extension of the reedbed downstream. Excavation of rhizomes in the Letaba River (Kotschy, 2001) revealed that the majority of rhizomes at reedbed edges and in areas of adjacent sediment are indeed oriented in the direction of flow.

3.4.3 Size

Reedbed lengths and edge:area ratios were measured by Kotschy (2001) in the Letaba River. Measurements were made on digitised aerial photographs using GIS software (PCI-ILWIS, version 2.1). Two sets of photographs were used, from September 1988 and September 1996. Reedbed lengths were measured from one 300m stretch of the river only. Fifty measurements were made for each date. Length was measured along the long axis of the reedbed, with a reedbed being identified as a group of contiguous reed pixels separated from other reed pixels by sand or water.

Stratified random sampling was used to select 12 sites for calculating edge:area ratios - two or three sites were randomly selected per 300m stretch of the study section of the river. Measurements were made at the same sites for each of the two dates. This provided a measure of spatial as well as temporal variation in reedbed sizes.

Mean reedbed length was around 10m, but could be as much as 33m (Table 3.4). Further study is needed to determine why reedbed length does not increase indefinitely. Tsujimoto et al (1996) found that the area of sediment deposited behind *Salix* bushes decreases with the length of the vegetation patch. With long patches the minimum velocity occurs halfway along the patch instead of behind it, and velocity actually increases in the lee zone. This inhibits deposition in the lee of the patch. It is not certain how such ideas would apply to *Phragmites* reedbeds which are not growing on bars within a channel.

Table 3.4 Lengths and edge:area ratios of reedbeds in the Letaba River measured from digitised aerial photographs from 1988 and 1996. Sampling was done in an alluvial section of the river between Engelhardt and Mingerhout Dams.

Characteristic	Measure	1988	1996
Reedbed length (m)	Mean±SE	9.0±0.72	10.3±0.98
	Range	1.5-23.9	1.9-33.1
Edge:area ratio	Mean±SE	2.65±0.17	2.49±0.18
	Range	1.2-4.1	1.1-4.3

The mean edge:area ratio of reedbeds across all sites and dates was 2.5. The decrease in edge:area recorded between 1988 and 1996 indicates that reedbeds became more consolidated during this period, probably as a result of clonal growth.

3.4.4 Nature of Reedbed Boundaries

The smoothness of a reedbed boundary depends on the extent to which that reedbed has expanded

clonally. During clonal expansion, colonising rhizomes extend from the reedbed into the surrounding sediment. These rhizomes give rise to shoots, but at a much lower density than in the established part of the reedbed (Table 3.2). This serves to "blur" the boundary of the reedbed and increase the form resistance. Where reedbeds grow directly adjacent to deep water, however, the boundaries are more distinct because the growth of colonising rhizomes generally requires exposed sediment (see Fig. 3.8).

Kotschy (2001) found that the density of colonising stems at the boundaries of reedbeds could be directly related to the amount of Nitrogen present in the sediment (Fig. 3.6). She also found that the magnitude of change in the density of colonising stems between the beginning and end of the wet season could be predicted from the magnitude of change in the level of the water table at a particular site (Fig. 3.7). The largest increases in density of colonising stems occurred where the water table was much closer to the surface than it had been at the beginning of the wet season.

It is likely that clonal expansion of reedbeds occurs mainly during the dry season, when colonising rhizomes are not disturbed by flow and the sediment is not anoxic. Since these colonising rhizomes are only found in the top 60 cm of sediment (Kotschy, 2001), it is possible that their growth during low-flow periods may be constrained by water availability, although no data are available to test this hypothesis.

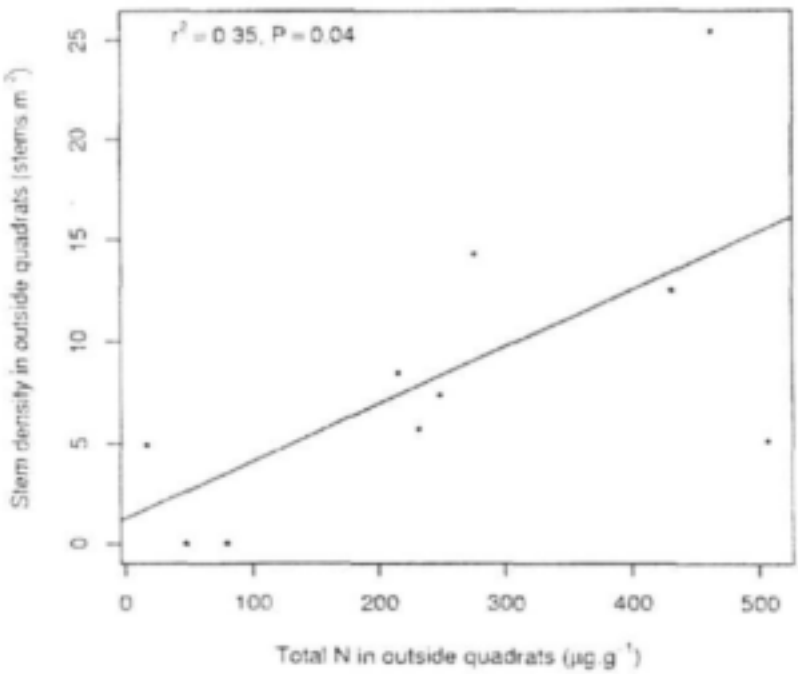

Figure 3.6 Relationship between soil nitrogen and density of colonising stems in reedbeds from the Letaba River

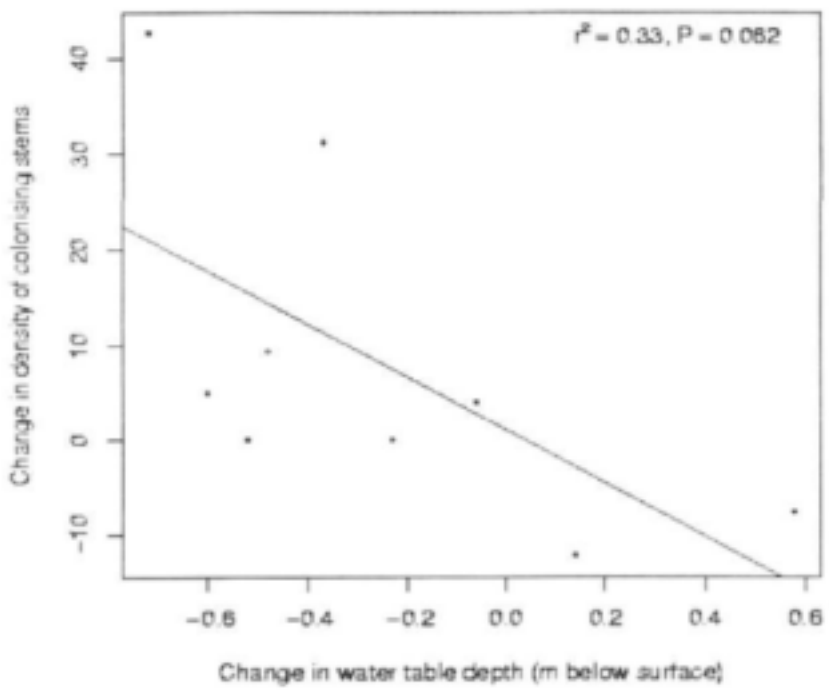

Figure 3.7 Relationship between change in water table depth and change in colonising stem density in reedbeds in the Letaba River

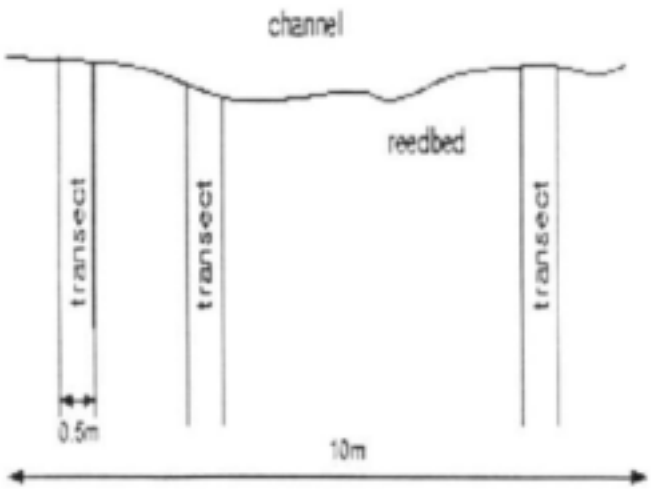

Figure 3.8 Transect layout at study sites

The hypothesis is presented here that reedbed boundaries are more distinct after high flows as a result of the mechanism described in Section 3.4.2, and more diffuse after periods of minimal hydrological disturbance, when clonal expansion of reedbeds is allowed to proceed.

3.5 SEDIMENT MOVEMENT AROUND INDIVIDUAL REEDBEDS

Differences in elevation between reedbeds and their surroundings give an indication of the extent to which reedbeds trap and stabilise sediment.

Profiles showing relative elevation were constructed from surveyed transects in the Letaba River (Kotschy, 2001). The transects were placed perpendicular to the long axis of the reedbed, starting in the centre of the reedbed and extending to the furthest extent of the rhizomes colonising the adjacent sediment (Fig. 3.8). Three transects were placed randomly at each of four sites.

The mean height of the reedbeds above the surrounding sediment was 0.27 m. Comparing the elevational profiles before and after the summer high flows (September 1998 and May 1999) gives some insight into the effect of high flows on the distribution of sediment around reedbeds. The mean elevation of the reedbed relative to the surrounding sediment increased from 0.2 m at the beginning of the wet season to 0.34 m after the summer high flows. Changes in the general shape of the profiles reflect changes in the distribution of sediment across the reedbed boundary (Fig. 3.9). The change in shape of the profiles in Fig. 3.9 suggests that sediment surrounding the reedbed was removed, especially at the upstream end. Such scouring is commonly observed at the upstream end of channel obstructions.

As the profiles indicate only relative elevation, it could not be determined whether changes in profile shape were due to accumulation of sediment within the reedbed or to the removal of surrounding sediment, but both are likely to have occurred. The following mechanism is proposed. Firstly, during high flows, sediment suspended in the water is deposited within and near the reedbed because of local reductions in flow velocity. Secondly, during high flows large volumes of sediment become "fluidised" and transported downstream (K.H. Rogers, pers. comm.). Sediment within reedbeds is less easily removed than uncolonised sediment. Thus reedbeds become higher than their surroundings both because they cause sediment to be deposited within them and because they prevent it from being removed during high flows.

3.6 EFFECTS OF FLOW ON INDIVIDUAL REEDBEDS

Because of the active role played by reeds in morphological change in semi-arid rivers, any model of such change must include rules describing the response of reeds to flow and sediment deposition. Although much work is still needed, this section contains a framework on which such rules may be based (Fig. 3.10). It is essentially a series of hypotheses relating changes occurring within reedbeds to flow conditions. These hypotheses are based on the data presented above, and are focussed at the scale of individual reedbeds.

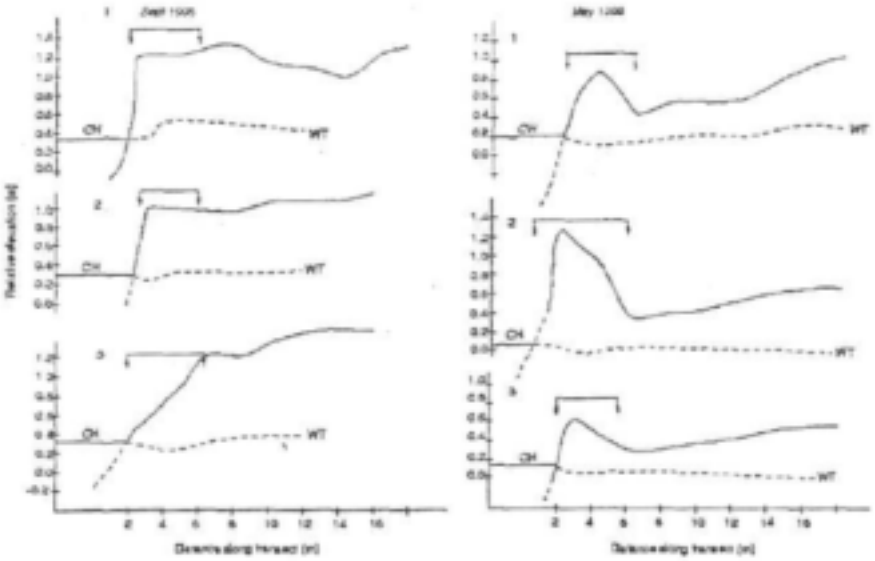

Figure 3.9 Profiles showing relative elevation of a reedbed before and after the summer high flows in the Letaba River. Transects 1 to 3 are progressively further downstream. The transects for the two dates are from the same reedbed but not from identical locations within it. Arrows mark the position of the reeds. WT: water table, CH: channel.

The generic flow states in Figure 3.10 are defined as follows: high flow; where the reed stems are partially or completely inundated; medium flow, where the water level is close to the reedbed surface; and low flow, where the water table is below the reedbed surface. In the most simple seasonal cycle, high flows would occur primarily in the wet season (summer), medium flows as the floodwaters subside, and low flows primarily in the dry season (winter).

Reed stems are most likely to be damaged by browsing during winter because reedbeds are more accessible to herbivores such as elephant and buffalo when water levels are low. Elephant in particular tend to remain closer to water during winter and thus depend more heavily on reed vegetation for food.

The work of Kotschy (2001) in the Letaba River has shown that the sediment beneath reedbeds contains a significantly larger proportion of fine silt and clay particles than uncolonised sediment, and that the clay particles tend to descend through the profile to form consolidated clay "cores". The results further suggest that the amount of clay accumulated beneath a reedbed is time-dependent. These clay cores could have an important influence on reed growth by increasing the water retention capacity of the sediment. They may also play an important role in reducing the chances of a reedbed being removed by floodwaters. The relationship between clay cores and reed growth and persistence thus merits further attention.

The changes to reedbeds listed in Fig. 3.10 have been related to river flow in a very simplistic manner. The actual effects of a "high", "medium" or "low" flow on a reedbed depend on the magnitude of the discharge, as well as on the channel morphology, the elevation of the reedbed, its position in relation to other reedbeds, and the flow history previously experienced by that reedbed. All of these factors need to be taken into account when developing model rules.

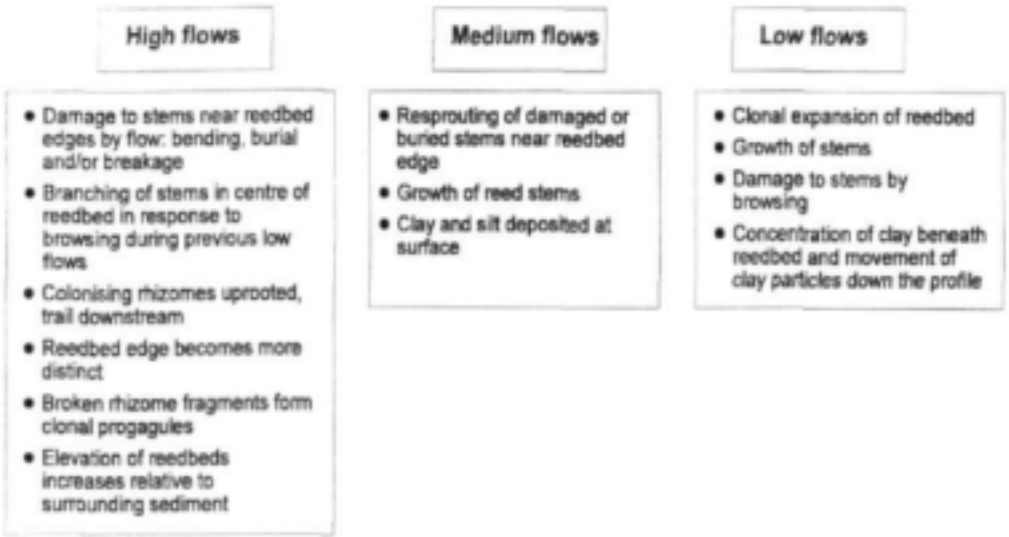

Figure 3.10 Summary of changes occurring within reedbeds at each of three generic flow states.

Chapter 4

BASIC RESISTANCE DUE TO REEDS - EXPERIMENTAL INVESTIGATIONS

4.1 INTRODUCTION

An experimental programme was carried out to investigate the influence of reed characteristics (such as stem diameter, density and morphology) on the basic flow resistance of a reedbed. The experiments were all conducted in laboratory flumes under controlled and idealized conditions in order to obtain a clear understanding of the influences of the different factors. This was intended to enable critical assessment of existing resistance equations and to contribute to the development of reliable resistance prediction procedures. No field testing or large scale laboratory testing with real vegetation was possible within this project, but data from other sources are available, and some of these are presented in section 4.2.3.

The resistance phenomenon depends on flow condition, and particularly on whether the tops of the stems are below or protrude through the water surface. Both of these conditions occur in rivers and the experiments were designed to measure basic resistance of reedbeds under both submerged and emergent conditions.

Resistance in reedbeds is dominated by stem drag, which depends strongly on the morphology of stems. Tests were therefore carried out using stems with different cross-sectional shapes. Most existing methods for estimating stem drag are based on discharge coefficient values for individual stems. Drag coefficient values were therefore measured for single stems with different shapes and morphologies, including real reed stems with branches and leaves.

This experimental work confirms that Manning's equation is inappropriate for flow through vegetation, and two alternatives are presented in Chapter 5 for emergent conditions - one accounting for stem drag only, and the other for bed shear and stem drag combined.

4.2 FLOW RESISTANCE EXPERIMENTS

Basic resistance tests were carried out in two different flumes with different widths using different stems, bed roughnesses and flow conditions. The experimental conditions are summarized in Table 4.1. The procedures and results for the different sets of experiments are described separately in the following sections.

4.2.1 Series A Experiments

4.2.1.1 Experimental Procedure

The first series of experiments (Series A) was conducted to establish the effects of stem density and shape on flow resistance under different hydraulic conditions determined by bed slope and discharge.

The experiments were done in a 0.10 m wide, 3.0 m long, glass-sided tilting flume. The bed was artificially roughened by gluing down a layer of angular silica sand (grain size diameter ranging from 2.4 mm to 4.8 mm). Uniform flow depth was ensured by adjustment of an overflow weir at the downstream end of the flume, and discharge was measured volumetrically. Local velocities were measured using a miniature propeller meter or a pitot-static tube connected to a pressure transducer, and water surface levels were measured with a pointer gauge. Reed stems were simulated using rigid steel rods arranged in a staggered grid pattern with equal longitudinal (a) and transverse (b) spacings (Fig. 4.1).

Table 4.1 Experimental conditions

Test	Stem Spacing (mm)	Stem Type	Bed Slope	Discharge (l/s)	Stem Submergence
A1	-	-	0.002	0.963 - 0.859	-
A2	25	round	0.010	0.125 - 1.642	emergent
A3	25	round	0.002	0.126 - 0.726	emergent
A4	50	round	0.002	0.164 - 1.986	emergent
A5	75	round	0.002	0.306 - 2.073	emergent
A6	25	square	0.010	0.136 - 1.612	emergent
A7	25	square	0.002	0.128 - 0.726	emergent
A8	50	square	0.002	0.161 - 1.852	emergent
A9	75	square	0.002	0.310 - 2.173	emergent
A10	25	diagonal	0.010	0.133 - 1.626	emergent
A11	25	diagonal	0.002	0.130 - 0.772	emergent
A12	50	diagonal	0.002	0.166 - 1.889	emergent
A13	75	diagonal	0.002	0.262 - 2.250	emergent
A14	25	round	0.002	0.107 - 1.989	submerged & emergent
A15	50	round	0.002	0.441 - 2.029	submerged & emergent
A16	75	round	0.002	0.996 - 2.082	submerged & emergent
B1	25	round	0.0118	0.00246	emergent
B2	25	round	0.0145	0.00246	emergent
B3	25	round	0.0160	0.00246	emergent
B4	25	round	0.0184	0.00246	emergent
B5	25	round	0.0165	0.00131	emergent
B6	25	round	0.0140	0.00206	emergent
B7	25	round	0.0130	0.00421	emergent
B8	25	round	0.0130	0.00604	emergent
B9	25	round	0.0130	0.00702	emergent

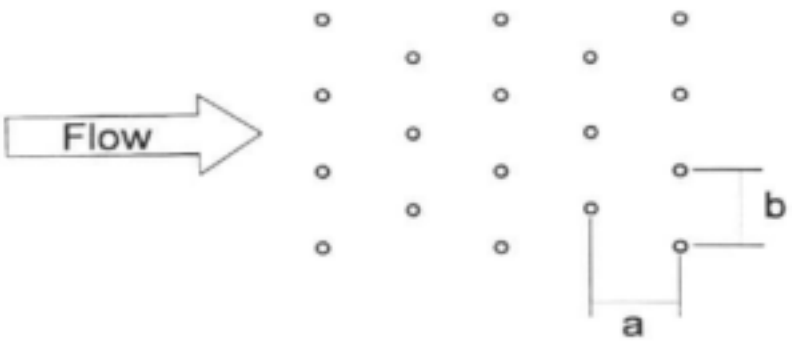

Figure 4.1 Stem arrangement used in experiments

Three different stem spacings and two different bed slopes were used, as listed in Table 4.1, and a range of discharges tested for each condition. The effective roughness of the bed was determined by running two discharges through the flume without the stem rods installed (Test A1). The vertical velocity profile was also measured for the greater of these discharges to allow the shear velocity and effective bed roughness to be determined.

Tests were carried out with three different stem shapes, all with the same staggered arrangement patterns. Round, 5 mm diameter rods were used to represent the stems in Tests A2 to A6 and A14 to A16 used, while 5 mm square section steel rods were used in Tests A6 to A13. In Tests A6 to A9 the rods were oriented with their faces parallel and normal to the flow direction (to be referred to as "square" orientation) and in Tests A10 to A13 they were oriented with their diagonal axes parallel and normal to the flow direction (to be referred to as the "diagonal" orientation).

Tests A2 to A13 were all carried out under emergent conditions, i.e. the stems penetrated the water surface. In Tests A14 to A16 the flow depths and discharges imposed resulted in both emergent and submerged conditions. Velocity profiles were measured for the two less dense stem arrangements (it was not possible to insert the probes for the most dense arrangement). It should be noted that the rough bed for Tests A14 to A16 was not the same one used for the other tests because the rods could not be supported from the top for submerged conditions. A new bed was laid and the rods inserted and glued into drilled holes; the rods were 0.094 m high for the 25 mm and 50 mm spacing arrangements and 0.090 m high for the 75 mm spacing arrangement. The same material was used for this bed as for the emergent tests, but no further measurements were taken without stems.

The data measured in the Series A experiments are listed in Appendix A.1.

4.2.1.2 Bed Friction

Assessment of the influence of stem drag on flow resistance requires knowledge of the resistance characteristics of the bed, so that the effects can be separated and that the bed can be represented correctly in model calibration applications. Test A1 was conducted in the roughened flume without stems in order to determine the bed friction factor. Two discharges were used and the corresponding flow depths measured. The vertical velocity distribution was also measured for the higher discharge.

Because the flume is narrow relative to the flow depth, the influence of the resistance of the glass side walls must be accounted for in determining the friction of the bed in the absence of stems. This has been done using the side-wall correction procedure of Vanoni and Brooks (1957), as follows.

The Reynolds number for the wall (Re_w) may be rearranged as follows:

$$Re_w = \frac{4U_w R_w}{\nu} = \frac{4U_w R_f}{\nu}\frac{R_w}{R_f} = Re_f \frac{R_w}{R_f} \qquad 4.1$$

where U is depth-averaged velocity, R is hydraulic radius, and the subscripts w and f refer to the wall and flume (composite wall and bed) sections, respectively. Applying the Darcy-Weisbach resistance equation for the wall and bed sections, and assuming equal flow velocities in these sections, leads to

$$\frac{R_w}{R_f} = \frac{f_w}{f_f} \qquad 4.2$$

where f is the friction factor. Combining equations 4.1 and 4.2 gives

$$\frac{Re_w}{f_w} = \frac{Re_f}{f_f} \qquad 4.3$$

For a hydraulically smooth wall, equation 4.3 is solved simultaneously with either the Blasius equation (equation 4.4) for $Re_w < 10^5$ or equation 4.5 for $Re_w \geq 10^5$.

$$f_w = \frac{0.316}{Re_w^{0.25}} \qquad 4.4$$

$$\frac{1}{\sqrt{f_w}} = 2\log\left(\frac{Re_w\sqrt{f_w}}{2.51}\right) \qquad 4.5$$

For a rectangular cross-section, applying the Darcy-Weisbach friction equation and the sum of the contributing wall and bed areas leads to the following relationships for the friction factor and hydraulic radius of the bed:

$$f = f_f + \frac{2y}{W}\left(f_f - f_w\right) \qquad 4.6$$

where y is the flow depth and W is the flow width, and

$$R = R_f \frac{f}{f_f} \qquad 4.7$$

The effective roughness of the bed (k_s) may be determined through rearrangement of the Colebrook-White equation, i.e.

$$\frac{1}{\sqrt{f}} = -2\log\left(\frac{k_s}{12R} + \frac{2.51}{Re\sqrt{f}}\right) \qquad 4.8$$

to give

$$k_s = 12R\left(10^{\frac{1}{-2\sqrt{f}}} - \frac{2.51}{Re\sqrt{f}}\right) \qquad 4.9$$

The results of the above analysis for the artificially roughened bed are given in Table 4.2.

Table 4.2 Hydraulic parameter values and friction factor

Discharge, Q (l/s)	0.963	0.859
Flow depth, y (m)	0.0428	0.0434
Energy slope, S_f	0.002	0.002
Hydraulic radius (flume), R_f (m)	0.0231	0.0232
Hydraulic radius (bed), R (m)	0.0338	0.0346
Friction factor (bed), f (m)	0.105	0.110
Effective bed roughness, k_s (m)	0.0125	0.0130

The bed shear and effective roughness may also be determined from the log-law relationship (equation 4.10), using the measured velocity profile.

$$\frac{u}{u_*} = 2.44\, ln\left(\frac{y}{k_s}\right) + 8.5 \qquad 4.10$$

in which u is the local velocity, u_* is the shear velocity and y is the elevation above the bed.

This analysis was done for the test with $Q = 0.963$ l/s. The measured velocity profile is plotted in dimensionless form in Fig. 4.2, together with equation 4.10. The dimensionless velocity (u^+) is defined as u/u_*, and the dimensionless elevation above the bed (z^+) is defined as yu_*/v, where v is the kinematic viscosity of the water. The result obtained through this analysis and the Colebrook-White equation are compared in Table 4.3. For analysis of the results of the combined bed and stem resistance experiments, k_s was assumed to be 0.0125 m. This value of k_s, together with the corresponding shear velocity value u_* = 0.026 m/s, implies a value of shear Reynolds number ($Re^* = u_* k_s/v$) of over 300, indicating hydraulically rough turbulent flow. It can therefore be assumed that the value of $f = 0.105$ determined for this bed will not vary significantly with flow condition in Test A1. In the tests with stems in place the velocities and boundary shear values are much lower, and f is estimated by the Colebrook-White equation (equation 4.8).

Table 4.3 Effective roughness determined using the Colebrook-White equation and through measurement of the velocity profile for $Q = 0.963$ l/s

Parameter	Colebrook-White	Velocity profile
Shear velocity, u_* (m/s)	0.0258	0.0260
Effective roughness, k_s (m)	0.0125	0.009

The influence of side wall friction on overall resistance in these experiments is illustrated in Fig. 4.3. Here a rating relationship derived using the side-wall correction procedure of Vanoni and Brooks (1957) is compared with one derived by application of Einstein's (1950) depth-averaged velocity equation,

$$V = 5.75u_*\, log\left(12.27\frac{Rx}{k_s}\right) \qquad 4.11$$

in which V is the depth-averaged velocity and x is a correction factor to account for wall roughness (see Chapter 6). In this application the channel section was assumed to be wide, and the hydraulic radius in equation (4.11) was replaced by the flow depth. The divergence of the curves becomes significant as flow depth increases, and indicates the necessity for carrying out the side-wall correction procedure described above.

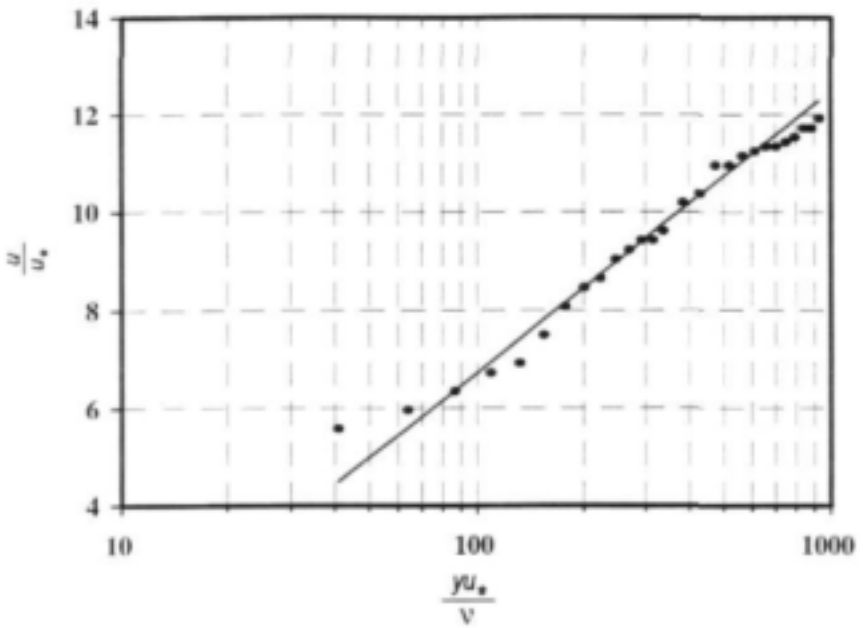

Figure 4.2 Dimensionless velocity profile used to calibrate the shear velocity and effective bed roughness in equation (4.10)

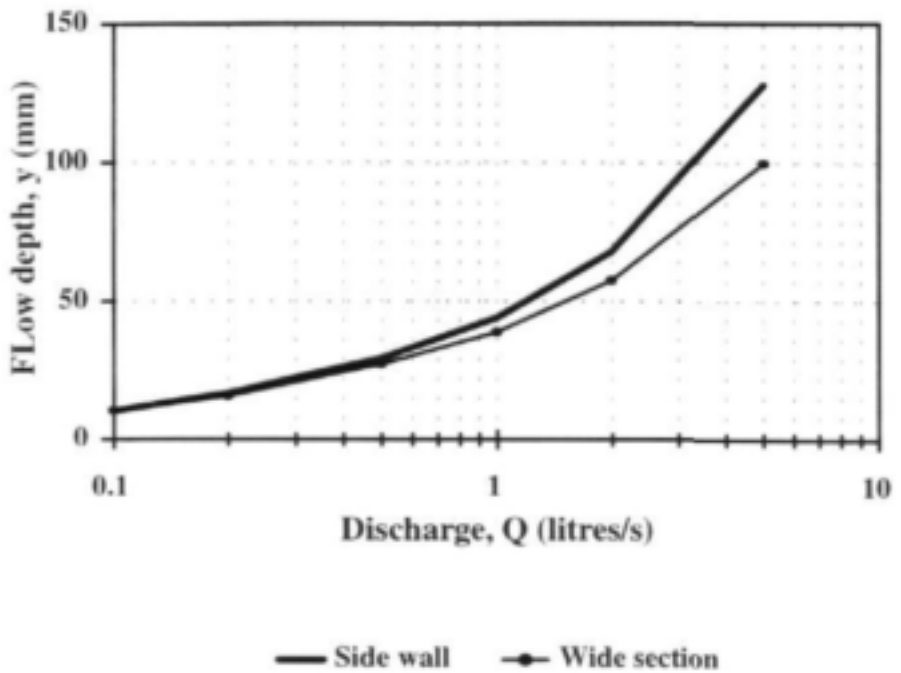

Figure 4.3 Modelling rating relationships for flow over the roughened flume bed (k_s=0.0125 m) applying the wall correction of Vanoni and Brooks (1957) and equation (4.11), assuming a wide channel section (S_o=1/500)

4.2.1.3 Influence of Stem Density on Resistance

Tests A3, A4 and A5 were conducted with the same bed slope and stem type, but with different stem spacings, to enable the density effects to be isolated in emergent flow. As expected, the flow depth for any given discharge is increased significantly by an increased stem density (Fig. 4.4).

The effect of stem density on flow resistance is expressed in terms of Manning's n in Fig. 4.5. In this analysis n was calculated using the flow depth in place of the hydraulic radius, implying an assumption that the resistance afforded by the glass side walls is relatively insignificant. Again, this shows that resistance increases with stem density, but importantly that Manning's n varies significantly with flow condition.

The effect of stem density on resistance in submerged flow was investigated in Tests A14, A15 and A16. Results indicate that the relationship between resistance and stem density persists to a similar extent once the water level rises above the tops of the stems (Fig. 4.6).

The relationship between stage and discharge is a reflection of the influence of resistance on flow velocity. In order to provide a basis for more fundamental consideration of resistance, the variation of local velocity with elevation was measured for different flow conditions in Tests A15 and A16 (Figs 4.7 and 4.8).

These velocity distributions show a tendency towards uniformity in the stem region, under the influence of stem drag, but this is significantly modified by momentum transfer in the vicinity of the stem tops. Above the stem tops the distribution is more similar to that in normal, boundary shear resisted flow, and could probably be described by conventional equations provided an effective roughness could be specified.

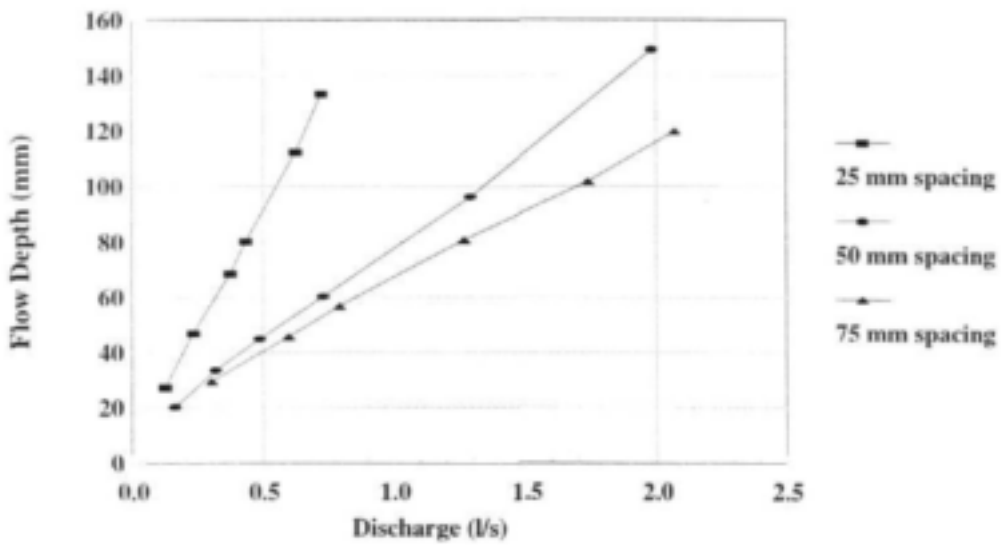

Figure 4.4 Effect of stem density on stage-discharge relationship for emergent flow

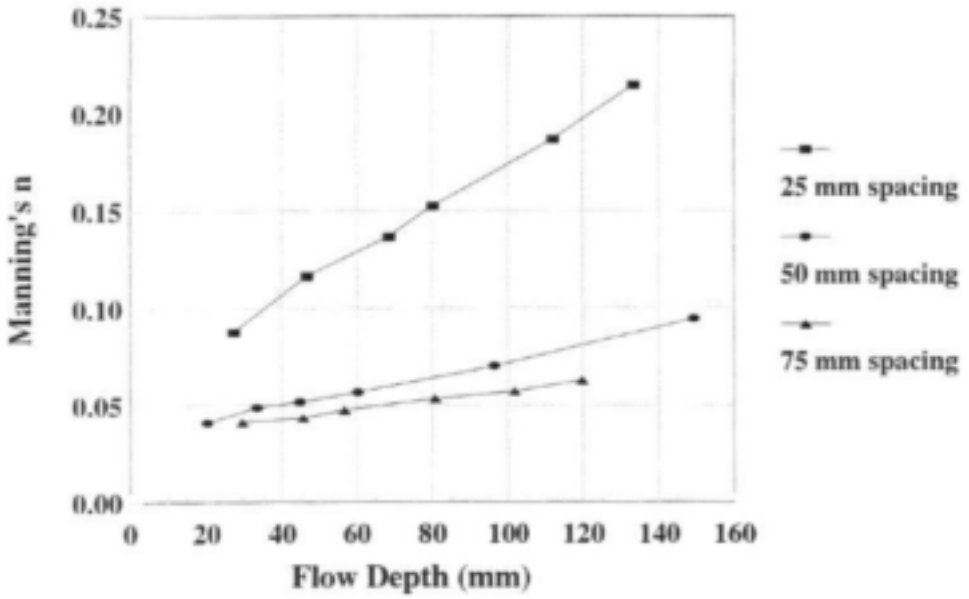

Figure 4.5 Effect of stem density on Manning's *n*

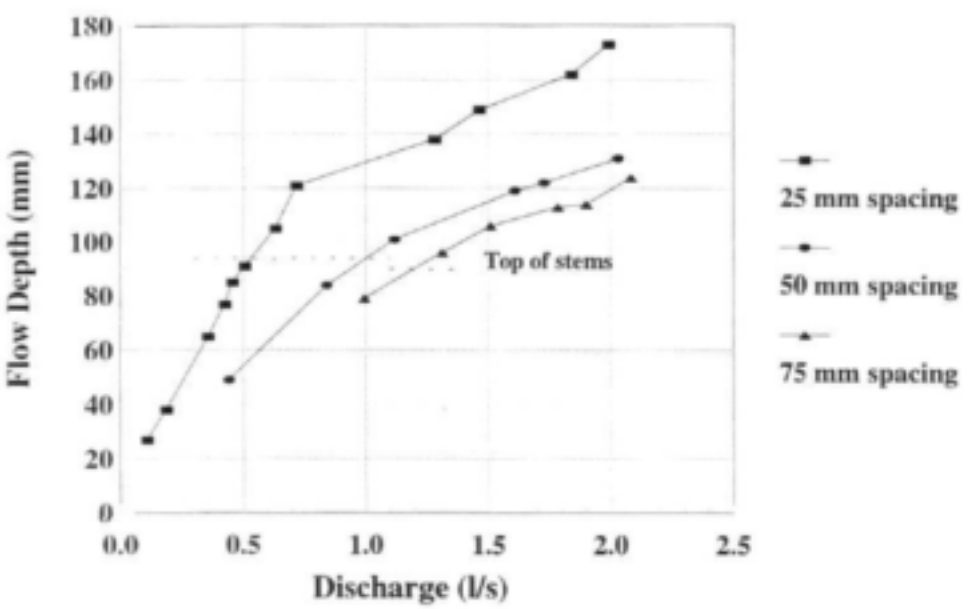

Figure 4.6 Effect of stem density on stage-discharge relationship for submerged flow

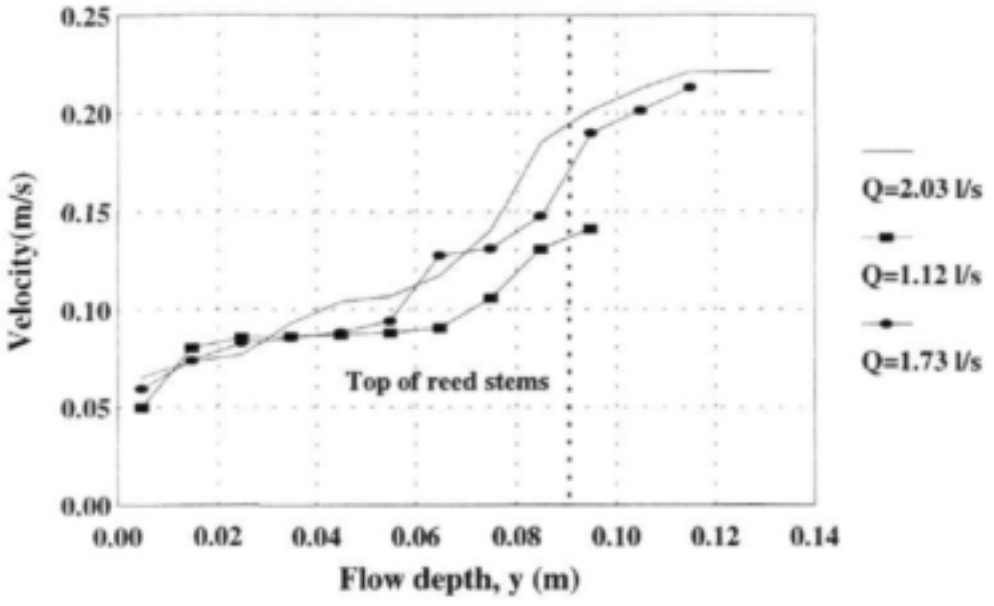

Figure 4.7 Vertical velocity distribution under submerged flow for 50 mm stem spacing

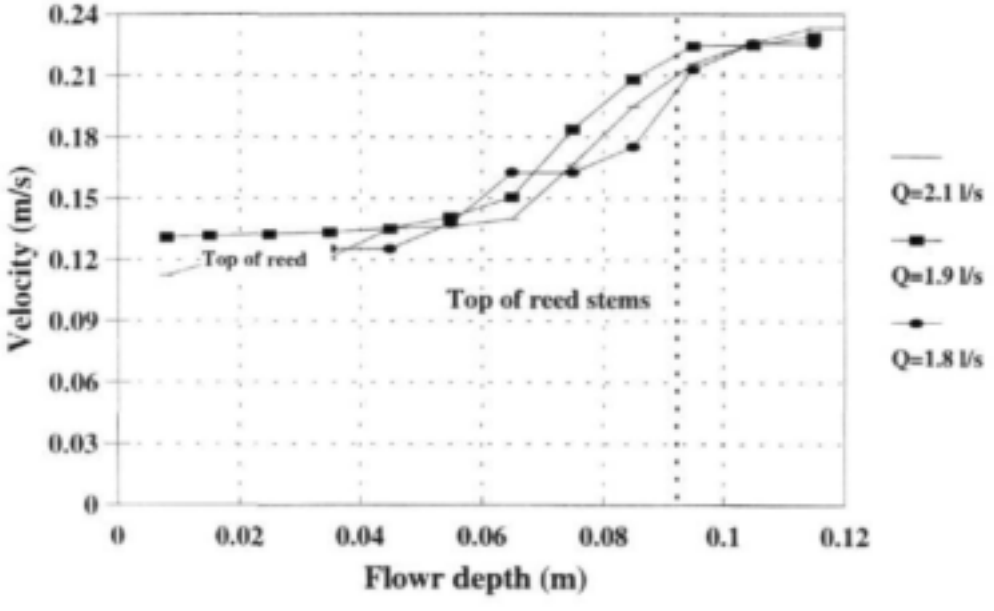

Figure 4.8 Vertical velocity distribution under submerged flow for 70 mm stem spacing

4.2.1.4 Influence of Stem Shape on Resistance

The experiments described above for investigating the effect of stem density on resistance for emergent flows were all carried out with stems represented by round, cylindrical rods. This is obviously an unrealistic simplification, and the influence of stem shape was investigated by repeating all the experiments with stems represented by 5 mm square section rods in both the "square" and "diagonal" orientations. These shapes are also unrealistic and the intention was not to represent real reeds, but rather to obtain an indication of the sensitivity of resistance to stem shape. This would give an idea of the importance of accounting for shape in predicting resistance, and how this might be done.

The effect of stem shape on stage-discharge relationship is shown in Figs 4.9 to 4.12 for the different stem density and channel slope conditions. The same results in terms of Manning's n are presented in Figs 4.13 to 4.16. For the steeper channel slope (Tests A2, A6 and A10, Figs 4.9 and 4.13) the effect of the tested stem shapes on resistance is significant, with Manning's n being increased by about 30% for a change in shape from circular to diagonal. The diagonal shape imposes the highest resistance, which is inconsistent with relative drag coefficient values measured for single cylinders (Albertson et al, 1960, Table 9-1). The effect is much less at the lower slope, however, (Tests A3, A7 and A11, Figs 4.10 and 4.14), and is largely independent of stem density at this slope (Figs 4.10, 4.11 and 4.12 and Figs 4.14, 4.15 and 4.16). At the milder slope the square rods produced slightly greater resistance than the diagonal ones, which is consistent with measured single cylinder drag coefficient values. The implications of these results are that relatively small variations in stem shape do not produce significant changes in resistance behaviour at low slopes (and hence velocities). Of course, the leaves and branches on natural reed stems will present much greater shape differences than those tested here. The main purpose of these experiments was to obtain data to test the ability of the model presented in Chapter 6 to account for shape differences. As these are specified in terms of drag coefficient (C_D), further experiments were carried out to determine values of C_D for these and more realistic stems. The results of these experiments are presented in section 4.3.

4.2.1.5 Influence of Channel Slope on Resistance

Series A experiments were conducted at two different slopes (0.01 and 0.002) for each stem type at the maximum density (25 mm spacing). The results in terms of Manning's n variation with flow depth for each stem type and channel slope are presented in Figure 4.17. The results suggest that channel slope has an influence on resistance, although this is inconsistent: the n values are higher for the milder slope for the round and square rods, but lower for the diagonal rods. The effect of slope on flow conditions is not direct, however, and the resistance effect may be a response to a change in velocity, Reynolds number, or stem drag coefficient. It may be possible to reconcile the apparent inconsistency of effects for the different stem shapes through more detailed knowledge of the consequences of slope on these variables.

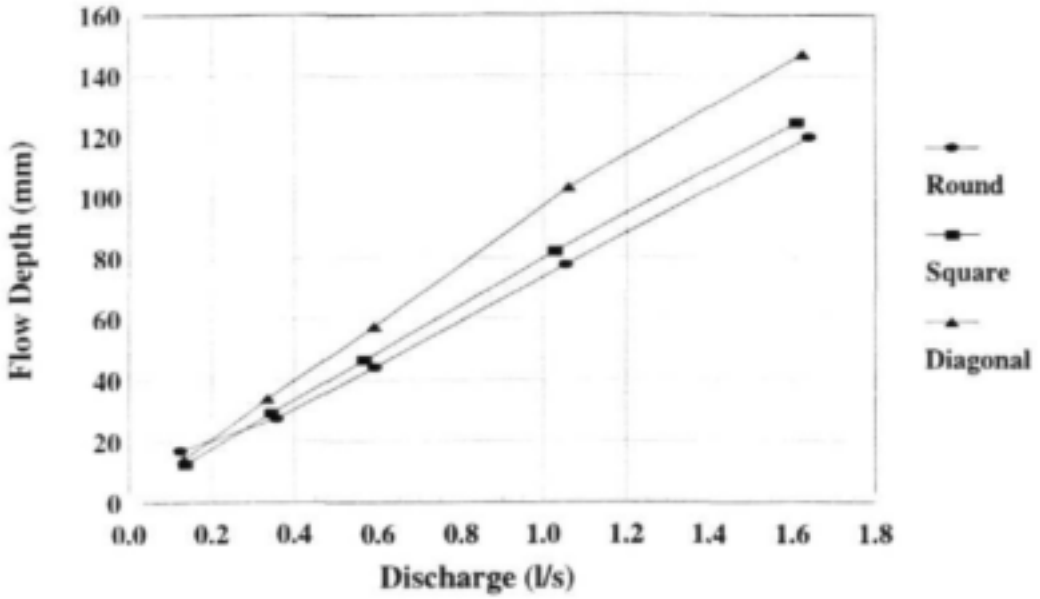

Figure 4.9 Influence of stem shape on stage-discharge relationship for slope=0.01, stem spacing=25 mm

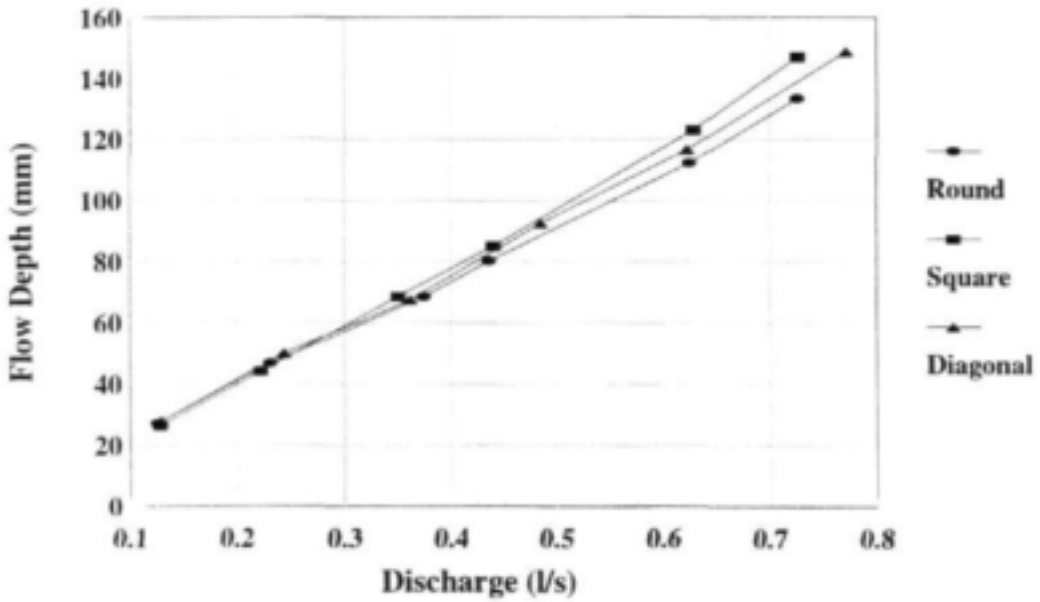

Figure 4.10 Influence of stem shape on stage-discharge relationship for slope=0.002, stem spacing=25 mm

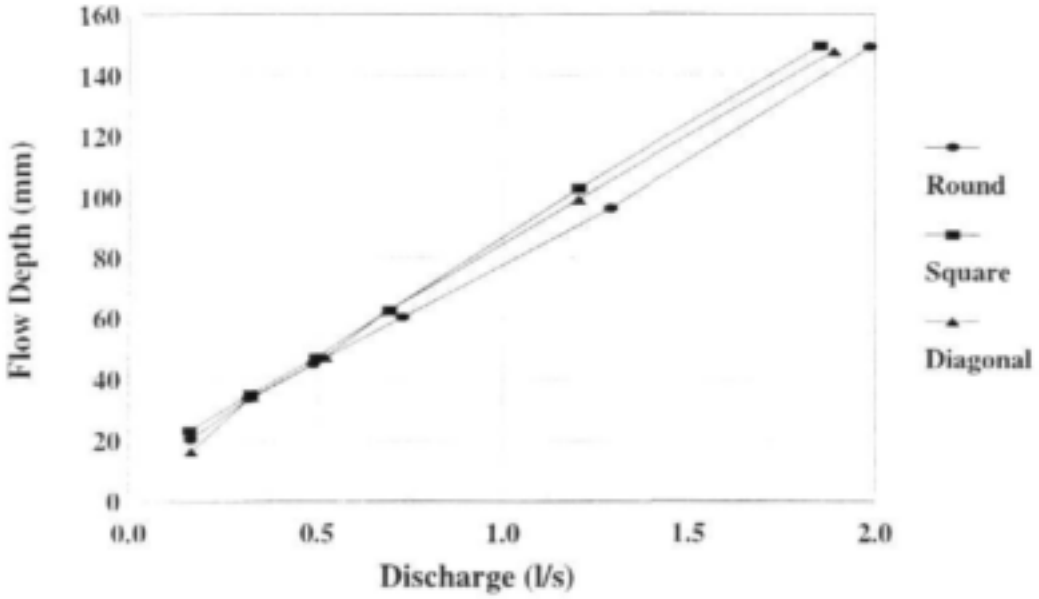

Figure 4.11 Influence of stem shape on stage-discharge relationship for slope=0.002, stem spacing=50 mm

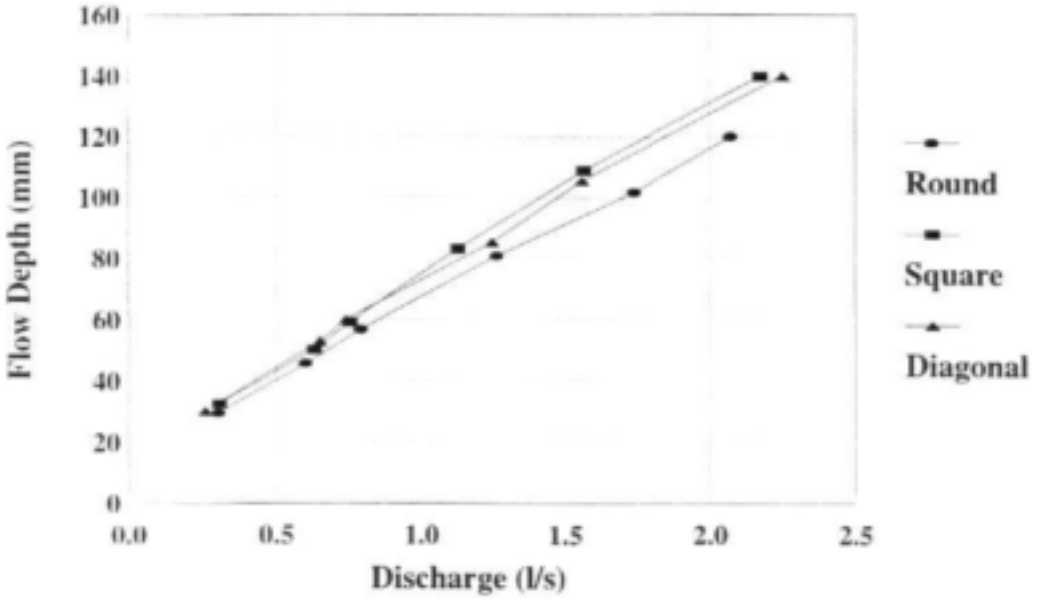

Figure 4.12 Influence of stem shape on stage-discharge relationship for slope=0.002, stem spacing=75 mm

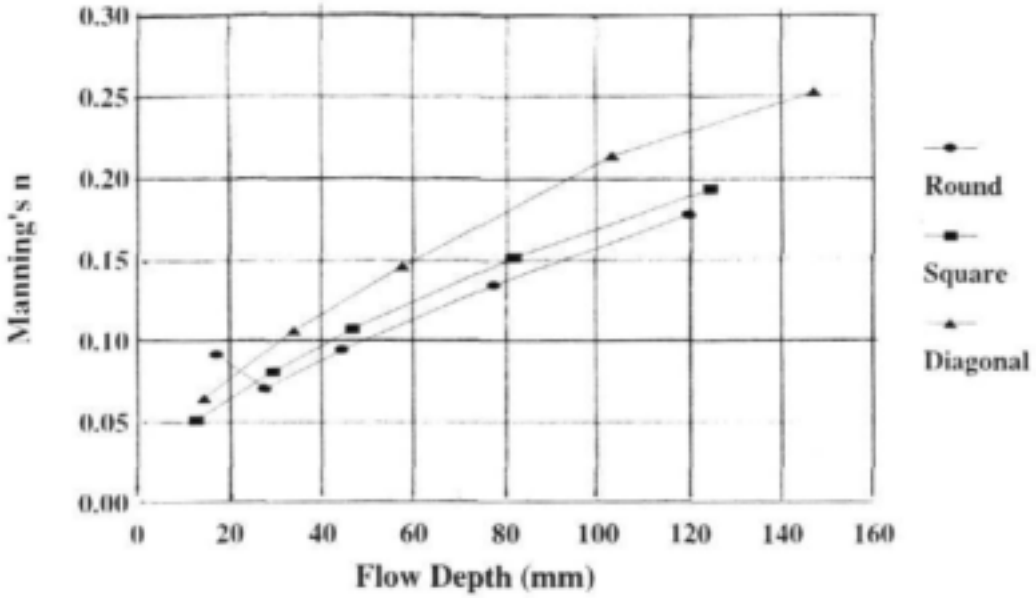

Figure 4.13 Influence of stem shape on Manning's *n* for slope=0.01, stem spacing=25 mm

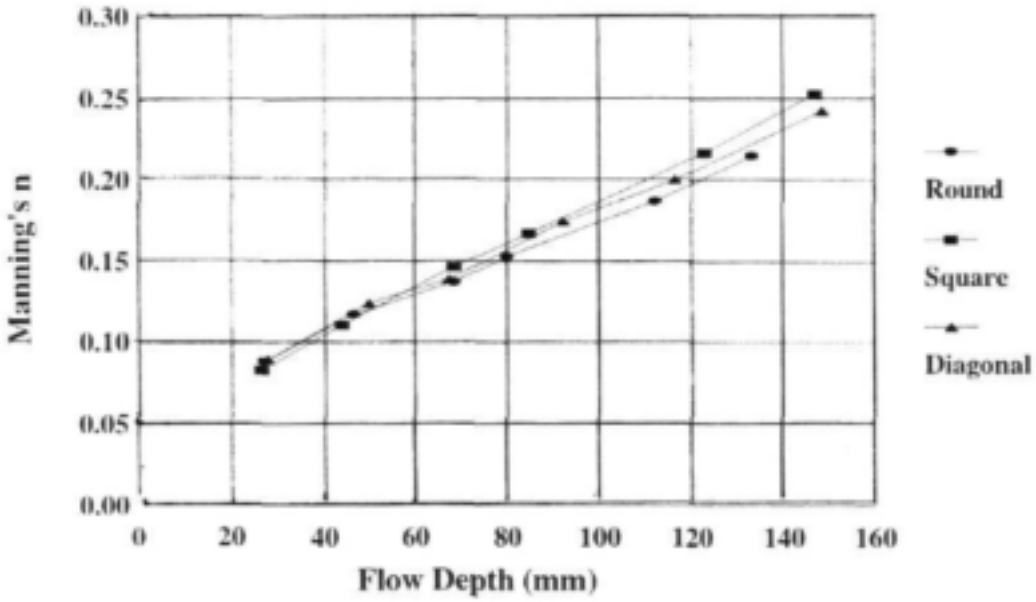

Figure 4.14 Influence of stem shape on Manning's *n* for slope=0.002, stem spacing=25 mm

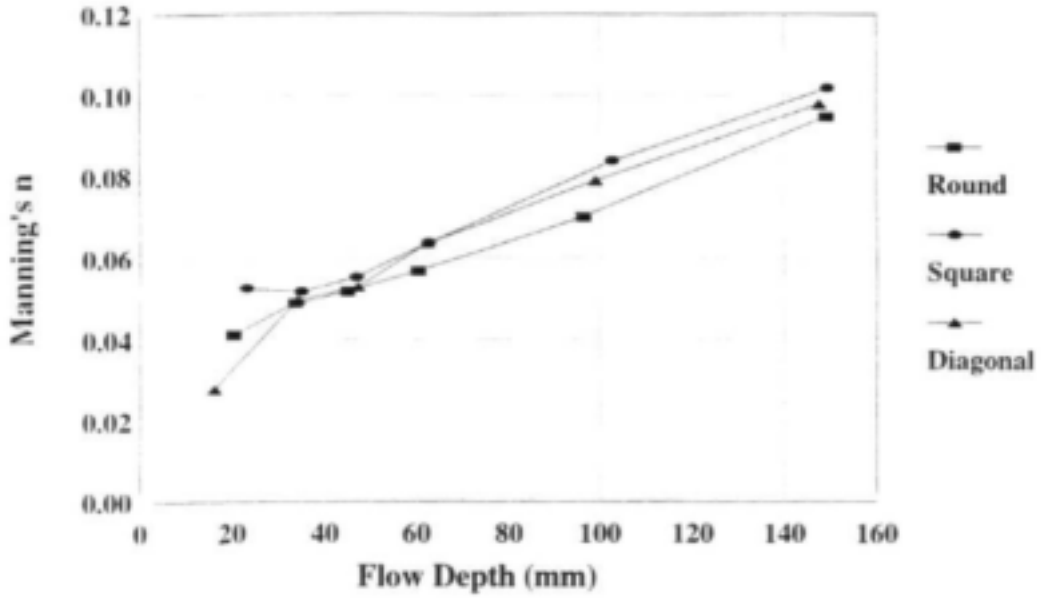

Figure 4.15 Influence of stem shape on Manning's *n* for slope=0.002, stem spacing=50 mm

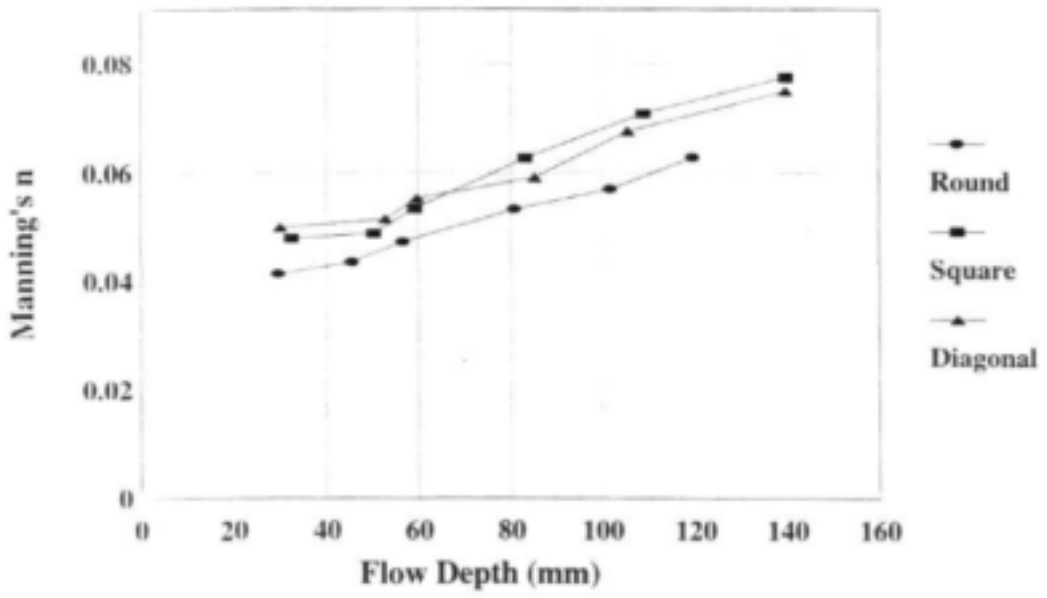

Figure 4.16 Influence of stem shape on Manning's *n* for slope=0.002, stem spacing=75 mm

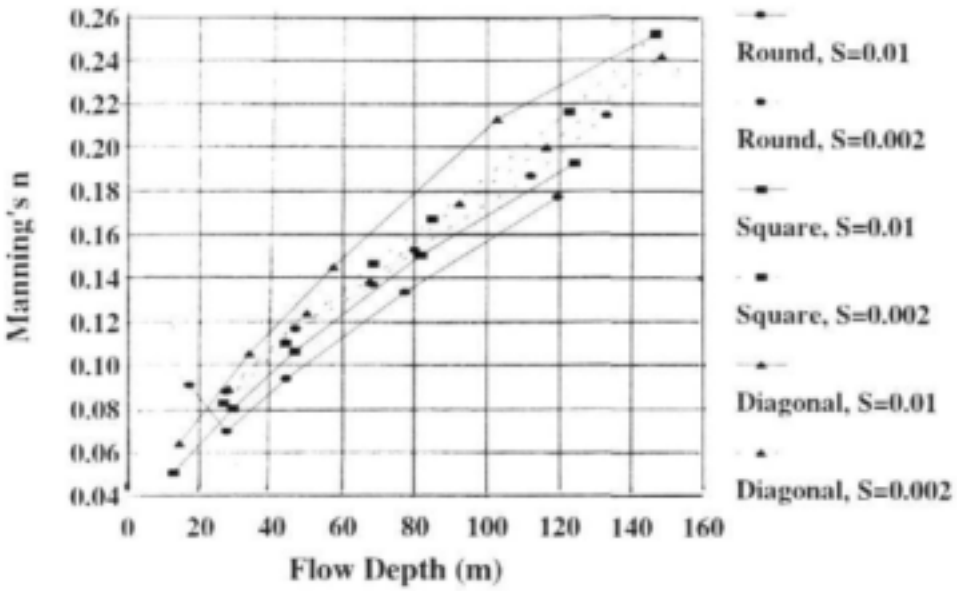

Figure 4.17 Influence of channel slope on Manning's *n* for Series A experiments with different stem shapes, stem spacing=25 mm

4.2.2 Series B Experiments

4.2.2.1 Experimental Procedure

The investigation of sedimentation in reedbeds, described in Chapter 10, provided opportunity for further flow resistance data collection (Series B). The experiments were conducted in a 0.38 m wide tilting flume but, because the bed was mobile, the slope was a dependent variable and could not be set. Uniform flow was ensured by setting an adjustable weir at the downstream end of the flow, and water levels were measured on scales fixed to the glass sides of the flume. Discharge was measured using a calibrated V-notch weir below the flume outlet. The stems were the same as the round, 5 mm rods used in Series A, but extended over a greater width (380 mm compared with 100 mm in Series A). The same stem arrangement was used, but only with the 25 mm stem spacing. The full experimental procedure is described in Chapter 10 and the tests relevant to the resistance investigation are listed in Table 4.1.

4.2.2.2 Results

The series B experiments produced measurements of flow depth and discharge which are useful for flow resistance interpretation. These are listed in Appendix A.2.

No analysis of bed friction characteristics is possible, because mobile bed experiments were only

conducted with the stems in place. Without the stems, bed forms would have developed and imposed significant form resistance. The bed consisted of loose sand with a mean diameter of 0.45 mm. This size cannot be used to characterize the effective roughness, however, because surface irregularities resulting from local scour around the stem bases during transport would have made an additional contribution to resistance over and above the shear associated with the grain roughness.

It is not possible to compile stage-discharge relationships from the Series B data because slope was a dependent variable and each experiment represented a unique combination of flow depth, discharge and slope. The resistance characteristics can, however, be represented by Manning's n, which shows variation with flow depth similar to the Series A results (Fig. 4.18). Here, Manning's n was calculated using the flow depth (y) to represent the hydraulic radius (R), which implicitly assumes that the resistance of the walls is negligible compared with that of the bed. (The average channel slope was 0.0145 and the range was 0.0118 to 0.0184).

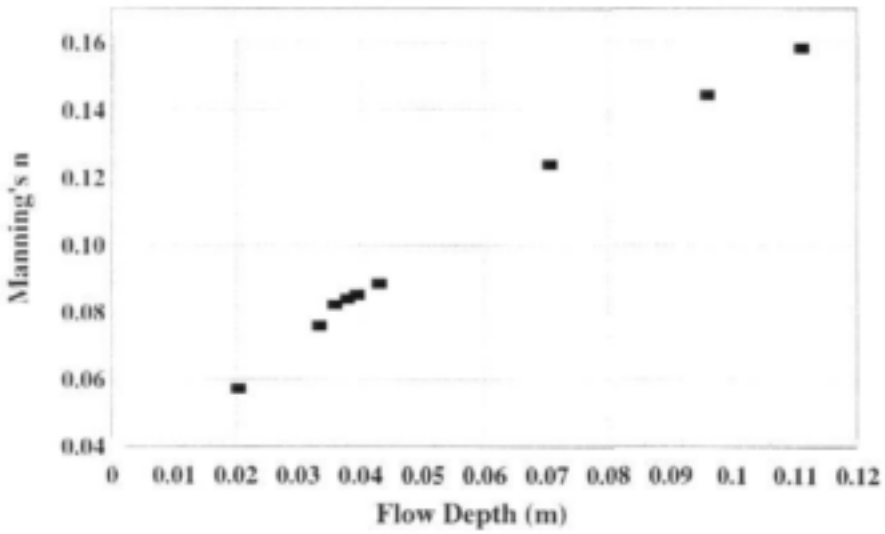

Figure 4.18 Influence of channel slope and flow depth on Manning's n for Series B experiments, stem spacing=25 mm

4.2.3 Data from Other Sources

Little information is available regarding flow resistance measurements through emergent vegetation, particularly with corresponding description of stem characteristics or drag coefficient values. The following sources have been identified, however, as being potentially useful for contributing to development and calibration of prediction models.

4.2.3.1 Waterways Experiment Station (1994)

Hall and Freeman (Waterways Experiment Station,1994) measured flow depths and discharges through a dense stand of bulrushes (*Scirpus validus*) grown over a length of approximately 15 m in a 1.2 m wide concrete drainage channel. A bulkhead was installed at the downstream end of the test section to enable the tailwater depth to be varied. Tests were conducted at different growth stages. In July 1992 the stem density was 403/m^2 and the stem diameter was 7.0 mm. Two tailwater conditions were imposed for the July tests by installing one and two 0.15 m high stoplogs above the bed level in the bulkhead; these two conditions are referred to as the "low" and "high" tailwater conditions respectively. In November 1992 the stem density had increased to 807/m^2 and the stem diameter to 7.6 mm. The November tests were conducted with the "high" tailwater condition only. The flow was obviously nonuniform during the tests, and the water level was measured at 5 locations in the July tests and at the upstream and downstream ends in the November tests. The slopes assigned to each test in the reported results are presumably averages of these measurements. Velocities were measured at different depths using a flow meter, and cross-sectional average velocities calculated from the measured discharges and flow depths. The stage-discharge data presented in Table 4.4 are derived from their reported results by calculating flow depth from the measured discharges and cross-sectional average velocities (assuming that the cross-sectional flow area is not significantly reduced by the stems).

Table 4.4 Stage-discharge data from the Waterways Experiment Station (1994) experiments

Tests	Depth (m)	Discharge (m^3/s)	Slope
July 1992 Tests (low tailwater)	0.103	0.009	0.0088
	0.215	0.026	0.0105
	0.268	0.044	0.0145
	0.306	0.057	0.0145
July 1992 Tests (high tailwater)	0.313	0.009	0.0010
	0.339	0.026	0.0035
	0.403	0.044	0.0040
	0.432	0.057	0.0050
November 1992 Tests	0.347	0.010	0.0028
	0.374	0.026	0.0085
	0.417	0.044	0.0120
	0.448	0.064	0.0198

4.2.3.2 Turner and Chanmeesri (1984)

Turner and Chanmeesri (1984) carried out experiments on flow through crops of wheat grown in two flumes. The first set of experiments were in a fixed-slope (0.001), 80 m long, 0.78 m wide flume. The length was divided into 8 sections, each 6 m long, in each of which different densities and arrangements of plants were grown and tested at different growth stages. Unfortunately, not all data are presented and the details of the reported results are inconsistent so that some conditions are ambiguous. However, stage-discharge measurements (for flow depths less than 100 mm) for two conditions (stem densities of 1650/m^2 and 1020/m^2, "diagonal" arrangement, and stem diameters of 2.72 mm and 2.89 mm) are presented with sufficient information to enable interpretation. The stage-discharge data for these tests, as extracted from their Fig. 3, are listed in Table 4.5.

The second set of experiments were carried out in a variable-slope flume that was 4 m long (with a 2.5 m long test section) and 0.45 m wide. Stage-discharge data are presented for one plant condition (stem density = 2200/m^2, "square" arrangement) and four different slopes (ranging from 0.002 to 0.01).

Table 4.5 Stage-discharge data from experiments of Turner and Chanmeesri (1984)

Location	Depth (m)	Discharge (l/s)	Slope
Section B	0.0161	0.71	0.002
	0.0247	1.08	
	0.0328	1.45	
	0.0445	2.00	
	0.0555	2.46	
	0.0665	3.10	
	0.0750	3.55	
	0.0860	4.00	
Section H	0.0140	1.01	0.0028
	0.0220	1.52	
	0.0260	1.83	
	0.0360	2.55	
	0.0415	3.20	
	0.0495	3.55	
	0.0535	4.00	
	0.0585	4.55	
	0.0670	4.85	

4.3 STEM DRAG EXPERIMENTS

The results of the Series A experiments confirmed that resistance to flow through stems is affected by stem shape. This effect is commonly accounted for in prediction models through specification of a drag coefficient, C_D, as discussed in Chapter 2. In anticipation of similar development based on these results, and extension and application to more natural stems, Series C experiments were undertaken to determine the values of C_D corresponding to the stem shapes used in Series A, and some typical values for real reed stems.

4.3.1 Experimental Procedure

Drag force experiments were carried out in a 24 m long, 0.915 m wide, horizontal flume. A length of the stem to be tested was attached to the lower end of a 1.410 m high, rectangular, aluminium frame extending across the width of the flume and with a pivot axis 770 mm above the attachment level (Fig. 4.19). The rotation of the frame under the influence of drag on the stem was balanced by filling with water a container attached by a line passing over a pulley to the top of the frame. Application of moment equilibrium enabled the drag force to be calculated from the weight of the water in the container. Corrections were made for the force exerted on the vertical members of the frame, which was measured without the stem in place.

Flow velocities were measured at the test stem level, with the stem removed, at the centre of the section and 250 mm from each side, using a Valeport electromagnetic flow meter. The average of these three measurements was used to represent velocity in the calculation of drag coefficient.

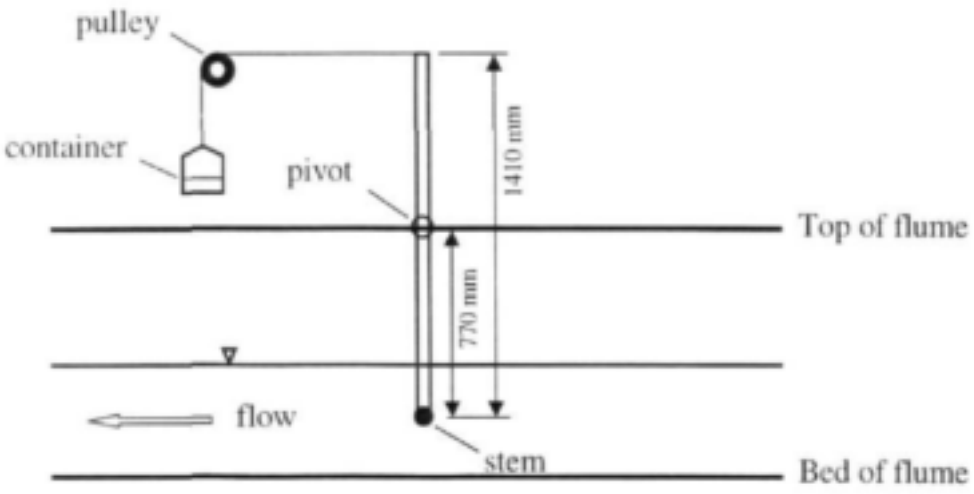

Figure 4.19 Apparatus for measuring drag force

The characteristics of the stems tested are listed in Table 4.6. Stem types tested included the 5 mm round, square and diagonal rods used in test Series A, as well as some real, freshly cut reed and bulrush stems. The reed and bulrush stems were harvested from stands of *Phragmites australis* and *Typha capensis* in the Braamfontein Spruit, north of Johannesburg. Two reed stems (Figs 4.20 and 4.21) and one bulrush stem (Fig. 4.22) were tested. In Tests C6 to C9, the stem of reed 2 was progressively stripped of leaves and branches to determine the relative contributions of the main stem and the foliage on drag. First, the stem was tested with all leaves and branches (Test 6), then with just 6 leaves (Test 7), then with 3 leaves (Test 8) and finally with only the bare stem (Test 9). The foliage areas of the stems were measured by tracing the outlines on to squared paper.

The measured data are listed in Appendix A.3.

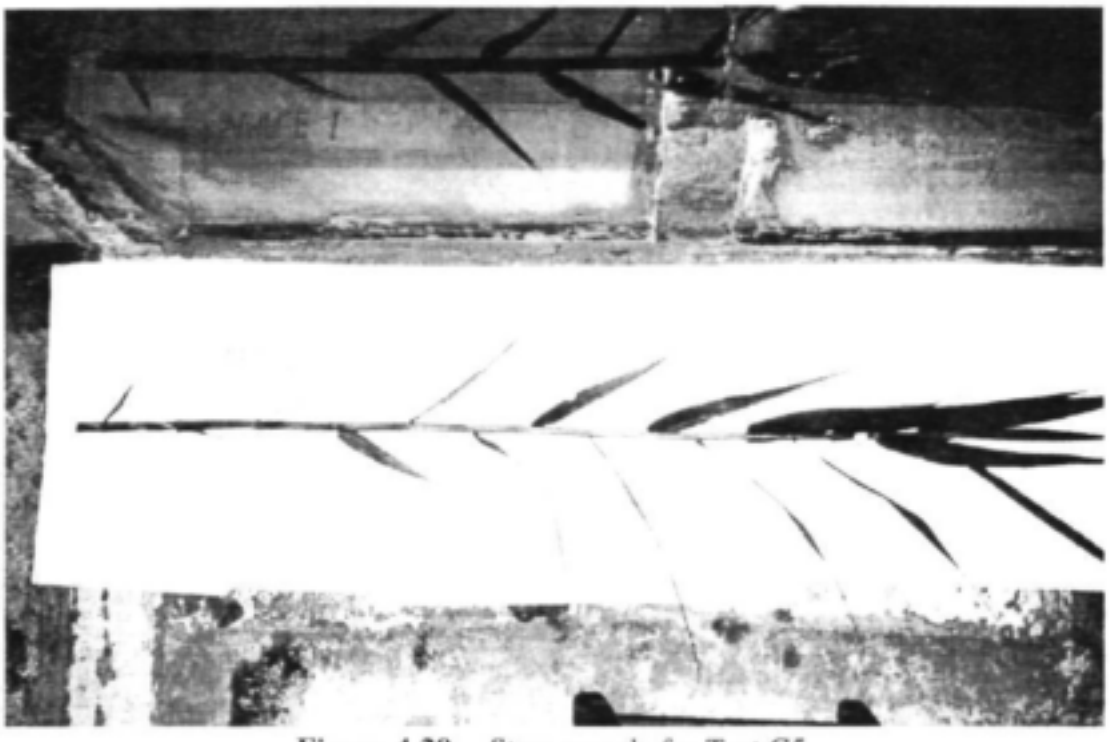

Figure 4.20 Stem sample for Test C5

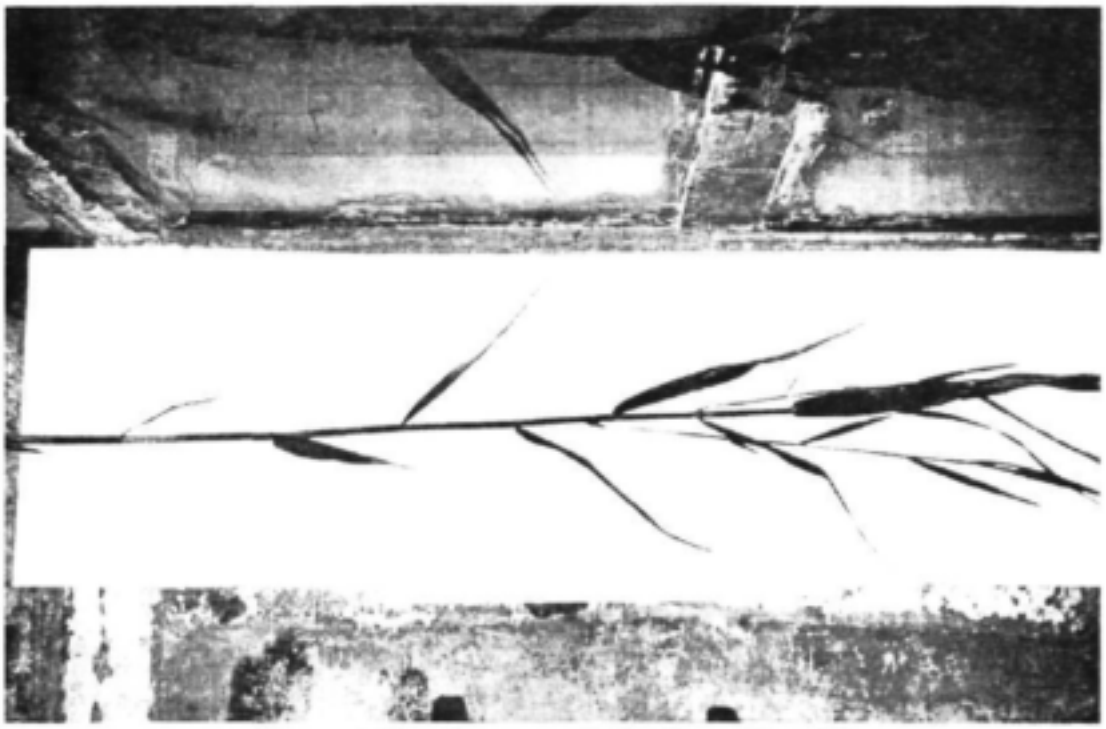

Figure 4.21 Stem sample for Tests C6 to C9

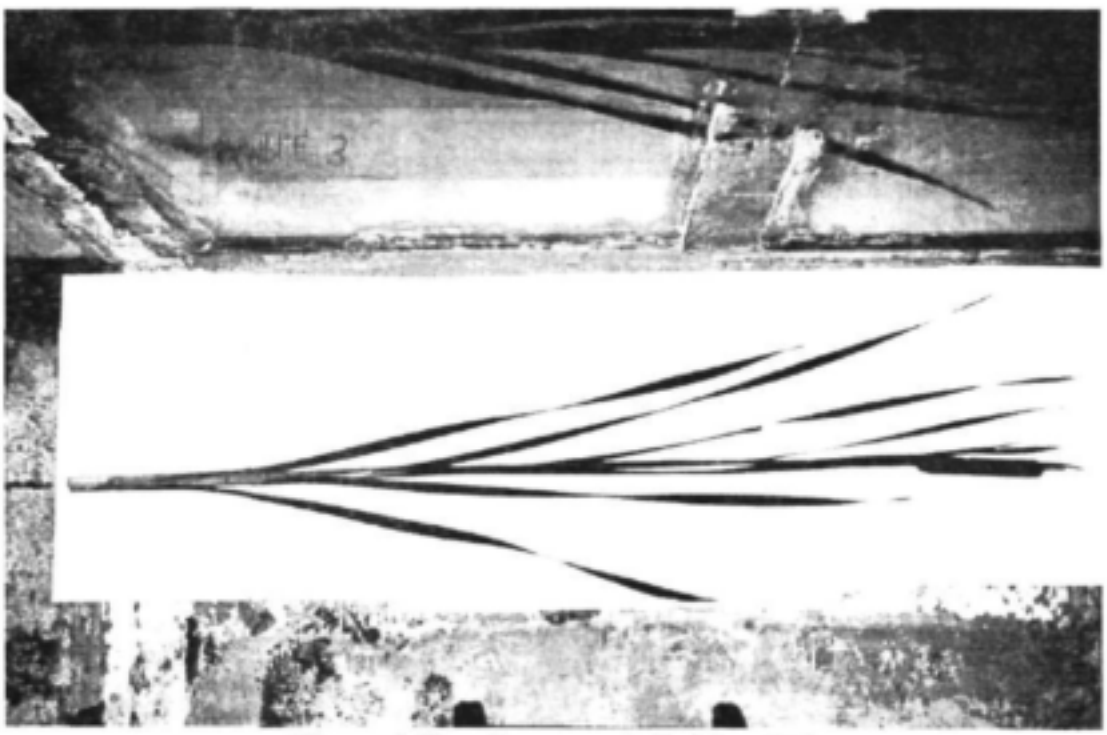

Figure 4.22 Stem sample for Test C10

Table 4.6 Stem drag experiments

Test	Stem Type	Stem Length (m)	Stem Diameter (mm)	Foliage Area (m^2)
C1	round	0.895	5	-
C2	square	0.895	5	-
C3	square	0.895	25	-
C4	diagonal	0.895	5	-
C5	reed 1	0.880	10.8	0.0292
C6	reed 2	0.860	8.40	0.0340
C7	reed 2	0.860	8.40	0.0318
C8	reed 2	0.860	8.40	0.0158
C9	reed 2	0.860	8.40	0
C10	bulrush	0.865	11.57	0.0339

4.3.2 Results

The drag force (F_D) of a stem is related to flow condition by

$$F_D = C_D A \frac{1}{2} \rho V^2 \qquad 4.12$$

in which A is the stem area projected in the flow direction, ρ is the water density, V is the local flow velocity, and C_D is the drag coefficient. C_D depends on the stem size and shape and the Reynolds number in terms of the stem diameter, d, i.e.

$$Re = \frac{Vd}{\upsilon} \qquad 4.13$$

in which υ is the kinematic viscosity of the water.

Values of C_D have been determined experimentally for a variety of cylinder shapes and are commonly expressed as graphical or tabular functions of Re, such as by Albertson et al (1960). The data collected in the experiments described above enable similar relationships to be established for the stems used in Series A and B experiments, as well as for the real reed and bulrush stems tested. For each experiment, the value of C_D was determined through application of equation 4.12, and Re by equation 4.13 (using a constant value of υ = 1.14x10^{-6} m^2/s, corresponding to the measured temperature of about 20°C). For the real stems the projected area was defined by the main stem only, as the actual projected area would be difficult to determine in practice, and would vary with flow condition as leaves deflect.

The derived values of C_D and corresponding Re for the stems used in test Series A are listed in

Table 4.7, and plotted in Fig. 4.23, together with the standard relationship for infinitely long circular cylinders as presented by Albertson et al (1960). The measured values for the round rod coincide closely with the standard curve for $Re > 200$, confirming the reliability of the experiments in this range. The measured point at $Re = 59$ appears to be erroneous, and this is attributed to the error in measuring the very small mass (0.2 g) and velocity (0.0135 m/s). The C_D values for the square and diagonal stems also appear to be exaggerated for Re less than about 1000. These results are not sufficiently precise to permit accurate specification of C_D values for the square and diagonal stems, but suggest that they are only slightly higher than for the round stem. For Re between 1000 and 10000, C_D for the square and diagonal stems appear to be respectively about 30% and 50% higher than for the round stem. This is considerably different from the corresponding 80% and 43% implied by Albertson et al (1960) in their Table 9-1 (C_D = 2.0 and 1.6 respectively).

Table 4.7 Drag coefficient values for cylindrical stems

Round		Square		Diagonal	
Re	C_D	***Re***	C_D	***Re***	C_D
d = 5 mm		**d = 5 mm**		**d = 5 mm**	
59	4.68	53	15.2	342	2.91
250	1.31	254	3.00	684	1.46
572	1.13	452	2.07	1163	1.18
949	1.00	608	1.82	1768	1.15
1601	1.02	899	1.36	2581	1.35
2177	1.04	1458	1.25	3029	1.39
2585	0.966	1589	1.15	3744	1.37
3001	0.910	2848	0.998	4376	1.33
3852	0.916	3070	1.03	4830	1.29
		3596	1.19		
		d = 25 mm		**d = 25 mm**	
		321	1.96	910	1.25
		614	1.29	2254	1.02
		1484	0.975	4456	1.28
		2259	0.961		
		3297	1.10		

The C_D values for the real reed (Tests C5 and C6) and bulrush (Test C10) stems are listed in Table 4.8. The values for the different stems, all with full foliage, are shown in Fig. 4.24, and the effect of foliage stripping for the second reed stem (Tests C6 to C9) in Fig. 4.25. These results show that foliage on natural stems increases the value of C_D considerably. Also, C_D for natural

stems appears to show dependency on *Re* at higher values of *Re* than the cylinders presented in the standard relationships by Albertson et al (1960), for example. Development of resistance equations based on stem drag quantification should therefore be accompanied by extensive experimental determination of C_D for relevant vegetation type

Table 4.8 Drag coefficient values for reed and bulrush stems

Reed 1 (Test C5)		Reed 2, full foliage (Test C6)		Reed 2, 6 leaves (Test C7)		Reed 2 3 leaves (Test C8)		Reed 2 stem only (Test C9)		Bulrush (Test C10)	
Re	C_D	Re	C_D	Re	C_D	Re	C_D	Re	C_D	Re	C_D
638	3.46	457	6.79	246	16.2	246	16.2	255	4.34	501	5.34
1257	2.43	820	5.35	874	4.19	764	2.45	911	1.72	961	2.56
1928	2.64	1535	3.70	1351	2.73	1368	2.20	1326	1.62	1867	3.09
3046	1.82	2149	2.50	2139	2.29	2127	1.69	2211	1.62	2882	2.94
3837	1.57	2804	2.29	2660	2.03	2947	1.51	2800	1.49	4070	2.73
4838	1.35	3483	1.88	3569	1.59	3542	1.44	3684	1.41	4831	2.51
		4347	1.75	4347	1.55	4731	1.27	4686	1.25	5981	2.22

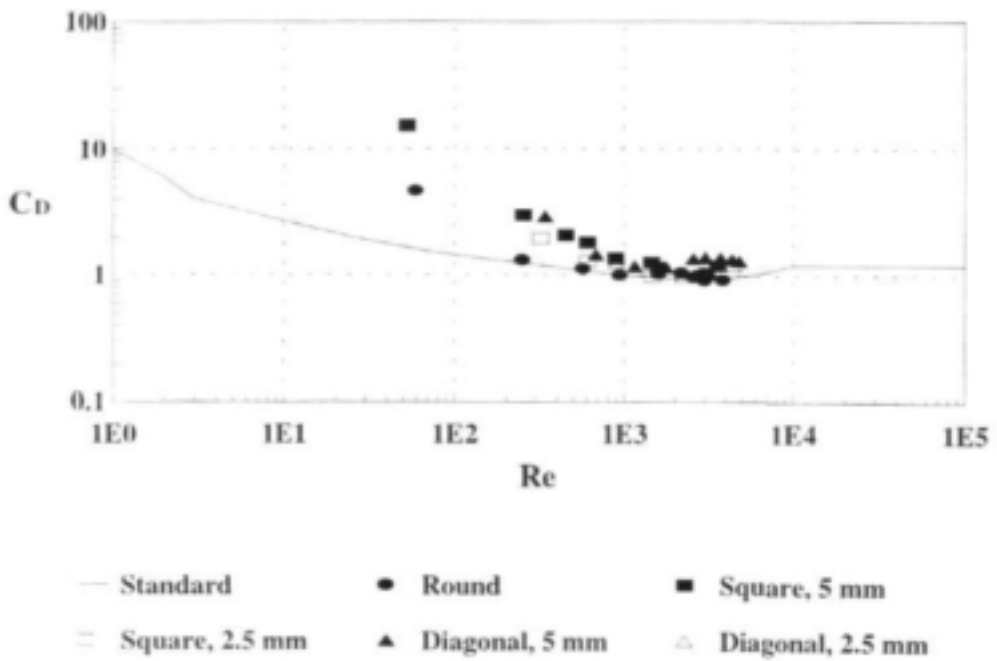

Figure 4.23 Drag coefficients for round, square and diagonal stems

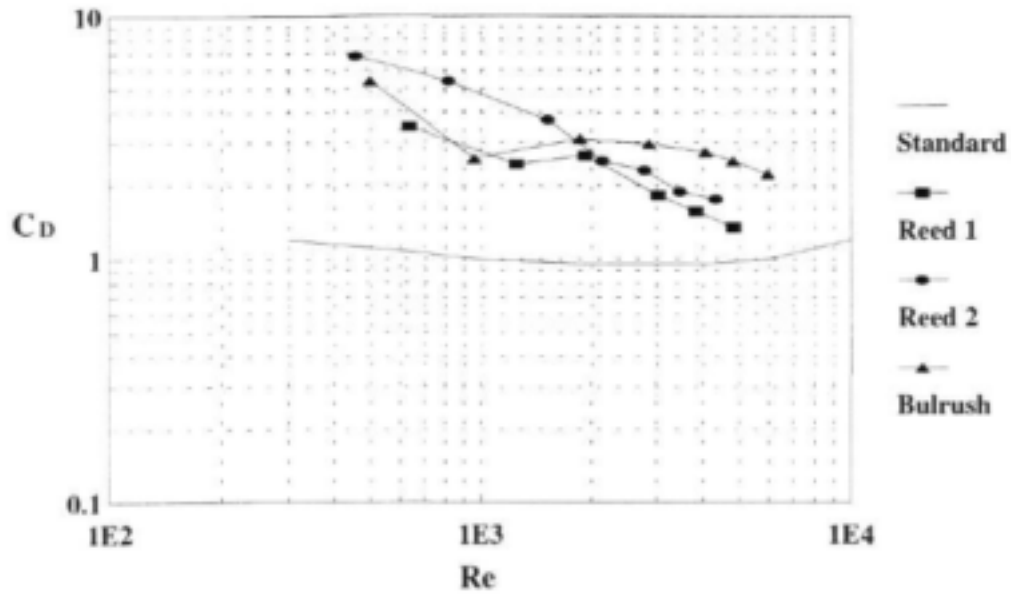

Figure 4.25 Drag coefficients for natural stems

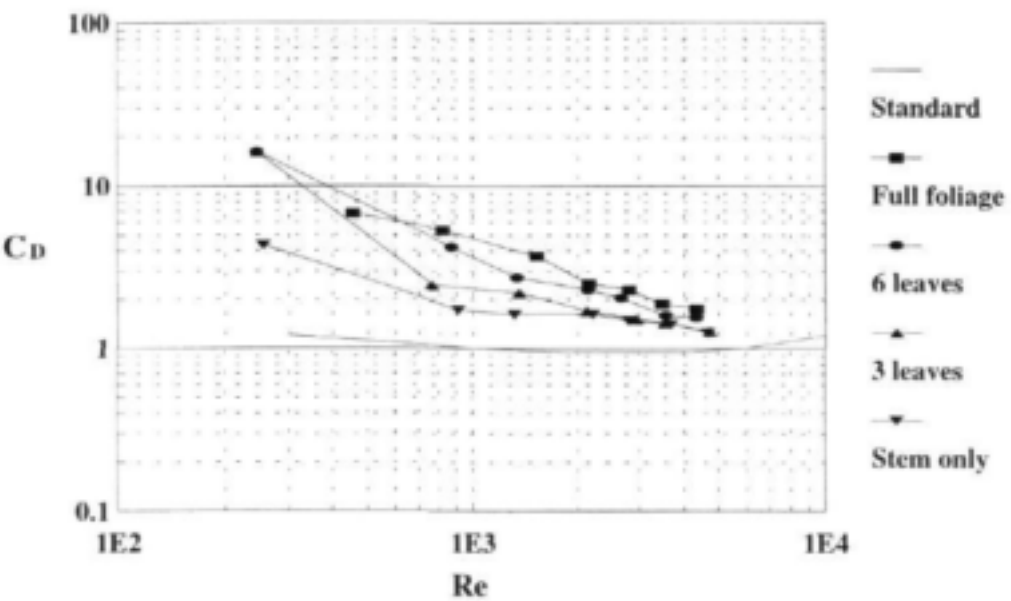

Figure 4.25 Variation of drag coefficient with degree of foliage

4.4 CONCLUSION

The experiments described in this chapter have provided data which enable the influence of vegetation stem characteristics on flow resistance to be elucidated, and to be quantified for relatively simple situations.

Resistance depends strongly on stem density. It may also depend on stem diameter, but this was not investigated experimentally; it is likely to be accounted for through C_D. Channel slope appears to have a minor influence on resistance, but this is most likely due to associated changes in velocity, and hence Re, with consequent influence on C_D.

The results for different stem shapes show that relatively small shape variations have little influence on resistance at low slopes, and the C_D measurements confirmed that the values were not significantly different for the round and square rods. The effect of foliage on C_D, however, has been shown to be significant and a relationship between C_D and a leaf area index for reeds should be able to be determined. For natural stems, C_D showed a significant dependence on Re at much higher values of Re than for smooth circular cylinders, as presented on the standard curve of Albertson et al (1960).

For submerged conditions the velocity profile within the stem zone is mostly uniform, but increases towards the stem tops through momentum transfer from the less resisted flow above. Above the stem tops the velocity distribution is similar to boundary resisted flow.

The results show that Manning's n varies significantly with flow condition in flow through stems, even when the other factors determining resistance are constant. This suggests that Manning's equation is inappropriate where the dominant flow resisting force arises from stem drag, rather than bed friction. The reason for this is explored in the following chapter and an alternative form of equation is proposed.

Chapter 5

RESISTANCE PREDICTION FOR FLOW THROUGH EMERGENT REEDS

5.1 INTRODUCTION

In the interpretation of the experimental results in Chapter 4, the flow resistance was expressed and presented in terms of Manning's n, because this is the most familiar and widely used form for free surface flow. In this form, the influence of stem density and shape on flow resistance can be clearly seen. However, the results also show that Manning's n for vegetated channels varies very significantly with flow depth. This arises because Manning's and similar resistance equations were developed for, and strictly apply only to, situations where flow is controlled by boundary shear. The dominant resistance in vegetated channels arises from stem drag, which is applied throughout the flow depth, and its effects should be described by a different form of equation.

Notwithstanding their inapplicability, the Manning, Darcy-Weisbach and Chézy equations have been widely applied to vegetated channels, and various attempts have been made to recommend appropriate coefficient values. Approaches include direct calibration from laboratory or field measurements (e.g. Waterways Experiment Station, 1994; Starosolszky, 1983; Gáspár, 1983), and adjustment of basic values based on vegetation characteristics (e.g. Petryk and Bosmajian, 1975; Christensen, 1996; Klaassen and van der Zwaard, 1974). The variation of n with flow condition has been expressed as a correlation with the product VR, (e.g. Ree and Crow, 1977), leading to the development of standard curves with wide application (Smith et al, 1990). This correlation is confirmed by our data, as shown in Fig. 5.1 for the Series B experiments (using y for R), but does not appear to be superior to the simpler relationships with y presented earlier (such as Fig. 4.18 for Series B). There are, however, conceptual and practical difficulties in applying such relationships, as discussed by Smith et al, 1990.

Recognition of the inapplicability of Manning's equation for vegetated channels is not new. Turner and Chanmeesri (1984) proposed an equation of the form

$$q = G^{-1} y^{m} S^{0.5} \qquad 5.1$$

in which q is the unit width discharge, y the flow depth, S the channel slope, and G a roughness coefficient that is independent of slope. They determined coefficient values from experimental results and, on the basis of these recommended changing the exponent of S to 0.35.

Kadlec (1990) recommended a similar form, i.e.

$$q = K y^{\beta} S^{\alpha} \qquad 5.2$$

in which K needs to be determined from field data. He recommended that $\alpha = 1.0$ if the stem Reynolds number is in the laminar range and $\alpha = 0.5$ if it is in the turbulent range.

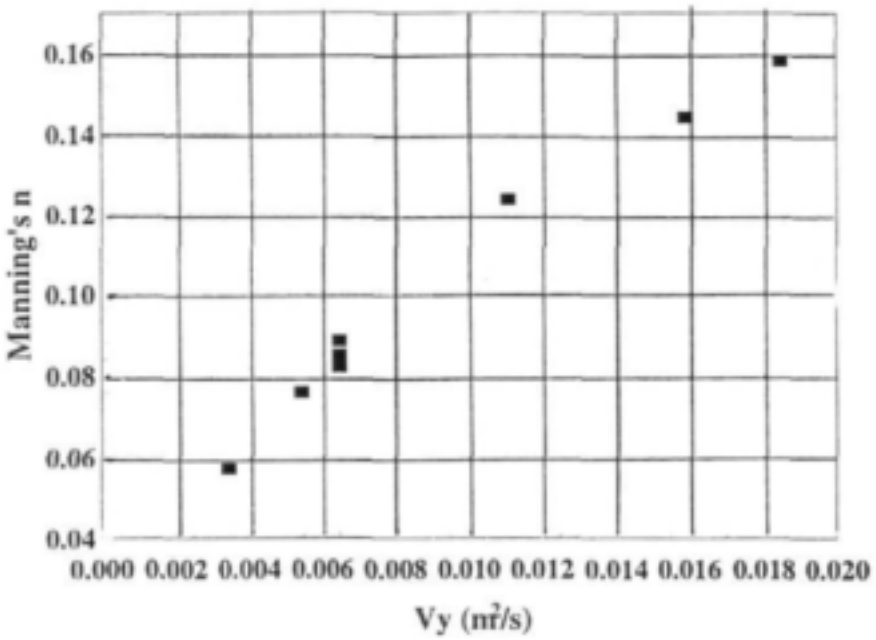

Figure 5.1 Correlation of Manning's n with Vy for Series B data

Smith et al (1990) used the same form of equation, and determined coefficient and exponent values from experimental results for a number of vegetation types. Their correlations produced values of the exponent to S in the range 0.83 to 2.6 and similarly wide variations for the other parameters. They concluded that widespread adoption of the equation was impeded by the dependence of the parameter values on vegetation type, geometry and flow condition, and the requirement for their experimental determination for each situation.

While recognising Smith et al's (1990) reservations concerning the generality of equation (5.2), it is undoubtedly preferable to the conventional resistance equations (Manning, Chézy and Darcy-Weisbach) because it is more compatible with the nature of the resistance phenomenon. It is therefore of value to attempt to reduce the uncertainty of the parameter values by providing a theoretical justification for the equation form, and to express it in a way that determination of parameter values for a particular situation does not require full stage-discharge measurement experiments. Ideally the equation should have as few empirical parameters as possible, and these should be able to be related to measurable plant characteristics.

5.2 THEORETICAL DEVELOPMENT

The conventional free surface flow resistance equations are founded on the balance of the forces driving and resisting the water movement. The driving force originates in the downslope weight component of the water, and the resisting force in the shear stress imposed by the boundary. The balance of these forces leads to a dependence of the boundary shear stress on flow depth, and the

assumed relationship between boundary shear stress and velocity underlies the dependence of velocity on flow depth in the conventional resistance equations. If the resistance to flow is exerted by stem drag rather than boundary shear, however, the velocity is independent of flow depth. This can be shown by considering the steady, uniform flow of a unit width element in stem-dominated flow (Fig. 5.2).

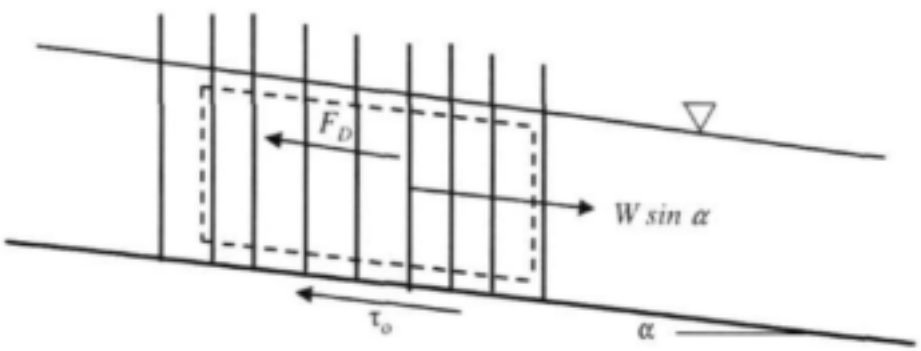

Figure 5.2 Forces on flow through stems

The driving force for the flow situation shown in Fig. 5.2 is the downflow weight component of the element, W. This is given by

$$W = V_{el} \gamma \sin \alpha \qquad 5.3$$

in which V_{el} is the volume of the element, γ is the unit weight of water, and α is the slope of the channel. For small slopes $\sin\alpha$ can be approximated by $\tan\alpha$, which is the channel slope S. The volume is given by the product of the cross-sectional area and the element length, L, reduced by the volume of stems within the element, i.e.

$$V_{el} = y\left(L - \frac{n\pi d^2}{4}\right) \qquad 5.4$$

The driving force is then

$$W = \gamma y\left(L - \frac{n\pi d^2}{4}\right)S \qquad 5.5$$

The force resisting motion of the element is the sum of drag forces from all the stems within the element, i.e.

$$F_D = C_D \frac{1}{2} \rho (nyd) V^2 \qquad 5.6$$

in which (nyd) is the projected area of all the stems.

Equating the driving and resisting forces, and expressing the number of stems in terms of the density (number of stems per unit area), N, i.e. $n = NL$, gives an equation for the flow velocity:

$$V = \sqrt{\frac{2g}{C_D N d}\left(1 - \frac{N \pi d^2}{4}\right)} \sqrt{S} \qquad 5.7$$

Equation (5.7) suggests that the exponent of S in equation (4.15) should be 0.5, and that the flow velocity is independent of depth if the resistance is caused exclusively by stem drag. This means that flow depth appears in equation (5.2) for continuity purposes only, and that its exponent should be 1.0. A general form of resistance equation for flow through vegetation can therefore be written as

$$V = \frac{1}{F} \sqrt{S} \qquad 5.8$$

with

$$F = \frac{1}{\sqrt{\frac{2g}{C_D N d}\left(1 - \frac{N \pi d^2}{4}\right)}} \qquad 5.9$$

constituting a resistance coefficient that depends on the stem density, diameter and drag coefficient. The resistance coefficient is expressed in inverse form in order to preserve proportionality of its value with resistance, as with Manning's n and the Darcy-Weisbach f, but unlike the Chézy C.

Nuding (1994) used an equation similar to equation (5.7), excluding the stem volume term, based on substitution into the Darcy-Weisbach equation an expression for f given by Lindner (1982) and Kaiser (1984). Tsujimoto and Kitamura (1994) used the Chézy equation with C given by a relationship similar to $1/F$, again ignoring the stem volume influence.

Experimental values of F have been calculated from the Series A round stem experimental results, as well as theoretical values from the stem characteristics using equation (5.9). Values of C_D were determined from the standard curve for infinitely long circular cylinders presented by Albertson et al (1960). The theoretical and measured values are plotted as functions of flow

depth (the heavy curve) in Fig. 5.3 (the graph for the steeper slope with 25 mm spacing is similar to the one shown for the milder slope, but about 10% lower). The resistance coefficient F is clearly much more independent of flow depth than is Manning's n, becoming constant as flow depth increases. The flow depth at which F becomes constant increases with stem spacing, indicating that equation (5.8) is more reliable for high stem density, where the contribution of bed shear to resistance is small. The theoretical values of F agree remarkably well with the measured values once they become constant. Equation (5.8) with F given by equation (5.9) therefore works well with the ideal stems and arrangements used in the experiments for high stem densities and relatively deep flows.

For low flow depths, sparse stem densities and very rough boundaries the influence of bed shear on overall resistance can be expected to be important, as reflected by the increasing values of F with decreasing flow depth in Fig. 5.3. Under these conditions an equation that accounts for bed shear is therefore necessary.

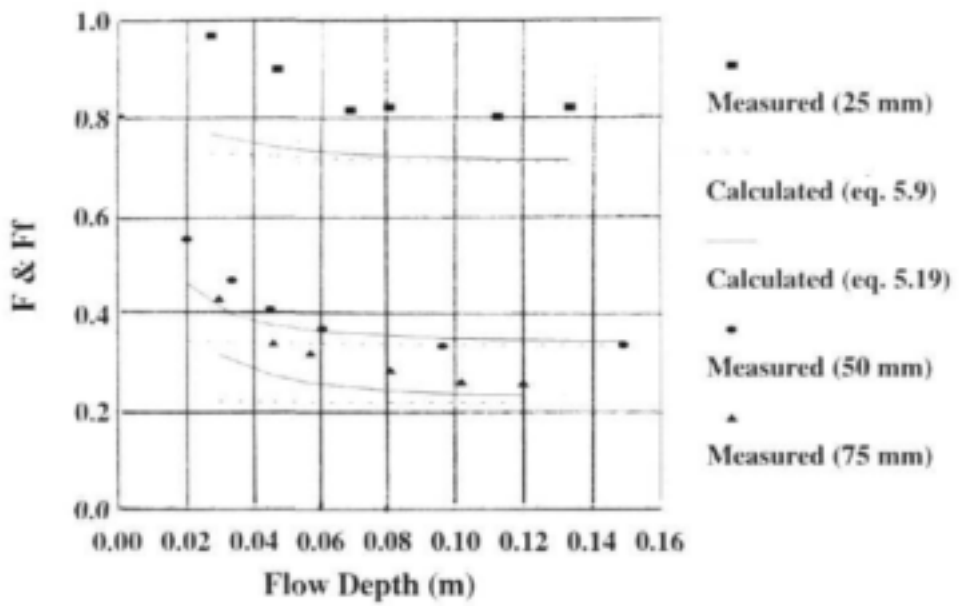

Figure 5.3 Measured and calculated resistance coefficients for Tests A3-A5

In the absence of stems, the shear stress in free surface flow increases linearly with flow depth to a maximum value at the bed, where it is balanced by the shear stress imposed by the bed on the flow. For unit width within a wide flow the bed shear is given by

$$\tau_0 = \gamma y S \qquad 5.10$$

In the presence of stems, some of the downslope weight component of the flow will be carried by the stems, and the force resisted by bed shear will be reduced. If it is assumed that this

reduction can be represented by the total stem drag force (equation (5.6)) divided by the plan area of flow, the bed shear can be expressed as

$$\tau_0 = \gamma y S \frac{A_{bed}}{A} - \frac{F_D}{A} \qquad 5.11$$

in which A_{bed} is the net area of the bed over which the shear stress acts, and A is the total plan area. The net area is given by the total area less the area occupied by the stems. Therefore

$$\tau_0 = \left(1 - \frac{n\pi d^2}{4A}\right)\gamma y S - C_D \frac{1}{2}\rho n y d V^2 \frac{1}{A} \qquad 5.12$$

which can be expressed in terms of the stem density (N) as

$$\tau_0 = \left(1 - \frac{N\pi d^2}{4}\right)\gamma y S - C_D \frac{1}{2}\rho N y d V^2 \qquad 5.13$$

The conventional free surface flow resistance equations are based on an assumed proportionality between boundary shear and average flow velocity (e.g. Henderson, 1966) , i.e.

$$\tau_0 = a\rho V^2 \qquad 5.14$$

If it is assumed that this proportionality holds in the presence of stems, in terms of the reduced bed shear given by equation (5.13), an equation for velocity can be derived which accounts for both bed shear and stem drag. Combining equations (5.13) and (5.14) gives

$$a\rho V^2 = \left(1 - \frac{N\pi d^2}{4}\right)\gamma y S - C_D \frac{1}{2}\rho N y d V^2 \qquad 5.15$$

which can be rearranged as

$$V = \sqrt{\left(\frac{1 - \frac{N\pi d^2}{4}}{a + C_D \frac{1}{2} N y d}\right) g y \sqrt{S}} \qquad 5.16$$

If equation (5.14) is recast as the Darcy-Weisbach equation, the parameter a can be represented

by

$$a = \frac{f}{8} \tag{5.17}$$

The equation for velocity under the influence of bed shear and stem drag can therefore be written as

$$V = \frac{1}{F_f}\sqrt{S} \tag{5.18}$$

with

$$F_f = \frac{1}{\sqrt{\left(\frac{1 - \frac{N\pi d^2}{4}}{\frac{f}{8} + \frac{1}{2} C_D N y d}\right) g y}} \tag{5.19}$$

As for equation (5.8), the resistance coefficient F_f is expressed in reciprocal form to maintain proportionality with resistance.

In practical applications there is probably a preference for describing bed resistance in terms of Manning's n rather than f. In this case the bed resistance term in equation (5.19) can be replaced by the corresponding Manning formulation, i.e.

$$\frac{f}{8} = \frac{g n^2}{y^{1/3}} \tag{5.20}$$

Values of F_f have been calculated for the Series A experimental conditions, and are plotted (as the fine line) together with the measured and calculated values of F on Fig. 5.3. In the calculation of F_f the value of f was determined using the Colebrook-White equation (equation (4.8)) with a value for k_s of 0.0125 m, as determined from the results of Test A1. Again, C_D was estimated using the standard relationship for infinitely long cylinders presented by Albertson et al (1960). It can be seen that equation (5.19) describes the combined resistance of stems and bed roughness realistically. The increase of resistance coefficient with decreasing flow depth is reproduced well in trend, although not quite as well in magnitude. The resistance for the most dense stem arrangement is not predicted accurately, particularly at low flow depths. This may be a reflection of underestimation of C_D using the standard relationship with Re for infinitely long single stems. The local approach velocity associated with drag becomes significantly different from the average velocity at high stem densities (Li and Shen, 1973), and additional drag associated with surface distortion would be expected to contribute significantly at low flow depths.

5.3 EQUATION CONFIRMATION

The performance of the proposed equations and resistance coefficients has been assessed by comparison of measured and predicted stage-discharge relationships for the Series A and B experiments, and some results presented by Turner and Chanmeesri (1984) and Hall and Freeman (1994).

Predicted stage-discharge relationships using the resistance coefficients presented in Fig. 5.3 are compared with the measured values for Tests A3, A4 and A5 in Figs 5.4, 5.5 and 5.6 respectively. The absolute errors for these predictions are listed in Table 5.1. Although the errors are fairly large, with discharge almost invariably overpredicted, the slopes of the curves are accurately reproduced, implying that the forms of the equations are sound. As expected, the predictions of equations (5.8) and (5.18) are very similar where stem density is high (Test A3) and the bed shear contribution is relatively small, but become progressively more different as the stem density decreases (Tests A4 and A5).

Table 5.1 Prediction errors in application of equations (5.8) and (5.18) to Series A and B tests

Measure	Equation (5.8)				Equation (5.18)		
	Test A3	Test A4	Test A5	Series B	Test A3	Test A4	Test A5
Average Absolute Error (%)	19.2	21.4	44.4	9.64	16.8	8.9	20.9
Standard Deviation (%)	7.3	21.6	26.5	4.26	5.2	7.2	8.8

Discharges have also been predicted for the Series B experiments. Only equation (5.8) could be applied in this case, because the roughness of the bed was not measured. Again, C_D was estimated using the relationship presented by Albertson et al (1960). The average absolute error for all the experiments was 9.64%, with a standard deviation of 4.26%, confirming reasonable performance. As in most of the Series A applications, the discharge was always overpredicted by equation (5.8). This is unlikely to be because the bed resistance component was neglected, because of the close similarity of equation (5.8) and (5.18) predictions for the same stem density in Test A3. It appears, therefore, that the stem drag is underestimated by using the standard $C_f(Re)$ relationship, with Re in terms of the average velocity. It should be noted that the bed slope in the Series B tests was much higher than for Tests A3 to A5, and the performance of equation (5.8) for both series confirms its reliability over a wide range of slopes.

Rigorous testing of equations (5.8) and (5.18), together with the resistance coefficients defined by equations (5.9) and (5.19) is not possible for natural conditions because no field data are

known where both the overall resistance (e.g. in the form of stage-discharge relationships) and the values of C_D for the individual stems were measured. Turner and Chanmeesri (1984), however, have presented some stage-discharge data for flow through crops of wheat in a flume, and these can be used to give some confirmation of the equations. They presented suitable stage-discharge data for two of their cases (Table 4.5). Their Section B and H data represent flow through diagonally arranged plants with average stem densities (N) of 1650/m^2 and 1020/m^2 respectively. Stem diameter varied with growth stage in their experiments, and it is not clear exactly what values correspond to the data presented; "mature" values of 2.72 mm and 2.89 mm, as listed in their Table III were assumed for the Section B and H conditions respectively. Confirmation of equation (5.8) with F given by equation (5.9) was sought by reproducing the stage-discharge relationships by adjusting the input value of C_D only. The stage-discharge data are listed in Table 5.2, together with the C_D values required to ensure accurate reproduction and corresponding values of Re. Equation (5.18) was not tested against these data because no information is available about the bed roughness. The fitted C_D values are compared with the standard curve (Albertson et al, 1960) in Fig. 5.7. The true values of C_D for these experiments were not measured, and the foliage and condition of the plants are not reported, so it is not possible to estimate values. However, the fitted values are fairly consistent for each set, and are reasonable if compared with those for reed stems (Figs 4.24 and 4.25) and the standard curve, particularly considering that little foliage was likely to be present at the low flow depths tested. The trend of the two sets with Re is also realistic.

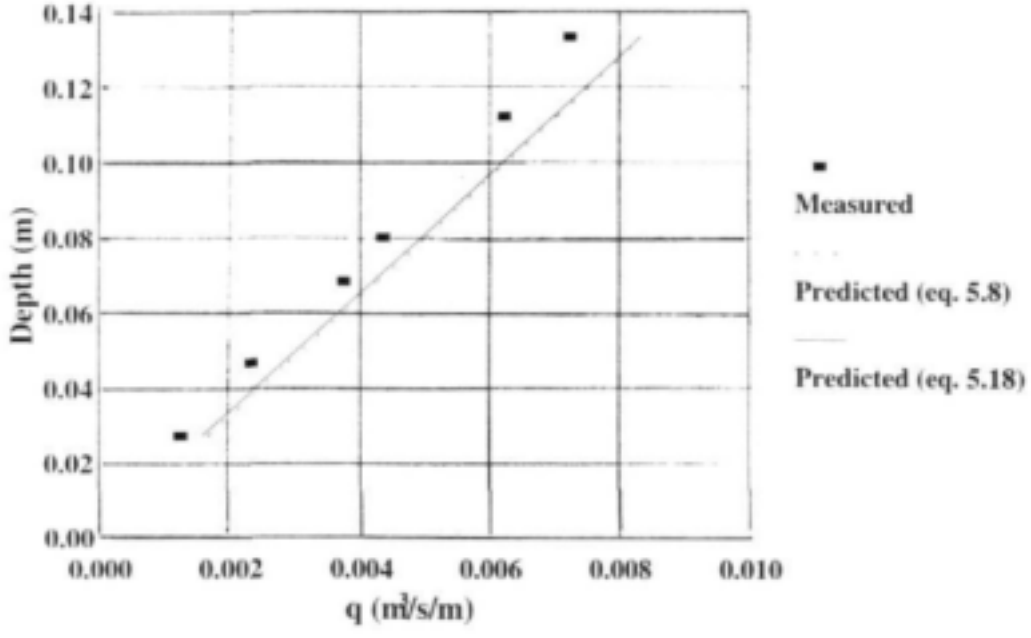

Figure 5.4 Measured and predicted stage-discharge relationship for Test A3

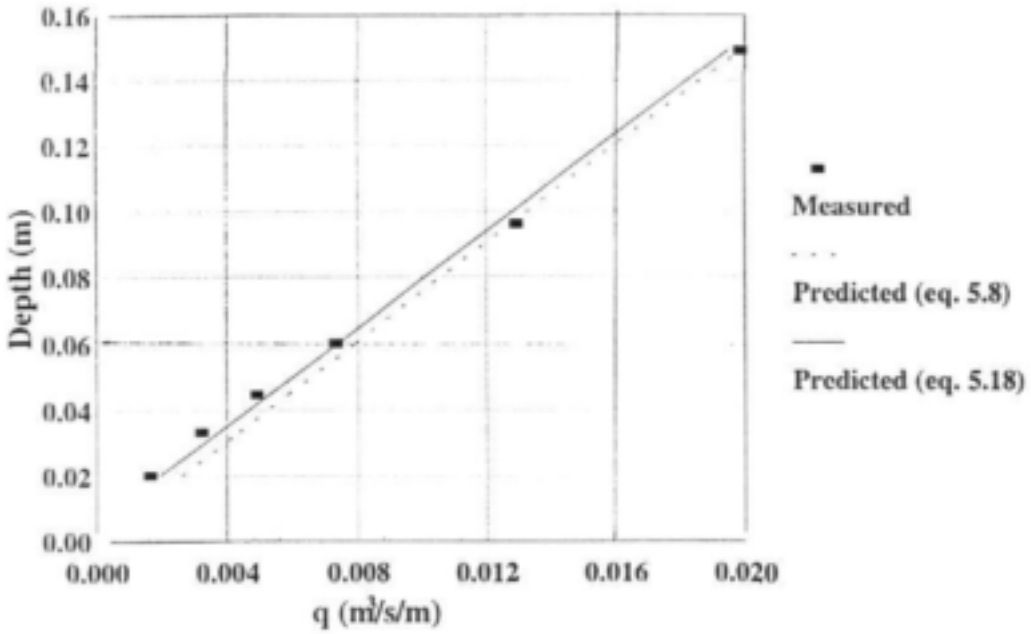

Figure 5.5 Measured and predicted stage-discharge relationship for Test A4

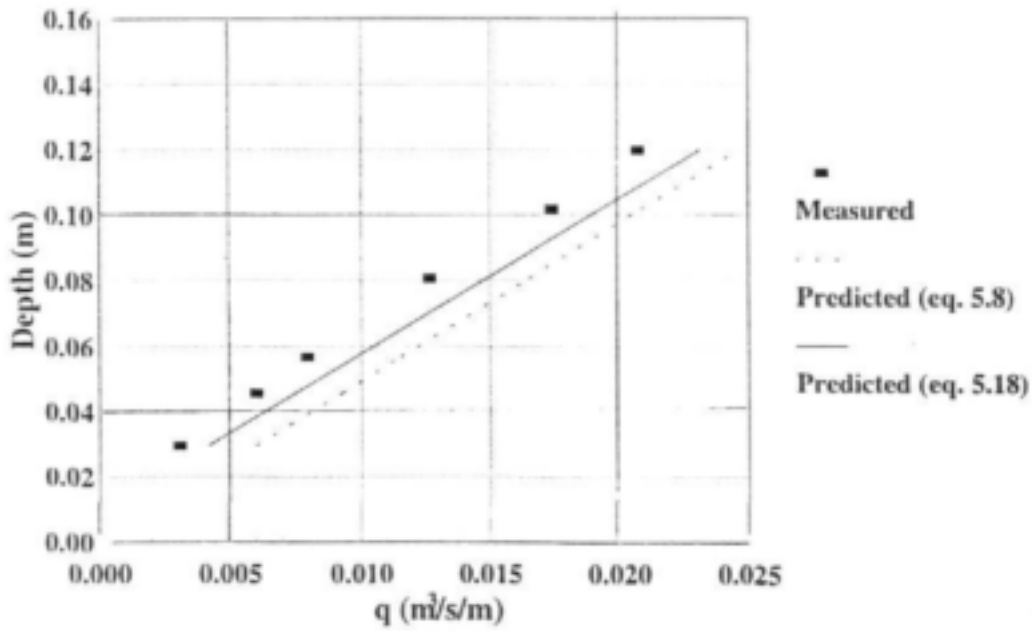

Figure 5.6 Measured and predicted stage-discharge relationship for Test A5

Table 5.2 **Values of C_D required to reproduce stage-discharge data of Turner and Chanmeesri (1984)**

Depth (m)	Discharge (l/s)	C_D	*Re*
Section B			
0.0161	0.71	2.70	154
0.0247	1.08	2.75	152
0.0328	1.45	2.69	154
0.0445	2.00	2.60	157
0.0555	2.46	2.68	155
0.0665	3.1	2.40	163
0.0750	3.55	2.35	165
0.0860	4.00	2.44	162
		Ave: 2.58	
		S. Dev: 0.15	
Section H			
0.0140	1.01	2.16	267
0.0220	1.52	2.35	256
0.0260	1.83	2.27	261
0.0360	2.55	2.24	262
0.0415	3.20	1.89	285
0.0495	3.55	2.19	266
0.0535	4.00	2.01	277
0.0585	4.55	1.86	288
0.0670	4.85	2.15	268
		Ave: 2.12	
		S. Dev: 0.16	

The same procedure was also applied to the data of the Waterways Experiment Station (1994) where, again, stage-discharge data are available and the stem densities and diameters are known, but not actual values of C_D. The fitted values of C_D and corresponding values of *Re* are listed in Table 5.3, and plotted for comparison with the standard curve in Fig.5.8. Again, although there is no basis for estimating C_D accurately, the fitted values conform closely with the values measured for real reed and bulrush stems in terms of both magnitude and trend with *Re*. The differences in values for the three test conditions are not understood at present, but could arise from a vertical variation of foliage density. This would result in a dependency of C_D on flow depth, and different ranges of depths were used in the tests. The estimation of gradient as the average of water surface slopes in the nonuniform flow conditions could also introduce some error and be reflected in the C_D values.

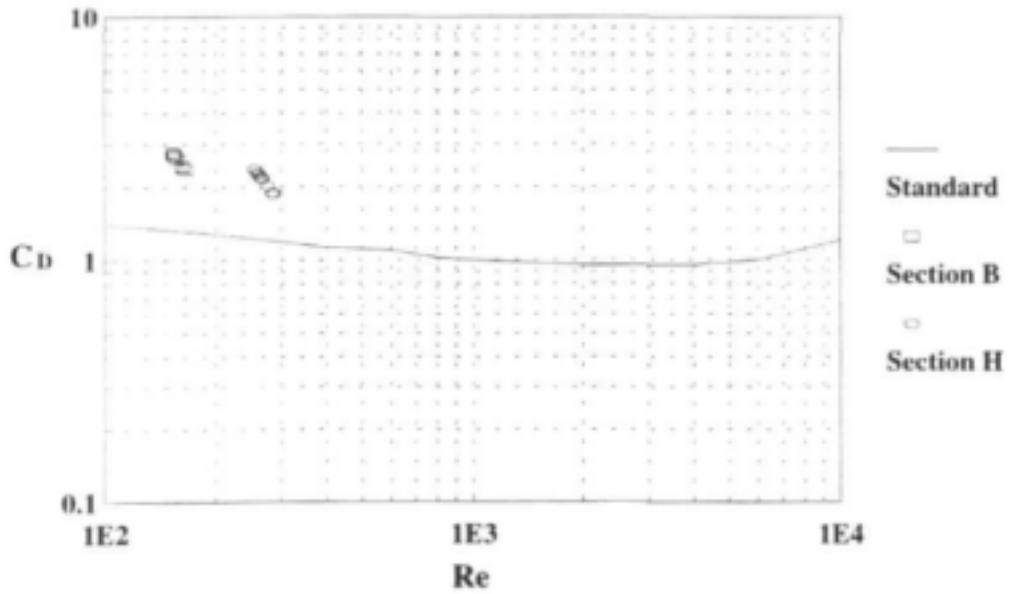

Figure 5.7 Values of C_D implied by equation (5.8)for data of Turner and Chanmeesri (1984)

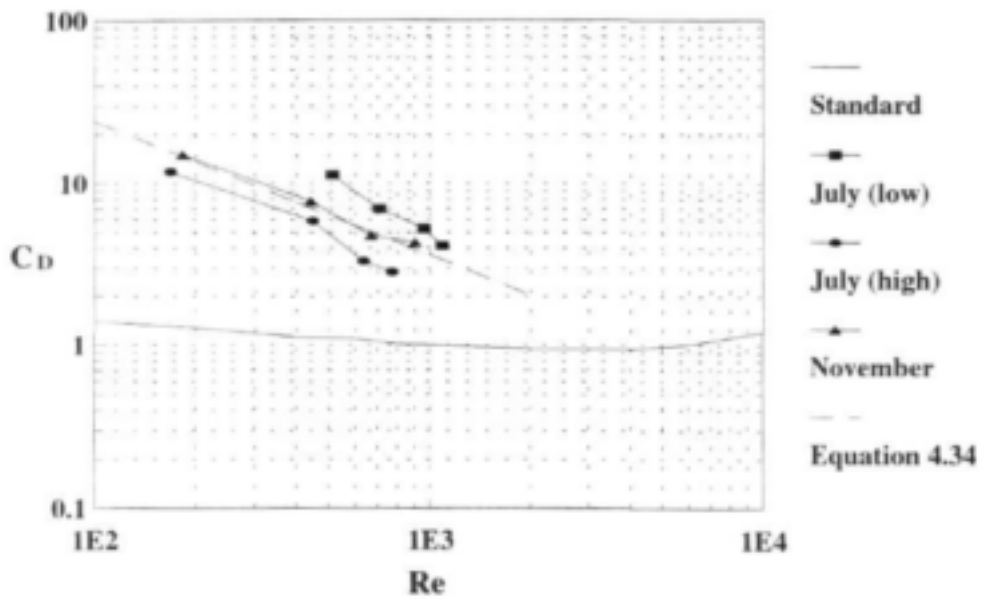

Figure 5.8 Values of C_D implied by equation (5.8) for data of Hall and Freeman (1994)

Table 5.3 **Values of C_D required to reproduce stage-discharge data of Hall and Freeman (1994)**

Tests	Depth (m)	Discharge (m^3/s)	C_D	Re
July 1992 Tests (low tailwater)	0.103	0.009	11.3	511
	0.215	0.026	7.00	707
	0.268	0.044	5.27	959
	0.306	0.057	4.13	1085
July 1992 Tests (high tailwater)	0.313	0.009	11.8	168
	0.339	0.026	5.85	448
	0.403	0.044	3.30	637
	0.432	0.057	2.83	770
November 1992 Tests	0.347	0.010	15.0	182
	0.374	0.026	7.80	441
	0.417	0.044	4.77	669
	0.448	0.064	4.30	904

5.4 SENSITIVITY ANALYSIS

Application of the proposed resistance equations requires estimation of the vegetation density (N), stem diameter (d), drag coefficient (C_D), and - where appropriate - the bed resistance in terms of f or n. There are many recommendations for estimating f or n through descriptions of surface roughness, either qualitatively or more objectively in terms of the effective roughness, k_s (Chow, 1959; Henderson, 1966). The stem diameter and density can be measured in the field with little difficulty. The most difficult parameter to determine is the drag coefficient. At present, there are very few experimental results on which to base estimates, and case-specific testing is required. Should the equations become widely accepted and used, tables of values of C_D for different vegetation characteristics, preferably with accompanying photographs, could be compiled as results become available. These could be presented in much the same way as the many recommendations for estimating values of Manning's n.

However the parameter values are estimated, it is useful to have an indication of the sensitivity of predictions to these estimates. This will serve as a guide to the accuracy required in their determination. To this end, the sensitivity of predictions of discharge using equation (5.8), with F given by equation (5.9), has been examined. The prediction of discharges for the Waterways Experiment Station (1994) November Tests described in section 5.3 above is used as a basis for comparison. The relationship between C_D and Re for these tests, as shown in Fig. 5.8, was expressed mathematically as

$$C_D = 1067\, Re^{-0.824} \qquad 5.21$$

Using this equation in evaluating F enabled the stage-discharge relationship to be reproduced with an average absolute error of only 5.85% (Fig. 5.9). The calculations were repeated with each of the parameters C_D, d, and N varied systematically, with the others kept constant. The average absolute errors in predicting discharge for each measured flow depth are listed in Table 5.4, for a range of deviations from the initial estimates of each of the parameters (d = 7.6 mm, N = 807/m^2, and C_D according to equation 4.34). Variations of C_D were made by including an additional factor in equation (5.21). Because of the dependence of C_D on Re, the solution is iterative, and was obtained by iterating with C_D until it conformed with equation (5.21). The effect of the parameter deviations tested on the stage-discharge relationship are shown in Figs 5.10 to 5.12.

Table 5.4 Sensitivity of discharge predictions to estimation of C_D, d, and N

Parameter	Parameter deviation (%)	Error in discharge prediction (%)
C_D	+10	-7.77
	+20	-14.36
	+50	-29.16
	+100	-44.54
	-10	+9.42
	-20	+20.86
	-50	+80.46
d	+10	-2.11
	+20	-4.07
	+50	-9.71
	+100	-18.70
	-10	+2.21
	-20	+4.59
	-50	+13.6
N	+10	-8.09
	+20	-14.90
	+50	-30.32
	+100	-46.34
	-10	+9.76
	-20	+21.7
	-50	+83.3

These results show that discharge predictions using equation (5.8) with F given by equation (5.9) are relatively insensitive to estimation of stem diameter, but very sensitive to estimates of drag coefficient and stem density. Sensitivity of depth prediction for given discharge is considerably less, as can be seen in Figs 5.10 to 5.12, but is still significant. It is therefore important in practical application that C_D and N be estimated accurately. Collection and compilation of appropriate C_D values are therefore required for effective use of the equation.

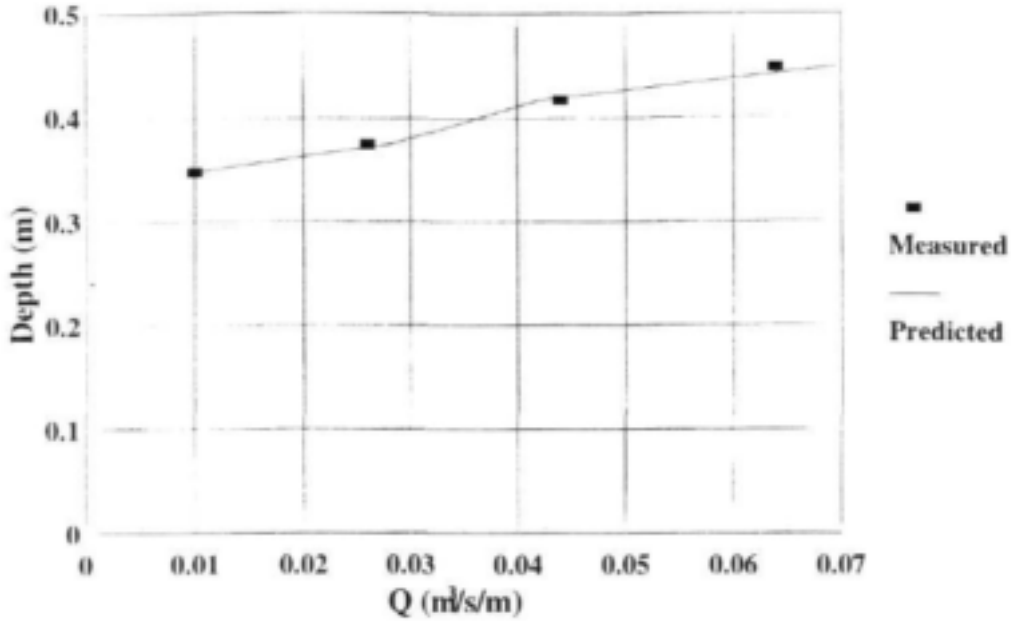

Figure 5.9 Stage-discharge relationship for Waterways Experiment Station (1994) November tests

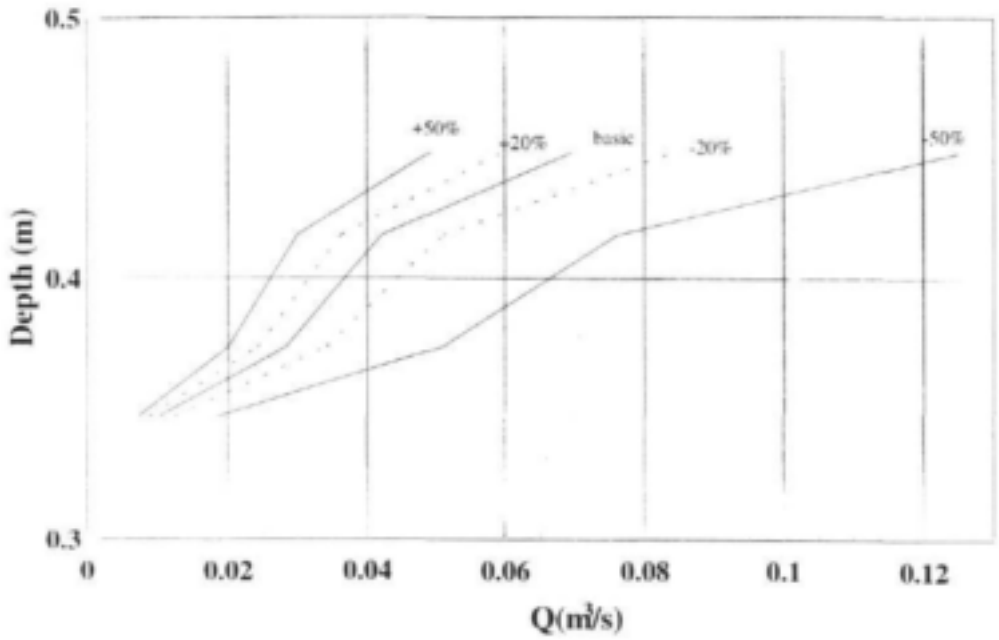

Figure 5.10 Effects of C_D estimation on prediction of stage-discharge relationship for Waterways Experiment Station (1994) November tests

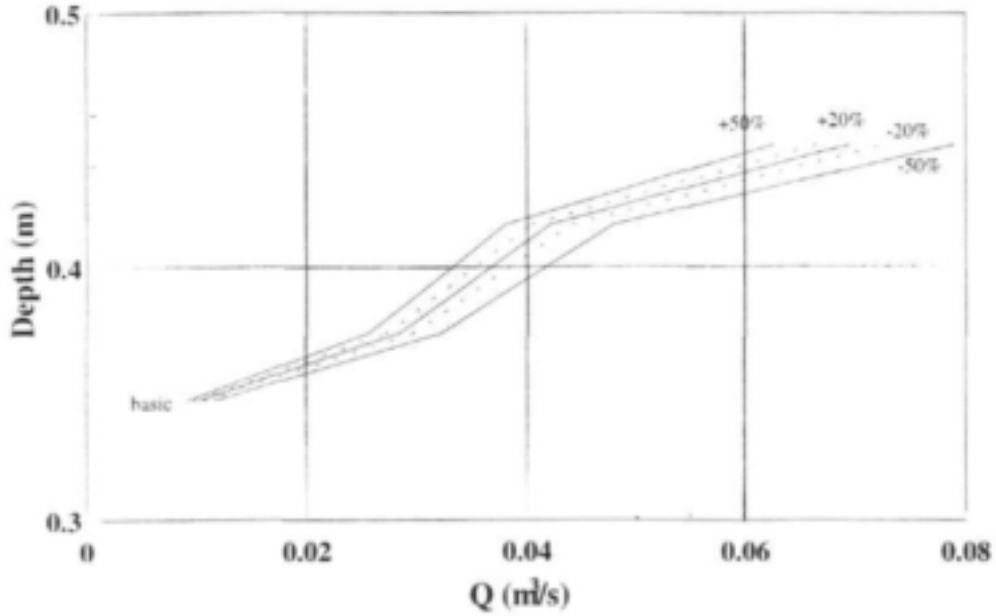

Figure 5.11 Effect of stem diameter estimation on prediction of stage-discharge relationship for Waterways Experiment Station (1994) November tests

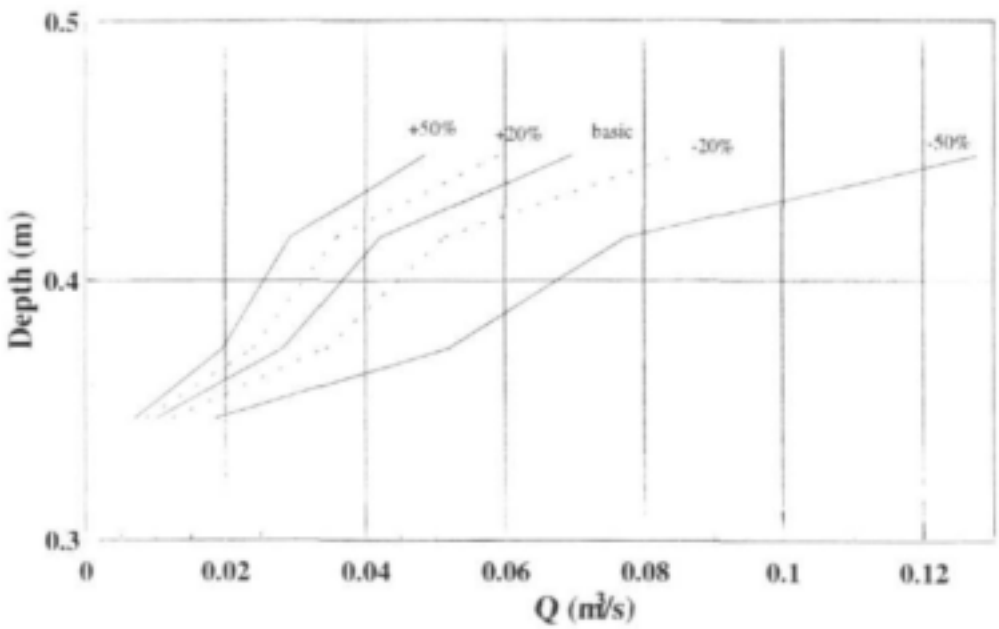

Figure 5.12 Effect of stem density estimation on prediction of stage-discharge relationship for Waterways Experiment Station (1994) November tests

The formulations for resistance coefficient given by equations (5.9) and (5.19) include a term for reducing the total flow volume by the volume occupied by the stems ($1 - N\pi d^2/4$). The stage-discharge predictions for the Waterways Experiment Station (1994) November tests (Fig. 5.9) were repeated with this term excluded. This produced an average absolute error over the full range of 0.85%, indicating that this term can be neglected to simplify the equation with no significant loss in accuracy.

5.5 EQUATION SELECTION

Presentation of two methods for estimating a resistance coefficient (equations (5.9) and (5.19)), one of which is simpler to apply than the other, raises the question of which to use in a particular situation. The deviations between F and F_f shown in Fig. 5.3 imply that ignoring bed shear resistance is acceptable for some conditions but not for others. Clearly, the higher the flow depth, the less the influence of the bed roughness on average velocity. It is not possible to specify a critical flow depth below which bed roughness should be accounted for, however, because the deviation becomes significant at different flow depths for the different stem densities. The condition where bed resistance becomes important is therefore dependent on (at least) the flow depth and the stem density. If the error in specifying the resistance coefficient as F rather than the more complete F_f is plotted against the product Ny (Fig. 5.13), it can be seen to increase rapidly for Ny values below a fairly well defined threshold. (The plot is in terms of $-(F - F_f)F_f$, as the actual error will always be an underestimate). As a rough guide, it would appear that bed resistance should be accounted for (i.e. through equation (5.19)) if the value of Ny is less than about 50. The influence of bed resistance might also be expected to depend on f, C_D, and stem diameter, d, but their inclusion led to less satisfactory criteria in the range of conditions represented by the Series A experiments.

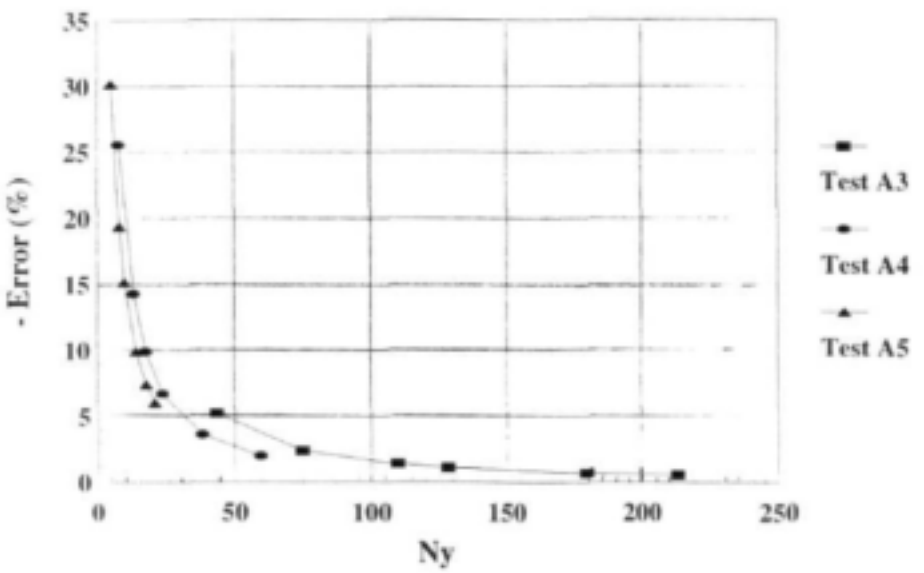

Figure 5.13 Error introduced to resistance coefficient by excluding bed shear

5.6 CONCLUSION

The results of Chapter 4 confirmed that Manning's equation is inappropriate where the dominant resistant force arises from stem drag, as opposed to bed friction. Equation (5.8) provides a theoretically sound alternative form, in which average flow velocity is (correctly) independent of flow depth and proportional to the square root of channel gradient. Equation (5.18) allows the influence of bed friction to be included, and it is shown that this is appropriate when the product of stem density and flow depth (Ny) is below some threshold (provisionally estimated as 50). The theoretical formulation of resistance coefficient for stem-dominated flow (given by equation (5.9)) shows it to be dependent on the diameter, density and drag coefficient of the stems, which can be determined without stage-discharge measurements. Bed friction is introduced into the combined resistance coefficient (equation (5.19)) through the Darcy-Weisbach friction factor or Manning's n.

The confirmation applications presented in this chapter show that the theoretical resistance formulations perform well for simple stem shapes in regular arrangements, and are realistic for natural conditions. The formulations therefore constitute a sound basis for development for practical application, and it should be possible to determine reliable resistance coefficient values based on measurable vegetation characteristics. At present, few measurements of drag coefficient are available for natural vegetation, but these are easier to determine than completely empirical resistance coefficients.

Sensitivity analysis of the equation (5.8) with F given by equation (5.9) showed that accurate determination of stem density and drag coefficient are essential, but that stem diameter is a relatively insensitive parameter.

The theoretical basis for the proposed equations is sound, but simplified. They do not account for the effect of stem arrangement, and it is known that this is significant (Li and Shen, 1973). The use of single stem drag coefficients in terms of the cross section average velocity is also potentially problematic, and the relationship between local velocity near stems and the cross section average needs to be examined. For these reasons a more detailed model is developed in Chapter 6, which can be applied parametrically (Chapter 7) to extend the validity of the forms of the equations presented in this chapter.

Chapter 6

MODELLING FLOW THROUGH REEDS

6.1 INTRODUCTION

The contribution to flow resistance of inundated reeds needs to be quantified in order to predict the local flow velocity, flow depth and bed shear stress resulting from discharge in open channels. Computational models for predicting the total flow resistance of a stand of uniform reed elements are developed in this chapter and verified using the experimental flume data described in Chapter 4. Uniform flow conditions within a homogenous arrangement of stems are assumed in the development of the computational models. The hydraulics of partially reeded channels is addressed in Chapter 8 (experimental) and Chapter 9 (analysis and modelling).

Different approaches have been developed for estimating the flow resistance of vegetation, and are presented in the literature survey (Chapter 2). These methods are generally based on the conventional open channel equations, with effective resistance coefficients determined experimentally or through estimation of the drag coefficient for vegetational elements. The methods apply strictly to conditions where flow is controlled by bed resistance (roughness and form drag), implying a logarithmic velocity distribution and linear shear stress distribution above the bed. For flow through dense vegetation, however, the velocity distribution above the bed is more nearly uniform (Kutija and Hong, 1996), as illustrated in Fig. 6.1 for rigid vertical cylindrical elements (Lindner, 1982). Chapter 5 describes the theoretical development and testing of a set of easy-to-apply equations for predicting resistance and stage-discharge relationships for flow through vertical rigid emergent reeds, taking account of both bed and vegetational resistance. The formulation is based on the balance of applied hydraulic and resisting bed shear and vegetational drag components. This approach has been widely applied in the development of resistance models for flow through vegetation (e.g. Li and Shen, 1973; Petryk and Bosmajian, 1975; Christensen, 1976; Lindner, 1982; and Kosorin, 1983), and its value lies in the potential for developing models that have general applicability. A number of empirical studies are described in the literature where effective resistance coefficients are correlated with various hydraulic determinants (refer to Chapter 2), making transferability between different systems and experimental conditions difficult to achieve.

The force balance approach is applied here to develop computational models for quantifying flow through reed-type vegetation. This approach, however, requires simplified conditions to be initially considered. Although this may be limiting in its application to natural river systems, it allows an understanding of the significant parameters contributing to flow resistance to be established. Based on sound physical principles, the models may then be extended to include conditions more indicative of flow through vegetation under field conditions.

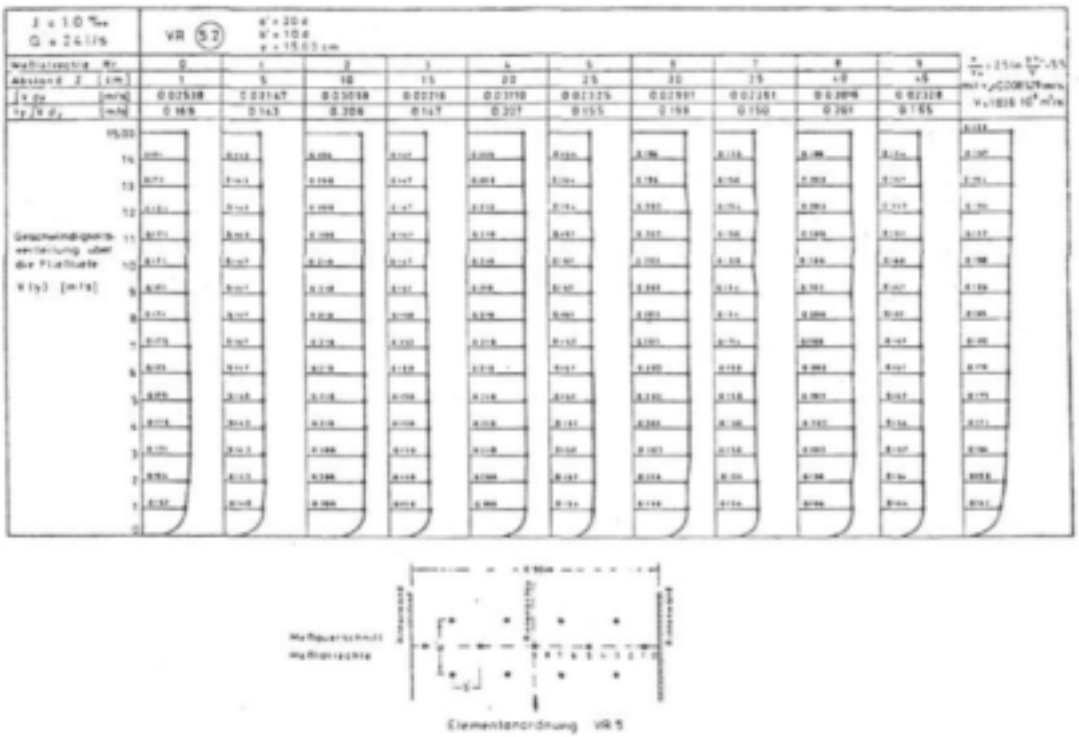

Figure 6.1 Velocity profiles between the centre and wall of a 0.9 m wide channel (after Lindner, 1982)

6.2 DETERMINANTS CONTRIBUTING TO FLOW RESISTANCE IN REEDS

The significant hydraulic, sedimentological and biological (vegetational) determinants likely to contribute to the flow resistance of reed beds are given in Table 6.1, and need to be accounted for in the computational model.

Table 6.1 Determinants contributing to flow resistance within reeds

Hydraulic	Energy slope Flow depth Local flow velocity
Sedimentological	Skin friction (bed roughness) Form drag (bedforms)
Biological	Geometric arrangement or pattern Stem diameter Stem height Flexural rigidity of reed stems Characteristics of leaves & litter

6.3 FLOW THROUGH EMERGENT REEDS

6.3.1 Model Development

A model is initially developed for uniform flow conditions within homogeneous arrangements of emergent, rigid, vertical stems. Submerged vegetation, the effects of bending (Section 6.4.1.4), and additional flow resistance imparted by leaves along the plant stem and litter at the base of the stand (Section 6.4.1.5) are addressed at a later stage of the model development.

The fundamental equation for the balance of applied (hydraulic) and resisting forces is given by

$$F_A = F_B + F_V \qquad 6.1$$

where F_A is the applied (hydraulic) force per unit plan area (N/m^2), F_B is the resisting force contributed by the bed per unit plan area (N/m^2), and F_V is the resisting force contributed by the vegetation per unit plan area (N/m^2). Methods for quantifying the applied and resisting forces in equation (6.1) are developed in the following sections.

6.3.1.1 Applied Hydraulic Force

The applied force per unit plan area is given by

$$F_A = \gamma y S_f (1 - mn\frac{\pi d^2}{4}) \qquad 6.2$$

where γ is the unit weight of water (9810 N/m^3), y is the flow depth (m), S_f is the energy slope, m and n are the number of stems in the longitudinal (x) and lateral (y) directions, respectively, and d is the stem diameter (m). As implied by equation (6.2), the stems are treated using cylindrical elements.

6.3.1.2 Vegetational Resistance

The resisting force of the vegetation (F_V) is determined by applying the empirical drag force relationship for vertical cylinders, given by

$$F_V = \frac{1}{2} C_{de} \rho y d m n u_{a\infty}^2 \qquad 6.3$$

where C_{de} is the effective drag coefficient and $u_{a\infty}$ is the asymptotic approach velocity (m/s).

The drag force coefficient (C_d) for a cylindrical element in idealised two-dimensional flow is given graphically in Fig. 6.2. The coefficient reduces with increasing Reynolds number (Re_d), reaching an approximately constant value of 1.0 for Re_d in the range $8\text{x}10^2$ to $8\text{x}10^3$, increasing to 1.2 in the range $8\text{x}10^3$ to $2\text{x}10^5$. The drag coefficient reduces sharply for $Re_d > 2\text{x}10^5$. The

cylinder Reynolds number is defined as

$$Re_d = \frac{u_a d}{\nu} \qquad 6.4$$

where u_a is the approach velocity (m/s), and ν is the kinematic viscosity (1.14×10^{-6} m^2/s for water at a temperature of 15 °C)

According to Petryk (1969) the following four effects may significantly alter the drag force and therefore coefficient from the two-dimensional situation depicted in Fig. 6.2:

- Open channel turbulence
- Water surface effects
- Non-uniform velocity profile
- Effect of blockage

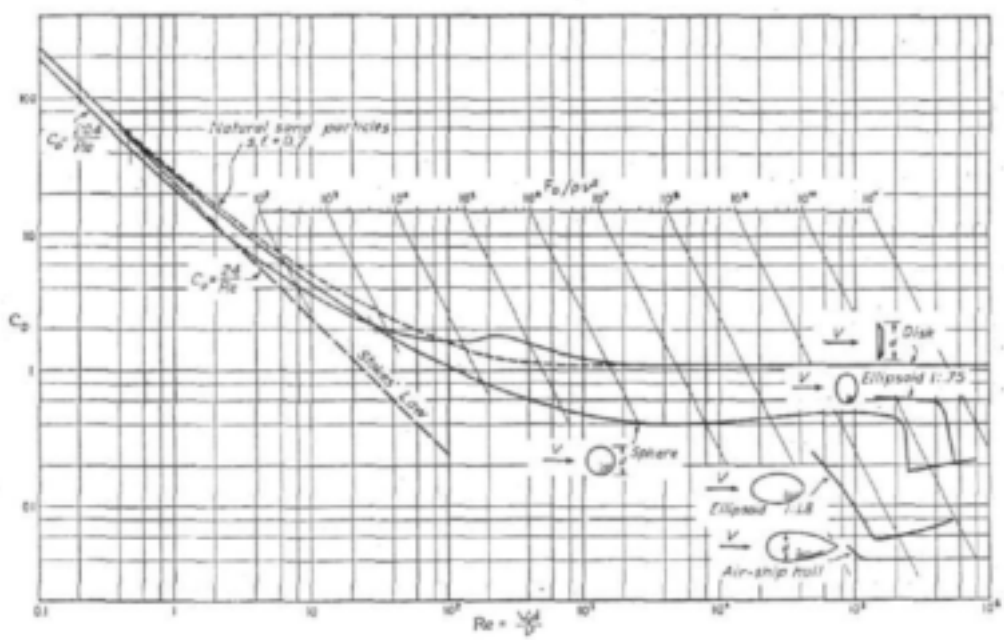

Figure 6.2 Drag force coefficient as a function of Reynolds number for a cylinder in two-dimensional uniform flow (after Albertson *et al.*, 1960)

When free-surface flow is disturbed by an unsubmerged obstacle, the water surface develops deformations, the characteristics of which are a function of the Froude number, representing the ratio of velocity to the celerity of a small wave. As the Froude number approaches unity, a marked change in the flow pattern becomes apparent (Hsieh, 1964) and a standing wave is formed that augments the drag due to the differential head upstream and downstream of the obstruction.

Petryk concluded from experimental data (Petryk (1969), Hsieh (1964), Isaacs (1965), and Dalton and Masch (1968)) that subject to the condition of no aeration being present immediately downstream of the obstruction, the best estimate of the drag coefficient is the two-dimensional value of 1.2 ($8\text{x}10^3 < Re_d < 2\text{x}10^5$). The condition pertaining to aeration (or water surface effects) is expressed by:

$$Fr_d = \frac{u_a}{\sqrt{gd}} < 1 \qquad 6.5$$

where Fr_d is the Froude number based on stem diameter, and g is the acceleration due to gravity (m/s^2).

The approach velocity to a vertical cylinder (or stem) in a stand of elements may differ significantly from the uniform velocity (U, in m/s) given by the ratio of discharge (Q, in m^3/s) to cross-sectional flow area (A, in m^2). This is due to the separation characteristics of the cylinder boundary layer and the development of a wake (and reduced velocity) immediately downstream of the obstruction. In order to determine the drag force imposed by rigid vertical stems (using equation (6.3)), it is necessary to predict the approach velocity to each stem, or the asymptotic value attained within a large stand of reeds.

From limited experimental results, Petryk (1969) provided the following relationships for the rate of spread and decay of a wake:

$$u_d = \frac{u_{max}}{2}\left(1 + \cos\left(\frac{\pi y}{s/2}\right)\right) \qquad 6.6$$

$$\frac{u_{max}}{u_a} = -0.9\left(\frac{x}{C_{ds}d}\right)^{-0.7} \qquad 6.7$$

$$\frac{s/2}{C_{ds}d} = -0.48\left(\frac{x}{C_{ds}d}\right)^{0.59} \qquad 6.8$$

where u_d is the flow velocity defect (m/s) at a distance y from the obstruction, u_{max} is the maximum velocity defect at a distance x from the upstream obstruction (m/s), y is the lateral distance relative to the obstruction, s is the spread of the wake (m), and C_{ds} is the drag coefficient for a single element within the stand. The variables in equations (6.6) to (6.8) are defined in Fig. 6.3.

Although the empirical equations (6.6 to 6.8) were derived based on limited experimental data, Li and Shen (1973) note that they are similar to the relationships developed by Eskinazi (1959).

Wakes spread and decay faster in fully developed open channel flow than under idealised two-dimensional (negative pressure gradient) conditions (Li and Shen, 1973). Petryk (1969) modified

equation 6.7 for free-surface conditions to give

$$\frac{u_{max}}{u_a} = -0.9\left(\frac{x}{C_{ds}d}\right)^{-0.7}\left(\frac{1}{1+\frac{gxS_o}{u_a^2/2}}\right)^{1.5} \qquad 6.9$$

where S_o is the bed slope.

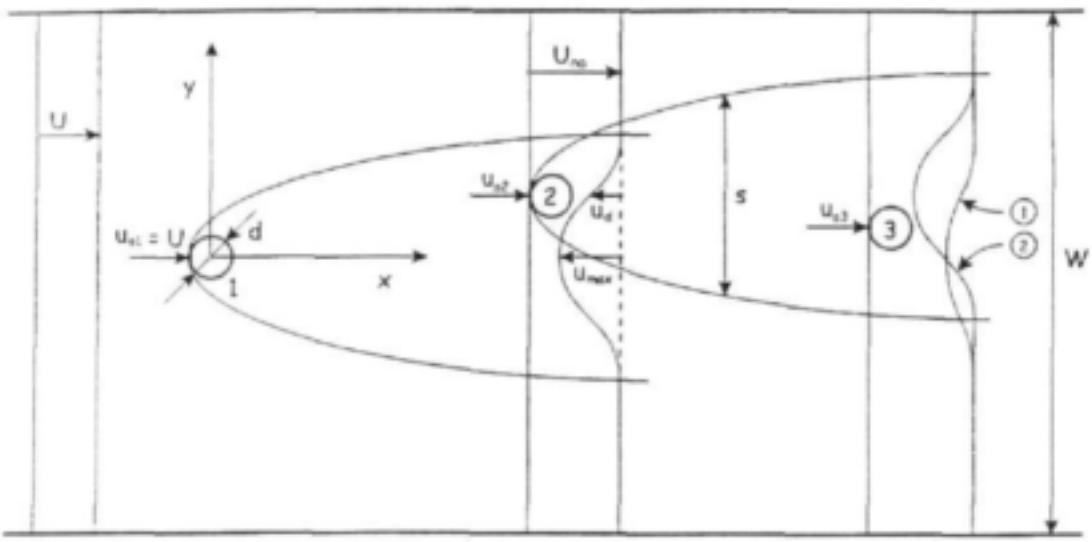

Figure 6.3 Definition of variables for the spread and decay of wakes

The effect of slope on the spread of a wake is assumed to be negligible. Equations (6.6), (6.8) and (6.11) completely define the two-dimensional (x-y) velocity distribution for open channel flow within a stand of vertical stems of given spatial arrangement. For a specific geometric pattern, the approach velocity to a stem is computed by deducting the point velocity defect contributed by all upstream elements from the reference free stream velocity, U_∞ (Fig. 6.3). The superposition of velocity defects is illustrated in Fig. 6.3. The free stream reference velocity at a longitudinal position (x) is computed by deducting the sum of the velocity defects arising from all upstream elements, per unit flow width, from the average free-stream velocity (U), i.e.

$$U_\infty = U - \frac{1}{W}\int_{-s/2}^{s/2} u_d \, dy \qquad 6.10$$

where W is the flow width (m). The integral of the velocity defects from a single upstream element is given by

$$\int_{-s/2}^{s/2} u_d \, dy = \frac{u_{max}}{2}\left(y + \frac{s/2}{\pi}\sin\left(\frac{\pi y}{s/2}\right)\right)_{-s/2}^{s/2} = \frac{u_{max} s}{2} \qquad 6.11$$

Alternative expressions for the distribution of velocity defect across the wake width were given by Schlichting (1930) (equation (6.12)) and Reichardt (1941) (equation (6.13)), and are plotted in Fig. 6.4 together with equation (6.6). The functions do not deviate significantly, and accordingly, Petryk's model is applied in the existing application since it can readily be integrated within a finite boundary (the wake width) to obtain an analytical expression for the velocity defect downstream of an obstruction.

$$u_d = u_{max}\left(1 - \left(\frac{y}{0.568s}\right)^{3/2}\right)^2 \qquad 6.12$$

$$u_d = u_{max} e^{-0.69\left(\frac{y}{s/4}\right)^2} \qquad 6.13$$

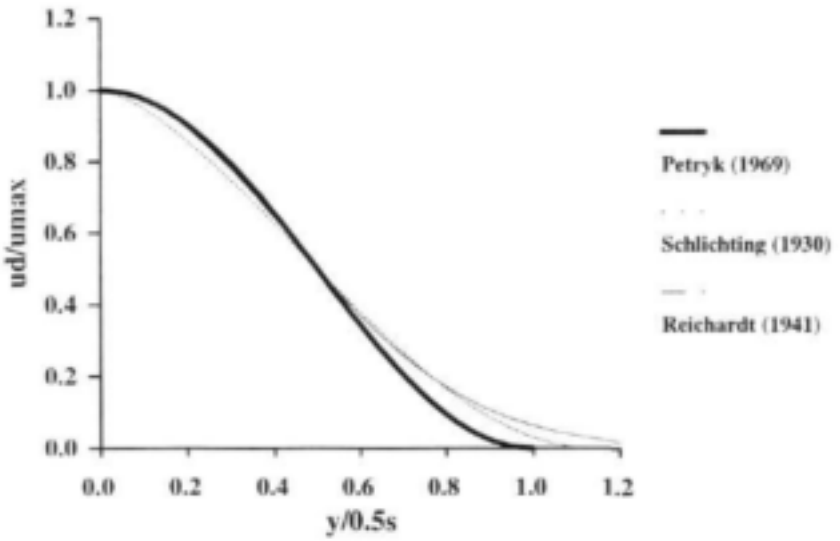

Figure 6.4 Alternative expressions for the distribution of velocity defect across the wake created by an upstream obstruction, after Lindner (1982)

Two geometric patterns of stem alignment within reed stands have been considered in the development of computational models of flow through vegetatively roughened channels, including parallel and staggered arrangements (Li and Shen, 1973 and Lindner, 1982), and are illustrated in Fig. 6.5. The parallel arrangement consists of equally spaced rows and columns of stems, whereas in the staggered formation, the columns are offset by half the distance between rows (i.e. $b/2$). The flow patterns and resistance of these two arrangements differ considerably. In the parallel arrangement, sub-channels of increased velocity are developed between adjacent rows, whereas in the staggered pattern, the offset stems act to deflect the flow laterally. Vertical aerial stems are likely to be arranged in a more random manner in natural reed stands, although the vegetative expansion of reed beds has been noted to display linear patterns through trailing of uprooted rhizomes following flood events. This mechanism relates to the growth of reed beds, however, and not directly to the geometric structure of aerial stems within a stand. The staggered arrangement is adopted in the resistance model as the structured pattern that most closely resembles the arrangement of stems within a naturally developed reed stand.

Lindner (1982) modified the drag coefficient for a single cylinder in idealised two-dimensional flow (Fig. 6.2) to account for blockage due to the influence of adjacent obstructions and surface wave effects. The influence of adjacent obstructions in a multi-stem arrangement was accounted for by adjusting the two-dimensional drag force coefficient (C_d) using the empirical relationship proposed by Richter (1973),

$$C_{de} = \left(1 + 1.9C_d\left(\frac{d}{b}\right)\right)C_d \qquad 6.14$$

Lindner does not describe the influence of geometric pattern on the applicability of equation (6.14), and the integrity of the function could not be verified within this study. Consequently, results are presented both incorporating and omitting equation (6.14) to demonstrate the effect of applying this function.

The influence of increased drag force through surface wave effects has been discussed with reference to the Froude number based on stem diameter, Fr_d. Lindner proposed that equation (6.14) be modified to account for this phenomena through the addition of a differential drag force coefficient, ΔC, given by

$$\Delta C = \frac{2}{Fr^2}\left(\frac{y_d}{y_u} - 1\right) \qquad 6.15$$

where the Fr is the Froude number based on flow depth, and y_u and y_d are the flow depths upstream and downstream of the local obstruction, respectively.

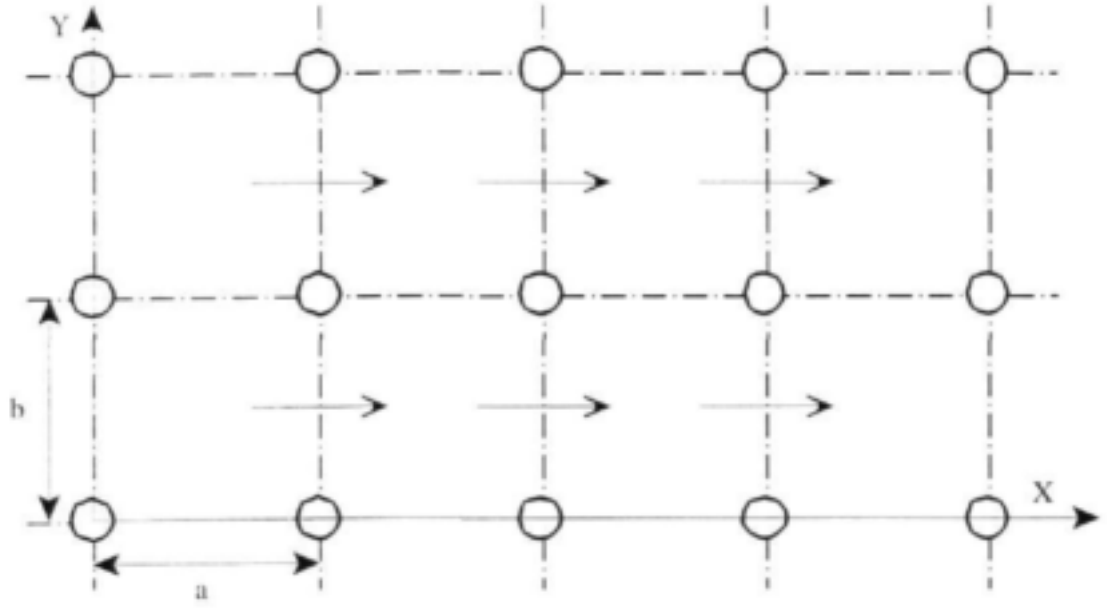

Parallel arrangement

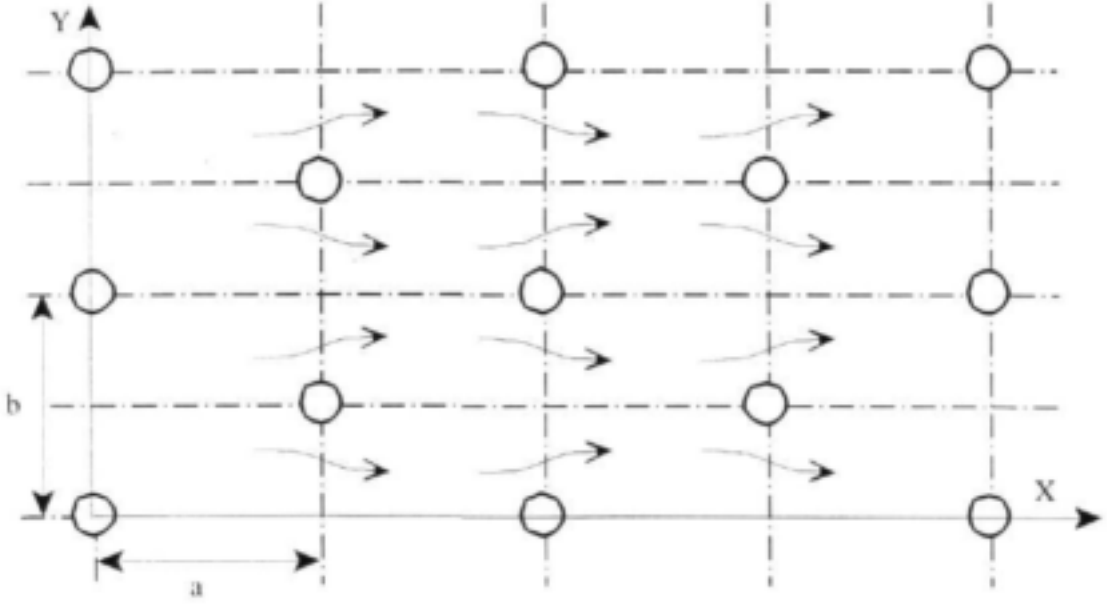

Staggered arrangement

Figure 6.5 Two geometric patterns of stem alignment

Lindner provides the following expression for the Froude number based on upstream and downstream flow depths, as well as the lateral spacing between and diameter of the stems,

$$Fr^2 = \frac{\frac{y_d}{y_u}\left(\left(\frac{y_d}{y_u}\right)^2 - 1\right)}{\left(\frac{y_d}{y_u} - \frac{b}{b-d}\right)} \qquad 6.16$$

The Froude number in equations (6.15) and (6.16) is based on average flow depth (y) , i.e.

$$Fr = \frac{U}{\sqrt{gy}} \qquad 6.17$$

Equation (6.16) was originally developed for free surface flow through a channel of reducing width (b to b-d) (Chow, 1959). Lindner has applied the theory to flow through localised constrictions between vertical elements, and the difference in water surface depth (and hence hydrostatic pressure force) has been used to compute the additional drag force coefficient, ΔC, in equation (6.15). The use of equation (6.16) to define the additional drag force due to surface wave effects is questionable for the following reasons:

- The constriction between vertical cylindrical elements is localised and not continuous as implied in the derivation of equation (6.16).
- The maximum constriction (b-d) occurs at half the stem diameter, and therefore the hydrostatic pressure force corresponding to the "downstream" flow depth is perpendicular to the flow and does not act in an upstream direction as implied in the application.

Consequently, the additional drag force arising from surface wave effects as proposed by Lindner has been disregarded in this study, and the recommendation of Petryk (1969) is applied, i.e. subject to the validity of equation (6.5) the additional drag force arising from surface wave effects is neglected.

It is desirable to base an effective drag coefficient (C_{de}) on the average velocity (U) rather than the asymptotic approach velocity ($u_{a\infty}$), since the former is more easily defined. Based on the form of the drag force relationship (equation (6.3)), the effective drag coefficient based on average velocity is given by equation (6.18), incorporating Lindner's (1982) empirical function (equation (6.14)) accounting for blockage.

$$C_{de} = \left(1 + 1.9C_d\left(\frac{d}{b}\right)\right)\left(\frac{u_{a\infty}}{U}\right)^2 C_d \qquad 6.18$$

Figure 6.6 is a plot of effective drag force coefficient against relative spacing for staggered and parallel arrangements of cylindrical stems in a two-dimensional (x-y) flow system applying the superposition of velocity defect principle as described. The drag force coefficient for a single stem is also indicated. The results show that the effective drag force based on average velocity decreases significantly with relative spacing for a staggered arrangement and increases for a parallel pattern. This is due to the reduction in approach velocity within a parallel arrangement, whereas for a staggered pattern the offset elements act to deflect the flow laterally thereby increasing the approach velocity. Incorporating Lindner's (1982) empirical function for blockage increases the effective drag coefficient by up to 37% for a relative stem spacing (a/d) of 5.

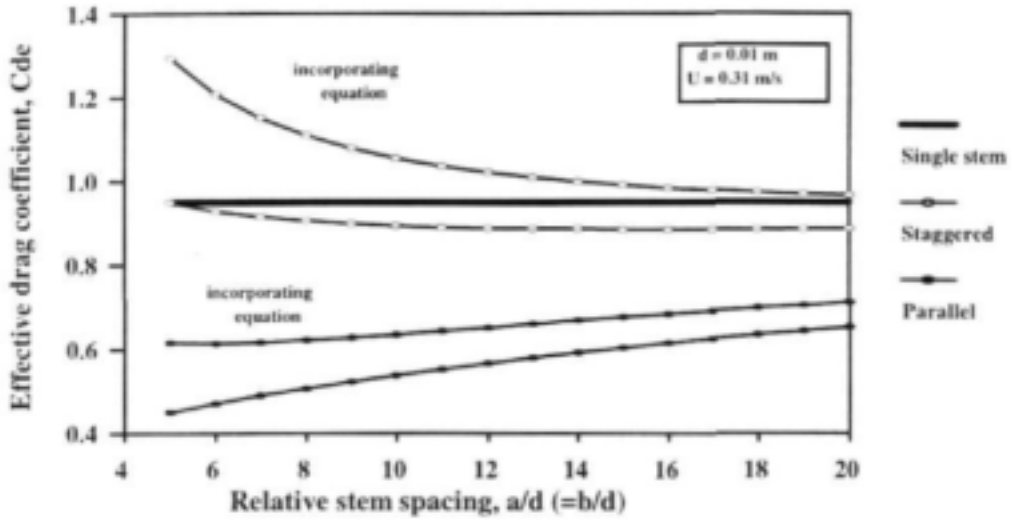

Figure 6.6 Effective asymptotic drag coefficient for rigid vertical stems in parallel and staggered geometric arrangements, incorporating and omitting equation (6.14)

Pasche and Rouvé (1984) provided the following empirical expression for the square of the ratio of asymptotic approach to average velocity in equation (6.18),

$$\left(\frac{u_{a\infty}}{U}\right)^2 = 0.923\left(\frac{l_e}{a}\right)^{0.374} + 0.610\left(\frac{s_e}{b}\right)^{1.33} \qquad 6.19$$

where l_e and s_e are the effective wake length and spread, respectively, and a and b are the distance between the reed stems in the longitudinal (x) and lateral (y) directions, respectively.

According to Lindner (1982), the velocity defect may be neglected at distances downstream of the obstruction where the ratio of the maximum defect to the approach velocity is less than 3%.

This condition is used by Pasche and Rouvé (1984) to define the effective wake dimensions, i.e. 0.03 is substituted for u_{min}/u_a in equation (6.7) or (6.9), and the corresponding effective spread of the wake is given by equation (6.8). Using the superposition of velocity defect principle and effective wake dimensions, Pasche and Rouvé presumably (the method by which equation (6.19) was developed as well as the geometric arrangement of stems are not described by the authors) developed the empirical correlation. In the present study, equation (6.19) could not be confirmed for a staggered arrangement of stems, and consequently the velocity defect model is applied.

6.3.1.3 Bed Roughness

The resisting force contributed by the bed includes both skin friction due to bed roughness as well as form drag arising from the presence of bedforms. The influence of bedforms is disregarded in the analysis, since the potential occurrence and nature of bedforms will be influenced by the existence of vegetation through the reduction and altered distribution of local bed shear stress (refer to series B flume experiments in Chapter 10). The frictional force due to bed roughness (per unit plan area) as expressed in equation (6.1) is given by

$$F_B = \tau_B(1 - mn\frac{\pi d^2}{4}) \qquad 6.20$$

where τ_B is the bed shear stress (N/m^2), and may be expressed as

$$\tau_B = u_*^2\rho \qquad 6.21$$

where u_* is the shear velocity (m/s), and ρ is the density of water (1000 kg/m^3).

In the absence of additional resistance (non-bed related such as vegetation), the applied hydraulic force (equation (6.2)) is balanced entirely by the resisting force along the wetted boundary (perimeter) of the cross-section, and equation (6.21) reduces to the well known relationship for bed shear stress, viz.

$$\tau_B = \gamma RS_f \qquad 6.22$$

where R is the hydraulic radius (m), given by the ratio of the cross-sectional flow area (A, in m^2) to the wetted perimeter (P, in m).

Momentum transfer between the bed and water surface in open channel flows determines the shape of the (temporally averaged) velocity profile. It is therefore necessary to review the theory developed for describing velocity profiles in open channel turbulent flow, since the vertical distribution of velocity is necessary to compute the vertical distribution of drag force applied to reed stems, as well as for defining the bed shear force.

Velocity profiles in open channel turbulent flow

The wall region

In turbulent flow, momentum transfer takes place by molecular exchange arising from fluid viscosity as well as turbulent diffusion by bulk fluid movement in eddies or vortices. The total shear stress across a shearing plane in turbulent flow is the sum of the viscous shear and turbulent shear (or Reynolds shear), given by

$$\tau = \rho\nu\frac{\partial u}{\partial z} - \rho\overline{u'w'} \qquad 6.23$$

where u is the average velocity (root mean square) (m/s), z is the height above the bed (m), u' and w' are the velocity fluctuations in the longitudinal (x) and vertical (z) directions, respectively (m/s).

In fully developed, two-dimensional (x-z) flow over a smooth bed, the equation of motion reduces after integration to the following linear variation of the total shear stress (Nezu and Rodi, 1986)

$$\tau = \rho u_*^2(1 - \xi) \qquad 6.24$$

where ξ is the dimensionless distance from the bed (expressed as z/y).

Equation (6.24) indicates a linear distribution of shear stress from the bed ($z = 0$) to the water surface ($z = y$). Applying the concept of momentum exchange due to turbulent velocity components, Prandtl (1925) developed a "mixing theory" expressing the shear stress in terms of the velocity gradient and mixing length,

$$\tau = \rho l^2\left(\frac{du}{dz}\right)^2 \qquad 6.25$$

where l is the mixing length (m).

Substituting for the Reynolds shear stress in equation (6.23) using Prandtl's mixing length theory gives

$$l^2\left(\frac{du}{dz}\right)^2 + \nu\frac{du}{dz} = u_*^2(1 - \xi) \qquad 6.26$$

which has root

$$\frac{du^+}{dz^+} = \frac{2(1 - \xi)}{1 + \sqrt{1+4l^{+2}(1 - \xi)}} \qquad 6.27$$

where u^+ is the dimensionless velocity, given by u/u_*, z^+ is the dimensionless z-ordinate, given by zu_*/ν, l^+ is the dimensionless mixing length, given by lu_*/ν.

Prandtl's formulation assumed that the mixing length is directly proportional to the height above the bed, i.e.

$$l = \kappa z \qquad 6.28$$

where κ is the von Kármán constant.

In the wall region ($\xi < 0.2$), the linear mixing length distribution of Prandtl can be applied, modified by the Van Driest's (1956) damping function in the near wall region,

$$l^+ = \kappa z^+ \Gamma \qquad 6.29$$

where Γ is the Van Driest damping function, given by

$$\Gamma = 1 - e^{(-z/B)} \qquad 6.30$$

and B is the damping factor.

The value $B = 26$ was obtained empirically for boundary layers by Van Driest and confirmed by Nezu and Rodi (1986). Integration of equation (6.27) and applying equation (6.28) yields for the viscosity dominated region very close to the wall,

$$u^+ = z^+ \qquad z^+ \ll B \qquad 6.31$$

and beyond the viscosity influenced region of the wall,

$$u^+ = \frac{1}{\kappa} \ln z^+ + A \qquad B < z^+ < 0.2R_* \qquad 6.32$$

where A is the integration constant and R_* is the shear Reynolds number (u_*y/ν).

Equation (6.31) is the "viscous-sublayer" relationship and equation (6.32) is the "log-law" formulation, and both apply to the wall region of flow which is governed by the variables ν and u_*. Equation (6.27) (subject to equations (6.28) and (6.29)) applies to flow in the entire wall region, whereas equations (6.31) and (6.32) may be derived independently by considering only the viscous component in the case of the near wall flow characteristics and only the Reynolds shear stress for flow in the region dominated by turbulent diffusion.

Reichardt (1951) (cited by Schlichting, 1979) presented a continuous velocity distribution for hydraulically smooth flow in the wall region:

$$u^+ = \frac{1}{\kappa}\ln(z^+ + 1) - 7.47\left(1 - e^{-\frac{z^+}{11.6}} - \frac{z^+}{11.6}e^{-0.33z^+}\right) \qquad 6.33$$

Smooth bed Equation (6.32) applies to turbulent flow structures over smooth beds in open channels, although the relations may be modified for flow over beds influenced by wall roughness. According to Nezu and Nakagawa (1993), the von Kármán constant κ and the integral constant A have universal values, regardless of the Reynolds and Froude numbers. Nezu and Nakagawa (1993) obtained values for κ and A of 0.41 and 5.29, respectively, for open channel flows and they compared these with the following results from the literature:

- $\kappa = 0.41, A = 5.0$ Boundary layers (Coles, 1968)
- $\kappa = 0.41, A = 5.17$ Closed-channel flows (Dean, 1978)
- $\kappa = 0.41, A = 5.2$ Boundary layers (Brederode and Bradshaw, 1974)

Nikuradse (1933), found $\kappa = 0.4$ and $A = 5.5$ for smooth turbulent flow in pipes. Adopting the constants of Nezu and Nakagawa (1993), equation (6.32) becomes using natural logarithms

$$\begin{aligned} u^+ &= 2.44 \ln\left(\frac{u_*}{\nu} z\right) + 5.29 \\ &= 2.44 \ln\left(\frac{8.75u_*}{\nu} z\right) \end{aligned} \qquad 6.34$$

or using logarithms to the base 10,

$$\begin{aligned} u^+ &= 5.61 \log\left(\frac{u_*}{\nu} z\right) + 5.29 \\ &= 5.61 \log\left(\frac{8.75u_*}{\nu} z\right) \end{aligned} \qquad 6.35$$

Rough bed The effects of roughness elements are generally classified as follows:

- Hydraulically smooth bed $k_s^+ < 5$
- Transitional or incompletely rough bed $5 \le k_s^+ \le 70$
- Completely rough bed $k_s^+ > 70$

where $k_s^+ = k_s u_*/\nu$, and k_s is the equivalent sand roughness.

Roughness effects disappear if the bed is hydraulically smooth due to the formation of a viscous sub-layer and viscous effects dissipate in the case of a completely rough bed since the roughness elements penetrate the fully turbulent flows. An incompletely rough bed is the transition between these and is a function of both viscosity and roughness.

Two issues require consideration for flow over rough beds:

- The parameter to be used to represent the size of the roughness elements.
- The location of the wall, i.e. where $z = 0$.

In addressing the first issue, Nikuradse used the equivalent sand roughness, utilising the particle diameter for a bed composed of uniform grain sizes. The relation between equivalent roughness and particle size varies widely in the literature, with the relative roughness given by

- $1.25D_{65}$ (Einstein, 1950)
- $2D_{65}$ (Engelund and Hansen, 1967)
- $5.1D_{84}$ (Mahmood, 1971)
- $1.25D_{35}$ (Ackers and White, 1973)
- $2D_{90}$ (Kamphuis, 1974)
- $3.5D_{84}$ (Hey, 1979)
- $3D_{90}$ (Van Rijn, 1982)

where D_i is the particle size for which i % of the particles (by mass) are finer.

The need to determine the equivalent (uniform) roughness is often circumvented by computing k_s from the mean velocity distribution where it coincides with the log-law relationship.

Rearranging the log-law for a smooth bed (equation (6.32)),

$$u^+ = \frac{1}{\kappa}\ln\,(z/k_s) + A_r \qquad 6.36$$

where

$$A_r = \frac{1}{\kappa}\ln\,k_s^+ + A \qquad 6.37$$

Although A_r complies with equation (6.37) over a smooth bed, it gradually decreases as k_s^+ increases (transitional conditions) and becomes constant (equal to 8.5) for a completely rough bed. For a completely rough bed, equation (6.36) reduces to

$$u^+ = 2.44 \ln (z/k_s) + 8.5$$
$$= 2.44 \ln \left(\frac{32.6z}{k_s}\right) \qquad 6.38$$

No standard exists as yet for the location of the wall in a rough bed (Nezu and Nakagawa, 1993). According to equation (6.38), the velocity reduces to zero at a distance $k_s/32.6$ from the bed. The theoretical level can be set a height δ below the top of the roughness elements with $0 < \delta < k_s$. The parameter value of δ may be included in the integration constant (equation (6.36)) by calibrating experimental mean velocity distribution data to fit the log-law relationship. Experimental data for the location of the wall differ and the range of δ/k_s is approximately 0.15 - 0.3 for sand grain roughness (Nezu and Nakagawa, 1993). Cebeci and Chang (1978) introduced a modified mixing length approach to account for the vertical ordinate shift in the flow depth for near wall conditions, with the dimensionless distance z^+ replaced by $(z^+ + \Delta z^+)$. This implies that the velocity reduces to zero when $z^+ + \Delta z^+ = 1$. The empirical relationship for the ordinate shift given by

$$\Delta z^+ = 0.9(\sqrt{k_s^+} - k_s^+ e^{-k_s^+/6}) \qquad 6.39$$

resulted from fitting the mean velocity data to the log-law. According to Nezu and Nakagawa (1993), the relation between Δz^+ and the theoretical displacement δ is not yet clear.

Christensen (1971) proposed the following modification to equation (6.38)

$$u^+ = 2.44 \ln (z/k_s + 0.0307) + 8.5$$
$$= 2.44 \ln \left(\frac{32.6z}{k_s} + 1\right) \qquad 6.40$$

which implies zero velocity at the bed (no slip condition) and approaches equation (6.38) at greater distances from the bed ($z/k_s >> 1$).

Einstein (1950) proposed a turbulent velocity profile equation applicable to hydraulically smooth, transitional and rough flow conditions, i.e.

$$u^+ = 5.75 \log \left(\frac{30.2x}{k_s} z \right) \qquad 6.41$$

where x is a correction factor obtained from Fig. 6.7 as a function of k_s/δ, where δ is the height of the viscous sublayer and can be estimated from

$$\delta = \frac{11.5\nu}{u_*} \qquad 6.42$$

Einstein (1950) also presented an integrated form of equation (6.41) to predict the average flow velocity

$$U = 5.75u_* \log\left(12.27\frac{Rx}{k_s}\right) \qquad 6.43$$

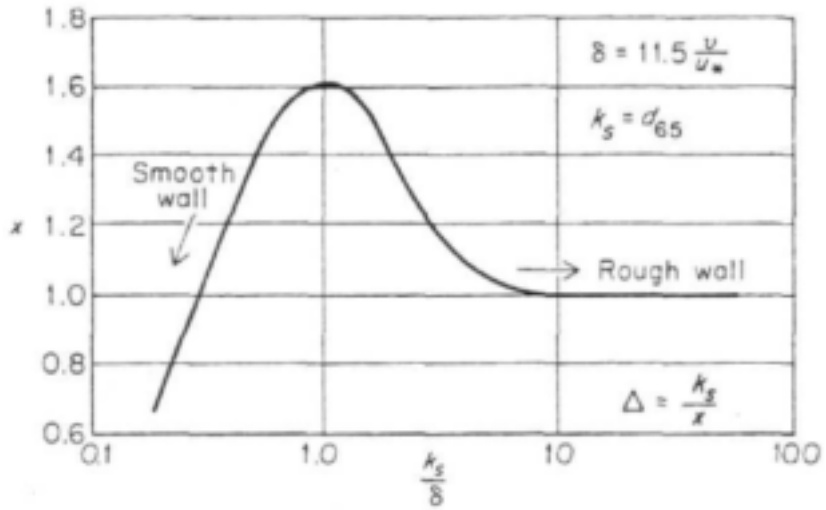

Figure 6.7 Correction factor in Einstein's velocity distribution (after Einstein, 1950)

The wake region

Recent studies have shown that the log-law is valid only in the wall region (Coleman, 1981 and Zippe and Graf, 1983). Deviations from the log-law in the outer region ($\xi > 0.2$) have often been accounted for by adjusting the von Kármán (κ) and the integration (A) constants and following Keulegan's (1938) recommendation, i.e. the log profile is applied to describe the mean velocity distribution over the entire depth for open channel flows. Deviations from the log profile in the outer region should not be accounted for by adjusting κ and A. According to Nezu and Nakagawa (1993) these should rather be treated as universal constants. Instead, a wake function should be added to equation (6.32) thereby increasing the range of applicability

$$u^+ = \frac{1}{\kappa}\ln z^+ + A + w(\frac{z}{y}) \qquad B < z^+ < y^+ \qquad 6.44$$

Coles (1956) proposed the following empirical relationship for the wake function

$$w(\frac{z}{y}) = \frac{2\Pi}{\kappa}\sin^2\left(\frac{\pi z}{2y}\right) \qquad 6.45$$

where Π is the Coles wake strength parameter.

The Coles wake function appears to be the most acceptable extension of the log-law, although several other empirical formulae have been proposed for the outer region. The wake function has lower limit 0 ($z = 0$) and upper limit $2\Pi/\kappa$ ($z = y$). The value of the wake strength parameter is determined by calibration using experimental data in the free-surface region and ranges from 0 ($R_* < 500$) to 0.2 ($R_* > 2000$) for open channel flow (Nezu and Nakagawa, 1993).

Deviations of the velocity profile from the log-law are likely to be even more apparent for flow through vegetation, since momentum transfer within the vegetated region will be governed by turbulent diffusion associated with the vegetational elements rather than the bed roughness. Consequently, a modified shear stress approximation is strictly applicable within this outer region. Wantanabe and Kondo (1990) modified the mixing length expression (equation (6.28)) for the vegetated region, whilst Kutija and Hong (1996) used the eddy-viscosity theory applied by Tsujimoto and Kitamara (1990).

In the present model development (REEDFLO v1), the log-law is assumed to extend throughout the flow depth. This assumption produces realistic velocity profiles for sparse vegetation, with reduced accuracy concomitant with increased stem density. The inability to accurately describe the velocity profile for densely vegetated stands may not be problematic, however, since the primary objective of the basic resistance component of the broader study is to determine the effective resistance to flow through reed stands as well as estimating the bed shear for sediment transport computations.

Lindner (1982) presented plots (Fig. 6.1) of measured velocity profiles between the centre-line and wall of a 0.9 m wide channel as well as the theoretical log-law for a hydraulically smooth bed using constants as given by Nikuradse (1933). The measured velocity profiles are remarkably uniform throughout the flow depth (15.03 cm), with depth averaged values ranging from 0.143 to 0.207 m/s. The theoretical (log) relationship has a maximum flow velocity of 0.199 m/s at the water surface, reducing to 0.141 m/s at 1 cm above the bed. For this particular density (a/d =10, b/d = 20), the log-law provides an acceptable "spatially averaged" approximation to the measured velocity profiles in the vegetated region. It does, however, provide an underestimate of the average bed shear along the line of measured velocity profiles (Fig. 6.1), a consequence of a steeper velocity gradient above the bed in the observed data.

6.3.1.4 REEDFLO v1

A resistance model for flow through reeds (REEDFLO v1) has been coded in QBASIC, and the flow chart describing computational procedures is given in Fig. 6.8. The input data necessary to run REEDFLO v1 are given in Table 6.2, as are the main output parameters. The code is reproduced in Appendix E.

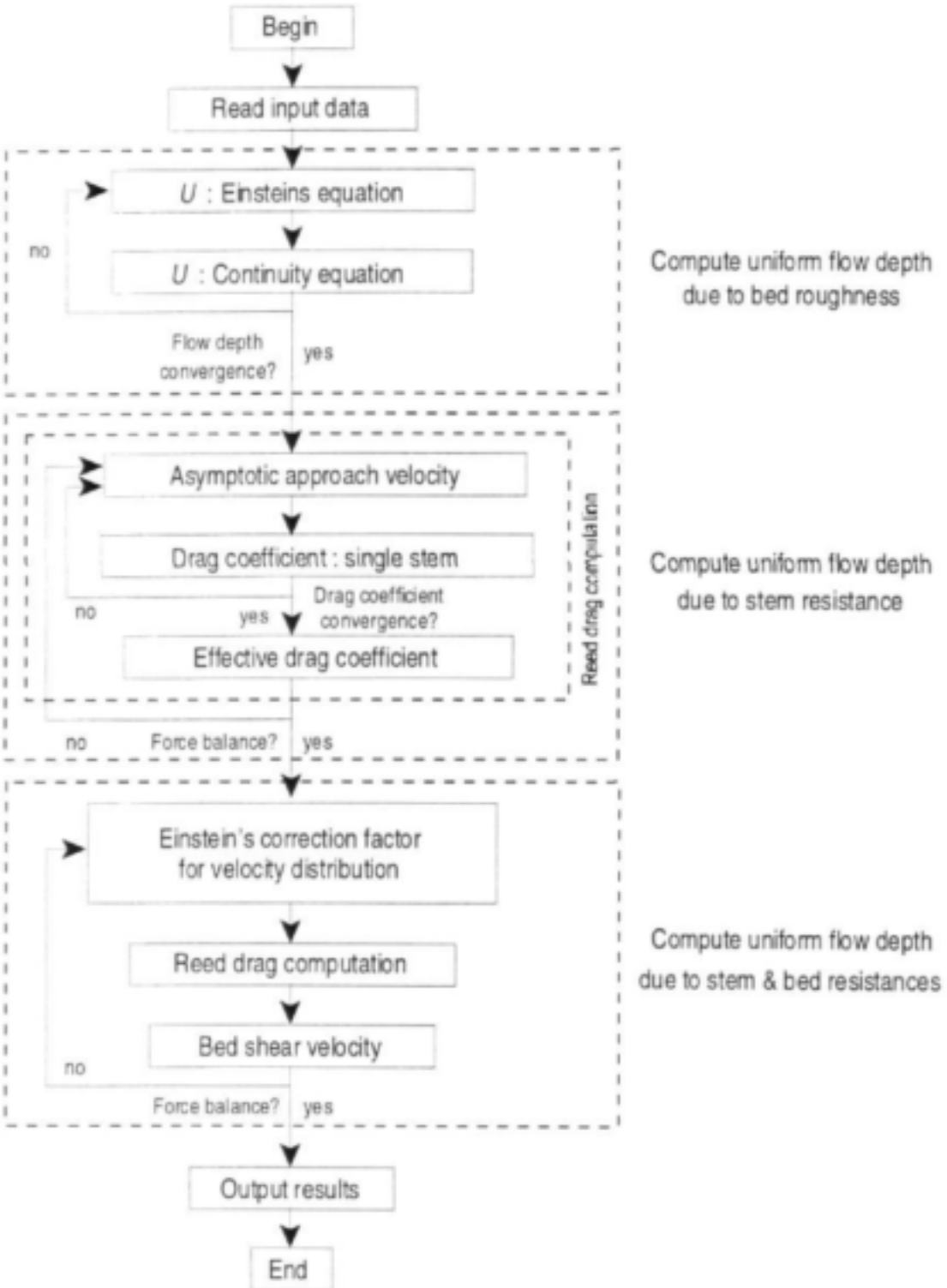

Figure 6.8 Flow chart describing computational procedures within REEDFLO v1

Table 6.2 REEDFLO v1 model input data and output parameters

Input data
Discharge per unit width, q ($m^3/s/m$)
Bed slope, S_o
Effective roughness of bed, k_s (m)
Stem arrangement: staggered or parallel
Shape of stem (i.e. cylindrical or other)
Stem diameter, d (m)
Distance between stems, a & b (m)
Output parameters
Flow depth, y (m)
Effective drag force coefficient, C_{de}
Bed shear stress, τ_B (N/m^2)
Force applied to stems per unit area of bed (N/m^2)
Effective resistance coefficients (f, n and C)

6.3.2 Model Verification

The series of experiments (A3, A4 and A5) performed to assess the influence of energy slope and stem density on resistance for emergent conditions are described in Chapter 4. The measured and modelled rating data are given in Appendix A1.

The rating data are plotted in Figs. 6.9 and 6.10 for two different energy slopes and three different relative spacings between stems, respectively. Incorporating equation (6.14), which accounts for blockage due to the influence of adjacent obstructions and surface wave effects, increases the estimate of the drag coefficient and modelled flow depths. Omitting this empirical function produces underestimates of the measured stages, whilst including the relationship provides overestimates, which increase with increased stem density. Figure 6.11 is a plot of the measured versus modelled flow depths (with equation (6.14) included in the model), and indicates a good correlation between observed and predicted values.

The change in flow depth as a function of relative spacing between stems (i.e. a/d) are given in Appendix A1, and are plotted in Fig. 6.12 for a discharge of 0.5 l/s (The measured values are interpolated from the experimental data). The modelled flow depths corresponding to bed friction and stem resistance are indicated, and as expected the predicted flow depths approach these lower limits at sparse and dense configurations, respectively. The modelled values are marginally lower than the depth due to bed friction for $a/d > 25$ due to the side wall correction applied in the computation of the latter condition. The predicted data compares reasonably with the measured values for the three stem densities, with increasing underestimates concomitant with reduced stem density. This may be attributed to general experimental inaccuracies, increased relative influence of side wall effects with reduced stem density, and difficulty in the estimation of effective flow depths over the rough bed (i.e. determination of the zero velocity boundary).

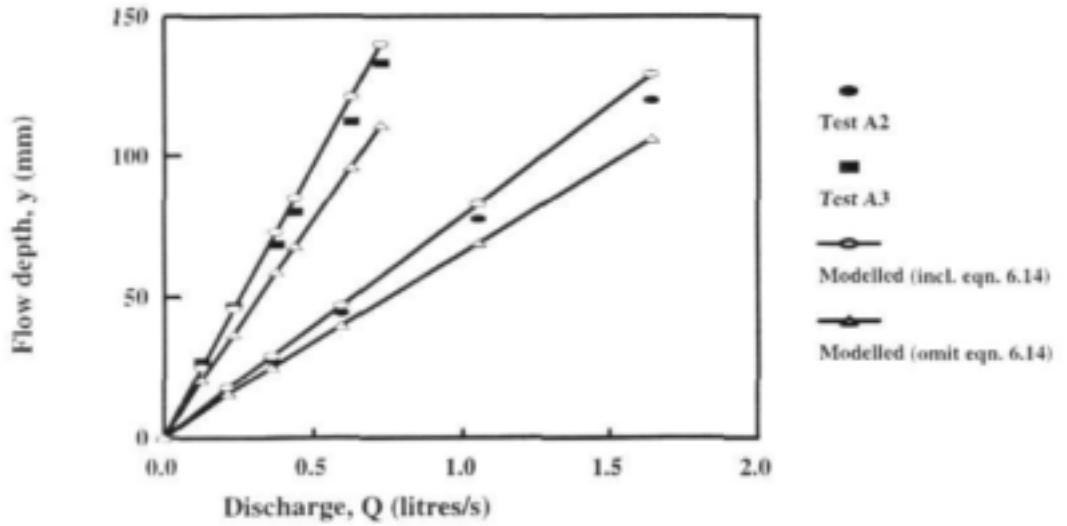

Figure 6.9 Measured rating data and modelled (REEDFLO v1) relationships for Tests A2 and A3

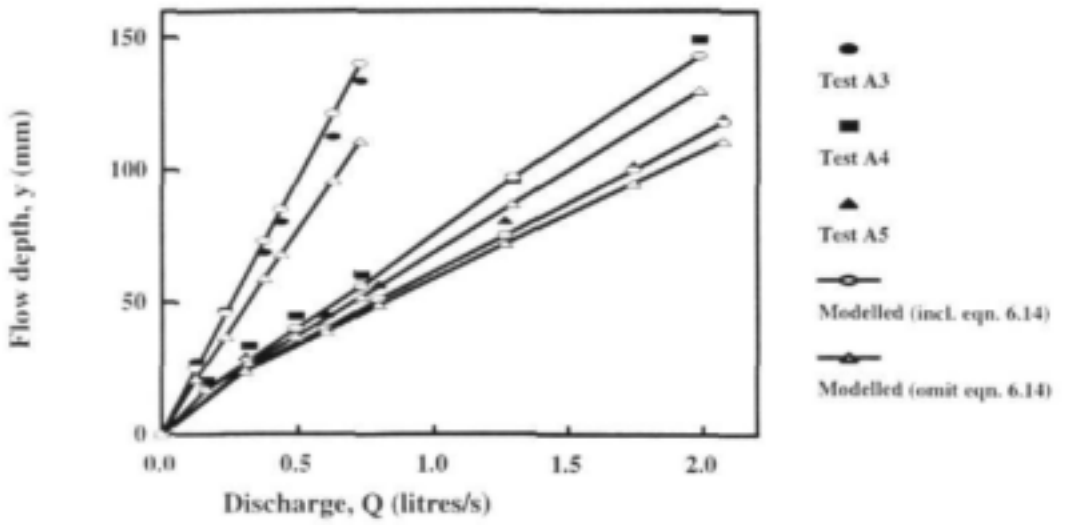

Figure 6.10 Measured rating data and modelled (REEDFLO v1) relationships for Tests A3, A4 and A5

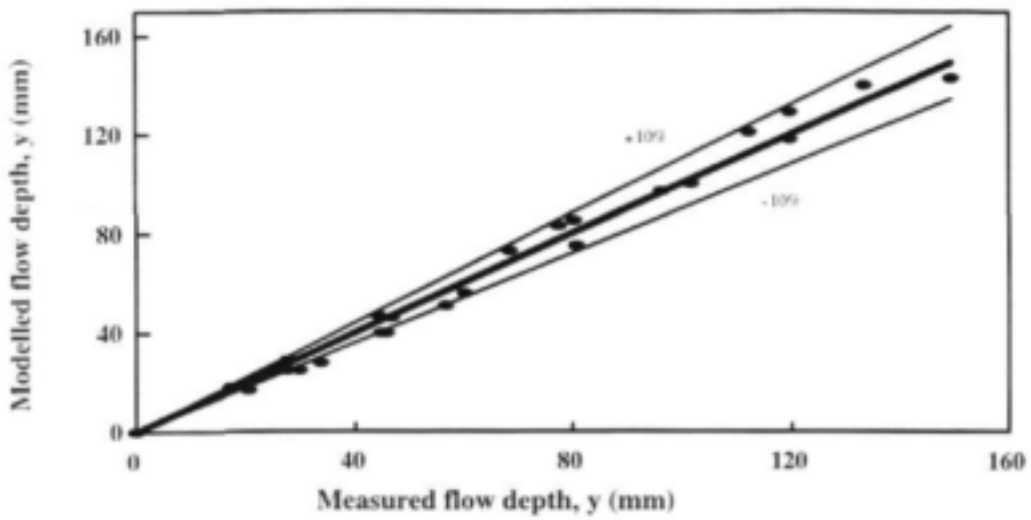

Figure 6.11 Measured versus modelled (REEDFLO v1 incorporating equation (6.14) flow depth for the four unsubmerged Series A tests

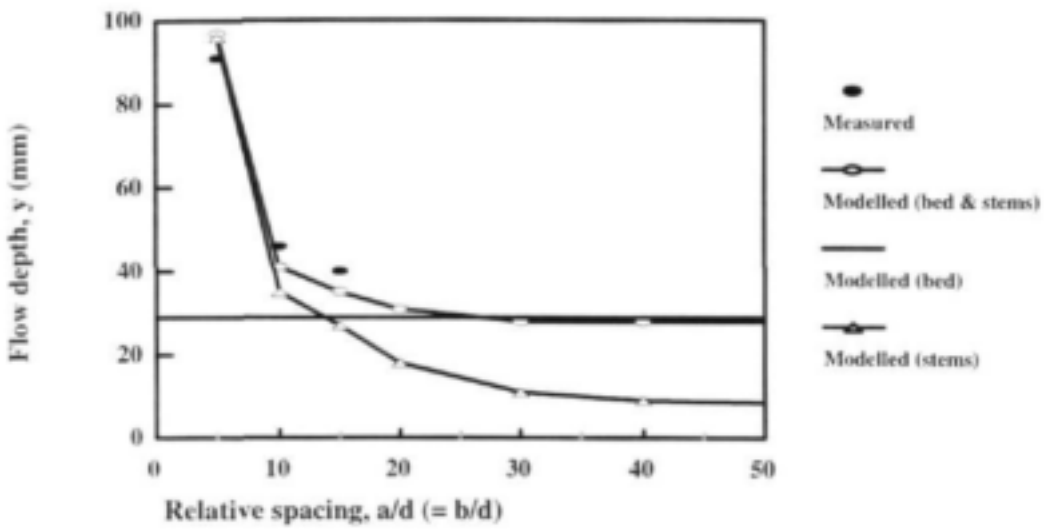

Figure 6.12 Measured and modelled (REEDFLO v1) changes in flow depth as a function of relative spacing for a staggered arrangement (Q=0.5 l/s, S_o=1/500, k_s=0.0125m)

6.3.3 Comparison With Models Published in the Literature

Various analytical models for predicting the effective resistance of a bed roughened with cylindrical type resistance elements are described in Chapter 2. These estimates are compared with the results of REEDFLO v1 (incorporating equation (6.14)), and the effective resistance determined from selected experimental data (Appendix A1) are plotted in Fig. 6.13. To facilitate comparisons with experimentally determined data, the stem density ($m.n$) is reduced from 400/m^2 to 300/m^2 to account for the missing "half" stems at the wall position of the 0.1 m wide flume along each alternate row.

The basic resistance coefficient in the computation according to Petryk and Bosmajian (1975) was determined for the bed friction condition by applying the side wall correction of Vanoni and Brooks (1957). The method of Nnaji and Wu (1973) accounts for resistance due to stem drag only, and the resistance coefficient from this method was added to the bed friction value to obtain an effective resistance.

The major differences between the analytical models presented in the literature and REEDFLO v1 are that the former methods apply a constant single-stem drag coefficient ($C_{de} = C_d$) with the drag force (equation (6.3)) based on the average flow velocity (Q/A) rather than the approach velocity. Although these assumptions may be reasonable for certain conditions, for others they may not, as illustrated in Fig. 6.6 where the effective drag coefficient deviates from the single stem value. In order to make comparisons between the different model predictions meaningful, an effective single stem value (for the range of Reynolds numbers developed) is applied in the calculations ($C_d = 1.15$). An exception is the model of Ackers (1991), where an empirical equation is used for calculation of an effective drag coefficient based on the ratio of flow depth to stem diameter.

An iterative procedure is required to obtain solutions for the effective resistance coefficients plotted in Fig. 6.13. The expressions given in Chapter 2 are used to calculate the resistance coefficient for a given flow depth estimate, and a resistance equation (Darcy-Weisbach for the friction factor, f) is applied to confirm the rating (stage-discharge) data for the effective resistance coefficient.

The modelled effective resistance coefficients in Fig. 6.13 underestimate the values determined experimentally. With the exception of the predictions of Nnaji and Wu (1973) (the most empirical of the models presented) the effective resistances are comparable at discharges above 0.75 l/s, but display a fair amount of scatter at low discharges (0.19 to 0.38 at 0.1 l/s). The rating data are plotted in Fig. 6.14 for the conditions described by the parameter values in Fig. 6.13. Figure 6.14 shows that errors in the estimate of flow depth are less significant than errors in effective resistance. This is because the friction factor (f) is proportional to the cube of the flow depth (y) for a wide channel.

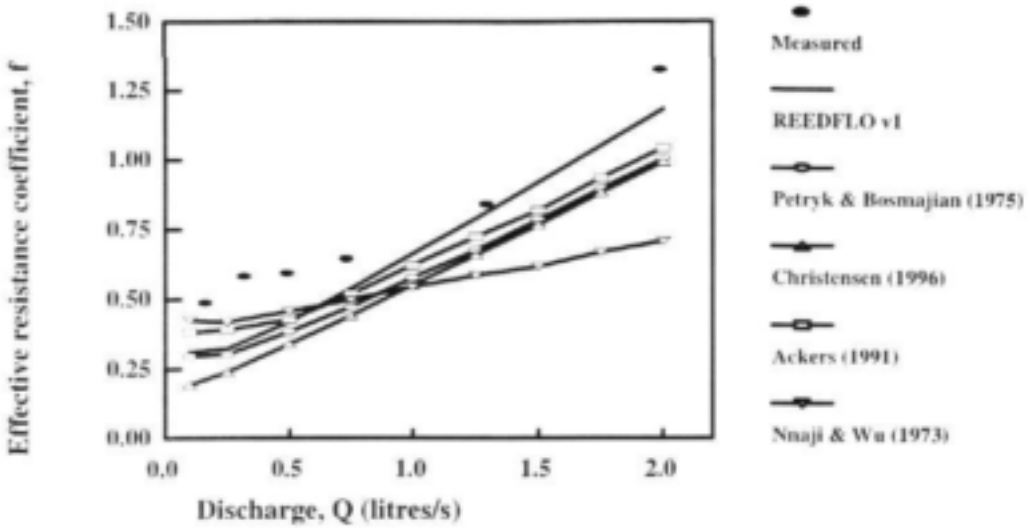

Figure 6.13 Measured and predicted (REEDFLO v1) variation in effective resistance coefficient (f) as a function of discharge for flow over an artificially roughened bed with rigid stem-type resistance elements arranged in a staggered pattern (d=0.005 m, a=0.05 m, S_o=1/500, $m.n$=300/m^2, k_s=0.0125 m)

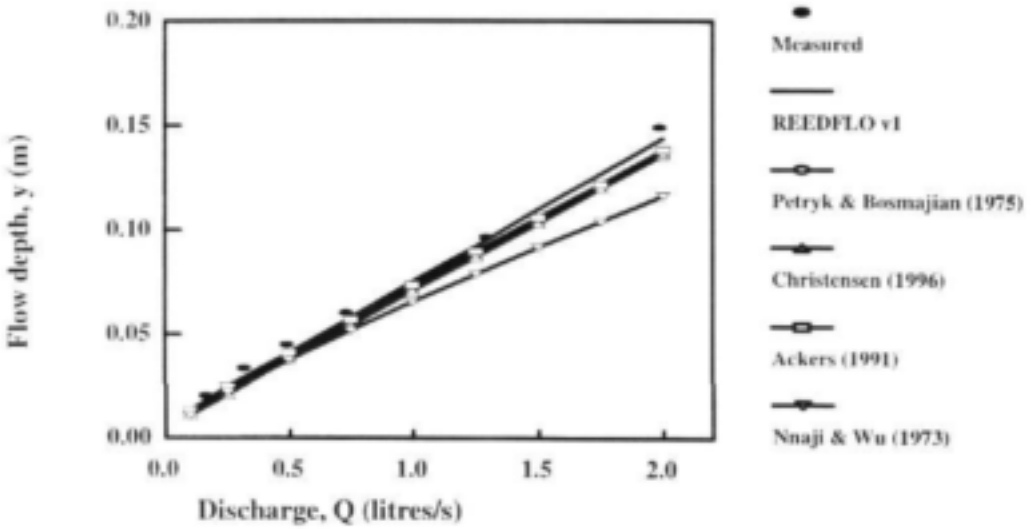

Figure 6.14 Measured and predicted (REEDFLO v1) rating data for the flow system described by the parameter values given in Fig.6.13

6.4 FLOW THROUGH SUBMERGED REEDS

The computational model developed for flow through emergent rigid vertical reeds stands (REEDFO v1) applies a non-uniform "logarithmic" distribution of velocity above the bed based on the mixing length theory of Prandtl. Measured velocity profiles (Lindner, 1982) and model verification using experimental data (Section 6.3.2) confirms the accuracy of the model for predicting stage-discharge relationships for emergent conditions. Einstein's (1950) turbulent velocity profile function (equation (6.41)) has been used to obtain an analytical solution for the vertical velocity distribution, and the integrated form of this relationship provides the depth averaged approach velocity (equation (6.43)), used in drag force computations (refer to Fig. 6.8).

For submerged conditions, the vertical distribution of velocity will deviate more significantly from a logarithmic distribution. This is because momentum transfer within the vegetated region is governed by turbulent diffusion associated with the vegetational elements, whilst above the vegetation, diffusion is associated with an "effective" roughness related to the vegetation surface, rather than the channel bed. The approach developed here for characterising the velocity and shear stress profiles is based on that of Kutija and Hong (1996), where different shear stress-velocity relationships are used to describe conditions below and above the vegetation, and these are solved numerically. A computational model (REEDFLO v2) has been developed for modelling flow through submerged reeds, and is also applicable for emergent reeds.

6.4.1 Model Development

For steady uniform flow and neglecting convective momentum considerations, the partial differential-difference equation describing the force balance is given by (Kutija and Hong, 1996)

$$\frac{\partial \tau}{\partial z} + \frac{Fx}{\Delta z} = -\gamma S_o \qquad 6.46$$

where Fx is the drag force per unit plan area of reed stand. Expressing equation (6.46) in finite-difference form using the notation given in Fig. 6.15,

$$\frac{\tau_{j+1} - \tau_j}{\frac{z_{j+1} - z_{j-1}}{2}} + \frac{Fx_j}{\frac{z_{j+1} - z_{j-1}}{2}} = -\gamma S_o \qquad 6.47$$

The drag force at the j^{th} node is given by

$$Fx_j = \frac{\rho C_{dv} du_j^2}{2ab} \frac{z_{j+1} - z_{j-1}}{2} \qquad 6.48$$

The drag force exerted on the reeds stems is a function of the approach velocity, and in order to solve equation (6.48) it is necessary to express the shear stress in terms of flow velocity (or *vice versa*).

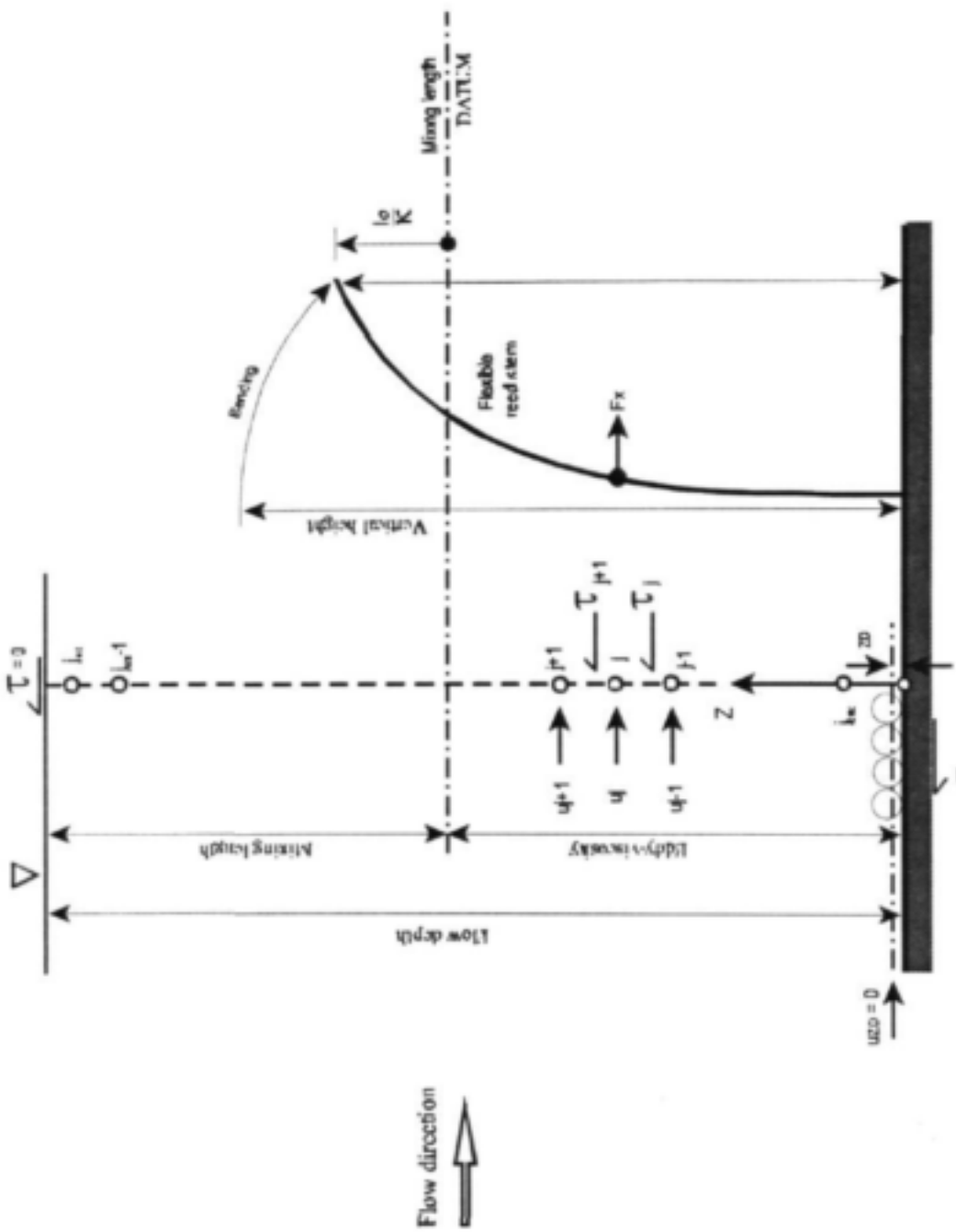

Figure 6.15 Finite-difference grid applied for the computation of the vertical distribution of flow velocity (u) and shear stress (τ)

6.4.1.1 Flow Through the Vegetation

For dense vegetation represented by both rigid and flexible rods, the velocity distribution above the channel bed has been shown to be nearly uniform (Lindner, 1982 and Kutija and Hong, 1996, respectively). Although a logarithmic distribution of velocity provides reasonable results for emergent conditions (Lindner, 1982 and Section 6.3), this study and others (Tsujimoto and Kitamura, 1990) show that for flow through submerged dense vegetation, the velocity in the vegetated zone is significantly less than that above the vegetation. Consequently, the logarithmic distribution derived from Prandtl's mixing length theory is inappropriate. Watanabe and Kondo (1990) modified the mixing length for the vegetated region, whilst Tsujimoto and Kitamaru (1990) modelled it using eddy-viscosity theory. The latter option was also adopted by Kutija and Hong (1996), and is applied here. The shear stress is given by

$$\tau = \rho\alpha a u \frac{\partial u}{\partial z} \qquad 6.49$$

where α is an empirical coefficient, typically calibrated using measured data. According to a sensitivity analysis undertaken by Kutija and Hong (1996), the significant range for α is between 0.001 and 0.01, with little influence on the results outside this range. Kutija and Hong used "s" rather than "a" in equation (6.49) to denote the spacing between the stems. Although the spacing in the lateral direction (refer to Fig. 6.16) is applied in equation (6.49), an effective spacing is likely to range between a and $2a$, and this can be incorporated in the calibration parameter α.

Expressing equation (6.49) in finite-difference form for the j^{th} node of the vertical finite-difference grid in Fig. 6.15, leads to

$$\tau_j = \rho\alpha a \frac{u_j + u_{j-1}}{2} \frac{u_j - u_{j-1}}{z_j - z_{j-1}}$$
$$\tau_{j-1} = \rho\alpha a \frac{u_{j-1} + u_j}{2} \frac{u_{j-1} - u_j}{z_{j-1} - z_j} \qquad 6.50$$

Substituting equation (6.48) for the drag force and equation (6.49) for the shear stress-velocity relationship in the force balance relationship (equation (6.47)), and rearranging terms gives

$$Au_{j-1} + Bu_j + Cu_{j-1} = D \qquad 6.51$$

where

where u_j^* is the velocity at the j^{th} node provided by the previous iteration (refer to the solution procedure in 6.4.1.6). Equation (6.51) is written for the nodes within the vegetated zone where the eddy-viscosity approximation is relevant.

$$A = \frac{\alpha a}{2}\frac{u_j^* - u_{j-1}^*}{z_j - z_{j-1}}$$
$$C = \frac{\alpha a}{2}\frac{u_{j+1}^* - u_j^*}{z_{j+1} - z_j} \qquad 6.52$$
$$B = -A - C + \frac{C_{de} du_j^*}{2ab}\left(\frac{z_{j+1}-z_{j-1}}{2}\right)$$
$$D = -gS_o\frac{z_{j+1}-z_{j-1}}{2}$$

6.4.1.2 Flow Above the Vegetation

For flow above the reeds, it is reasonable to model the turbulent shear stress using Prandtl's mixing length theory, i.e.

$$\tau = \rho l^2 \frac{\partial u}{\partial z}\left|\frac{\partial u}{\partial z}\right| \qquad 6.53$$

Expressed in finite-difference terms (with reference to the notation in Fig. 6.15),

$$\tau_j = \rho l_j^2 \frac{u_j - u_{j-1}}{z_j - z_{j-1}}\left|\frac{u_j - u_{j-1}}{z_j - z_{j-1}}\right|$$
$$\tau_{j+1} = \rho l_{j+1}^2 \frac{u_{j+1} - u_j}{z_{j+1} - z_j}\left|\frac{u_{j-1} - u_j}{z_{j-1} - z_j}\right| \qquad 6.54$$

Substituting equations (6.48) and (6.54) in equation (6.47) and rearranging terms leads to

$$Au_{j-1} + Bu_j + Cu_{j+1} = D \qquad 6.55$$

where

$$A = l_j^2 \left| \frac{u_j^* - u_{j-1}^*}{(z_j - z_{j-1})^2} \right|$$
$$C = l_{j-1}^2 \left| \frac{u_{j-1}^* - u_j^*}{(z_{j-1} - z_j)^2} \right| \qquad 6.56$$
$$B = -A - C + \frac{C_{de} du_j^*}{2ab} \left(\frac{z_{j+1} - z_{j-1}}{2} \right)$$
$$D = -gS_o \frac{z_{j+1} - z_{j-1}}{2}$$

where u_j^* is the velocity at the j^{th} node provided by the previous iteration (refer to the solution procedure in 6.4.1.6). Equation (6.55) is written for each of the nodes where the mixing length approximation is applied to provide a relationship between shear stress and velocity. The drag force coefficient (C_{de}) is present in equation (6.56), since the mixing length approximation may be applied a certain distance below the effective reed height (refer to Fig. 6.15).

6.4.1.3 Boundary Conditions

To solve the set of finite-difference equations generated by equations (6.51) and (6.55) for flow through reeds, it is necessary to establish the boundary conditions prevalent at the channel bed, water surface, and the internal boundary delineating the zone above and within the vegetation where the mixing length and eddy-viscosity relationships are applied, respectively. Although the finite-difference model has been developed to describe flow under submerged conditions, it is also applicable for emergent conditions with the eddy-viscosity approximation being applied between the channel bed and water surface. To allow for these different conditions and develop a general model for flow through reeds, the boundary conditions at the channel bed and water surface need to be determined for both the eddy-viscosity and mixing length approximations.

Channel bed

Kutija and Hong (1996) approximated the shear stress at the bed using a resistance coefficient (Chézy's) and applying the average flow velocity. Presumably, Chézy's resistance equation was used to calculate the energy slope and hence shear stress. The authors remark that this approach is not entirely satisfactory, but nevertheless justify its use by considering the reduced influence of bed shear compared with the additional resistance introduced by the vegetation. Kutija and Hong (1996) recommend that a more accurate way to model the lower boundary is to introduce a no-slip condition. This approach is applied here with a zero velocity prescribed at a distance zo from the channel bed. Assuming hydraulically rough flow conditions, the zero velocity level may be set to $ks/30.2$, where ks is the equivalent roughness of the bed material. The shear stress at the bed is then calculated by extrapolating the shear stress distribution computed numerically at the nodes above the bed level.

For the node j_{bed} directly above the bed level, the following boundary equation applies

$$Bu_{jbed} + Cu_{jbed+1} = D \tag{6.57}$$

where for the eddy-viscosity approximation,

$$\begin{aligned} C &= \frac{\alpha a}{2} \frac{u_{jbed+1}^{*} - u_{jbed}^{*}}{z_{jbed+1} - z_{jbed}} \\ B &= -C + \frac{C_{de} du_{jbed}^{*}}{2ab} \left(\frac{z_{jbed+1} - zo}{2} \right) \\ D &= -gS_o \frac{z_{jbed+1} - zo}{2} \end{aligned} \tag{6.58}$$

and for the mixing length approximation,

$$\begin{aligned} C &= l_{jbed+1}^{2} \frac{\left| u_{jbed+1}^{*} - u_{jbed}^{*} \right|}{(z_{jbed+1} - z_{jbed})^{2}} \\ B &= -C + \frac{C_{de} du_{jbed}^{*}}{2ab} \left(\frac{z_{jbed+1} - zo}{2} \right) \\ D &= -gS_o \frac{z_{jbed+1} - zo}{2} \end{aligned} \tag{6.59}$$

Water surface

The boundary condition at the water surface is the slip condition (velocity > 0) with a zero shear stress. For the node j_{ws} directly below the water surface, the following boundary equation applies

$$Au_{jws-1} + Bu_{jws} = D \tag{6.60}$$

where for the eddy-viscosity approximation,

$$\begin{aligned} A &= \frac{\alpha a}{2} \frac{u_{jws}^{*} - u_{jws-1}^{*}}{z_{jws} - z_{jws-1}} \\ B &= -A + \frac{C_{de} du_{jws}^{*}}{2ab} \left(y - \frac{z_{jws} + z_{jws-1}}{2} \right) \\ D &= -gS_o \left(y - \frac{z_{jws} + z_{jws-1}}{2} \right) \end{aligned} \tag{6.61}$$

and for the mixing length approximation,

$$A = l_{jws}^{\,2} \left| \frac{u_{jws}^{\,*} - u_{jws-1}^{\,*}}{(z_{jws} - z_{jws-1})^2} \right|$$

$$B = -A + \frac{C_{de} du_{jws}^{\,*}}{2ab} \left(y - \frac{z_{jws} + z_{jws-1}}{2} \right) \qquad 6.62$$

$$D = -gS_o \left(y - \frac{z_{jws} + z_{jws-1}}{2} \right)$$

Internal boundary demarcating the change in modelled shear stress functions for the zones below and above the vegetation

Kutija and Hong (1996) noted from the experimental data of Tsujimoto and Kitamura (1990) that the eddy-viscosity approximation was unsuitable for the entire vegetated region. This arises from an increase in the momentum transfer (and hence velocity) below the top of the vegetated layer, which the eddy-viscosity approximation does not adequately account for. The authors treated this deficiency by introducing an additional calibration factor, representing the proportion of the effective reed height that is modelled using the eddy-viscosity approximation. They noted that the factor is a function of reed density, diameter and stiffness, and stated that investigations are being directed to establish these relationships. No further studies on this have been found in the literature.

Figure 6.16 shows various hypothetical relationships for mixing length as a function of height above the bed, including those according to Prandtl, Prandtl's displaced vertically by the effective height of the reed stems (*he*), Prandtl's displaced vertically by *he-lo*/κ, and Kutija and Hong (1996). *lo* is defined as the mixing length at the effective height of the reeds. Kutija and Hong (1996) apply a modified form of Prandtl's relationship (Fig. 6.16) that reduces to zero at the water surface. Although this may represent an improvement of the classical linear function (i.e. $l \propto z$), the fact that the datum lies at the channel bed may be somewhat unrealistic.

Based on physical constraints due to the reed stems, the maximum mixing length of an eddy that may be generated within the reeds and diffuse into the region above the vegetation is limited by the diameter and spacing between adjacent reeds to between *a-d* and 2*a-d* (Fig. 6.16) Assuming that mixing length is proportional to vertical height and the proportionality is given by the von Kármán constant (κ), the mixing length datum (Fig. 6.16) should therefore be positioned between (*a-d*)/κ and (2*a-d*)/κ below the effective height of the reeds. It may be expected that the mixing lengths associated with turbulent structures generated below this "mixing length datum" are limited in dimension to the spacings between reed stems.

This modified datum for Prandtl's mixing length approximation appears reasonable, and requires a lower limit at the channel bed for low stem density where *lo*/κ approaches the effective height of the reed stems (*he*). As stem density increases, the datum increases in height above the bed and approaches the top of vegetation, as expected.

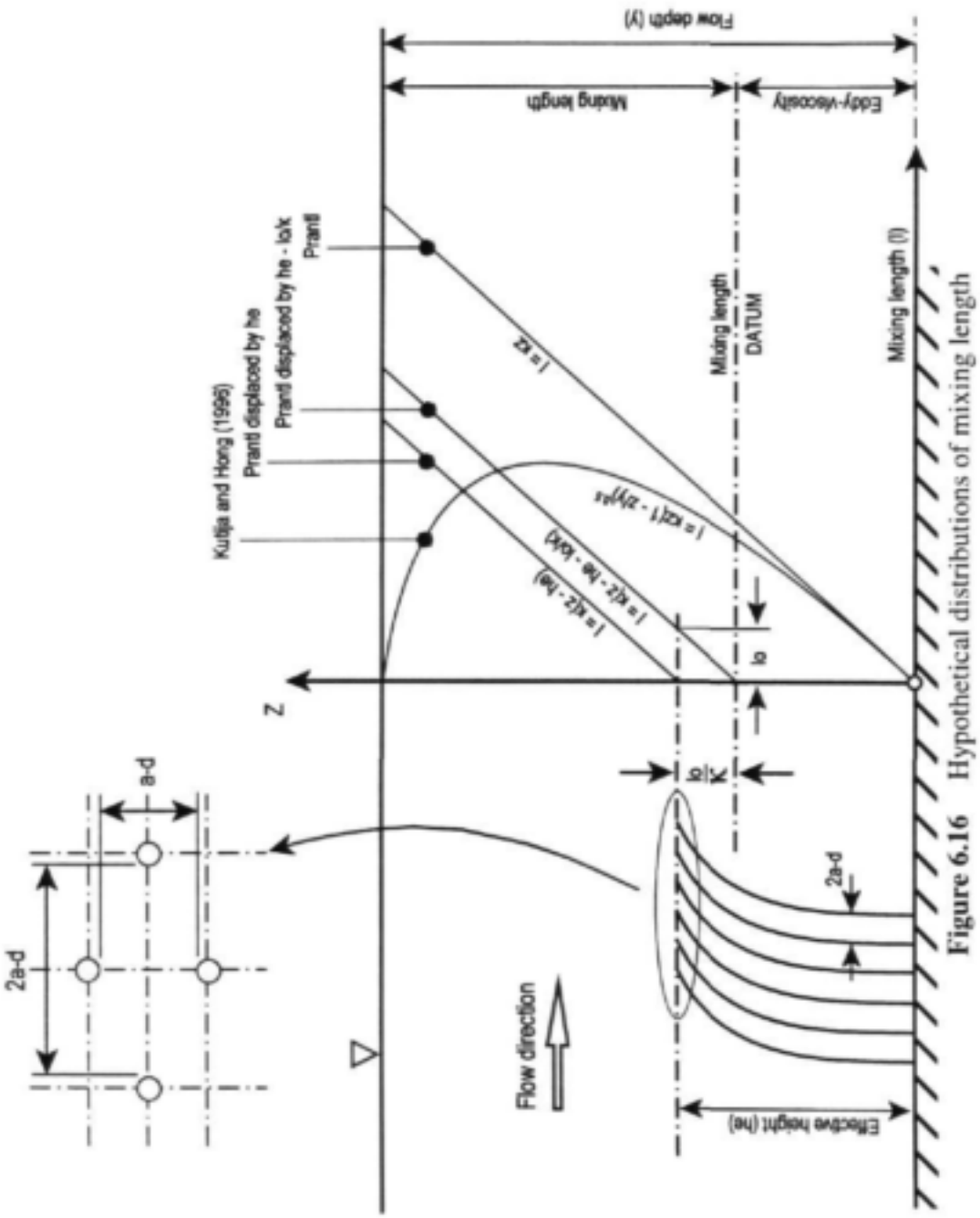

Figure 6.16 Hypothetical distributions of mixing length

The velocity coefficients at the nodes directly below (equation (6.51)) or above (equation (6.55)) the change in shear stress approximation from the eddy-viscosity to the mixing length models require modification. A is computed using equation (6.52), C is computed using equation (6.56), and B and D remain unchanged (as given in equations (6.52) and (6.56), respectively).

The various hypothetical models for describing the mixing length relationship and the position of the internal boundary between shear stress approximations are assessed using experimental data in Section 6.4.1.10.

6.4.1.4 Flexural Rigidity of Reed Stems

It is necessary to account for the bending of reed stems in the flow resistance model, since this has been observed in the field under relatively high flow conditions in many rivers across Southern Africa. A relatively simplistic model for reed bending is incorporated in the model, with the reed stems treated as elastic vertical cantilevers without permanent (plastic) deformation after the loading is removed. It may be necessary to refine this approach by including pivoting about the base of the reed stems to account for permanent deformation.

The horizontal displacement (δ_z) at a vertical height above the base of the stem is given by

$$\delta_z = \frac{UDL}{EI}\left(6he^2z^2 - 4hez^3 + z^4\right) \qquad 6.63$$

where E is Young's modulus for the reed stem (N/m^2), I is the second moment of area (m^4), and UDL is the equivalent uniformly distributed load (N/m) given by

$$UDL = \frac{\rho C_{de} u_{reed}^2}{2} \qquad 6.64$$

where u_{reed} is the average velocity in the reed zone (m/s).

This bending model applies an equivalent uniformly distributed load (UDL), rather than the using the velocity profile, to compute the vertical load distribution. It is simpler to apply the UDL arrangement, and this is considered appropriate within the context of the uncertainty in other determinants effecting resistance, including for example, the variance in stem diameter, flexural rigidity (EI) and leaf density with reed height. The change in cross-sectional (horizontal) shape of the bent reed stem (i.e. elliptical rather than circular) is also neglected in computing the drag force coefficient, and a circular stem section is applied.

An iterative solution is necessary to solve equation (6.63) for a given average velocity in the reed zone (i.e. known UDL), since the effective height (he) is a function of the deflected reed stem. An initial value for the effective stem height is assumed, and successive calculations provide a convergent solution. The equilibrium shape of the deflected stem is computed by determining the horizontal displacement at vertical increments along its length, and computing the height above the bed where the deflected stem length is equivalent to the vertical (unloaded) stem length.

The velocity in the reed zone is, however, a function of the effective reed height, and an additional iterative procedure is required to solve for bending while also satisfying the continuity equation (refer to Fig. 6.20).

The flexural rigidity (EI) may be calibrated by applying loads to reed stems (of varying diameters, and lengths) and measuring the resultant deflection. It will also be valuable to verify the bending model by performing experiments using flexible elements, not covered within the scope of this study.

6.4.1.5 Influence of Leaves and Litter

Leaves add additional resistance to the flow by increasing the drag force. Two simple means of incorporating leaves within the resistance model may be to adjust (increase) the drag force coefficient for the stems to provide an effective reed (i.e. stem and leaf) drag force coefficient, or to introduce an additional physical drag force element for the leaves. Although the latter method may be physically more rigorous, it will be difficult to implement, since the orientation of the leaves within the flow will vary with the flow velocity. It is therefore proposed that the former more empirical method be applied, at least initially, and that the additional drag force introduced by leaves be experimentally determined for different reed morphologies (i.e. reed age, leaf density and height above the basal position). Experiments performed to calibrate effective drag coefficients for various stem shapes and leaf densities have been described in Chapter 4.

The litter that occurs at the bed of reed stands is more difficult to incorporate in the resistance model because of the heterogeneity that occurs under field conditions. Methods of incorporating litter include the addition of further resistance elements at the base of the stand, the adjustment of the drag force (through an effective drag force coefficient) in the region directly above the bed, and adjustment of the height of the zero velocity boundary (no-slip condition) above the bed. The merits of each of these approaches needs to be considered using experimental or field data to obtain vertical velocity profiles against which modelled results can be assessed.

6.4.1.6 Solution of Simultaneous Equations

A set on n simultaneous equations for n unknown point velocities along the vertical profile is developed by writing equations (6.51) and (6.55) for each of the finite-difference nodes, and incorporating the relevant boundary conditions. The resultant set of equations represents a tridiagonal system (i.e. with a maximum of three adjacent unknowns point velocities in each of the n expressions).

LU (Lower and Upper) decomposition with implicit partial pivoting as described by Press *et al.* (1989) has been used to solve the set of simultaneous equations.

It is not possible to obtain a direct solution for velocity from equation (6.47) due to the non-linearity inherent in equations (6.48), (6.50) and (6.54). This non-linearity has been dealt with by treating one of the two velocity products as a known value derived from an estimate or the

previous iteration (refer to equations (6.52) and (6.56)). Consequently, an iterative solution is required to solve the system of simultaneous equations and obtain convergent values for the point velocities. Furthermore, successive iterative computations are required to satisfy the continuity equation and to determine the effective height of the vegetation for flexible stems, thereby providing a balance between applied and resisting forces acting on the system.

6.4.1.7 Determination of the Empirical Coefficient α

The computational model (REEDFLO v2) developed for submerged conditions (but also applicable to flow through emergent vegetation) incorporates three model parameters that need to be assessed. These are the empirical coefficient α in the eddy-viscosity relationship describing flow through the vegetation (equation (6.49)) (submerged and emergent conditions), the mixing length function in the zone above the vegetation (equation (6.53)) (submerged conditions), and the internal boundary between these two shear stress-velocity models.

The empirical coefficient α alters the gradient of the velocity profile directly above the bed, as illustrated in Fig. 6.17 for two different parameter values. It accounts for momentum transfer between the channel bed and the region of flow influenced entirely by vegetation, and therefore determines the predicted bed shear. Although bed shear may not significantly influence overall flow resistance under certain conditions (e.g. dense vegetation and high flow depths), it determines sediment transported as bed load - an important determinant contributing to the growth and reduction of reed beds in river systems. The model should therefore provide the ability to predict bed shear with reasonable confidence, and suitable values for α are required for this purpose.

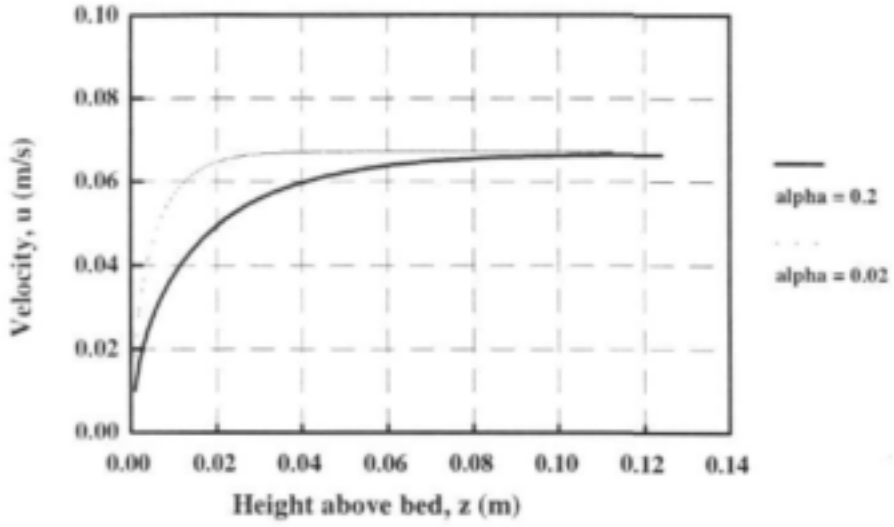

Figure 6.17 Influence of the empirical coefficient α in the eddy-viscosity relationship (equation (6.49)) on the modelled velocity profile for two different parameter values of α

Calibration of α using fixed bed flume data

No data are available from direct measurement of bed shear for calibration of the empirical coefficient, α, and an indirect method is therefore applied. Using Series A experimental data (Chapter 4) for emergent flow conditions over a roughened fixed bed, α was calibrated to provide agreement between the measured and modelled flow depths. This method is not entirely satisfactory, since flow depth is not particularly sensitive to variations in α. An improvement of this method would be to use direct measurements of bed shear.

A multiple regression using these α values provides the following empirical relationship

$$\alpha = 34.71 \frac{y^{0.961}\, k_s^{0.525}}{(a/d)^{2.427}\, S^{0.506}} \qquad 6.65$$

where y is the flow depth (m), k_s is the effective roughness of the bed (m), a/d is a measure of the stem density, and S is the slope.

Figure 6.18 is a plot of α values from equation (6.65) against calibrated values in the flow resistance model (REEDFLO v2), yielding $R^2 = 0.90$. The B Series experimental data plotted in Fig. 6.18 have not been included in the data set used to develop equation (6.65). Although equation (6.65) is based on experimental results for two bed roughnesses ($k_s = 0.0125$ and 0.0375) and slope values (0.002 and 0.010), the wide range of α values used (0.006 to 0.5) provides reasonable confidence in the applicability of the empirical relationship.

Model testing using mobile bed flume data

The applicability of equation (6.65) has been tested using experimental data from the Series B mobile bed experiments. The experimental procedure is described in Chapter 4, and reedbed sedimentation is addressed in Chapter 10. The bed consisted of loose sand with a median grain diameter 0.45 mm, and the effective roughness of the bed was estimated according to van Rijn (1982), i.e. $k_s = 3D_{50}$. The irregularities in the bed surface resulting from scour around the bases of the rods contribute to the bed resistance, but have been neglected for the purpose of estimating an effective roughness in equation (6.65). Figure 6.19 is a plot of the modelled versus measured flow depths for the nine mobile bed experiments, showing excellent agreement ($R^2 = 0.99$). The maximum and average absolute errors in the prediction of flow depth are 11% and 5%, respectively.

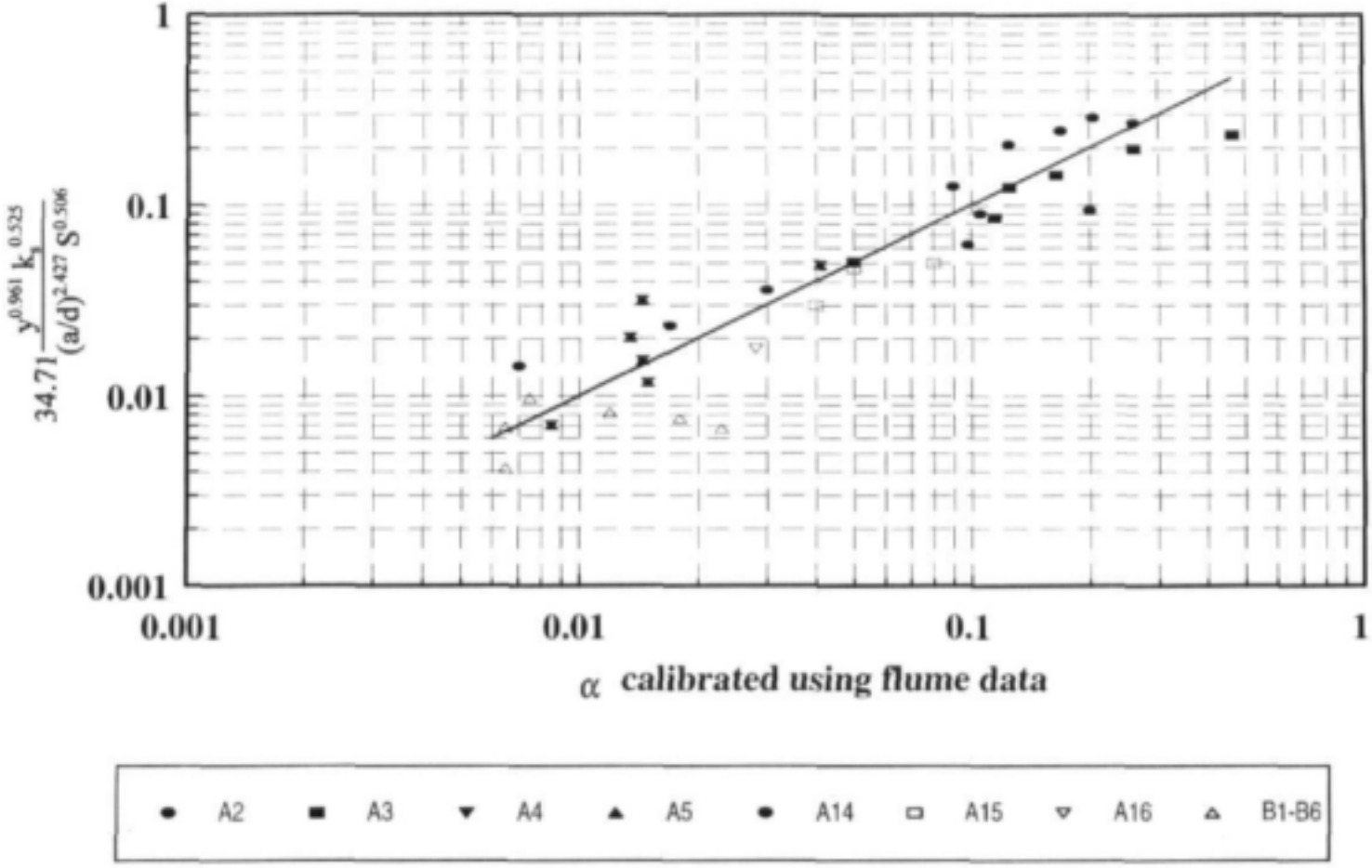

Figure 6.18 Plot of the empirical coefficient α determined from equation (6.65) against calibrated varues from REEDFLO v2 using fixed bed flume data

6.4.1.8 REEDFLO v2

REEDFLO v2 is applicable for submerged conditions as well as for flow through emergent vegetation, but requires further calibration of the mixing length parameters for submerged conditions. Table 6.3 lists the input parameters and output data provided by model. The bottom portion of the flow chart in Fig. 6.8 describes the steps for computing the uniform flow depth due to combined stem and bed resistances in REEDFLO v1, and has been modified for submerged conditions and flexible stems (Fig. 6.20).

Table 6.3 REEDFLO v2 model input data and output parameters

Input data
Discharge per unit width, Q (m^2/s)
Bed slope, S_o
Effective roughness of bed, k_s (m)
Stem arrangement - staggered/parallel
Shape of stem (i.e. cylindrical, etc.)
Stem diameter, d (m)
Distance between stems , a & b (m)
Flexural rigidity of stems, EI (Nm^2)
Mixing length at top of reeds, lo (m)*
Finite-difference parameter
Vertical height increment, dz (m)
Output parameters
Flow depth, y (m)
Velocity (average and through reeded zone), m/s
Vertical distribution of velocity (m/s)
Bed shear stress, τ_B (N/m^2)
Vertical distribution of shear stress (N/m^2)
Effective reed height, he (m)
Effective drag force coefficient, C_{de}
Reynolds and Froude no's (based on stem diameter)
Force applied to bed and stems per unit area of bed (N/m^2)
Bed and effective resistance coefficients(f, n and C)

*requires calibration using experimental data (refer to section 6.4.1.10).

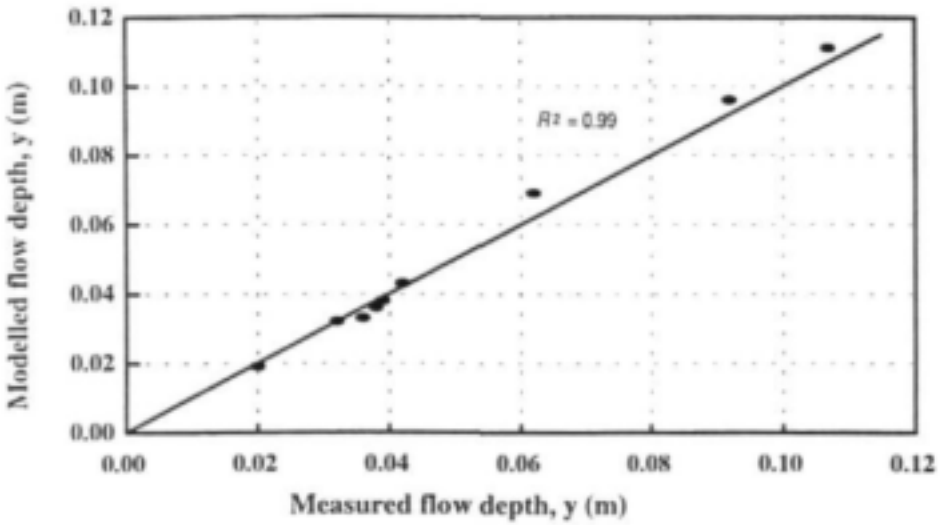

Figure 6.19 Measured versus modelled (REEDFLO v2) flow depths for the Series B flume data from mobile bed experiments

6.4.1.9 Sensitivity to Vertical Height Increment (dz) for Emergent Conditions

The finite-difference method used to solve the partial differential-difference equation (6.46) requires the discretisation of the vertical space dimension into nodes, as illustrated in Fig. 6.15. The vertical distance between nodes (dz) is a model input parameter (Table 6.3), the value of which effects the accuracy of the solution. The results of a sensitivity analysis show that flow depth (y) is relatively insensitive to dz for $dz < 0.1y$. The solution may be more sensitive, however, where shear stress and velocity gradients are high. Furthermore, the bed shear stress is calculated by extrapolating the shear stress profile down to bed level, and therefore requires accurate computation of shear stresses immediately above the bed. It is therefore advisable to check the sensitivity of the solution to the choice of vertical height increment for the flow condition being modelled.

6.4.1.10 Parameter Calibration

A series of experiments (A14, A15 and A16 - refer to Appendix A1) were performed to obtain data for submerged conditions. The experiments were conducted in a 0.1 m wide flume with a roughened bed, and rod heights of 0.094 m for Series A14 and A15 tests and 0.090 m for Series A16. Local velocities along a vertical profile were measured at different discharges to obtain data for calibration of the computational model (REEDFLO v2) under submerged conditions. The measured local velocity data are plotted in Figs 6.21(a), (b) and (c) for rod spacings of 25 mm (Test A14), 50 mm (Test A15) and 75 mm (Test A16), respectively.

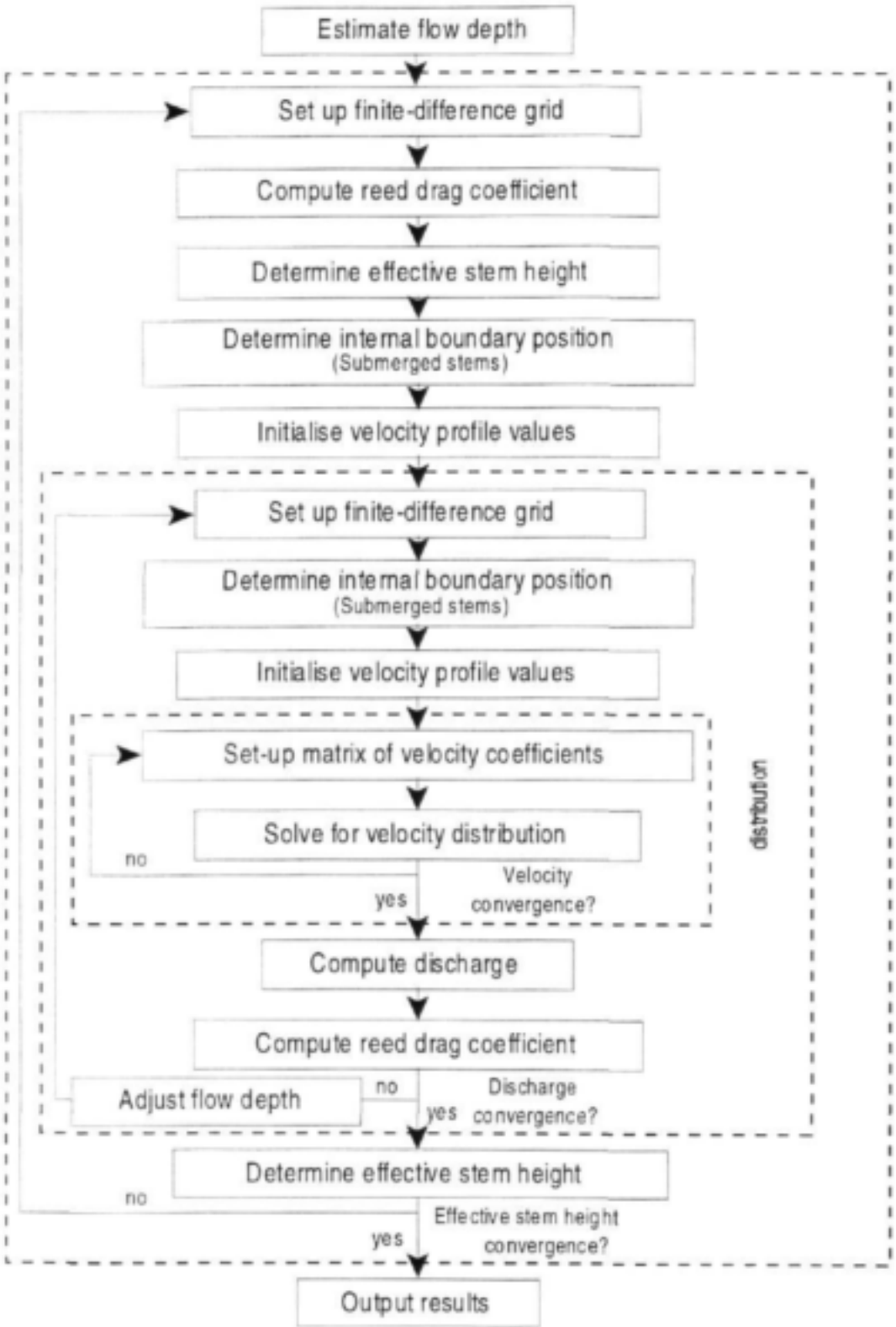

Figure 6.20 Flow chart describing computational procedures within REEDFLO v2 for combined stem and bed resistances, incorporating bending of the reed stems

Velocities were calculated from pitot-static tube and miniature propeller meter measurements. Temporally averaged velocity measurements are required because of strong fluctuations associated with turbulent structures within this flow region. The use of the available instrumentation for measuring velocities in the region below the top of the rods was unsatisfactory, since accurate temporal recording of velocities was not possible. For the 25 mm rod spacing (Test A14), velocities between the rods were too small to obtain accurate measurements, and data are only available in the region above the rods (Fig. 6.21(a)). The difference in velocity measurements obtained from the two sets of instrumentation is illustrated in Fig. 6.21(b). The pitot-static tube was used to measure velocities for the discharge of 1.61 l/s, and gives higher measurements in the rod zone, compared to, for example, the profile corresponding to a discharge of 1.73 l/s which was measured with the miniature propeller meter. Velocity measurements were taken at a position along the centre line of the flume (in the wake zone of the centre rod). The computational model, however, predicts average velocities at any given height within the vegetated region. A direct comparison between the measured and modelled values below the top of the rods is therefore not possible with the data presented in Figs 6.21. Velocity measurements taken above the rods and rating data from these experiments are nevertheless useful in providing submerged data for preliminary calibration of REEDFLO v2.

Modelled velocity profiles for three selected discharges are plotted in Figs 6.22(a) to (c) for the three rod spacings used in the experiments. The calibration parameters discussed in Section 6.4.1.3 were adjusted to provide predictions of velocity (above the rods) and flow depth that agreed with measured values. As expected, modelled (average) velocities in the rod zones are higher than measured (local) values (Figs 6.22(b) and (c)). The requirement for higher modelled values is supported by continuity, since discharge is calculated from the area under the velocity profile integrated across the width of the flume. For the 50 mm and 75 mm rod spacings, calculation of discharge from the measured velocity profiles provides an underestimate, indicating that these velocities are lower than average values in the rod zone.

The velocity profiles and inferred flow depths in Figs 6.22 have been modelled using the following parameters: a mixing length (lo) at the top of the rods given by a-d, which supports the proposal in Section 6.4.1.3., i.e. a-d to 2a-d; a corresponding mixing length datum of lo/κ below the top of the rods; von Kármán's constant (κ) was reduced from the boundary layer value of 0.41 (refer to Section 6.3.1.3) to 0.2 to agree more closely with the measured velocity profiles above the rods; the internal boundary demarcating the change in modelled shear stress functions (eddy-viscosity and mixing length functions) was positioned at the top of the vegetation. Finally, α was increased to twice the value given by equation (6.65), which was derived from emergent flow conditions.

For submerged conditions, α adjusts the shape of the profile within the vegetated zone, and indirectly determines the scale of the velocity profile in the region above the vegetation. α should ideally be defined by a single relationship for both emergent and submerged conditions. This may possibly be achieved by incorporating a function of the ratio of flow depth to the effective height of the vegetation, i.e. $(y/he)^e$, in equation (6.65), where e is an exponential coefficient determined empirically using measured data. This will be consistent with the application of equation (6.65) for emergent vegetation, since for emergent conditions, flow depth and effective height of the vegetation are equivalent. High quality spatially averaged velocity data in the vegetated region are required to confirm and refine this further.

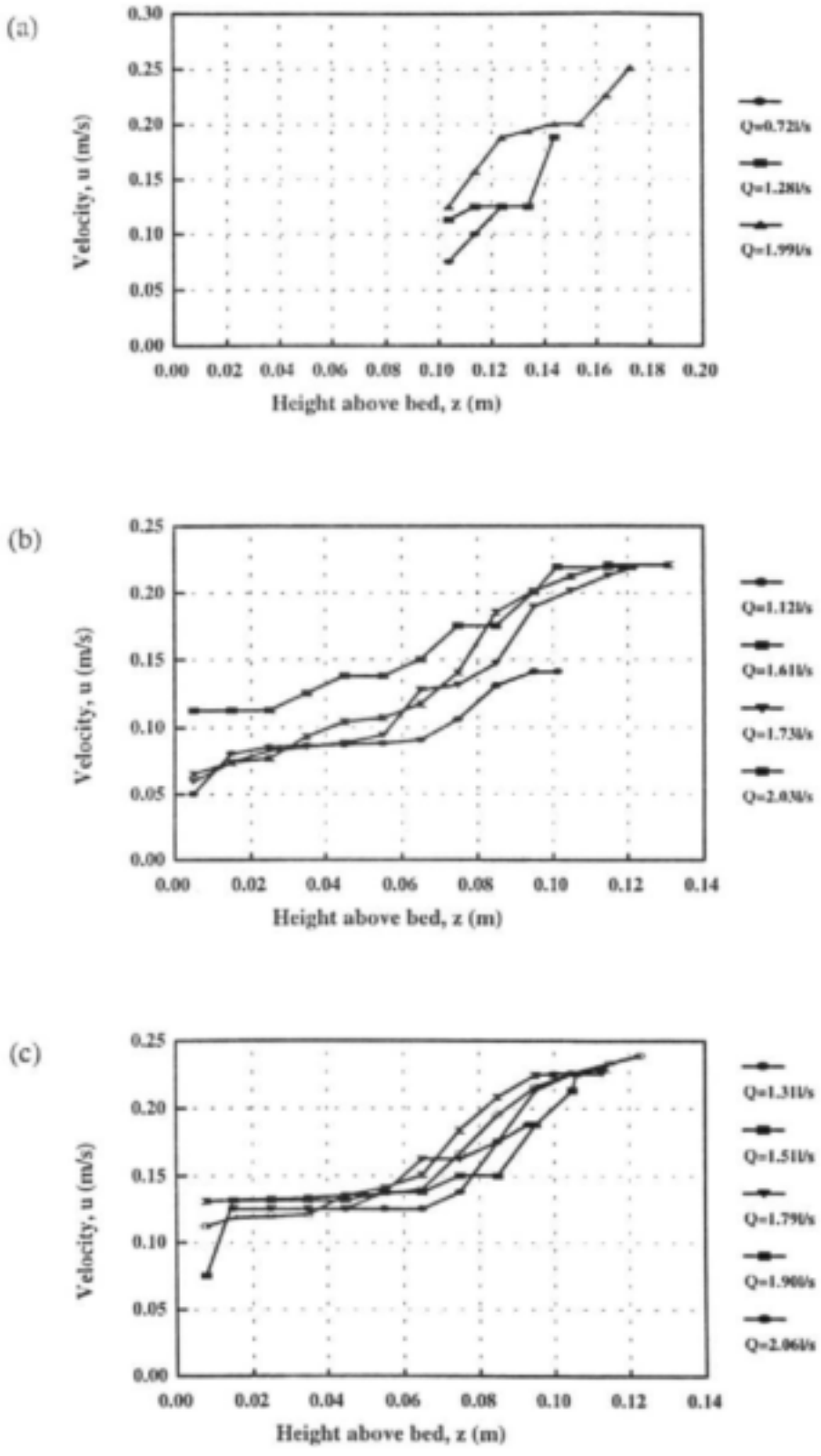

Figure 6.21 Measured local velocity data under submerged condition for rod spacing of (a) 25 mm, (b) 50 mm and (c) 75mm

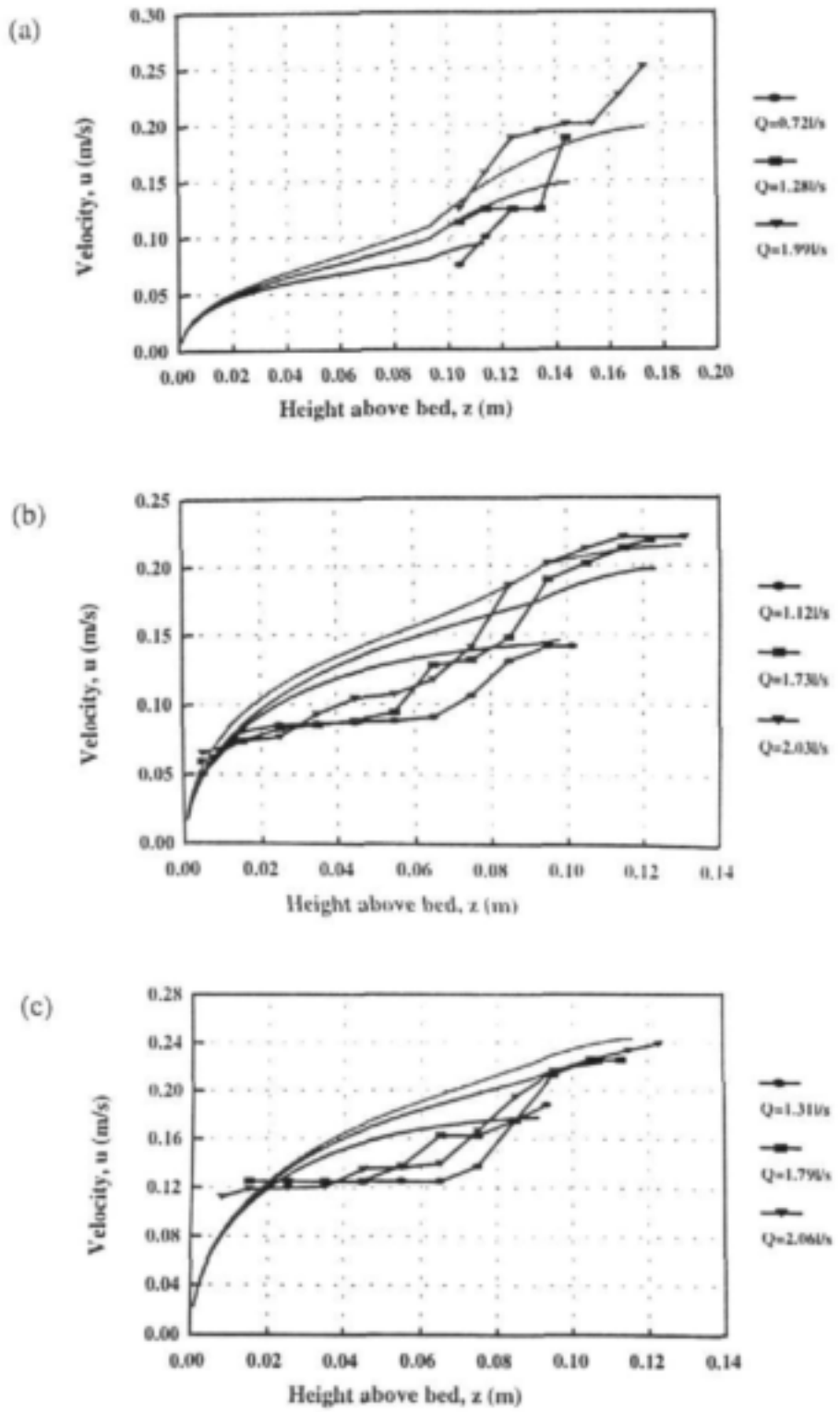

Figure 6.22 Plots of selected modelled velocity profiles (REEDFLO v2) against measured local velocities under submerged conditions for rod spacing of (a) 25mm, (b) 50 mm and (c) 75 mm

Figure 6.23 is a plot of the velocity and corresponding shear stress profiles for a discharge of 1.99 l/s under Test A14 conditions. The shear stress displays a reasonably complex distribution with height above the bed. As expected, a linear variation occurs in the region above the vegetation with a maximum value at the top of the vegetation. The shear stress reduces below the top of the vegetation, increasing again closer to the bed.

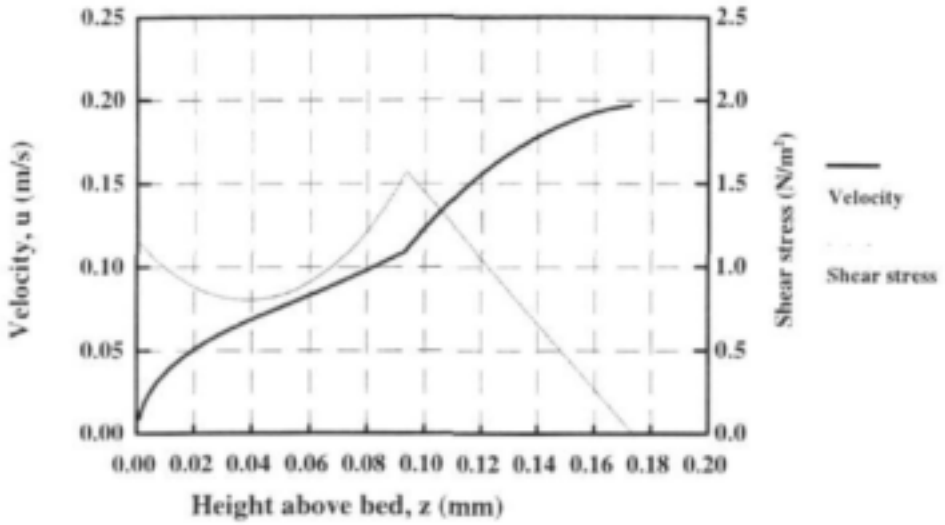

Figure 6.23 Modelled distribution of velocity and shear stress for Test A14 with a discharge of 1.99 l/s

Figure 6.24 is a plot of the modelled rating relationships (REEDFLO v2) and experimental data for emergent and submerged conditions. These measured data have been used to calibrate various model parameters. Therefore, conclusions on the accuracy of the computational resistance model, based on the plots in Fig. 6.24, are not justified.

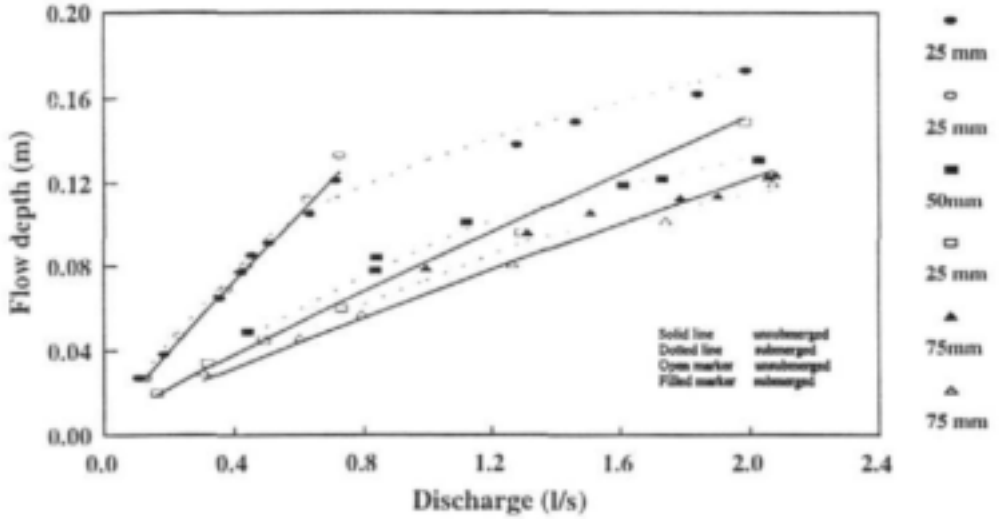

Figure 6.24 Measured rating data and modelled (REEDFLO v2) relationships for the three different rod spacings (d=0.005 m, S_o=1/500, k_s=0.0125 m (emergent) and k_s=0.0130 m (emergent and submerged))

6.5 SUMMARY AND CONCLUSIONS

Force balance principles can be applied to model the resistance characteristics of flow through reed beds, with modest data requirements. These requirements are the discharge, channel bed slope, effective roughness of the bed, and reed density and stem diameter. Resistance models have been developed for emergent and emergent/submerged conditions, and account for both bed roughness and vegetational resistance due to drag on flexible stems.

The drag force imposed by reed stems is modelled using the drag force relationship, which requires an estimate of the drag coefficient and approach velocity within a large reed stand. The velocity field resulting from flow through vegetation is complex due to the separation

characteristics of boundary layers and the development of wakes downstream of submerged elements. The velocity defect model of Petryk (1969) has been successfully incorporated in the resistance models to predict approach velocity. The drag force coefficient depends on the cross-sectional shape of the submerged vegetation and may be adjusted to account for leaves, litter on the bed, as well as different types of vegetation.

A resistance model (REEDFLO v1) has been developed for flow through emergent reeds and applies a logarithmic distribution of velocity, consistent with that for open channel flow resisted

by channel boundary friction. The accuracy of this assumed velocity function reduces with increased reed density, where velocities in the vegetated region become more uniform. Measured data for verification of model results has been obtained from uniform flow experiments with rigid vertical rods of varying density, positioned on a roughened flume bed. Modelled rating relationships compare well with experimental data when accounting for blockage effects with the use of an empirical function published in the literature. The applicability of this function, however, could not be confirmed experimentally. Comparison between the results of the resistance model, five model solutions published in the literature, and experimental data, demonstrates the improved performance of REEDFLO v1.

The resistance model for emergent vegetation was further developed for submerged conditions (REEDFLO v2). REEDFLO v2 is also applicable for emergent conditions, and therefore supercedes REEDFLO v1. The model uses numerical techniques to obtain solutions to the finite-difference equations describing the balance of applied and resisting forces acting on the flow system. REEDFLO v2 predicts, as a function of the data requirements described previously, the flow depth; vertical distribution of average velocity and shear stress; shear stress applied to the channel bed; the force resisted by the reeds and the effective height of flexible stems; the effective drag coefficient based on the average velocity through the reeds; and the effective channel boundary resistance (e.g. Manning's n or the friction factor, f). Flow through and above the vegetated region is modelled using eddy-viscosity and mixing length functions, respectively. Empirical coefficients and boundary conditions in the resistance model have been calibrated using experimental data collected in this study. These include the coefficient α in the eddy-viscosity function; the mixing length lo at the top of the reeds and the value of von Kármán constant in the mixing length function; and the internal boundary demarcating the change in modelled shear stress functions. The flow depths predicted by the resistance model show excellent agreement with experimental data collected for reedbed sedimentation (Chapter 10) under emergent conditions. Further data are required for confirmation of the calibrated resistance model for submerged conditions.

The resistance model (REEDFLO v2) is applied in Chapter 7 to generate data for developing a simpler method for computing effective boundary resistance under emergent flow conditions.

Chapter 7

APPLICATION OF REED FLOW MODEL FOR EMERGENT REEDS

7.1 INTRODUCTION

The resistance model for flow through reeds (REEDFLO v2) has been developed for uniform flow conditions within homogeneous arrangements of rigid, vertical stems, and coded in QBASIC. The detailed explanation of the model is provided in Chapter 6. The model gives a realistic description of the resistance phenomenon and can account for the influential parameters at high level of detail. It is, however, too complex and cumbersome for practical application, and provide a high resolution description that would usually be required. It has therefore been applied hypothetically to develop a general resistance equation which accounts for the important parameters that determine resistance.

7.2 FLOW RESISTANCE MODEL

7.2.1 Model Development

The model is based on a force balance approach (Li and Shen,1973; Petryk and Bosmajian,1975; Christensen, 1976; Linder, 1982 and Kosorin, 1983), in which the applied force is balanced against the bed resisting forces and vegetation drag components as follows

$$F_A = F_B + F_V \tag{7.1}$$

where F_A is the applied force per unit plan area, F_B is the resisting force contributed by the bed per unit plan area, and F_V is the resisting force contributed by the vegetation per unit plan area. The applied force per unit plan area is given by

$$F_A = \gamma y S_f (1 - mn\frac{\pi D^2}{4}) \tag{7.2}$$

where γ is the unit weight of water, y is the flow depth, S_f is the energy slope, m and n are the number of stems in the longitudinal and lateral directions, respectively, and D is the stem diameter. The resistance force of the vegetation is determined by applying the empirical drag force relationship for vertical cylinders,

$$F_V = \frac{1}{2} C_{De} \rho y D m n u_{a-} \tag{7.3}$$

where u_{a-} is the asymptotic approach velocity, and C_{De} is the effective drag coefficient proposed by Richter (1973), i.e.

$$C_{D_r} = \left(1 + 1.9 C_D \left(\frac{D}{b}\right)\right) C_D \qquad 7.4$$

where b is distance between reed stems in the lateral direction, and C_D is the drag force coefficient for a cylindrical element and is a function of the cylinder Reynolds number. The resisting force contributed by the bed is given by

$$F_B = \tau_B (1 - mn \frac{\pi d^2}{4}) \qquad 7.5$$

where τ_B is the bed shear stress.

7.2.2 Sensitivity Analysis of the Mathematical Model

Utilization of the mathematical model (REEDFLO v2) for the development of a general resistance equation for practical application requires an estimation of factors determining flow resistance. For this reason, various conditions were simulated for a wide range of input variables. The variables were varied systematically to explore their effects on flow resistance. The variables and their ranges are given in Table 7.1.

Table 7.1 Ranges of variable values for simulation

Variable	Range
Stem diameter, D (m)	0.005 - 0.02
Stem spacing, a (m)	0.05 - 0.45
Bed slope, S	0.0005 - 0.005
Bed roughness, k_s (m)	0.0125 - 0.0.03
Drag coefficient, C_D	1 - 2.2
Discharge, q (m^3/s/m)	0.01 - 0.05

The sensitivity of the model to the first five variables in Table 7.1 was investigated over the discharge range of 0.010-0.05 m^3/s/m. In the first series of investigations the variables were increased up to 75 %. The resulting changes of flow depth at discharge of 0.01 m^3/s/m are presented in Fig.7.1. The range of variables shown in Fig.7.1 is listed in Table 7.2

It can be observed in Fig.7.1 that different parameters have different effects on flow resistance. Different stem diameters and spacing between stems had significant influences on flow resistance. When the diameter was increased by 75 % the flow depth increased by 40 %. When the stem spacing was increased by 75 % the depth decreased by 40 %. The bed roughness, k_s,

had no significant influence on flow resistance. Increasing bed roughness, k_s by 75 %, increased the depth by only 3 %.

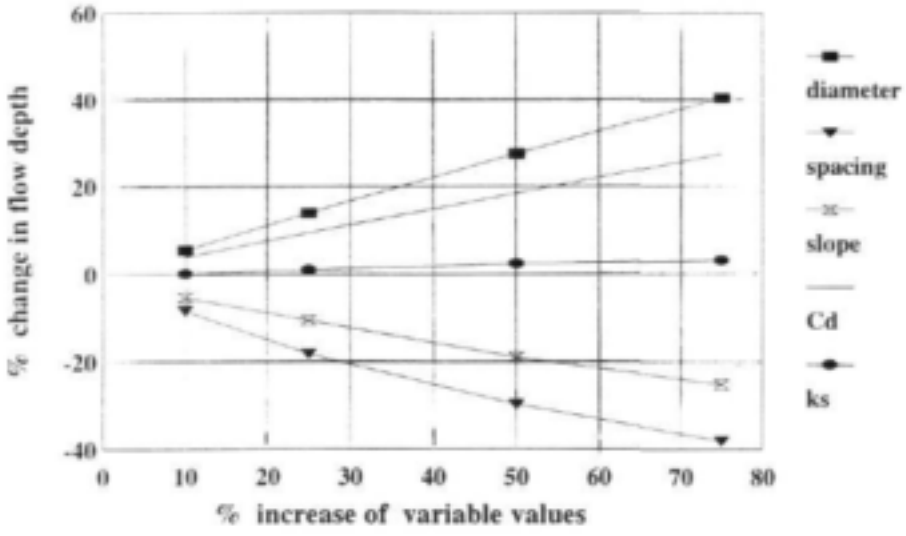

Figure 7.1 Effect of increasing variable values on change of flow depth for q=0.01 m^3/s/m

In the second series of investigations the variables were decreased by 75 %. The effects on flow depth are shown in Fig.7.2. The variables shown in Fig.7.2 are listed in Table 7.3.

The stem spacing curve (Fig.7.2) for a decrease in stem spacing of 75 % demonstrates a significant increase in flow depth. The slope curve (Fig.7.2) shows that a decrease in bed slope of 75 % results in an increase in flow depth of 100 %. As in Fig. 7.1 the bed roughness curve (Fig.7.2) shows little effect on flow depth.

Table 7.2 Variables range for Figure 7.1

Variable	Base value	Range
Stem diameter, D (m)	0.005	0.0055 - 0.00875
Stem spacing, a (m)	0.05	0.055 - 0.0875
Bed slope, S	0.001	0.0011 - 0.00175
Bed roughness, k_s (m)	0.0125	0.01375 - 0.02188
Drag coefficient, C_D	1.15	1.265 - 2.0125

Table 7.3 Variables range for Figure 7.2

Variable	Base value	Range
Stems diameter, D (m)	0.005	0.00125 - 0.0045
Stem spacing, a (m)	0.05	0.0125 - 0.045
Bed slope, S	0.001	0.00025 - 0.0009
Bed roughness, k_s (m)	0.0125	0.0313 - 0.01125
Drag coefficient, C_D	1.15	0.2875 - 1.035

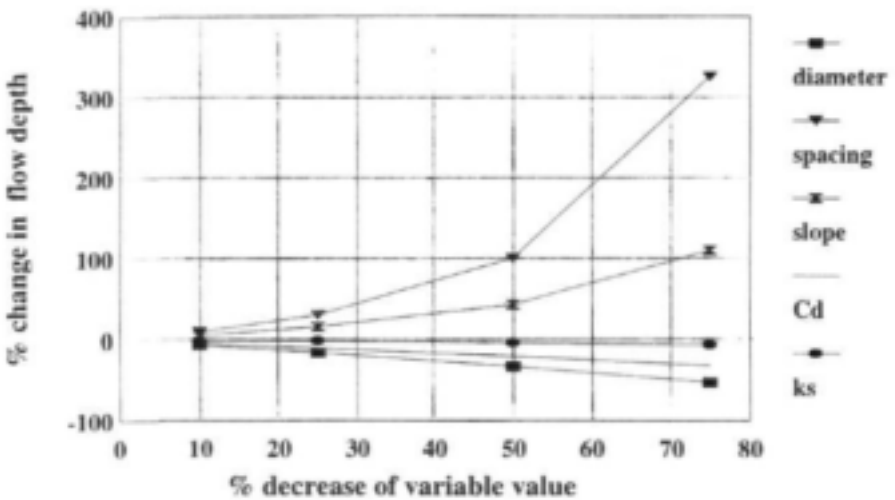

Figure 7.2 Effect of decreasing variable values on change of flow depth for q=0.01 m^3/s/m

The influence of three diameter values (D=0.005 m, D=0.01 m and D=0.02 m) at a slope of 0.0005 and a discharge of 0.05 m^3/s/m for stem spacings in the range of 0.02 to 0.18 on flow resistance is presented in Fig.7.3. From these curves, it can be seen that the diameter significantly influences flow depth, but this effect decreases with increased stem spacing.

From Fig.7.3 it can be seen that relative spacing, a/D, influences flow resistance differently, depending on absolute stem spacing and diameter. For example, for spacing of 0.1 m and diameter of 0.02 m (relative spacing of 5) the flow depth is about 1.3 m. For the same relative spacing, but with stem spacing and stems diameter of 0.05 and 0.01 respectively, however, the depth is 1.75 m.

The effect of bed roughness, k_s on flow resistance for three different stem spacings, at slope of 0.0005 and discharge of 0.05 m^3/s m, is presented in Fig.7.4. From these curves it can be concluded that a decrease in stem spacing results in an increase in flow resistance, while the changes in values of bed roughness in the range 0.0075 m to 0.0525 m did not influence flow resistance significantly for any one of three stem spacings. It is clear (Fig.7.4) that the effect of different bed roughness for three stem spacings (a= 0.05 m, a=0.15 m and a= 0,45 m) on flow resistance is similar.

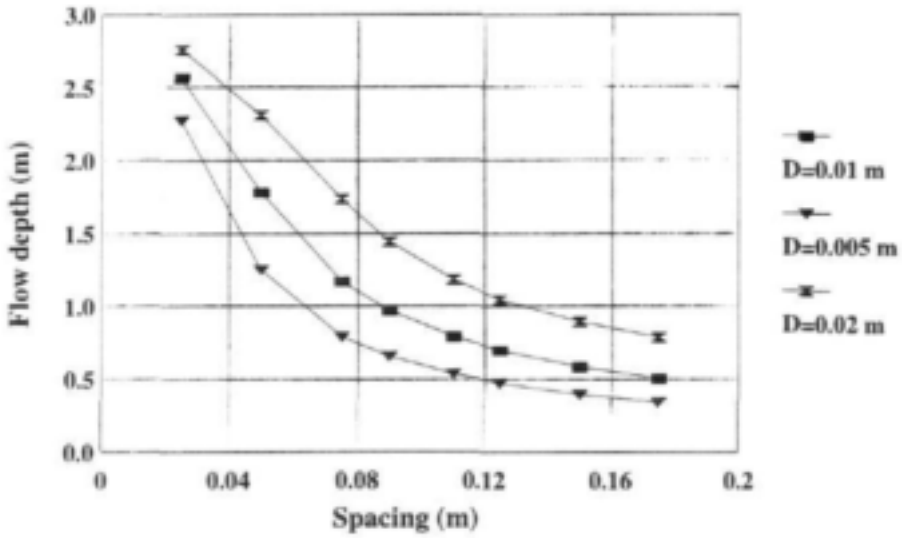

Figure 7.3 Effect of stem spacing on flow depth for stem diameters of 0.005 m, 0.01 m and 0.02 m for slope=0.0005 and q=0.05 $m^3/s/m$

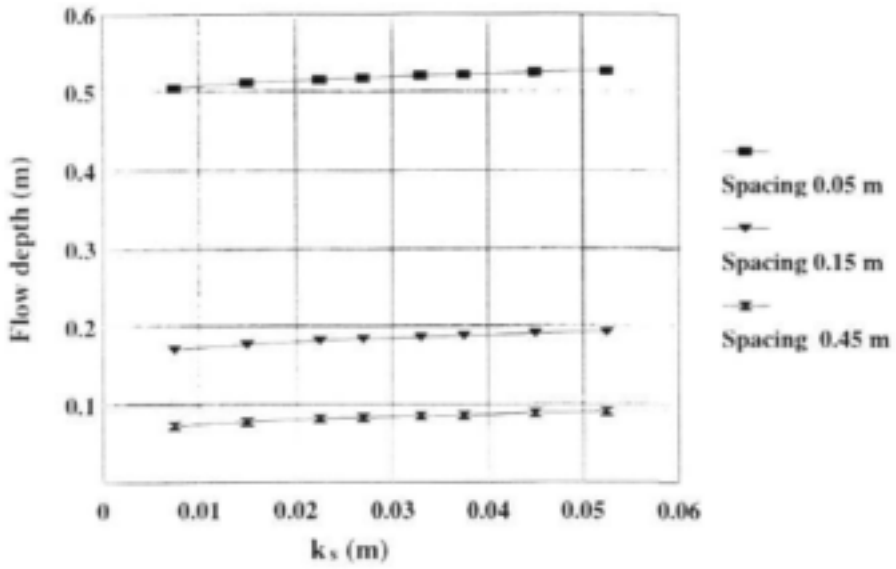

Figure 7.4 Effect of bed roughness, k_s on flow depth for stem spacing 0.05 m, 0.15 m and 0.45 m for slope=0.005 and q=0.05 $m^3/s/m$

7.3 RESISTANCE EQUATION FOR FLOW THROUGH EMERGENT REEDS

The factors determining flow resistance were identified in the previous section as bed slope, stem diameter, stem spacing and drag coefficient. The influence of bed roughness, k_s, was found to be not a significant factor in flow resistance.

Recognition of the irrelevance of Manning's equation for channels with vegetation suggested developing a resistence equation in the form of a discharge-depth equation similar to the equation proposed by Turner and Chanmeesri (1984), and Smith et al (1990). The discharge-depth equation offered by Turner and Chanmeesri (1984) is given by

$$q = G^{-1} y^m S^{0.5} \qquad 7.6$$

where q is the discharge per unit width, G is a coefficient of roughness which is independent of slope, y is the flow depth, and S is the channel slope. Roughness coefficient, G, and exponent, m, values were determined from experimental results.

Smith et al (1990) recommended an equation similar to Turner and Chanmeesri's(1984) resistance equation, which they expressed as

$$q = a S_f^{\ b} y^c \qquad 7.7$$

in which a, b and c are fitted parameters. However, the equation has been deduced based on experiments for a particular crop type, geometry and flow conditions, and this limits the scope of use for the equation.

Utilization of the mathematical model (REEDFLO v2) provides a possibility for developing resistance equation for a wide rang of conditions. The proposed stage-discharge equation is given by

$$q = F^{-1} y S^{0.5} \tag{7.8}$$

where y (m) is flow depth, S is bed slope and F (s/m) is a resistance coefficient dependent on stem diameter, stem density and drag coefficient. The resistance coefficient, F, was expressed in term of dimensionless parameters, and the most suitable form was found to be given by

$$F = fn\left(\frac{a}{D}, \frac{D}{y}, C_D\right) \tag{7.9}$$

where a (m) is stem spacing, D (m) is stem diameter and C_D is drag coefficient. The functional relationship (Eq. 7.9) was evaluated by subjecting the results of all the simulated runs for wide range of the input variables to multiple regression analysis. The ranges of the input variables were chosen according to real field conditions. The variables describing reed characteristics were chosen to correspond with field data of reeds from the Sabie, Letaba and Sand Rivers within the Kruger National Park (Kotschy, in preparation, Carter,1995 and van Coller et al, 1997). The range of input variables used in the simulation runs are given in Table 7.4.

Table 7.4 Run simulations input variables

Input Variable	Range
Discharge, q ($m^3/s/m$)	0.005 - 0.5
Bed slope, S	0.0005 - 0.002
Stem diameter, D (mm)	0.005 - 0.02
Stem spacing, a (m)	0.05 - 0.1
Drag coefficient, C_D	0.98 - 7

The following relationship was derived for conditions listed in Table 7.4

$$F = 1.885\left(\frac{a}{D}\right)^{-0.653}\left(\frac{D}{y}\right)^{0.071} C_D{}^{0.483} \qquad 7.10$$

with r^2 equal to 0.95. This equation reproduces the results simulated by REEDFLO v2 with an average absolute error of 11.46 per cent, a standard deviation of 8.38 per cent and a maximum error of + 33.28 %. A plot of absolute errors against the number of simulations is presented in Fig.7.5. Figure 7.6 which is plot of the modelled (REEDFLO v2) versus predicted (equation (7.10)) resistance coefficients, F, indicates a good correlation between the values modelled by REEDFLO v2 and values predicted by equation (7.10).

7.4 EQUATION EXAMINATION

The proposed stage-discharge equation (7.8) with resistance coefficient, F (equation (7.10)), was evaluated by comparison of experimental and predicted resistance coefficients for the Series A and B experiments (Chapter 4.2), as well as with some experimental data presented by Turner and Chanmeesri (1984) and Hall and Freeman (1994).

7.4.1 Experimental Data

Experimental values of F were estimated from the experimental results of Series A and B experiments. Predicted values of F were calculated using equation (7.10). Values of drag coefficient (C_D) were estimated from a standard curve for cylindrical elements in idealised two-dimensional uniform flow presented by Albertson et al (1960). The predicted and experimental values of resistance coefficient, F, are plotted against flow depths for a slope of 0.002 with 25 mm spacing (Test A3) in Fig. 7.7. Figure 7.8 and 7.9 are graphs of the experimental and predicted resistance coefficient, F, versus flow depths for spacing of 50 mm (Test A4) and 70 mm spacing (Test A5) respectively. Figure 7.10 is a plot of experimental and predicted (equation (7.10)) resistance coefficient, F, values for Series B experiments. From these plots (Figures 7.7, 7.8, 7.9 and 7.10) it can be seen that correlations between predicted and experimental values of resistance coefficient, F, are better for spacing of 50 mm and 75 mm than for 25 mm, which is beyond the range of spacing (Table 7.2) for which the theoretical equation (equation (7.10)) was developed. The predicted values of resistance coefficient, F, correspond quite well (Figures 7.8 and 7.9) when they become constant at relatively large flow depths. Prediction errors incurred by applying equation (7.10) to the results of Series A and B experiments are provided in Table 7.5.

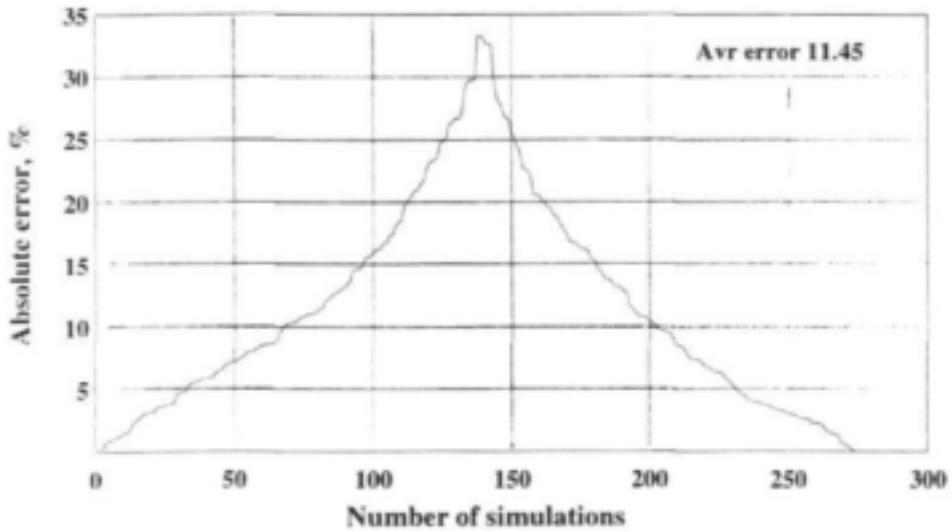

Figure 7.5 Absolute errors of theoretical reproduction of REEDFLO v2 simulations

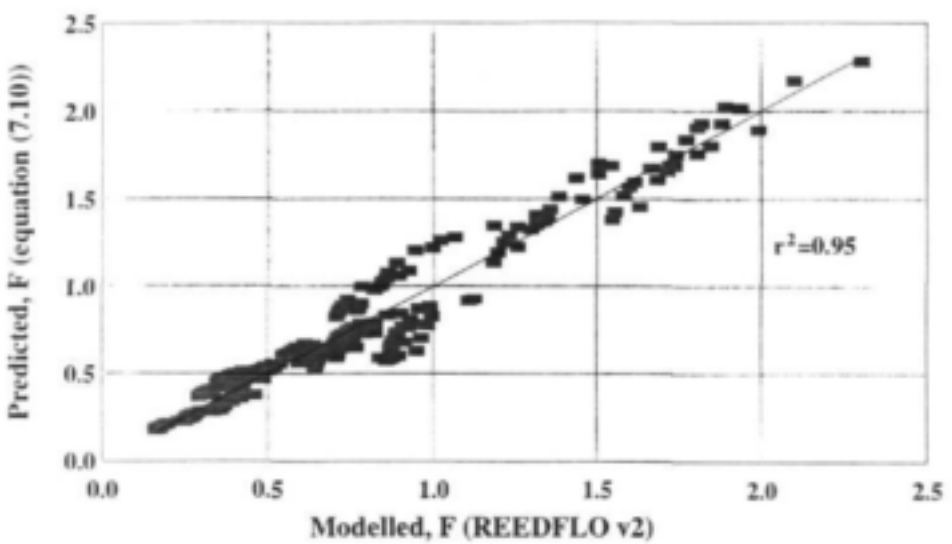

Figure 7.6 Predicted (equation (7.10)) and modelled (REEDFLO v2) resistance coefficients, *F*

Table 7.5 Prediction errors in application of equation (7.10) to Series A and B tests

Error and Standard Deviation	Series A3 25 mm spacing	Series A4 50 mm spacing	Series A5 75 mm spacing	Series B 25 mm spacing
Average Absolute Error (%)	29.44	10.15	11.36	22.33
Standard Deviation (%)	2.14	9.03	10.39	1.11

Figures 7.11 to 7.14 are plots of the measured discharge values versus values predicted by equation 7.8 for Tests A.3, A.4 and A.5, and for Series B experiments, respectively. On each plot the line of perfect correlation, as well as various percentile accuracy limits are shown.

7.4.2 Turner and Chanmeesri (1984), and Hall and Freeman (1994) Experimental Data

Examination of the proposed stage-discharge equation (7.8) with resistance coefficient, F, for natural conditions is not possible, as no field data for values of drag coefficient, C_D, for single stems are available. Turner and Chanmeesri (1984), and Hall and Freeman (1994) presented some experimental data for flow through crops of wheat and bulrushes, respectively. Their observation can be utilized for some confirmation of the equation.

Turner and Chanmeesri (1984) carried out laboratory experiments in a long concrete channel of fixed slope, and in a smaller flume having variable slope. Crops of wheat were selected for testing. The tests were carried out for different sowing patterns, stem densities, stages of growth, and different slopes. The experimental data applicable for the examination of equation (7.8) was extracted from their observations and are given in Table 7.6.

Table 7.6 Turner and Chanmeesri experimental data

Test section	Discharge, q ($l\ s^{-1}\ m^{-1}$)	Flow depth, y (mm)	Stem diameter, D (mm)	Density, No. of stems per m^2	Slope	Grid pattern
B	0.97	20	2.72	1650	0.002	diagonal
	2.24	40	2.72	1650	0.002	diagonal
	3.66	60	2.72	1650	0.002	diagonal
H	1.26	20	2.89	1020	0.0028	diagonal
	3.01	40	2.89	1020	0.0028	diagonal
	4.99	60	2.89	1020	0.0028	diagonal

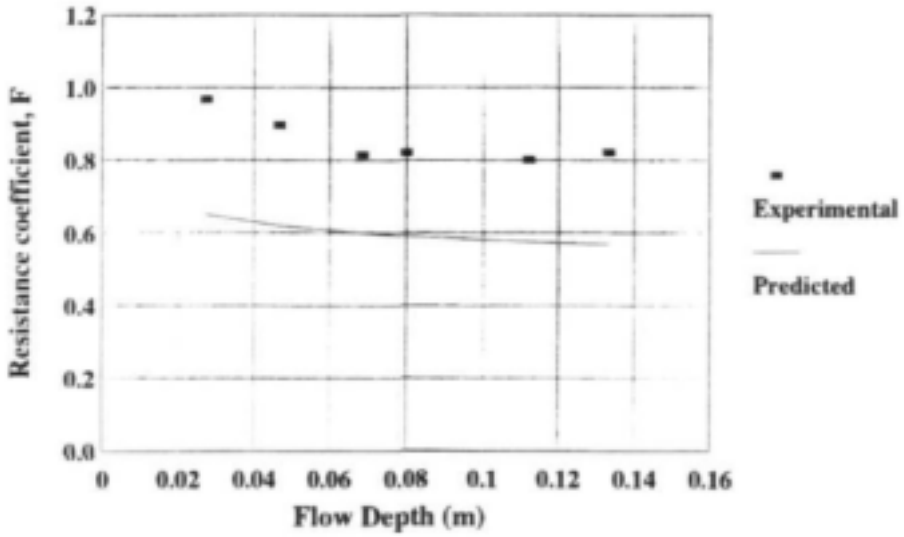

Figure 7.7 Experimental and predicted resistance coefficients, F, for Series A3 experiments

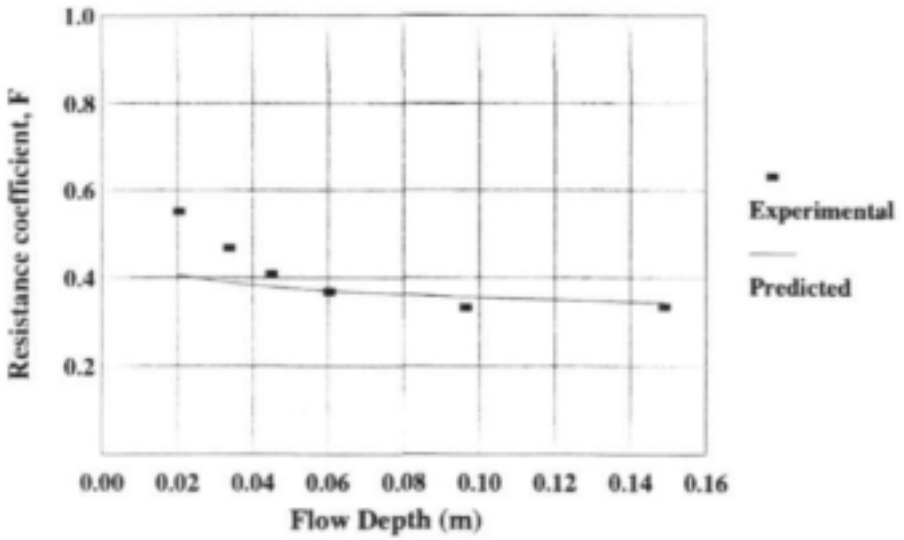

Figure 7.8 Experimental and predicted resistance coefficients, F, for Series A 4 experiments

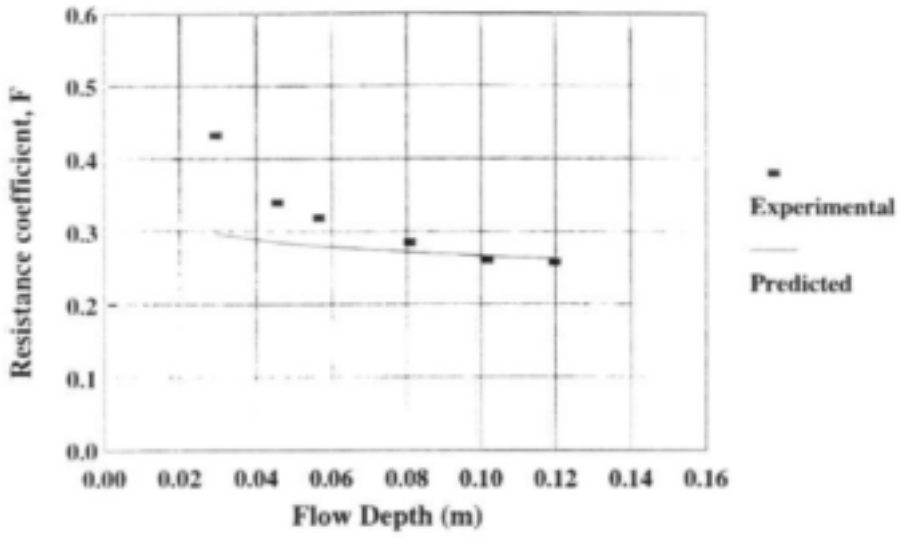

Figure 7.9 Experimental and predicted resistance coefficients, F, for Series A5 experiments

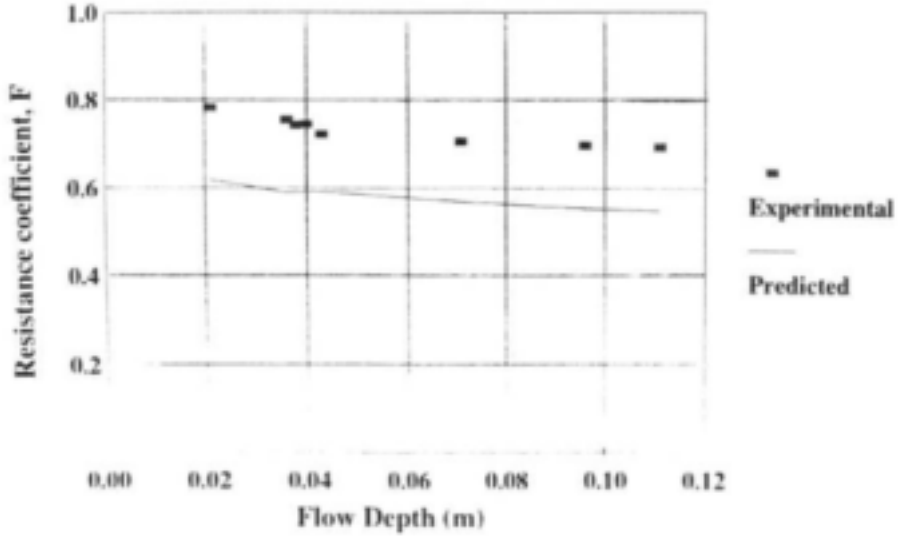

Figure 7.10 Experimental and predicted resistance coefficients, F, for Series B experiments

Examination of equation (7.8) with resistance coefficient, F given by equation (7.10) was obtained by reproducing the stage-discharge relationships listed in Table 7.4. Experimental resistance coefficients were calculated from stage-discharge data for Test sections B and H. Predicted values of F were adjusted to be equal to the experimental ones by altering input values of C_D only. The stage-discharge data and the values of C_D required for reproducing it as well as corresponding Re number are presented in Table 7.7. The required C_D values are plotted together with experimental C_D values for Reed 2 (full foliage and stem only) and Reed 1 (Chapter 4, Stem Drag Experiments) and with the standard curve (Albertson et al, 1960) in Fig.7.15, and show a reasonable relation with measured values of C_D for reed stems and with the standard curve for cylinder elements in idealised two-dimensional uniform flow. It is not possible to make any further conclusion about estimated values of C_D for crop stems because the foliage and condition of tested plants were not reported.

Table 7.7 Values of C_D required for reproducing stage-discharge data of Turner and Chanmeesri (1984)

Section	Discharge, q (l/s/m)	depth, y (mm)	C_D	Re
B	0.97	20	6.00	116
	2.24	40	4.91	134
	3.66	60	4.37	146
H	1.26	20	6.20	160
	3.01	40	4.80	191
	4.99	60	4.13	211

Hall and Freeman (1994) carried out laboratory experiments on flow through bulrushes (*Scirpus validus*) at different growth stages, in a 150 m long concrete lined drainage channel. A weir installed downstream of the channel was used to control backwater. The test section was approximately 15 m long where soft stem bulrushes were planted in late April 1992. The first two sets of experiments were conducted in July for "low" and "high" tailwater conditions. In the July tests the stem diameter was 7.0 mm and the density of the stems was 403 per square metre. The next additional set of tests were run in November when the stem diameter was 7.6 mm and the stem density was 807 stem per square metre. The tests were conducted for "high" tailwater conditions only. The same approach for examination of proposed stage-discharge equation 7.8 was applied. The experimental stage-discharge data and the values of C_D required for reproducing it as well as corresponding Re number are presented in Table 7.8. The fitted values of C_D for three sets of experiments and experimental values of C_D for Reed 2 (stem only) and

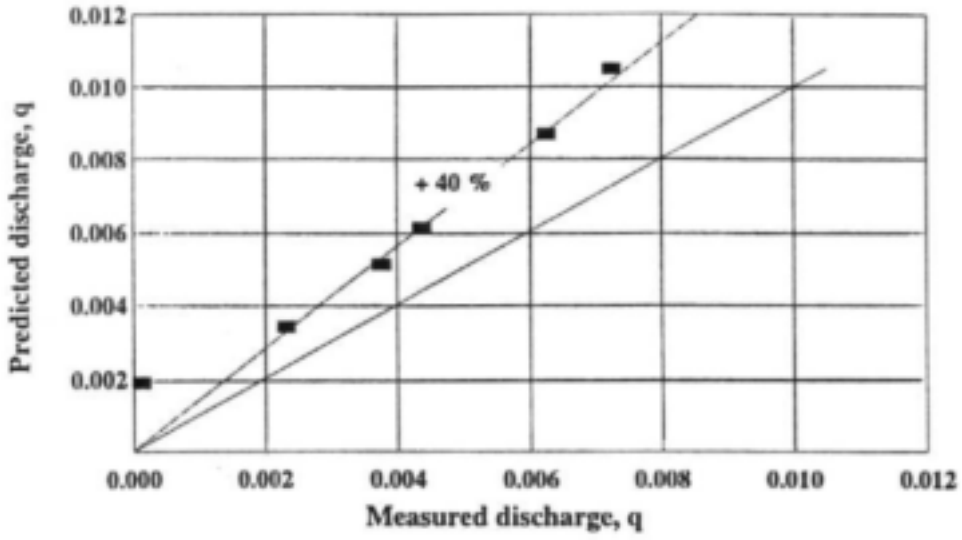

Figure 7.11 Measured and predicted discharge, q ($m^3/s/m$) for Series A3 experiments

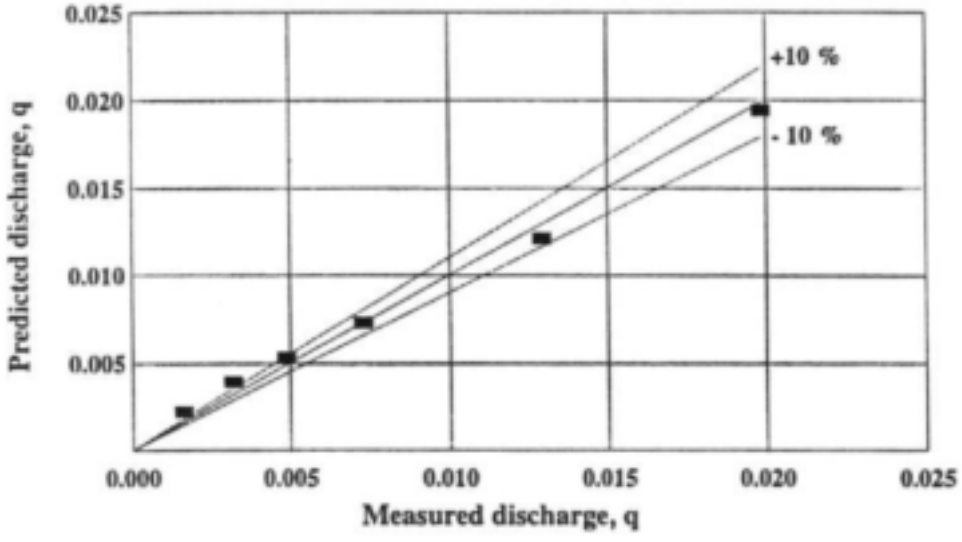

Figure 7.12 Measured and predicted discharge, q ($m^3/s/m$) for Series A4 experiments

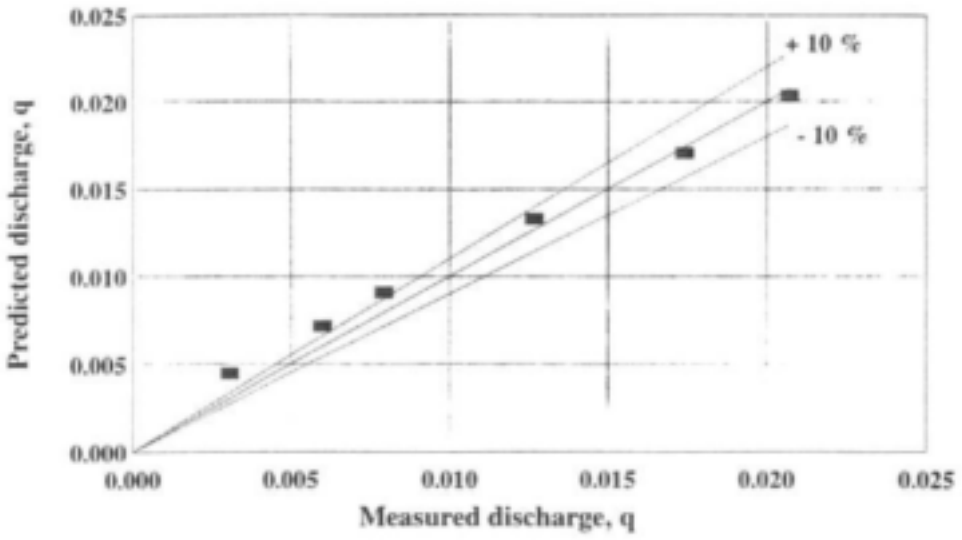

Figure 7.13 Measured and predicted discharge, q ($m^3/s/m$) for Series A 5 experiments

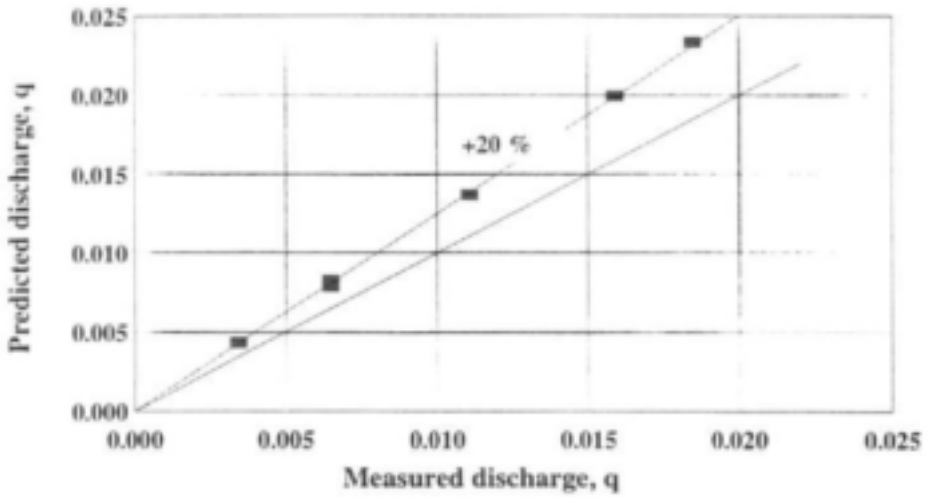

Figure 7.14 Measured and predicted discharge, q ($m^3/s/m$) for Series B experiments

Reed 1 (Chapter 4) plotted together with standard curve in Fig.7.16. Comparison of the fitted values of drag coefficient, C_D for bulrushes with the experimental values of drag coefficient, C_D for reed stems show reasonable relationships.

Table 7.8 Fitted values of C_D for reproducing Hall and Freeman (1994) stage-discharge data

Test	Discharge, Q (m^3/s)	Depth, y (mm)	C_D	Re
July 1992	0.009	0.103	9.53	448
Tests	0.026	0.215	6.52	620
(low tailwater)	0.044	0.268	5.00	841
	0.057	0.306	3.95	952
July 1992	0.009	0.312	11.83	147
Tests	0.026	0.339	5.74	393
(high tailwater)	0.044	0.403	3.26	559
	0.057	0.432	2.81	675
November 1992	0.010	0.347	19.27	160
Tests	0.026	0.374	9.90	387
(high tailwater)	0.044	0.417	6.06	587
	0.064	0.448	5.50	793

7.5 CONCLUSION

The REEDFLO v2 model was utilized for development of a general equation for practical application. Sensitivity analysis of REEDFLO v2 showed bed roughness, k_s to be not significant for vegetated stream where stem drag resistance dominates. The proposed stage-discharge equation is given by equation (7.8) where resistance coefficient is a function of stem spacing, stem diameter and stem drag coefficient. The proposed equation (7.10) of resistance coefficient can be used for determining resistance coefficient without stage-discharge measurements.

The examination of the proposed stage-discharge and resistance coefficient equations show a reasonable correlation between theoretical and experimental results for simple stems as well as for natural conditions.

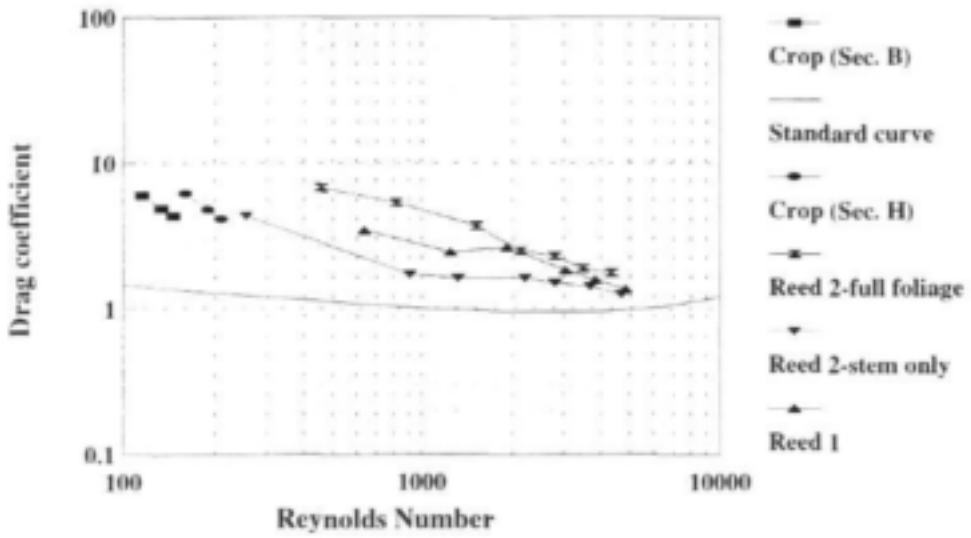

Figure 7.15 Fitted values of drag coefficient C_D for data of Torner and Chanmeesri (1984)

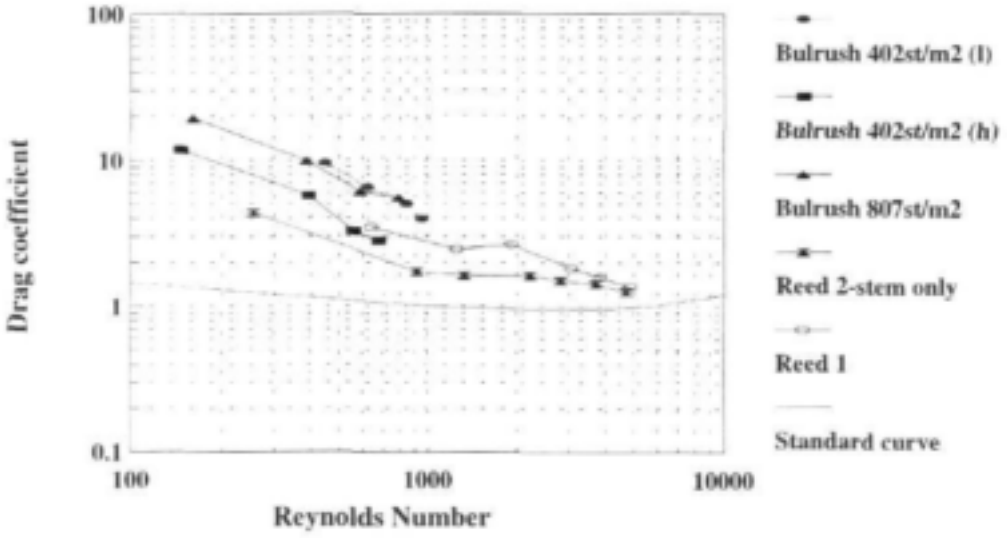

Figure 7.16 Fitted values of drag coefficient C_D for data of Hall and Freeman (1994)

Chapter 8

HYDRAULICS OF PARTIALLY REEDED CHANNELS - EXPERIMENTAL INVESTIGATIONS

8.1 INTRODUCTION

The investigations and results presented in Chapters 4 to 7 quantify and enable prediction of resistance in extensive expanses of emergent reeds, such as occur in marsh or swamp type wetlands and riverine flood plains. In river corridors reeds commonly occur in strips along the channel margins, or in strips or patches within the active channel. The basic resistance phenomena (as described in Chapters 4 to 7) operate within these reedbeds, but overall channel resistance and sediment behaviour is likely to be significantly influenced by the boundary characteristics imposed by marginal strips and discrete roughness effects associated with instream patches. This chapter presents laboratory investigations of the influence of reedbed distribution on overall resistance and flow characteristics in partially reeded river channels. The first part deals with longitudinally uniform distribution patterns comprising strips along the channel margins and within the channel. The second part deals with patterns that vary discretely in the streamwise direction as well as across the channel. In both cases only emergent stems are considered, with only one stem density.

8.2 LONGITUDINAL STRIP REED DISTRIBUTIONS

8.2.1 Experimental Procedure

Experiments were carried out in a 12.26 m long, 1.0 m wide, rectangular channel lined with cement plaster and set on a slope of 0.00107. Water was supplied to the channel from an elevated constant head tank, and controlled by a valve upstream of the head of the channel. Discharge was measured with two triangular weirs installed in parallel in a forebay between the control valve and the head of the channel. The head on these weirs was measured in a piezometer tube connected to the forebay and the rating relationship determined by volumetric measurement. Uniform flow was ensured by adjustment of a hinged overflow gate downstream of the channel. Water surface elevations were measured along the channel centre line using a pointer gauge mounted on a travelling instrument bridge, and depths calculated by subtracting bed elevations.

Reed stems were simulated using the same 5 mm diameter steel rods as for the basic resistance experiments described in Chapter 4. The rods were arranged in the same staggered grid pattern as before (Fig. 4.1), with longitudinal and transverse spacings of 25 mm. The rods were secured above the water surface in wooden frames, each 1.0 m long and 0.125 m wide and holding 200 rods, to enable their arrangement in different strip widths. The frames were arranged to create the 7 distribution patterns shown in Fig. 8.1, all of which extended over a distance of 11.0 m. All the patterns contain the same total number of stems with the same local density and the same overall coverage (50% of the channel area) - it is only the overall distribution pattern that differs.

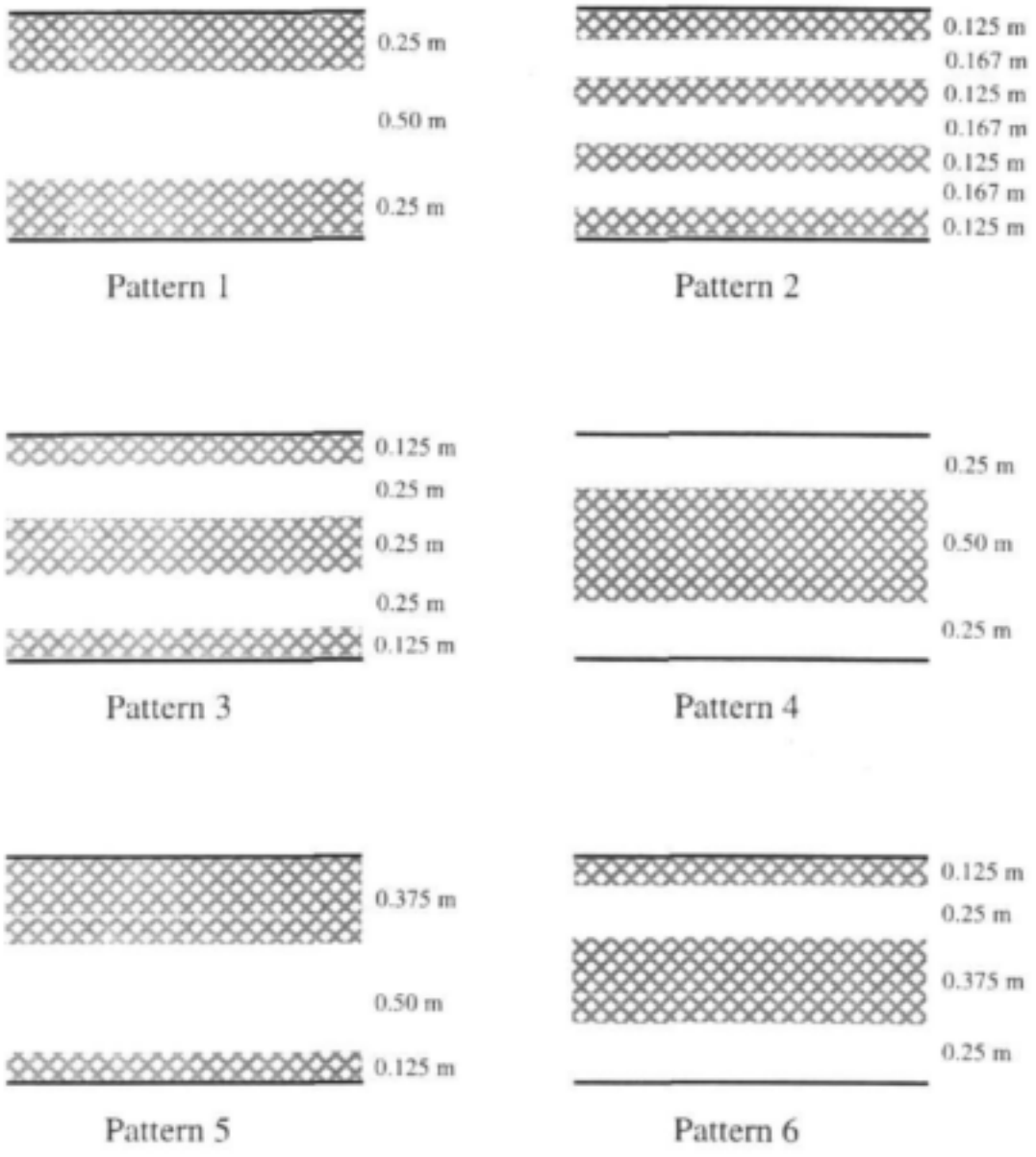

Figure 8.1 Longitudinal strip distribution patterns (in plan)

Stage-discharge measurements were taken for all the distribution patterns, and also for the channel with no stems to enable the basic resistance characteristics to be determined. For the basic channel, flow depths were measured for discharges from 5 l/s up to 35 l/s. For the vegetated channels, flow depths were measured at discharges of 5 l/s, 10 l/s, 12.5 l/s and 15 l/s for all the patterns, and up to 22.5 l/s for Pattern 1 and 20 l/s for Pattern 5. Longitudinal flow velocities were also measured at one cross section in the clear channels to enable the clear channel discharges to be determined by integration and the velocity distributions to be documented. Flow velocities were measured with a miniature propeller meter connected to an analogue indicator that integrated signals to give an average over 10 seconds. Velocities were measured at a number of vertical sections across the clear channel, the spacing depending on the total width. At each vertical section the velocity was measured at three depths: 0.2, 0.4 and 0.8 of the total depth from the bed. The depth-averaged velocity (V) for the section was then calculated as (Gordon et al, 1992)

$$V = \left(V_{0.2} + 2V_{0.4} + V_{0.8}\right) / 4 \qquad 8.1$$

in which the subscripts indicate the relative elevation of the point measurement.

No velocities were measured amongst the stems because instrumentation for measuring the very low, highly nonuniform and unsteady velocities in these regions was not available. Water temperatures were measured at all conditions to enable viscosities to be determined. Further details of these experiments are given by Makoa (2001).

Some additional experiments were done with strips along the sides of the channel only, to describe the velocity distributions at a higher resolution and to investigate the effect of marginal strip width on clear channel hydraulics. In these experiments water levels were measured in stilling pots connected to piezometers at 1.50 m spacings along the centre line of the channel. Velocities were measured with a pitot-static tube connected to a pressure transducer. Boundary shear stresses were measured using the pitot-static tube as a Preston tube, and using the calibration relationships of Patel (1965) to relate shear stress to dynamic pressure head. Velocity and bed shear profiles were measured at three flow discharges each for marginal strip widths of 0.250 m (as for Pattern 1), 0.125 m and 0.050 m. Depth-averaged velocities were measured and calculated as described above at varying increments across the clear channel, from 10 mm increments close to the boundaries to 100 mm increments in the central region. Further details of these experiments are given by Nagdi and Sharpe (2000).

The measured data are presented in Appendix B.

8.2.2 Basic Resistance

The stage-discharge data obtained for the basic channel enabled the frictional resistance characteristics of the surface to be established. For each measurement the average flow velocity was calculated as the discharge divided by the flow area, and the hydraulic radius from the flow depth and channel width. The friction factor, f, was then calculated from the Darcy-Weisbach equation (equation (2.4)). This is plotted against the Reynolds number ($4VR/\nu$) in Fig. 8.2,

showing the variation characteristic of smooth to transitional turbulent flow. Manning's n was found, using the same information, to be almost constant at 0.0102 over the entire range of conditions, with no discernable trend. The value of k_s was estimated through the Colebrook-White equation (equation (4.8)) to be approximately 0.0002 m.

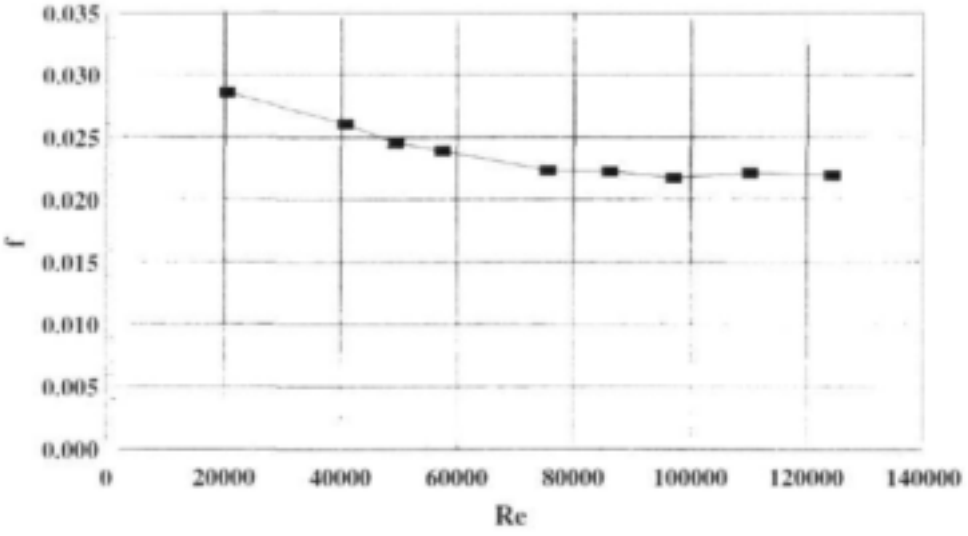

Figure 8.2 Friction factor for basic channel

8.2.3 Effect of Reed Strip Pattern on Resistance

The stage-discharge relationships for the basic channel and the different strip patterns are presented in Fig. 8.3. It is clear that the distribution pattern of the stems has a significant effect on overall resistance. The curves for Patterns 1, 2 and 3 show that subdivision of the strips and clear channel areas significantly increases the resistance, and that this effect becomes greater with increasing discharge. The total stem and clear channel areas for these three patterns are the same, but the number of strips and clear channels increases progressively, and their widths decrease correspondingly, from Pattern 1 to Pattern 3 to Pattern 2. The number of stem-clear water interfaces increases from two for Pattern 1 to four for Pattern 3 to six for Pattern 2. The progressive increase in overall resistance for these three patterns suggests that transfer of momentum across the interfaces between the relatively high velocity flow in the clear areas and the relatively low velocity within the stems is a major source of resistance in partially reeded channels. It is also significant that the solid channel side wall offers substantially less resistance to clear channel flow than a stem-water interface. This can be seen by comparing the curve for Pattern 2 (with six interfaces) with that for Pattern 7 (with five interfaces and one solid boundary) and the curve for Pattern 3 (with four interfaces) with that for Pattern 4 (with two solid

boundaries and two interfaces). In each comparison replacement of a stem-water interface with a solid boundary reduces the resistance. The close correspondence of the curves for Patterns 1 and 5, which both have two stem-water interfaces and differ only in strip thicknesses, suggests that the thickness of the strips, at least when greater than some minimum value, is not a significant parameter. (This issue is addressed further in the higher resolution experiments described in the following section).

The resistance characteristics of the different distribution patterns are presented in terms of Manning's n and its variation with flow depth in Fig. 8.4. In addition to the effects described above, it can be seen that where stem boundaries exist the value of Manning's n varies strongly with flow condition, similarly to the variation found in the basic stem resistance investigation described in Chapter 4. It is therefore not sound practice to assign a single value of n to a partially reeded river. It is also evident from Fig. 8.4 that the variation in resistance associated with a change in the strip distribution pattern can be at least as great as the increase in resistance caused by introducing bank strips to a clear channel.

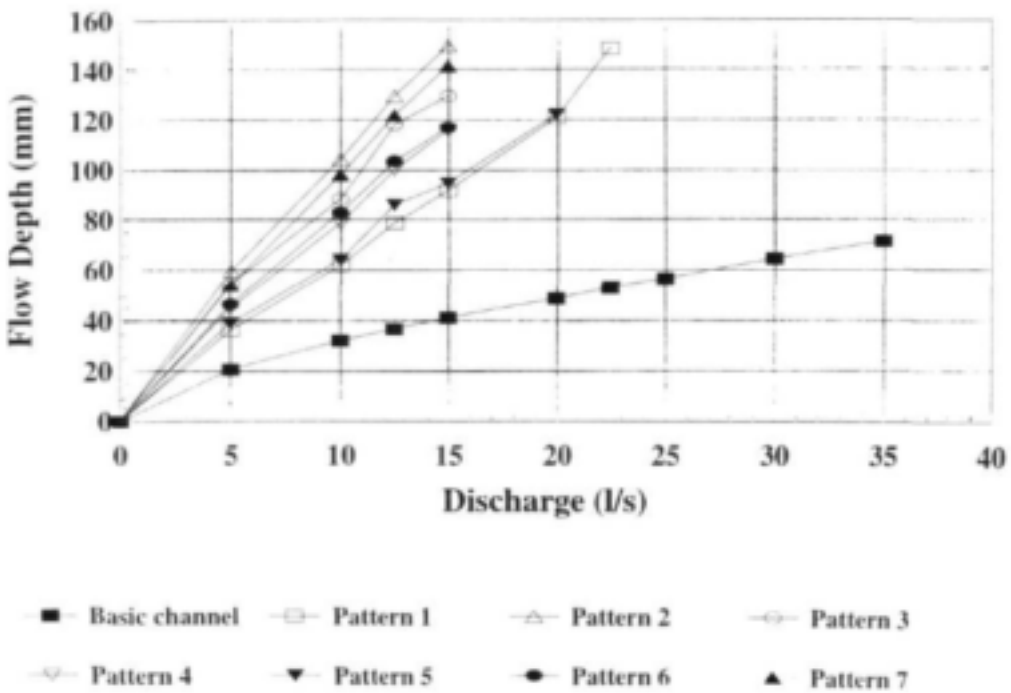

Figure 8.3 Stage-discharge relationships for basic channel and strip patterns

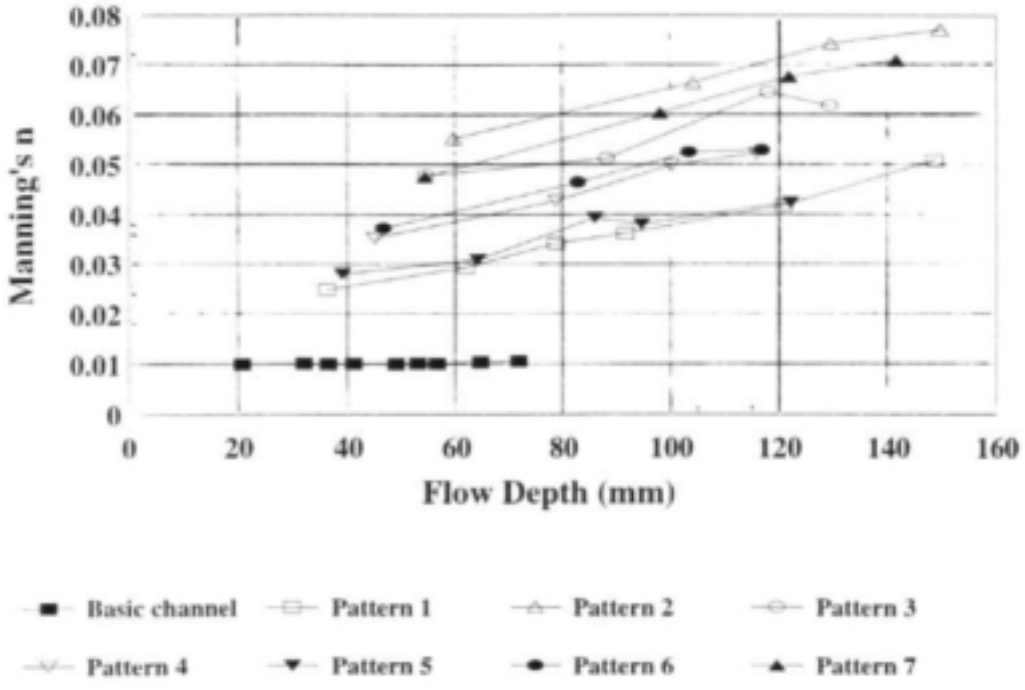

Figure 8.4 Manning's n variation with flow depth for basic channel and strip patterns

8.2.4 Effect of Reed Strips on Flow Velocity and Bed Shear

The velocity measurements enabled the distribution of depth-averaged velocity to be described for the clear channels in all the strip patterns shown in Fig. 8.1. These are presented in Figs 8.5 to 8.12 and all show discernable peaks at the centres of the channels, even for the basic channel where no stems are present. (For the basic channel, velocities were measured over only half the channel width, and Fig. 8.5 shows an assumed symmetrical distribution). This implies that the velocity is influenced by the lateral boundaries or stem-water interfaces all the way across the clear channel in every case, and that even for the basic channel the width is insufficient for the central region velocity to be controlled by the bed resistance only. Because the stem-water interfaces afford greater resistance than the solid boundaries, their influence on the velocity distributions is stronger, and the maximum velocities in the clear channels are significantly reduced as the width of the clear channel decreases and the transverse profiles from opposite sides intersect at lower values. The high resistance of the stem-water interfaces also means that the immediately adjacent velocities are much lower than for the solid boundaries (for example, see Fig. 8.12 for pattern 7, where the velocity close to the solid boundary on the right is about 2.5 times that close to the stem boundaries). These low boundary velocities and the intensity of the shear zones extending into the clear channels mean that the introduction of stem-water interfaces results in a much greater range of velocity within the clear channels. The results also show that

the magnitude of velocity does not vary as much with discharge where it is strongly influenced by stems (compare the distribution of the basic channel (Fig. 8.5) with that for Pattern 1 (Fig. 8.6), for example). The greater range of velocity across a channel and the lesser variation with discharge in reed-influenced channels must have significant implications for habitat character and sediment dynamics.

Clear channel discharges were determined by integrating the velocity profiles shown in Figs 8.5 to 8.12. This enabled the proportion of the total discharge flowing within the clear channels to be determined. The proportion varied very little with total discharge, and the average for all discharges is shown for each pattern in Fig. 8.13. As shown in Fig. 8.14, this proportion correlates very closely with the number of stem-water interfaces.

The velocity profiles presented in Figs 8.5 to 8.12 all show increases to maxima at the clear channel centres. The measuring resolution is very coarse, however, and the inferred trend could be misleading. The additional experiments undertaken with strips along the sides only enabled more detailed transverse velocity profiles to be defined, as shown in Figs 8.15 to 8.17 for strip widths of 0.250 m, 0.125 m and 0.050 m respectively on each side. These profiles all show a rapid initial increase in velocity away from the stem-water interface, followed by an apparently uniform and sometimes slightly depressed velocity over the central part of the channel. The distance over which the initial increase takes place is surprisingly constant for all strip widths and flow depths (the average distance estimated from the velocity distribution plots is 118 mm, with a standard deviation of 9 mm). The form of the distribution suggests that the zone of rapidly increasing velocity is a transition zone in which the flow is resisted primarily by the stems, and beyond this zone the flow is resisted primarily by the bed friction. Comparison of the profiles for similar depths with different strip widths (Figs 8.18 to 8.20) shows, however, that the central velocities are significantly different and inversely proportional to the strip width. They can therefore not be controlled by the bed resistance only, indicating that the stem resistance influences the flow over a considerable distance, and well beyond the point where the profile appears to level off. The width of the side strips therefore has a significant effect on the whole clear channel velocity profile. It is noticeable that the profiles for the different strip widths at the lowest flow depth (Fig. 8.18) are very much closer together than the others, indicating that the stem-water interfaces are less influential at low depths than at high depths, as would be expected.

The boundary shear stress distributions across the clear channels are presented in Figs 8.21 to 8.23, and show similar variations with transverse distance and strip thickness to the velocity distributions. The erratic variations in some regions are associated with irregularities in the plaster finish of the channel bed.

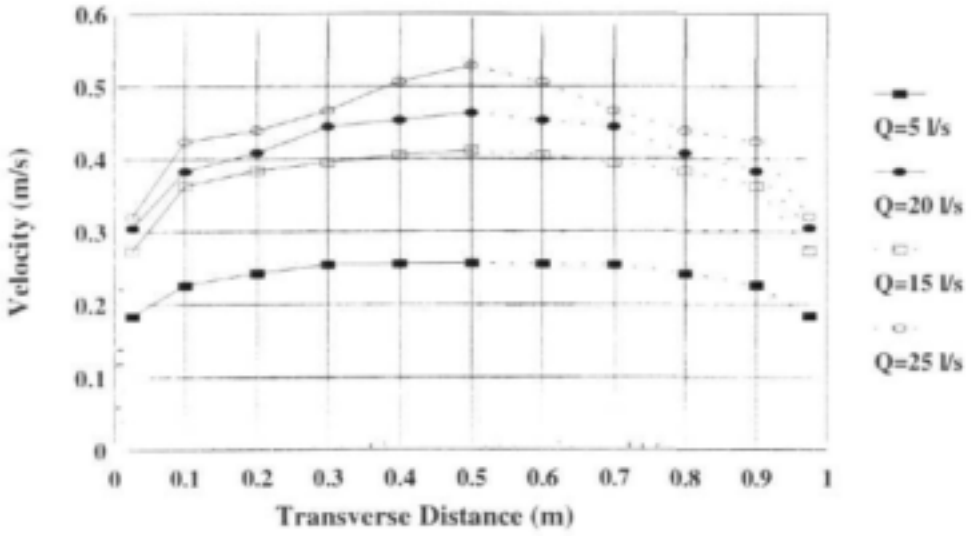

Figure 8.5 Transverse velocity distributions for basic channel

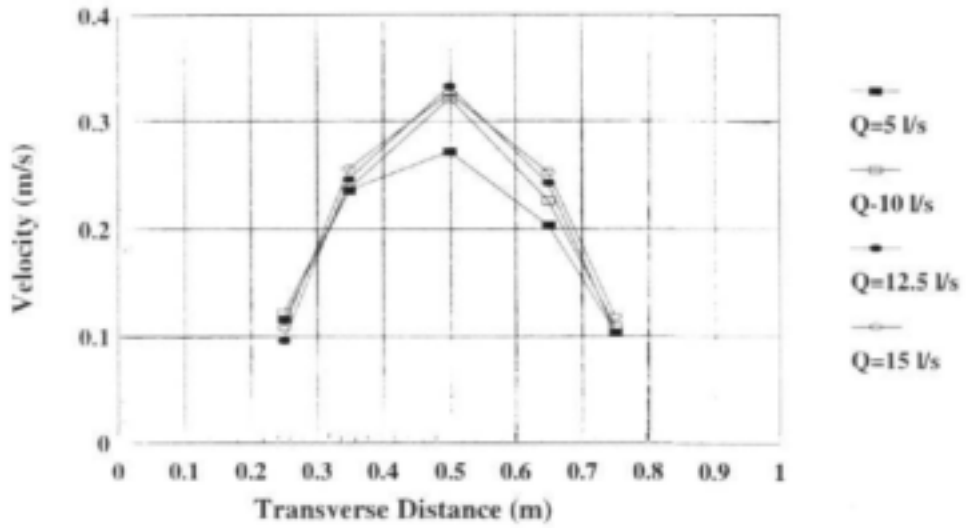

Figure 8.6 Clear channel transverse velocity distributions for Pattern 1

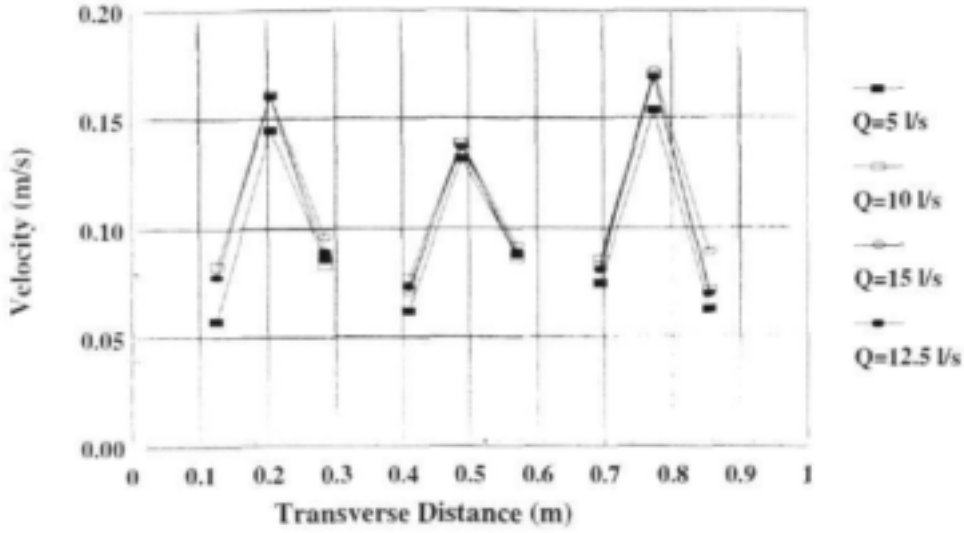

Figure 8.7 Clear channel transverse velocity distributions for Pattern 2

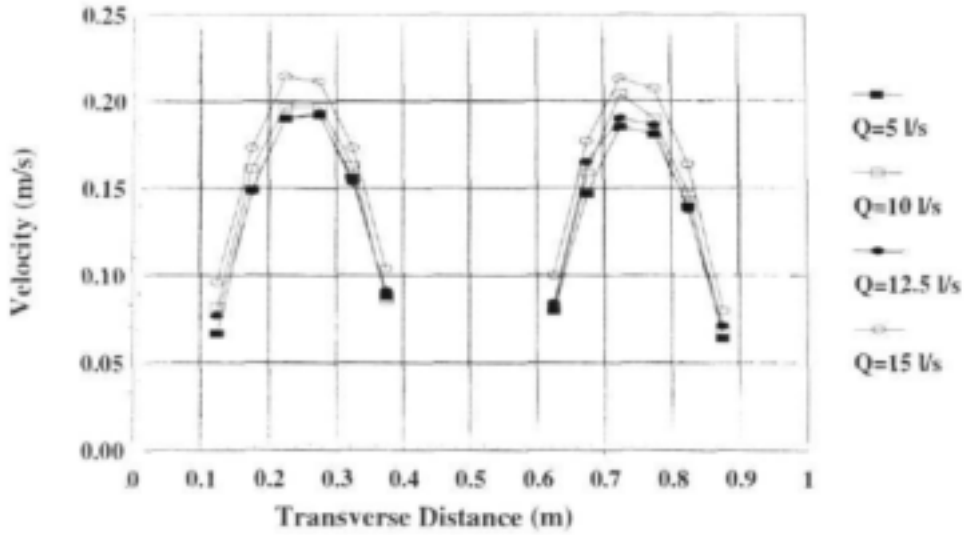

Figure 8.8 Clear channel transverse velocity distributions for Pattern 3

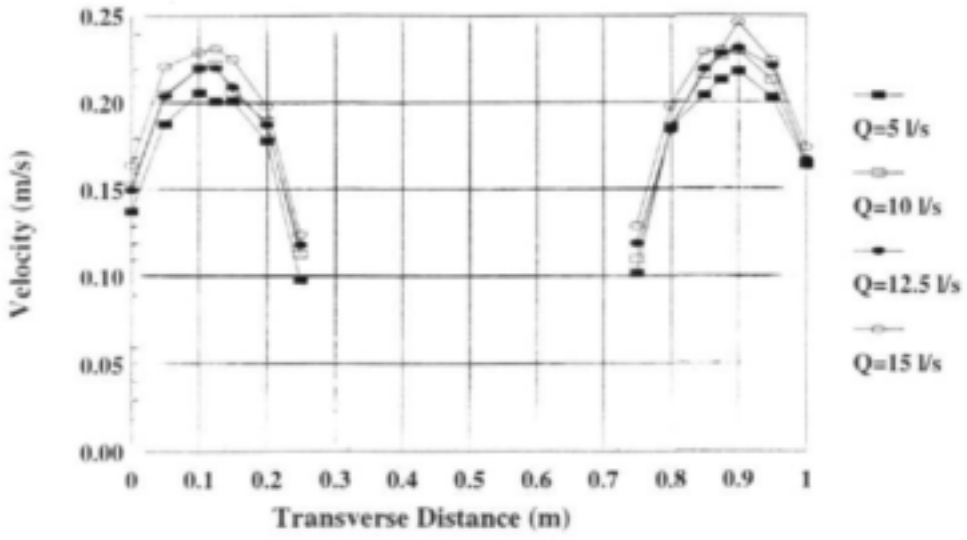

Figure 8.9 Clear channel transverse velocity distributions for Pattern 4

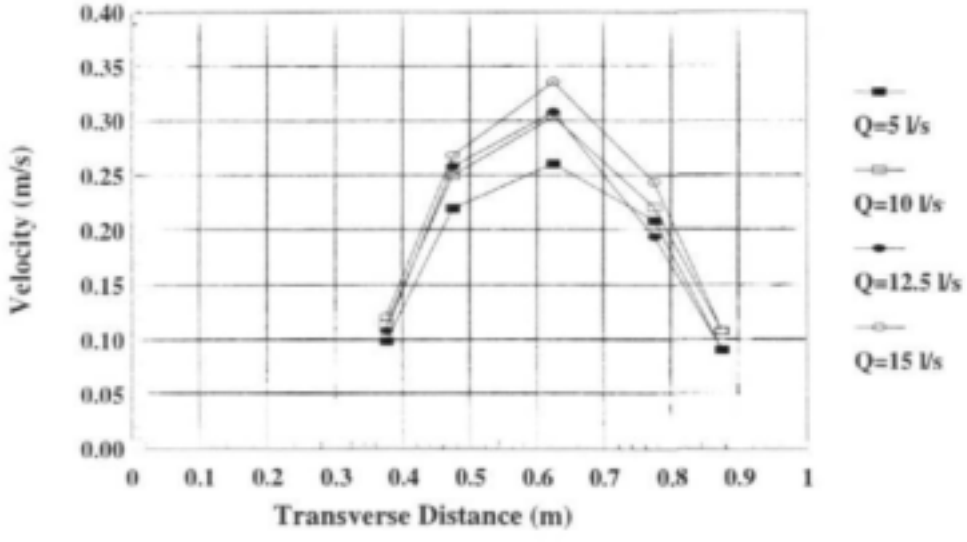

Figure 8.10 Clear channel transverse velocity distributions for Pattern 5

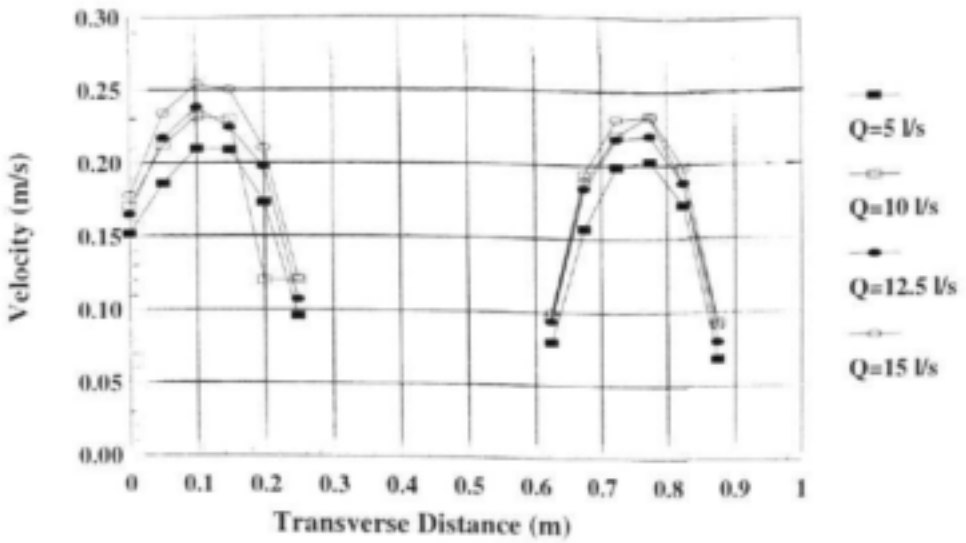

Figure 8.11 Clear channel transverse velocity distributions for Pattern 6

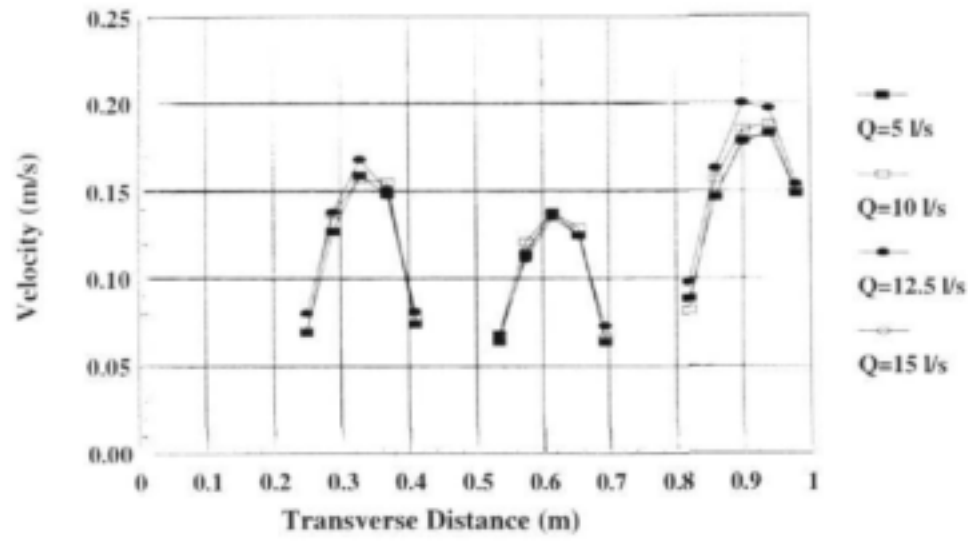

Figure 8.12 Clear channel transverse velocity distributions for Pattern 7

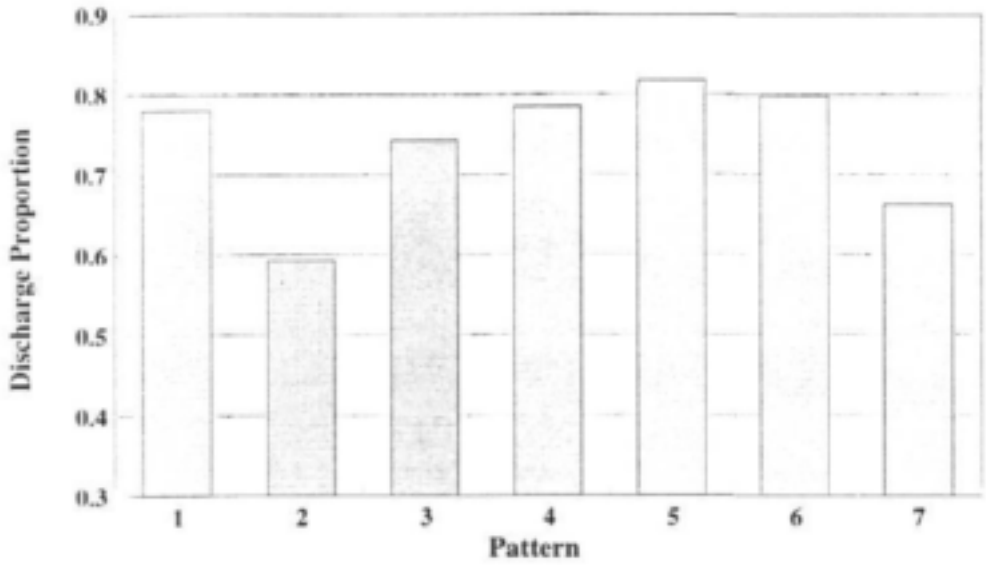

Figure 8.13 Proportion of total discharge in clear channels for strip patterns

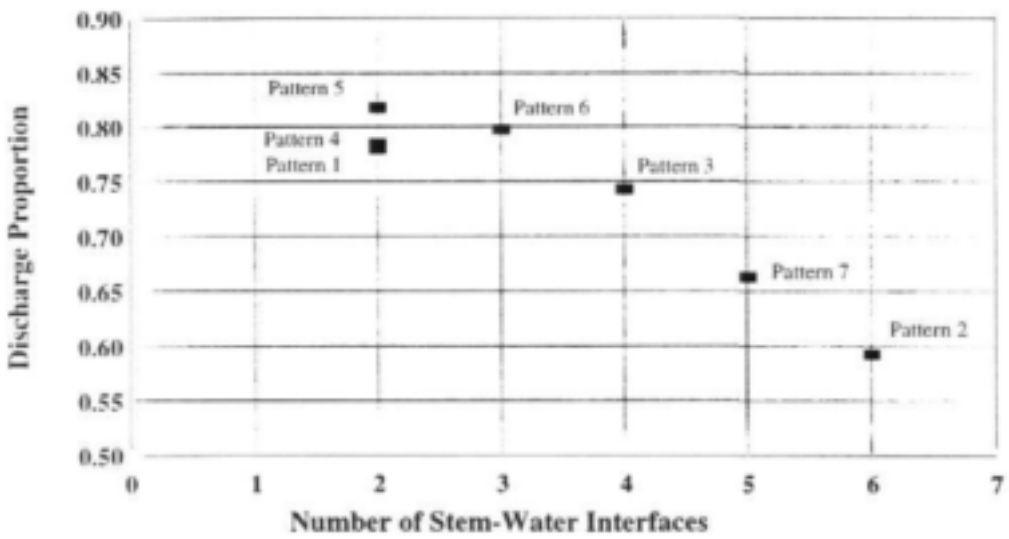

Figure 8.14 Influence of number of stem-water interfaces on proportion of total discharge in clear channels

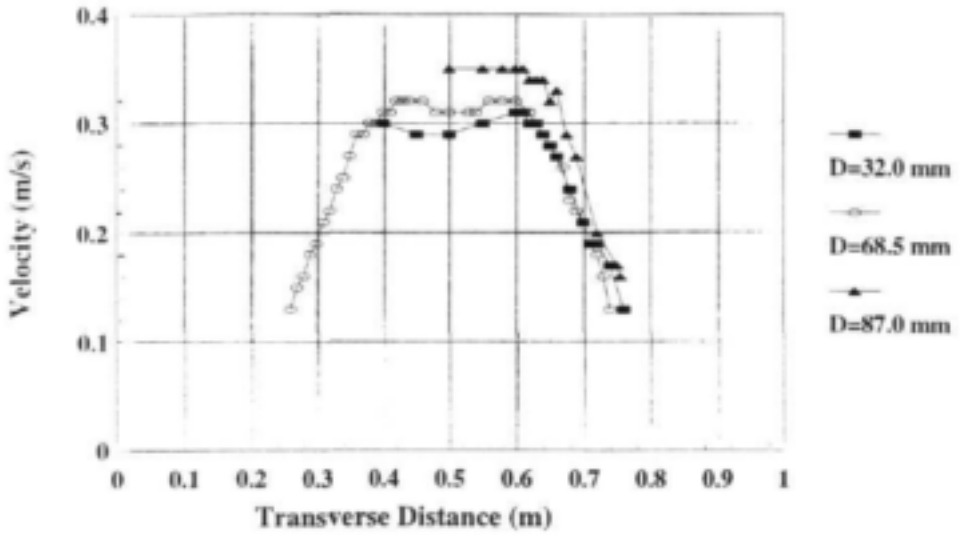

Figure 8.15 Transverse velocity distribution with 0.25 m side strips

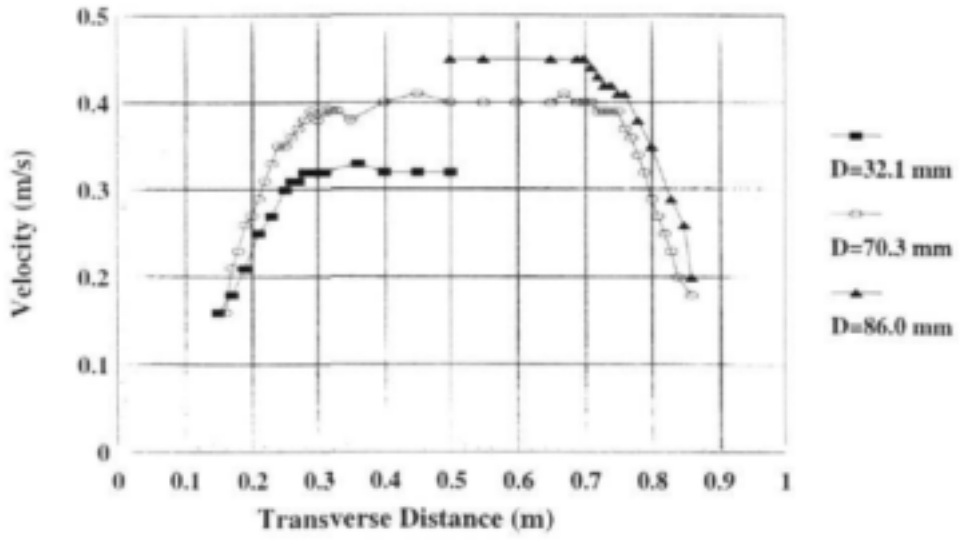

Figure 8.16 Transverse velocity distribution with 0.125 m side strips

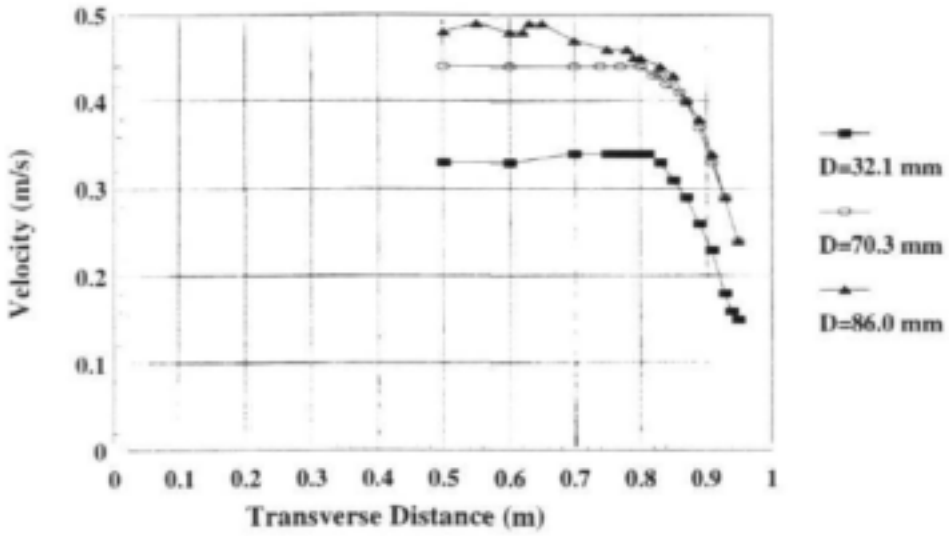

Figure 8.17 Transverse velocity distribution with 0.05 m side strips

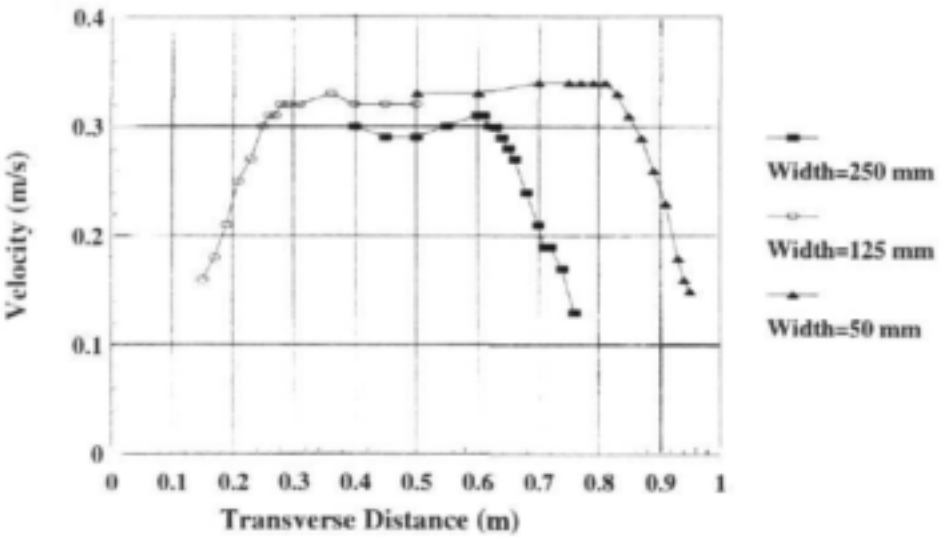

Figure 8.18 Comparison of transverse velocity profiles with side strips for flow depth approximately 33 mm

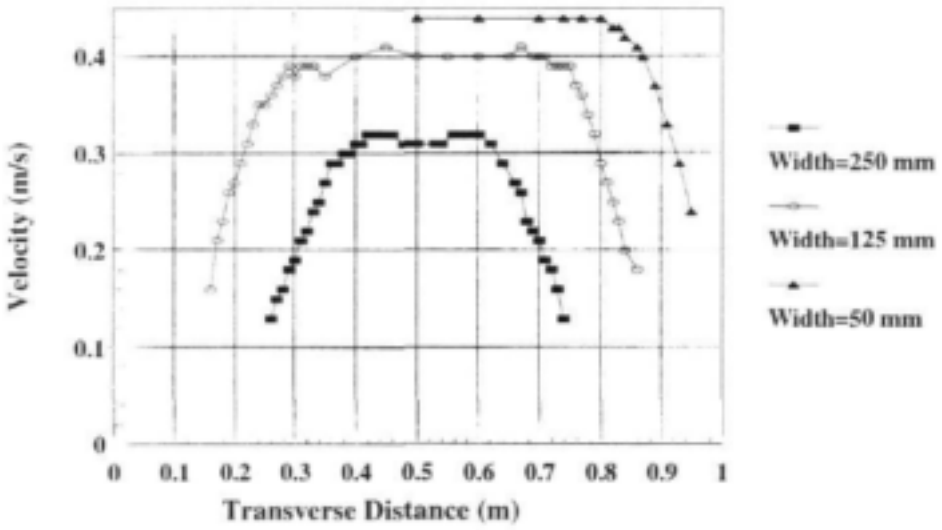

Figure 8.19 Comparison of transverse velocity profiles with side strips for flow depth approximately 70 mm

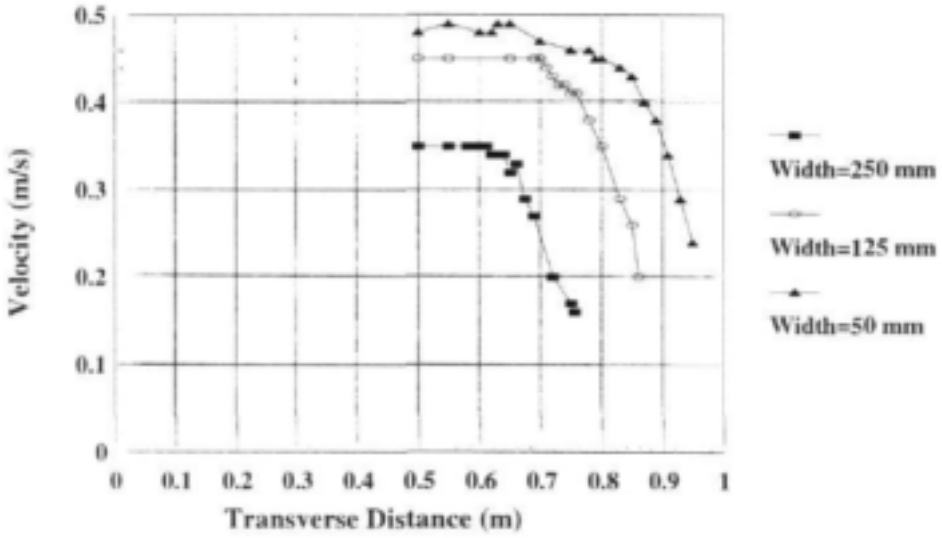

Figure 8.20 Comparison of transverse velocity profiles with side strips for flow depth approximately 88 mm

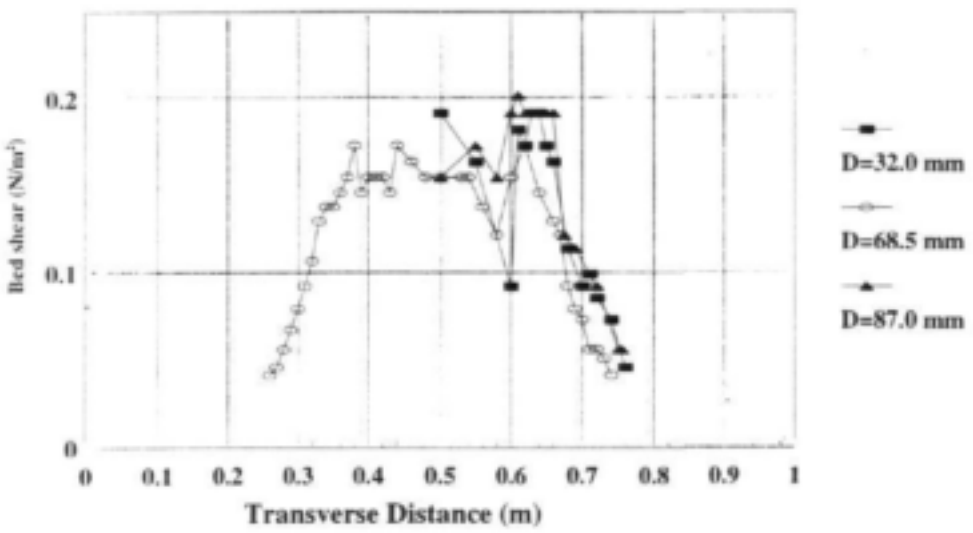

Figure 8.21 Bed shear stress distribution with 0.25 m side strips

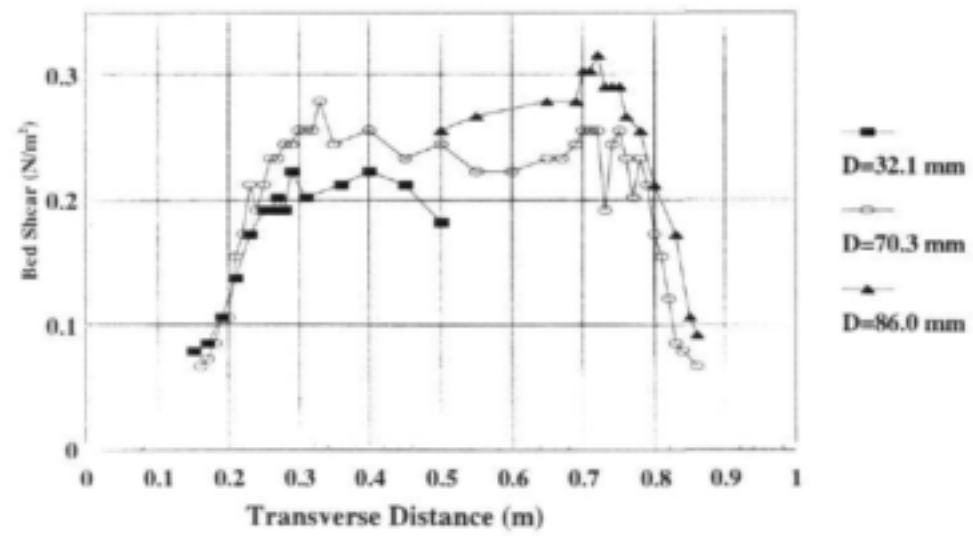

Figure 8.22 Bed shear stress distribution with 0.25 m side strips

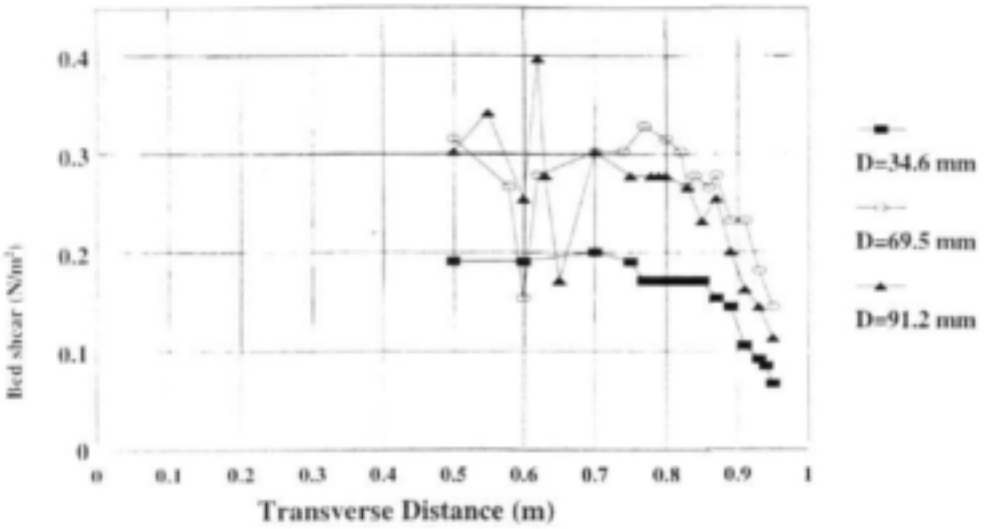

Figure 8.23 Bed shear stress distribution with 0.125 m side strips

8.3 DISCRETE PATCH REED DISTRIBUTIONS

8.3.1 Experimental Procedure

The discrete patch experiments were carried out in the same facility used for the longitudinal strip experiments. In this case, water surface elevations were measured piezometrically as well as by pointer gauge. Eight small aluminium tubes were placed on the bed at the centre of the channel at 1.5 m intervals along the length of the channel and connected via plastic pipes to stilling pots. These were used to check uniform flow as well as to measure flow depth.

The reed bed was simulated using the same rods as for the longitudinal strip experiments. The frames, or roughness units, were arranged in 15 different patterns as shown in Fig.8.24. The patterns varied discretely in the longitudinal direction as well as across the channel. The number of roughness units used to arrange the different patterns also varied. The minimum number of roughness units used to design the pattern was 12 and the maximum was 44. The area covered by the roughness units was therefore different for the different patterns. The maximum total channel area covered by the roughness units was 50%, while the minimum was 12.5%. The number of roughness units used for each pattern as well as a percentage of total area covered by reeds are presented in Table 8.1.

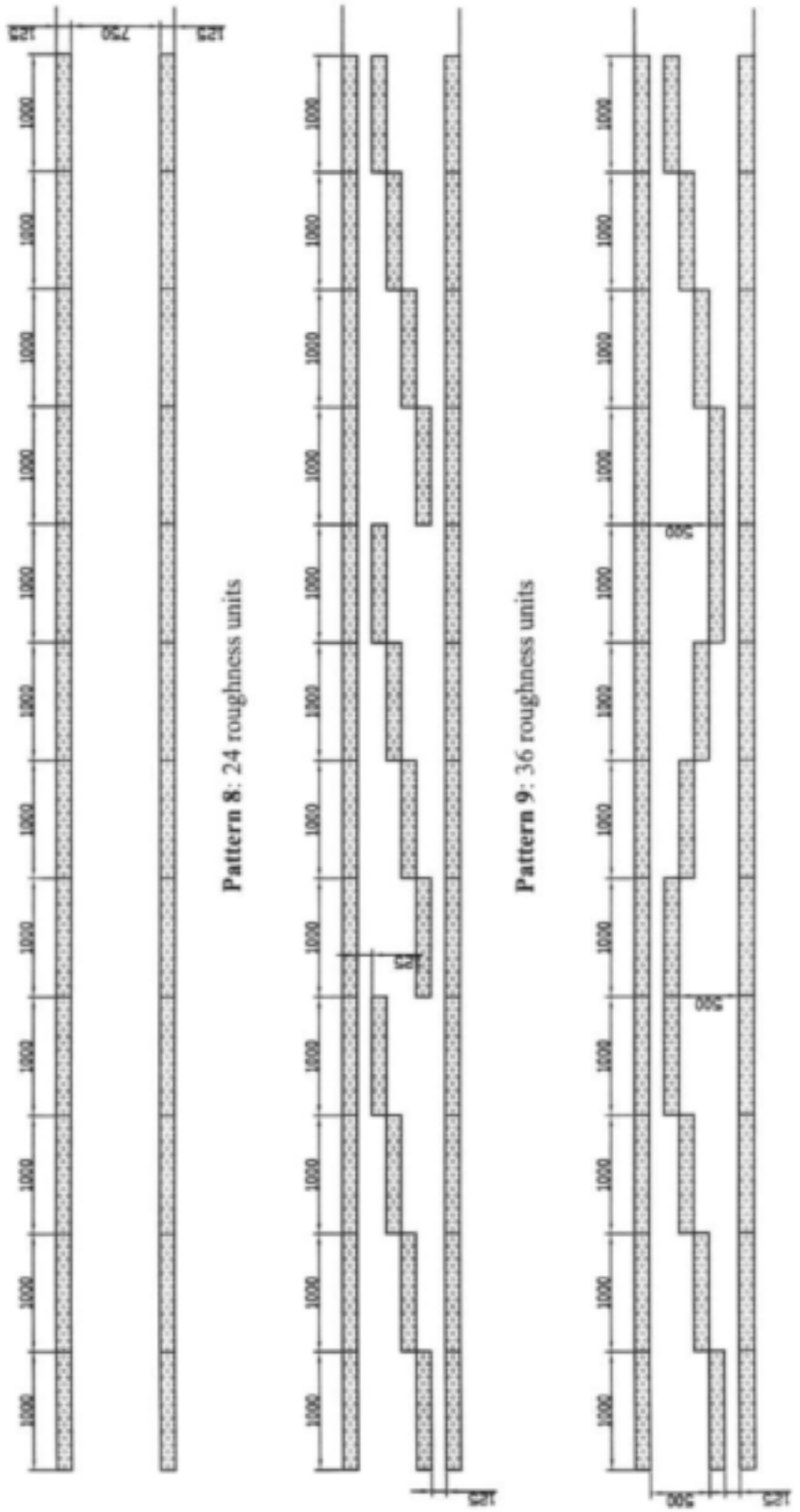

Figure 8.24 Discrete patch distribution patterns (sheet 1 of 5)

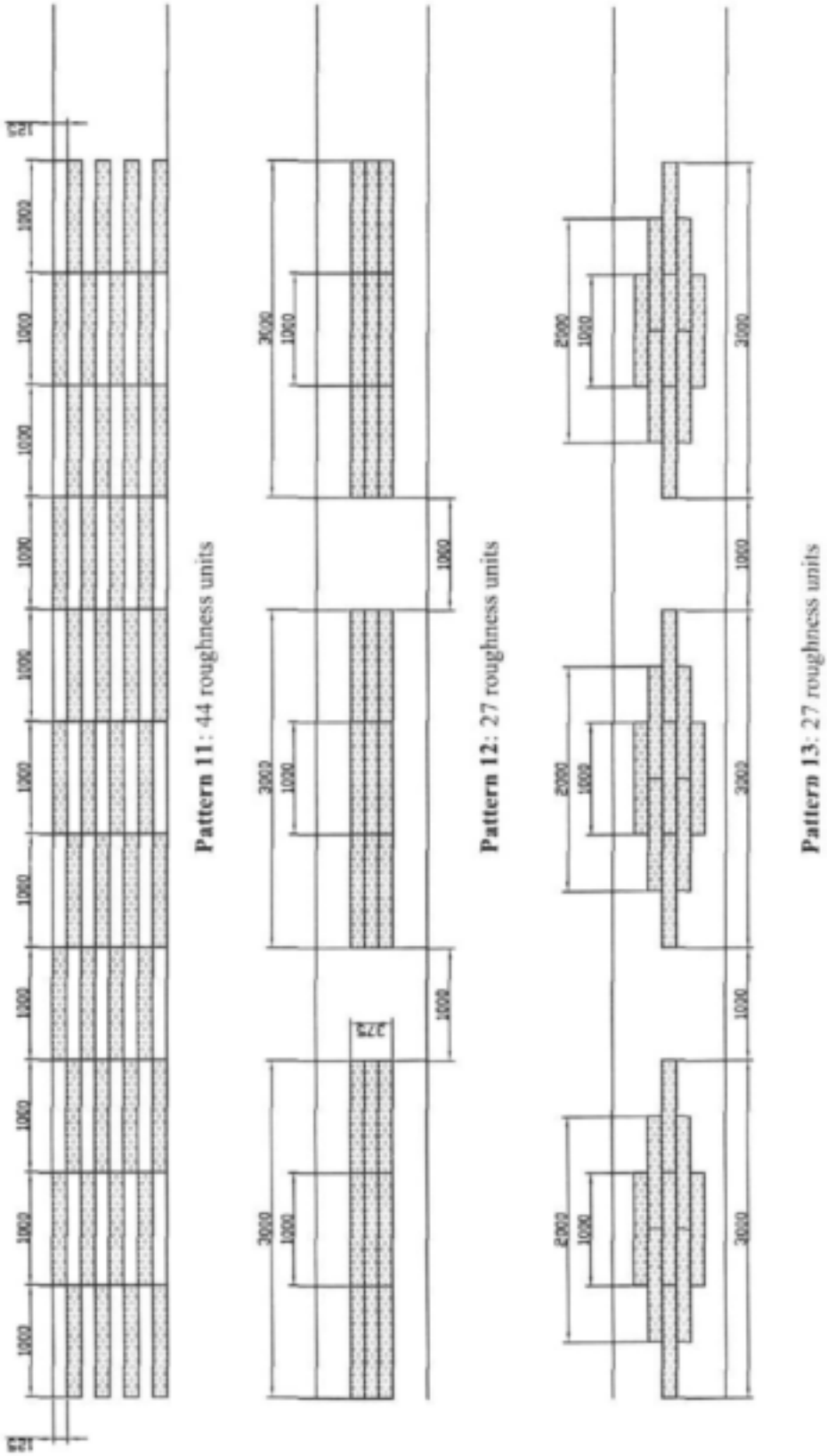

Figure 8.24 Discrete patch distribution patterns (sheet 2 of 5)

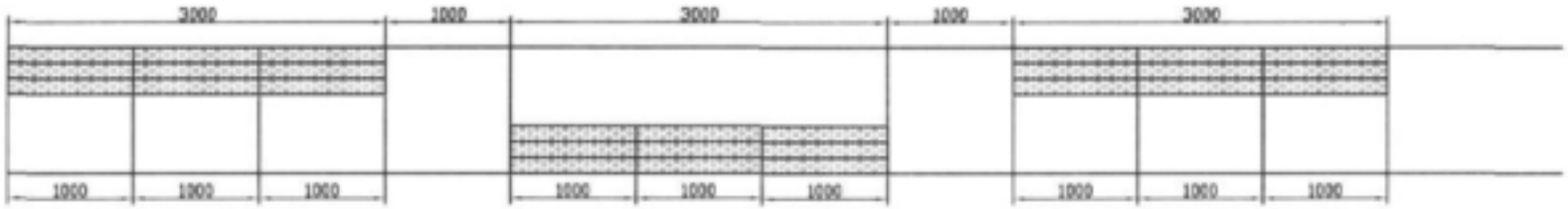

Pattern 14: 27 roughness units

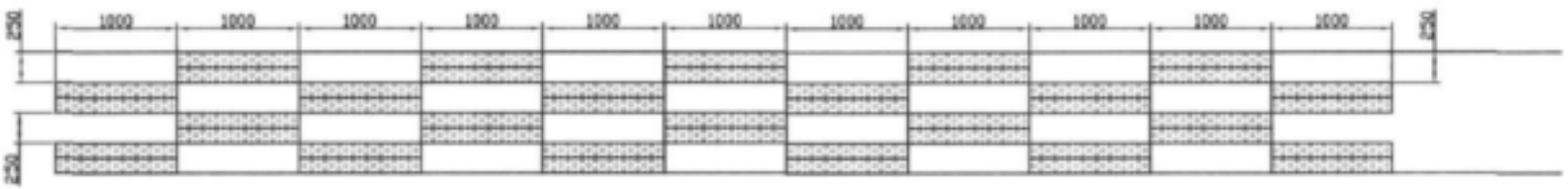

Pattern 15: 44 roughness units

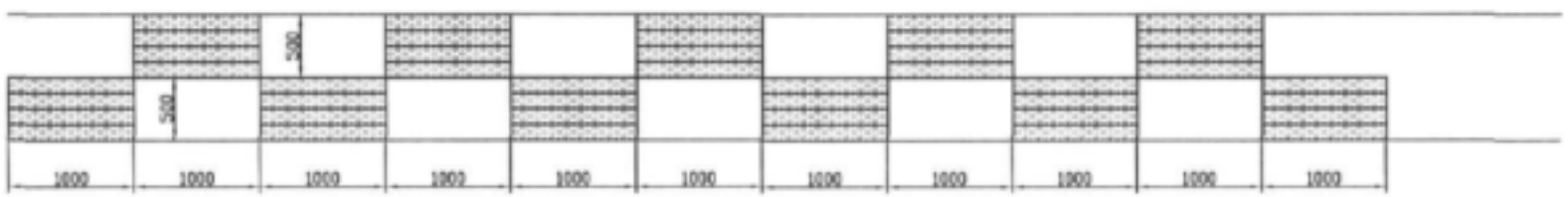

Pattern 16: 44 roughness units

Figure 8.24 Discrete patch distribution patterns (sheet 3 of 5)

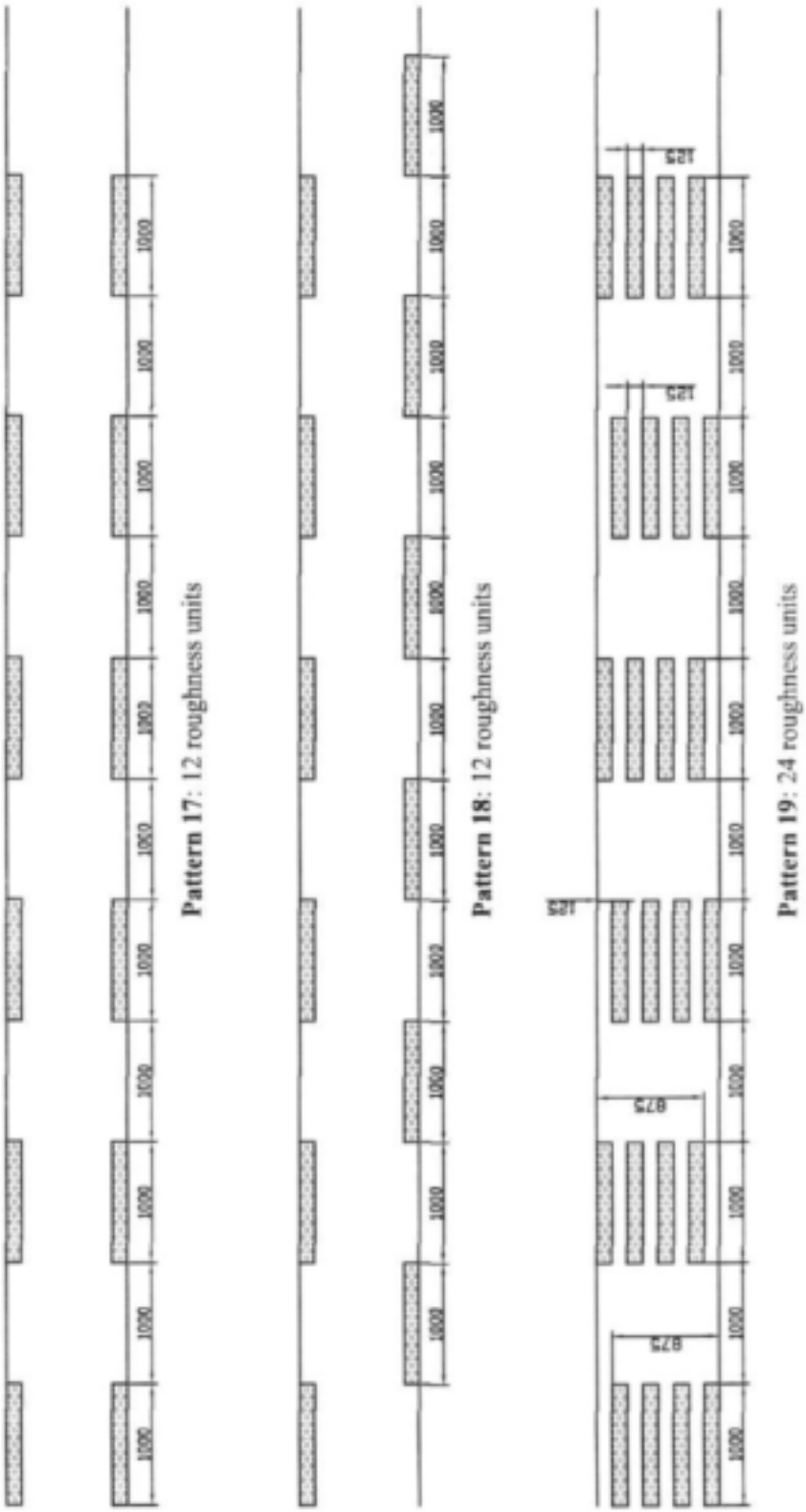

Pattern 17: 12 roughness units

Pattern 18: 12 roughness units

Pattern 19: 24 roughness units

Figure 8.24 *Discrete patch distribution patterns (sheet 4 of 5)*

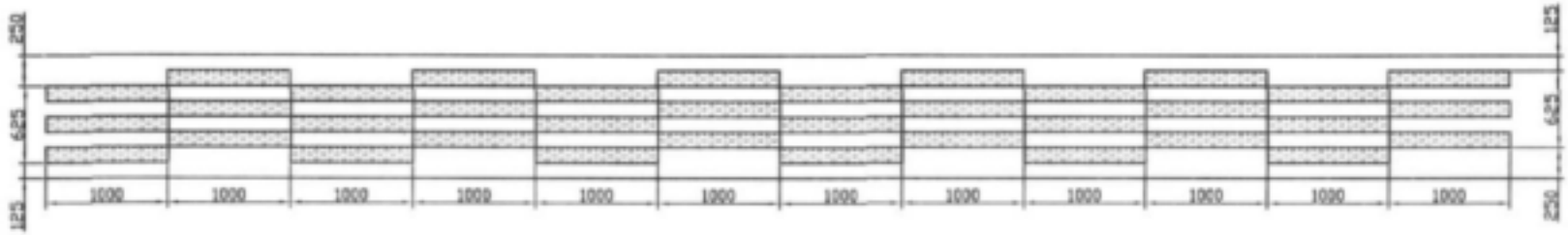

Pattern 20: 36 roughness units

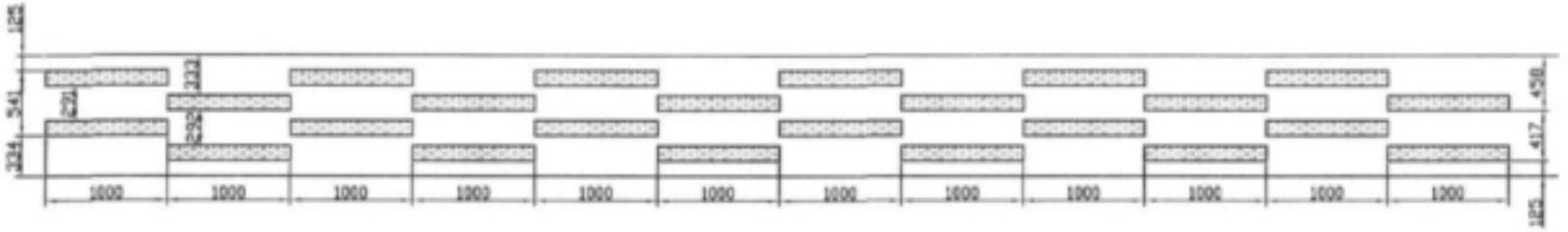

Pattern 21: 24 roughness units

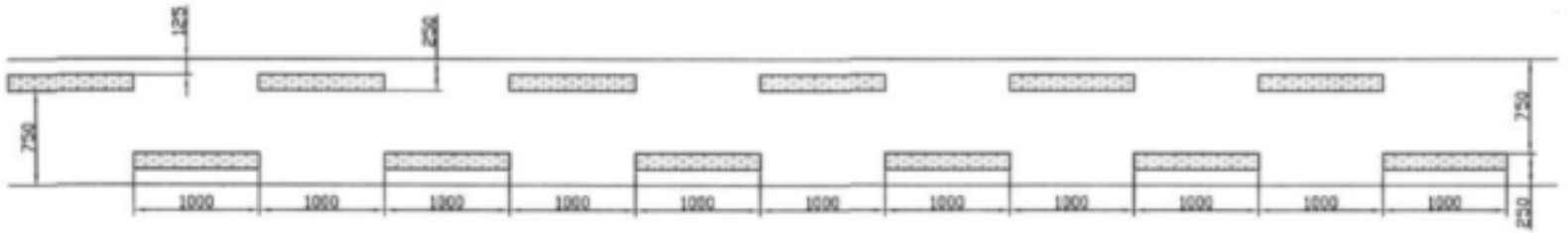

Pattern 22: 12 roughness units

Figure 8.24 Discrete patch distribution patterns (sheet 5 of 5)

Table 8.1 Reed Patterns

Pattern	Number of roughness units	% of total area covered by reeds	Range of discharge, Q (l/s)
Pattern 8	24	25.000	5-20.0
Pattern 9	36	37.500	5-20.0
Pattern 10	36	37.500	5-20.0
Pattern 11	44	50.000	5-11.0
Pattern 12	27	28.125	5-20.0
Pattern 13	27	28.125	5-20.0
Pattern 14	27	28.125	5-20.0
Pattern 15	44	50.000	5-11.0
Pattern 16	44	50.000	5-11.0
Pattern 17	12	12.500	5-20.0
Pattern 18	12	12.500	5-20.0
Pattern 19	24	25.000	5-12.5
Pattern 20	36	37.500	5-12.5
Pattern 21	24	25.000	5-12.5
Pattern 22	12	12.500	5-12.5

Flow depths were measured at different discharges for the different patterns. The range of discharges for each pattern is shown in Table 8.1. The measured stage-discharge data and the average velocity and Manning's n for each measurement are presented in Appendix B.4.

8.3.2 Effects of Discrete Reed Patches on Resistance

The influence of discrete patches of reeds on the flow resistance was investigated through the laboratory experiments. Fifteen different distribution patterns, shown in Fig.8.24, were tested in the experimental channel as explained in the previous section. The stage-discharge data obtained for each different pattern were used to establish the resistance characteristics in terms of Manning's n, i.e.

$$n = \frac{A R^{2/3} S^{1/2}}{Q} \qquad 8.2$$

where A is flow area (calculated as measured flow depth, y, multiplied by the channel width), R is hydraulic radius (obtained as A/P, where P is wetted perimeter), S is channel slope and Q is

measured discharge. The average flow velocity was calculated for each measurement as

$$V_{avr} = \frac{Q}{A} \qquad 8.3$$

To obtain a clear understanding of the influence of different parameters of discrete reed patches on flow resistance, the experimental results were compared on the basis of shape, size, number of discrete patches, and similarity of pattern. The distribution patterns were therefore divided into the following groups:

- Patterns with 44 roughness units (Patterns 11, 15 and 16)
- Patterns with 36 roughness units (Patterns 9, 10 and 20)
- Patterns with 27 roughness units (Patterns12 and 14)
- Patterns with 27 roughness units (Patterns12 and 13)
- Patterns with 24 roughness units (Patterns 8, 19 and 21)
- Patterns with12 roughness units (Patterns 17, 18 and 22)
- Patterns with 44 and 24 roughness units (Patterns11and 19)
- Staggered patterns (Patterns 11, 20, 21 and 22)

8.3.2.1 Effects of Distribution of Discrete Patches on Resistance

The influence of the distribution of discrete patches was investigated through arrangements of 36 roughness units as shown for Patterns 9, 10 and 20. The effects of these distributions on flow resistance are presented in Fig. 8.25. Patterns 9 and 10 are very similar, whereas Pattern 20 is different (Fig. 8.24) in that it has six stem-clear water interfaces plus two solid boundaries rather than the four stem-clear water interfaces for Patterns 9 and 10. The curves for Patterns 9, 10 and 20 (Fig. 8.25) show that the highest flow resistance is for Pattern 20 and the lowest for Pattern 10. The similar distribution of the discrete patches for Patterns 9 and 10, which both have four stem-clear water interfaces and differ only in design of the middle strip, offers different overall resistence. The difference between the overall resistance for these two patterns which have equal number of stream-clear water interfaces suggests that the number of stem-clear water interfaces is not the only parameter that affects the overall resistance. It is evident that the discontinuity of the discrete patches of the middle strip in Pattern 9 has a significant effect on overall resistance. The resistance characteristics in terms of Manning's n and average velocity are plotted against flow depth in Figs 8.26 and 8.27 respectively. The overall Manning's n value (Fig. 8.26) varies significantly with flow depth for these distributions of discrete patches.

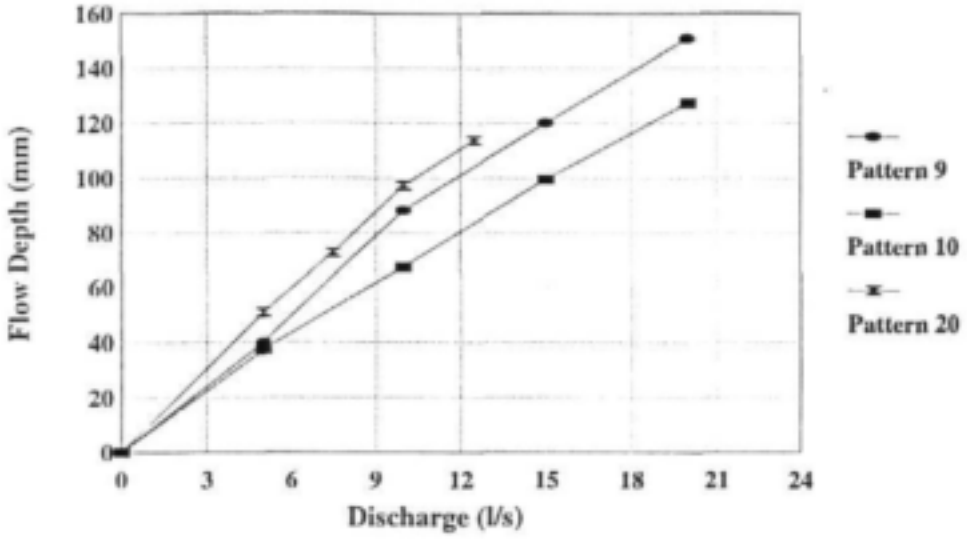

Figure 8.25 Stage-discharge relationships for Patterns 9, 10 and 20

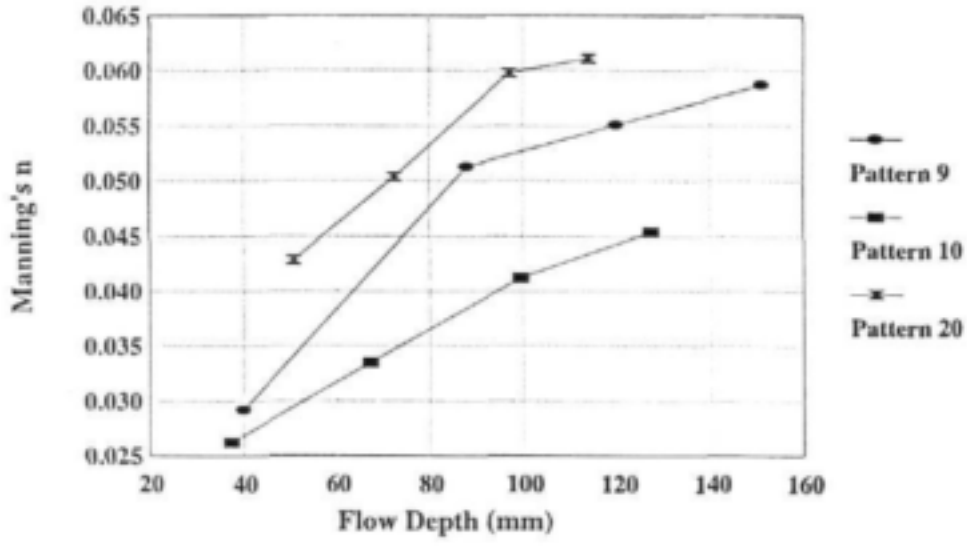

Figure 8.26 Manning's *n* variation with flow depth for Patterns 9, 10 and 20

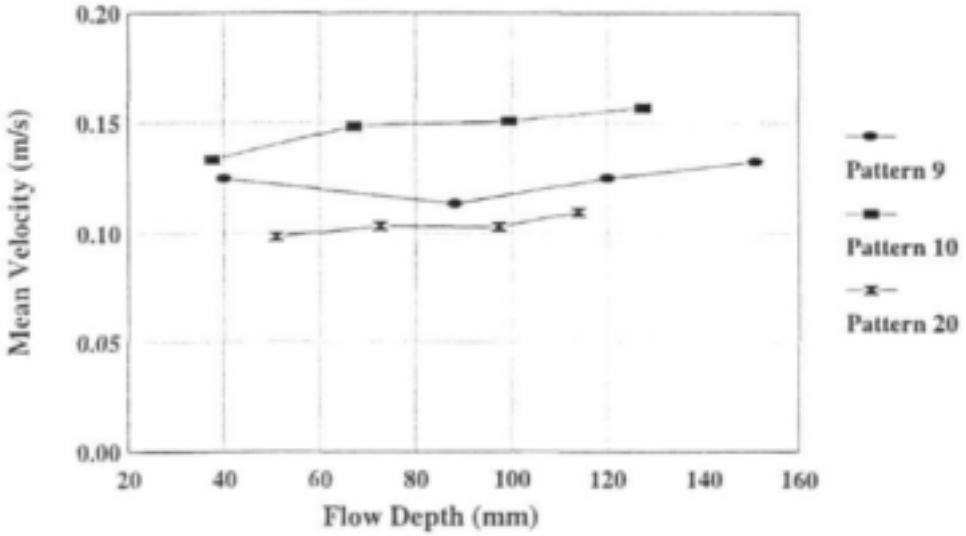

Figure 8.27 Mean velocity variation with flow depth for Patterns 9, 10 and 20

The influence of two different distributions of discrete patches, Pattern 12 and Pattern14, on flow resistance is shown in the stage-discharge relationships presented in Fig. 8.28. In Pattern 12, three patches of regular shape, consisting of nine roughness units each, were placed on the central line of the channel with free spaces of 1.0 m length between successive patches. For Pattern 14, these patches were situated on the margins of the channel (Fig. 8.24). The stage-discharge curves for Patterns 12 and 14 (Fig. 8.28) show that the general distribution pattern of discrete patches with the same shape and size is not a significant parameter in determining overall resistance. Variations of Manning's n and average velocity with flow depth are plotted in Figs 8.29 and 8.30 respectively.

Twenty four roughness units were arranged in Patterns 8, 19 and 21. The stage-discharge relationships for these patterns are presented in Fig. 8.31. From these curves it can be seen that flow resistance is higher for Patterns19 and 21, where the roughness units are within the channel, than for Pattern 8, with the roughness units positioned along the channel sides only. Comparison of the curves for Patterns 19 and 21, which both have the same patch size but a different distribution (Pattern 19 has four patches every second metre of the channel length, while Pattern 21 has two every metre), shows that the distribution of the discrete patches within the channel has an influence on overall resistance. The higher resistance for Pattern 19 may be attributed either to the discontinuity of the patch distribution or to the higher number of stem-clear water interfaces for Pattern 19. Overall Manning's n and its variation with flow depth is given in Fig. 8.32. From these curves it can be seen that the Manning's n values are around 0.015 for Pattern 8 while for Patterns 19 and 21 the values vary significantly with flow depth, because of the dominance of the stem drag contribution to resistance. The average velocity, calculated for each measurement, is plotted against flow depth in Fig. 8.33.

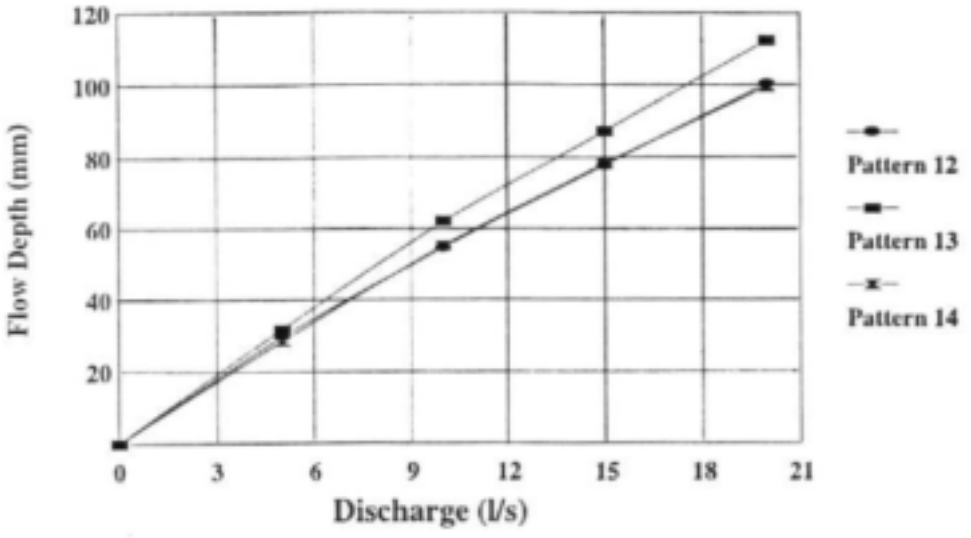

Figure 8.28 Stage-discharge relationships for Patterns 12, 13 and 14

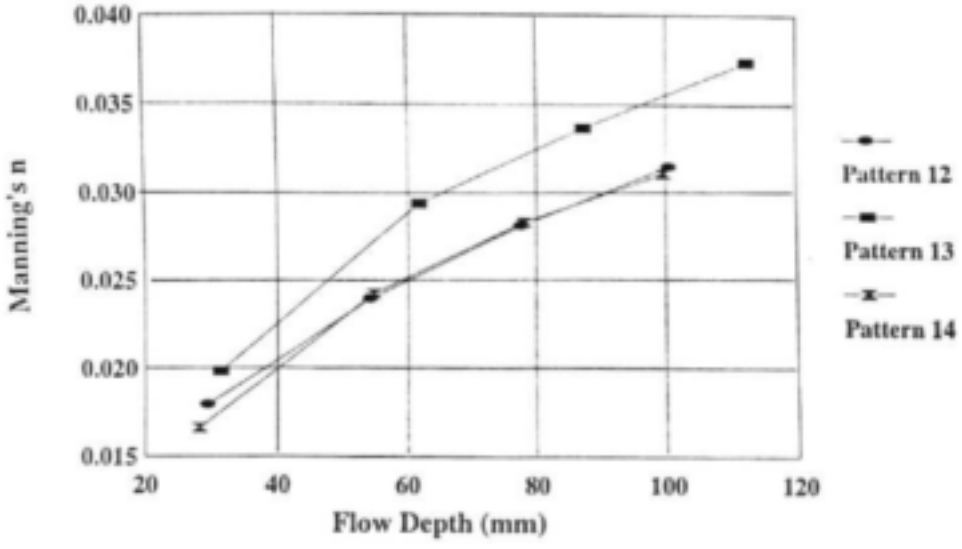

Figure 8.29 Manning's n variation with flow depth for Patterns 12, 13 and 14

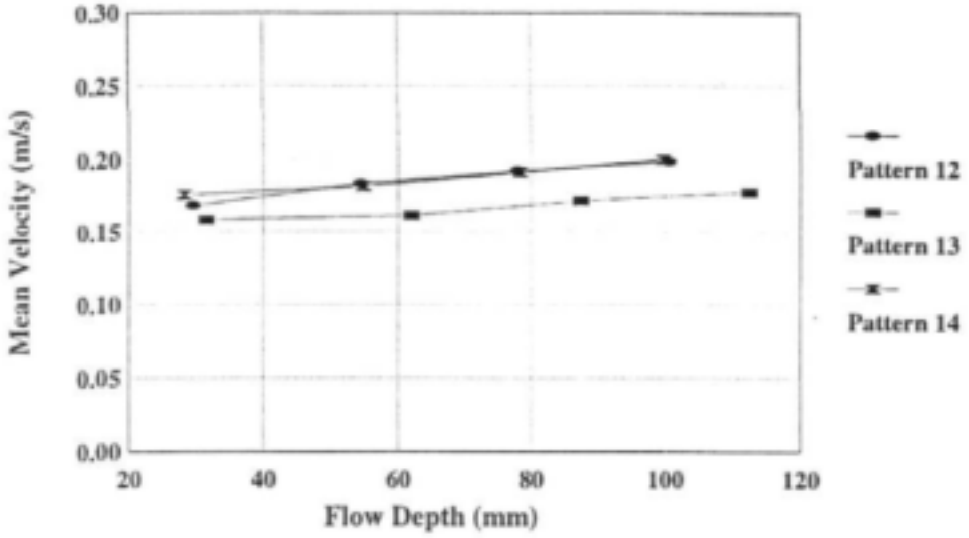

Figure 8.30 Mean velocity variation with flow depth for Patterns 12, 13 and 14

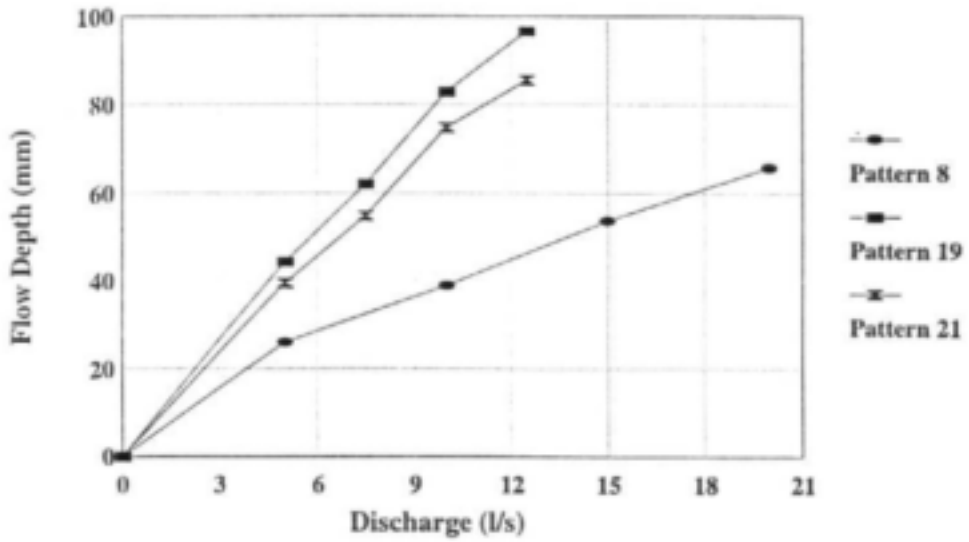

Figure 8.31 Stage-discharge relationships for Patterns 8, 19 and 21

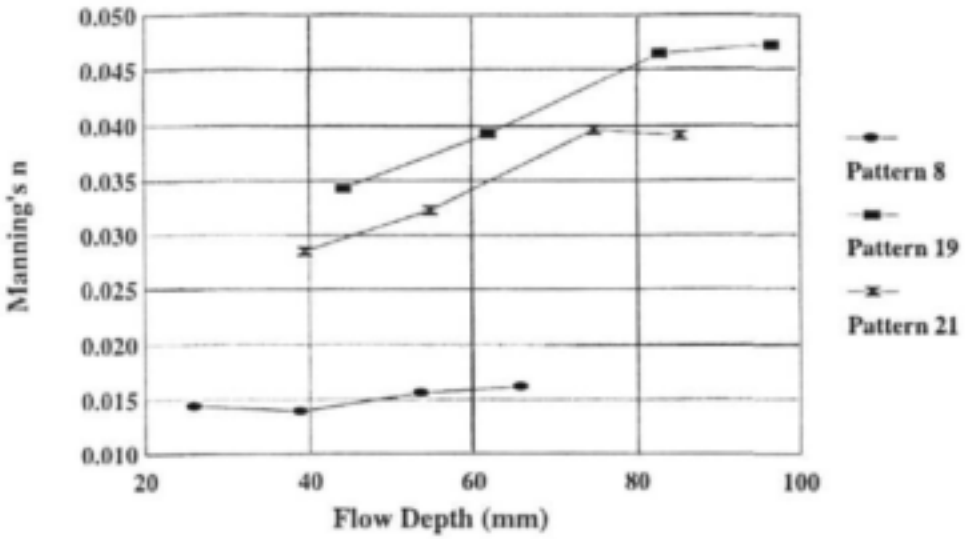

Figure 8.32 Manning's n variation with flow depth for Patterns 8, 19 and 21

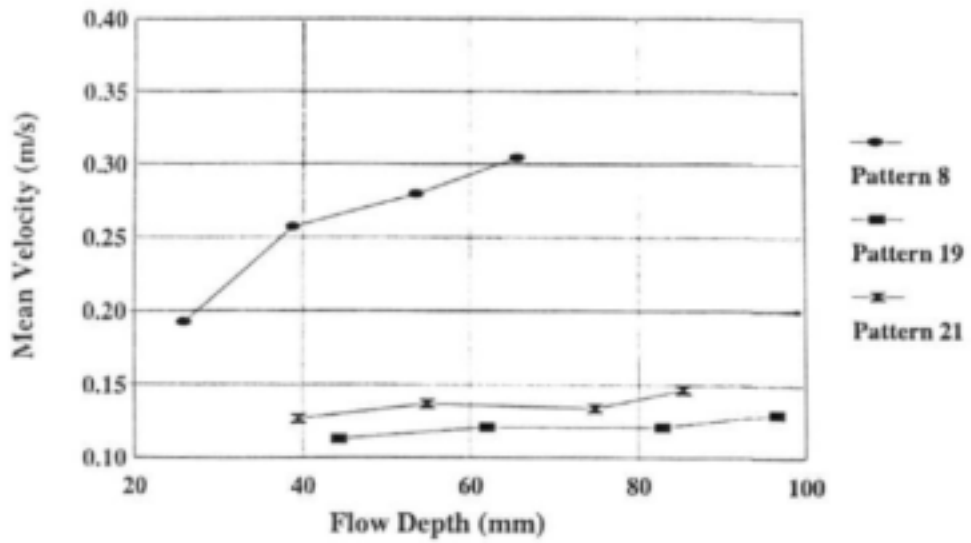

Figure 8.33 Mean velocity variation with flow depth for Patterns 8, 19 and 21

The effect of three different distributions of twelve roughness units (Patterns 17, 18 and 22) on overall resistance is shown in Fig. 8.34. The close correspondence of the curves for Patterns 17 and 18, which both have six patches along the channel margins and differ only in their arrangement along the sides (Pattern 17 has a parallel distribution and Pattern 18 an alternate one (Fig. 8.24)), suggests that this difference in the arrangement of the patterns is not a significant parameter in determining overall resistance. Comparison of the curves for Pattern 22 and Pattern18 (both have the alternate distribution of discrete patches and differ only in positions of the patches relative to the channel margin), shows that this difference does influence overall resistance. Overall resistance is higher for the pattern with discrete patches arranged some distance from the channel side. The resistance characteristics of this distribution pattern are presented in terms of Manning's n plotted against flow depth in Fig. 8.35. The average velocity and its variation with flow depth is given in Fig. 8.36.

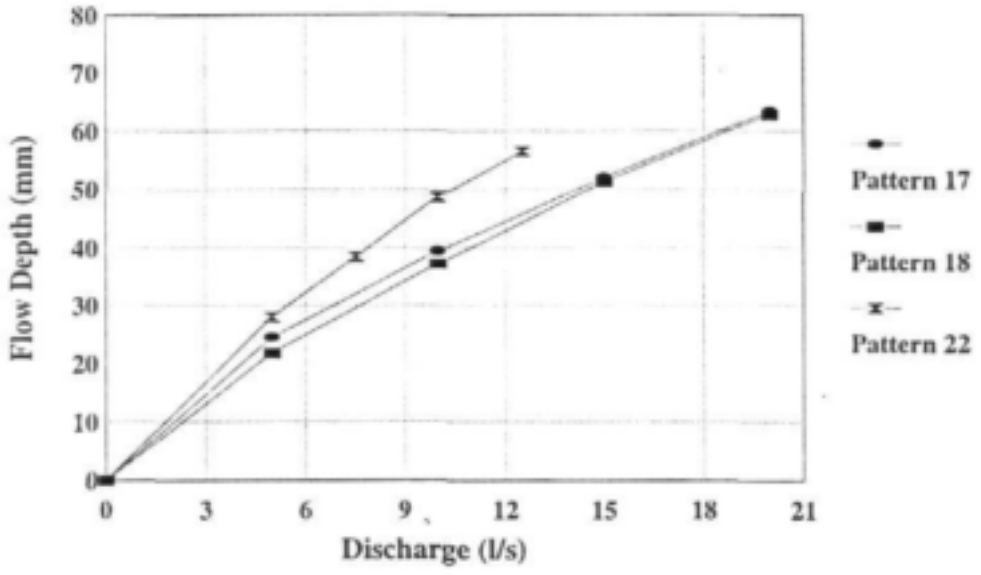

Figure 8. 34 Stage-discharge relationships for Patterns 17, 18 and 22

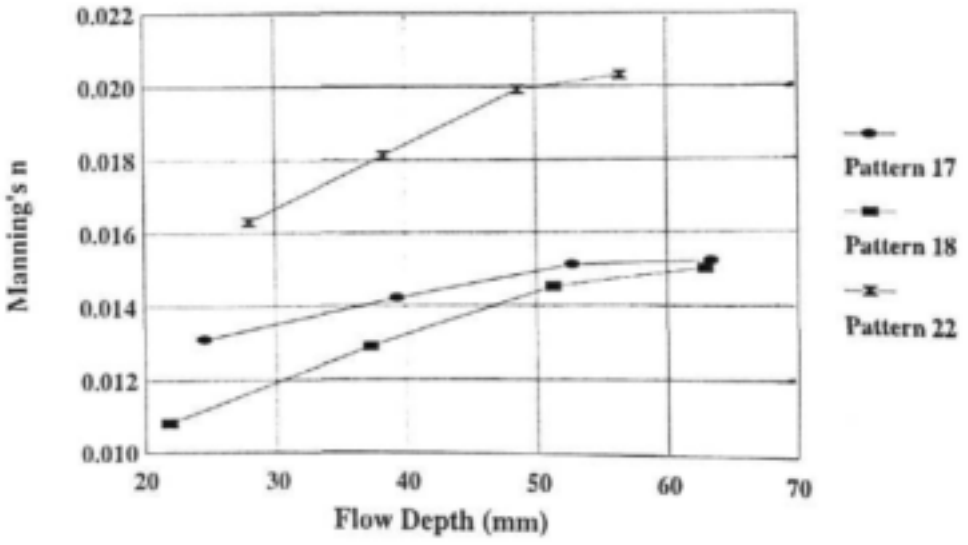

Figure 8.35 Manning's *n* variation with flow depth for Patterns 17, 18 and 22

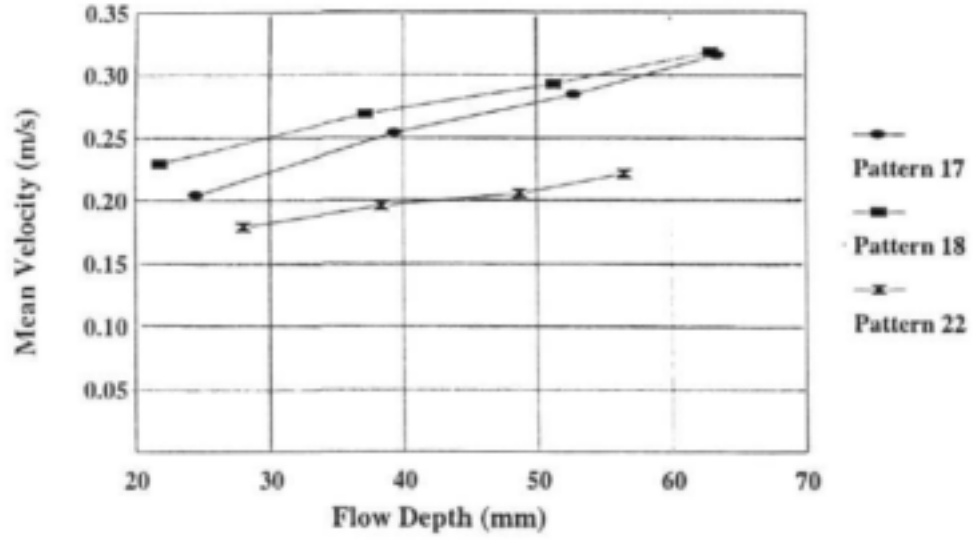

Figure 8.36 Mean velocity variation with flow depth for Patterns 17, 18 and 22

8.3.2.2 Effects of Size of Discrete Patches on Resistance

The influence of patch distribution on flow resistance was discussed in the previous section; this section presents the hydraulic effects of the size of reed patches on overall flow resistance.

The influence on stage-discharge relationship of three different sizes of discrete patches arranged with 44 roughness units (Patterns 11,15 and 16) is shown in Fig. 8.37. These three distribution patterns each have four roughness units per metre, however they differ in that the roughness units are arranged in a different way across the channel. Pattern 11 was arranged with each roughness unit separated from the next one by a clear channel with a width of one roughness unit. In this pattern, each patch had a size of one roughness unit. In Pattern 15, patches were created with two roughness units positioned together and separated from the following patch by a clear channel with a width of two roughness units. Four roughness units were placed together, covering half of the channel width, in Pattern 16, and in this pattern the size of one patch was four roughness units. The arrangement of the next metre of the channel length was mirror image of the previous one (Fig. 8.24). The number of stem-clear water interfaces decreases from seven in Pattern 11 to one in Pattern 16. Each of these patterns has one solid boundary at any longitudinal position. The size of discrete patches increases from one roughness unit for Pattern 11 to four for Pattern 16. It is evident (Fig. 8.37) that the overall resistance is higher for Pattern 16 than for Pattern 11, and this suggests that the size of the discrete patches has a significant effect on the overall resistance. Graphs of Manning's n against flow depth are given in Fig. 8.38. Average velocity and its variation with flow depth are presented in Fig. 8.39.

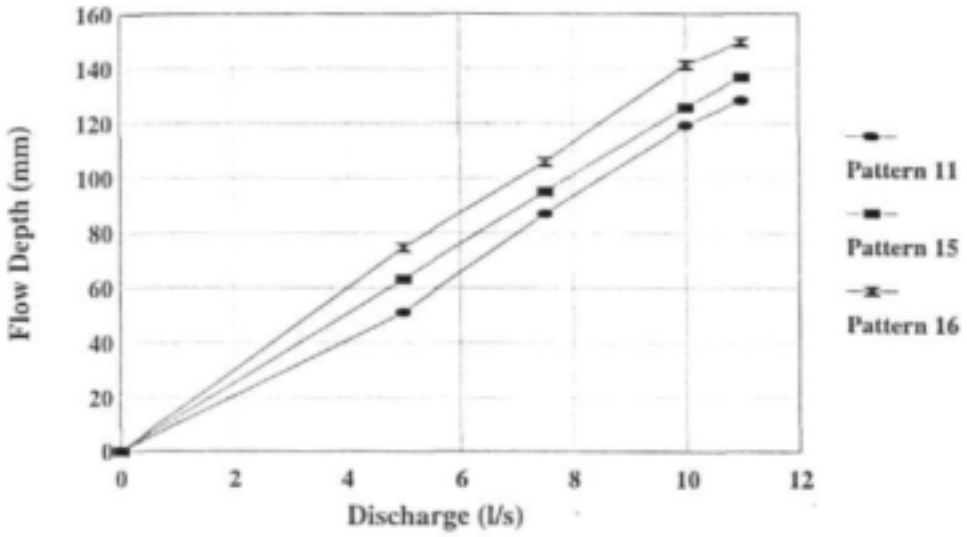

Figure 8.37 Stage-discharge relationships for Patterns 11, 15 and 16

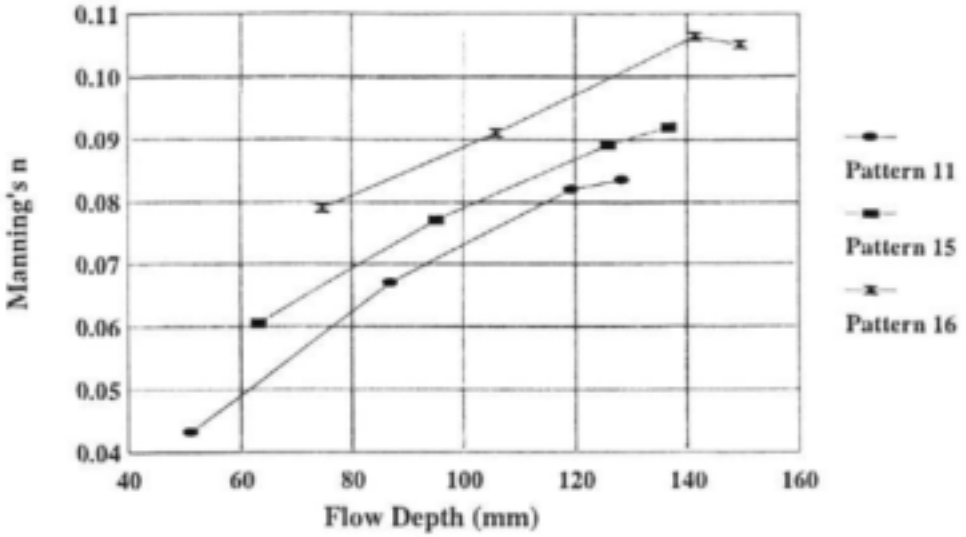

Figure 8.38 Manning's n variation with flow depth for Patterns 11, 15 and 16

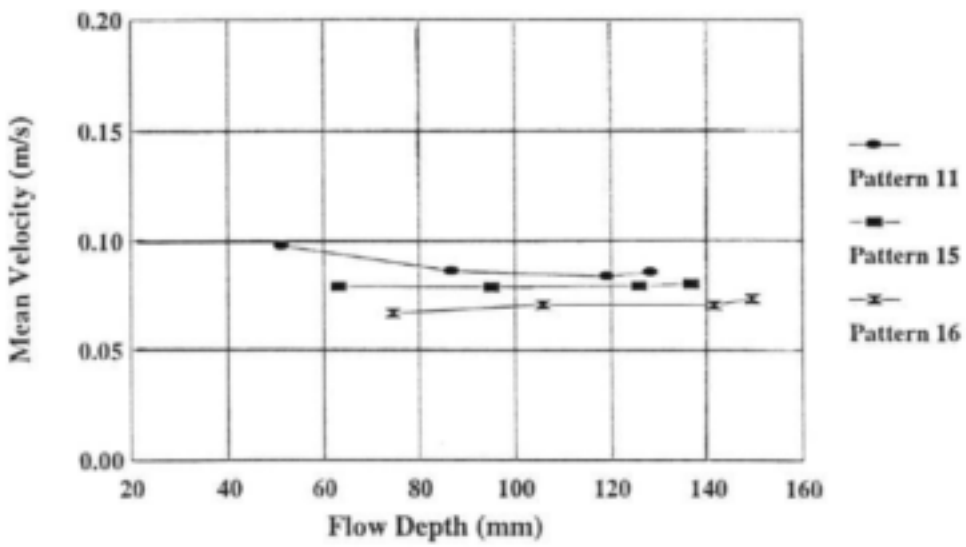

Figure 8.39 Mean velocity variation with flow depth for Patterns 11, 15 and 16

8.3.2.3 Effects of Number of Discrete Patches on Resistance

The influence of number of discrete patches on overall resistance was investigated through staggered arrangement of discrete patches. Staggered Patterns 11, 20, 21 and 22, were arranged with different numbers of discrete patches as shown in Fig. 8.24 and Table 8.1. The number of discrete patches used for these staggered patterns increases from 12 (one discrete patch per metre) for Pattern 22 to 44 (four discrete patches per metre) for Pattern 11. Stage-discharge relationships are presented in Fig. 8.40. It is clear that the overall resistance increases progressively with increasing stem area. Resistance characteristics in terms of Manning's n variation with flow depth are presented in Fig. 8.41. The average velocity calculated for each measurement is plotted against the flow depth in Fig. 8.42, indicating that the velocity variation is uniform for Pattern 11 and steeply increasing for Pattern 22. The maximum total area covered by discrete patches was 50% for Pattern 11, while the minimum was 12.5 % for Pattern 22. Manning's n and its variation with proportion of area covered by discrete patches are given in Fig. 8.43 for a discharge of 10 l/s. It is clear that for similar distribution patterns the proportions of area covered by discrete patches has a significant effect on overall resistance. The curves in Fig. 8.43 show that proportion of area covered by roughness unit increase the resistance, and that Manning's n is linearly related to the proportion of area covered by reeds.

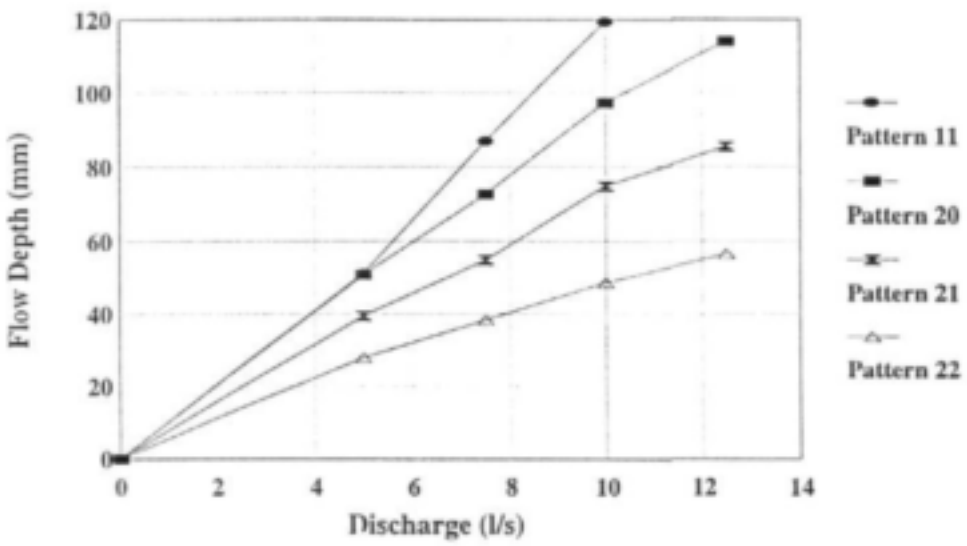

Figure 8.40 Stage-discharge relationships for Patterns 11, 20, 21 and 22

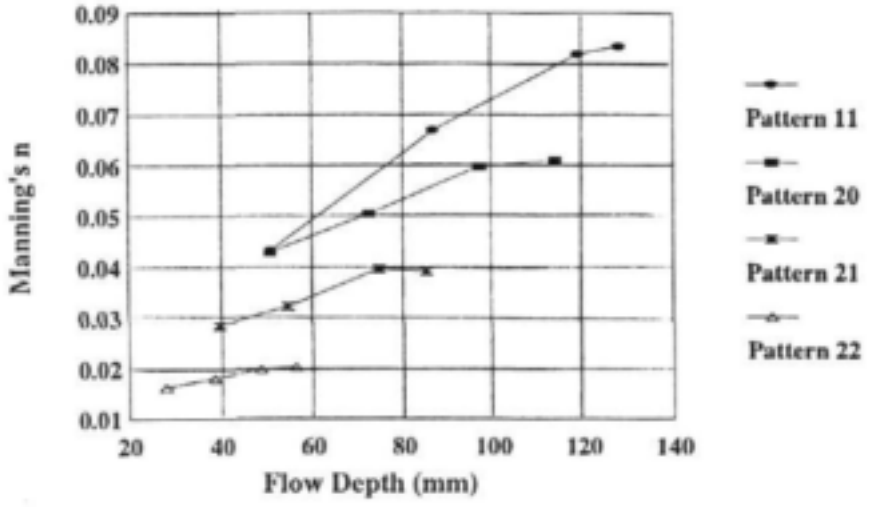

Figure 8.41 Manning's *n* variation with flow depth for Patterns 11, 20, 21 and 22

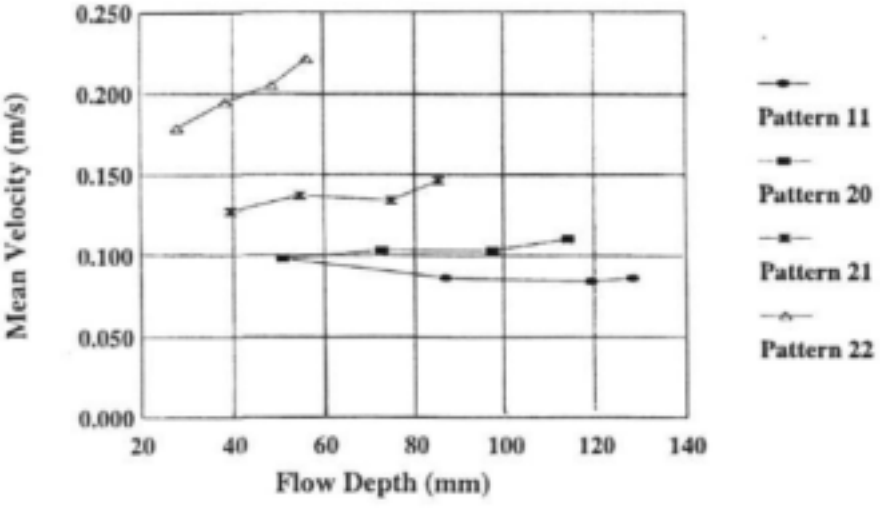

Figure 8.42 Mean velocity variation with flow depth for Patterns 11, 20, 21 and 22

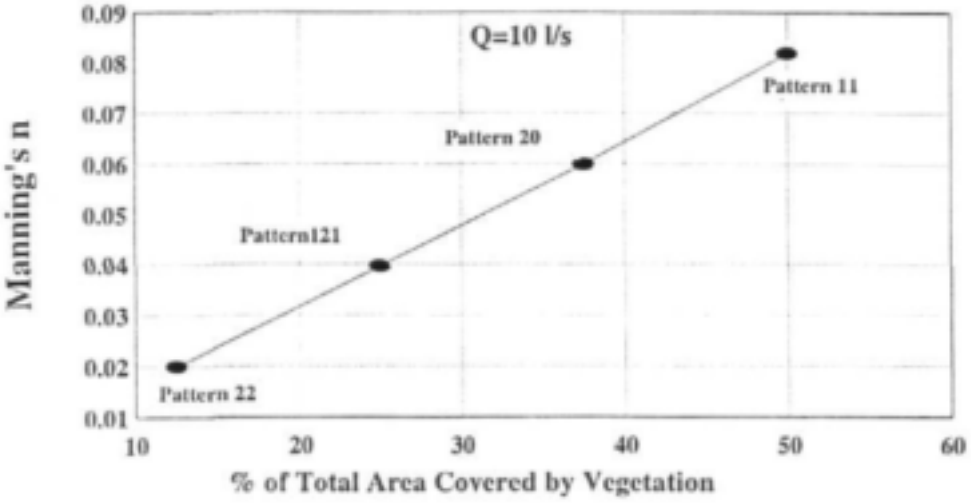

Figure 8.43 Manning's n variation with proportion of total area covered by roughness units for Patterns 11, 20, 21 and 22

The effect on flow resistance of an increase in number of discrete patches from 22 for Pattern 19 to 44 for Pattern 11 is presented in Fig. 8.44. The total area covered by roughness units is 50% for Pattern 11 and 25% for Pattern 19. The discrete patch distributions of these two patterns differ in that Pattern 19 is discontinuous along the channel length with 1.0 m intervals between successive patches (Fig. 8.24). The stage-discharge curve for Pattern11 (Fig. 8.44) shows that number of discrete patches along the channel significantly increases the resistance, and that this effect becomes greater with increasing discharge. Manning's n is plotted against flow depth in Fig. 8.45. The higher variation of Manning's n for Pattern 11 than for Pattern19 suggests the dominance of stem drag resistance in the whole channel. Calculated average velocity and its variation with flow depth are presented in Fig.8.46.

8.3.2.4 Effects of Shape of Discrete Patch on Resistance

The influence of shape of discrete patches on overall resistance was tested in Patterns 12 and 13. In Pattern 12, three patches with a regular shape consisting of nine roughness units were placed along the centre line of the channel with free spaces of 1.0 m between them, while in Pattern 13 the patches had an irregular shape situated in the same locations as in Pattern 12 (Fig. 8.24). The effect of this shape difference on overall resistance is shown by the stage-discharge relationships presented in Fig. 8.28. The curves for Patterns 12 and 13 show that irregularity of the shape of the patch significantly increases the resistance, and that this effect becomes greater with increasing discharge. The effect of the shape of discrete patches on overall resistance may be attributed to the change of form drag resulting from the change in the shape of the patch.

Variations of Manning's *n* and average velocity with flow depth are plotted in Figs 8.29 and 8.30 respectively.

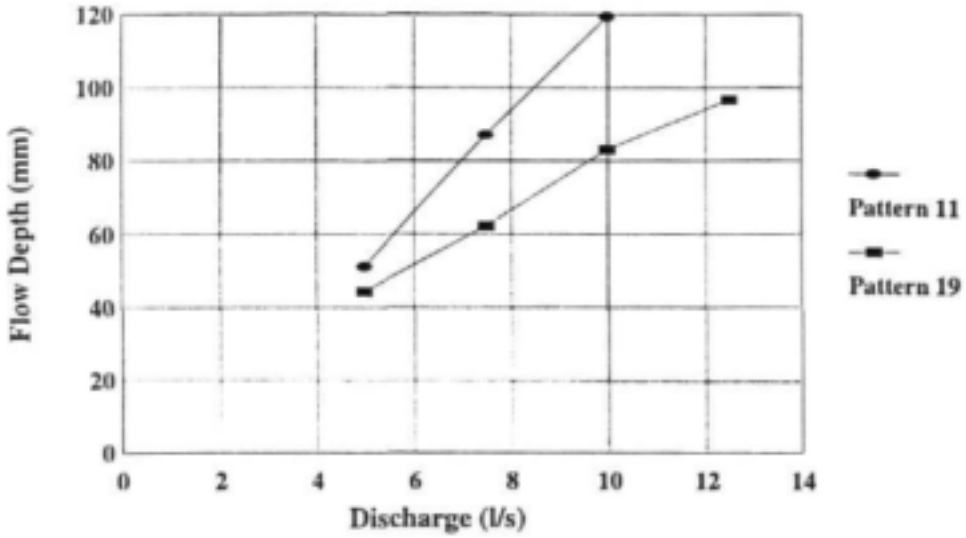

Figure 8.44 Stage-discharge relationships for Patterns 11 and 19

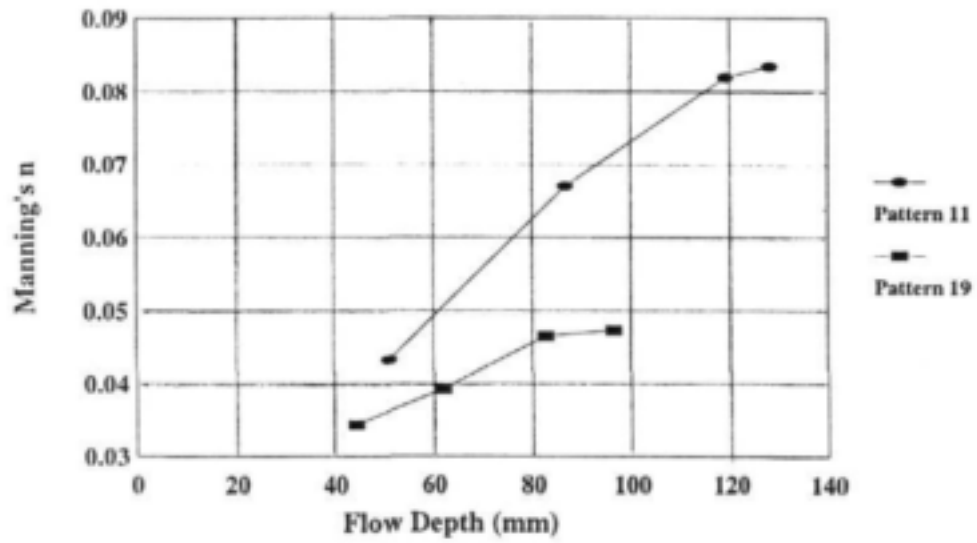

Figure 8.45 Manning's *n* variation with flow depth for Pattern 11 and 19

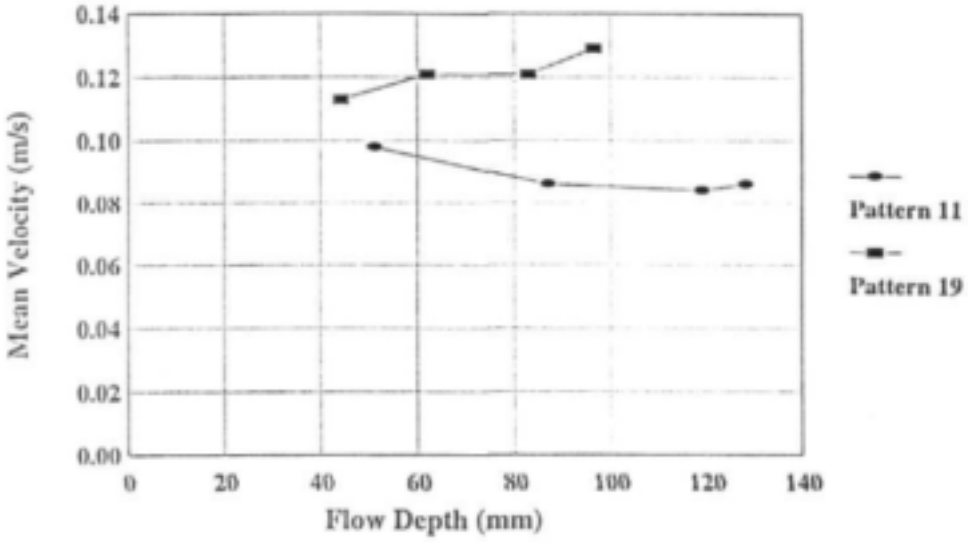

Figure 8.46 Mean velocity variation with flow depth for Patterns 11 and 19

8.3.2.5 Effects of Total Area of Discrete Patches on Resistance

For clear understanding of the influence of discrete patches on flow resistance, the measured depths at 10 l/s discharge were plotted against proportion of total area covered by reeds for all patterns in Fig. 8.47. From this plot, it is evident that resistance increases with increasing total area covered by vegetation, but it is also evident that resistance varies for a particular reed area over a very wide range. It is clear, therefore, that overall resistance depends not only on total area of discrete patches, but also significantly on different reedbed parameters such as size, shape, number and distribution of discrete patches. The dependence of Manning's n on proportion of area covered by discrete patches at 10 l/s discharge is presented in Fig. 8.48.

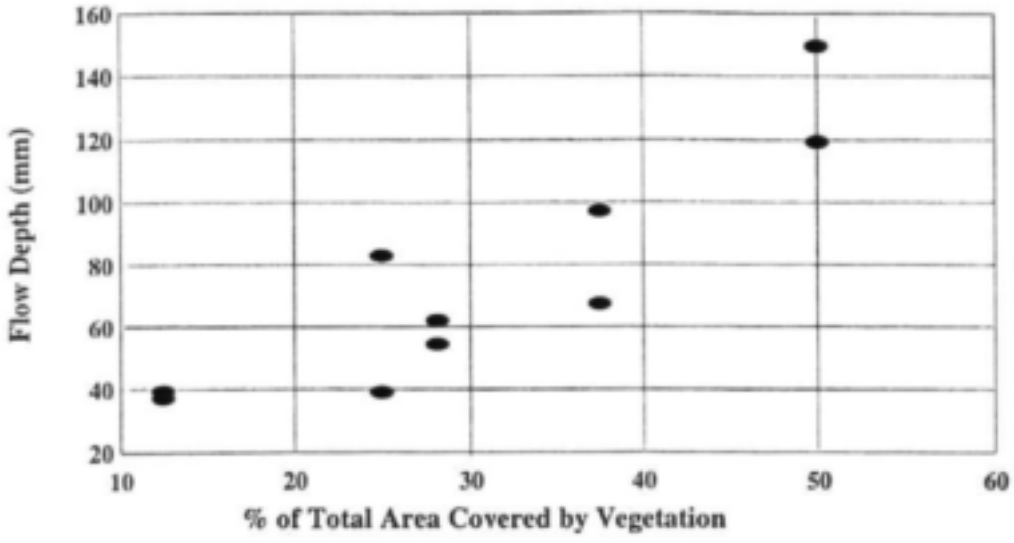

Figure 8.47 Flow depth variation with proportion of total area covered by roughness units for discrete patches, Q=10 l/s

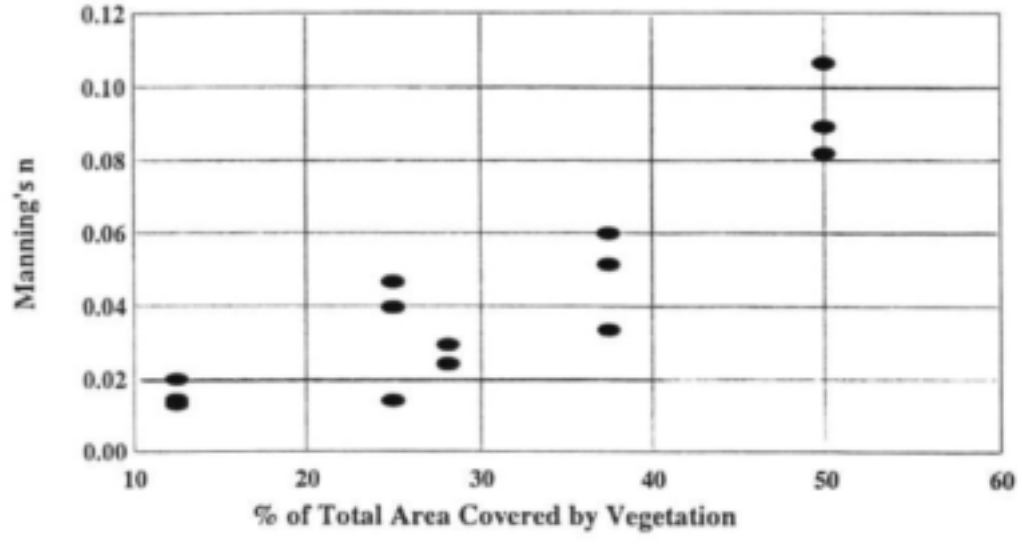

Figure 8.48 Manning's *n* variation with proportion of total area covered by roughness units for discrete patches, Q=10 l/s

8.4 CONCLUSION

The experiments presented in this chapter have enabled some hydraulic effects of the arrangement of reedbeds in partially reeded channels to be described. In particular, the influence of reedbed patterns on overall resistance and clear water velocity distributions has been demonstrated.

The resistance of partially reeded channels is significantly influenced by the distribution pattern of the reedbeds. Where reedbeds form longitudinal strips, the resistance is proportional to the number of stem-water interfaces, and the proportion of total discharge within the clear channel regions decreases consistently with increasing number of interfaces. Importantly, the overall Manning n value varies significantly with flow depth for all the longitudinal strip patterns investigated, reflecting the dominance of stem drag resistance in the whole channel, and confirming that specification of a single value of n in such channels is inappropriate.

The flow velocity in the clear channels between reedbed strips is affected by the strips for a considerable distance from the stem-water interface. Although the velocity increases rapidly away from the interface within a fairly narrow zone, the experimental results suggest that the apparently uniform velocity beyond this zone is still influenced by the vegetation and depends strongly on the width of the strip. The bed shear stress in the clear channels is similarly affected by the vegetation, and this has significant implications for understanding and describing sediment dynamics in partially reeded channels. The resistance of vegetation boundaries results in a much wider range of velocities in the channel than would otherwise occur, but much less variation of these velocities with changing discharge. As for fully vegetated channels, an increase in discharge is accommodated by an increase in flow depth more than an increase in velocity, as would occur without the vegetation. The effect of vegetation on velocity distribution and variation with discharge has important implications for riverine habitat definition.

If reedbeds form discrete, longitudinally discontinuous patches within a channel, the resistance is strongly influenced by the characteristics of the patches as well as the overall areal coverage. The resistance increases consistently with increasing areal coverage: for the same overall distribution pattern Manning's n varies linearly with the proportion of channel occupied by reedbed. However, for any particular coverage, the resistance also varies significantly with the overall distribution pattern of the patches, the size and shape of the patches, and the degree of fragmentation as reflected by patch discontinuity and the length of stem-clear water interface. As for the strip patterns, there is evidence that Manning's n varies significantly with depth where there is a strong stem drag contribution to overall resistance, resulting in almost constant average flow velocity at all flow depths. This is clearly apparent for all cases where areal coverage exceeds about 25%.

Chapter 9

CONVEYANCE PREDICTION FOR STRIP ROUGHNESS

9.1 INTRODUCTION

Vegetation has a significant influence on the overall resistance of a river channel, even if it occupies only a relatively small part of the channel, as has been demonstrated in Chapter 8. It has been shown that the resistance depends not only on the areal extent of the vegetation, but also significantly on its distribution pattern. Partially reeded rivers are common and there is therefore a need for conveyance prediction methods that account for these effects.

Two basic types of reedbed distribution patterns were considered in Chapter 8, namely continuous longitudinal strips and discrete patches. Both of these occur naturally in rivers and need to be accounted for in conveyance prediction. Their resistance processes differ, however, and therefore require different treatment. In the case of marginal and mid-channel strips the additional resistance afforded by the reedbeds is through momentum transfer across the interface between the reeded zones, where basic resistance is high and the velocity low, and the clear channel zone where the basic resistance is relatively low and the velocity relatively high. The effect of this momentum transfer is the imposition of an effective shear stress at the interface which can be treated, at least for the clear channel zone, as an effective surface roughness. For discrete reedbed patches there is also a significant form resistance contribution to overall resistance which is probably best addressed using a distributed drag force approach, similar to the treatment of individual stems in the basic reed resistance models, but at a larger scale.

This chapter addresses the problem of conveyance prediction for channels with continuous longitudinal strips of reeds. This applies particularly to the very common situation of rivers and streams with reedbeds along the banks. Discrete, mid-channel patch resistance has not been considered and requires further investigation.

9.2 PREDICTION APPROACHES

Rigorous explanation and description of the flow in partially vegetated rivers would require detailed computational modelling of the processes involved. Computational methods are excluded from consideration here, however, as the prime need is for a simple hand calculation method that could also be incorporated reasonably easily into practical river hydraulics modelling software.

Various approaches could be adopted to develop such a method. The most direct would be to consider the channel cross section as an entirety, and to develop an empirical relationship between a resistance coefficient (such as Manning's n) and the measurable channel characteristics. Such a relationship would include basic values of n for the reeded and clear channel areas, the flow depth (the importance of which has been shown for both basic stem resistance and resistance in partially reeded channels), and a description of the distribution pattern of the reed strips. The pattern could be described by parameters such as the widths of the strips and clear channels and

the number of stem-water interfaces. Clearly, an equation incorporating all relevant parameters would be complex and would need to draw on a large data base to be reliable. The data currently available are limited, especially on a natural river scale, and this puts severe limitations on development and application of a purely empirical method. A method with a more rational basis would be preferable, as this could be more generally applied with less stringent requirements for calibration.

The well-structured distributions of roughness presented by the strip patterns appear to correspond well with the composite roughness interpretation underlying the equivalent resistance coefficient formulations of Horton (1933), Einstein and Banks (1950), Colebatch (1941), Lotter (1933) and others, as reviewed in Chapter 2. These methods would not be successful in direct application to this situation, however. They are all based on a subdivision of the channel cross section into regions associated with different bed roughnesses, with no consideration of the flow interaction between them. For partially reeded channels, the extreme difference between the resistance of the reeded and clear channel areas causes significant flow interaction, as shown by the velocity distributions in Figs 8.5 to 8.12 and 8.15 to 8.17 and the boundary shear stress distributions in Figs 8.21 to 8.23.

Explicit subdivision of the channel cross-section into zones with different characteristics would enable the resistance effects within the reeds and the clear channels to be treated separately, and the flow interaction between them to be accounted for. Two different approaches to channel subdivision have been identified. The first is a physical subdivision, where discharges are calculated separately for the reeded and clear channel zones. The second is a hydraulic subdivision, based on the form of the cross-sectional velocity distribution. The velocity distribution across the interface between a reeded and a clear channel area is shown schematically in Fig. 9.1. For Zone 1, the conveyance is defined by the basic stem resistance, as described in Chapters 4 to 7. In Zone 4, the resistance is exerted exclusively by bed friction, and standard methods can be applied. The conveyances of the transition Zones 2 and 3 are defined by the form of the velocity profile, which is determined by the resistance characteristics of the reedbed and the clear channel, as well as the channel slope and flow depth. While this approach holds promise, the form of the velocity profile and its dependence on the physical characteristics of the two outer zones are not yet understood sufficiently well. The extents of the transition zones remain uncertain and require further investigation, both experimentally and through turbulence modelling.

The physically based divided channel approach is convenient and reasonable, provided flow interaction is accounted for, and is pursued here. Following this approach, the discharges in the clear channels and reeded zones are computed separately and then added.

9.3 CLEAR CHANNEL ZONE DISCHARGE

The clear channel zones are considered as independent, rectangular channels. The flow interactions with the reeded zones can be accounted for by recognising the existence of shear stresses over the interfaces between the zones. The interfaces can then be represented by vertical boundaries with effective roughnesses and corresponding resistance coefficients. A clear channel

zone can then be considered as a composite channel with different roughnesses on the sides and bed. If flow areas within the clear channel associated with these different resisting surfaces can be defined by interfaces over which there is negligible shear, then the equivalent resistance coefficient formulations for composite channels are applicable.

Application of the equivalent resistance methods requires knowledge of resistance coefficient values for the different surfaces, in this case of the plaster finish of the basic channel for the bed and solid side boundaries, and of the stem-water interfaces. The friction factor, f, and Manning's n for the basic channel were presented in Section 8.2.2, and apply to the bed and solid side boundaries. The resistance coefficients for the stem-water interfaces can be determined from the experimental results through an inverse application of the side-wall correction procedure developed by Vanoni and Brooks (1957) and modified for rough side walls by Brownlie (1981).

The basic procedure of Vanoni and Brooks, presented in Section 4.2.1.2, was extended by Brownlie (1981) to include a friction factor diagram for a range of surface roughnesses and Reynolds numbers. The method depends on the relationships

$$\frac{Re}{f} = \frac{Re_w}{f_w} = \frac{Re_b}{f_b} \qquad 9.1$$

and

$$\frac{R}{f} = \frac{R_w}{f_w} = \frac{R_b}{f_b} \qquad 9.2$$

in which the subscripts w and b refer to the wall and bed respectively; unsubscripted variables apply to the whole channel. The procedure given by Brownlie (1981) for estimating bed characteristics is as follows:

1. Calculate Re and f for the whole cross section and compute Re_w/f_w, which is equal to Re/f according to equation (9.1).

2. Plot $Re_w/f_w = Re/f$ = constant on the friction factor diagram (Fig. 9.2) as a straight line with a slope of 1 in log units, and with the intercept at $f = 0.01$ at $0.01Re/f$. The desired values of f_w and Re_w lie on this line.

3. Select a trial value of R_w, compute $4R_w/k_{sw}$ (where k_{sw} is the effective roughness of the walls), and determine f_w from Fig. 9.2.

4. Compute $R_w = (R/f)f_w$ and compare with the selected value. Iterate to convergence.

5. Calculate f_b and R_b from equations (9.2) and

$$Pf = P_b f_b + P_w f_w \qquad 9.3$$

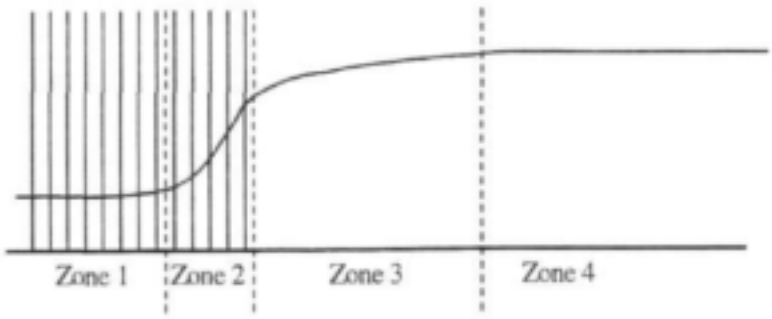

Figure 9.1 Form of velocity distribution across a stem-water interface

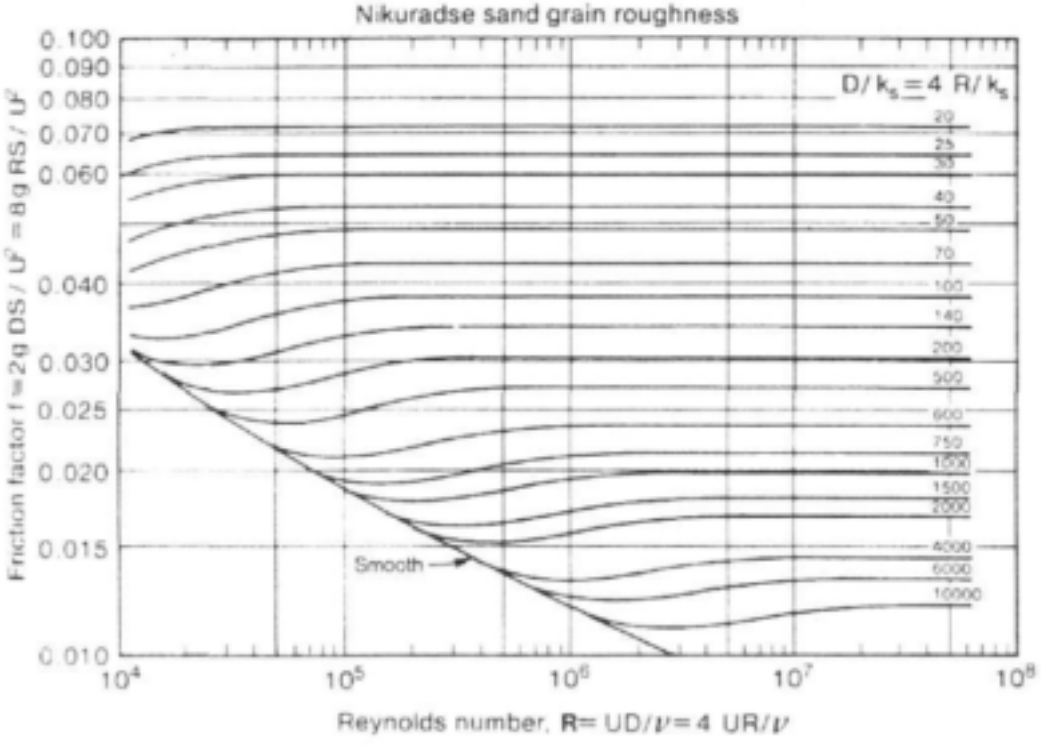

Figure 9.2 Friction factor diagram (Brownlie, 1981)

In this application k_{sw} is not known and the procedure was carried out the other way round, using a trial value of R_b and following the procedure from step 3 to produce values for f_w and R_w. This was done using the integrated clear channel discharges and corresponding flow depths obtained for Patterns 1, 3 and 5. The values of f_b resulting from this analysis are plotted against Re_b on Fig. 9.3, where they are compared with the basic channel results to confirm consistency; the relationship of f_b with Re_b implied by the pattern data appears to merge with the relationship for the basic channel at higher values of Reynolds number. The relationship produced for the friction factor of the stem-water interface (f_w) is shown on Fig. 9.4. Although dependence of the friction factor on Reynolds number appears to persist to higher values of Reynolds number than for the bed, the method implicitly assumes that the velocities in the sub-areas controlled by the bed and sides are the same, which is not really true, as can be seen from the velocity profiles (Figs 8.6, 8.8 and 8.10). The velocities and hence the Reynolds numbers associated with the f_w values are therefore probably exaggerated.

Corresponding values of Manning's n for the stem-water interfaces were calculated by equating the Manning and Darcy-Weisbach formulae to give

$$n_w = R_w^{1/6}\left(\frac{f_w}{8g}\right)^{1/2} \qquad 9.4$$

The calculated values of n_w range from 0.0390 to 0.0474, with an average of 0.0432 and standard deviation of 0.0024. There is no discernible trend of n_w with flow condition, so the average is assumed to be representative for all conditions.

The friction factor for the stem-water interface was also estimated from the data measured for the additional side strip experiments, which included boundary shear measurements. The shear force at the interface was calculated from a balance of forces for uniform flow: the downslope component of the weight of the water in a clear channel is balanced by the sum of the shear force exerted by the bed (F_{bed}) and the shear force exerted by the two stem-water interfaces (Fw), i.e.

$$W \sin\theta = F_{bed} + F_w \qquad 9.5$$

in which W is the weight of the water over a certain length of channel, and θ is the channel slope. The weight of the water (W) can be calculated from the measured flow depth, clear channel width and unit weight of water. The shear force exerted by the bed (F_{bed}) is determined by integration of the measured bed shear stress distributions (Figs 8.21 to 8.23). The shear force exerted by the interfaces (F_w) can then be calculated from equation (9.5), and converted to a shear stress (τ_w) by dividing by the interface area, as determined by the flow depth. From the Darcy-Weisbach equation it can be shown that the friction factor, f, can be related to boundary shear stress (τ_o) by

$$f = \frac{8\tau_o}{\rho V^2} \qquad 9.6$$

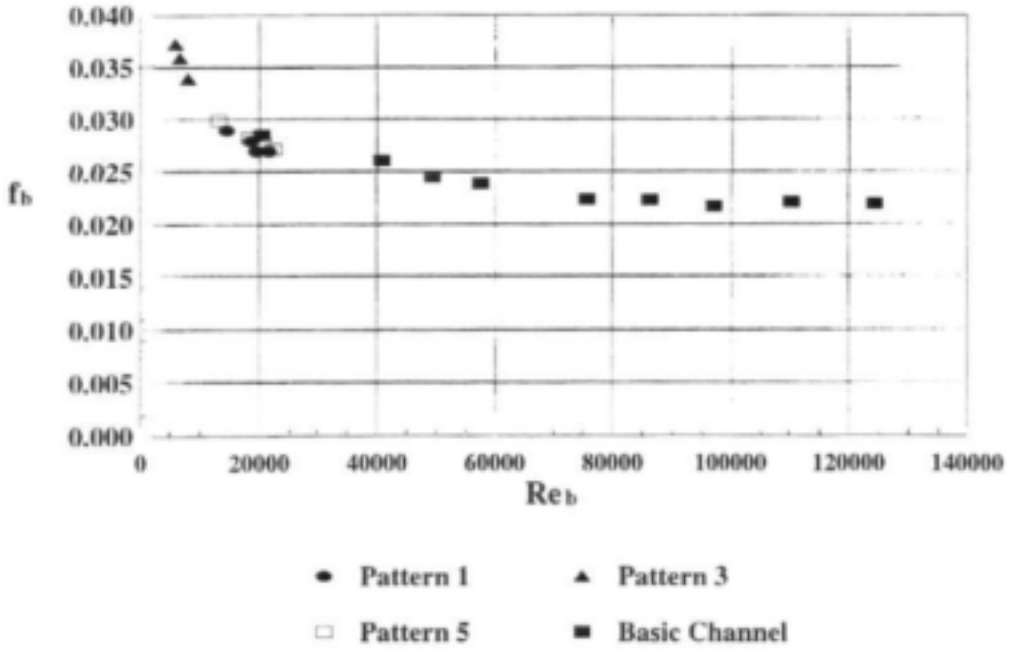

Figure 9.3 Friction factor for clear channel bed

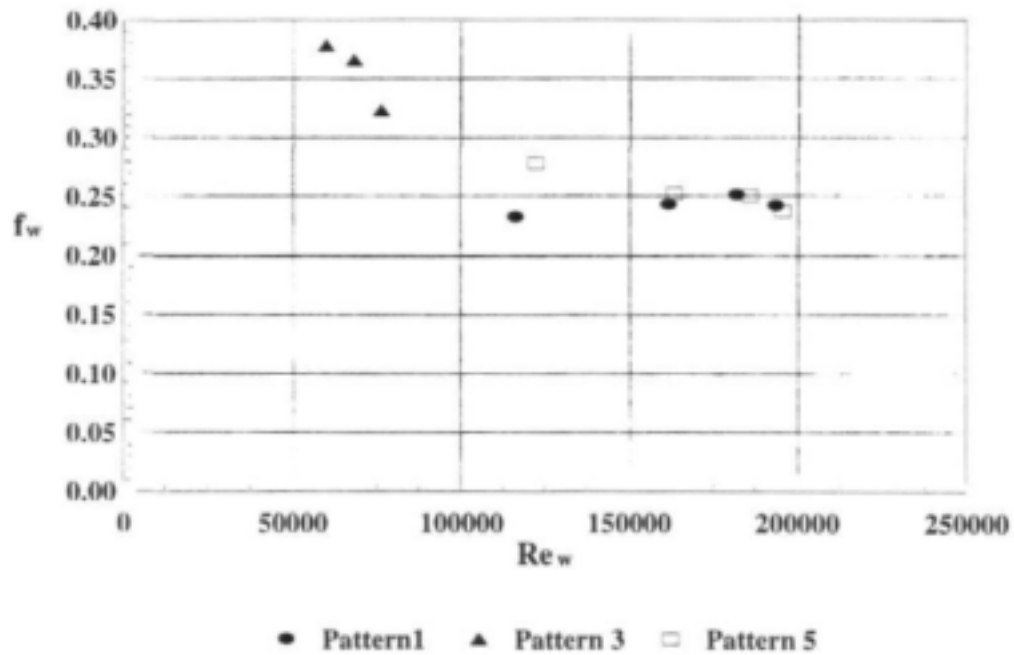

Figure 9.4 Effective friction factor values for stem-water interfaces

Assuming that equation (9.6) applies to components of composite resistance, it can be applied to calculate the friction factor of the stem-water interfaces (f_w) from the interface shear stress. This procedure was applied to the three flow depths for each of the three strip patterns tested. It is not possible to assign *Re* values to the interface-influenced flow regions using this approach, but the resulting values for f_w are plotted against flow depth in Fig. 9.5. The values determined by the side-wall correction approach for the one common situation (Pattern 1) are also plotted here for comparison. The two approaches produce remarkably similar results. The values obtained from the shear stress integration approach suggest that they depend on the thickness of the strip, which is consistent with the interpretation of the velocity distributions. The values for the 0.250 m and 0.125 m strips suggest a variation with depth producing a maximum at an intermediate depth, but this is contradicted by the values for the 0.050 m strips. The influence of the stem-water interface on clear channel flow characteristics clearly requires further investigation.

In the following analyses resistance is described in terms of Manning's n. The value for the basic channel was found to be essentially constant at 0.0102, and is adopted for the bed. The value of n used for the stem-water interfaces is the average determined from the data for Patterns 1, 3 and 5, i.e. 0.0432. Although the experiments for different strip widths suggest that the value depends on this width, insufficient data are available to quantify the dependence, and the single value is used throughout.

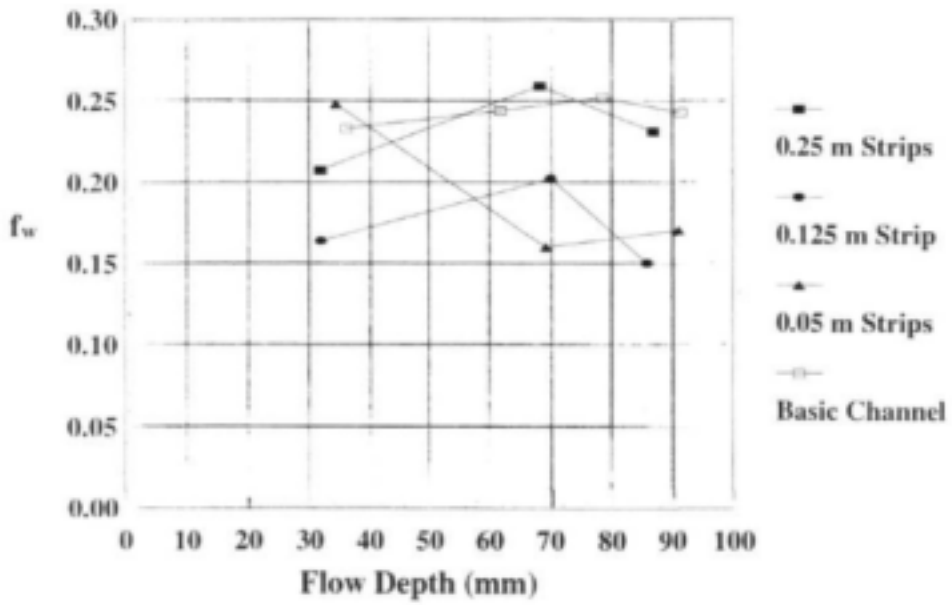

Figure 9.5 Dependence of effective friction factor for stem-water interfaces on flow depth and stem strip width

The stage-discharge relationships for total clear channel flow has been predicted for all the strip patterns using the equivalent resistance coefficient formulae of Horton (1933), Einstein and Banks (1950), Lotter (1933), and Colebatch (1941). These formulae give the equivalent value of Manning's n in terms of subdivided cross section characteristics as follows.

Horton (1933):

$$n_e = \left(\frac{\sum_{i=1}^{N} \left(P_i n_i^{3/2} \right)}{P} \right)^{2/3} \qquad 9.7$$

Einstein and Banks (1950):

$$n_e = \left(\frac{\sum_{i=1}^{N} \left(P_i n_i^{2} \right)}{P} \right)^{1/2} \qquad 9.8$$

Lotter (1933):

$$n_e = \frac{P R^{5/3}}{\sum_{i=1}^{N} \frac{P_i R_i^{5/3}}{n_i}} \qquad 9.9$$

Colebatch (1941):

$$n_e = \left(\frac{\sum_{i=1}^{N} \left(A_i n_i^{3/2} \right)}{A} \right)^{2/3} \qquad 9.10$$

In equations 9.7 to 9.10 n_c is the equivalent Manning resistance coefficient for the whole cross section, P is the wetted perimeter, A is the flow area, and R is the hydraulic radius. The subscript i indicates the subdivision value and unsubscripted variables represent the entire cross section. N is the number of subdivisions, which is three in these applications.

The clear channel subdivision is made by bisecting the wall-bed angle (90° in these cases), and projecting the intersection of the subdivision planes from either side vertically in cases where the intersection point is below the water surface (as done by Flintham and Carling (1991) in a study of composite roughness with simple, solid boundary channels). Implicit in these methods is that there is no interaction between the subareas, which means that there is no shear stress on the subdivision planes. Such planes exist, but their forms and locations can only be determined by more detailed velocity distribution description than can be obtained from the experiments conducted. The angle-bisector subdivisions are therefore approximations to shear-free surfaces, and their correctness is unknown. However, Flintham and Carling (1991) investigated the effect of replacing the angle-bisector planes with planes defined by assumed velocity contours, ensuring no shear stress, and found that predictions were not sensitive to the location of the planes.

The measured and predicted clear channel discharges are compared in Table 9.1, and the average absolute errors in discharge for these predictions are listed in Table 9.2. It is clear that the method of Lotter (1933) is unsatisfactory; it always overpredicts discharge (by over 200% in one case) with inconsistent errors both within and between pattern conditions. (Flintham and Carling (1991) also found this method to be unsatisfactory for their experimental conditions). Colebatch's (1941) formula produces consistent overprediction errors, averaging 15.12% over all the patterns, with a standard deviation of 8.10%. The relatively high overall and individual pattern standard deviations shows less consistency than the two better methods. The method of Einstein and Banks (1950) performs best overall, with an overall average absolute error of 7.32% and standard deviation of absolute errors of 4.68%. It also performs best for most patterns, being inferior to Horton's method only for Patterns 1 and 5. Discharge predictions are both over and under the measured values. Horton's (1933) method is also satisfactory, with an overall average absolute error of 8.68% and standard deviation of errors of 6.41%, again with discharge being both under- and overpredicted. It performs better than Einstein and Banks's method for Patterns 1 and 5, suggesting that it may be superior for channels with bank reeds only, although these are two of the three patterns used for estimating the stem-water interface resistance in the first place. It is concluded that both the methods of Einstein and Banks (1950) and Horton (1933) give satisfactory results, and there is little to choose between them. On the basis of these applications, the Horton (1933) equation may be preferable for relatively wide clear channels, such as those with bank reeds only, while the Einstein and Banks (1950) may be superior for more complex patterns, i.e. those with multiple strips and different side surfaces.

Table 9.1 **Comparisons of predictions for clear channel discharges (Q is discharge in l/s, E is error in %)**

Pattern	Depth (m)	Measured Discharge (l/s)	Einstein & Banks (1950)		Horton (1933)		Colebatch (1941)		Lotter (1933)	
			Q (l/s)	E (%)	Q (l/s)	E (%)	Q (l/s)	E (%)	Q (l/s)	E (%)
1	0.0363	4.00	3.30	-17.5	3.70	-7.50	4.33	8.25	5.70	42.5
	0.0619	7.50	6.40	-14.7	7.22	-3.73	8.57	14.3	12.75	70.0
	0.0786	9.80	8.60	-12.2	9.60	-2.04	11.35	15.8	17.93	83.0
	0.0916	11.80	10.30	-12.7	11.48	-2.71	13.47	14.2	22.11	87.4
2	0.0596	3.10	3.37	8.71	3.66	18.1	3.92	26.5	7.21	133
	0.1041	5.90	6.26	6.10	6.64	12.5	6.34	7.46	10.33	75.1
	0.1295	7.30	7.93	8.63	8.35	14.4	7.85	7.53	11.92	63.3
	0.1496	8.70	9.26	6.44	9.70	11.5	9.08	4.37	13.21	51.8
3	0.0545	4.10	3.98	-2.93	4.41	7.56	5.11	24.6	8.75	113
	0.0882	7.00	6.94	-0.86	7.55	7.86	8.17	16.7	15.04	115
	0.1181	9.00	9.63	7.00	10.36	15.1	10.51	16.8	18.91	110
	0.1293	11.10	10.65	-4.05	11.41	2.79	11.31	1.89	19.85	78.8
4	0.0451	4.10	4.14	0.98	4.66	13.7	5.25	28.0	9.36	128
	0.0786	7.60	8.08	6.32	9.09	19.6	9.84	29.5	23.40	208
	0.1000	9.60	10.70	11.5	12.00	25.0	12.53	30.5	34.37	258
	0.1159	11.80	12.66	7.29	14.17	20.1	14.40	22.0	43.19	266
5	0.0391	4.10	3.61	-12.0	4.07	-0.73	4.79	16.8	6.39	55.9
	0.0640	7.70	6.68	-13.2	7.51	-2.47	8.92	15.8	13.38	73.8
	0.0859	10.80	9.54	-11.7	10.65	-1.39	12.55	16.2	20.27	87.7
	0.0945	12.30	10.68	-13.2	11.90	-3.25	13.94	13.3	23.06	87.5
6	0.0466	4.00	3.81	-4.75	4.27	6.75	4.89	22.3	8.51	113
	0.0828	8.10	7.52	-7.16	8.35	3.09	9.05	11.7	19.80	144
	0.1033	9.90	9.70	-2.02	10.71	8.18	11.16	12.7	26.70	170
	0.1169	11.90	11.15	-6.30	12.28	3.19	12.47	4.79	31.27	163
7	0.0543	3.40	3.36	-1.18	3.71	9.12	4.02	18.2	8.43	148
	0.0979	6.40	6.53	2.03	7.08	10.6	7.47	16.7	19.13	199
	0.1218	8.40	8.30	-1.19	8.94	6.43	8.42	0.24	21.78	159
	0.1416	10.10	9.70	-3.96	10.48	3.76	9.48	-6.14	24.09	139

Table 9.2 **Average absolute prediction errors (%) for clear channel discharges (standard deviations in parentheses)**

Pattern	Einstein & Banks (1950)	Horton (1933)	Colebatch (1941)	Lotter (1933)
1	14.28 (2.07)	4.00 (2.11)	13.12 (2.89)	70.71 (17.49)
2	7.47 (1.21)	14.12 (2.50)	11.45 (8.75)	80.70 (31.06)
3	3.71 (2.22)	8.33 (4.40)	15.00 (8.23)	104.3 (14.81)
4	6.51 (3.73)	19.60 (4.02)	27.52 (3.29)	215.1 (54.82)
5	12.51 (0.71)	1.96 (0.97)	15.56 (1.33)	76.20 (13.03)
6	4.64 (1.82)	5.30 (2.22)	12.87 (6.22)	147.4 (22.04)
7	2.09 (1.13)	7.48 (2.62)	10.33 (7.46)	161.1 (23.00)
All Patterns	7.32 (4.68)	8.68 (6.41)	15.12 (8.10)	122.2 (57.7)

9.4 REEDED ZONE DISCHARGE

In most partially reeded channels the discharge through the reeded zones would be expected to be small in comparison with that through the clear channel zones. In the main experiments carried out in this study the proportion of channel occupied by stems was 50%, which would be relatively high in natural rivers (Chapter 3; Kotschy et al, 2000). In the experimental channels the discharge through the stem zones was not insignificant, as shown in Fig. 8.13, and significant errors would result from ignoring the stem zone contribution for some patterns. Although less important than for the clear channel zones, it is therefore necessary to be able to predict the stem zone discharges reliably.

Various strategies can be followed to develop a method for estimating stem-zone discharges. The simplest would be to ignore any interaction between the clear channel and stem zones. As discussed in section 9.2, this has been shown by the experimental results to be unrealistic and would certainly be unacceptable for the clear channels. However, because of the relatively greater resistance of the stem zones, the interaction would have less influence within these zones than within the clear channel zones. The error introduced would therefore be less than for the clear

channels and, considering the lower proportional discharge within the stems, it may not contribute a significant error to the total channel discharge.

The stem-zone discharges have been calculated on this basis for all the patterns tested. Manning's equation was applied to the stem zones, using the values of Manning's n determined for this stem density (25 mm spacing) in the basic resistance experiments described in Chapter 4.2.1.3, and presented in Fig. 4.5. Although the bed roughness in the basic resistance equations was different from that in the pattern experiments, the resistance is dominated by stem drag (as shown in Chapter 5), and the difference in bed roughness will have insignificant effect on the results. The predictions are compared with the measured values in Table 9.3, and the average absolute errors are summarized in Table 9.4. The measured discharges were determined by subtracting the integrated clear channel discharges from the measured total discharges. As expected, this approach underestimates the discharge considerably in all but one case, and this exception is attributed to data inaccuracy.

The discharge within a stem zone is underestimated by ignoring the interaction with an adjacent clear channel because the momentum transfer from the clear channel will enhance the velocity within the stems over some distance. This could be accounted for through knowledge of the form of the transverse velocity profile across the interface. Experiments reported by Tsujimoto and Kitamura (1994) and Tsujimoto and Shimizu (1994) show that the profile changes from a constant value in the clear channel to a constant value within the stems, and that the ratio of the width of the interaction zone within the stems (Zone 2 in Fig. 9.1) to the total interaction zone width (Zones 2 and 3 in Fig. 9.1) is relatively constant and lies between 0.20 and 0.30. The detailed velocity distributions reported in Section 8.2.4 (and shown in Figs 8.15 to 8.20) indicated a relatively constant width of Zone 3 of 118 mm. This information, together with the assumption that the constant velocities within each zone are undisturbed values determined by local conditions only, enabled the velocity profiles to be approximated for all conditions. It was further assumed that local velocities could be used to estimate local values of Manning's n, and hence the distributions of n could be described, and average values for the stem zones determined. This approach was applied to the conditions of Pattern 1, but produced negligible improvement over the assumption of no interaction effect, and was not pursued further. The failure of this approach is attributed to the assumption that the constant velocity values on either side of the transition zone are undisturbed values. As discussed in Section 8.2.4, the experimental results suggest that the transition zone extends well beyond the region of rapid velocity change, and the apparently constant values are, in fact, strongly influenced by the zonal interaction. Until further knowledge enables better description of the velocity profiles, their use for calculating zonal discharges will remain unsatisfactory.

Table 9.3 Comparison of predictions for stem-zone discharges

Pattern	Depth (m)	Measured	No Interaction		Interaction Included	
		Discharge (l/s)	Discharge (l/s)	Error (%)	Discharge (l/s)	Error (%)
1	0.0363	1.0	0.651	-34.9	1.314	31.4
	0.0619	2.5	1.267	-49.3	2.248	-10.1
	0.0786	2.7	1.573	-41.7	2.836	5.00
	0.0916	3.2	1.845	-42.3	3.318	3.70
2	0.0596	1.9	1.153	-39.3	1.832	-3.49
	0.1041	4.1	2.129	-48.1	3.199	-21.9
	0.1295	5.2	2.582	-50.3	3.937	-24.2
	0.1496	6.3	2.959	-53.0	4.587	-27.1
3	0.0545	0.9	1.042	15.8	1.847	105.1
	0.0882	3.0	1.764	-41.2	2.949	-1.75
	0.1181	3.5	2.422	-30.8	3.784	8.07
	0.1293	3.9	2.575	-34.0	4.355	11.6
4	0.0451	0.9	0.827	-8.1	1.430	58.8
	0.0786	2.4	1.573	-34.5	2.458	2.4
	0.1000	2.9	2.037	-29.8	3.065	5.68
	0.1159	3.2	2.384	-25.5	3.603	12.6
5	0.0391	0.9	0.695	-22.8	1.345	49.4
	0.0640	2.3	1.278	-44.4	2.266	-1.47
	0.0859	1.7	1.688	-0.7	3.033	78.4
	0.0945	2.7	1.920	-28.9	3.371	24.9
6	0.0466	1.0	0.858	-14.2	1.593	59.3
	0.0828	1.9	1.671	-12.1	2.883	51.9
	0.1033	2.6	2.101	-19.2	3.491	34.1
	0.1169	3.1	2.381	-23.2	4.032	30.2
7	0.0543	1.6	1.035	-35.3	1.753	9.73
	0.0979	3.6	2.013	-44.1	3.098	-14.0
	0.1218	4.1	2.447	-40.3	3.904	-4.73
	0.1416	5.0	2.700	-46.0	4.582	-6.34

Table 9.4 **Average absolute prediction errors (%) for stem zone discharges (standard deviations in parentheses)**

Pattern	No Interaction	Interaction Included
1	42.1 (5.10)	12.5 (11.12)
2	47.7 (5.14)	19.2 (9.24)
3	30.4 (9.27)	31.6 (42.6)
4	24.5 (9.96)	19.9 (22.8)
5	24.2 (15.70	38.5 (28.6)
6	17.2 (4.34)	43.9 (12.09)
7	41.4 (4.08)	8.71 (3.56)
All patterns	32.5 (13.60)	24.9 (25.58)

The effect of the momentum transfer from a clear channel to an adjacent stem zone can also be described by assigning a shear stress to the interface. This stress will have the same value as determined for the clear channel sides in Section 9.3, but will be applied in the direction of flow, hence enhancing the downslope weight component of the flow, and effectively reducing the resistance. Ignoring the influence of bed shear within the stem zone, the force balance for the movement of a flow element can then be written as

$$W \sin\theta + F_w = F_D \qquad 9.11$$

in which W is the weight of a flow element on a bed slope θ, $\sin\theta$ can be represented by the channel slope, S, as before, F_w is the shear force on the interface, and F_D is the total drag force exerted by the stems. This force balance can be formulated into a resistance equation just as was done for basic resistance in Chapter 5.2, assuming in this case that the volume of stems is negligible. The shear force, F_w, can be evaluated as the product of the wall shear stress, τ_w, and the flow depth (for unit length of interface). The shear stress is related to the wall friction factor, f_w, as before, by

$$\tau_w = \frac{f_w \rho V_c^2}{8} \qquad 9.12$$

in which V_c is the velocity in the clear channel (as implicit in the side-wall correction procedure used to determine f_w, it is assumed that the velocity in the wall and bed zones are equal). By equating the Manning and Darcy-Weisbach equation to relate their respective coefficients, the wall shear can also be related to the Manning coefficient for the wall, n_w, by

$$\tau_w = \frac{n_w \rho g V_c^2}{R_w^{1/3}} \qquad 9.13$$

in which R_w is the hydraulic radius associated with the wall in the clear channel. As in the application of the composite roughness methods, the area associated with the wall is defined by the bisector of the angle between the bed and the wall, and the vertical from the intersection of the bisectors from opposite walls for narrow channels.

The total drag force of the stems in unit length of channel, F_D, is given by

$$F_D = C_D N L_g y d \frac{1}{2} \rho V^2 \qquad 9.14$$

in which C_D is the stem drag coefficient, N is the number of stems per unit area, L_g is the width of the stem zone, y is the flow depth, and d is the stem diameter.

The weight of a flow element of unit length (neglecting the volume occupied by the stems) is

$$W = \rho g L_g y \qquad 9.15$$

By substituting equations (9.15), (9.14) and (9.12) into the force balance equation (9.11) and rearranging, a resistance equation for the stem zone similar to that for the basic stem resistance (equation (5.8)) can be obtained, i.e.

$$V = \frac{1}{F_c} \sqrt{S} \qquad 9.16$$

with

$$F_c = \frac{1}{\sqrt{\frac{2\left(g + \frac{f_w V_c^2}{8 L_g S}\right)}{C_D N d}}} \qquad 9.17$$

Using equation (9.13) instead of (9.12) in the above derivation gives

$$F_c = \frac{1}{\sqrt{\frac{2\left(g + \frac{n_w^{\,2} V_c^{\,2}}{R_w^{\,1/3} L_g S}\right)}{C_D N d}}} \qquad 9.18$$

Equations (9.17) and (9.18) apply to stem zones with a clear water interface on one side only. For strips with two interfaces, the term containing the interface resistance coefficient should be multiplied by 2.

Equations (9.16) and (9.18) have been applied to the stem zones of all the experimental patterns. In these applications a constant value of $n_w = 0.0432$ was used, as determined for the sides of the clear channels. The clear channel velocity, V_c, was calculated in each case from the experimental integrated discharge and corresponding flow depth. The calculated stem zone discharges are listed in Table 9.3, and the average absolute errors summarized in Table 9.4. These predictions are generally significantly better than those made without consideration of interaction effects, with some anomalies. Some large errors most likely result from inaccurate data: for example the high positive errors for the lowest flow depth for Pattern 3 and the second highest for Pattern 5 reflect the apparent underestimate of measured discharge, shown by irregularities on the stage-discharge relationships (Fig. 8.3). Both methods, but particularly equations (9.16) and (9.18), appear to produce relatively more positive errors for the lowest flow depths. This is probably due to the neglect of bed shear in the derivation of the equations which was shown in Chapter 5 to be significant at low depths. Inclusion of bed shear would have resulted in a much more complicated form of equation for the resistance coefficient, however, similar to the more complicated form presented in Chapter 5. The only patterns for which equations (9.16) and (9.18) perform distinctly worse than if flow interaction is not accounted for are Patterns 5 and 6. As already mentioned, some error for Pattern 5 is attributable to inaccurate data, which makes comparative interpretation of the predictions difficult. The poor performance of equations (9.16) and (9.18) for Pattern 6 is puzzling, considering the relatively good performance for Patterns 3 and 4, with similar strip types, and has not been explained. Overall, the use of equations (9.16) and (9.18) is preferable to ignoring flow interaction, except for very low flow depths.

9.5 TOTAL DISCHARGE

The total channel discharges, including both clear channel and stem zone contributions, have been computed for all the patterns using the methods described above. Assuming no interaction effects for the stem zone enables the zonal discharges as computed above to be simply added. Allowing for the interaction (using equations (9.16) and (9.18)) requires recalculation of the stem zone discharges because the computations depend on the magnitude of the clear channel average flow velocity; in the above calculations the values were derived from the experimental measurements, but in predictions will be determined by the clear channel calculations. The clear channel

discharges have been calculated by the composite roughness formulae of Einstein and Banks (1950), Horton (1933) and Colebatch (1941); the formula of Lotter (1933) has been rejected because of its consistently poor performance.

The predicted discharges and their errors for the different methods and patterns are presented in Table 9.5, and the average absolute errors summarized in Table 9.6. Overall the best approach appears to be to use the composite roughness formula of Einstein and Banks (1950) for clear channel discharges, and to include flow interaction when calculating stem zone discharges. This produces an overall average absolute error of 6.61%, with a standard deviation of 4.38%. The composite roughness formula of Horton (1933) is, however, superior when the clear channels are wide, such as when stem zones are on the banks only. Ignoring flow interaction when computing stem zone discharges does not produce unacceptable errors, although there is a degree of error compensation because the stem zone discharges will always be underestimated (Tables 9.2 and 9.3) and clear channel discharges are often overestimated, particularly by application of Horton's (1933) formula. The measured stage-discharge relationships are compared in Figs 9.6 to 9.12 with those calculated for each pattern using the composite roughness formulae of Einstein and Banks (1950) and Horton (1933) for the clear channel discharge calculations, and both ignoring and including the zonal flow interaction for the stem zone discharges.

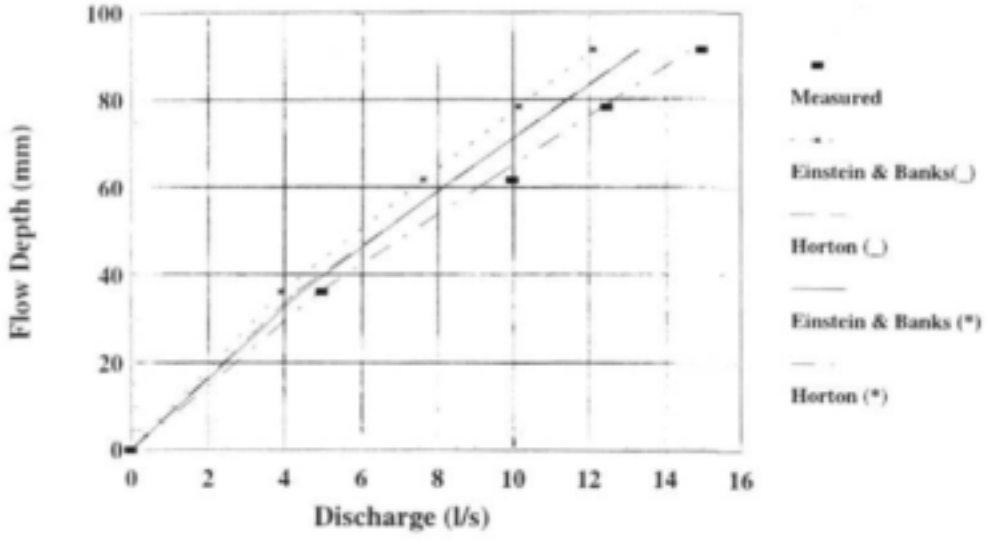

Figure 9.6 Measured and predicted stage-discharge relationships for Pattern 1. (_) indicates zonal interaction ignored, (*) indicates zonal interaction included.

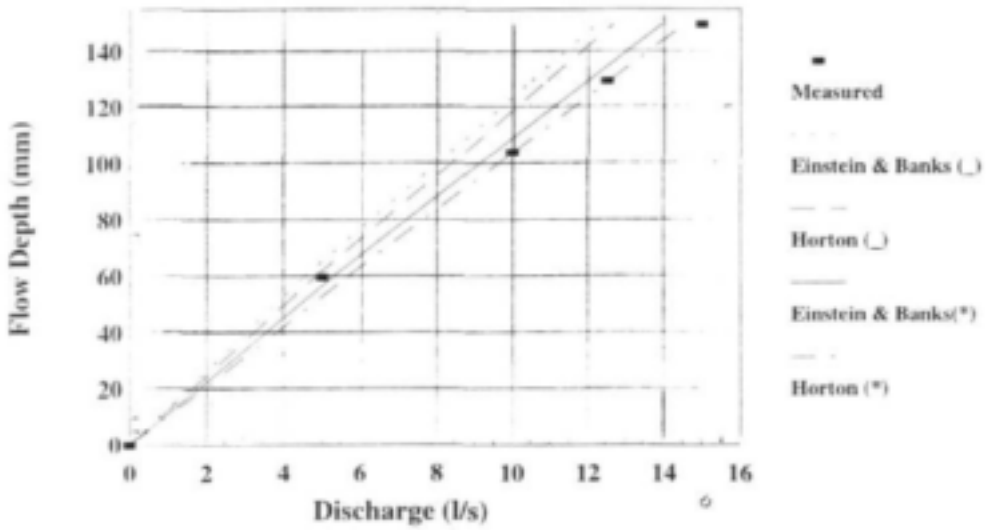

Figure 9.7 Measured and predicted stage-discharge relationships for Pattern 2. (_) indicates zonal interaction ignored, (*) indicates zonal interaction included.

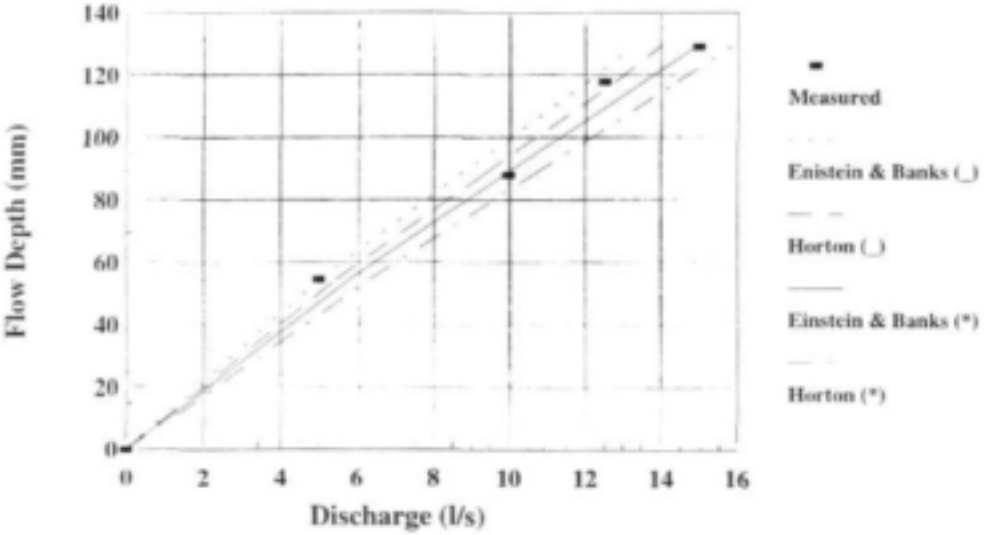

Figure 9.8 Measured and predicted stage-discharge relationships for Pattern 3. (_) indicates zonal interaction ignored, (*) indicates zonal interaction included.

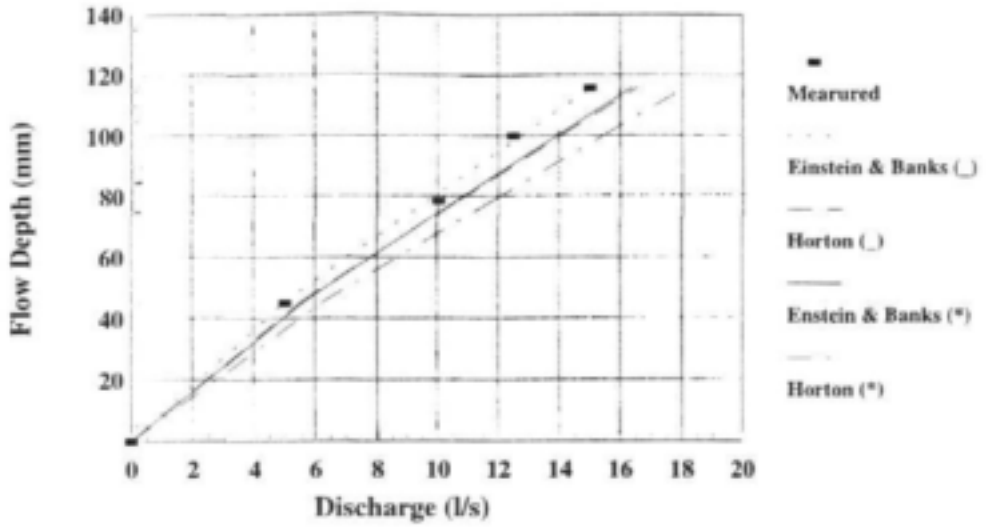

Figure 9.9 Measured and predicted stage-discharge relationships for Pattern 4. (_) indicates zonal interaction ignored, (*) indicates zonal interaction included.

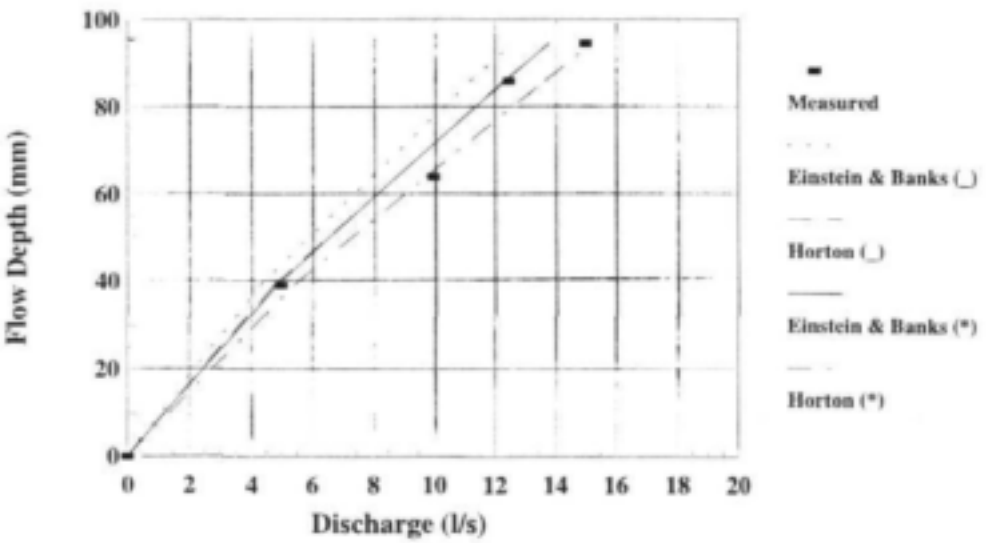

Figure 9.10 Measured and predicted stage-discharge relationships for Pattern 5. (_) indicates zonal interaction ignored, (*) indicates zonal interaction included.

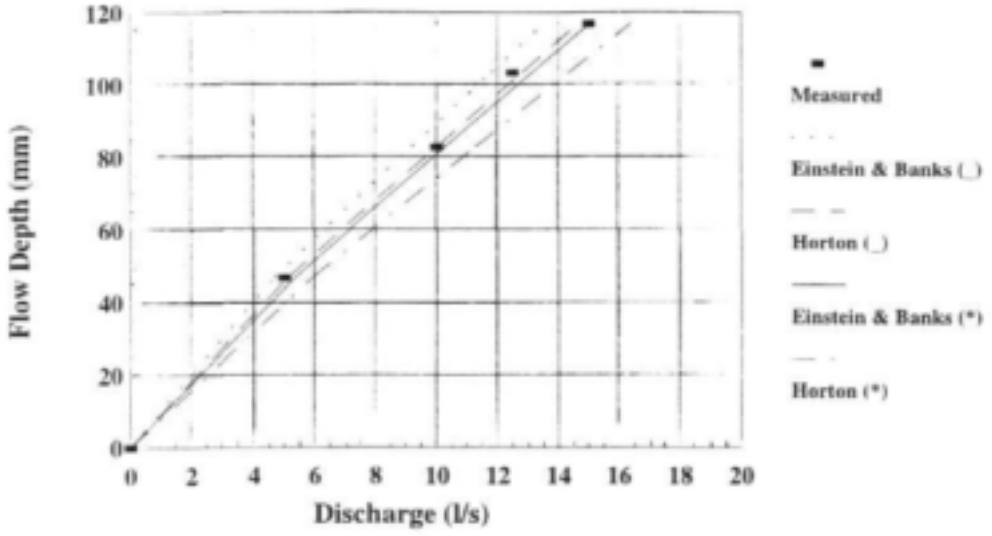

Figure 9.11 Measured and predicted stage-discharge relationships for Pattern 6. (_) indicates zonal interaction ignored, (*) indicates zonal interaction included.

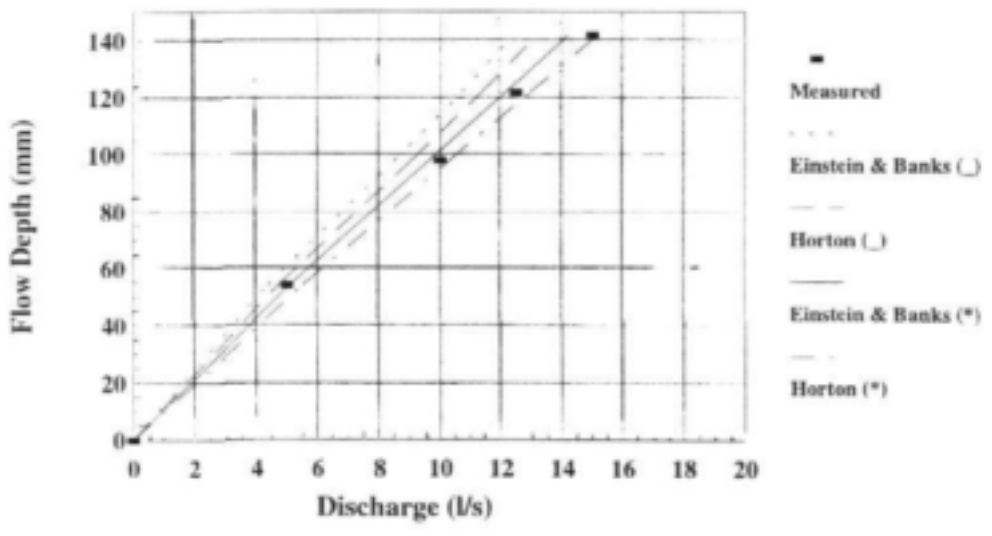

Figure 9.11 Measured and predicted stage-discharge relationships for Pattern 6. (_) indicates zonal interaction ignored, (*) indicates zonal interaction included.

Table 9.5 Comparison of predictions for total discharges (Q is discharge in l/s, E is error in %)

Pattern	Depth (m)	Measured Discharge (l/s)	No Interaction						Interaction Included					
			Einstein & Banks (1950)		Horton (1933		Colebatch (1941)		Einstein & Banks (1950)		Horton (1933		Colebatch (1941)	
			Q (l/s)	E (%)	Q (l/s)	E (%)	Q (l/s)	E (%)	Q (l/s)	E (%)	Q (l/s)	E (%)	Q (l/s)	E (%)
1	0.0363	5.0	3.951	-21.0	4.351	-13.0	4.981	-0.38	4.475	-10.5	4.949	-1.01	5.713	14.2
	0.0619	10.0	7.667	-23.3	8.487	-15.1	9.837	-1.63	8.442	-15.6	9.411	-5.89	11.031	10.3
	0.0786	12.5	10.173	-18.6	11.173	-10.6	12.923	3.38	11.214	-10.3	12.391	-0.86	14.480	15.8
	0.0916	15.0	12.145	-19.0	13.325	-11.2	15.315	2.10	13.349	-11.0	14.734	-1.78	17.099	14.0
2	0.0596	5.0	4.523	-9.54	4.813	-3.74	5.073	1.46	5.270	5.39	5.658	13.2	5.993	19.9
	0.1041	10.0	8.389	-16.1	8.769	-12.3	8.469	-15.3	9.541	-4.59	10.039	0.39	9.664	-3.36
	0.1295	12.5	10.512	-15.9	10.932	-12.5	10.432	-16.5	12.008	-3.94	12.558	0.46	11.937	-4.51
	0.1496	15.0	12.219	-18.5	12.659	-15.6	12.039	-19.7	13.971	-6.86	14.548	-3.01	13.779	-8.14
3	0.0545	5.0	5.022	0.44	5.452	9.04	6.152	23.0	5.799	16.0	6.341	26.8	7.243	44.9
	0.0882	10.0	8.704	-13.0	9.314	-6.86	9.934	-0.66	9.876	-1.24	10.628	6.28	11.409	14.1
	0.1181	12.5	12.052	-3.58	12.782	2.26	12.932	3.46	13.536	8.29	14.426	15.4	14.610	16.9
	0.1293	15.0	13.225	-11.8	13.985	-6.77	13.885	-7.43	14.917	-0.55	15.841	5.6	15.717	4.78
4	0.0451	5.0	4.967	-0.66	5.487	9.74	6.077	21.5	5.577	11.5	6.191	23.8	6.899	38.0
	0.0786	10.0	9.653	-3.47	10.663	6.63	11.413	14.1	10.608	6.08	11.787	17.9	12.677	26.8
	0.1000	12.5	12.737	1.90	14.037	12.30	14.567	16.5	13.917	11.33	15.430	23.4	16.052	28.4
	0.1159	15.0	15.044	0.29	16.554	10.36	16.784	11.9	16.381	9.21	18.133	20.9	18.402	22.7
5	0.0391	5.0	4.305	-13.9	4.765	-4.7	5.485	9.70	4.866	-2.67	5.407	8.14	6.264	25.3
	0.0640	10.0	7.958	-20.4	8.788	-12.1	10.198	1.98	8.779	-12.2	9.745	-2.55	11.408	14.1
	0.0859	12.5	11.228	-10.2	12.338	-1.30	14.238	13.9	12.374	-1.01	13.661	9.29	15.885	27.1
	0.0945	15.0	12.600	-16.0	13.820	-7.87	15.860	5.73	13.800	-8.00	15.212	1.41	17.594	17.3
6	0.0466	5.0	4.668	-6.64	5.128	2.56	5.748110	15.0	5.359	7.18	5.927	18.5	6.699	34.0
	0.0828	10.0	9.191	-8.09	10.021	0.2	721	7.21	10.285	2.85	11.293	12.9	12.147	21.5
	0.1033	12.5	11.801	-5.59	12.811	2.49	13.261	6.09	13.144	5.15	14.362	14.9	14.907	19.3
	0.1169	15.0	13.531	-9.79	14.661	-2.26	14.851	-0.99	15.038	2.52	16.393	9.29	16.622	10.8
7	0.0543	5.0	4.395	-12.1	4.745	-5.10	5.055	1.10	5.104	2.07	5.551	11.0	5.942	18.8
	0.0979	10.0	8.543	-14.6	9.093	-9.07	9.483	-5.17	9.656	-3.44	10.343	3.43	10.829	8.30
	0.1218	12.5	10.747	-14.0	11.387	-8.90	10.867	-13.1	12.183	-2.53	12.976	3.81	12.330	-1.36
	0.1416	15.0	12.400	-17.3	13.180	-12.1	12.18	-18.8	14.200	-5.34	15.161	1.07	13.929	-7.14

Table 9.6 **Average absolute prediction errors (%) for total discharges (standard deviations in parentheses)**

Pattern	No Interaction			Interaction Included		
	Einstein & Banks (1950)	Horton (1933)	Colebatch (1941)	Einstein & Banks (1950)	Horton (1933)	Colebatch (1941)
1	20.5 (1.87)	12.5 (1.77)	1.87 (1.08)	11.85 (2.2)	2.39 (2.05)	13.6 (2.02)
2	15.0 (3.33)	11.05 (4.42)	13.3 (7.00)	5.19 (1.09)	4.26 (5.25)	8.97 (6.53)
3	7.20 (5.32)	6.23 (2.47)	8.65 (8.65)	6.52 (6.25)	13.5 (8.6)	20.2 (14.9)
4	15.8 (12.4)	9.76 (2.04)	16.0 (3.58)	9.54 (6.25)	21.5 (2.38)	29.0 (5.61)
5	15.1 (3.70)	6.50 (3.99)	7.83 (4.44)	5.97 (4.43)	5.35 (3.42)	20.9 (5.40)
6	7.52 (1.58)	1.88 (0.97)	7.31 (5.00)	3.86 (2.59)	13.9 (3.34)	21.4 (8.29)
7	14.5 (1.87)	8.80 (2.49	9.53 (6.86)	3.35 (1.25)	4.83 (3.72)	8.91 (6.31)
All Patterns	11.6 (6.68)	8.10 (4.34)	9.21 (7.09)	6.61 (4.38)	9.40 (7.97)	17.6 (10.46)

9.6 CONCLUSION

The conveyance of channels with longitudinal strips of reeds can be estimated by adding together the discharges of reeded zones and clear water zones, calculated separately. The discharge in clear water zones can be determined reliably by application of the composite roughness formulae of Einstein and Banks (1950) and Horton (1933), with different resistance coefficient values and flow areas assigned to the bed and sides. The flow areas associated with these surfaces can be defined by separation planes along the bisectors of the bed-wall angles, and a vertical plane through the intersection point if the planes from opposite sides intersect before reaching the water surface. For the experimental conditions, the resistance coefficient of the stem surfaces was determined by application of Brownlie's (1981) side-wall correction procedure and from measurements of the bed shear stress. Field investigations are necessary to determine representative stem surface resistance coefficients for practical applications. The discharge in reeded zones, accounting for the effect of zonal flow interaction, can be determined by a modified form (including the stem surface resistance coefficient) of the basic resistance

relationship for flow through stems presented in Chapter 5. Depending on the extent of reed cover and the corresponding proportion of flow within the reedbeds, ignoring the zonal flow interaction may not introduce significant error. Application of these procedures to the experimental conditions suggest that the formula of Horton (1933) is preferable for channels with reedbeds along the banks only and relatively wide clear water zones, while the formula of Einstein and Banks (1950) is better for more complex arrangements with narrow clear water zones.

Chapter 10

SEDIMENTATION IN REEDBEDS

10.1 BASIC SEDIMENTATION

10.1.1 Introduction

The influence of riverbed vegetation on sediment transport capacity for the purpose of predicting sediment deposition and/or erosion in vegetated areas has became one of the most interesting topics in hydraulics. Many researchers have performed laboratory experiments and proposed methods for determining hydraulic resistance of vegetated streams. There are many formulae proposed for the prediction of the rate of sediment transport in rivers (Vanoni, 1977). However, only a few investigations have been performed on the interaction between sediment and vegetation.

A series of experiments were carried out in the laboratory to investigate and predict bed load discharge in a vegetated stream. Experiments were aimed at establishing how hydraulic parameters such as bed slope and flow depth are influenced by sediment transport and flow rate through vegetation.

10.1.2 Sediment Experiments

10.1.2.1 Experimental Set Up

Sediment tests were carried out in an experimental flume which had a width of 0.38 m, a height of 0.66 m and a length of 15.0 m. A tailgate fixed downstream of the flume was used to control the flow depth in the channel to ensure uniform flow. Water was supplied to the flume through a closed circulation system. The water was pumped from an underground sump to a constant head tank and then fed from the constant head tank to the flume. Two valves situated in the supply pipe at the head of the experimental flume were used to control the discharge.

A V-notch weir (at the end of the flume) was used to determine the discharge. The V-notch was positioned at the outlet of the stilling basin at the end of the flume. A transparent rectangular tube connected to the tank was placed on the outside wall of the tank. The level of the water in the transparent tube indicated the depth of flow over the V-notch. A calibration curve of the V-notch was used to determine the discharge.

A belt feeder was used to supply sediment to the flume. It was installed at the upstream end of the experimental length of the flume, on the top of the flume walls. Sediment was loaded onto the feeder via a hopper. Sediment discharge rates were controlled by adjusting the size of the opening at the base of the hopper, and by changing the speed of the belt. The belt feeder does not have the facility to measure sediment discharge, which was therefore determined by collecting sediment over a fixed period of time observed with a stopwatch, and then weighing. The sediment discharge rate was expressed as weight of sediment per unit time. Different sediment feed rates were tested, as described in the Section 10.1.2.2.

In order to develop predictive and realistic relationships between vegetation characteristics, sediment transport and hydraulic parameters, it is desirable to have a test section of natural vegetation in which all variables can be controlled. Due to the biological variability of natural vegetation (such as the differing diameters of individual stems, varying stem density, variability of size and number of leaves on individual stems) this degree of control is not feasible when using real vegetation. For this reason artificial vegetation was used in the experiments. The vegetation was simulated by cylindrical 5 mm metal rods fixed in wooden frames (125 mm by 1000 mm) sized to fit the experimental flume. The metal rods were arranged in a staggered type distribution (Fig. 4.1), spaced at 25 mm (centre to centre).

The frames were arranged in the flume with three frames positioned across the width, and nine frames along the flume. They were positioned with the wooden part on top.

Sediment used for the testing was graded silica non-cohesive sand with 0.3-0.65 mm diameter, produced by the South African company Eggo Sand. A particle distribution analysis was performed (by sieve techniques) before using the sand in the experiments. The results of the analysis of particle size distribution are given in Table 1, Appendix C, and the particle size distribution curve No.1 is presented in Fig.10.1.

It was found that a very fine fraction was present in the material. It was assumed that this fraction would be washed out during the experiments, changing the particle size distribution. To ensure that particle size distribution was the same for all experiments, the fine fraction was, therefore, eliminated by sieving and the sediment prewashed. The size analysis for the sieved washed sediment is presented in Table 2, Appendix C. The granulometric curve No. 2 of sieved sand is shown in Fig.10.1. The D_{50} was 0.45 mm.

10.1.2.2 Experimental Procedure

All experiments were performed until conditions of equilibrium were attained. To ensure this condition, the transported sediment was collected in a bag fastened to the downstream end of the flume. The mass of sediment being fed into and flowing out of the test section could thus be compared, the respective mass being measured volumetrically. The duration of the sediment collection period was recorded by a stopwatch, and the water temperature measured by a thermometer. The length of the flume was subdivided into reaches of 1.0 m length, so defining the location of observation points. Flow depth was measured using scales fixed at every half metre along the length of the flume to ensure the uniform flow.

The series of experiments are presented in Table 10.1. The experiments can be divided into two series: Series B1 had a constant flow with various sediment feed rates, and Series B2 had a constant sediment discharge with various rates of flow.

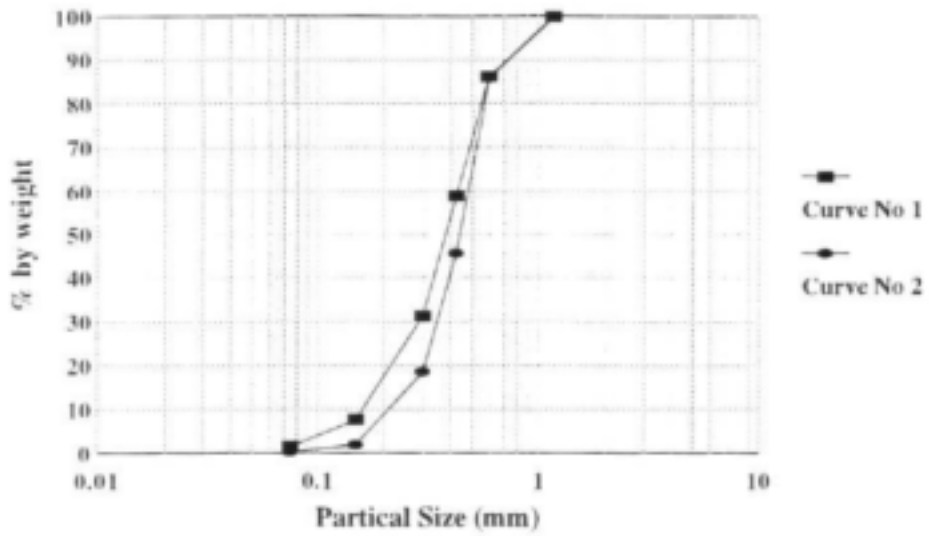

Figure 10.1 Granulometric curve for used sediment

Table 10.1 **Series B 1 and B 2 experiments**

Number of experiments	Flow rate q ($m^3/s/m$)	Sediment feed rate q_s (kg/s/m)
Series B1		
B 1.1	0.0065	0.005
B 1.2	0.0065	0.0097
B 1.3	0.0065	0.0131
B 1.4	0.0065	0.0186
Series B2		
B 2.1	0.0034	0.0085
B 2.2	0.0054	0.0085
B 2.3	0.0111	0.0085
B 2.4	0.0159	0.0085
B 2.5	0.0185	0.0085

Maximum flow retardation and minimum sediment carrying capacity occur during emergent flow. In the natural environment vegetation remains erect until submergence is complete. The experiments were thus conducted for flow through emergent rigid stems. The experimental programme was thus divided into two sections, Series B1 and Series B2. Each of these two sets of experiments is described in turn below.

10.1.2.3 Series B1 Experiments

The first series of experiments (Series B1) was conducted to establish the effect of sediment rate on flow depth and bed slope under constant discharge. Experiments were performed under constant flow with various sediment discharge rates. The aim of the experiments was to investigate the relationship between bed load discharge and hydraulic parameters such as bed slope and flow depth for given flow.

A 25 mm layer of sediment was spread over the flume bed before the artificial vegetation was placed in the flume as described in the Section 10.1.2.1. The discharge was set by adjusting the upstream control valve and determined by the V-notch weir measurements. The flow depth was checked at every half metre along the length of the flume and the downstream tailgate adjusted to maintain uniform flow before each test as well as during the tests.

Four sediment discharge rates were tested for a given flow rate in order to obtain a range of bed slope profiles. Each sediment feed rate was set (see Section 10.1.2.2) before testing and was also checked after testing to ensure that the sediment feed rate did not change. Each sediment experiment was run until the sediment input rate equalled the output rate. After equilibrium conditions were first attained the test was continued for some time to ensure stability. The bed slope was obtained from height differentials over 1 m lengths for each of the four tests. The measurement of the bed heights along the experimental flume are presented in Table 3, Appendix C. Flow depth and water temperature were also measured for each test and are listed in Table 5 in Appendix C.

Results of Series B1 Experiments

The bed slope and flow depth controlled by the different sediment discharges were measured in the flume under equilibrium conditions during each experiment.

The bed profile was determined by taking seven measurements of the bed height along the channel at 1 m intervals for each test. The measurements were taken at the equilibrium condition. The bed slopes were derived from a linear regression analysis of the measured heights of the bed profile for each test. The correlation coefficients ranged from 0.992 to 0.998 (Table3, Appendix C). The bed profiles were plotted against longitudinal distance along the flume for all experiments of Series B1 and are presented in Fig.10.2. The influence of sediment feed rate on the bed slope gradient is illustrated in Fig.10.3. It is clear that higher sediment feed rates form steeper bed gradients for a given discharge.

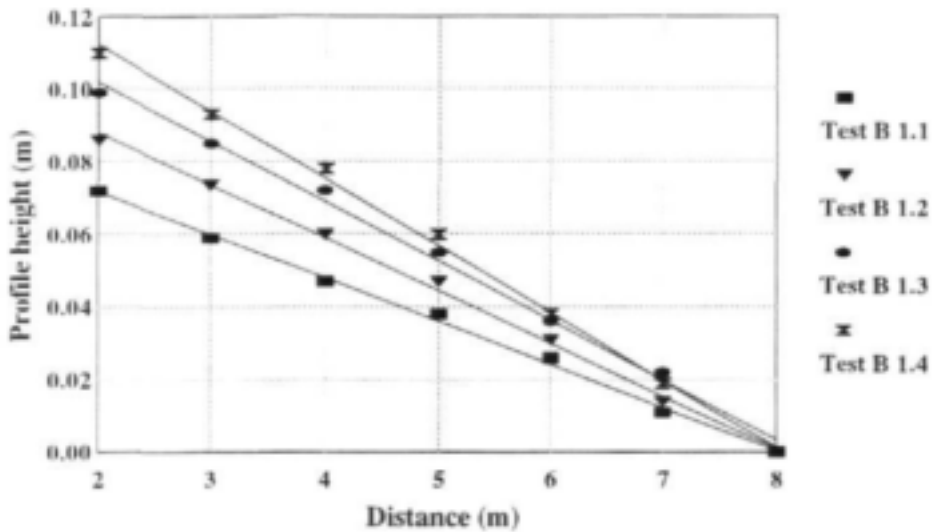

Figure 10.2 Measured bed profiles for Series B1 experiments

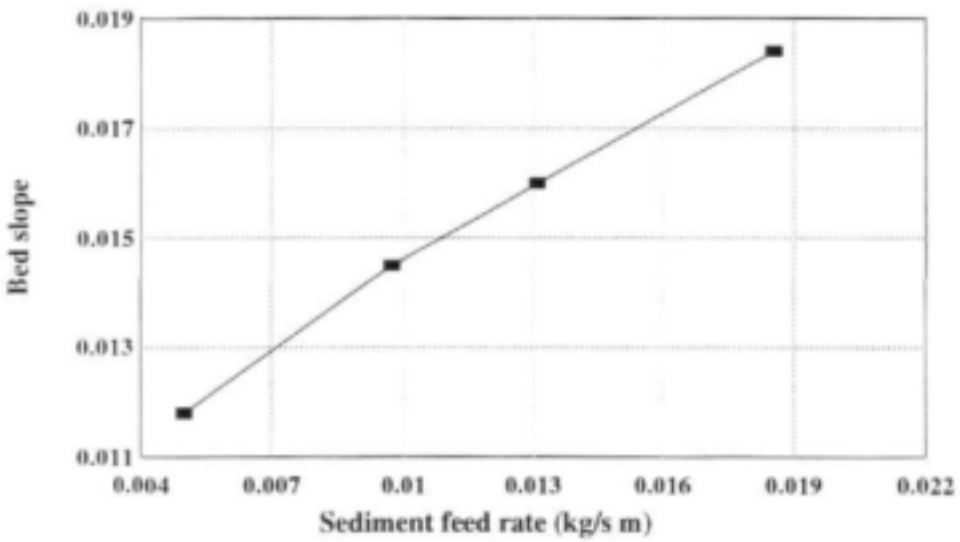

Figure 10.3 Influence of sediment feed rate on bed slope, q=0.0065 $m^3/s/m$

Uniform flow was maintained by adjusting the downstream tailgate during the experiments, and the uniform depth was measured for each experiment. The measured depths are listed in Table5 (Appendix C). The influence of sediment feed rate on stage is illustrated on Fig.10.4, showing that flow depth decreases with increasing sediment feed rate.

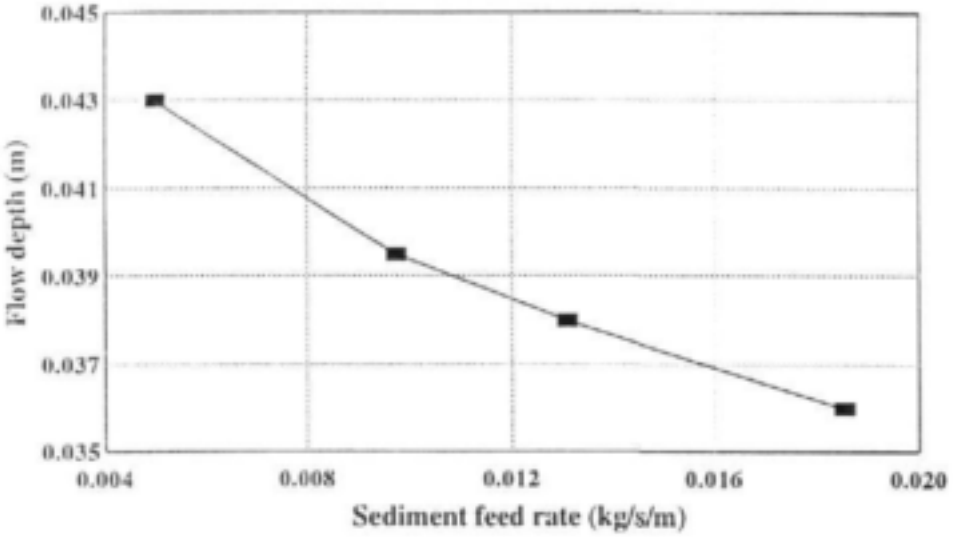

Figure 10.4 Influence of sediment feed rate on flow depth (q=0.0065 $m^3/s/m$)

10.1.2.4 Series B 2 Experiments

The second set of experiments comprised a constant sediment load discharge rate combined with various flow rates. The aim of these experiments was to investigate how hydraulic parameters (bed slope and flow depth) change with different flow rates for a given sediment discharge rate. The sedimentation feed rate was set before testing and was checked before and after each experiment to ensure that it remained the same. Flow rate was controlled by the upstream valve and was measured using the V-notch weir. The experimental procedure and measurement methods were the same as those under constant flow rate, as described above. The measured heights of the bed profile and flow depth for each test are listed in Tables 4 and 5 respectively in Appendix C.

Results of Series B2 Experiments

In this set of experiments bed slope and flow depth were controlled by the discharges. Measurements of the flow depth and the bed slope were taken under equilibrium condition during each test.

The bed profiles were determined by measuring the bed heights along the channel at 1 m intervals. The bed slopes were derived from a linear regression analysis of the measured heights of the bed profile with correlation coefficients from 0.987 to 0.999 (Table 4, Appendix C). Figure 10.5 is a plot of measured bed profiles against longitudinal distance for the experimental flume. The influence of the discharge on the bed slope gradients for a given sediment feed rate is shown in Fig.10.6. The results of the experiments presented in Fig.10.6 show that for a given sediment discharge the bed slope gradient decreases with increase of the flow rate. At a certain stage (Fig.10.6), however, further increase in the flow rate has no influence on the bed slope gradient, indicating that the incremental resistance is almost all from stem drag and that bed shear does not increase. This demonstrates the effectiveness of vegetation in protecting the bed from erosion at high flows.

The measurements of the depths are presented in Table 5 (Appendix C). A stage-discharge relationship for a given sediment feed rate is plotted in Fig.10.7.

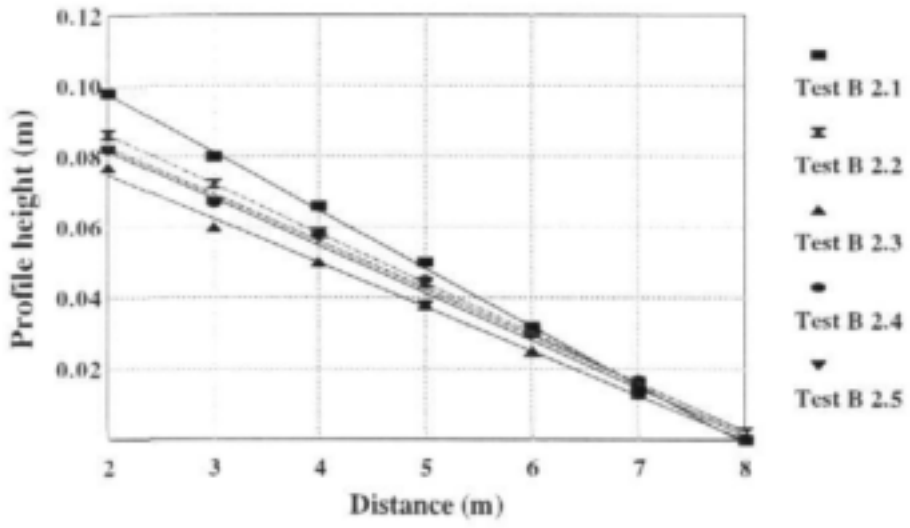

Figure 10.5 Measured bed profiles for Series B2 experiments

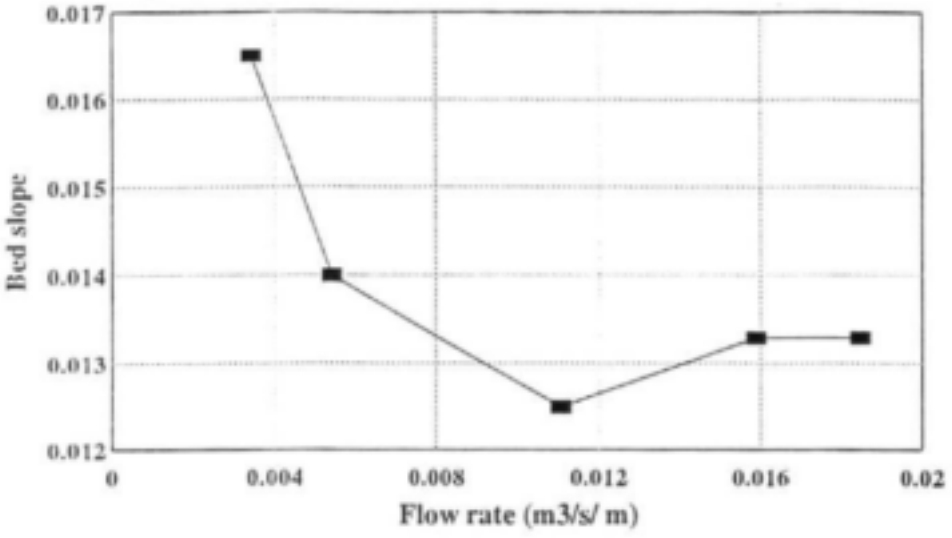

Figure 10.6 Influence of flow rate on bed slope (q_s=0.0085 kg/s/m)

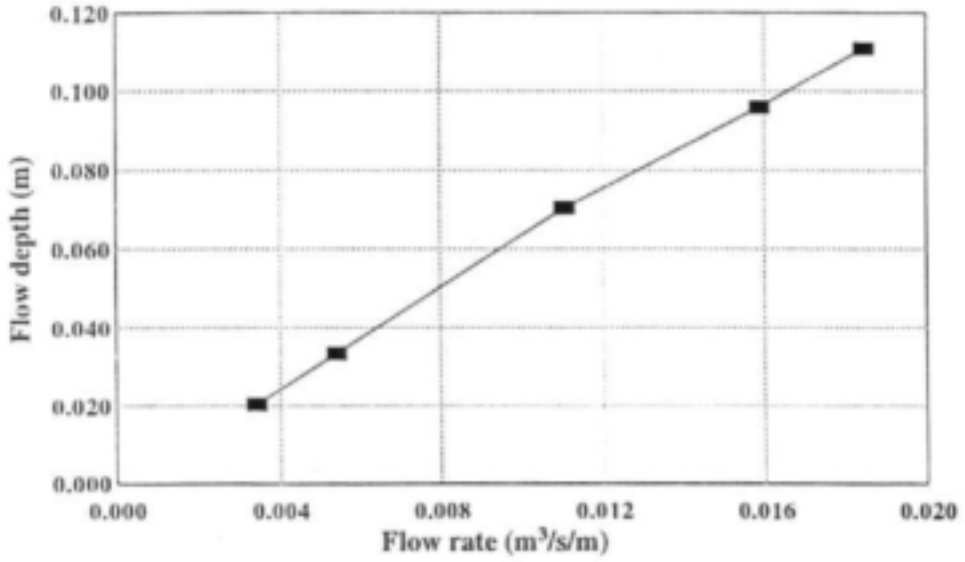

Figure 10.7 Stage-discharge relationship for Series B2 experiments (q_s=0.0085 kg/s/m)

10.1.3 Sediment Equation for Emergent Flow

10.1.3.1 Sediment Transport

The amount of bed material a stream can carry is determined by the size of bed material (sometimes represented by the fall velocity of the particles), the slope of the stream or the average stream velocity, and nature of the channel, including the depth, size, shape and roughness of its bed and banks (Lane and Borland, 1950).

There are a number of bed load equations which have been developed for predicting the bed load of a stream. More than hundred yeas ago du Boys (1879) advanced a model of sediment transport based on assumption that the sediment moves in layers of thickness ε. The shear stress applied to the bed is balanced by the sum of the resistance forces between the layers,

$$\tau_0 = c_f n \varepsilon (\gamma_s - \gamma) \tag{10.1}$$

where c_f is a friction coefficient, and γ_s and γ are the unit weights of the sediment and water respectively. The velocity of the surface layer is $(n-1)\, v_s$, where v_s is the velocity increment between layers. If the layers between the first and n^{th} layers moves according to a linear distribution, then the volumetric sediment transport rate per unit width is given by

$$q_s = \varepsilon v_s \frac{n(n-1)}{2} \tag{10.2}$$

The critical condition will occur when the top layer begins to move, when n=1, and in this case equation (10.1) becomes

$$\tau_c = c_f \varepsilon (\gamma_s - \gamma) \tag{10.3}$$

and

$$\tau_0 = n \tau_c \tag{10.4}$$

Introducing $n = \tau_0/\tau_c$ into equation (10.2) the following is obtained

$$q_s = \left(\frac{\varepsilon v_s}{2 \tau_c^2} \right) \tau_c (\tau_0 - \tau_c) \tag{10.5}$$

where $\varepsilon v_s / 2\tau_c^2 = \chi$ is a characteristic sediment coefficient. The total amount of bed load transport Q_s is given by

$$Q_s = \chi \int_{x_1}^{x_2} \tau_0 (\tau_0 - \tau_c) dx \qquad 10.6$$

where x is the width of the channel.

O'Brien and Rindlaub, (1934) generalized the du Boys equation (equation (10.5)) and the following relationship was proposed

$$q_s = \chi' (\tau_0 - \tau_c)^m \qquad 10.7$$

where χ' and m are parameters in functional relationship with the median diameter. The U. S. Waterways Experimental Station (1935) independently found the values of the exponent m to range from 1.5 to 1.8 for sand mixtures where $0.025<D<0.560$ mm.

10.1.3.2 Sediment Deposition in Simulated Grass Filters

Tollner et al. (1977) developed a model describing sediment deposition profiles in a rigid grass medium with uniform flow. Twenty experimental tests were performed to validate the sediment profile model in simulated cylindrical and flat bladed medium. The duration of each test was in the range the of 1-3 min. Flow rate, inflow sediment concentration and size, and medium density were systematically varied in order to obtain a wide range of results. The outflow was collected and weighed in a weigh tank. Flow rate and concentration data were used for determination of the rate of deposition. The sediment slope was obtained from profile height differentials over 30 cm lengths. After conducting the different experiments it was observed that when a steady flow of water and sediment were introduced into the medium, a triangular shaped wedge formed. When the flow duration was long enough, the wedge height increased up to the top of the medium height while leading edge of the sediment progressed downslope. In all cases the slope of the leading edge was nearly constant for a given hydraulic condition. This fact simplified the problem, making it possible to model it. The model is based on mass continuity and estimates the rate of advance of the leading edge of the sediment.

The mathematical model proposed by Barfield et al (1979) was developed to predict the outflow sediment load, q_{so}, resulting from a given incoming sediment load, q_{si}. The trapping efficiency, T_e, is given by

$$T_e = 1 - \frac{q_{sd}}{q_{si}} \left[1 - \frac{q_{sd} - q_{so}}{q_{sd}} \right] \qquad 10.8$$

where q_{sd} is the sediment load transported immediately downstream of the deposition wedge. Based on the experimental data collected in cylindrical media sediment transport in zone $D_{(t)}$ (Fig.1, Barfield et al, 1979) is given by

$$\frac{q_{sd} - q_{so}}{q_{sd}} = exp\left[-1.05 \times 10^{-3}\left(\frac{VR_s}{\nu}\right)^{0.82}\left(\frac{L_e V}{V_s d_f}\right)^{-0.91}\right] \qquad 10.9$$

where V is the mean flow velocity, V_s is the terminal settling velocity of the sediment particles, d_f is the depth of flow, L_e is the effective length of filter, and R_s is defined as the spacing hydraulic radius given by

$$R_s = \frac{b d_f}{2d_f + b} \qquad 10.10$$

where b is the spacing of the filter medium elements. Using the spacing radius the mean flow velocity can be obtained by

$$V = \frac{1}{n} R_s^{2/3} S_c^{1/2} \qquad 10.11$$

where S_c is channel slope and n is Manning's roughness coefficient.

The assumption that the spacing hydraulic radius can be used in place of the hydraulic radius to calculate tractive force was used. New calibration curves between the parameters were developed where the spacing hydraulic radius was substituted for flow depth in the parameters for each of the relationships studied. Einstein's (1942) transport relationship was used, and the modified equation for grass filters is given by

$$\psi = 1.08\,\phi^{-0.28} \qquad 10.12$$

where ψ is the shear intensity parameter and ϕ is the Einstein bed load transport factor, defined by equations (10.13) and (10.14) respectively, i.e.

$$\psi = \frac{\rho_s - \rho}{\rho} \frac{d_p}{S_c R_s} \qquad 10.13$$

and

$$\phi = \frac{q_{sd}}{\rho_s \sqrt{\frac{\rho_s - \rho}{\rho} g d_p^3}} \qquad 10.14$$

where d_p is particle diameter, and q_{sd} is equilibrium sediment load per unit channel width.

Equation (10.13) and equation (10.14) are proposed to predict the sediments load downstream from the deposition wedge if the spacing hydraulic radius is known.

The model based on the modified Einstein procedure for calculating sediment load has not been evaluated independently of the data used to develop the model.

Tollner et al (1982) examined the sediment transport relationships developed by Tollner et al (1977) and Barfield et al (1979) for their suitability as predictors of sediment transport through a vegetated medium. In an attempt to reduce the complexity of analytically describing the flow through a vegetated medium an analogy between flow of depth d_f through a medium with a spacing of b and the flow through a deep, narrow rectangular channel with the same flow depth, d_f, and a width equal to b was proposed. The resulting shear on the channel is proposed as

$$\tau_b = \rho g R_s S_e \qquad 10.15$$

where R_s is equivalent hydraulic radius as in equation (10.10).

Equation (10.15) was used to calculate the bed shear for the all experimental runs. Calculated bed shear was used in an analysis made of the suitability of the relationship developed by Einstein (1942) and Graf (1971) for predicting sediment transport in a simulated medium. The relationship between the shear intensity parameter, ψ, and the Einstein bed load transport factor, ϕ , as modified for vegetated media for the total load given in equation (10.12) and for bed load is

$$\psi = 1.02\,\phi_b^{-0.413} \qquad 10.16$$

Observed and predicted values demonstrated good agreement, and therefore it was considered as being useful for research and design applications.

10.1.3.3 Flow Resistance in Vegetated Streams

Flow resistance through a given vegetated area is a function of many variables including flow velocity, distribution of vegetation, roughness of the channel boundary, and plants properties. The pressure forces applied per unit plan area are balanced (Petryk and Bosmajian,1975) by the resistance forces contributed by wall roughness and drag force of the plants

$$\gamma A L S = \tau_o P L + \sum D_i \qquad 10.17$$

where γ is the specific weight of liquid, A is the cross-sectional area of flow, L is the length of

channel, S is the bed slope of channel, D_i the drag force on the i^{th} plant, τ_o is the shear force per unit area on the channel boundary, and P is the wetted perimeter of the channel.

The drag force on each plant is given by

$$D_i = \frac{C_d \gamma V_i^2 A_i}{2g} \qquad 10.18$$

where C_d is the drag coefficient for the vegetation, V_i is the average approach velocity to the i^{th} plant (assumed to be equal the mean velocity), A_i is the projected area of the i^{th} plant in the streamwise direction.

The drag coefficient of the n^{th} stem is given by (Li and Shen, 1973)

$$\overline{C}_{dn} = \frac{U_{on}^2}{U_o^2} C_d \qquad 10.19$$

where C_d is the drag coefficient on an individual cylinder without any influence by other cylinders, U_{on} is the average approach velocity to the i^{th} cylinder, and U_o is mean velocity of flow based on channel flow area.

10.1.3.4 Proposed Sediment Equation

Application of Tollner et al's (1982) Sediment Prediction Model

For steady uniform flow in vegetated streams total flow resistance may be divided into boundary resistance and vegetation resistance. The boundary resistance is the result of shear and pressure forces acting on the grains comprising the boundary, whereas the vegetation resistance is due to the drag of the vegetation. The total shear stress τ may likewise be separated into bed shear stress, τ_b and shear stress contributed by the vegetation, τ_v. Bed load transport capacity is controlled by the bed shear stress. Tollner et al's (1982) sediment prediction model (the only one available for predicting the sediment transport potential of flow through the vegetation) was used to examine experimental data of Series B1 experiments. The bed shear stress for each experiment as well as the equivalent hydraulic radius (spacing hydraulic radius) were obtained by equation (10.15) and equation (10.10) respectively. The experimental data and the predicted (equation (10.16)) shear intensity parameters, ψ are listed in Table 10.2. Figure 10.8 presents a plot of calculated (equation (10.15)) bed shear stresses against the experimental sediment discharge rate. A critical shear stress of 0.933 N/m^2 was deduced as a value of the stress for zero sediment discharge obtained by extrapolating a graph (Fig.10.8) of observed sediment discharge versus calculated (equation (10.15)) shear stress. A dimensionless shear stress relevant to the critical shear stress of 0.933 N/m^2 is plotted against the boundary Reynolds number together with the Shields diagram

in Fig.10.9. Figure10.9 shows that application of Tollner et al's (1982) model to the experimental data resulted in a significant deviation from the Shields curve. The experimental shear intensity parameter, ψ, as well as that predicted by equation (10.16) are plotted together with Tollner et al's line of best fit of their experimental data (Tollner et al, 1982, Fig.4, page 1523) for the bed load relationship in Fig.10.10. From Fig. 10.10 it is clear that the experimental data of Series B1 (Tests B1.1, B1.2, B1.4 and B1.4) experiments do not have a good correlation with Tollner et al's results. It can be concluded therefore that Tollner et al's sediment prediction model is not applicable in this case.

Table 10.2 Application of Tollner et al's (1982) model

Characteristics	B1.1	B1.2	B1.3	B1.4
Flow depth (m)	0.0430	0.0395	0.0380	0.0360
Slope, S_b	0.0118	0.0145	0.1600	0.0184
Sediment discharge, q_s (kg/s /m)	0.0050	0.0097	0.0132	0.0184
Spacing, a (m)	0.025	0.025	0.025	0.025
Spacing hydraulic radius, R_s (m)	0.0097	0.0095	0.0094	0.0093
Bed shear stress, τ_b (N/m^2)	1.12	1.35	1.48	1.67
Particle diameter, d_{50} (m)	0.00045	0.00045	0.00045	0.00045
Shear intensity parameter, ψ	6.50	5.39	4.93	4.35
Einstein bed load transport factor, φ	0.05	0.10	0.13	0.18
Predicted Einstein's, ψ	3.54	2.69	2.37	2.07
Critical shear stress, τ_{cr} (N/m^2)	0.933			
Dimensionless shear stress	0.128			
Shear velocity (m/s)	0.031			
Boundary Reynolds Number, R_*	12.06			

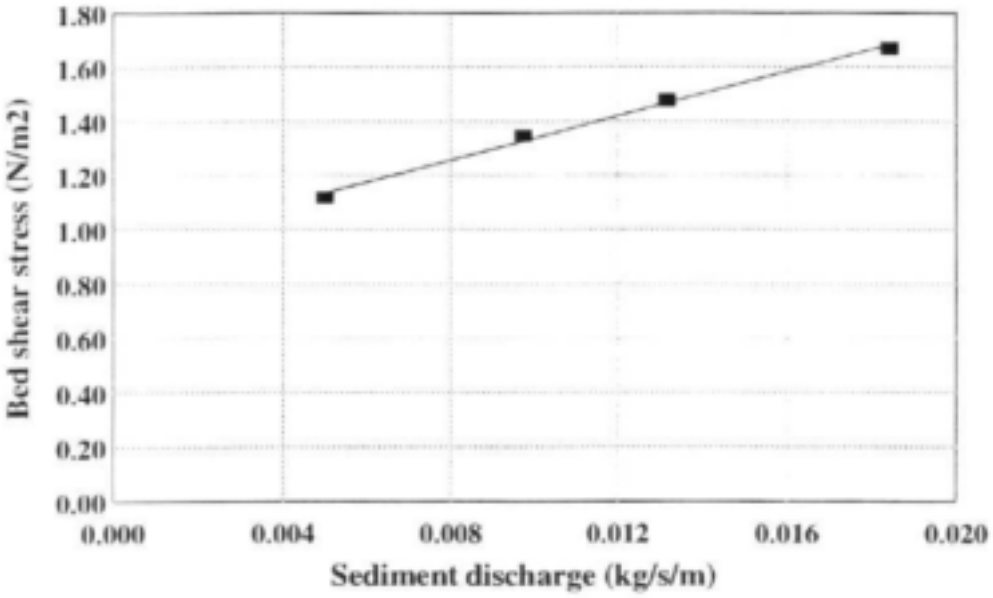

Figure 10.8 Calculated bed shear stress for Series B1 experiments using Tollner et al's (1982) model

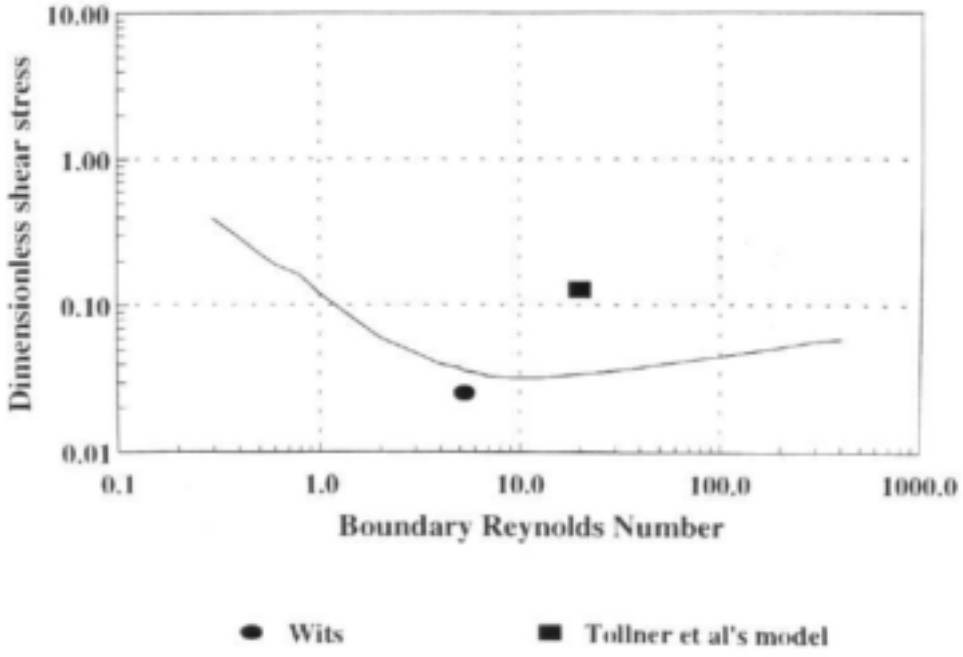

Figure 10.9 Critical shear stress for Series B1 experiments using Tollner et al's model and the proposed approach with the Shields curve

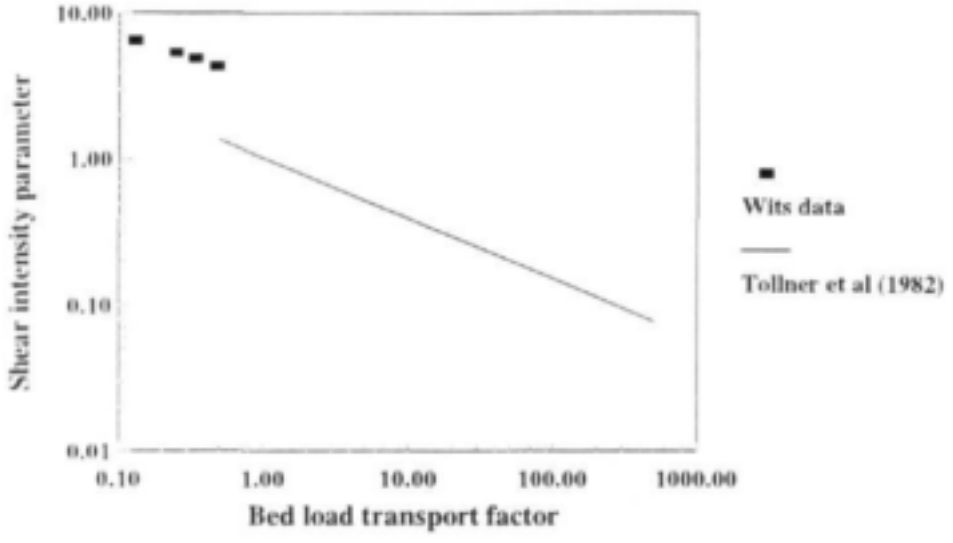

Figure 10.10 Experimental shear intensity parameter values compared with Tollner et al's (1982) line of best fit for their experimental data

Proposed Approach

The proposed equation for bed load sediment transport in vegetated streams takes the form of the du Boys type (equation (10.7)) equation,

$$q_s = k\left(\tau_b - \tau_c\right)^b \qquad 10.21$$

where τ_b and τ_c are the bed and the critical shear stresses, respectively, k and b are parameters in functional relationship with d_{50} diameter. The resistance force contributed by the bed is a part of the total pressure forces applied per unit plan of vegetated stream (Petryk and Bosmajian,1975). The resistance contributed by the drag force of the plants is given by equation (10.18). The drag coefficient for the vegetation is expressed by equation (10.19).

From equation (10.19) it can be seen that to derive the drag coefficients for the vegetation the approach velocity should be known. The approach velocity to a vertical stem in a stand of elements is different from the average velocity. This can be attributed to the development of a wake immediately downstream of the abstraction. A mathematical model (Li and Shen, 1973) of velocity in the wake behind roughness elements was utilized for developing an approach velocity equation for conditions listed in Table 10.3. The most suitable form of approach velocity

equation was found to be

$$V_{apr} = fn(\frac{a}{D}, D, V_{avr}) \qquad 10.22$$

where V_{apr} is the approach velocity, a is stem spacing, D is stem diameter and V_{avr} is the average velocity. The functional relationship for the adjustment factors presented in equation (10.22) was derived by subjecting the results of the simulated runs to multiple regression analysis.

Table 10.3 Ranges of variable values for simulation

Variable	Range
Stem diameter, D (m)	0.005 - 0.04
Stem spacing, a (m)	0.025 - 0.2
Bed slope, S_b	0.0005 - 0.005
Average velocity, V_{avr} (m/s)	0.1 - 0.7

The proposed approach velocity equation is valid for conditions listed in Table 10.3, and is represented by

$$V_{apr} = 1.0756\, D^{0.0065} \left(\frac{a}{D}\right)^{-0.0174} V_{avr}^{0.9895} \qquad 10.23$$

with r^2 equal to 0.99. The proposed equation generated the results simulated by the mathematical model with an average absolute error of 3.53%, a standard deviation of 1.13% and a maximum error of -5.56%.

The experimental values of the bed shear stresses were calculated from the Series B1 experimental results and are listed in Table 10.4. The drag coefficients for the vegetation were determined by Eq.10.19 and the approach velocities by Eq.10.23. The sediment discharges are plotted against the calculated bed shear stresses in Fig.10.11. A value of the critical shear stress (Table 10.4) is deduced as a value of the stress for zero sediment discharge from Fig. 10.11.

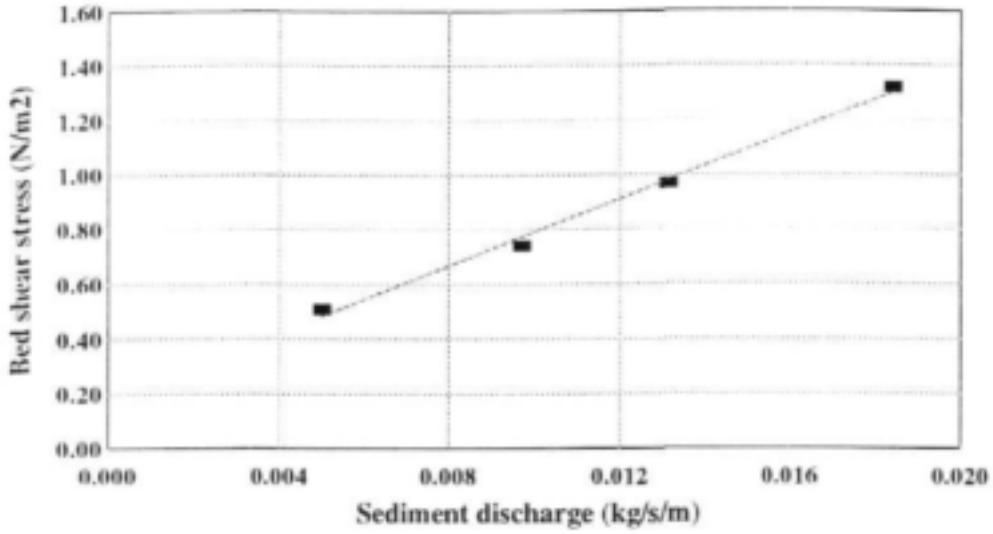

Figure 10.11 Calculated bed shear stress for Series B1 experiments using proposed approach

A dimensionless shear stress relative to critical shear stress is plotted against the boundary Reynolds number in the Shields diagram (Fig.10.9) manifesting a good correlation with Shields's results.

The functional parameters of the proposed sediment equation (equation (10.21)) were obtained by fitting the experimental data of the Series B1 experiments to the regression relationship. The regression coefficients in equation (10.21) are given by

$$q_s = 0.017\left(\tau_b - \tau_c\right)^{1.047} \qquad 10.24$$

with r^2 equal to 0.99. The average absolute error for the Series B1 experiments was 4.54%, with a maximum error of -6.5% and standard deviation of 2.16%, confirming reasonable representation. The measured sediment discharge values versus those predicted by equation (10.24) values for the Series B1 experiments are presented in Fig.10.12. The line of perfect correlation and 10 % accuracy limits are also shown (Fig.10.12).

Table 10.4 Series B1 experiments

Characteristics	B1.1	B1.2	B1.3	B1.4
Flow depth (m)	0.0430	0.0395	0.0380	0.0360
Slope, S_b	0.0118	0.0145	0.0160	0.0184
Sediment discharge, q_s (kg/s /m)	0.0050	0.0097	0.0132	0.0184
Flow discharge, q (m^3/s/ m)	0.0065	0.0065	0.0065	0.0065
Spacing, a (m)	0.025	0.025	0.025	0.025
Stem diameter, D (m)	0.005	0.005	0.005	0.005
Temperature (C^0)	23	18	19	20
Reynolds number	799	776	826	893
Average velocity, V_{avr} (m/s)	0.151	0.164	0.170	0.180
C_D from standard curve	1.058	1.064	1.050	1.031
Approach velocity V_{apr} (m/s)	0.155	0.169	0.175	0.185
Approach drag coefficient, C_{Di}	1.124	1.129	1.112	1.091
Total applied force (N/m^2)	4.82	5.44	5.78	6.30
Vegetation resistance force (N/m^2)	4.33	4.73	4.84	5.02
Bed shear stress (N/m^2)	0.51	0.74	0.97	1.32
Critical shear stress, τ_{cr} (N/m^2)	0.180			
Dimensionless shear stress	0.025			
Shear velocity (m/s)	0.013			
Boundary Reynolds Number, R_*	5.30			

Equation Examination

The performance of the proposed sediment equation (10.24) was based on analysing the Series B1 experimental results. The examination of the proposed equation (equation (10.24)) was performed by comparison of measured and predicted sediment discharge for the Series B2 experiments. The Series B2 experiments were accomplished under constant sediment feed rate (Table 10.1). Bed load sediment transport is controlled by bed shear stress. Therefore it is assumed that if sediment discharge is the same for all experiments of Series B2, the bed shear stress should also be the same. The same approach for the bed shear stress calculation as for the

Series B1 experiments was applied. The calculated bed shear stresses for each experiment of the Series B2 are listed in Table 10.5. The average bed shear stress for the Series B2 experiments is equal to 0.66 N/m^2 with a standard deviation of 0.035 N/m^2.

Table 10.5 Series B2 experiments

Characteristics	B2.1	B2.2	B2.3	B2.4	B 2.5
Flow depth (m)	0.0205	0.0335	0.0705	0.0960	0.1110
Slope, S_b	0.0165	0.0140	0.0125	0.0133	0.0133
Sediment discharge, q_s (kg/s /m)	0.0085	0.0085	0.0085	0.0085	0.0085
Flow discharge, q (m^3/s/ m)	0.0034	0.0054	0.0111	0.0159	0.0185
Spacing, a (m)	0.025	0.025	0.025	0.025	0.025
Stem diameter, D (m)	0.005	0.005	0.005	0.005	0.005
Temperature (C ^{0})	20.5	22	21	22	21
Reynolds number	845	841	798	860	446
Average velocity, V_{avr} (m/s)	0.168	0.162	0.157	0.166	0.166
C_D from standard curve	1.044	1.046	1.058	1.04	1.044
Approach velocity V_{apr} (m/s)	0.173	0.167	0.162	0.170	0.171
Approach drag coefficient, C_{Di}	1.107	1.109	1.123	1.103	1.107
Total applied force (N/m^2)	3.22	4.46	8.38	12.14	14.03
Vegetation resistance force (N/m^2)	2.54	3.84	7.72	11.46	13.44
Bed shear stress (N/m^2)	0.70	0.63	0.68	0.69	0.61

The proposed sediment equation (10.24) was applied to predict the sediment discharge of the Series B2 experiments. The proposed sediment equation predicts the measured sediment discharges with an average absolute error of 7.18 %, a standard deviation of 6.82 % and a maximum error of 17.35 %. The predicted sediment discharges with the bed shear stresses and the absolute errors are listed in Table 10.6.

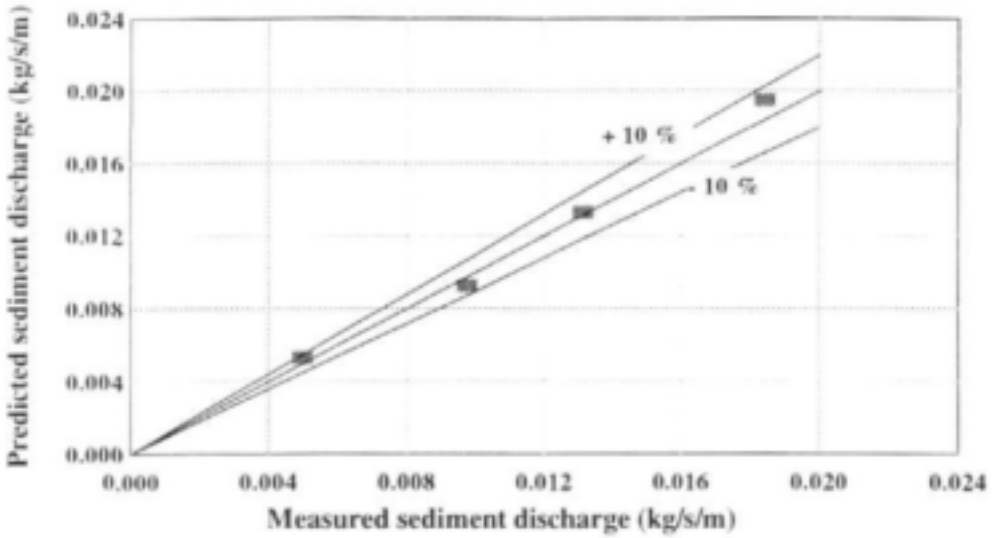

Figure 10.12 Measured and predicted sediment discharge with 10% accuracy limits

Table 10.6 Predicted sediment discharge

Test	Bed sheas stress, τ_b (N/m^2)	Predicted sediment discharge, q_s (kg/s/m)	Absolute error, (%)
B 2.1	0.70	0.0086	0.85
B 2.2	0.63	0.0074	13.33
B 2.3	0.68	0.0082	3.21
B 2.4	0.69	0.0084	1.18
B 2.5	0.61	0.0070	17.35
		Average error	7.18
		Standard Deviation	6.82

10.1.4 Conclusion

A number of experiments (Series B1 and B2) were performed in the hydraulics laboratory to investigate sedimentation processes in a vegetated stream. The study was undertaken to obtain a general knowledge of how sediment transport is influenced by vegetation. An equation for the prediction of sediment transport in vegetated stream was presented.

The amount of sediment a vegetated stream can carry is determined by the bed shear stress. A procedure for practical estimation of bed shear stress was developed. The procedure relies on the difference between the total shear stress and the shear stress contributed by the vegetation. The bed shear stress contributed by the vegetation is a function of the vegetation characteristics such as a vegetation density, vegetation stem diameter and drag coefficient of vegetation. The drag coefficient of the vegetation is in turn a function of approach velocity. The equation for calculation of the approach velocity as a function of a relative stem spacing, stem diameter and average velocity was derived.

The flow depth and bed slope are significantly influenced by the sediment discharge. The experiments carried out under the constant flow condition show that the flow depth decreases with increasing sediment rate and the highest sediment rates form steeper bed gradients. The experiments conducted to determine the influence of flow discharges on bed gradient under constant sediment rate show that the bed slope decreases with increase of the flow rate. However, at a certain stage further increases in the flow rate have no influence on the bed gradient.

An equation for prediction of sediment transport in vegetated stream was developed based on the Series B1 experiments. The results of the Series B2 experiments were used to validate the proposed equation, and good correlation was obtained. The experiments were performed for one sediment size and one stem spacing only, and therefore further investigation for confirmation of the proposed equation for practical application is necessary.

10.2 SEDIMENTATION IN PARTIALLY REEDED CHANNELS

10.2.1 Introduction

A streambank's and streambed's vegetation plays an important role in the riparian stream ecosystem. The riparian-stream is a crucial component for the restoration or reestablishment of streambank and streambed as well as for providing environmentally favourable spaces for aquatic species. Sediment deposition in a degraded stream system is essential to channel morphology. It is therefore necessary to be able to predict sediment entrapment and sediment retention in streambank and streambed vegetation.

Vegetation is a key component in river management (Tsujimoto, 1999). The management of fluvial processes should include multi-functional aspects such as safety against floods, water resource utilization and ecological preservation. To achieve this, a clear understanding of hydraulic processes of flow with vegetation and the interaction between vegetation and sediment

required for aquatic habitat formation and ecological functioning is required. The key to modelling vegetation in hydraulics is quantifying spatial drag due to vegetation elements and additional production of turbulent energy. Tsujimoto (1999) explained how to treat flow with vegetation, and used a 2D analysis of fluvial processes related to flow with vegetation.

The presence of vegetation significantly enhances the deposition of sediment in a channel. The height of vegetation influences the amount of sediment deposition. Abt et al (1994) performed a series of laboratory experiments to test sediment entrapment and retention potential in a simulated stream system as a function of discharge and vegetation blade length. Four series of tests were carried out in a trapezoidal channel which had a width of 5.5 m and a length of 18.9 m. The first series of tests attempted to ascertain where deposition would occur in a simulated stream system without the presence of vegetation. The second series of tests attempted to test sedimentation potential due the presence of vegetation. The third series attempted to estimate the entrapment potential of vegetation during flushing (flushing is a simulation of the recession limb of a hydrograph). The fourth series was aimed at ascertaining the difference between wider bladed vegetation and bluegrass in enhancing sediment deposition. The results of four series of tests indicated that the presence of vegetation enhances deposition, and that the amount of sediment trapped is a function of flow and vegetation blade length.

The ability of vegetation to entrap and retain sediment is related to the length and cross-sectional area of vegetation. A sedimentation factor (Thornton et al, 1997) could be introduced as a predictor for the sediment deposition expected in a stream system given by

$$S_d = \frac{\left(\frac{A}{P}\right)L}{F_r D d^4} \qquad 10.25$$

where A is cross-sectional area of vegetative stem (cm^2), P is circumference of vegetative stem (cm), L is length of vegetation (cm), F_r is Froude Number, D is density of vegetation (number of stems per cm^2) and d is flow depth (m). The amount of sediment deposited in vegetated bed is given by

$$D_s = 1.856\, S_d^{-0.218} \qquad 10.26$$

where D_s is deposited sediment in kg/m^2. The percent sediment retained in flexible and rigid vegetation is presented by

$$R_s = 42.835 + (1.097\, L) \qquad 10.27$$

where R_s is percent of sediment retained and L is length of vegetation (cm). The relationship expressed in equation (10.27) is based on vegetation lengths ranging from 1.3 cm to 35.56 cm.

The amount of sediment entrapped by the vegetation is given by

$$E_s = R\, D_s \qquad 10.28$$

where E_s is entrapped sediment (kg/m^2), R is the fraction of sediment retained (in decimal form) and D_s is amount of sediment deposited (kg/m^2).

The results of the study indicated that the vegetation could retain between 30% and 70% of the deposited sediment.

Tsujimoto and Kitamura (1994) studied flow and sediment transport in a channel with a longitudinally continuous zone of vegetation. In a channel with a vegetated zone, the water flows in the vegetated areas, and it influences the flow in the main channel. The flow near the interface between vegetated and non-vegetated zone is identified by fluctuations of the water surface. The faster flow in the channel is laterally mixed with the slow flow in the vegetated areas. The mixing of momentum causes an increase in the flow resistance and the lateral deposition of the sediment. This phenomenon was reproduced in the laboratory flume in an idealized condition. A process observed in a laboratory flume was described by the non-equilibrium bed load transport model and shows a good correlation with the observed results.

10.2.2 Sediment Experiments

A series of experiments were performed in an experimental flume to investigates sedimentation processes in a partially vegetated stream. The influence of vegetation strips on entrapment and retention of sediment were researched as a function of the discharge. In order to understand the morphodynamics around the vegetation, a series of experiments were carried out for three different lengths of isolated patches. A deposited volume of sediment and a decay rate of sediment were studied as a function of the discharge.

10.2.2.1 Experimental Set Up

All experiments were conducted in the same flume where the experiments of the basic sedimentation were performed. The flow rate in the flume was controlled by the opening or closing of two control valves situated on the upstream end of the flume. The V-notch weir installed at the outlet of the stilling basin was used for flow measurement.

A belt feeder mounted upstream at the top of the experimental flume was used to supply the sediment. Sediment discharge rates were controlled by the speed of the belt.

Details of experimental set up have been presented in section 10.1.2.1.

10.2.2.2 Longitudinal Strip Reed Sedimentation

Experimental Procedure

Longitudinal strips of vegetation were imitated by wooden frames into which were inserted 5 mm metal rods at 25 mm spacing (centre to centre). These were installed in the left side of the flume covering one third of the cross sectional area of the flume. The frames (125 by 1000 mm) were positioned with the wooden parts on the top. The metal rods were arranged in a staggered pattern (Fig. 4.1).

The sediment tested was the same as at the basic sedimentation experiments. The analysis of particle size distribution is presented in Table 1, Appendix C, and the particle size distribution curve is given in Fig.10.1. The sediment being fed into and flowing out of the flume was collected in a bag fixed at the downstream outlet of the flume, and measured volumetrically.

All experiments were performed under uniform flow conditions. Flow depth was measured at every half metre along the length of the flume to ensure uniform flow.

The testing programme comprised two test series: Series B 3 consisted of three tests to evaluate the sediment entrapment potential of the longitudinal strip during the deposition of sediment (Table 10.7). Series B 4 consisted of three tests conducted to investigate the sediment retention potential of the longitudinal strip during the erosion process as a function of discharge (Table10.8).

Series B 3 Experiments and Results

The Series B 3 experiments were conducted to investigate how discharge influences the sediment entrapment potential of the longitudinal strip for a given sediment rate. Tests B 3.1, B 3.2 and B 3.3 were characterized by feeding a constant rate of sediment (Q_s=8.4 g/s) for 80, 100 and 120 minutes respectively. The tested discharges were 3.2, 5.2 and 7.47 l/s (Table 10.7) for tests B 3.1, B 3.2 and B 3.3 respectively.

Table 10.7 Series B3 sediment entrapment experiments

Test	Time, T (min)	Discharge, Q (l/s)	Q_s / Q (g/l)	Deposited / Input sediment volume (%)
B 3.1	80	3.20	2.47	7.56
B 3.2	100	5.20	1.62	12.76
B 3.3	120	7.47	1.14	11.49

The testing procedure was consistent for each of the experiments. The artificial vegetation was installed along the left side of the flume. The sediment hopper was filled and the sediment rate was calibrated by adjusting the speed of the belt. The desired discharge was set by opening or closing the control valves. Uniform depth was maintained by the tailgate fixed downstream of the flume.

Three flow rates were tested for a given sediment rate in order to obtain the entrapment potential of the longitudinal strip as a function of the flow rate. The mass of sediment being fed into the flume was calculated and is listed in Table 6, Appendix C. The mass of sediment flowing out of the flume was collected in the bag per time period and measured. The mass of the sediment deposited in the stems was measured at the end of each test.

The results in terms of the volume of sediment deposited for each test are presented in Table 6, Appendix C. The sediment-time deposition graphs are given in Figs10.13, 10.14 and 10.15 for experiments B 3.1, B 3.2 and B 3.3 respectively. From these figures it is observed that the deposition of sediment is higher at the beginning of the tests and it decreases with time. The influence of the flow rate on the sediment deposition for a given sediment discharge is illustrated in Fig.10.16. It is obvious (Fig.10.16) that flow rate affects the deposition of sediment, the highest discharge resulting in the highest sediment deposition. The relationship of the ratio of the deposited sediment to fed sediments versus the flow rate is given in Fig. 10.17. From Fig. 10.17 it can be concluded that the ratio tends to stay approximately constant (10%) with an increase in the flow rate (additional experiments will be required to investigate it for a wider range of flow rate and a sediment ratios).

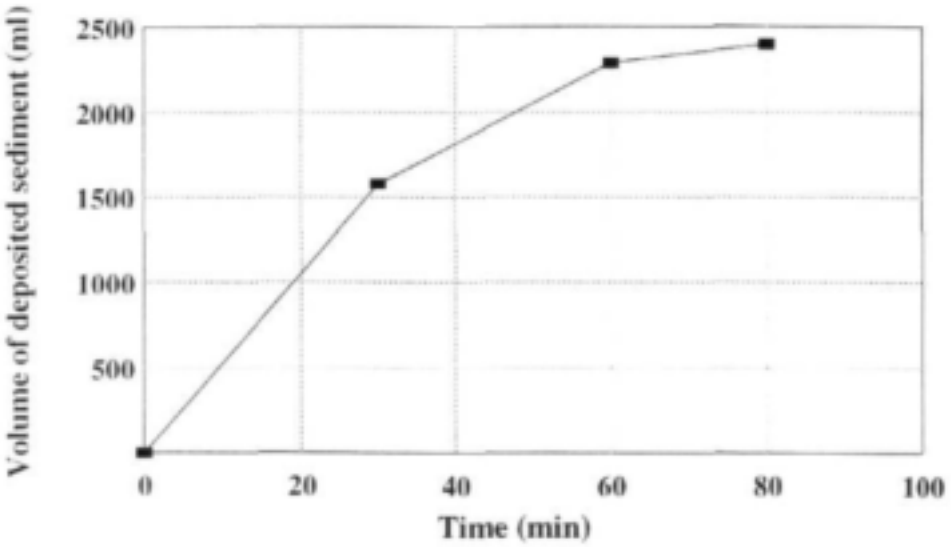

Figure 10.13 Sediment-time deposition relationship for Series B3.1 experiment

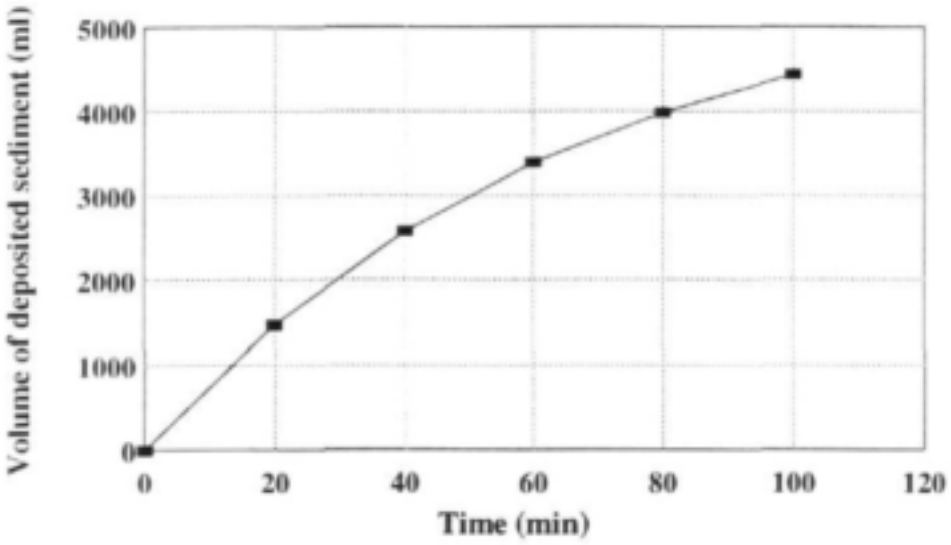

Figure 10.14 Sediment-time deposition relationship for Series B3.2 experiment

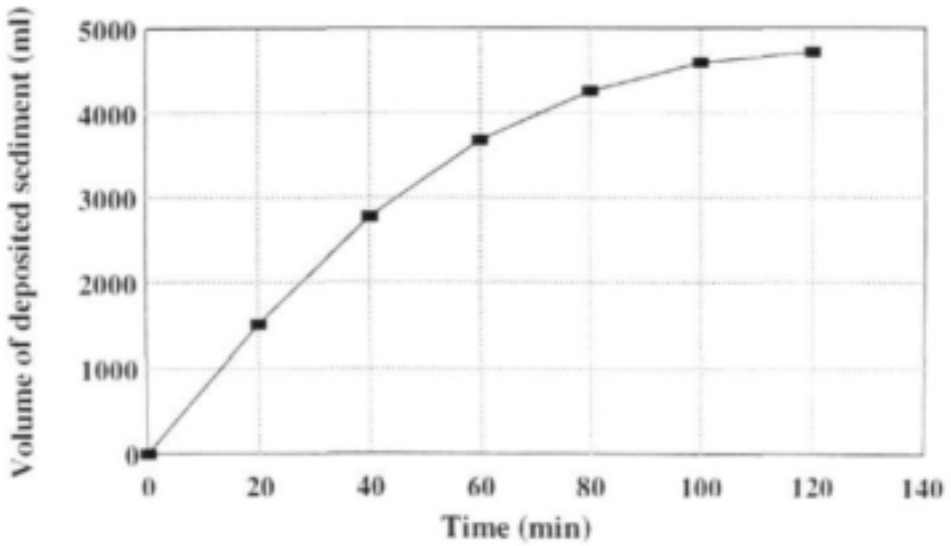

Figure 10.15 Sediment-time deposition relationship for Series B3.3 experiment

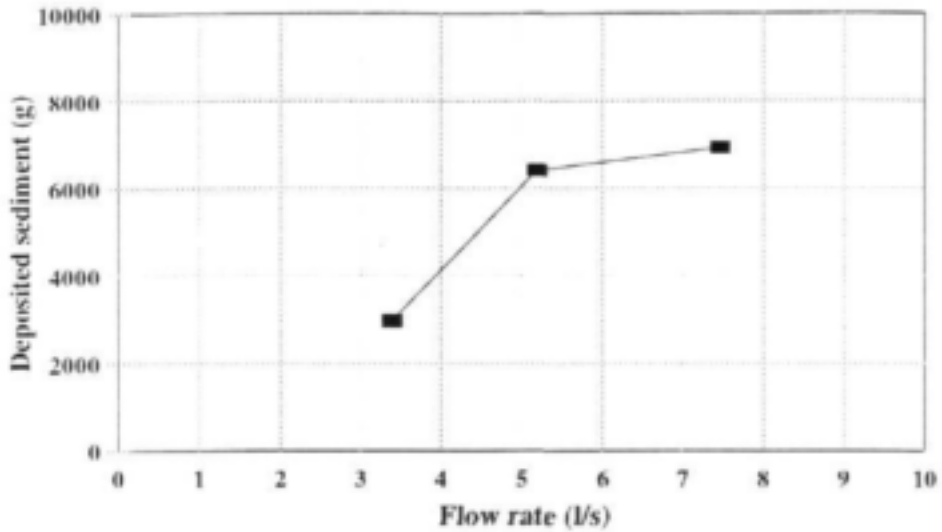

Figure 10.16 Influence of flow rate on sediment deposition (Q_s=8.4 g/s)

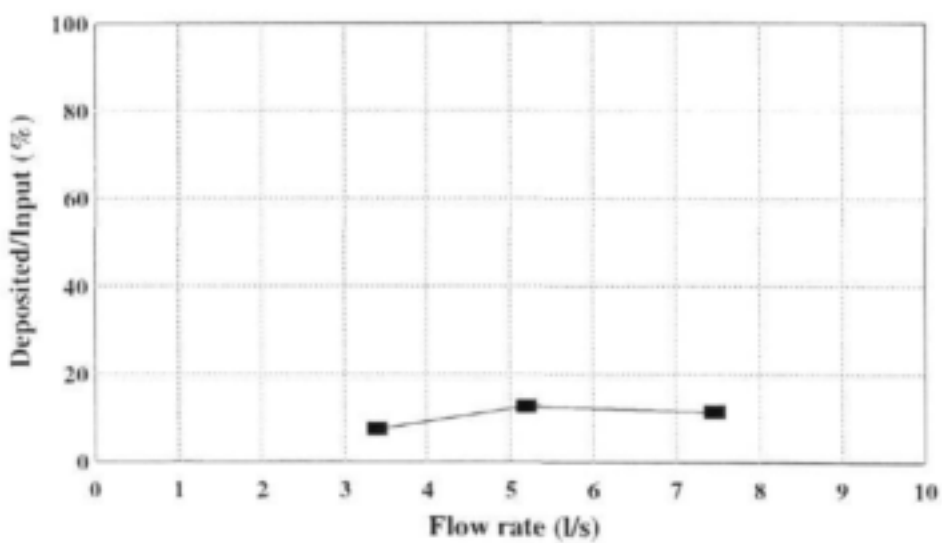

Figure 10.17 Relationship of flow rate and ratio of deposited to input sediment

Series B 4 Experiments and Results

The Series B 4 experiments were performed to establish the effect of vegetation on sediment retention. Experiments were performed at various discharge rates (Table 10.8). The aim of the experiment was to investigate the relationship between flow discharge and retained sediment in a simulated stream system.

Table 10.8 Series B4 retention potential experiments

Test	Time, T (min)	Discharge, Q (l/s)	Retained sediment (%)
B 4.1	400	1.79	70.68
B 4.2	630	5.20	60.80
B 4.3	960	7.47	52.44

A given volume of sediment (Table 7, Appendix C) was spread over the left side of the flume bed before inserting the artificial strips of vegetation. The flow was introduced slowly in the flume by adjusting the upstream control valve.

Three discharge rates were tested in order to obtain a range of retention volumes of sediment. Each experiment was run until the volume of eroded sediment equalled approximately zero. Duration of each test is listed in Table 10.8. The experiments were terminated when the erosion process was completed. The artificial strips were then taken out of the flume and the volume of the retained sediment was measured volumetrically.

The results of the sediment retention experiments are presented in Table 7, Appendix C. The results are given in terms of the volume of retained sediment as well as the initial sediment volume placed in the flume before each test. The sediment-time erosion diagrams are given in Figs10.18, 10.19 and 10.20 for experiments B 4.1, B 4.2 and B 4.3 respectively. From these diagrams it is obvious that the maximum erosion occurs at the beginning of the tests and it decreases with time. The influence of the flow rate on the retention of sediment by the vegetation is illustrated in Fig.10.21. It is observed (Fig.10.21) that sediment retention varied from 52% to 70 %. The volume of retained sediment for each test is presented in Table 7, Appendix C. The percent sediment retained after introducing different discharges is listed in Table 10.8.

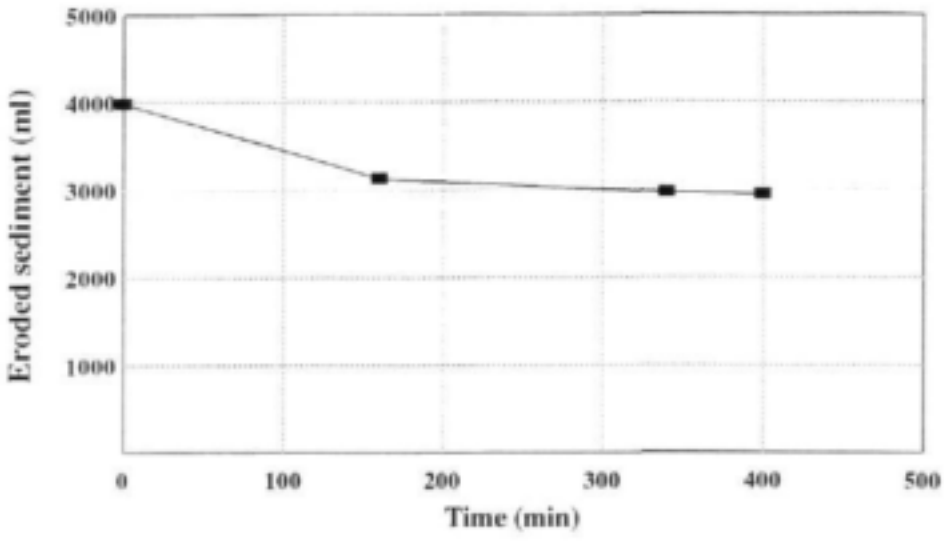

Figure 10.18 Sediment-time erosion relationship for Series B4.1 experiment

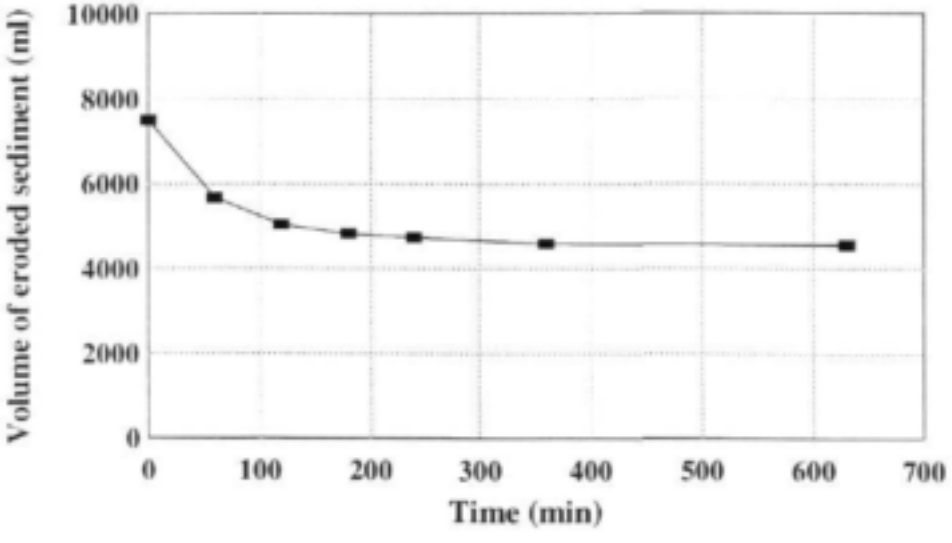

Figure 10.19 Sediment-time erosion relationship for Series B4.2 experiment

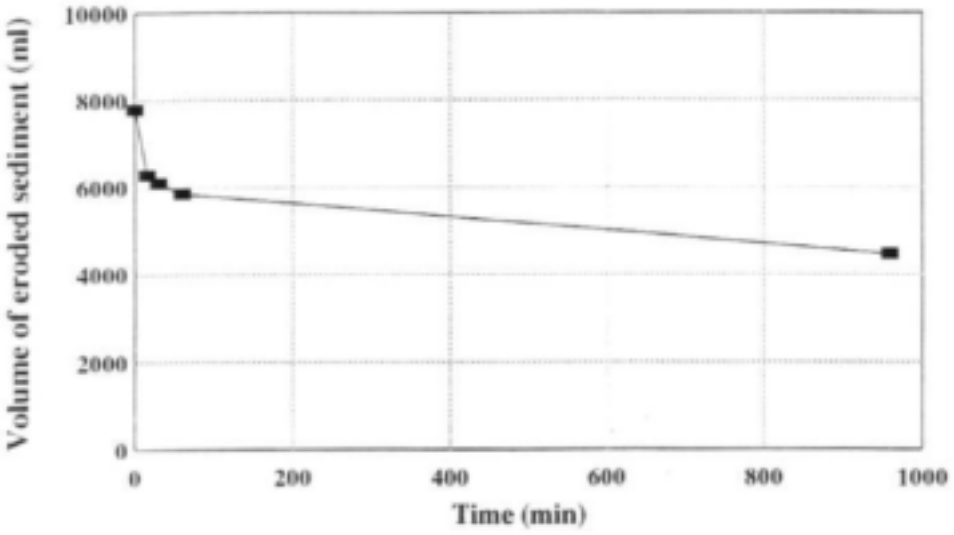

Figure 10.20 Sediment-time erosion relationship for Series B4.3 experiment

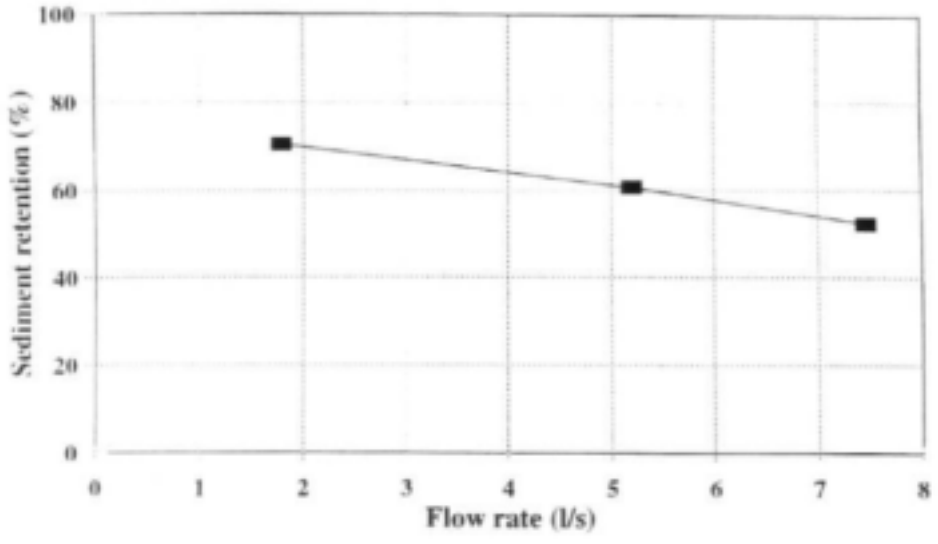

Figure 10.21 Influence of flow rate on retention of sediment (Series B4 experiments)

10.2.2.3 Isolated Patch Reed Sedimentation

Experimental Procedure

The idealised vegetation patches were made from perspex blocks which held apart 1.6 mm diameter copper rods with a 14 mm spacing. The diameter of the rods and the spacing were chosen to have the same density of the vegetation in terms of λ. λ is vegetation density defined as the projected area of vegetation to the flow per unit volume of water (Tsujimoto and Shimizu, 1994). Three lengths of the isolated patches were tested, full, half and quarter length. The width of the vegetation patches was the same (70 mm), and the length of each investigated patch (L) is given in Table 10.9.

Table 10.9 Series B5 deposition experiments

Test	Q (l/s)	L (mm)	Q_s (g/s)	Q_s/Q (kg/l)
B 5.1	5.26	140	9	0.00171
B 5.2	6.88			0.00131
B 5.3	8.93			0.00101
B 5.4	4.43	280	9	0.00203
B 5.5	6.73			0.00134
B 5.6	9.10			0.00099
B 5.7	5.13	560	9	0.00175
B 5.8	6.31			0.00143
B 5.9	9.54			0.00094

Sediment used for the testing was coal with d_{50} of 1 mm. Coal was used because its relatively low density (1500 kg/m^3) enhanced mobility at the low flow velocities used in the experiments. A particle distribution analysis was performed by sieve techniques and the results are presented in Table 8. Appendix C. The granulometric curve of the sediment used is shown in Fig. 10.22.

The experiments were performed in the same flume where the previous experiments were conducted. The flume and feeder were cleaned and all sand particles were taken out so as not to influence test results. A grid 50 mm by 50 mm was drawn on the flume bed surface for scaling purposes.

The laboratory testing consisted of two series of tests, namely Series B5 and B6 (Tables 10.9 and 10.10). Series B5 consisted of nine tests which investigate the relationship between flow rate and deposited volume of sediment for three different lengths of vegetation patches. The tests for each vegetation length consisted of three different flow rates. These flow rates were approximately 5, 7 and 9 litres per second. Series B 6 consisted of three tests which investigated the decay rate of the deposited sediment for the three lengths of vegetation patches. The decay rate of the sediment occurs when the deposited bar size decreases in the absence of sediment supply during flooding.

All experiments were run until equilibrium condition was reached (when no more net deposition in and around the vegetation occurred). The tests were stopped when the equilibrium stage was reached and the width of the deposited strip was measured at the 50 mm chainages to determine the deposited plan area. The plan area and weight of the deposited sediment were compared with the different flow rates and lengths of vegetation patches.

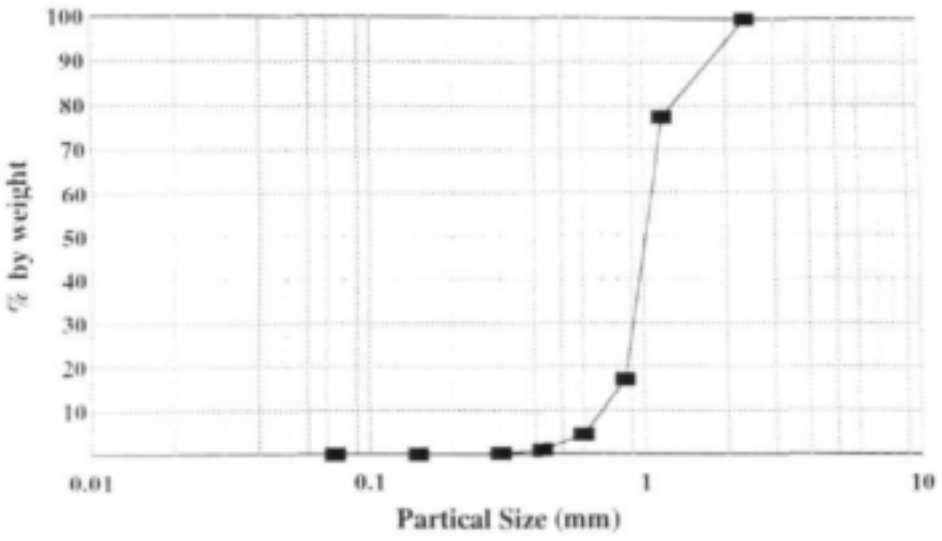

Figure 10.22 Granulometric curve for used coal

Table 10.10 Series B 6 Decay experiments

Test	Q (l/s)	L (mm)	Time, T (min)
B 6.1	5.01	140	0
B 6.2			6
B 6.3			17
B 6.4			25
B 6.5			45
B 6.6			55
B 6.7	5.01	280	0
B 6.8			7
B 6.9			18
B 6.10			30
B 6.11			50
B 6.12			65
B 6.13			75
B 6.14	5.01	560	0
B 6.15			5
B 6.16			10
B 6.17			20
B 6.18			30
B 6.19			55

Series B 5 Experiments and Results

The deposition experiments were carried out to investigate influence of flow rates on sediment deposition around the isolated vegetation patches with three different lengths (Table 9, Appendix C). From the experiments conducted on the equilibrium deposits, it was observed (Fig. 10.23) that as the flow rate increased the weight of deposited material decreased. From Fig. 10.23 it can be seen the relationship between flow rate and deposited weight of sediment is almost exponential, becoming asymptotic to some limit. The increase in vegetation length resulted in increased sediment deposition.

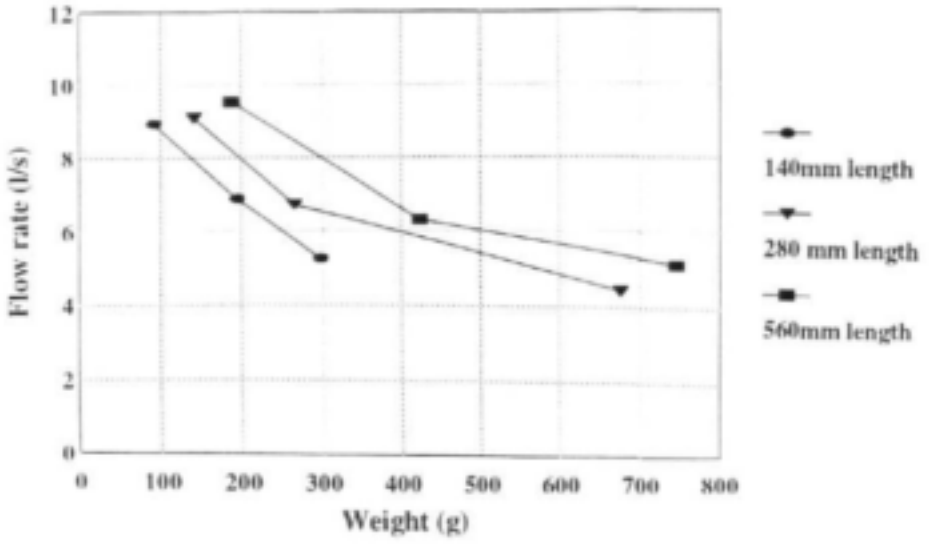

Figure 10. 23 Influence of flow rate on deposited weight (Series B5 experiments)

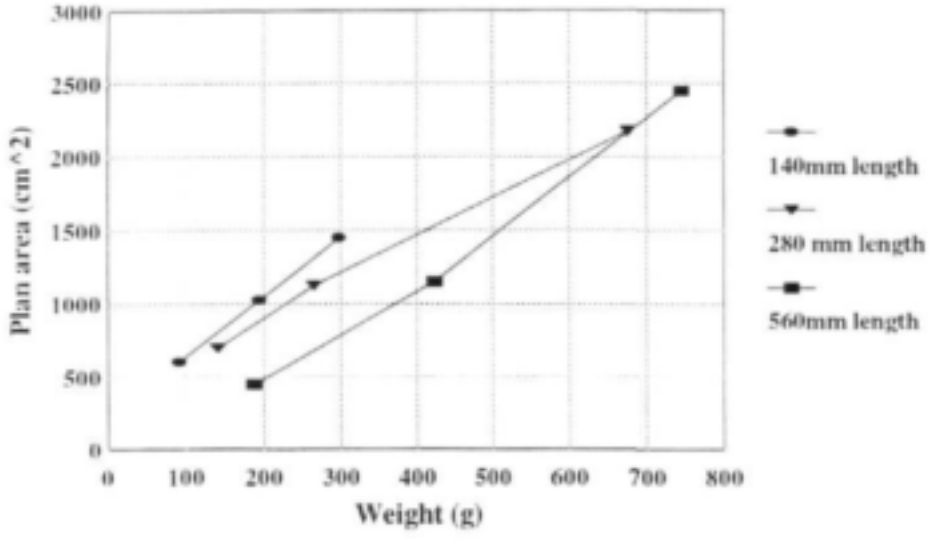

Figure 10.24 Relationship of deposited weight of sediment and deposited plan area

The relationship of deposited weight versus deposited plan area is presented in Fig. 10.24. From this figure it obvious that deposited plan area increases with increasing deposited weight of sediment.

The relationship of the ratio of constant sediment feed rate to varying flow rate versus the deposited weight of sediment shows (Fig. 10.25) that the deposited weight increases with an increase in this ratio.

For the full length of patch it was found that the sediment deposited in the patch itself, while for the half and quarter length this did not occur. It was found as well that when the flow rate for the full length of vegetation was decreased, the amount of deposited sediment in the vegetation increased.

Series B 6 Experiments and Results

The decay experiments were conducted to study how the depositional bar would decrease in size in the event of a flood passing through a river system with the absence of sediment supply.

Three decay experiments were conducted. Initially the net depositional bar was formed, the sediment switched off and the experiment was run until sediment formed an equilibrium decay bar. The experiments were performed under constant flow rate of 5 l/s.

The relationship of the plan area of the decay deposit against time is plotted in Fig.10.26. It can be seen that the plan area of the decayed equilibrium deposit increases as the length of the vegetation increases, but they are close in magnitude to one another.

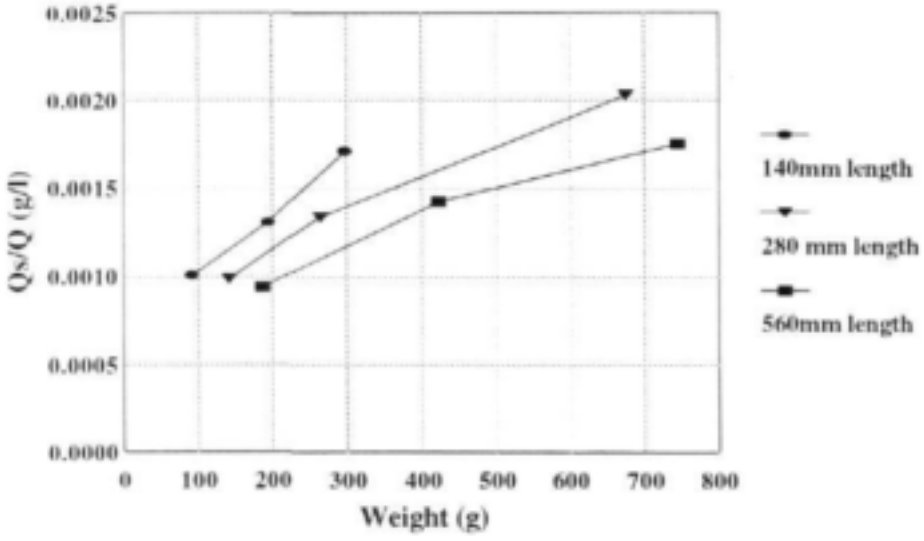

Figure 10.25 Relationship of deposited weight of sediment and ratio of constant sediment feed rate to varying flow rate

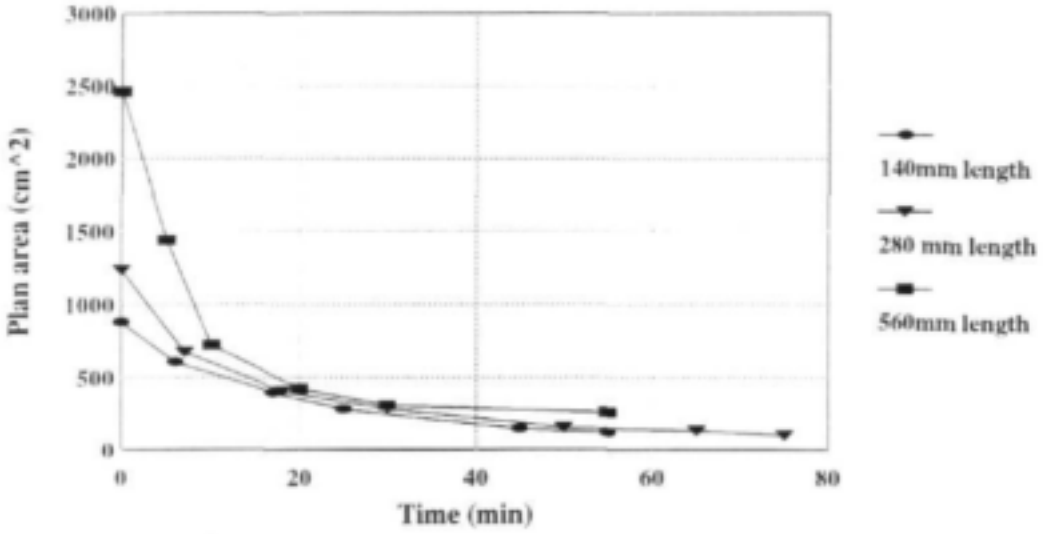

Figure 10.26 Plan area-time decay deposition relationship (Series B6 experiments)

10.2.3 Conclusion

Laboratory tests were performed to investigate the entrapment and retention potential of longitudinal strips and patches of vegetation. Through the experiments it was observed that vegetation plays an important pole in entrapment and retention processes of sediment.

From the results of Series B 3 tests it was found that the longitudinal strips of vegetation can trap approximately 10 % of the fed sediment. The highest rate of sediment deposition occurs at the beginning of the test and it decreases with time. The influence of flow discharge on the sediment deposition was studied for a given sediment rate. It was found that the highest flow discharge results in the highest sediment deposition.

The percent of sediment retained in the longitudinal strips (Series B 4 experiments) was observed to vary between 52 and 70 % with the flow rate. The maximum erosion took place at the beginning of the tests and it decreased with time.

The weight of deposited sediment around the vegetation patch (Series B 5 tests) increases with the ratio of the sediment feed rate to the flow rate and with an increase in the length of the vegetation patch.

For the decay experiments (Series B 6), the sediment deposit volume decayed exponentially and the equilibrium deposit size increased with an increase in the length of vegetation, but they were all close to one another in magnitude.

The experiments on the influence of vegetation strips on sedimentation process were carried out for one width of strip, one vegetation density, one feed sediment rate and one sediment size only. Therefore additional tests to upgrade the understanding of sedimentation processes in longitudinal strips of vegetation are required.

The decay rate experiments of interaction between bed load sediment and isolated vegetation patches were performed for a single density, patch width, sediment size and flow rate only. Additional tests to extend the knowledge and to confirm some of the results are therefore required.

Chapter 11

MODELLING MORPHOLOGICAL CHANGE IN REEDED RIVERS

11.1 INTRODUCTION

The interaction of sediment with flow in a river gives rise to patterns of erosion and deposition that determine the overall channel morphology. The patterns may develop through purely alluvial processes, but are influenced strongly by outcrops of bedrock and the presence of vegetation, such as reeds. Reedbeds influence erosion and deposition patterns directly by stabilizing existing deposits and trapping transported sediment, and indirectly by modifying the hydraulics of the flow and hence its sediment transport characteristics. The occurrence of reedbeds is itself influenced by the distribution of sediment and the flow conditions, which define habitat for establishment and growth. There is therefore a strong feedback interaction between reedbed dynamics, hydraulics and sedimentation processes, which must be accounted for when predicting changes of river morphology in response to different flow management scenarios.

Studies of some of the relevant biotic, hydraulic and sedimentation processes have been presented in previous chapters, but the kind of knowledge obtained from such isolated studies needs to be integrated for realistic description of the feedback interactions. This is most effectively done through simulation modelling, such as proposed in this chapter. A hypothetical, prototype model is presented for simulating morphologic change in vegetated, bedrock-controlled rivers, as exemplified by the Sabie River in the Kruger National Park, South Africa. Process descriptions in this model are inferred largely from observations in the Sabie River; they are speculative and are certainly inadequate for practical application, but the approach provides a useful framework for future development. More details of the ideas presented here are provided by Nicolson (1999).

11.2 MODELLING APPROACH

Models which relate the morphological characteristics of rivers to their flow regimes can be divided into two types: *static* models, which apply to stable, equilibrium channels (i.e. the largely empirical "regime" approach) and *dynamic* models, which simulate channel changes through time. Static models cannot be used to describe transient change, and therefore have limited predictive usefulness. Dynamic simulation models are able to describe transient responses to changes in flow regime, but require rather simplified process descriptions in order to produce tractable solutions. Examples of such models are HEC-6 (Hydrologic Engineering Center, 1977), MOBED (Krishnappan, 1981), TABS (Thomas, 1982), IALLUVIAL (Karim and Kennedy, 1982) and FLUVIAL-11 (Chang, 1984). These dynamic models are essentially sediment routing models, utilizing fairly complex partial differential equations to represent water continuity, water motion and sediment continuity.

Conventional dynamic simulation models are widely used to predict change in alluvial rivers, but they are not well-suited to bedrock-influenced rivers with semi-arid flow regimes for the following reasons:

They do not cope well with the spatial variability of bedrock rivers: Rivers with bedrock influence usually have complex geometries, varying in cross section over very short distances and in many cases exhibiting anabranched distributary channels. Description of this variation in sufficient detail for conventional modelling is practically infeasible over extended distances.

Hydraulic parameters are difficult to determine from discharge values: The high degree of irregularity and the presence of vegetation makes estimation of friction factors and their variation with stage extremely difficult in bedrock-controlled channels.

Sediment transport is often supply limited: In alluvial channels the sediment transport rate is generally determined by the transport capacity of the flowing water. In bedrock-controlled channels transport capacity can be extremely high, exceeding the supply rate, and transport rate is then determined by the supply rate rather than the transport capacity. Conventional sediment transport equations deal better with the former conditions than the latter.

Sediment transport is episodic: Sediment transport in alluvial channels in humid regions is usually a slow, continuous process, which is well suited to description by the partial differential equations expressing rates of change. Semi-arid rivers have highly variable flow regimes with very abrupt changes, and most sediment is transported during short, discontinuous portions of the flow hydrograph.

Vegetation has significant influence: Inclusion of the feedback interactions between reedbed dynamics, hydraulics and sediment transport in conventional computational models would require inclusion of partial differential equations describing rates of change of reedbeds in terms of environmental conditions. This is not yet possible with current knowledge and, even if the equations could be formulated they would most likely require more data than could be practically acquired.

Process descriptions are scale-dependent: Processes responsible for cause-and-effect at one time and space scale do not necessarily apply in the same way at other scales. Conventional computational models apply process descriptions that have been established at small scales, e.g. the relationship between bed load transport rate and boundary shear stress, and the continuous nature of this transport. There is increasing evidence that these descriptions are unreliable at the natural river scale (Nicolson, 1999). An illustrative example of contrasting causality at different scales is the response of a channel to sediment overloading. In a laboratory flume the response would be a steepening of the channel bed, which is well described by conventional models. However, channel steepening in response to sediment overload does not appear to be the natural response in rivers - most documented cases report response by anabranching or braiding.

These considerations suggest that adaptation of existing computational models to describe morphological change in semi-arid, bedrock-controlled, vegetated rivers is unlikely to be a fruitful pursuit. As an alternative, a qualitative, rule-based approach is proposed, which we believe is more appropriate for modelling change at low resolution and large scale.

The concepts of qualitative modelling originated in the field of artificial intelligence during the 1970s, and the approaches presented here are a logical development from expert systems

applications. The essential differences between qualitative and computational modelling are the replacement of real number variables by qualitative states for describing the system, and the replacement of differential equation solutions for determining variable values by logical rules to specify states. Instead of calculating changes in variables from one time step to the next using mathematical operators and rate equations (i.e. differential or difference equation), logical operators are used in the form of IF-THEN rules: IF(some condition is met) THEN(adjust the qualitative variable representing the system component from one state to another). Whereas conventional models may represent time either as being continuous (using differential equations) or discrete (using difference equations), rule-based models are always event-driven and are therefore always discrete models (Starfield et al, 1989).

This approach has been successfully applied in physics (e.g. de Kleer, 1975; Hollan et al, 1984; Forbus, 1995) and ecology (e.g. Starfield et al, 1989, 1993; Tester et al, 1997). Since rivers share many of the attributes which make other natural systems amenable to qualitative modelling, the approach should also be useful for modelling river change. Qualitative modelling has the following advantages over conventional computational approaches for river applications.

Qualitative states are appropriate for describing complex systems: While it is seldom easy to describe natural systems simply in terms of numbers, qualitative patterns are often relevant and relatively easy to describe. Natural rivers are complex in terms of the distribution of sedimentary features and vegetation, but functionally can be described in terms of the low resolution, qualitative, terminology used in classification schemes. For example, describing a river reach as "braided" is sufficient for many purposes, and the number and dimensions of individual bars are superfluous. An approach which is based on low resolution variables therefore matches the way we think about and describe river channel complexity.

Low resolution models are appropriate for representing large spatial and temporal scales: River modelling requires description of morphology over large distances and changes over long time periods. Representation of these systems using conventional computation modelling has to be at resolutions that require vast amounts of information, which is difficult and expensive to acquire, manipulate and interpret. A simpler, low resolution representation matches the nature of many issues that are important for management and enables inexpensive, practical prediction.

IF-THEN rules are well suited to modelling disturbance-driven systems: The conventional modelling approach is appropriate to systems which are driven continuously, but inappropriate for systems which experience unpredictable disturbance. Early studies treated rivers as equilibrium systems, but it has become increasingly apparent that they are strongly influenced by large magnitude flow events. Disturbance, and not equilibrium, is therefore a suitable paradigm for modelling river change. Qualitative, rule-based modelling is better suited to this paradigm than computational modelling.

Natural systems are often understood in a qualitative way: Geomorphology cannot usually be described in the same precise, quantitative way as, for example, physics and chemistry (Schumm, 1983). Conventional modelling is precise, and cannot easily incorporate qualitative information and expert opinion as can low resolution, rule-based modelling.

Qualitative modelling fosters understanding of system behaviour: Understanding of natural systems is often piecemeal, and it is difficult to incorporate incomplete knowledge in conventional computational models. Rule-based modelling is ideal for developing understanding as rule sets can be speculative and easily adjusted to examine influences of poorly understood processes. The model can therefore be used as a tool for setting and testing hypotheses about system behaviour, and hence to guide continuing research. As will be seen in the application to follow, individual rules are easy to understand in isolation, but their interactions can lead to non-intuitive results.

Qualitative models enhance interdisciplinary communication: Computational models are difficult to understand by people from different disciplines, who are then unable or reluctant to provide input for their improvement. IF-THEN rules are generally stated in fairly simple language, rather than mathematics, which is a significant aid to communication between scientists with different areas of expertise, as well as managers.

The qualitative, rule-based modelling approach clearly has many features which make it suitable for modelling complex, dynamic river change.

11.3 PROTOTYPE MODEL

A prototype model based on the principles outlined above has been developed to demonstrate the approach's suitability for simulating the morphologically significant interaction between sediment and reeds in a mixed bedrock/alluvial river, as typified by the Sabie River in the Kruger National Park, South Africa. The present state of knowledge about vegetative and sedimentary processes is far from adequate for reliable modelling, and the prototype model presented involves speculation concerning some of the processes. The purpose at this stage is not to present an operational model, but to show that the rule-based approach allows vegetation to be modelled as an integral part of the fluvial system, and to show clearly the impact that vegetation can be expected to have on river morphology.

11.3.1 Characteristics of a Vegetation-Morphology Model

The nature and structure of any model must be appropriate to the kinds of questions to be addressed, and for the kinds of processes operating within the system. These requirements can be applied as criteria for planning and evaluating models.

In terms of the first criterion, the model must address the nature of the problem to be solved (in this case to predict morphological changes under different flow regime scenarios), and must have the following characteristics.

The model must be driven by flow regime: The primary questions the model must answer relate to how morphological and habitat conditions in a river will change in response to upstream management, such as dam construction or land use changes. It must therefore be capable of running several different flow regime scenarios to enable comparison of their effects on

sedimentary change along the river. Dealing with flow regime scenarios also requires that the model should simulate fairly long time periods, since the river is likely to have a highly variable flow pattern from one year to another. To capture this kind of naturally inherent variability, model periods of at least five to ten years are necessary.

The model should be capable of simulating long reaches of river: Effective management of a bedrock/vegetation-influenced river must be concerned with diversity of channel types that extend over reaches with lengths from a few hundred metres to several kilometres. The model should therefore "see" reasonably long lengths of river, and not just cross sections or short reaches.

The model must be spatially explicit: Nicolson (1999) has demonstrated clearly through application of rule-based models that the spatial sequence of different types of reach has significant impact on sediment movement and storage, and it cannot be assumed that all reaches of the same type will respond similarly to an imposed flow regime. The model must therefore be able to account for the morphological characteristics of the different reach types and their spatial arrangement.

The model must represent vegetation in some way: The importance of vegetation in river morphology processes has already been highlighted, and the vegetation characteristics that affect erosion and deposition processes must be represented in a way that enables their influence to be accounted for. The representation depends on the type of vegetation (e.g. bank grasses, reeds, or riparian trees) and the resolution of description required (from simply presence or absence in a reach at one extreme, to numbers and locations of individuals at the other).

According to the second criterion, the model must describe the relevant processes appropriately. This requires selection of appropriate temporal and spatial scales, driving variables, and representation of the physical system (i.e. which components of the system the model can and cannot "see").

The model should include sediment input from upstream tributaries: The morphology of a river is highly dependent on the sediment input, and describing morphological dynamics requires budgeting the inputs and internal transfers. Unfortunately the sediment input is a major area of uncertainty at present. Van Niekerk and Heritage (1993) used a geographic information systems approach to quantify crudely the total sediment yield from the Sabie River catchment. Based on Rooseboom's (1992) sediment yield chart and certain topographical features of the Sabie River catchment, they estimated the average annual sediment yield to be 300 t/km^2/a, but were unable to describe the annual variability or quantify the relative inputs of different tributaries. Donald (1997) addressed these shortcomings by applying a modification of the CALSITE model (Bradbury, 1995), which enable distributed catchment sediment delivery to be determined. No direct monitoring of Sabie tributaries has been done, however, and estimates have not been reliably confirmed.

The model should reflect the episodic, event-driven nature of sediment movement: Sediment movement is an episodic process, occurring mostly in response to individual flow events in the long term hydrograph. For the Sabie River, flow events are concentrated mostly between

November and March and are generally of the order of a few days to a week in duration. It is therefore unnecessary to simulate large parts of the hydrograph, but during the sediment moving events the simulation time step should be a day at most.

The model should reproduce differences in sediment transport rates along a river's length: The different channel types found in the Sabie and similar rivers have different capacities for transporting sediment by virtue of different gradients and morphologies. Simulating these differences is fundamental to achieving the spatially explicit modelling requirement stipulated above.

The model needs to track how stored sediment is distributed in a reach: As vegetation is closely associated with particular morphological units (van Coller, 1993; Carter, 1995), it is not sufficient simply to keep track of the total volume of sediment stored in a reach. The model must be able to allocate stored sediment to morphological units, such as bars or pools, to provide a basis for predicting vegetation response.

The model must relate vegetation changes to flow regime: Although the processes that drive riparian distribution and growth are not yet fully understood, it is indisputable that the occurrence of water in terms of its magnitude, timing and frequency (i.e. the flow regime) plays an important role. The magnitude of flows determines river stage and hence area of inundation, thereby determining areas of suitable habitat and disturbance. The frequency of inundation can affect the supply of groundwater to plants, thus influencing their growth (Hupp, 1990; Carter, 1995), and large, high-energy flood events can rip vegetation out and wash it downstream (Yanosky, 1982).

The model must account for feedbacks between vegetation and sediment dynamics: Part of the complexity of the problem of predicting morphological change in vegetation-influenced rivers is that vegetation is an integral component of the system, and its presence in a reach can alter the flow characteristics. This in turn has an effect on the movement of sediment, since it is the energy of the flowing water that is responsible for sediment movement. In addition, the presence of vegetation on alluvial features tends to stabilize them (Thorne, 1988; Witt, 1985; Hickin, 1984), and can also enhance the rate of sediment deposition on them (Dietz, 1952; Graf, 1978; Abt et al., 1994). Vegetation can therefore not be treated simply as an extrinsic factor when modelling morphological change.

The model should be able to incorporate existing knowledge of fluvial processes and be easy to improve as fluvial processes become better understood: A model cannot be effective if it does not account for the important processes involved in the system. Unfortunately the processes underlying morphological dynamics are poorly understood at the scale of interest for ecological management. The rule-based approach has the advantage over more conventional approaches, however, that current understanding can be incorporated, even if it is incomplete and non-quantitative. There is an iterative relationship between modelling and the development of understanding: modelling, even when rudimentary and crude, helps to identify critical areas of uncertainty which require focussed attention through field work or theoretical development.

The model should not be so complex that intellectual control over its results is lost: The characteristics listed above may seem to imply that their inclusion requires an extremely detailed

and complex model. The major disadvantage of this would be the associated requirement for huge amounts of data to describe the channel geometry, hydraulic characteristics and flow regime - with no guarantee that these data will illuminate rather than obscure what is happening. It is often very difficult to understand how models such as this actually work. Moreover, if there are no data against which the model performance can be tested (as in our case), it can be extremely difficult to evaluate whether or not it is producing sensible and valid results. It is important that the logic and key processes of the model can be traced through retrospectively to check their validity and to understand why the model produces the results it does. It is easy to lose intellectual control if the model is too detailed and too complex: simple models are to be preferred over complex ones.

The characteristics outlined above do not resolve precisely every detail of the model, but provide a set of guiding principles regarding the kind of model that is required, given the nature of the questions to be answered and the nature of the geomorphological processes involved.

11.3.2 Prototype Model Overview

11.3.2.1 The Sediment Budget

The basic idea underpinning the model is very simple. The channel is represented as a series of cells, each connected to the cells immediately upstream and downstream. A certain amount of sediment is stored in each cell, and at every time step the model calculates how much sediment is removed from a given cell and transported to the one(s) downstream of it. In this way, the spatial distribution of sediment along the length of the river changes through time in response to the flow regime and the input of sediment to the upstream end of the channel.

The first task at every time step is to determine how much sediment the flow will remove from each cell. This depends not only on the flow, but also on the sediment availability. Accordingly, the model requires three variables to be computed for each cell: *potential*, *available* and *remove*. The variable *potential* is a function only of the flow and the geometry of the reach; it represents the upper limit of the amount of sediment which could be removed from that cell during the given time step if there were no constraint on availability (i.e. the sediment transport capacity of the flow). Because it is possible that the transport capacity exceeds the amount of sediment stored in that reach, the variable *available* is needed to represent the amount of sediment in each cell that is actually available for transport. If *available* is less than *potential*, then sediment movement is supply limited and the variable *remove* is set equal to the amount of sediment *available*. If *available* exceeds *potential*, then the amount of sediment *removed* from the cell is set equal to *potential* (i.e. it is not supply limited). The variable *remove* is therefore determined by the lesser of *available* and *potential*. The units of these three variables are either mass per model time step or volume per model time step; which of the two chosen is immaterial since they are related by the unit density of sediment, i.e. its mass per unit volume.

After computing the amount of sediment removed from each cell, the next task is to transport the amount *remove* from each cell into the one(s) downstream of it. The most straight forward way to do this is simply to shift all removed sediment from cell i into cell $i+1$. This, however, sets

the velocity of the sediment slug to the ratio of cell length to time step and requires that the cell length be chosen to ensure a realistic velocity. An alternative way of setting the sediment velocity is to move a proportion of the *removed* sediment from cell *i* into cell *i+1* and the remaining proportion into cell *i+2* (or cells *i+2, i+3, ... i+n*). This increases the rate at which a slug of sediment advances through the system and also results in dispersion of the slug as it advances. The control of slug velocity and dispersion can therefore be easily incorporated in a model, but should be seen as a refinement, as little is known about these characteristics in real rivers.

Application of the simple sediment budgeting procedure at each time step enables the movement of sediment from one cell to another along the river to be simulated, and the time variation of sediment stored in each of the cells to be described.

11.3.2.2 Representation of the River Characteristics

The river is represented in the model as a series of contiguous cells, with each cell having distinctly different functional characteristics from those upstream and downstream. The functional characteristics are those that determine the available storage volume, the sediment transport capacity (to define the *potential* variable value) and velocity of sediment movement. These all depend on the morphological characteristics of the reach, including cross-sectional shape, longitudinal gradient, the occurrence and form of bedrock, and the occurrence, location and type of vegetation. For a bedrock-influenced river like the Sabie, the channel type classification of van Niekerk et al (1995) (alluvial, pool-rapid, bedrock anastomosing, etc) provides an appropriate basis for specifying cell representation, as there is evidence that sediment behaviour is distinctly different in each of these types. The bedrock anastomosing reaches, for example, are significantly steeper than the other channel types, with water surface slopes of up to 0.010. This means that they have relatively high energy and can easily transport large amounts of sediment. The pool-rapid reaches, on the other hand, are like a series of sediment-trapping reservoirs. They consist of large pools which dam up behind bedrock outcrops in the river, so the pools are deep and have slow-moving water. At low flows the pool sections have very mild water surface slopes and are low energy environments, but at high flows the rapids drown out and the water slope is more uniform throughout the entire pool-rapid reach. Alluvial reaches differ from both of these two channel types: firstly, they always contain a store of sediment which may be eroded, and secondly they lie between the other two types in their water surface slopes, so have an intermediate amount of energy for sediment movement. Nicolson (1999) has discussed the description of bedrock-influenced cell types in greater detail and demonstrated how their functional differences influence morphological dynamics; the focus in this chapter will be on the influence of vegetation, which is discussed further in sections 11.3.2.4/5.

The behaviour of the cells is encapsulated in a look-up table of sediment transport capacities (*potential* values) for each cell type and flow condition (as described in section 11.3.2.3 below). (An example of such a table for a vegetated cell is given in Table 11.1). At each simulation time step the table is interrogated to determine the *potential* value to assign each cell for the prevailing flow category for the sediment budget calculations. The actual values of sediment transport to insert in the table are obviously very difficult to specify accurately, given the high degree of uncertainty associated with sediment transport prediction even for highly simplified conditions.

They could be determined by field measurement, experimentation or detailed analytical modelling. However, for predicting morphological response for management purposes a high degree of accuracy is probably not necessary. More important than actual sediment transport values are the relative relationships between values for different cell types and flow categories. Even rough estimates by experts can be used in a model application to yield useful prediction of general trends under different scenarios and, very importantly, to develop insight of system behaviour.

Table 11.1 Look-up table for sediment transport capacity in tons per day as a function of reed state and flow category

Reed State	Flow Category				
	Base	Small rise	Medium rise	Small drop	Large rise
None/rhizomes	0	10	10	4	20
Young stems	0	14	14	6	20
Dense reedbed	0	9	10	6	15

Application of the sediment budget enables the change in sediment storage within a cell to be simulated over time. For some river types and applications this may be all that is necessary, but in some cases it may be important to describe the distribution of sediment storage within a reach. This may be extremely nonuniform in bedrock-influenced channels. Whether to include this extension or not depends largely on the problems being addressed and the purpose of the simulation. For modelling the dynamics of reed growth and its influence on morphological dynamics it is essential because the extent and distribution of reed coverage is closely related to the distribution of deposited sediment.

In an alluvial reach, sediment is stored in two places: on the river bed, and in alluvial bars. The sediment available for transport will depend on the relative amounts in these different storages, as well as the flow condition. At low flows the sediment stored in bars may be mostly above the water level and the only sediment available will be that on the bed between the bars. At progressively higher flows more of the sediment stored in bars will be accessible. Accounting for the distribution of sediment between bars and the bed will add realism to the model and can be quite easily done by the introduction of a few additional rules and defining two separate storage units for the bed and the bars. The sediment budget specifies the amount of sediment entering a cell, Q_i, say. The proportion of this to be allocated to bar storage can be calculated by multiplying the total amount by a proportionality factor, p_b. The allocation to the bars is then $p_b Q_i$ and the allocation to the bed is $(1-p_b)Q_i$. The value of p_b could be dependent on flow condition to reflect the different behaviour at different flow magnitudes. The relative erosion of

bars and bed can be treated similarly by specifying an erosion proportionality factor for the bars, p_e: if the total sediment transport potential for a particular cell and event is P_t, then the model will subtract $p_e P_t$ from the bars and $(1-p_e)P_t$ from the bed. A further rule could be added to the effect that if insufficient sediment is stored in bars at a particular time, the excess transport potential can be applied to move sediment from the bed. Vegetation influences are also closely related to the distribution of sediment within a reach. Reeds establish and grow on bars rather than on the river bed, and will afford additional stability and resistance to erosion of the bars during floods. How this can be accounted for is described in section 11.3.2.5.

11.3.2.3 Representation of the Hydrograph

Model applications to predict morphological and vegetation changes in a river must simulate behaviour over time periods of at least 5 to 10 years. It has been established that significant movement of sediment is not continuous over long periods, but takes place only during brief events of high magnitude. It is therefore unnecessary to simulate the flow in the river continuously, and the model can be event driven. Because an average flow condition over the simulation period must be specified and because the variation of sediment transport over small ranges of discharge is less significant than the differences between no event and a flood event, it is appropriate for this type of modelling to specify flows in magnitude categories for a simulation period rather than as continuous, instantaneous discharges. For example, in a particular reach the threshold discharge for sediment movement could be estimated and all flows below this can be ignored. The flood events that cause sediment movement could be categorized as *small*, *medium* or *large* in terms of the discharge values associated with different frequencies of occurrence. These categories should reflect the peak and duration of the events, so that they are functionally different in the simulations. As an example, Nicolson (1999) modelled sediment movement through Sabie River cells using three flow categories: *small floods* with peaks less than 20 m^3/s and durations of about 1 day for the rising limb and 2 to 3 days for recession, *medium floods* with peaks between 20 m^3/s and 42 m^3/s and durations of 1 to 2 days for the rising limb and about 5 days for recession, and *large floods* with peaks above 42 m^3/s and durations of 1 to 2 days for the rising limb and more than a week for recession.

Representing the sediment movement of a flood event in terms of discharge is a simplification, however, even when applied in the many computational models that do not account for unsteady behaviour rigorously. Field evidence confirms that sediment movement cannot be neatly correlated with discharge, but depends strongly on whether the river stage is rising or falling. This is probably due to the fact that sediment transport depends on stream power, involving the energy gradient of the flow as well as the discharge (stream power is given by γQS_f, where γ is the specific gravity of water, Q is the discharge, and S_f is the energy gradient). The energy gradient is related differently to discharge on the rising and falling limbs of a hydrograph, being significantly greater on the rising limb (this can be shown theoretically, as in most standard texts, such as Henderson (1966)). Because sediment transport is related to stream power, it is to be expected that it will be greater on the rising limb than on the falling limb. A more realistic representation of the driving hydrograph for the model than that given above would therefore specify separately the two parts of the hydrograph in the definition of the sediment-moving events, i.e. as *small rise*, *small drop*, *medium rise*, *medium drop*, etc. The sediment transport

capacities for different reach characteristics are therefore related to these event characteristics in the look-up table for defining the *potential* values, as for example, in Table 11.1 for a vegetated alluvial reach.

11.3.2.4 Representation of Reedbed Dynamics

It has been established that the movement and storage of sediment in a river is strongly influenced by the occurrence of vegetation, and particularly reeds. It is also obvious that the life history characteristics of stands of reeds, such as areal distribution, stem density and extent of foliage must be influential. A realistic sediment budget must take these factors into account and, as they are time dependent, some dynamic description of reedbed characteristics must be included in the model.

The response of reeds to channel morphology and flow regime characteristics is complex. Some advances in the understanding of the relationship between reedbed characteristics and the physical environment have been made (Chapter 3), but a complete and adequate description is not yet available. The description used in this model is rudimentary and based on the following highly simplified and speculative interpretations. The main purpose of the model is to demonstrate that realistic behaviour can be simulated using a semi-qualitative, rule-based approach. The rules and details can be refined, extended, or even radically revised as new understanding and information are obtained and incorporated, but the basic approach can provide a sound framework at all stages of development.

Reeds are most abundant - and therefore most important as agents of morphological change - in reaches with high proportions of alluvial bars, and are less commonly found in bedrock reaches. They are affected by flooding, with the depth, timing, and duration of each flood event playing a role in their growth and removal. One mechanism of bar colonization by reeds is by redistribution of rhizomes, by deposition on exposed sediment surfaces during flood recession or surface floating from the river bank to an alluvial bar. Once rhizomes are present on a bar, the reeds establish by clonal reproduction and a network of rhizomes will extend over the bar. This network will be fairly resistant to subsequent flooding and not easily destroyed. Once the rhizomes are in place, reeds can begin to grow their leafy aerial stems. The reedbed requires periodic inundation to supply water and nutrients to the alluvial substrate of the bar, but large floods can have sufficient power to bend the reeds, which may be broken off and removed. The timing and frequency of floods are also important: frequent inundation will not allow reeds to recover between events, and may subject them to intolerable stress. Long-lasting high water levels can also cause anaerobic conditions in the root zone, which would affect the processes of nutrient and water uptake. Under these conditions the reeds may die off, so the duration of inundation is also a factor that should be accounted for.

Translating information such as this about the reed dynamics into a simulation model requires description of the possible states of the reeds and specification of rules for the transition between the states, in relation to the flow regime. The different stages of reed development are defined in terms of three possible states. The first state, *rhizomes*, indicates that rhizomes have established in the bar alluvium, but aerial shoots are not yet evident. The second state, *young*

stems, describes a reedbed that has begun to grow aerial stems. This stage will last for the first year under normal conditions and has stems that are more flexible than when fully grown and fairly sparse in terms of areal density. The final state, *dense reedbed*, represents a fully developed stand of reeds; the stems are stronger and taller than in the previous state, the stem density is higher and foliage on the stems is well developed. In addition to these three growth states, the state of an unvegetated alluvial bar is defined as *none*.

Specification of rules to describe the transitions between these states requires definition of the rate of reed growth, with the implication of choosing an appropriate time scale for updating reed state. *Phragmites mauritianus* is adapted to the annual cycle of summer flooding and winter low flow, and grow primarily during the dry season. The model therefore updates the reed state at the beginning of each water year (i.e. October), to reflect the growth during the preceding months. Because of the effect of large floods on reeds, the model also checks for the occurrence of floods and adjusts the state accordingly. The normal cycle of reed growth in response to flow regime characteristics is as follows:

1. The variable *reeds* is changed from *none* to *rhizomes* after a moderate-sized event, provided the bar size is above some threshold (representing the surface area of the bar above water level).

2. If *rhizomes* are present at the end of one wet season, the reed state will be updated to *young stems* at the beginning of the following wet season.

3. The *young stems* can be destroyed by a large flood event, in which case the reed state is reset to *none*. This is because the sparse density of stems in this state does not increase the flow resistance substantially, and the bar is likely to be eroded and the rhizomes with it.

4. If the *young stems* remain in place for an entire wet season, and if there are at least two moderate floods which inundate the bar to provide water and nutrients, the *young stems* are updated at the beginning of he following wet season to become a *dense reedbed* growing on the bar.

5. A *dense reedbed* can only be removed by the second of two large floods in a single wet season. This reflects the fact that reeds have some resilience to high energy events, but this resilience is reduced by the stress of one such event and more than part of a season is required for recovery. Therefore, if a second large event occurs within the same wet season, it will be able to rip out the reedbed.

These rules are summarized in Fig. 11.1.

Figure 11.1 Diagrammatic summary of the reed states and rules

11.3.2.5 Representation of Reedbed-Sediment Interaction

The procedures in the previous sections enable the dynamics of both bars and reeds in a river reach to be simulated independently, but the way in which the presence of reeds alters the sediment dynamics has not yet been included. This model accounts for three principal mechanisms by which reeds can affect the sedimentary processes in a river reach:

- Reedbeds can change the overall sediment transport capacity (*potential*) of a reach by changing the hydraulic resistance and hence altering the overall magnitudes and distributions of flow velocity and shear stress.

- Reeds can reduce the erodibility of alluvial bars by reducing the boundary shear stress on the sediment surface, and by stabilizing the sediment with roots and rhizomes.

- Reeds can enhance deposition of sediment on the bar by slowing down sediment-carrying water flowing through or over the reedbed and allowing suspended or bedload sediment to settle out and deposit.

All of these mechanisms can easily be incorporated into the structure of the model. The model allows for the transport capacity to be specified for each reach as a function of the type of flow on a given day; this can be extended so that transport capacity is specified in terms of the reach geometry *and* the state of the reedbed. This additional effect can be incorporated in the look-up

table for transport capacity. As before, the values in this table can be determined by field measurement, detailed modelling or expert opinion. An example of such a table for an alluvial reach is given in Table 11.1, which is used to obtain the modelling results presented in the following section. Because the effect of reeds on sediment transport is likely to vary with discharge, each combination of reed state and flow type must be described. When the state of reeds is *none* or *rhizomes*, there is no increase or decrease in the overall transport capacity at any flow level, but for an incipient reedbed of *young stems* the transport capacity for the reach is assumed to increase slightly because the water will be channelled into a smaller flow area and will move faster. For a *dense reedbed* it is assumed that the additional roughness causes a decrease in transport capacity for large flood events.

The model structure is also well-suited to inclusion of the effect of reeds on bar erodibility and the rate of deposition. The rule for removing sediment from a reach states simply that a certain proportion of the total sediment within a reach would be taken from the bar (if a bar is present in the reach) and the remaining proportion would be removed from the bed. When dense reeds are present, the proportion of sediment removed from a bar is reduced, so the bar is eroded less than it would have been in the absence of reeds. Similarly the variable that determines the proportion of sediment moved into a reach that is stored in bars can be adjusted to determine the amount of deposition on the bar. Table 11.2 gives speculated values for these two variables for different reed states.

Table 11.2 Bar erosion (p_e) and deposition (p_b) factors for different reed states

Reed State	p_e	p_b
None/rhizomes	0.4	0.3
Young stems	0.4	0.4
Dense reedbed	0.05	0.6

The values in the table reflect the fact that the presence of rhizomes makes no substantial difference to the amount of sediment eroded or deposited on bars, that young reeds do not help much to stabilize sediment (although they enhance deposition slightly), and that dense reeds stabilize the bar almost completely as well as enhancing further deposition.

11.3.3 Model Application

The concepts described above have been coded as a prototype model to illustrate the rule-based approach for simulating the interaction between reeds and sediment in an alluvial channel reach. The model logic is shown by the flowchart in Fig. 11.2 and the code is reproduced in Appendix

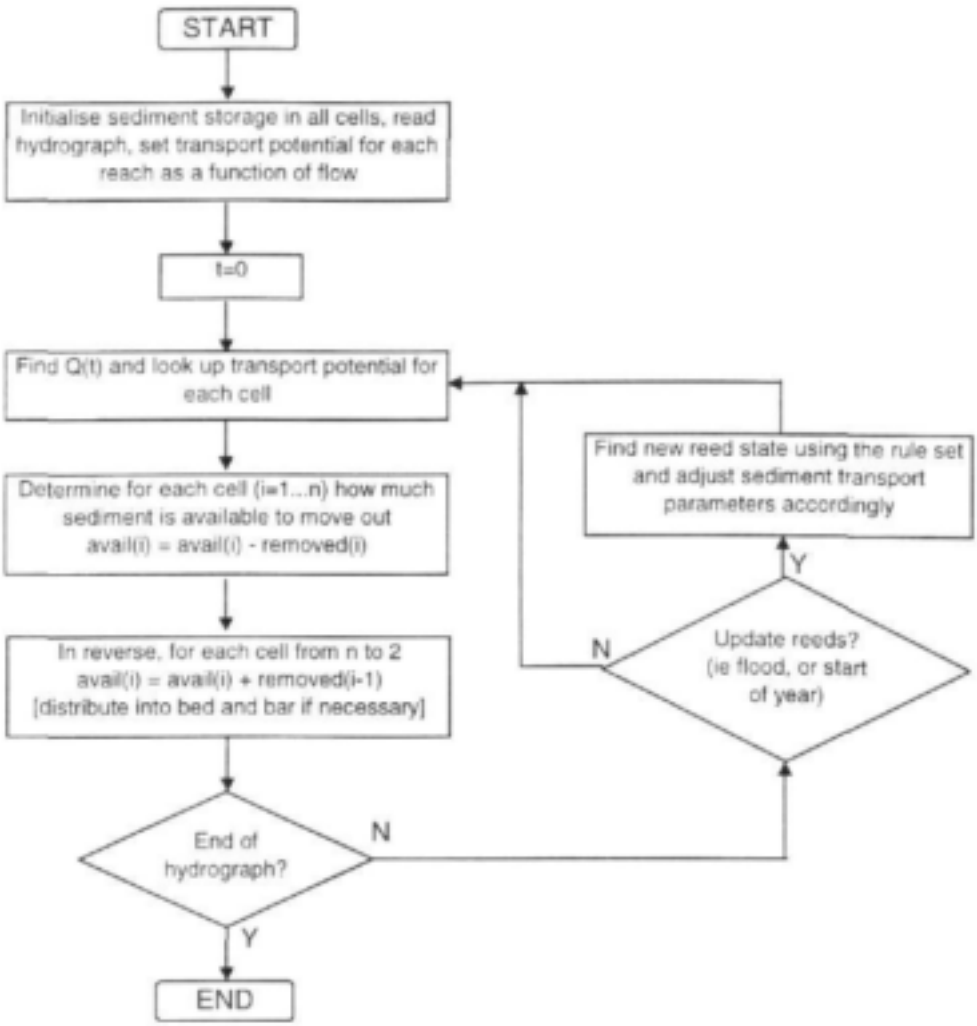

Figure 11.2 Flowchart outlining the model procedures

The model is applied to some simple situations to demonstrate the capabilities of the approach. Realistic predictions would require better understanding of physical behaviour than is currently available, and these examples use the speculative rules and values presented above.

The first example shows how the development of bars in a river can be simulated. Bars do not necessarily develop in all reaches of a river, and the rules are applied here to allow bar growth in just one of 10 cells in a hypothetical river. The driving hydrograph for this simulation is shown in Fig. 11.3, and runs over a period of 8 years, representing flow measurements on the Sabie River from 1981 to 1988. Only the rainy seasons are considered and only the flood events within these are included in the hydrograph, in accordance with the representation described above. The floods are represented as small, medium and large events. Below each hydrograph is a bar graph showing the total sediment stored in each of the 10 cells at the end of each year. For the fifth cell

(marked by an arrow), storage is allowed to be in bars (the upper portion) or on the bed (the lower portion). In some years (e.g. years 1981 and 1983) bars develop when there were none the previous year, and in some years (e.g. years 1982 and 1988) existing bars are removed completely by large floods. In the other years the bar deposition increases and decreases depending on the nature of the flow regime for the year.

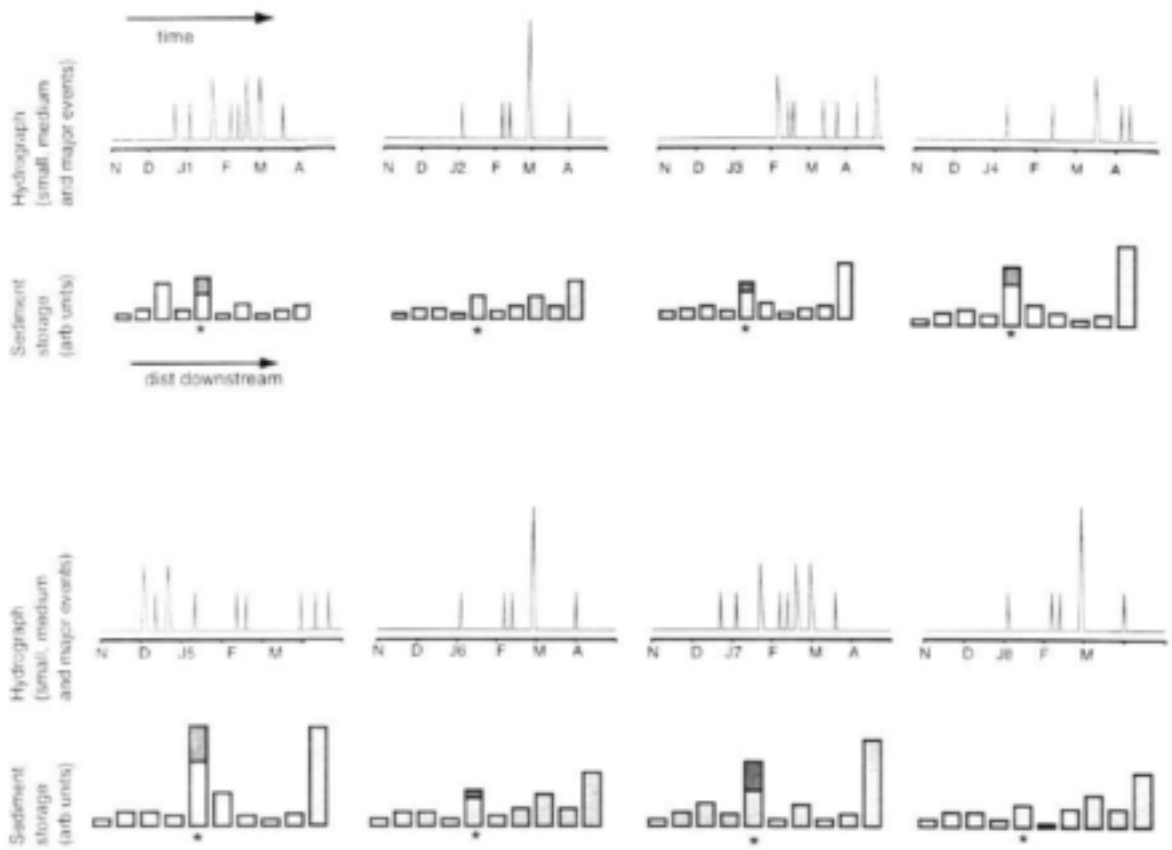

Figure 11.3 An eight-year input hydrograph and sediment storage response of a model that accounts for bar development, but not reed influences

To illustrate the effect of the bar rules, the simulated results for the fifth cell are shown in Fig. 11.4 with and without the bar rules invoked, i.e. with and without the deposition and erosion proportionalities of Table 11.2 applied. The overall amount of sediment in storage is the same for the two simulations, but the proportions stored in the bars and on the bed are shown for the simulation in which they are specified. Note that these proportions are not constant from year to year, but depend on the hydrograph characteristics.

The second example extends the first by including the rules describing reedbed dynamics and the influence of the reeds on sediment erosion and deposition. In Fig. 11.5 the effect of the reeds is shown by comparing the storage dynamics of the fifth cell with and without the reed rules

included. The results show similar behaviour until the reeds have had a chance to establish (in year 1985). At this time they begin to be able to stabilize the bars, so that almost all of the sediment removed from the reach is taken from the bed. In years 1986 to 1988 the reeds have promoted sediment deposition on the bars and stabilized them so effectively that the large event in 1988 is not able to remove the bars, as without the reeds. Both the total amount of sediment stored in the reach and its distribution between bars and bed have clearly been influenced by the presence of the reeds.

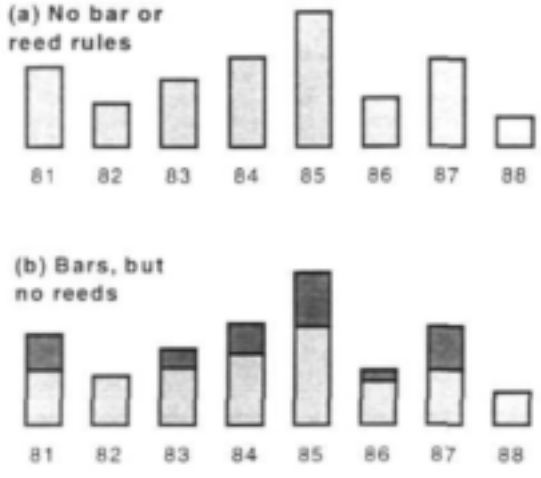

Figure 11.4 The effect of adding bar rules on the sediment storage dynamics of the fifth cell in the hypothetical river

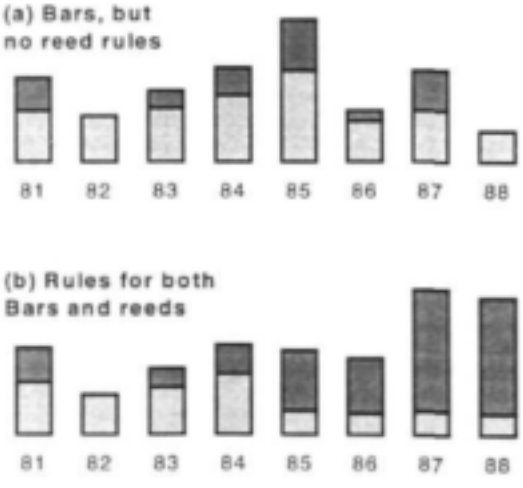

Figure 11.5 The effect of adding reed rules on the sediment storage dynamics of the fifth cell in the hypothetical river

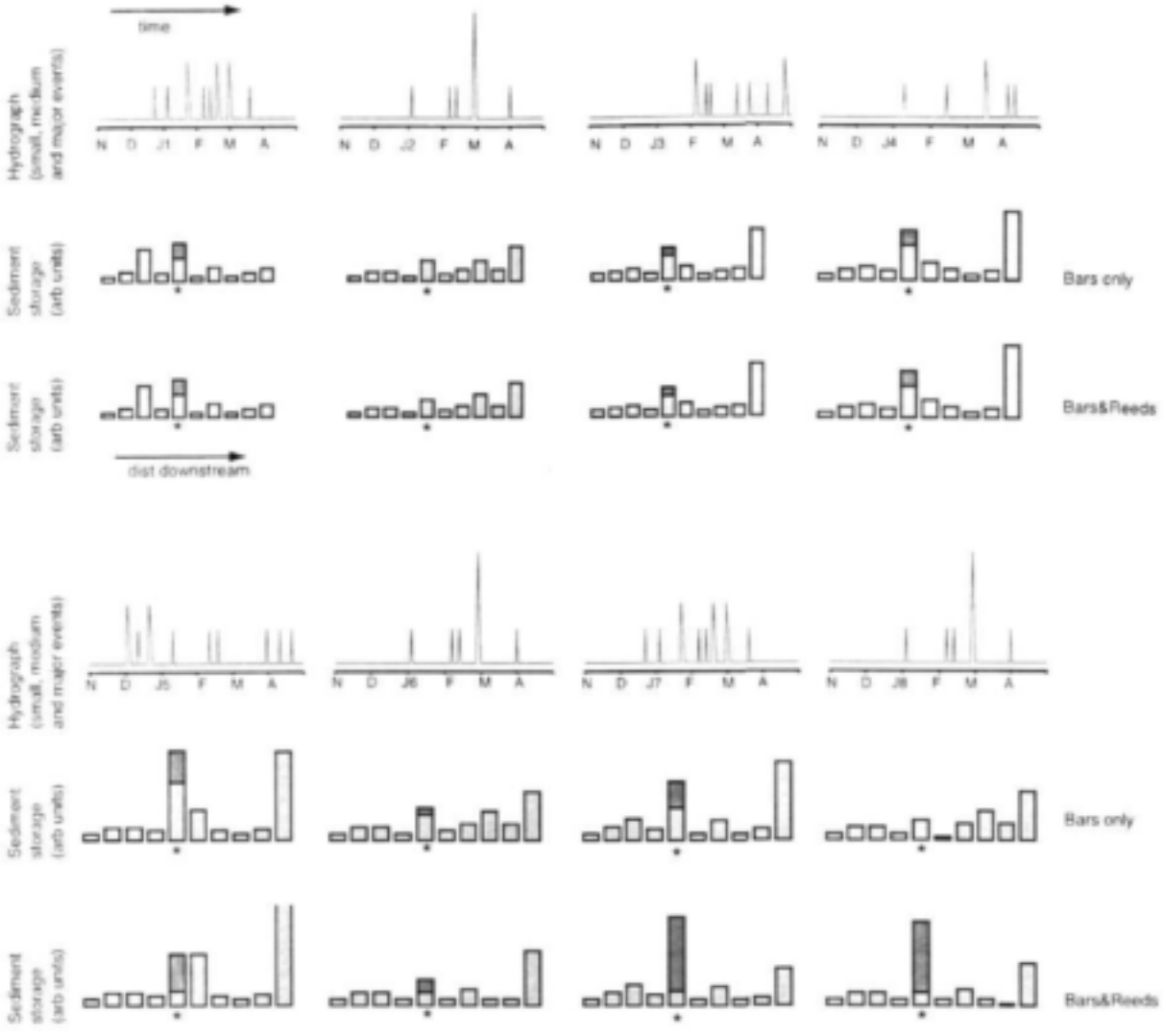

Figure 11.6 Comparison of simulations of the sediment storage dynamics of the hypothetical river with and without reed rules

Although hypothetical, this example shows how application of even a simple set of rules can produce a realistic description of the co-evolution of bars and reeds in a river. It shows that modelling morphological change over several years without accounting for vegetation effects ignores a component that can have a profound effect. In the simulation presented above, the reeds not only change the morphological state of the reach in which they are present but, by influencing the sediment dynamics of that reach, they also determine how much sediment can be moved into subsequent reaches. The model therefore shows that reeds can affect the morphological state of the river downstream as well as in the reach where they are growing. This is illustrated in Fig. 11.6, which again compares two model simulations, the first without reed rules in the fifth cell and the second including them. Figure 11.6 presents for comparison the overall sediment balance

for all 10 cells used in the model with the same 8-year input hydrograph. Although the reed rules are only applied to the fifth cell, their influence is noticeable as far as the tenth cell further down the river.

11.4 DISCUSSION

The model presented in this chapter is clearly inadequate for practical application. It is hypothetical and intended only to demonstrate that it is possible to simulate the dynamic interaction between vegetation and morphology in a fairly simple way.

The way in which the model simulates the development of morphological units by allocating sediment in a particular proportion between bars and the bed is obviously simplistic, as is the method used for describing the effect of reeds on bar erosion and deposition. However, these simplifications reflect our inadequate understanding of the processes rather than an inadequate modelling strategy. A better understanding of the processes that determine sediment distribution within a reach would enable better rules to be specified and more realistic simulations to be achieved. It would seem that our ability to model morphological processes is further advanced than our understanding of the processes.

The lack of data and knowledge available to use a basis for defining model rules has arisen, at least in part, because data collection and river process studies are planned in the context of existing hypotheses and their anticipated application in models. Existing information has therefore generally been compiled to serve the needs of the conventional modelling paradigm. The new approach presented here requires different types of information because it looks at the river in a somewhat different perspective. This is a major reason why the model presented has not been developed to a more realistic, useable stage.

The purpose of this chapter has been to show that rule-based modelling provides an appropriate framework for the simulation of river change because it allows for the incorporation of vegetation as an integral component of the system, i.e. a component that itself responds to the system's driving forces (in this case the flow regime), and which also alters the system's internal processes. We believe that the framework is sound, and that the details within the framework can be improved on as our understanding develops of sediment movement through a reach, factors influencing reed growth, and the interaction between reeds and sediment dynamics. The key process have been identified, and we have the potential to model them. However, the model is only as good as its rules, and these have as yet little scientific foundation.

Although not yet developed to the stage of being useful for management applications, the model has been useful in demonstrating the importance of the role of vegetation in shaping fluvial forms and processes. Model development should proceed in tandem with process understanding, as conjectural applications of the type presented in this chapter are very useful in the identification of important processes that need further theoretical, experimental or field investigation. A particular model formulation can be regarded as an expression of a hypothesis to be tested.

Chapter 12

CONCLUSIONS AND RECOMMENDATION

This project aimed at enhancing our understanding of river function by elucidating the interaction of sediment, water and vegetation. The results will contribute to environmentally sound river management through their addition to our knowledge of the characteristics and dynamics of reedbeds in semi-arid rivers, improved ability to predict the influences of reedbeds on the hydraulic conditions that determine habitat characteristics and sediment dynamics, improved understanding and predictive capability of the movement of sediment by bed load through emergent reeds, and the establishment of a modelling framework for simulating the interaction of reedbed dynamics and morphological processes.

The main conclusions of the study are summarized in the following paragraphs. The issues that have been investigated are important individually but, because of the emphasis on their integration, the depth of the research was not as great as it would have been if attention had been focussed on any one aspect only. Some remaining deficiencies are therefore identified as requiring further investigation before the modelling framework can be applied effectively in practice.

The biological work described in Chapter 3 addresses the specific objectives related to Reedbed Dynamics (outlined in Chapter 1) as modified in consultation with the Steering Committee. This work meets the original objectives related to describing the reed life history characteristics that influence hydraulics and sedimentation by documenting stem characteristics and their variations with season and age of reedbed. The hydraulically relevant characteristics of reedbeds were also documented and used to guide the laboratory investigations on hydraulics of partially reeded channels. Some preliminary understanding of reedbed dynamics was also obtained, which throws new light on the processes involved, but is not yet sufficient for reliable modelling. The local hydraulic conditions and sedimentation states conducive to reedbed establishment, maintenance, expansion and contraction have not been reliably established and require further investigation.

The objectives related to Hydraulics have been achieved to a high degree. The experiments on basic resistance of reeds (Chapter 4) established that resistance depends strongly on stem density and drag coefficient, but not independently on stem diameter or channel slope. It was shown that the velocity profile amongst the stems under emergent conditions is essentially uniform. For submerged flow the velocity distribution is mostly uniform below the stem tops, and similar to boundary resisted flow above the tops. It was shown clearly that Manning's n varies significantly with flow condition, suggesting that this equation is not appropriate where the dominant flow resisting force arises from stem drag rather than bed friction. A theoretically sound alternative equation form is proposed (Chapter 5), in which average flow velocity is (correctly) independent of flow depth and proportional to the square root of channel gradient. An enhancement of this equation allows the influence of bed friction to be included in terms of either the Darcy-Weisbach f or Manning's n, and a preliminary criterion is proposed to indicate the conditions under which this effect should be accounted for. The new equations are confirmed by application to the data collected, and it is shown that stem density and drag coefficient must be accurately specified. Drag coefficient values were measured for typical reed stems, showing that this information can be acquired relatively easily.

The new equations do not account for all influences of vegetation on flow resistance, for example the areal distribution pattern of stems and stem bending, or for submerged flow conditions. Our approach to generalizing the results has been analytical, rather than by extending the experimental data base. A rigorous simulation model (REEDFLO) has been developed that predicts vegetative resistance by accounting for fundamental processes (Chapter 6). The model is based on force balance principles. The classic drag force equation is used to describe stem drag, using the defect model of Petryk (1969) to determine local approach velocity. Both submerged and emergent conditions can be accounted for, using eddy-viscosity and mixing length functions to describe flow through and above the stem zone. Empirical coefficients and boundary conditions were calibrated using experimental results obtained in this study. The model predicts flow depth, vertical distribution of average velocity and shear stress, bed shear stress, total stem drag and effective height of flexible stems, effective drag coefficient based on average velocity, and the effective channel boundary resistance (in terms of Manning's n or Darcy-Weisbach friction factor, f). Input requirements are discharge, channel bed slope, effective bed roughness, reed stem density and stem diameter. The flow depths predicted by the model show excellent agreement with the experimental data collected in the reedbed sedimentation experiments (Chapter 10) under emergent conditions. Further data are required for confirmation of the calibrated resistance model for submerged conditions.

The REEDFLO model is too computationally intensive for routine application, and it was therefore applied hypothetically to develop a simple resistance relationship for flow through emergent vegetation stems (Chapter 7). The form of this relationship is consistent with the theoretical equations of Chapter 5, and also requires reliable specification of drag coefficient.

This work on basic resistance through stems meets the intentions of the first specific Hydraulics objective (see Chapter 1). Its practical usefulness, however, requires additional measurement of drag coefficient values for reeds and other vegetation types. This would enable a resource base (similar to the tables of Manning's n for different channel characteristics) to be established and possible relationships between drag coefficient and leaf area index developed. It is recommended that a project be initiated to enable this work to be carried out.

The experimental work described in Chapter 8 demonstrates the significant dependence of conveyance in partially reeded channels on the distribution pattern of the reedbeds. Where reedbeds form longitudinal strips, resistance is proportional to the number of stem-water interfaces. For the strip patterns investigated, the overall value of Manning's n for the channel was found to vary strongly with flow depth, indicating that specification of a single value of n is inappropriate for channels with significant reed influence, even with only partial coverage. The conveyance of channels with strips of vegetation (including the important case of vegetated banks) can be predicted by calculating separately the discharges of vegetated and clear zones, and adding them together (Chapter 9). The discharge in clear water zones can be reliably estimated by application of the composite roughness formulae of Einstein and Banks (1950) and Horton (1933) with appropriate resistance coefficients assigned to the bed and sides. The flow areas associated with these surfaces is defined by the bisectors of the bed-side angles, and a vertical plane through the intersection point if the planes from opposite sides intersect below the water surface. The discharge in the vegetated zones can be estimated by a modified form (including the stem surface resistance coefficient) of the basic resistance relationship presented in Chapter 5.

Application of these procedures in practice will require specification of a resistance coefficient for the stem surface. This was easily determined in the laboratory, but the values are not representative of natural channels. It is recommended that field data are obtained to enable representative values to be established.

If reedbeds form discrete, longitudinally discontinuous patches within a channel, the resistance is strongly influenced by the shape and distribution pattern of the patches as well as the overall areal coverage (Chapter 8). While overall resistance (in terms of Manning's n) varies approximately linearly with areal coverage for similar reedbed distribution patterns, it also depends strongly on the distribution pattern, patch size and shape, and the degree of reedbed fragmentation as reflected by patch discontinuity and length of stem-clear water interface. As for the strip patterns it appears that Manning's n varies significantly with depth (for areal coverage greater than 25% for the cases tested). No method was developed for predicting conveyance for channels with this type of reedbed distribution. This warrants further research, which could be included in a more general study of discrete element roughness.

The second Hydraulics objective (see Chapter 1) has therefore been substantially achieved, but additional field data are required for determination of effective resistance coefficients of lateral vegetation boundaries, and methods need to be developed for describing discrete roughness effects.

The work on basic resistance and partially reeded channels also addressed the third Hydraulics objective (Chapter 1) of describing ecologically relevant and sediment-related hydraulic conditions. The important hydraulic variables in this context are flow depth, velocity and boundary shear stress, and these need to be described both within reed stands and in the clear channel areas of partially reeded channels. Flow depths and cross-sectional average velocities can be determined through the resistance equations and prediction methods discussed above.

The average bed shear stress in a clear channel area can be determined from the general shear stress equation (equation (6.22)), using the hydraulic radius defined by the area allocated to the bed in the composite resistance procedure. More accurately, this could be done by applying a side-wall correction procedure, as outlined in Chapter 9. The average bed shear within the stems can be estimated from a force balance in which the downslope component of weight is known and the total drag of stems can be calculated (Chapter 10). Estimation of bed shear amongst the stems is inherently inaccurate because it constitutes only a small part of total resistance and the large stem drag component will always be highly variable and uncertain in natural situations.

For both ecological and sediment dynamics purposes, the distributions of velocity and boundary shear stress also need to be described. The experiments on strip roughness showed that the resistance of vegetation boundaries results in a much wider range of velocities in a channel than would otherwise occur, but much less variation of these velocities with changing discharge. The results showed that flow velocity increases rapidly away from a vegetation boundary before levelling off, but there is some evidence that the velocity beyond the zone of rapid increase still depends on the vegetation strip characteristics for some distance. The bed shear stress in the clear channels is similarly affected by vegetation. Velocity and boundary shear stress distributions were measured for some laboratory situations to enable these conclusions to be drawn, but no

generally applicable, quantitative description of velocity distribution was developed. It is recommended that the distribution of velocity and bed shear stress in partially vegetated channels be investigated further by high resolution experimentation and computational modelling.

The work carried out to address the Sedimentation objectives is described in Chapter 10. Only sediment movement by bed load was considered, and further work on suspended sediment is recommended. Experiments were carried out to determine the rate of bed load transport through stems, and the data were used to develop an equation for its calculation. The experiments were done for only one sediment size and one stem density, and further experiments to generalize the results are recommended. These results address the second Sedimentation objective (Chapter 1), as they can be interpreted to define the incipient motion condition as well as to describe the influence of vegetation on transport rate. The first objective (the trapping effectiveness of reedbeds and the influence of reedbed characteristics on trapping) was addressed in a semi-quantitative way only, but the effectiveness of vegetation strips on trapping and stabilizing sediment was clearly demonstrated. It was found that the rate of sediment transfer into vegetation strips increases with discharge, and decreases with time as the sediment accumulates and eventually reaches an equilibrium state. Similar trends were observed for erosion of sediment from within the vegetation strips. Experiments on the formation of lee bars associated with vegetation patches showed the size and extent of deposition to depend on flow condition as well as the patch size and shape. Importantly, it was shown that the bar zones are active, representing a dynamic equilibrium of erosion and deposition; a change in sediment supply with constant hydraulics results in a change in the bar size. The characteristics of residual bars therefore reflect the sediment supply conditions during their formation as well as the hydraulics. The experiments were undertaken with only one stem density, one sediment size, and a limited range of discharges; further investigations of this type are recommended.

A modelling framework for simulating the interaction of water flow, reedbed dynamics and sediment movement was developed to enable reedbed and channel morphology changes to be predicted under modified hydrological regimes (Chapter 11). This addresses the Modelling objectives (Chapter 1), as modified by the Steering Committee. The model presented is not sufficiently developed for practical application, but the deficiencies are more related to inadequate understanding of processes than the model itself. We believe the framework to be sound and capable of incorporating new knowledge as it becomes available, and therefore do not recommend further model development until substantial progress has been made in process description along the lines of the recommendations made above. Even in its present rudimentary form, however, the model was able to demonstrate the importance of accounting for vegetation sediment interaction in modelling morphological change, and provides a useful means of identifying particular research needs for process description.

Chapter 13

REFERENCES

Abt, S R, Clary, W P and Thornton, C I (1994) Ability of streambed vegetation to entrap fine sediments, Journal of Irrigation and Drainage Engineering, Vol. 120, No. 6, pp 1098-1111.

Ackers, P (1958) Resistance to fluids flowing in channels and pipes, Hydraulics Research Paper No. 1, H.M.S.O., London.

Ackers, P (1991) Hydraulic design of straight compound channels, Report SR 281, HR Wallingford, UK.

Ackers, P And White, W R (1973) Sediment transport: New approach and analysis, Journal of the Hydraulics Division, ASCE, Vol. 99, No. HY11, pp 2041-2060.

Albertson, M L, Barton, J R and Simons, D B (1960) Fluid Mechanics for Engineers, Prentice Hall.

Andrews, E D (1984) Bed-material entrainment and hydraulic geometry of gravel-bed rivers in Colorado, Geological Society of America Bulletin, Vol. 95, pp 371-378.

ASCE Task Force on Friction Factors in Open Channels (1963) Friction factors in open channels, Journal of the Hydraulics Division, ASCE, Vol. 89, No. HY2, pp 97-143.

Ashton, P (1987) Reedbed encroachment processes in relation to the rivers of the Kruger National Park, Unpublished document, National Institute for Water Research, CSIR, Pretoria.

Barfield, B J, Tollner, E W and Hayes, J C (1979) Filtration of sediment by simulated vegetation, I. Steady-state flow with homogeneous sediment, Transactions, ASAE, Paper No. 77-2023, pp 540-548.

Barnes, H H (1967) Roughness characteristics of natural channels, US Geological Survey Water-Supply Paper 1849, United States Government Printing Office, Washington.

Birkhead, A L, Olbrich, B W, James, C S and Rogers, K H (1997) Developing an integrated approach to predicting the water use of riparian vegetation, Water Research Commission Report 474/1/97.

Bradbury, P A (1995) CALSITE VERSION 3.1, Calibrated simulation of transported erosion, Overseas Development Unit, HR Wallingford, UK.

Brederode, V and Bradshaw, P (1974) A note on the empirical constants appearing in the logarithmic law for turbulent wall flows, Aero. Report 74-03, Imperial College, U.K.

Brownlie, W R (1981) Re-examination of Nikuradse roughness data, Journal of the Hydraulics Division, ASCE, Vol. 107, No HY1, pp 115-119.

Carter, A J (1995) A Markovian approach to investigating landscape change in the Kruger National Park rivers, PhD thesis, University of the Witwatersrand, Johannesburg, South Africa.

Carter, A J and Rogers, K H (1989) Phragmites reedbeds in the Kruger National Park: The complexity of change in riverbed state, Proceedings of the Fourth South African National Hydrological Symposium, Pretoria, S Kienzle and H Maaren (Eds), pp 339-346.

Carter, A and Rogers, K (1995) A Markovian approach to investigating landscape change in the Kruger National Park Rivers, Report No. 2/95, Centre for Water in the Environment, University of the Witwatersrand, Johannesburg.

Cebeci, T and Chang, K C (1978) Calculation of incompressible rough-wall boundary layer flows AIAA Journal, Vol. 16, pp 730-735.

Chang, H H (1984) Modeling of river channel changes, Journal of Hydraulic Engineering, Vol. 110, No. 2, pp 157-172.

Charlton, F G, Brown, P M and Benson, R W (1978) The hydraulic geometry of some gravel-bed rivers in Britain, Report INT-180, Hydraulic Research Station, Wallingford, UK.

Chow, Ven Te (1959) Open Channel Hydraulics, McGraw-Hill, New York, 680 pp.

Christensen, B A (1971) Incipient motion of cohesionless channel banks, Sedimentation Symposium to Honor H.A. Einstein, Berkeley, California.

Christensen, B A (1976) Hydraulics of sheet flows in wetlands, Proceedings of the 3rd Annual Symposium of the Waterways, Harbors and Coastal Division of ASCE, Colorado State University, Fort Collins, Colorado, 10-12 August, 1976, pp 746-759.

Christensen, B A (1996) Estimating Manning's n in wetlands and vegetated flood plains, Proceedings of the Sixteenth Annual American Geophysical Union Hydrology Days, Colorado State University, Fort Collins, Colorado, April, Hydrology Days Publications, pp 75-85.

Clifton, C (1989) Effects of vegetation and land use on channel morphology, In Practical Approaches to Riparian Resource Management: An Educational Workshop, Billings, Montana, pp 121-129.

Colebatch, G T (1941) Model tests on the Liawanee Canal roughness coefficients, Journal of the Institute of Civil Engineers (Australia), Vol. 13, pp 27-32.

Coleman, N L (1981) Velocity profiles with suspended sediment, Journal of Hydraulic Research, Vol. 19, pp 211-229.

Coles, D (1956) The law of the wake in the turbulent boundary layer, Journal of Fluid Mechanics, Vol. 1, pp 191-226.

Coles, D (1968) The young person's guide to the data, Proc. of AFOSR-IFR Stanford Conference on Computation of Turbulent Boundary Layers, Coles, D and Hirst (Eds), Vol. 2, pp 1-45.

Dalton, C and Masch, F P (1968) Influence of secondary flow on drag forces, Journal of the Engineering Mechanics Division, ASCE, Vol. 94, No. EM5, pp 1249-1257.

Darby, S E and Thorne, C R (1996) Predicting stage-discharge curves in channels with bank vegetation, Journal of Hydraulic Engineering, Vol. 122, No. 10, pp 583-586.

Dawson, F H and Charlton, F G (1988) Bibliography on the hydraulic resistance or roughness of vegetated watercourses, Freshwater Biological Association, Occasional Publication No. 25.

Dean, R B (1978) Reynolds number dependence of skin friction and other bulk flow variables in two-dimensional rectangular duct flow, Journal of Fluids Engineering, ASME, Vol.100, pp 215-223.

de Kleer, J (1975) Qualitative and quantitative knowledge in classical mechanics, Technical Report No. 352, Artificial Intelligence Laboratory, MIT, Cambridge, Massachusetts, USA.

Dietz, R A (1952) The evolution of a gravel bar, Annals of the Missouri Botanical Garden, Vol. 39, pp 249-254.

Donald, P D (1997) GIS Modelling of erosion and sediment yield in a semi-arid environment, MSc (Eng) dissertation, University of the Witwatersrand, Johannesburg, South Africa.

Du Boys, M P (1879) Le Rhone et les Rivieres a Lit affouillable, Met.Doc.,Ann. Pont et Chaussees, ser. 5. Vol. XVIII.

Einstein, H A (1942) Formulas for the transportation of bed load, Transactions, ASCE, Vol. 107, pp 561-577.

Einstein, H A (1950) The bed-load function for sediment transportation in open channel flows, Technical Bulletin No. 1026, United States Department of Agriculture, Soil Conservation Service, Washington, DC.

Einstein, H A and Banks, R B (1950) Fluid resistance of composite roughness, Transactions of the American Geophysical Union, Vol. 31, No. 4, pp 603-610.

Engelund, F And Hansen, E (1967) A monograph on sediment transport in alluvial streams, Teknik Vorlag, Copenhagen, Denmark.

Eschner, T R, Hadley, R F and Crowley, K D (1983) Hydrological and geomorphic changes in channels of the Platte River basin in Colorado, US Geological Survey, Professional Paper 1277A.

Eskinazi, S (1959) Mixing of wakes in a turbulent shear flow, NASA TN-D-83, National

Aeronautics and Space Administration.

Everitt, B L (1979) Fluvial adjustment to the spread of Tamarisk in the Colorado plateau region: Discussion and reply, Geological Society of America Bulletin, Vol. 90, pp 1183-1184.

Fathi-Maghadam, M and Kouwen, N (1997) Nonrigid, nonsubmerged, vegetative roughness on floodplains, Journal of Hydraulic Engineering, Vol. 123, No. 1, pp 51-57.

Fisher, K R (1993) Spatial variations of in-bank hydraulic roughness in channels, Report Sr 357, HR Wallingford, Wallingford, UK.

Flintham, T P and Carling, P A (1988) The prediction of mean bed and wall boundary shear in uniform and compositely rough channels, International Conference on River Regime, W R White (Ed.), John Wiley & Sons, New York, pp 267-287.

Flintham, T P and Carling, P A (1991) Manning's n of composite roughness in channels of simple cross section, in "Channel Flow Resistance: Centennial of Manning's Formula", B C Yen (Ed.), Water Resources Publications, Littleton, Colorado, USA.

Forbus, K D (1995) *Qualitative spatial reasoning: framework and frontiers, In J Glasgow, H* Narayanan and B Chandrasekaren (Eds), Diagrammatic Reasoning: Computational and Cognitive Perspectives, AAAI Press, Chicago, Illinois, USA.

French, R H (1985) Open Channel Hydraulics, McGraw-Hill.

Garbrecht, J and Brown, G O (1991) Calculation of total conveyance in natural channels, Journal of Hydraulic Engineering, Vol. 117, No. 6, pp 788-798.

Gáspár, J (1983) Circulation in reed-overgrown lakes, Proceedings of the 20th IAHR Congress, Moscow, pp 536-537.

Gibbs Russell, G, Watson, L, Koekemoer, M., Smook, L, Barker, N, Anderson, H and Dallwitz, M (1990) Grasses of Southern Africa, Memoirs of the Botanical Survey of South Africa No. 58, National Botanic Gardens/Botanical Research Institute.

Gordon, N D, McMahon, T A and Finlayson, B L (1992) Stream Hydrology: An Introduction for Ecologists, Wiley.

Gordon-Gray, K and Ward, C (1971) A contribution to knowledge of Phragmites (Gramineae) in South Africa, with particular reference to Natal populations, Journal of South African Botany, Vol. 37, No. 1, pp 1-30.

Graf, W (1978) Fluvial adjustment to the spread of tamarisk in the Colorado Plateau region, Geological Society of America Bulletin, Vol. 89, pp 1491-501.

Graf, W H (1971) Hydraulics of Sediment Transport, McGraw-Hill, New York.

Graf, W L (1988) Fluvial Processes in Dryland Rivers, Springer-Verlag, New York, 356 pp.

Hadley, R F (1961) Influence of riparian vegetation on channel shape, northeastern Arizona, US Geological Survey Professional Paper 424-C, 66 pp.

Hall, B R and Freeman, G E (1994) Study of hydraulic roughness in wetland vegetation takes new look at Manning's n, The Wetlands Research Program Bulletin, Vol. 4, No. 1, pp 1-4.

Harvey, M D and Watson, C C (1986) Fluvial processes and morphological thresholds in incised channel restoration, Water Resources Bulletin, Vol. 22, pp 359-368.

Haslam, S (1969) The development and emergence of buds in *Phragmites communis* Trin., Annals of Botany, Vol. 33, pp 289-301.

Henderson, F M (1966) Open Channel Flow, Macmillan.

Heritage, G L, van Niekerk, A W, Moon, B P, Broadhurst, L J, Rogers, K H and James, C S (1997) The geomorphological response to changing flow regimes of the Sabie and Letaba River systems, Water Research Commission Report 376/1/97.

Hey, R D (1979) Flow resistance in gravel-bed rivers, Journal of the Hydraulics Division, ASCE, Vol. 105, No. HY4, pp 365-379.

Hey, R D (1988) Bar form resistance in gravel-bed rivers, Journal of Hydraulic Engineering, Vol. 114, No. 12, pp 1498-1508.

Hickin, E J (1984) Vegetation and river channel dynamics, Canadian Geographer, Vol. 28, pp 111-126.

Hickin, E J and Nanson, G C (1984) Lateral migration rates of river bends, Journal of Hydraulic Engineering, Vol. 110, pp 1557-1567.

Hollan, J, Huchins, E and Weitzman, L (1984) STEAMER: An interactive inspectable simulation-based training system, AI Magazine, Vol. 5, No. 2, pp 15-27.

Horton, R E (1933) Separate roughness coefficients for channel bottom and sides, Engineering News Record, Vol. III, No. 22, pp 652-653.

Hsieh, T (1964) Resistance of cylindrical piers in open channel flow, Proceedings of the Hydraulics Division, ASCE, Vol. 90, No. HY1, pp 161-173.

Hupp, C R (1990) Vegetation patterns in relation to basin hydrogeomorphology, In J B Thornes (Ed), Vegetation and Erosion: Processes and Environments, Wiley, Chichester, pp 217-237.

Hydrologic Engineering Center (1977) Scour and deposition in rivers and reservoirs. HEC-6 Users Manual, HEC, Davis, California, USA.

Isaacs, L T (1965) Hydrodynamic forces on surface piercing cylindrical cylinders and flat plates, Thesis presented to the University of Queensland at St. Lucia, Brisbane, Australia.

James, C S (1998) The role of hydraulics in understanding river processes, Abstracts, National Rivers Initiative, Southern African Society of Aquatic Scientists, Pietermaritzburg, South Africa, 29 June - 1 July, p10.

James, C S, Liu, W and Myers, W R C (2001) Effects of marginal vegetation on conveyance in meandering channels, Proceedings of the Institution of Civil Engineers, Water and Maritime Engineering, Vol. 148, Noo. 2, pp 97-106.

Kadlec, R H (1990) Overland flow in wetlands: vegetation resistance, Journal of Hydraulic Engineering, Vol. 116, No. 5, pp 691-706.

Kamphuis, J W (1974) Determination of sand roughness for fixed beds, Journal of Hydraulic Research, Vol. 12, No. 2, pp 193-203.

Kaiser, W (1984) Fließwiderstandsverhaltern in Gerinnen mit durchströmten Ufergehölzzonen, Wasserbau-Mitteilungen der TH Darmstadt, Heft 23.

Karim, M F and Kennedy, J F (1982) IALLUVIAL: A computer-based flow- and sediment-routing model for alluvial streams and its application to the Missouri River, IIHR Report 250, Iowa Institute for Hydraulic Research, Iowa City, Iowa, USA.

Keulegan, G H (1938) Laws of turbulent flow in open channels, Journal of Research of the National Bureau of Standards, Vol. 21, pp 707-741.

Klaassen, G J and van der Zwaard, J J (1974) Roughness coefficients of vegetated flood plains, Journal of Hydraulic Research, Vol. 12, No. 1, pp 43-63.

Kosorin, K (1983) Turbulent shear stress and velocity distribution in vegetated zone of open channel, Proceedings, 20th IAHR Congress, Moscow, pp 572-579.

Kotschy, K (2001) Clonal growth and colonisation of sediment by reeds (*Phragmites mauritianus*) in the Letaba River, Kruger National Park, MSc dissertation, University of the Witwatersrand, Johannesburg.

Kotschy, K, Rogers, K and Carter, A (2000) Patterns of change in reed cover and distribution in a seasonal riverine wetland in South Africa, Folia Geobotanica, Vol. 35, pp 363-373.

Kouwen, N (1988) Field estimation of the biomechanical properties of grass, Journal of Hydraulic Research, Vol. 26, No. 5, pp 559-568.

Kouwen, N and Li, R-M (1980) Biomechanics of vegetative channel linings, Journal of the Hydraulics Division, ASCE, Vol. 106, No. HY6, pp 1085-1103.

Kouwen, N, Unny, T E and Hill, A M (1969) Flow retardance in vegetated channels, Journal of the Irrigation and Drainage Division, ASCE, Vol.95, No. 2, pp 329-342.

Krishnamurthy, M and Christensen, B A (1972) Equivalent roughness for shallow channels, Journal of the Hydraulics Division, ASCE, Vol. 98, No. HY12, pp 2257-2262.

Krishnappan, B G (1981) MOBED: Unsteady, non-uniform, mobile boundary flow model. User's Manual, National Water Research Institute, Burlington, Ontario, Canada.

Kutija, V and Hong, H T M (1996) A numerical model for assessing the additional resistance to flow introduced by flexible vegetation, Journal of Hydraulic Research, Vol. 34, No. 1, pp 99-114.

Lane, E W and Borland, W M (1950) Estimating bed load, Paper Presented at the Annual Meeting of the American Geophysical Union, May 1-3.

Li, R-M and Shen, H W (1973) Effect of tall vegetations on flow and sediment, Journal of the Hydraulics Division, ASCE, Vol. 99, No. HY5, pp 793-814.

Lindner, K (1982) Der Strömungswiderstand von Pflanzenbeständen, Mitteilung des Leichtweiß-Institutes für Wasserbau der TU Braunschweig, Heft 75.

Liu, W (1997) Effects of floodplain geometry and marginal vegetation on the conveyance of meandering compound channels, PhD thesis, University of the Witwatersrand, Johannesburg, South Africa.

Lotter, G K (1933) Considerations on hydraulic design of channels with different roughness of walls, Transactions, All-Union Scientific Research Institute of Hydraulic Engineering, Leningrad, Vol. 9, pp 238-241.

Mackenzie, J A, van Coller, A L and Rogers, K H (1997) A general guide to the reed, *Phragmites*, Internal Report, Centre for Water in the Environment, University of the Witwatersrand, Johannesburg.

Mahmood, K (1971) Flow in sand bed channels, Water Management Technical Report No. 11, Colorado State University, Fort Collins, Colorado.

Makoa, M J (2001) Flow resistance in partially reeded channels, MSc(Eng) project report, University of the Witwatersrand, Johannesburg, South Africa.

Masterman, R and Thorne, C R (1992) Predicting influence of bank vegetation on channel capacity, Journal of Hydraulic Engineering, Vol. 118, No. 7, pp 1052-1058.

Masterman, R and Thorne, C R (1994) Analytical approach to flow resistance in gravel-bed channels with vegetated banks, in "Process Models and Theoretical Geomorphology", M J Kirkby (Ed.), John Wiley & Sons Ltd, pp 201-218.

Motayed, A K and Krishnamurthy, M (1980) Composite roughness of natural channels, Journal of the Hydraulics Division, ASCE, Vol. 106, No. HY6, pp 1111-1115.

Nanson, G C (1981) New evidence of scroll-bar formation on the Beatton River, Sedimentology, Vol. 28, pp 889-891.

Nagdi, F I and Sharpe, R (2000) The effect of bank vegetation on flow resistance in river channels, Final Year Investigational Project Report, Department of Civil Engineering, University of the Witwatersrand, Johannesburg, South Africa.

Neill, C R (1967) Mean velocity criterion for scour of coarse uniform bed material, Proceedings of the 12th Congress, Vol. III, International Association for Hydraulic Research, Fort Collins, Colorado, USA, pp 46-54.

Nezu, I and Nakagawa, H (1993) Turbulence in open-channel flows, IAHR Monograph, A A Balkema, Rotterdam, Netherlands, 281pp.

Nezu, I and Rodi, W (1986) Open-channel flow measurements with a laser Doppler anemometer, Journal of Hydraulic Engineering, Vol. 115, No. 2, pp 335-355.

Nicolson, C R (1999) Qualitative rule-based modelling of geomorphological change in semi-arid bedrock-influenced rivers, PhD thesis, University of the Witwatersrand, Johannesburg, South Africa.

Nikuradse, J (1933) Strömungsgesetze in rauhen Röhren, VDI Forschungsheft 361 (English translation, Laws of flow in rough pipes, NACA Tech. Memo. 1292, Natl Advis. Comm. for Aeron., Washigton, D.C., 1950).

Nnaji, S and Wu, I-P (1973) Flow resistance from cylindrical roughness, Journal of the Irrigation and Drainage Division, ASCE, Vol. 99, No. IR1, pp 15-26.

Nuding, A (1994) Hydraulic resistance of river banks covered with trees and brushwood, Proceedings, 2nd International Conference on River Flood Hydraulics, York, England, pp 427-437.

O'Brien, M P and Rindlaub B D, (1934) The transportation of bed-load by streams, Transections of the American Geophysical Union.

Ostendorp, W (1991) Damage by episodic flooding to Phragmites reeds in a prealpine lake - Proposal of a model, Oecologia, Vol. 86, No. 1, pp 119-124.

Parker, G and Peterson, A W (1980) Bar resistance of gravel-bed streams, Journal of the Hydraulics Division, ASCE, Vol. 106, No. HY10.

Pasche, E and Rouvé, G (1985) Overbank flow with vegetatively roughened flood plains, Journal of Hydraulic Engineering, Vol. 111, No. 9, pp 1262-1278.

Patel, V C (1965) Calibration of the Preston tube and limitations on its use in pressure gradients, Journal of Fluid Mechanics, Vol. 23, Part 1, pp 185-208.

Petryk, S (1969) Drag on cylinders in open channel flow, PhD thesis, Colorado State University, Fort Collins, Colorado, USA.

Petryk, S and Bosmajian, G (1975) Analysis of flow through vegetation, Journal of the Hydraulics Division, ASCE, Vol. 101, No. HY7, pp 871-884.

Poff, N L, Allan, J D, Bain, M B, Karr, J R, Prestegaard, K L, Richter, B D, Sparks, R E and Stromberg, J C (1997) The natural flow regime: a paradigm for river conservation and restoration, BioScience, Vol. 47, No. 11, pp 769-784.

Prandtl, L (1925) Über die ausgebildete turbulenz, ZAMM, Vol. 5, 131.

Press, W H, Flannery, B P, Teukolsky, S A, and Vetterling, W T, (1989) Numerical Recipes - The Art of Scientific Computing (FORTRAN version), Cambridge University Press, Cambridge, 702 pp.

Prestegaard, K (1983) Bar resistance in gravel bed streams at bankfull stage, Water Resources Research, Vol. 19, No. 2, pp 472-476.

Ree, W O and Crow, F R (1977) Friction factors for vegetated waterways of small slope, Agricultural Research Series, ARS-S-151, USDA, Washington.

Reichardt, H (1941) Über eine neue Theorie der freien Turbulenz, ZAMM Vol. 21, 257 pp.

Reichardt, H (1951) Vollstandige darstellung der turbulenten geschwindigeitsverteilung in glatten leitungen. Z. Angew. Math. Mech., Vol. 31, No. 7, pp 208-219.

Richter, A (1973) Stömungskräfte auf starre Kreiszylinder zwischen parallelen Wänden. Diss., Universität Karlsruhe.

Rooseboom, A (1992) Sediment transport in rivers and reservoirs - A South African perspective, WRC Report No. 297/1/92, Water Research Commission, Pretoria, South Africa.

Rowntree, K (1991) An assessment of the potential impact of alien invasive vegetation on the geomorphology of river channels in South Africa, South African Journal of Aquatic Science, Vol. 17, pp 28-43.

Sayre, W W and Albertson, M L (1961) Roughness spacing in rigid open channels, Journal of the Hydraulics Division, ASCE, Vol. 87, No. HY3, pp 121-150.

Schlichting, H (1930) Über das ebene Windschatten problem. Ingenieur-Archiv, I. Band.

Schlichting, H (1979) Boundary-Layer Theory, 7th edition, McGraw-Hill, New York.

Smith, D G (1976) Effect of vegetation on lateral migration of a glacial meltwater river, Geological Society of America Bulletin, Vol. 87, pp 857-860.

Smith, R J, Hancock, N H and Ruffini, J L (1990) Flood flow through tall vegetation, Agricultural Water Management, Vol. 18, pp 317-332.

Soil Conservation Service (1963) Guide for selecting roughness coefficient "n" values for channels, US Department of Agriculture, Soil Conservation Service, Washington, D.C.

Starfield, A M, Cumming, D H M, Taylor, R D and Quadling, M S (1993) A frame-based paradigm for dynamic ecosystem models, AI Applications, Vol. 7, Nos 2&3, pp 1-15.

Starfield, A M, Farm, B P and Taylor, R H (1989) A rule-based ecological model for the management of an estuarine lake, Ecological Modeling, Vol. 46, pp 107-119.

Starosolszky, Ö (1983) The role of reeds in the shaping of currents, Proceedings, 20th congress, International Association for Hydraulic Research, Moscow, pp 498-509.

Tester, J R, Starfield, A M and Frelich, L E (1997) Modeling for ecosystem management in Minnesota pine forests, Biological Conservation, Vol. 80, pp 313-324.

Thomas, D S G and Tsoar, H (1991) The geomorphological role of vegetation in desert dune systems, In J B Thornes (Ed.), Vegetation and Erosion: Processes and Environment, Wiley, Chichester, pp 471-490.

Thomas, W A (1982) Mathematical modelling of sediment movement. In R D Hey, J C Bathurst and C R Thorne (Eds), Gravel Bed Rivers, Wiley, Chichester, pp 487-508.

Thompson, G T and Roberson, J A (1976) A theory of flow resistance for vegetated channels, Transactions of the American Society of Agricultural Engineers, Vol. 19, No. 2, pp 288-293.

Thompson, K (1985) Emergent plants of permanent and seasonally-flooded wetlands, in: The Ecology and Management of African Wetland Vegetation, Denny, P(Ed.), Junk, Dordrecht.

Thorne, C R (1978) Processes of bank erosion in river channels, PhD thesis, University of East Anglia, Norwich, UK.

Thorne, C R (1982) Processes and mechanisms of river bank erosion, in R D Hey, J C Bathurst and C R Thorn (Eds), Gravel Bed Rivers, Wiley, Chichester, pp 227-271.

Thorne, C R (1988) The influence of bank stability on regime geometry of natural channels, In W R White (Ed.), International Conference on River Regime, Wiley, Chichester, pp 135-148.

Thorne, C R (1990) Effects of vegetation on riverbank erosion, in J B Thornes (Ed.), Vegetation and Erosion: Processes and Environments, Wiley, Chichester, pp 125-144.

Thorne, C R, Hey, R D and Chang, H H (1988) Prediction of hydraulic geometry of gravel-bed rivers using the minimum stream power concept, International Conference on River Regime, Wiley, Chichester, pp 29-40.

Thornes, J B (Ed.) (1991) Vegetation and Erosion: Processes and Environment, Wiley, Chichester.

Thornton, C I, Abt, S R and Clary, W P (1997) Vegetation influence on small stream siltation, Journal of the American Water Resources Association, Vol. 33, No. 6, pp 1279-1288.

Tollner, E W, Barfield, B J and Hayes, J C (1982) Sedimentology of erect vegetal filters, Journal of the Hydraulics Division, ASCE, Vol.108, No. HY12, pp 1518-1531.

Tollner, E W, Barfield, B J, Vachirakornwatana, C and Haan, C T (1977) Sediment deposition patterns in simulated grass filters, Transactions, ASAE Vol. 20, No. 5 pp 940-944 .

Trissler , K E and Stevens, E G (1994) Hydraulic relationships between vegetation patterns and channel friction, Final Year Investigational Project, Department of Civil Engineering, University of the Witwatersrand, Johannesburg.

Tsujimoto, T (1999) Fluvial processes in streams with vegetation, Journal of the Hydraulic Research, Vol. 37, No. 6, pp 789-803.

Tsujimoto, T and Kitamara, T (1990) Velocity profile of flow in vegetated-bed channels, KNL progressive report, Hydraulics Laboratory, Kanazawa University, Japan.

Tsujimoto, T and Kitamura, T (1994) Lateral bed load transport due to organized fluctuation of flow in open-channel with vegetation zone, Proceedings, 1st International Symposium on Habitat Hydraulics, Trondheim, Norway, pp 185-198.

Tsujimoto, T and Kitamura, T (1996) River-bed degradation influenced by growth of vegetation along a stream, in Leclerc, M et al (Eds), Proceedings of the 2nd IAHR Symposium on Habitat Hydraulics, Ecohydraulics 2000, Quebec, pp A389-A394.

Tsujimoto, T and Kitamura, T and Murakami, S (1996) Basic morphological process due to deposition of suspended sediment affected by vegetation, in Leclerc, M et al (Eds), Proceedings of the 2nd IAHR Symposium on Habitat Hydraulics, Ecohydraulics 2000, Quebec, pp A395-A405.

Tsujimoto, T and Shimizu, Y (1994) Flow and suspended sediment in a compound channel with vegetation, KHL Hydraulic Research '94, Hydr. Lab., Kanazawa University, Japan.

Tsujimoto, T, Shimizu, Y and Nakagawa, H (1991) Concentration distribution of suspended sediment in vegetated sand bed channel, International Symposium on the Transport of Suspended Sediment and its Mathematical Modelling, Florence, Italy.

Turner, A K and Chanmeesri, N (1984) Shallow flow of water through non-submerged vegetation, Agricultural Water Management, Vol. 8, pp 375-385.

van Coller, A L (1993) Riparian vegetation of the Sabie River: relating spatial distribution patterns to characteristics of the physical environment, MSc dissertation, University of the Witwatersrand, Johannesburg, South Africa.

van Coller, A and Rogers, K (1996) A basis for determining the Instream Flow Requirements of the riparian vegetation along the Sabie River within the Kruger National Park, Report No. 2/96, Centre for Water in the Environment, University of the Witwatersrand, Johannesburg.

van Coller, A L, Rogers, K H and Heritage, G L (1997) Linking riparian vegetation types and fluvial geomorphology along the Sabie River within the Kruger National Park, South Africa, African Journal of Ecology, Vol. 35, pp 194-212.

Van Driest, E R (1956) On turbulent flow near a wall, J. Aeron. Sci., Vol. 23, pp 1007-1011.

van Niekerk, A W and Heritage, G L (1993) Geomorphology of the Sabie River: overview and classification, Report 2/93, Centre for Water in the Environment, University of the Witwatersrand, Johannesburg, South Africa.

van Niekerk, A W, Heritage, G L and Moon, B P (1995) River classification for management: the geomorphology of the Sabie River in the Eastern Transvaal, South African Geographical Journal, Vol. 77, pp 68-76.

Vanoni, V A (Ed.) (1977) Sedimentation Engineering, Manuals and Reports on Engineering Practice, No.54, ASCE.

Vanoni, V A and Brooks, N H (1957) Laboratory Studies of the Roughness and Suspended Load of Alluvial Streams, Sedimentation Laboratory Report No. E68, California Institute of Technology, Pasadena, California, USA.

Van Rijn, L (1982) Equivalent roughness of alluvial bed, Journal of Hydraulic Engineering, Vol. 108, No. 10, pp 1215-1218.

Viles, HA (Ed.) (1988) Biogeomorphology, Blackwell, Oxford, 365 pp.

Waldron, L J (1977) Shear resistance of root permeated homogeneous and stratified soil, Soil Science Society of America Journal, Vol. 41, pp 843-849.

Walker, K F, Sheldon, F and Puckridge, J T (1995) A perspective on dryland river ecosystems, Regulated Rivers: Research & Management, Vol. 11, pp 85-104.

Wantanabe, T and Kondo, J (1990) The influence of canopy structure and density upon the mixing length within and above vegetation, J. Met. Soc. Japan, Vol. 68, No. 2, pp 227-235.

Wark, J B (1993) Discharge assessment in straight and meandering compound channels, PhD thesis, University of Glasgow.

Wark, J B, Slade, J E and Ramsbottom, D M (1991) Flood discharge assessment by the lateral distribution method, HR Wallingford Report SR 277.

Waterways Experiment Station (1994) Effects of vegetation on hydraulic roughness and sedimentation in wetlands, WRP Technical Note SD-CP-2.2.

Watts, J F and Watts, G D (1990) Seasonal changes in aquatic vegetation and its effect on river channel flow, in J B Thornes (Ed.), Vegetation and Erosion: Processes and Environments, Wiley, Chichester, pp 257-267.

Williams, G P (1978) The case of the shrinking channels - the North Platte and Platte Rivers in Nebraska, US Geological Circular 781.

Witt, A (1985) Vegetational influences on intrachannel deposition: evidence from the Konczak stream, Greater Poland Lowlands, Western Poland, Quaestiones Geographicae, Vol. 9, pp 145-160.

Yanosky, T M (1982) The effects of flooding on woody vegetation, US Geological Survey Professional Paper 1206, 21 pp.

Zippe, H J and Graf, W H (1983) Turbulent boundary-layer flow over permeable and non-permeable rough surfaces, Journal of Hydraulic Research, Vol. 21, No. 1, pp 51-65.

Appendix A

Experimental Data for Basic Stem Resistance

Series A Data

Test A1: Rough bed, no stems

Spacing (mm)	Slope	Q (l/s)	Depth (m)
	0.002	0.963	0.0428
	0.002	0.859	0.0434

Test A2: Round stems

Spacing (mm)	Slope	Q (l/s)	Depth (m)
25	0.01	0.125	0.0171
25	0.01	0.36	0.0275
25	0.01	0.593	0.0443
25	0.01	1.056	0.0775
25	0.01	1.642	0.1197

Test A3: Round stems

Spacing (mm)	Slope	Q (l/s)	Depth (m)
25	0.002	0.126	0.0273
25	0.002	0.233	0.0468
25	0.002	0.376	0.0686
25	0.002	0.437	0.0802
25	0.002	0.626	0.1123
25	0.002	0.726	0.1334

Test A4: Round stems

Spacing (mm)	Slope	Q (l/s)	Depth (m)
50	0.002	0.164	0.0203
50	0.002	0.32	0.0336
50	0.002	0.49	0.0449
50	0.002	0.731	0.0603
50	0.002	1.292	0.0963
50	0.002	1.986	0.1493

Test A5: Round stems

Spacing (mm)	Slope	Q (l/s)	Depth (m)
75	0.002	0.306	0.0296
75	0.002	0.6	0.0457
75	0.002	0.794	0.0568
75	0.002	1.267	0.0808
75	0.002	1.742	0.1018
75	0.002	2.073	0.1198

Test A6: Square stems

Spacing (mm)	Slope	Q (l/s)	Depth (m)
25	0.01	0.1364	0.0127
25	0.01	0.3473	0.0293
25	0.01	0.568	0.0466
25	0.01	1.029	0.082
25	0.01	1.612	0.1245

Test A7: Square stems

Spacing (mm)	Slope	Q (l/s)	Depth (m)
25	0.002	0.1284	0.0266
25	0.002	0.2235	0.0441
25	0.002	0.3518	0.0686
25	0.002	0.4408	0.085
25	0.002	0.6289	0.123
25	0.002	0.7264	0.1471

Test A8: Square stems

Spacing (mm)	Slope	Q (l/s)	Depth (m)
50	0.002	0.1607	0.0232
50	0.002	0.3251	0.0351
50	0.002	0.4961	0.047
50	0.002	0.695	0.0627
50	0.002	1.205	0.1028
50	0.002	1.852	0.1495

Test A9: Square stems

Spacing (mm)	Slope	Q (l/s)	Depth (m)
75	0.002	0.3101	0.0326
75	0.002	0.6298	0.0504
75	0.002	0.755	0.0593
75	0.002	1.131	0.0832
75	0.002	1.5674	0.1089
75	0.002	2.1732	0.1398

Test A10: Diagonal stems

Spacing (mm)	Slope	Q (l/s)	Depth (m)
25	0.01	0.133	0.0144
25	0.01	0.337	0.0339
25	0.01	0.5915	0.0575
25	0.01	1.063	0.103
25	0.01	1.6263	0.1471

Test A11: Diagonal stems

Spacing (mm)	Slope	Q (l/s)	Depth (m)
25	0.002	0.1295	0.028
25	0.002	0.2453	0.05
25	0.002	0.3627	0.0676
25	0.002	0.486	0.0925
25	0.002	0.6227	0.1166
25	0.002	0.7721	0.1488

Test A12: Diagonal stems

Spacing (mm)	Slope	Q (l/s)	Depth (m)
50	0.002	0.1664	0.0162
50	0.002	0.3259	0.0343
50	0.002	0.5218	0.0472
50	0.002	0.69	0.0624
50	0.002	1.205	0.0992
50	0.002	1.889	0.1477

Test A13: Diagonal stems

Spacing (mm)	Slope	Q (l/s)	Depth (m)
75	0.002	0.2622	0.0302
75	0.002	0.65	0.053
75	0.002	0.7414	0.0599
75	0.002	1.25	0.0853
75	0.002	1.56	0.1056
75	0.002	2.25	0.1399

Test A14: Round stems

Spacing (mm)	Slope	Q (l/s)	Depth (m)
25	0.002	0.107	0.027
25	0.002	0.185	0.038
25	0.002	0.356	0.065
25	0.002	0.423	0.077
25	0.002	0.454	0.085
25	0.002	0.506	0.091
25	0.002	0.631	0.105
25	0.002	0.715	0.121
25	0.002	1.281	0.138
25	0.002	1.462	0.149
25	0.002	1.841	0.162
25	0.002	1.989	0.173

Test A15:
Round stems

Spacing (mm)	Slope	Q (l/s)	Depth (m)
50	0.002	0.441	0.049
50	0.002	0.841	0.084
50	0.002	1.121	0.101
50	0.002	1.609	0.119
50	0.002	1.731	0.122
50	0.002	2.029	0.131

Test A16:
Round stems

Spacing (mm)	Slope	Q (l/s)	Depth (m)
75	0.002	0.996	0.079
75	0.002	1.311	0.096
75	0.002	1.506	0.106
75	0.002	1.787	0.113
75	0.002	1.901	0.114
75	0.002	2.082	0.124

Series B Data

Test	Spacing (mm)	Slope	Q (l/s)	Depth (m)
B1	25	0.0118	2.46	0.0430
B2	25	0.0145	2.46	0.0395
B3	25	0.0160	2.46	0.0380
B4	25	0.0184	2.46	0.0360
B5	25	0.0165	1.31	0.0205
B6	25	0.0140	2.06	0.0335
B7	25	0.013 0	4.21	0.0705
B8	25	0.013 0	6.04	0.0960
B9	25	0.013 0	7.02	0.1110

Sten Drag Data

Round Stems,
d=5 mm

Flow depth (mm)	Mass (g)	Force (N)	V (m/s)
190	0.2	0.00189	0.014
207	1.0	0.00943	0.057
235	4.5	0.04243	0.130
180	11.0	0.10371	0.216
162	32.0	0.30169	0.365
165	60.0	0.56567	0.496
160	78.7	0.74197	0.589
150	100.0	0.94278	0.684
120	165.8	1.56313	0.878

Square Stems, d=5 mm

Flow depth (mm)	Mass (g)	Force (N)	V (m/s)
195	0.5	0.00491	0.012
215	2.3	0.02256	0.058
235	5.0	0.04905	0.103
210	8.0	0.07848	0.139
190	13.0	0.12753	0.205
162	31.6	0.31000	0.332
151	34.3	0.33648	0.362
143	96.0	0.94176	0.649
138	115.0	1.12815	0.700
115	182.1	1.78640	0.820

Square Stems, d=25 mm

Flow depth (mm)	Mass (g)	Force (N)	V (m/s)
197	0.5	0.00471	0.015
190	1.2	0.01131	0.028
213	5.3	0.04997	0.068
205	12.1	0.11408	0.103
230	29.6	0.27906	0.150

Diagonal Stems, d=5 mm

Flow depth (mm)	Mass (g)	Force (N)	V (m/s)
210	3.0	0.02828	0.056
215	6.0	0.05657	0.111
210	14.0	0.13199	0.189
208	31.8	0.29980	0.288
183	79.0	0.74480	0.420
163	112.0	1.05591	0.493
130	168.8	1.59141	0.610
150	224.5	2.11654	0.713
135	264.8	2.49648	0.787

Diagonal Stems, d=25 mm

Flow depth (mm)	Mass (g)	Force (N)	V (m/s)
193	1.8	0.01697	0.029
195	9	0.08485	0.073
227	41	0.38654	0.144

Reed Stem 1 (Test C5)

Length (mm)	880
Diameter 1 (mm)	12.4
Diameter 2 (mm)	11.2
Diameter 3 (mm)	8.8
Kinematic viscosity (m2/s)	1.14E-06
Temperature (C)	19.5
Density (kg/m3)	1000

Flow depth (mm)	Mass (g)	Force (N)	Velocity (m/s)
210	7.9	0.07448	0.067
243	21.6	0.20364	0.133
210	55.1	0.51947	0.203
195	95.0	0.89564	0.322
195	129.6	1.22184	0.405
180	177.5	1.67343	0.511

Leaf characteristics:

no. of leaves 8

leaf no.	length (mm)	area (mm^2)
1	160	2024.48
2	210	2657.13
3	260	3100.00
4	290	3669.37
5	320	4048.96
6	340	4302.02
7	360	4555.08
8	390	4850.00
	total =	29207.04

Leaf area = 0.03 m2

Reed Stem 2 (Test C6)

Length (mm)	860
Diameter 1 (mm)	10.8
Diameter 2 (mm)	7.8
Diameter 3 (mm)	6.6
Kinematic viscosity (m2/s)	1.14E-06
Temperature (C)	20
Density (kg/m3)	1000

Flow depth (mm)	Mass (g)	Force (N)	Velocity (m/s)
210	10.0	0.09428	0.062
190	25.4	0.23947	0.111
210	61.5	0.57981	0.208
185	81.5	0.76837	0.292
200	127.1	1.19827	0.381
200	160.7	1.51505	0.473
175	233.3	2.19950	0.590

Leaf characteristics:

no. of leaves	6

leaf no.	length (mm)	area
1	200	3110
2	260	4043
3	340	5440
4	400	6300
5	410	6375.5
6	420	6531
	total	31799.5

Leaf area = 0.0317995 m2

Branch characteristics

no of branches	2

branch no	length	area (mm2)	diam. (mm)
1	370	1480	4
2	210	693	3.3
		2173	
	total (m^2)	0.002173	

Total =0.03397

Reed Stem 2 (Test C7)

Length (mm)	860
Diameter 1 (mm)	10.8
Diameter 2 (mm)	7.8
Diameter 3 (mm)	6.6
Kinematic viscosity (m2/s)	1.14E-06
Temperature (C)	20
Density (kg/m3)	1000
Leaf area = 0.0318	m2

Flow depth (mm)	Mass (g)	Force (N)	Velocity (m/s)
220	6.9	0.06505	0.033
240	22.6	0.21307	0.119
170	35.1	0.33092	0.183
220	73.9	0.69671	0.290
190	101.5	0.95692	0.361
180	142.7	1.34535	0.484
175	206.3	1.94495	0.590

Reed Stem 2 (Test C8)

Length (mm)	860
Diameter 1 (mm)	10.8
Diameter 2 (mm)	7.8
Diameter 3 (mm)	6.6
Kinematic viscosity (m2/s)	1.14E-06
Temperature (C)	20
Density (kg/m3)	1000
Leaf area = 0.0158	m2

Flow depth (mm)	Mass (g)	Force (N)	Velocity (m/s)
220	6.9	0.06505	0.033
230	10.1	0.09522	0.104
240	29.0	0.27341	0.186
195	54.1	0.51004	0.289
205	92.8	0.87490	0.400
190	127.1	1.19827	0.481
150	200.9	1.89404	0.642

Reed Stem 2 (Test C9)

Length (mm)	860
Diameter 1 (mm)	10.8
Diameter 2 (mm)	7.8
Diameter 3 (mm)	6.6
Kinematic viscosity (m2/s)	1.14E-06
Temperature (C)	20
Density (kg/m3)	1000

Flow depth (mm)	Mass (g)	Force (N)	Velocity (m/s)
195	2.0	0.01886	0.035
230	10.1	0.09522	0.124
180	20.1	0.18950	0.180
250	56.0	0.52796	0.300
215	82.5	0.77779	0.380
210	135.0	1.27275	0.500
175	194.0	1.82899	0.636

Bulrush Stem (C10)

Length (mm)	865
Diameter 1 (mm)	16.6
Diameter 2 (mm)	11.1
Diameter 3 (mm)	7
Temperature	20.5

Flow depth (mm)	Mass (g)	Force (N)	Velocity (m/s)
225	6.9	0.06505	0.049
230	12.2	0.11502	0.095
260	55.6	0.52419	0.184
200	125.8	1.18602	0.284
190	232.6	2.19290	0.401
205	301.7	2.84436	0.476
175	408.8	3.85408	0.589

<u>leaf characteristics</u>

no. of leaves 6

leaf no.	length (mm)	thickness (mm)	area (mm2)
1	780	14	10920
2	630	13	8190
3	530	12	6360
4	395	10	3950
5	350	9	3150
6	160	8.5	1360
		total	33930

Leaf area = 0.03393 m2

Appendix B

Experimental Data for Partially Reeded Channels

Strip Experimental Data

Stage-Discharge Data

Basic Channel **S =0.00107**

Q (m3/s)	Depth (m)	Temp (oC)	nu (10-6m2/s)	V (m/s)	R (m)	f	n	Re
0.0000	0.000							
0.0050	0.021	23	0.9424	0.242	0.0199	0.0286	0.0099	20377.87
0.0100	0.032	24	0.9236	0.312	0.0302	0.0261	0.0102	40697.86
0.0125	0.037		0.9424	0.342	0.0341	0.0246	0.0101	49435.12
0.0150	0.041	22	0.9626	0.365	0.0380	0.0239	0.0101	57594.34
0.0200	0.049	22	0.9626	0.409	0.0445	0.0224	0.0100	75701.22
0.0225	0.053		0.9424	0.425	0.0479	0.0223	0.0102	86344.30
0.0250	0.057	24	0.9236	0.442	0.0508	0.0218	0.0101	97283.62
0.0300	0.065	22	0.9626	0.465	0.0571	0.0222	0.0104	110413.81
0.0350	0.072	21	0.9842	0.489	0.0626	0.0220	0.0106	124434.30

Pattern 1

Q (m3/s)	Depth (m)	Temp (oC)	nu (10-6m2/s)	V (m/s)	R (m)	f	n	Re
0.0000	0.000							
0.0050	0.036	21	0.9842	0.138	0.0338	0.1498	0.0248	18946.39
0.0100	0.062	21	0.9842	0.162	0.0551	0.1772	0.0293	36166.40
0.0125	0.079	17	1.0834	0.159	0.0679	0.2255	0.0342	39880.14
0.0150	0.092	21	0.9842	0.164	0.0774	0.2424	0.0363	51526.11
0.0200	0.121	22	0.9626	0.165	0.0974	0.2988	0.0418	66922.85
0.0225	0.149	23	0.9424	0.151	0.1146	0.4196	0.0510	73617.63

Pattern 2

Q (m3/s)	Depth (m)	Temp (oC)	nu (10-6m2/s)	V (m/s)	R (m)	f	n	Re
0.0000	0.000							
0.0050	0.060	22	0.9626	0.084	0.0533	0.6354	0.0552	18563.44
0.0100	0.104	22	0.9626	0.096	0.0862	0.7841	0.0664	34391.99
0.0125	0.130	23	0.9424	0.097	0.1029	0.9271	0.0744	42139.62
0.0150	0.150	22	0.9626	0.100	0.1151	0.9618	0.0772	47974.60

Pattern 3

Q (m3/s)	Depth (m)	Temp (oC)	nu (10-6m2/s)	V (m/s)	R (m)	f	n	Re
0.0000	0.000							
0.0050	0.055	22	0.9626	0.092	0.0491	0.4903	0.0478	18734.17
0.0100	0.088	21	0.9842	0.113	0.0750	0.4898	0.0513	34549.30
0.0125	0.118	21	0.9842	0.106	0.0955	0.7161	0.0646	41097.51
0.0150	0.129	21	0.9842	0.116	0.1027	0.6410	0.0618	48439.29

Pattern 4

Q (m3/s)	Depth (m)	Temp (oC)	nu (10-6m2/s)	V (m/s)	R (m)	f	n	Re
0.0000	0.000							
0.0050	0.045	20	1.0070	0.111	0.0414	0.2826	0.0353	18217.73
0.0100	0.079	20	1.0070	0.127	0.0679	0.3524	0.0428	34325.91
0.0125	0.100	20	1.0070	0.125	0.0833	0.4479	0.0499	41377.03
0.0150	0.116	19	1.0312	0.129	0.0941	0.4717	0.0523	47237.29

Pattern 5

Q (m3/s)	Depth (m)	Temp (oC)	nu (10-6m2/s)	V (m/s)	R (m)	f	n	Re
0.0000	0.000							
0.0050	0.039	21	0.9842	0.128	0.0363	0.1862	0.0280	18847.99
0.0100	0.064	19	1.0312	0.156	0.0567	0.1952	0.0309	34389.42
0.0125	0.086	19	1.0312	0.146	0.0733	0.2907	0.0394	41380.00
0.0150	0.095	19	1.0312	0.159	0.0795	0.2649	0.0381	48937.68
0.0200	0.122	19	1.0312	0.164	0.0981	0.3071	0.0425	62355.35

Pattern 6

Q (m3/s)	Depth (m)	Temp (oC)	nu (10-6m2/s)	V (m/s)	R (m)	f	n	Re
0.0000	0.000							
0.0050	0.047	19	1.0312	0.107	0.0426	0.3109	0.0372	17742.07
0.0100	0.083	19	1.0312	0.121	0.0710	0.4090	0.0465	33280.08
0.0125	0.103	19	1.0312	0.121	0.0856	0.4910	0.0525	40186.54
0.0150	0.117	19	1.0312	0.128	0.0947	0.4832	0.0530	47160.72

Pattern 7

Q (m3/s)	Depth (m)	Temp (oC)	nu (10-6m2/s)	V (m/s)	R (m)	f	n	Re
0.0000	0.000							
0.0050	0.054	19	1.0312	0.092	0.0490	0.4851	0.0476	17495.61
0.0100	0.098	17	1.0834	0.102	0.0819	0.6589	0.0604	30874.26
0.0125	0.122	17	1.0834	0.103	0.0979	0.7809	0.0677	37109.44
0.0150	0.142	17	1.0834	0.106	0.1103	0.8258	0.0710	43157.08

Clear Channel Velocity Distributions

All velocities are depth-averaged values in m/s, calculated from measurements at 0.2, 0.4 and 0.8 of the depth from the bed, as described in the text

Basic Channel

Distance (m)	Q = 5 l/s	Q = 15 l/s	Q = 20 l/s	Q = 25 l/s
0.025	0.184	0.273	0.305	0.320
0.100	0.226	0.363	0.383	0.424
0.200	0.242	0.384	0.408	0.439
0.300	0.254	0.395	0.444	0.466
0.400	0.255	0.405	0.453	0.506
0.500	0.256	0.411	0.463	0.528

Pattern 1

Distance (m)	Q = 5 l/s	Q = 10 l/s	Q = 12.5 l/s	Q = 15 l/s
0.250	0.116	0.122	0.096	0.108
0.350	0.236	0.237	0.246	0.256
0.500	0.272	0.322	0.333	0.327
0.650	0.204	0.227	0.243	0.253
0.750	0.104	0.109	0.103	0.118

Pattern 2

Distance (m)	Q = 5 l/s	Q = 10 l/s	Q = 12.5 l/s	Q = 15 l/s
0.125	0.058	0.083	0.078	0.078
0.205	0.145	0.161	0.160	0.161
0.285	0.086	0.083	0.089	0.096
0.410	0.062	0.077	0.073	0.071
0.490	0.132	0.139	0.137	0.139
0.570	0.088	0.086	0.089	0.092
0.695	0.075	0.086	0.081	0.083
0.775	0.154	0.170	0.169	0.172
0.855	0.063	0.072	0.070	0.089

Pattern 3

Distance (m)	Q = 5 l/s	Q = 10 l/s	Q = 12.5 l/s	Q = 15 l/s
0.125	0.067	0.082	0.077	0.096
0.175	0.149	-0.161	0.148	0.173
0.225	0.190	0.197	0.190	0.214
0.275	0.192	0.197	0.193	0.211
0.325	0.156	0.163	0.153	0.173
0.375	0.088	0.086	0.091	0.104
0.625	0.080	0.081	0.084	0.100
0.675	0.147	0.159	0.165	0.177
0.725	0.185	0.204	0.190	0.213
0.775	0.181	0.190	0.186	0.207
0.825	0.140	0.147	0.138	0.164
0.875	0.064	0.068	0.071	0.080

Pattern 4

Distance (m)	Q = 5 l/s	Q = 10 l/s	Q = 12.5 l/s	Q = 15 l/s
0.000	0.138	0.152	0.150	0.164
0.050	0.188	0.205	0.204	0.221
0.100	0.206	0.220	0.220	0.229
0.125	0.201	0.222	0.220	0.231
0.150	0.201	0.206	0.209	0.225
0.200	0.178	0.189	0.187	0.198
0.250	0.098	0.113	0.118	0.124
0.750	0.102	0.110	0.119	0.129
0.800	0.185	0.186	0.184	0.198
0.850	0.204	0.216	0.219	0.229
0.875	0.213	0.227	0.228	0.230
0.900	0.218	0.230	0.231	0.246
0.950	0.203	0.213	0.221	0.224
1.000	0.164	0.165	0.167	0.174

Pattern 5

Distance (m)	Q = 5 l/s	Q = 10 l/s	Q = 12.5 l/s	Q = 15 l/s
0.375	0.099	0.114	0.108	0.121
0.475	0.220	0.250	0.258	0.268
0.625	0.261	0.304	0.308	0.336
0.775	0.209	0.221	0.194	0.244
0.875	0.091	0.108	0.091	0.108

Pattern 6

Distance (m)	Q = 5 l/s	Q = 10 l/s	Q = 12.5 l/s	Q = 15 l/s
0.000	0.152	0.171	0.165	0.178
0.050	0.186	0.212	0.217	0.234
0.100	0.210	0.232	0.238	0.254
0.150	0.209	0.230	0.224	0.250
0.200	0.173	0.120	0.197	0.210
0.250	0.096	0.120	0.107	0.121
0.625	0.080	0.097	0.094	0.100
0.675	0.157	0.188	0.184	0.194
0.725	0.199	0.220	0.218	0.231
0.775	0.203	0.234	0.220	0.233
0.825	0.173	0.199	0.188	0.188
0.875	0.069	0.093	0.080	0.091

Pattern 7

Distance (m)	Q = 5 l/s	Q = 10 l/s	Q = 12.5 l/s	Q = 15 l/s
0.250	0.069	0.070	0.080	0.069
0.290	0.127	0.137	0.138	0.127
0.330	0.159	0.157	0.168	0.159
0.370	0.148	0.155	0.151	0.148
0.410	0.074	0.077	0.081	0.074
0.535	0.064	0.068	0.068	0.064
0.575	0.114	0.121	0.111	0.115
0.615	0.138	0.138	0.135	0.138
0.655	0.125	0.129	0.125	0.125
0.695	0.064	0.066	0.073	0.064
0.820	0.089	0.082	0.098	0.089
0.860	0.147	0.157	0.163	0.147
0.900	0.179	0.185	0.200	0.178
0.940	0.183	0.188	0.197	0.183
0.980	0.149	0.150	0.154	0.149

Clear Channel Velocity Distributions
(Detailed Measurements with Marginal Strips)

All velocities are Depth-averaged values in m/s, calculated from measurements at 0.2, 0.4 and 0.8 of the depth from the bed, as described in the text

50 mm Strips

Flow Depth=34.6 mm

Dist. (m)	V (m/s)	B Shear (N/m2)
0.95	0.15	0.0674
0.94	0.16	0.0858
0.93	0.18	0.0925
0.91	0.23	0.1065
0.89	0.26	0.1460
0.87	0.29	0.1546
0.85	0.31	0.1728
0.83	0.33	0.1728
0.81	0.34	0.1728
0.79	0.34	0.1728
0.77	0.34	0.1728
0.75	0.34	0.1919
0.70	0.34	0.2019
0.60	0.33	0.1919
0.50	0.33	0.1919

Flow Depth=69.5 mm

Dist. (m)	V (m/s)	B Shear (N/m2)
0.95	0.24	0.1460
0.93	0.29	0.1822
0.91	0.33	0.2334
0.89	0.37	0.2334
0.87	0.40	0.2791
0.86	0.41	0.2673
0.84	0.42	0.2791
0.83	0.43	0.2673
0.82	0.43	0.3036
0.80	0.44	0.3163
0.77	0.44	0.3292
0.74	0.44	0.3036
0.70	0.44	0.3036
0.62		0.2791
0.60	0.44	0.1546
0.58		0.2673
0.50	0.44	0.3163

Flow Depth=91.2 mm

Dist. (m)	V (m/s)	B Shear (N/m2)
0.95	0.24	0.1139
0.93	0.29	0.1460
0.91	0.34	0.1636
0.89	0.38	0.2019
0.87	0.40	0.2557
0.85	0.43	0.2334
0.83	0.44	0.2673
0.80	0.45	0.2791
0.79	0.45	0.2791
0.78	0.46	0.2791
0.75	0.46	0.2791
0.70	0.47	0.3036
0.65	0.49	0.1728
0.63	0.49	0.2791
0.62	0.48	0.3980
0.60	0.48	0.2557
0.55	0.49	0.3424
0.50	0.48	0.3036

125 mm Strips

Flow Depth=32.1 mm

Dist. (m)	V (m/s)	B Shear (N/m2)
0.15	0.16	0.0794
0.17	0.18	0.0858
0.19	0.21	0.1065
0.21	0.25	0.1376
0.23	0.27	0.1728
0.25	0.30	0.1919
0.26	0.31	0.1919
0.27	0.31	0.2019
0.28	0.32	0.1919
0.29	0.32	0.2226
0.31	0.32	0.2019
0.36	0.33	0.2121
0.40	0.32	0.2226
0.45	0.32	0.2121
0.50	0.32	0.1822

Flow Depth=70.3 mm

Dist. (m)	V (m/s)	B Shear (N/m2)
0.16	0.16	0.0674
0.17	0.21	0.0733
0.18	0.23	0.0858
0.19	0.26	0.1065
0.20	0.27	0.1065
0.21	0.29	0.1546
0.22	0.31	0.1728
0.23	0.33	0.2121
0.24	0.35	0.1919
0.25	0.35	0.2121
0.26	0.36	0.2334
0.27	0.37	0.2334
0.28	0.38	0.2444
0.29	0.39	0.2444
0.30	0.38	0.2557
0.31	0.39	0.2557
0.32	0.39	0.2557
0.33	0.39	0.2791
0.35	0.38	0.2444
0.40	0.40	0.2557
0.45	0.41	0.2334
0.50	0.40	0.2444
0.55	0.40	0.2226
0.60	0.40	0.2226
0.65	0.40	0.2334
0.67	0.41	0.2334
0.69	0.40	0.2444
0.70	0.40	0.2557
0.71	0.40	0.2557
0.72	0.39	0.2557
0.73	0.39	0.1919
0.74	0.39	0.2444
0.75	0.39	0.2557
0.76	0.37	0.2334
0.77	0.36	0.2019
0.78	0.34	0.2334
0.79	0.32	0.2121
0.80	0.29	0.1728
0.81	0.27	0.1546
0.82	0.25	0.1215
0.83	0.23	0.0858
0.84	0.20	0.0794
0.86	0.18	0.0674

Flow Depth=86.0 mm

Dist. (m)	V (m/s)	B Shear (N/m2)
0.50	0.45	0.2557
0.55	0.45	0.2673
0.65	0.45	0.2791
0.69	0.45	0.2791
0.70	0.45	0.3036
0.71	0.44	0.3036
0.72	0.43	0.3163
0.73	0.42	0.2912
0.74	0.42	0.2912
0.75	0.41	0.2912
0.76	0.41	0.2673
0.78	0.38	0.2557
0.80	0.35	0.2121
0.83	0.29	0.1728
0.85	0.26	0.1065
0.86	0.20	0.0925

250 mm Strips

Flow Depth=32.0 mm

Dist. (m)	V (m/s)	B Shear (N/m2)
0.76	0.13	0.0463
0.74	0.17	0.0733
0.72	0.19	0.0858
0.71	0.19	0.0993
0.70	0.21	0.0925
0.68	0.24	0.1139
0.66	0.27	0.1636
0.65	0.28	0.1728
0.64	0.29	0.1919
0.63	0.30	0.1919
0.62	0.30	0.1728
0.61	0.31	0.1822
0.60	0.31	0.0925
0.55	0.30	0.1636
0.50	0.29	0.1919
0.45	0.29	
0.40	0.30	

Flow Depth=68.5 mm

Dist. (m)	V (m/s)	B Shear (N/m2)
0.26	0.13	0.0416
0.27	0.15	0.0463
0.28	0.16	0.0564
0.29	0.18	0.0674
0.30	0.19	0.0794
0.31	0.21	0.0925
0.32	0.22	0.1065
0.33	0.24	0.1294
0.34	0.25	0.1376
0.35	0.27	0.1376
0.36	0.29	0.1460
0.37	0.29	0.1546
0.38	0.30	0.1728
0.39	0.30	0.1460
0.40	0.31	0.1546
0.41	0.31	0.1546
0.42	0.32	0.1546
0.43	0.32	0.1460
0.44	0.32	0.1728
0.46	0.32	0.1636
0.48	0.31	0.1546
0.50	0.31	0.1546
0.53	0.31	0.1546
0.54	0.31	0.1546
0.56	0.32	0.1376
0.58	0.32	0.1215
0.60	0.32	0.1546
0.62	0.31	0.1728
0.64	0.29	0.1460
0.66	0.27	0.1294
0.67	0.26	0.1215
0.68	0.23	0.0925
0.69	0.22	0.0794
0.70	0.21	0.0733
0.71	0.19	0.0564
0.72	0.18	0.0564
0.73	0.16	0.0512
0.74	0.13	0.0416

Flow Depth=87.0 mm

Dist. (m)	V (m/s)	B Shear (N/m2)
0.50	0.35	0.1546
0.55	0.35	0.1728
0.58	0.35	0.1546
0.60	0.35	0.1919
0.61	0.35	0.2019
0.62	0.34	0.1919
0.63	0.34	0.1919
0.64	0.34	0.1919
0.65	0.32	0.1919
0.66	0.33	0.1919
0.68	0.29	0.1215
0.69	0.27	0.1139
0.72	0.20	0.0925
0.75	0.17	0.0564
0.76	0.16	0.0564

Discrete Reed Patches Stage-Discharge Data

	Q (m3/s)	depth (m)	T	viscosity m2/s	V (m/s)	R (m)	f	n	Re
Pattern 8	0.0050	0.0260	17	1.08344E-06	0.192	0.025	0.0561	0.0144	17547.3
	0.0100	0.0389	17	1.08344E-06	0.257	0.036	0.0459	0.0139	34254.4
	0.0150	0.0537	17	1.08344E-06	0.279	0.048	0.0522	0.0156	50008.3
	0.0200	0.0658	17	1.08344E-06	0.304	0.058	0.0529	0.0161	65251.8
Pattern 19	0.0050	0.0443	21	9.8416E-07	0.113	0.041	0.2683	0.0343	18667.9
	0.0075	0.0621	21	9.8416E-07	0.121	0.055	0.3180	0.0392	27115.1
	0.0100	0.0829	21	9.8416E-07	0.121	0.071	0.4104	0.0465	34863.4
	0.0125	0.0966	21	9.8416E-07	0.129	0.081	0.4060	0.0473	42578.6
Pattern 21	0.0050	0.0395	21	9.8416E-07	0.127	0.037	0.1919	0.0285	18834.0
	0.0075	0.0549	21	9.8416E-07	0.137	0.049	0.2226	0.0322	27467.0
	0.0100	0.0749	21	9.8416E-07	0.134	0.065	0.3069	0.0396	35348.6
	0.0125	0.0855	21	9.8416E-07	0.146	0.073	0.2869	0.0391	43385.8
Pattern 9	0.0050	0.0401	17	1.08344E-06	0.125	0.037	0.2005	0.0292	17089.2
	0.0100	0.0882	17	1.08344E-06	0.113	0.075	0.4898	0.0513	31383.4
	0.0150	0.1200	17	1.08344E-06	0.125	0.097	0.5201	0.0551	44660.6
	0.0200	0.1510	17	1.08344E-06	0.132	0.116	0.5551	0.0587	56711.9
Pattern 10	0.0050	0.0375	17	1.08344E-06	0.133	0.035	0.1648	0.0262	17171.8
	0.0100	0.0674	17	1.08344E-06	0.148	0.059	0.2266	0.0335	32533.9
	0.0150	0.0995	17	1.08344E-06	0.151	0.083	0.3066	0.0412	46187.8
	0.0200	0.1275	17	1.08344E-06	0.157	0.102	0.3467	0.0454	58835.8
Pattern 20	0.0050	0.0509	21	9.8416E-07	0.098	0.046	0.4020	0.0428	18444.3
	0.0075	0.0727	21	9.8416E-07	0.103	0.063	0.5008	0.0504	26613.3
	0.0100	0.0973	21	9.8416E-07	0.103	0.081	0.6475	0.0598	34022.9
	0.0125	0.1140	21	9.8416E-07	0.110	0.093	0.6484	0.0611	41371.9
Pattern 11	0.0050	0.0512	18	1.05664E-06	0.098	0.046	0.4090	0.0432	17169.7
	0.0075	0.0870	18	1.05664E-06	0.086	0.074	0.8374	0.0669	24183.9
	0.0100	0.1193	18	1.05664E-06	0.084	0.096	1.1512	0.0819	30563.4
	0.0110	0.1284	17	1.08344E-06	0.086	0.102	1.1689	0.0834	32313.3
Pattern 15	0.0050	0.0632	17	1.08344E-06	0.079	0.056	0.7528	0.0605	16388.2
	0.0075	0.0952	21	9.8416E-07	0.079	0.080	1.0820	0.0770	25607.2
	0.0100	0.1260	20.5	9.95415E-07	0.079	0.101	1.3417	0.0891	32096.0
	0.0110	0.1368	17	1.08344E-06	0.080	0.107	1.3950	0.0919	31887.1
Pattern 16	0.0050	0.0747	20	1.007E-06	0.067	0.065	1.2181	0.0789	17279.4
	0.0075	0.1060	20.5	9.95415E-07	0.071	0.087	1.4670	0.0910	24866.5
	0.0100	0.1415	20.5	9.95415E-07	0.071	0.110	1.8543	0.1064	31320.5
	0.0110	0.1495	20.5	9.95415E-07	0.074	0.115	1.7851	0.1051	34028.2
Pattern 12	0.0050	0.0297	17	1.08344E-06	0.168	0.028	0.0831	0.0179	17424.7
	0.0100	0.0545	17	1.08344E-06	0.183	0.049	0.1226	0.0239	33290.8
	0.0150	0.0779	17	1.08344E-06	0.193	0.067	0.1526	0.0281	47914.1
	0.0200	0.1006	17	1.08344E-06	0.199	0.084	0.1779	0.0315	61470.9

Pattern 13	0.0050	0.0316	17	1.08344E-06	0.158	0.030	0.0997	0.0198	17362.4
	0.0100	0.0620	17	1.08344E-06	0.161	0.055	0.1781	0.0294	32846.5
	0.0150	0.0874	17	1.08344E-06	0.172	0.074	0.2121	0.0337	47139.2
	0.0200	0.1125	17	1.08344E-06	0.178	0.092	0.2440	0.0374	60276.6
Pattern 14	0.0050	0.0284	16	1.11156E-06	0.176	0.027	0.0728	0.0166	17025.7
	0.0100	0.0550	16	1.11156E-06	0.182	0.050	0.1259	0.0242	32419.3
	0.0150	0.0783	16	1.11156E-06	0.192	0.068	0.1549	0.0283	46669.7
	0.0200	0.0998	16	1.11156E-06	0.200	0.083	0.1740	0.0311	59995.8
Pattern 17	0.0050	0.0245	21	9.8416E-07	0.204	0.023	0.0471	0.0131	19372.6
	0.0100	0.0394	21	9.8416E-07	0.254	0.037	0.0476	0.0142	37675.0
	0.0150	0.0528	21	9.8416E-07	0.284	0.048	0.0497	0.0151	55142.6
	0.0200	0.0634	21	9.8416E-07	0.315	0.056	0.0475	0.0152	72140.2
Pattern 18	0.0050	0.0218	21	9.8416E-07	0.229	0.021	0.0333	0.0108	19472.9
	0.0100	0.0372	21	9.8416E-07	0.269	0.035	0.0402	0.0129	37829.3
	0.0150	0.0513	21	9.8416E-07	0.292	0.047	0.0457	0.0145	55292.7
	0.0200	0.0629	21	9.8416E-07	0.318	0.056	0.0464	0.0150	72204.3
Pattern 22	0.0050	0.0280	21	9.8416E-07	0.179	0.027	0.0698	0.0163	19244.2
	0.0075	0.0384	21	9.8416E-07	0.195	0.036	0.0785	0.0181	28308.7
	0.0100	0.0487	21	9.8416E-07	0.205	0.044	0.0884	0.0199	37036.4
	0.0125	0.0565	21	9.8416E-07	0.221	0.051	0.0871	0.0203	45646.7

Appendix C

Experimental Data for Sedimentation in Reedbeds

Table 1 Particle size analysis for unsieved and unwashed sample

Sieve size	Mass retained	Retained	Passing
1.18	0.9	0.136	99.864
0.6	89.9	13.627	86.236
0.425	180.4	27.346	58.98
0.3	180.9	27.422	31.469
0.15	156.6	23.738	7.731
0.075	40.8	6.185	1.546
pan	9.6	1.455	0.091

Table 2 Particle size analysis for sieved sample

Sieve size	Mass retained	Retained	Passing
1.18	0	0	100
0.6	127.7	16.823	83.177
0.425	344.9	45.435	37.742
0.3	187.6	24.713	13.029
0.15	91.7	12.08	0.948
0.075	5.7	0.751	0.198
pan	0	0	0

Table 3 Measurements of bed heights of Series B 1 experiments

Number of	Flow rate,	Sediment	Distance	Bed height	Slope	
Series B 1						
1.1	0.0065	0.005	2	0.072	0.0118	0.992
			3	0.059		
			4	0.047		
			5	0.038		
			6	0.026		
			7	0.011		
			8	0		
1.2	0.0065	0.0097	2	0.086	0.0145	0.996
			3	0.0736		
			4	0.06		
			5	0.047		
			6	0.031		
			7	0.014		
			8	0		
1.3	0.0065	0.0131	2	0.099	0.016	0.995
			3	0.085		
			4	0.072		
			5	0.055		
			6	0.036		
			7	0.022		
			8	0		
1.4	0.0065	0.0186	2	0.11	0.0184	0.998
			3	0.093		
			4	0.078		
			5	0.06		
			6	0.038		
			7	0.019		
			8	0		

Table 4 Measurements of bed heights of Series B 2 experiments

Number of	Flow rate,	Sediment	Distance	Bed	Slope	
Series B 2						
2.1	0.0034	0.0085	2	0.098	0.0165	0.999
			3	0.08		
			4	0.066		
			5	0.05		
			6	0.031		
			7	0.014		
			8	0		
2.2	0.0054	0.0085	2	0.085	0.0143	0.998
			3	0.071		
			4	0.06		
			5	0.046		
			6	0.032		
			7	0.016		
			8	0		
2.3	0.0111	0.0085	2	0.077	0.0125	0.998
			3	0.06		
			4	0.05		
			5	0.038		
			6	0.025		
			7	0.013		
			8	0		
2.4	0.0159	0.0085	2	0.082	0.013	0.995
			3	0.067		
			4	0.058		
			5	0.045		
			6	0.03		
			7	0.017		
			8	0		
2.5	0.0185	0.0085	2	0.082	0.013	0.987
			3	0.067		
			4	0.057		
			5	0.038		
			6	0.032		
			7	0.015		
			8	0		

Table 5 Series B 1 and B 2 experimental results

Number of experiments	Flow rate q (m^3/s m)	Sediment rate q_s (kg/s m)	Flow depth y (m)	Slope S_o	Temperature T (°C)
Series B 1					
1.1	0.0065	0.005	0.043	0.0118	23
1.2	0.0065	0.0097	0.04	0.0145	18
1.3	0.0065	0.0131	0.038	0.016	19
1.4	0.0065	0.0186	0.036	0.0184	20.5
Series B 2					
2.1	0.0034	0.0085	0.021	0.0165	20.5
2.2	0.0054	0.0085	0.034	0.014	22
2.3	0.0111	0.0085	0.071	0.0121	21
2.4	0.0159	0.0085	0.096	0.0133	22
2.5	0.0184	0.0085	0.111	0.0133	21

Table 6 Series B 3 experimental results

Test	Time, T (min)	Discharge, Q (l/s)	Sediment rate, Q_s (g/s)	Input sediment volume (ml)	Deposited sediment volume (ml)	Flow depth (mm)
B 3.1	80	3.40	8.4	27840	2060	25
B 3.2	100	5.20	8.4	34800	4440	32
B 3.3	120	7.47	8.5	42480	4880	40

Table 7 Series B4 experimental results

Test	Time, T (min)	Discharge, Q (l/s)	Initial sediment volume (ml)	Retained sediment volume (ml)	Flow depth (mm)
B 4.1	400	1.79	3860	2820	16
B 4.2	630	5.20	7500	4560	32
B 4.3	960	7.47	7800	4090	40

Table 8 Coal particle size distribution

Sieve size	Mass retained	Retained	Passing
2.360	0.2	0.02	99.98
1.180	227.2	22.58	77.40
0.850	606.8	60.31	17.09
0.600	126.9	12.61	4.48
0.425	34.1	3.39	1.09
0.300	8.3	0.82	0.27
0.150	2.6	0.26	0.01
0.075	0.1	0.01	0.00
pan	0.0	0.0	0.0

Table 9 Series B5 deposition experiments

Test	Q	L	W	Upstream	Downstream	No.	Area,	Q,/Q
B 5.1	5.26	126	297.9	140	1980	58	1450	0.00171
B 5.2	6.88		195.3	160	2320	41	1025	0.00131
B 5.3	8.93		91.8	170	2280	24	600	0.00101
B 5.4	4.43	252	675.7	120	2500	87	2175	0.00203
B 5.5	6.73		265.1	260	2300	45	1125	0.00134
B 5.6	9.10		141.5	270	2270	28	700	0.00099
B 5.7	5.13	504	745.6	160	4900	98	2450	0.00175
B 5.8	6.31		422.9	200	3180	46	1150	0.00143
B 5.9	9.54		187.6	420	1660	18	450	0.00094

Table 10 Series B 6 Decay experiments

Test	Q	L	Time,	Number	Area,
B 6.1	5.01	140	0	35.2	880.0
B 6.2			6	24.2	605.0
B 6.3			17	15.8	395.0
B 6.4			25	11.3	282.5
B 6.5			45	5.9	147.5
B 6.6			55	4.8	120.0
B 6.7	5.01	280	0	49.6	1240.0
B 6.8			7	27.1	677.5
B 6.9			18	16.2	405.0
B 6.10			30	11.5	287.5
B 6.11			50	6.3	157.5
B 6.12			65	5.3	132.5
B 6.13			75	4.2	105.0
B 6.14	5.01	560	0	98.5	2462.5
B 6.15			5	57.6	1440.0
B 6.16			10	28.9	722.5
B 6.17			20	16.9	422.5
B 6.18			30	12.3	307.5
B 6.19			55	10.5	265.5

Appendix D

Coding of Rule-Based Vegetation-Morphology Model

This appendix contains the full listing of the Borland Delphi 2.0 computer code for the model described in Chapter 11. This model uses a conventional dynamic sediment budget approach, but has the following advancements:

- It has the ability to simulate the evolution of geomorphic features (bars) and vegetation (reeds) in one of the cells.
- It allows for large floods to be represented in the hydrograph in addition to minor events of the order of 8-20 m^3s^{-1} and moderate events of the order of 20-40 m^3s^{-1}.
- It has a user interface (see Figure below).

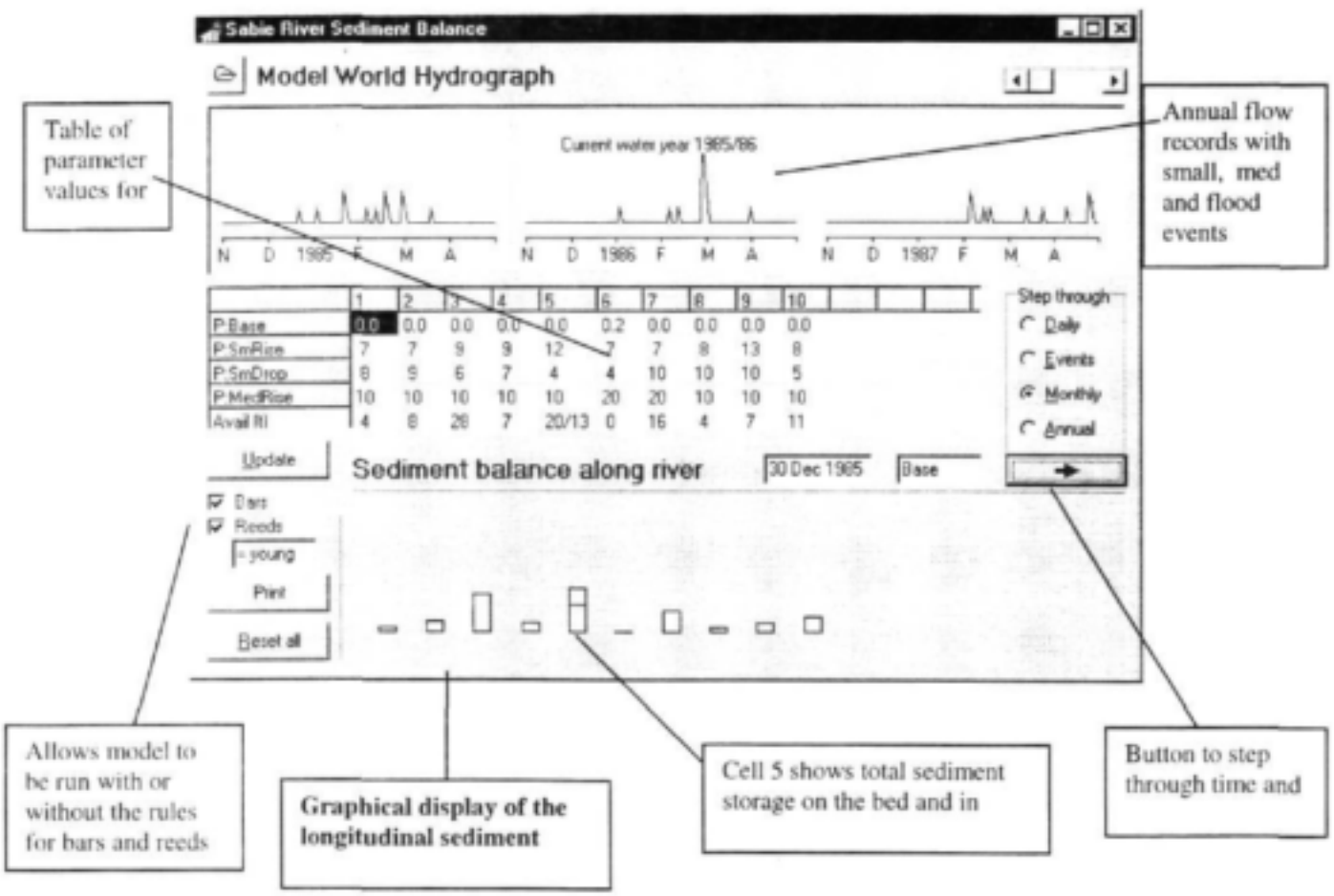


```
Much of the code here is devoted to user interface.  The key parts of the model are
the Procedure MoveSedi (which performs the computation of the dynamic longitudinal
sediment budget) and Procedure CheckReedUpdate (which adjusts the state of the
reeds based on the hydrograph - see transition rules in Chapter11)
```

```
unit SabieSimHome;

interface

uses
  Windows, Messages, SysUtils, Classes, Graphics, Controls, Forms, Dialogs,
  StdCtrls, Grids, ExtCtrls, ComCtrls, Buttons;

type
  TForm1 = class(TForm)
    Bevel1: TBevel;
    Bevel2: TBevel;
    DateBox: TEdit;
    OpenDialog1: TOpenDialog;
    Label1: TLabel;
    Label3: TLabel;
    StepOption: TRadioGroup;
    OpenFileBtn: TSpeedButton;
    FwdBtn: TBitBtn;
    ResetBtn: TButton;
    HydroScroll: TScrollBar;
    Edit1: TEdit;
    Results: TStringGrid;
    UpdateBtn: TButton;
    ReedRules: TCheckBox;
    Button1: TButton;
    BarBox: TCheckBox;
    RdState: TEdit;
    procedure OpenFileBtnClick(Sender: TObject);
    procedure HydroScrollChange(Sender: TObject);
    procedure FwdBtnClick(Sender: TObject);
    procedure ResetBtnClick(Sender: TObject);
    procedure UpdateBtnClick(Sender: TObject);
    procedure StartUpRoutine(Sender: TObject);
    procedure Button1Click(Sender: TObject);
    procedure ReedRulesClick(Sender: TObject);
    procedure BarBoxClick(Sender: TObject);
  private
    procedure CheckBars;
    procedure CheckReeds;
    procedure CheckEndofYear;
    procedure CheckReedUpdate;
    procedure ConvertToDate(d,y :Integer);
    procedure DrawHydro(yr,pos:Integer);
    procedure DrawRiver;
    procedure GenerateDailyHydro(yr:Integer);
    procedure InitialValues;
    procedure MoveSedi;
    procedure RedrawHydro(yr :Integer);
    procedure ReadHydroFile(infile :TFileName);
    procedure SaveResults;
    { Private declarations }
  public
    { Public declarations }
    procedure ResetAll;
  end;
```

```
var
  Form1: TForm1;
Type
  flowtype = (base, smrise, smdrop, medrise, flood, med);
  eventtype = Record


 startdate :Integer;
               magnitude : Integer;
             End;
  reedtype = (none, rhizomes, sparse, dense);
Var
  year : Array[1..10] Of Record
           floodevents :Integer;
           event :Array[1..15] Of eventtype;
         End;
  storedresults : Array[0..10] Of Record
             bedstorage :Array[1..20] Of Real;
             barstorage :Array[1..20] Of Real;
             reedstate :reedtype;
           End;
  cell : Array[1..20] Of Record
           dist :Integer;      {Chainage from upstream end}
           chantype :String;   {Channel type morphology}
           initbed :Real;      {Initial sedi storage on bed}
           initbar :Real;      {Initial sedi storage in bars}
           vegbar :Real;       {Sedi stored in vegetated features}
           availbed :Real;     {Sedi stored on bed at time t}
           availbar :Real;     {Sedi stored in bars at time t}
           potential :Array[1..5] Of Real; {Transport potential for var flows}
           bardep :Real;       {Proportion of sediment deposited in bars}
           remove :Real;       {Sediment moved from a cell at time t}
         End;
  reeds : Record
           state : reedtype;
           lastmed : Integer;
          End;
  dailyflow :Array[0..200] Of flowtype;
  prev :Array[1..20] Of Real;
  i, day, startyear, curryear, numyrs :Integer;
  barerode : real;
{$R *.DFM}


implementation

{-------------------------------------------------------------}

Procedure TForm1.CheckBars;
{If you switch reeds on, make sure that bars are on too, and
 if you switch reeds off, turn off the reed state label}
Begin
  If (ReedRules.Checked = True)
    Then Begin
      BarBox.Checked := True;
      RdState.Visible:=True;
    End;
  If (ReedRules.Checked = False)
    Then Begin
      RdState.Visible:=False;
    End;
```

```
End;

Procedure TForm1.CheckReeds;
{If you switch off bars, reeds must go off as well}
Begin
  If ((BarBox.Checked = False) and (ReedRules.Checked = True))
    Then Begin
      ReedRules.Checked := False;
      RdState.Visible:=False;
    End;
End;


Procedure TForm1.CheckEndofYear;
Var yearnum :Integer;
Begin
  If day > 180 Then Begin
    SaveResults;
    curryear:=curryear+1;
    yearnum:=curryear-startyear+1;
    GenerateDailyHydro(yearnum);
    RedrawHydro(yearnum);
    day:=1;
  End;
End;

Procedure TForm1.CheckReedUpdate;
Begin
  If ((day=1) and (reeds.state=sparse))
    Then Begin
      reeds.state:=dense;
      RdState.Text:='= dense';
      With cell[5] Do Begin
        potential[2]:=9;
        potential[3]:=10;
        potential[4]:=6;
        potential[5]:=15;
        bardep:=0.6;
        barerode:=0.05;
      End;
    End;
  If ((day=1) and (reeds.state=rhizomes))
    Then Begin
      reeds.state:=sparse;
      RdState.Text:='= young';
      With cell[5] Do Begin
        potential[2]:=10;
        potential[3]:=14;
        potential[4]:=6;
        bardep:=0.4;
      End;
    End;
  If ((dailyflow[day]=medrise) and (reeds.state=none) and (cell[5].availbar>=7))
    Then Begin
      {Reed rhizomes take root on the bar}
      reeds.state:=rhizomes;
      RdState.Text:='= rhizomes';
    End;
      If    ((dailyflow[day]=flood)    and    (dailyflow[day+1]=flood)    and
(reeds.state=rhizomes))
    Then Begin
      reeds.state:=none;
      RdState.Text:='= none';
```

```
    End;

If ((dailyflow[day]=flood) and (dailyflow[day+1]=flood) and (reeds.state=sparse))
    Then Begin
      reeds.state:=none;
      RdState.Text:='= none';
      With cell[5] Do Begin
        potential[2]:=12;
        potential[3]:=10;
        potential[4]:=4;
        bardep:=0.3;
      End;
    End;
End;


Procedure TForm1.ConvertToDate(d,y :Integer);
{Takes in the day number of the geomorph year and converts it to
 a date in the form dd MMM yr and writes it to DateBox}
Var
  month, counter :Integer;
  date :String;
Begin
  month := d div 30;
  If ((d mod 30)=0) Then month := month - 1;
  Case month of
    0: Begin date:='Nov'; End;
    1: Begin date:='Dec'; End;
    2: Begin date:='Jan'; End;
    3: Begin date:='Feb'; End;
    4: Begin date:='Mar'; End;
    5: Begin date:='Apr'; End;
  End;
  date := IntToStr(d - month*30) + ' ' + date + ' ';
  If month<=1
    Then date:=date + IntToStr(y)
    Else date:=date + IntToStr(y+1);
  datebox.Text := date;
  { draw a marker on the timeline to show current date
  canvas.Brush.Color:=clWhite;
  canvas.MoveTo(209+d,123); canvas.LineTo(209+d,127);
  canvas.Brush.Color:=clBlack;
  canvas.MoveTo(210+d,123); canvas.LineTo(210+d,127);
  canvas.Brush.Color:=clWhite;}
End;


Procedure TForm1.DrawHydro(yr,pos:Integer);
Var
  bottom, left, width, height,i,peaks, time :Integer;
  months :String;
Begin
  bottom := Bevel2.Top+Bevel2.Height-35;
  left := Bevel2.Left+10 + 200*pos;
  width := Bevel2.Width-20;
  height := Bevel2.height-40;
  canvas.Brush.Color:=clWhite;
  canvas.Pen.Color := clBlue;
  canvas.Pen.Width := 1;
    canvas.MoveTo(left,bottom);
  For i := 1 To year[yr].floodevents Do Begin
    time := year[yr].event[i].startdate-31;
    canvas.LineTo(left+time-1,bottom);
```

```
    If year[yr].event[i].magnitude = 1

Then Begin
        canvas.LineTo(left+(time),bottom-Trunc(0.15*height));
        canvas.LineTo(left+(time+2),bottom);
      End;
    If year[yr].event[i].magnitude = 2
      Then Begin
        canvas.LineTo(left+(time),bottom-Trunc(0.3*height));
        canvas.LineTo(left+(time+4),bottom);
      End;
    If year[yr].event[i].magnitude = 3
      Then Begin
        canvas.LineTo(left+time,bottom-Trunc(0.8*height));
        canvas.LineTo(left+time+3,bottom-Trunc(0.3*height));
        canvas.LineTo(left+time+5,bottom);
      End;
  End;
  canvas.LineTo(left+180,bottom);
  canvas.Pen.Color := clBlack;
  canvas.MoveTo(left,bottom+10);
  canvas.LineTo(left+180,bottom+10);
  canvas.LineTo(left+180,bottom+11);
  canvas.MoveTo(left,bottom+11);
  months := 'NDJFMA';
  For i:=0 To 6 Do Begin
    canvas.MoveTo(left+i*30,bottom+11);
    canvas.LineTo(left+i*30,bottom+14);
    If i=2
      Then canvas.TextOut(left+i*30-11,bottom+15,IntToStr(1985+yr-1))
      Else canvas.TextOut(left+i*30-3,bottom+15,Copy(months,i+1,1));
  End;
  If pos=1 Then canvas.TextOut(left+23,Bevel2.Top+20,'Current water year
'+IntToStr(1985+yr-2)+'/'+IntToStr(85+yr-1));
End;


procedure TForm1.DrawRiver;
const
  halfbarwidth = 6;
  bars = 0;
  lines = 1;
Var
  s :String;
  xpos, i :Integer;
  xscale,ymax :Real;
  bottom, left, width, height, barheight : Integer;
Begin
  Results.Cells[0,1]:='P:Base';
  Results.Cells[0,2]:='P:SmRise';
  Results.Cells[0,3]:='P:SmDrop';
  Results.Cells[0,4]:='P:MedRise';
  Results.Cells[0,5]:='Avail (t)';
  For i:=1 To 10 Do Begin
    Results.Cells[i,0]:=IntToStr(i);
    Str(cell[i].availbed:2:0,s);
    Results.Cells[i,5]:=s;
    If i=5 Then Begin
     Str(cell[5].availbar:2:0,s);
     Results.Cells[5,5]:=REsults.cells[5,5]+'/'+s;
    End;
  End;
  ymax:=80;
```

```
  bottom := Bevel1.Top+(Bevel1.Height - 20);

width := Bevel1.Width-20;
  left := Bevel1.Left + 10;
  height := (Bevel1.height) - 40;
  canvas.Brush.Color := clBtnFace;
  canvas.FillRect(Rect(left,bottom-height-2,left+width,bottom+height+2));
  xscale := width/16;
  {Draw bars for each section}
  canvas.Brush.Color := clYellow;
  For i:=1 To 10 Do Begin;
    barheight := Trunc(cell[i].availbed/ymax*height);
    If (i=5)
      Then barheight := barheight + Trunc(cell[5].availbar/ymax*height);
    If barheight > height Then barheight := height;
    If barheight < (-Height) Then barheight := (-height);
    xpos := left + Trunc(xscale*i) - 10;
    If barheight >= 0
      Then canvas.Rectangle(xpos-halfbarwidth,bottom-
barheight,xpos+halfbarwidth,bottom+1)
      Else canvas.Rectangle(xpos-halfbarwidth,bottom-
barheight,xpos+halfbarwidth,bottom);
    If (i=5)
      Then Begin
        Canvas.MoveTo(xpos-halfbarwidth,bottom-
Trunc(Cell[5].availbed/ymax*height));
        Canvas.LineTo(xpos+halfbarwidth,bottom-
Trunc(Cell[5].availbed/ymax*height));
      End; {Of drawing line between bed and bar for cell 5}
  End; {For i}
End;


Procedure TForm1.GenerateDailyHydro(yr:Integer);
Begin
  {My geomorph year starts on 1 Nov and goes on for 6 months,
   i.e. to April 30.  This is a total of 180 days, assuming
   each month is 30 days long, and ignoring leap years.
   This routine takes the events for a given year and generates
   a daily flow for each of the 180 days.}
  For i:=0 To 180 Do Begin
    dailyflow[i] := base;
  End;
  With year[yr] Do Begin
    For i:=1 To floodevents Do Begin
      Case event[i].magnitude Of
        1: Begin
             dailyflow[event[i].startdate-31]:=smrise;
             dailyflow[event[i].startdate-31+1]:=smdrop;
             dailyflow[event[i].startdate-31+2]:=smdrop;
           End;
        2: Begin
             dailyflow[event[i].startdate-31]:=medrise;
             dailyflow[event[i].startdate-31+1]:=smdrop;
             dailyflow[event[i].startdate-31+2]:=smdrop;
             dailyflow[event[i].startdate-31+3]:=smdrop;
           End;
        3:  Begin
             dailyflow[event[i].startdate-31]:=flood;
             dailyflow[event[i].startdate-31+1]:=flood;
             dailyflow[event[i].startdate-31+2]:=med;
             dailyflow[event[i].startdate-31+3]:=med;
             dailyflow[event[i].startdate-31+4]:=smdrop;
```

```
                dailyflow[event[i].startdate-31+5]:=smdrop;
              End;

End; {Of Case}
    End; {For i=each floodevent of the year}
  End; {With year[yr]}
End;


Procedure TForm1.InitialValues;
var
  s :String;
  j :Integer;
Begin
  reeds.state:=none;
  RdState.Text:='= none';
  CheckBars;
  CheckReeds;
  If (BarBox.Checked) Then barerode := 0.4 Else barerode := 0.0;
  {Initialise all the annual storedresults to 0}
  For i:=0 To 10 Do Begin
    With storedresults[i] Do Begin
      For j:=1 TO 20 Do Begin;
        bedstorage[j]:=0.0;
        barstorage[j]:=0.0;
        reedstate:=none;
      End;   {For j}
    End;  {With storedresults}
  End; {For i}
  {Initialise all the transport potentials}
  For i:=1 To 10 Do Begin
    cell[i].initbed:=0; cell[i].initbar:=0; cell[i].bardep:=0.0;
    cell[i].potential[5]:=20;
  End;
  If (BarBox.Checked)
    Then cell[5].bardep:=0.3
    Else cell[5].bardep:=0.0;
  With cell[1] Do Begin dist:=0 ; initbed:=20;
    potential[1]:=0 ; potential[2]:=7 ;potential[3]:=10 ;potential[4]:=8; End;
  With cell[2] Do Begin dist:=150 ; initbed:=10;
    potential[1]:=0 ; potential[2]:=7 ;potential[3]:=10 ;potential[4]:=9 ; End;
  With cell[3] Do Begin dist:=300 ;
    potential[1]:=0 ; potential[2]:=9 ;potential[3]:=10 ;potential[4]:=6 ; End;
  With cell[4] Do Begin dist:=450 ;
    potential[1]:=0 ; potential[2]:=9 ;potential[3]:=10 ;potential[4]:=7 ; End;
  With cell[5] Do Begin dist:=600 ;
    potential[1]:=0 ; potential[2]:=12 ;potential[3]:=10 ;potential[4]:=4 ; End;
  With cell[6] Do Begin dist:=750 ;
    potential[1]:=0.2 ; potential[2]:=7 ;potential[3]:=20 ;potential[4]:=4 ; End;
  With cell[7] Do Begin dist:=900 ;
    potential[1]:=0 ; potential[2]:=7 ;potential[3]:=20 ;potential[4]:=10 ;  End;
  With cell[8] Do Begin dist:=1050 ;
    potential[1]:=0 ; potential[2]:=8 ;potential[3]:=10 ;potential[4]:=10 ;  End;
  With cell[9] Do Begin dist:=1200 ;
    potential[1]:=0 ; potential[2]:=13 ;potential[3]:=10 ;potential[4]:=10 ;  End;
  With cell[10] Do Begin dist:=1350;
    potential[1]:=0 ; potential[2]:=8 ;potential[3]:=10 ;potential[4]:=5 ;
potential[5]:=35; End;
  For i:=1 To 10 Do Begin
    cell[i].availbed:=cell[i].initbed;
    cell[i].availbar:=cell[i].initbar;
    cell[i].vegbar:=0.0;
    Results.Cells[i,0]:=IntToStr(i); {cell numbers}
```

```
    Str(cell[i].potential[1]:2:1,s);
    Results.Cells[i,1]:=s; {base}

    Str(cell[i].potential[2]:2:0,s);
    Results.Cells[i,2]:=s; {smrise}
    Str(cell[i].potential[4]:2:0,s);
    Results.Cells[i,3]:=s;  {smdrop}
    Str(cell[i].potential[3]:2:0,s);
    Results.Cells[i,4]:=s;  {medrise}
  End;
End;


Procedure TForm1.MoveSedi;
  {This routine is the heart of the model.  It routes sediment down
   the river in response to the flow for a given day.  Its calculations
   are as follows:
     1. Get the transport potential for each cell as a fn of flow
     2. Compare each cell's potential to the amount available
     3. Amount removed from a cell = lesser of available and potential
     4. Subtract the amount removed from available
     5. Go from last cell to first adding removed[i-1] to available[i]}
Var
  limit,removebar,sparecap: Real;
Begin
  For i:=1 TO 20 Do Begin
    cell[i].remove := 0.0;
    prev[i]:=cell[i].availbed;
  End;
  For i:=1 To 20 Do Begin
    With cell[i] Do Begin
      If (dailyflow[day]=base) Then Begin
      limit:=potential[1];
        If (availbed>limit)
          Then remove:=limit
          Else remove:=availbed;
        availbed:=availbed - remove;
      End;
      If (dailyflow[day]=smrise) Then Begin
        limit:=potential[2];
        If (availbed>limit)
          Then remove:=limit
          Else remove:=availbed;
        availbed:=availbed - remove;
      End;
      If (dailyflow[day]=flood) Then Begin
        limit:=potential[5];
        removebar:=0.0;
        sparecap:=0;
        {Med flows can affect bars... begin by eroding the bars
         in the reach using a proportion of the potential}
        If (availbar > (barerode*limit))
          Then Begin (case where there is more bar than potential)
            removebar := barerode*limit;
            availbar := availbar-removebar;
            End
          Else Begin (case where bar gets removed completely and excess
                      potential is transferred to the bed)
            removebar := availbar;
            If ((limit=0) or (barerode=0))
              Then sparecap:=0.0
              Else sparecap := barerode * (1 - availbar/(barerode*limit));
            availbar := 0.0;
```

```
        End;
        If (availbed>((1-barerode+sparecap)*limit)) (Now remove from the bed)

Then Begin
             remove:= (1-barerode+sparecap)*limit (avail sed exceeds potential)
             End
           Else Begin
             remove:= availbed; (all avail sed removed from bed)
        End;
        availbed:=availbed - remove;
        remove:=remove + removebar;
      End; (Of the flood hydrograph)
      If (dailyflow[day]=smdrop) Then Begin
        limit:=potential[4];
        If (availbed>limit)
          Then remove:=limit
          Else remove:=availbed;
        availbed:=availbed - remove;
      End;
      If ((dailyflow[day]=medrise) or (dailyflow[day]=med)) Then Begin
        limit:=potential[3];
        If (availbed>limit)
          Then remove:=limit
          Else remove:=availbed;
        availbed:=availbed - remove;
      End;
    End; (Of with cell[i])
  End; (Of the for i loop);
  For i:=19 DownTo 1 Do Begin
      If ((dailyflow[day]=medrise) or (dailyflow[day-1]=medrise))
        Then Begin
          cell[i].availbar := cell[i].availbar + cell[i].bardep*cell[i-1].remove;
          cell[i].availbed := cell[i].availbed + (1-cell[i].bardep)*cell[i-
1].remove;
          cell[i-1].remove:=0;
          End
        Else Begin
          cell[i].availbed := cell[i].availbed + cell[i-1].remove;
      End;
  End; (For i)
  {Sedi input from upstream}
  If (dailyflow[day]=smrise) Then cell[1].availbed := cell[1].availbed+15;
  If (dailyflow[day-1]=smrise) Then cell[1].availbed := cell[1].availbed + 5;
  If (dailyflow[day]=medrise) Then cell[1].availbed := cell[1].availbed+20;
  If (dailyflow[day-1]=medrise) Then cell[1].availbed := cell[1].availbed + 10;
  If (dailyflow[day-1]=flood) Then cell[1].availbed:=cell[1].availbed + 15;
End; (of procedure MoveSedi)


procedure TForm1.RedrawHydro(yr:Integer);
Begin
  canvas.Brush.Color:=clWhite;
  canvas.FillRect(Rect(Bevel2.Left+1,Bevel2.Top+1,Bevel2.Left+Bevel2.Width-
1,Bevel2.Top+Bevel2.Height-1));
  canvas.MoveTo(Bevel2.left+1,Bevel2.Top+Bevel2.Height-2);
  canvas.LineTo(Bevel2.left+1,Bevel2.Top+1);
  canvas.LineTO(Bevel2.left+bevel2.width-2,Bevel2.top+1);
  canvas.Pen.Color:=clBtnFace;
  canvas.MoveTo(BEvel2.left+3,Bevel2.Top+Bevel2.Height-2);
  canvas.LineTo(Bevel2.left+Bevel2.width-2,Bevel2.Top+Bevel2.Height-2);
  canvas.LineTo(Bevel2.left+bevel2.width-2,Bevel2.top+1);
  canvas.MoveTo(Bevel2.left+200,Bevel2.top+10);
  canvas.LineTo(Bevel2.left+200,Bevel2.top+Bevel2.Height-10);
```

```
  canvas.MoveTo(Bevel2.left+400,Bevel2.top+10);
  canvas.LineTo(Bevel2.left+400,Bevel2.top+Bevel2.Height-10);

canvas.Pen.Color:=clBlack;
  If yr=1 Then Begin
    DrawHydro(1,1);
    DrawHydro(2,2);
  End;
  If yr=numyrs Then Begin
    DrawHydro(numyrs-1,0);
    Drawhydro(numyrs,1);
  End;
  If ((yr<>1) and (yr<>numyrs)) Then Begin
    DrawHydro(yr-1,0);
    DrawHydro(yr,1);
    DrawHydro(yr+1,2);
  End;
End;


Procedure TForm1.ReadHydroFile(infile: TFileName);
Var
  data_file :TextFile;
  i,j,nextint,numevents,yr :Integer;
  dummy,currdir :String;
  nextreal : Real;
begin
    AssignFile(data_file,'SabHydro.dat');
    Reset(data_file);
    Readln(data_file);
    Read(data_file,numyrs); Readln(data_file);
    HydroScroll.Max:=numyrs;
    Readln(data_file);Readln(data_file,dummy);
    For i:=1 To numyrs Do Begin
      With year[i] Do Begin
        Read(data_file,yr); Read(data_file,floodevents);
        For j:=1 To floodevents Do Begin
          Read(data_file,event[j].magnitude);
          Read(data_file,event[j].startdate);
        End; {For j}
        Readln(data_file);
      End; {With year[i]}
    End; {For i}
    CloseFile(data_file);
    day:=1;
    curryear:=1984;
    startyear:=1984;
    GenerateDailyHydro(1);
    ConvertToDate(day,curryear);
    If dailyflow[day]=base Then Edit1.Text:='Base';
    If dailyflow[day]=smrise Then Edit1.Text:='SmRise';
    If dailyflow[day]=medrise Then Edit1.Text:='MedRise';
    If dailyflow[day]=smdrop Then Edit1.Text:='SmDrop';
End;


procedure TForm1.OpenFileBtnClick(Sender: TObject);
begin
  If OpenDialog1.Execute Then Begin
    ReadHydroFile(OpenDialog1.Filename);
    RedrawHydro(1);
    InitialValues;
    DrawRiver;
```

```
  End;
end;


procedure TForm1.HydroScrollChange(Sender: TObject);
begin
  RedrawHydro(HydroScroll.Position);
end;

procedure TForm1.FwdBtnClick(Sender: TObject);
var yearnum :Integer;
begin
  yearnum:=curryear-startyear+1;
  If ((StepOption.ItemIndex=0) and (yearnum<=numyrs) and (day<=180)) Then Begin
    day:=day+1;
    CheckEndofYear;
    If ReedRules.Checked Then CheckReedUpdate;
    MoveSedi;
  End;
  If ((StepOption.ItemIndex=1) and (yearnum<=numyrs) and not ((yearnum=numyrs) and
(day=180))) Then Begin
    Repeat
      day:=day+1;
      CheckEndofYear;
      If ReedRules.Checked Then CheckReedUpdate;
      MoveSedi;
    Until (((dailyflow[day+1]=base) and (dailyflow[day]<>base)) or (day>=180) or
(day=1));
  End;
  If ((StepOption.ItemIndex=2) and (yearnum<=numyrs) and not ((yearnum=numyrs) and
(day=180))) Then Begin
    Repeat
      day:=day+1;
      CheckEndofYear;
      If ReedRules.Checked Then CheckReedUpdate;
      MoveSedi;
    Until (((day mod 30)=0) or (day=1));
  End;
  If ((StepOption.ItemIndex=3) and (yearnum<=numyrs) and not ((yearnum=numyrs) and
(day=180))) Then Begin
    Repeat
      day:=day+1;
      CheckEndofYear;
      If ReedRules.Checked Then CheckReedUpdate;
      MoveSedi;
    Until ((day=180) or (day=1));
  End;
  DrawRiver;
  ConvertToDate(day,curryear);
  If dailyflow[day]=base Then Edit1.Text:='Base';
  If dailyflow[day]=smrise Then Edit1.Text:='SmRise';
  If dailyflow[day]=medrise Then Edit1.Text:='MedRise';
  If dailyflow[day]=smdrop Then Edit1.Text:='SmDrop';
  If ((yearnum=numyrs) and (day=180))
    Then Begin
      SaveResults;
      ShowMessage('You are at the end of the hydrograph');
    End;
end;

procedure TForm1.ResetBtnClick(Sender: TObject);
begin
  ResetAll;
```

```
End;

Procedure TForm1.ResetAll;
Begin
  day:=1; curryear:=startyear;
  InitialValues;
  For i:=1 To 20 Do prev[i]:=cell[i].initbed;
  DrawRiver;
  GenerateDailyHydro(1);
  RedrawHydro(1);
  ConvertToDate(day,curryear);
  If dailyflow[day]=base Then Edit1.Text:='Base';
  If dailyflow[day]=smrise Then Edit1.Text:='SmRise';
  If dailyflow[day]=medrise Then Edit1.Text:='MedRise';
  If dailyflow[day]=smdrop Then Edit1.Text:='SmDrop';
end;

procedure TForm1.SaveResults;
Var yr :Integer;
Begin
  yr := curryear - startyear + 1;
  For i:=1 To 10 Do Begin
    storedresults[yr].bedstorage[i]:=cell[i].availbed;
    storedresults[yr].barstorage[i]:=cell[i].availbar;
    If (i=5) Then
      storedresults[yr].reedstate:=reeds.state;
  End;
End;

procedure TForm1.UpdateBtnClick(Sender: TObject);
var
  update :Real;
  code :Integer;
begin
  For i:=1 To 10 Do Begin
    With cell[i] Do Begin
      Val(Results.Cells[i,1],update,code);
      Potential[1]:=update; {base}
      Val(Results.Cells[i,2],update,code);
      Potential[2]:=update; {smrise}
      Val(Results.Cells[i,3],update,code);
      Potential[4]:=update; {smdrop}
      Val(Results.Cells[i,4],update,code);
      Potential[3]:=update; {medrise}
      Val(Results.Cells[i,5],update,code);
      availbed:=update;
    End;
  End;
  DrawRiver;
end;

procedure TForm1.StartUpRoutine(Sender: TObject);
begin
  ReadHydroFile('SabHydro.dat');
  RedrawHydro(1);
  InitialValues;
  DrawRiver;
end;

procedure TForm1.Button1Click(Sender: TObject);
begin
  PrintOutput.Visible:=True;
end;
```

```
procedure TForm1.ReedRulesClick(Sender: TObject);
begin
  CheckBars;
end;

procedure TForm1.BarBoxClick(Sender: TObject);
begin
  CheckReeds;
end;

end.
```

Appendix E

Coding of REEDFLO v2 Model

```
'-------------------------------------------------------------------------

'                              - R E E D F L O -

'                                 A.L. Birkhead

'                         Centre for Water in the Environment
'                           University of the Witwatersrand
'                                 1 Jan Smuts Avenue
'                                   Johannesburg

'                              Water Research Commission
'                                  Project No. 856


'                              Last modified : May 2000

'-------------------------------------------------------------------------

' Mathematical model for non-uniform flow through reeded vegetation of
given
' stem diameter, spacing, arrangement (staggered or horizontal) and
flexural
' rigidity.  The model makes allowance for a rough bed of given effective
' roughness (ks), and the stems are cylindrical.  Submerged and unsubmerged
' conditions are considered and the vertical distribution of velocity and
' shear stress are modelled using eddy-viscosity and mixing length theory
' approximations for below and above the reed zone, respectively.

' The model makes use of the following literature :

' Vedrana Kutija and Hoang Thi Minh Hong (1996).  A numerical model for
' assessing the additional resistance to flow introduced by flexible
' vegetation.  Journal of Hydraulic Research, Vol. 34, No. 1, 99-114.

' Li, R.M., and Shen, H.S. (1973).  Effect of tall vegetations on flow
' and sediment.  Journal of the Hydraulics Division, ASCE, No. HY5,
' 793-814.

' Lindner, K. (1982).  Der stromingwiderstand von pflanzenbestanden.
' Mitteilungen, Leichtweiss-Institut fur Wasserbau, TU Braunschweig,
' Heft 75.

' Pasche, E and Rouve, M. (1987).  Overbank flow with vegetatively
' roughened floodplains.  Journal of Hydraulic Engineering, Vol. 111,
' No. 9, 1262-1278

'-------------------------------------------------------------------------

  DECLARE SUB Bedroughness ()
  DECLARE SUB Stembending ()
  DECLARE SUB Linearinterp ()
  DECLARE SUB Einsteinsvelocity ()
  DECLARE SUB Sidewallcorrection ()
  DECLARE SUB Reeddragcoeff ()
  DECLARE SUB Forcebalance ()
  DECLARE SUB Einsteinscorrfac ()
  DECLARE SUB Dragshape ()
```

```
  DECLARE SUB Dischargecompute ()
  DECLARE SUB Effectres ()
  DECLARE SUB SolnMatrix ()
  DECLARE SUB SolveMatrix ()
  DECLARE SUB Shearstress ()
  DECLARE SUB Velconverg ()
  DECLARE SUB FDGrid ()
  DECLARE SUB Dischargeconverg ()
  DECLARE SUB Stembendconverg ()
  DECLARE SUB Outputresults ()

' Definition of variables and dimensioning

' TYPE INTEGERS

' Global

' heiter          - iteration no. for effective reed height
' jbot            - node directly above bed
' jsheardiv       - node at division between eddy viscosity
'                   and mixing length approximations
' jtop            - node directly below water surface
' jtopveg         - node directly below top of vegetation
' ni              - max no. of elements in the x-direction
' nCddatapts      - no. ordinates in drag coefficient file
' nxdatapts       - no. ordinates in Einstein's x file
' viter           - iteration no. for velocity
' yiter           - iteration no. for flow depth
' yitermax        - max no. of iterations no. for flow depth
' yroughiter      - iteration no. for flow depth: bed roughness only

  DIM SHARED jtop AS INTEGER, jbot AS INTEGER, jtopveg AS INTEGER
  DIM SHARED jsheardiv AS INTEGER
  DIM SHARED ni AS INTEGER
  DIM SHARED nCddatapts AS INTEGER
  DIM SHARED nxdatapts
  DIM SHARED viter AS INTEGER, heiter AS INTEGER, heitermax AS INTEGER
  DIM SHARED yiter AS INTEGER, yroughiter AS INTEGER, yitermax AS INTEGER

' Local

' j  - node in vertical (y) direction
' pt - counter for data points

  DIM j AS INTEGER, pt AS INTEGER

' TYPE REALS

' Global

' a, b          - distance c/c reeds in x-direction (m)
' alpha         - constant in eddy-viscosity relationship
' asym          - asymetric rod arrangement in narrow flume correction
factor
' C             - constant in height of viscous layer equation
' Cd            - drag coefficient of element as a fn of reed Re
' Cdreed        - effective asymptotic drag coefficient for element in reed
zone
' Cbed          - Chezy's resistance due to bed roughness
' Ceff          - effective Chezy's resistance (using wetted perimeter)
' d             - diameter of reed stem (m)
```

```
' delta          - height of viscous sub-layer (m)
' depx           - dependant variable x in linear interpolation
' dragcoeff      - tabulated drag coefficient data for given shape
' dy             - vertical height increment in finite-difference grid (FDG)
(m)
' dybot          - bottom (above bed) vertical height increment in FDG (m)
' dyTau          - vertical height difference between 1st & 2nd Tau nodes (m)
' dytop          - topmost vertical height increment in FDG (m)
' EI             - flexural rigidity, (Nm2)
' Einsteinsx     - Einstein's correction factor x = fn(ks/delta)
' Einsx          - Einstein's correction factor for modelled flow depth
' eta            - viscosity of water at 15degC
' f              - friction factor (bed & wall)
' fbed           - friction factor due to bed roughness
' feff           - effective friction factor (using wetted perimeter)
' flowidth       - width of rectangular river or flume (m)
' Forceappl      - force applied by flow per unit bed area (N/m2)
' Forcebalx      - previous estimates of the error in the force balance
(N/m2)
' Forcebalerr    - error in the balance of applied and resisting forces (%)
' Forcebed       - force resisted per unit bed area (N/m2)
' Forcereed      - force resisted by reeds per unit bed area (N/m2)
' Forceres       - resisting force (bed & reed or reed) (N/m2)
' Frd            - Froude no. based on stem diameter
' Fstem          - Force on unit bed area of reed stand (M/m2)
' g              - acceleration due to gravity (m/s2)
' gamma          - unit weight of water (N/m3)
' he, hv         - effective and vertical reed heights (m)
' hepr           - previous estimate of effective reed height (m)
' indx           - independant variable x in linear interpolation
' kappa          - von Karman's constant
' ks             - effective roughness of bed (m)
' ksdelta        - indepedant data set for Einstein's correction factor, x
' lo           - mixing length at the top of the reeds (m)
' lnfac          - conversion factor log bas 10 to log base e
' MatA/B/C(j)    - 3 columns of coeffiecints of velocity in tridiagonal
system
' MatR(j)        - column of constants in system of tridiagonal equations
' nbed           - Manning's resistance due to bed roughness
' neff           - effective Manning's resistance (using wetted perimeter)
' P              - perimeter (m)
' pi             - pi
' Q              - discharge per metre width (m2/s)
' Qbalx          - difference in discharge estimates (m3/s/m)
' Qit            - iterative discharge through reedbed (m3/s/m)
' R              - hydraulic radius bed & wall (m)
' ratioksdelta   - ratio ks to delta
' Rbed           - hydraulic radius of the bed using side wall correction (m)
' Re             - Reynolds no.
' Rebed          - Reynold's no. corrected for bed using side wall correction
' Rereed         - reed Reynolds no.
' Reshear        - shear Reynolds no.
' Rey            - Reynolds no. of which Cd is a function (tabulated data
set)
' rho            - density of water (kg/m3)
' So             - bed slope
' Tauj(x)        - shear stress at node x
' v              - average velocity due to bed roughness (m/s)
' uj(x)          - velocity at node x from soln of equations (m/s)
' vave           - average velocity as input to the reed drag model (m/s)
' vavebedonly    - average velocity due to bed roughness only (m/s)
```

```
' vEinstein     - average velocity due to Einsteins equation (m/s)
' vj(x)         - velocity at node x using previous estimates & uj(x) (m/s)
' vreed         - average velocity in the reed zone (m/s) (=Q/yreed)
' vshear        - shear velocity due to bed & wall effects (m/s)
' vshearbed     - shear velocity due to bed roughness (m/s)
' xsarea        - cross-sectional flow area (m2)
' y             - flow depth due to effect of reeds or reeds/bed (m)
' ybedonly      - flow depth due to bed roughness (m)
' yj(x)         - node elevations in y-direction (m)
' yo            - height above bed where velocity = 0 (m)
' ymldat        - elevation of the mixing length DATUM (m)
' yreedonly     - flow depth due to reed resistance only (m)
' ysheardiv     - elev of div betwn eddy viscosity & mixing length approxs
(m)
' yx/ypr        - previous estimates of flow depth (m)

  DIM SHARED a, alpha, asym, b, d
  DIM SHARED dy, dytop, dybot, dyTau
  DIM SHARED C
  DIM SHARED Cbed, Ceff
  DIM SHARED Cd, Cdreed
  DIM SHARED dragcoeff(20)
  DIM SHARED dep1, dep2, dep3, ind1, ind2, ind3
  DIM SHARED Einsx, Einsteinsx(20), EI
  DIM SHARED f, fbed, feff, Fstem
  DIM SHARED flowidth
  DIM SHARED forcebal1, forcebal2, forcebal3
  DIM SHARED Forceapp1, Forceres
  DIM SHARED Forcebed, Forcereed, Forcebalerr
  DIM SHARED Frd
  DIM SHARED g, lnfac, eta, pi, gamma, kappa
  DIM SHARED he, hv
  DIM SHARED ks, delta, ksdelta(20)
  DIM SHARED lo
  DIM SHARED MatA(1000) AS DOUBLE, MatB(1000) AS DOUBLE, MatC(1000) AS
DOUBLE
  DIM SHARED MatR(1000) AS DOUBLE
  DIM SHARED nbed, neff
  DIM SHARED q, qit, So
  DIM SHARED Qbal1, Qbal2, Qbal3
  DIM SHARED ratioksdelta
  DIM SHARED Re, Rebed, Rereed, Reshear, Rey(20)
  DIM SHARED r, Rbed, xsarea, P, rho
  DIM SHARED Tauj(1000)
  DIM SHARED v, vave, vEinstein, vshear, vshearbed, vreed
  DIM SHARED vavebedonly
  DIM SHARED vj(1000) AS DOUBLE, uj(1000) AS DOUBLE, hepr
  DIM SHARED y, yo, y1, y2, y3, y4, ybedonly, yj(1000) AS DOUBLE, ypr,
ymldat
  DIM SHARED yreedonly, ysheardiv

' arrangement     - arrangement or pattern of reeds
' comp            - type of computation (reedonly or reeds & bed)
' dragshapefile   - data for drag coefficient as a function of Re
' Einsteinsxfile - data for Einstein's correction factor, x
' forcebalan      - determines whether a balance of forces has been achieved
' heconverg       - defines whether the effective reed height has converged
' interpolatey    - defines whether an interpolation of flow depth is
required
' Outputfile      - data file for output of results
' path            - path to data files
```

```
' pathout          - path to output data
' Qconverg         - defines whether the discharge has converged
' sidewall         - apply side wall correction (yes/no)
' title            - title to input data files
' vconverg         - defines whether the velocities have converged

  DIM SHARED arrangement AS STRING
  DIM SHARED dragshapefile AS STRING
  DIM SHARED comp AS STRING
  DIM SHARED Einsteinsxfile AS STRING
  DIM SHARED forcebalan AS STRING
  DIM SHARED interpolatey AS STRING
  DIM SHARED outputfile AS STRING
  DIM SHARED path AS STRING, pathout AS STRING
  DIM SHARED Qconverg AS STRING
  DIM SHARED sidewall AS STRING
  DIM SHARED title AS STRING * 80
  DIM SHARED vconverg AS STRING
  DIM SHARED heconverg AS STRING

' Input variables

  arrangement = "S"   'staggered (S) or horizontal (H) arrangement
  d = .005            'diamater of cylindrical element (m)
  hv = .09             'vertical reed height (m)
  a = .075           'c/c spacing in streamwise direction (m)
  b = a               'c/c spacing in transverese direction (m)
  flowidth = .1        'width of rectangular section (m)
  So = .002       'bed = energy slope (uniform flow)
  ni = 50             'no. of rows of elements
  q = .002082 / .1     'discharge per unit width (m2/s)
  ks = .0125      'effective roughnesss of the bed (m)
  sidewall = "yes"    'side wall correction for bed roughness only ?
  asym = 1.5 / 1.33 'Symmetric correction for rods in narrow flume
  dy = .001           'vertical increment in finite-difference grid (m)
  EI = 200            'Flexural rigidity, EI (Nm2)
  temp = 21           'water temperature (deg C)

  alphadet$ = "Auto" 'input alpha manually = "Man" or allow the programme
                     'to compute it, i.e. = "Auto"
  alpha = .018       'value for alphadet$="Man" or initial estimate for
"Auto"

  heitermax = 20      'Maximum no. of iterations for effective veg. height
  yitermax = 20       'Maximum no. of iterations for flow depth

' Location of tabulated input data and output folders

  path = "c:\reedflow\reeds\model\"
  pathout = "c:\reedflow\reeds\model\"

' Naming of input and output files

  Einsteinsxfile = path + "Einstein.x"
  dragshapefile = path + "Circdrag.cof"
  outputfile = pathout + "Reedflo.txt"

' Constants

  pi = 3.1415926548
  C = 11.6              'constant in eqn for height of viscous sub-layer
```

```
  g = 9.81                'acceleration due to gravity (m2/s)
  kappa = .41             'von Karman's constant
  rho = 1000              'density of water (kg/m3)
  gamma = rho * g         'unit weight of water (N/m2)
  'viscosity of water at temp in degC (m2/s)
  eta = (1.741 - .0499 * temp + .00066 * temp ^ 2) * 10 ^ -6
  lnfac = 2.302585093#  'conversion factor log base 10 to log base e

'
'-------------------------------------------------------------------------

' Start of main programme

' Clear monitor
  CLS

  PRINT "Running Reedflo"

' Initial estimate for drag coefficient

  Cd = 1

' Read drag coefficient data from file

  OPEN dragshapefile FOR INPUT AS #1

  INPUT #1, title, title
  INPUT #1, nCddatapts

  FOR pt = 1 TO nCddatapts
    INPUT #1, Rey(pt), dragcoeff(pt)
  NEXT pt

  CLOSE #1

' Run model to compute uniform flow depth due to bed roughness only

  yroughiter = 0
  CALL Bedroughness

  vavebedonly = q / (flowidth * ybedonly)

' Run reed drag model to compute uniform flow depth due to reed drag only -
' uniform distribution of velocity

' Initial estimate of flow depth and effective reed height

  yreedonly = ybedonly

  he = hv

  interpolatey = "no"

  yiter = 1
  comp = "reedonly"

  DO

    vave = q / yreedonly
    vreed = vave
```

```
    y = yreedonly

    CALL Reeddragcoeff
    CALL Stembending

'   Hydraulic force applied to the reeds

    Forceappl = gamma * yreedonly * So * (1 * 1 - 1 / (a * b) * asym * pi *
d ^ 2 / 4)

'   Resisting drag force exerted by the reeds

    Forcereed = .5 * rho * Cdreed * (d * he) * vreed ^ 2 * (1 / (a * b) *
asym)

'   Resisting force

    Forceres = Forcereed

'   Iterate flow depth to achieve force balance

    y = yreedonly

    CALL Forcebalance

    yreedonly = y

    yiter = yiter + 1

  LOOP UNTIL forcebalan = "yes"

' Print results to screen
  PRINT
  PRINT "Flow depth bed only (m)  ", USING "#####.###"; ybedonly
  PRINT
  PRINT "Flow depth reed only (m) ", USING "#####.###"; yreedonly
  PRINT "Reed height (m)          ", USING "#####.###"; hv
  PRINT "Effective reed height (m)", USING "#####.###"; he

  'PRINT "press <ENTER> to continue"
  'INPUT keyin$

'
------------------------------------------------------------------------

' Start of program to compute uniform flow depth : bed roughness & reed
drag

' Intial estimates of velocity and depth - use largest depth from the bed
' or reed computations

  IF yreedonly > ybedonly THEN
    vave = q / yreedonly
    vreed = vave
    y = yreedonly
  ELSE
    vave = q / ybedonly
    vreed = vave
    y = ybedonly
  END IF
```

```
  interpolatey = "no"

  heiter = 1
  comp = "reedandbed"

' Loop (1) for effective reed height

  DO

'   Set-up finite difference grid (flow depth dependant)

    CALL FDGrid

    CALL Reeddragcoeff          'Cdreed = fn(vreed)

    CALL Stembending            'fn(Cdreed & vreed)

'   Mixing length above the reeds

'   *** This needs to be verified or calibrated using experimental flume
'   data. For example, von Prantl's mixing length equation could be offset
by
'   "he" to give lo=0 (I think that this represents the lowest value for
lo,
'   since it is likely that turbulence occuring above the reeds will be
'   generated some disctance below the top of the reeds, especially for low
'   densities). Kutija and Hoang Thi Minh Hong (1996) used
l=K.z(1-z/y)^0.5,
'   which is parabolic in shape and reduces to zero at the water surface.
'   It is independant of the height and density of the reeds, with the
DATUM
'   being at the bed of the channel(!).  I think that a function
'   taking reed density (and dia.?) into consideration will be more
reasonable
'   and physically meaningful, i.e. lo=a...2a or ka/d where k is calibrated
'   using the flume data.  a..2a physically represents the largest size of
'   an eddy or vorticy that may be accomodated between reeds stems at the
top
'   of the reed bed.  A reasonable range for lo is 0 (very dense reeds) to
K.he
'   (very sparse reeds). ***

    lo = 0

'   Limit to lo - see comment above

    IF lo > kappa * he THEN
      lo = kappa * he
    END IF

'   Find the node at the top of the vegetation

    jtopveg = jtop

    FOR j = jbot TO jtop
      IF yj(j) >= he THEN
        jtopveg = j - 1
        EXIT FOR
      END IF
    NEXT j
```

```
'   According to Kutija and Hoang Thi Minh Hong (1996), the mixing length
'   model applies some distance below the top of the vegetation - treated
'   as an additional unknown (p * he).  In the existing model, the change
'   from eddy-viscosity to mixing length function (ysheardiv) is assumed to
'   occur at a height (lo/kappa) below the top of the vegetation.

'   *** This will also require further consideration using experimental
'   data. ***

    IF he < y THEN
      ysheardiv = he
    ELSE
      ysheardiv = y
    END IF

'   Node at the shear division (jsheardiv)

    jsheardiv = jbot

    IF ysheardiv < 0 THEN
      ysheardiv = 0
      jsheardiv = jbot
    ELSE
      FOR j = jtopveg TO 1 STEP -1
       IF yj(j) <= ysheardiv THEN
         jsheardiv = j
         EXIT FOR
       END IF
      NEXT j
    END IF

'   Datum for the mixing length theory approximation

'   *** This relates directly to the definition of lo, and therefore
requires
'   further consideration using experimental data. ***

'   Shear division option
'   ymldat = he - lo / kappa
'   Channel bed option (y = 0)
    ymldat = 0

    IF ymldat < 0 THEN ymldat = 0

    IF jsheardiv = jbot THEN
'     Log-law throughout
      ymldat = 0
    END IF

'   Initialise velocity values - assume linear distribution

    FOR j = jbot TO jtop
      vj(j) = 2 * (yj(j) / (y - yo)) * (q / (y - yo))
    NEXT j

'   Boundary condition at bed : no-slip condition

    vj(jbot - 1) = 0

'   Loop (2) for flow depth using discharge convergence
```

```
    interpolatey = "no"

    yiter = 1

    DO

      CALL FDGrid

      jtopveg = jtop

      FOR j = jbot TO jtop
        IF yj(j) >= he THEN
          jtopveg = j - 1
          EXIT FOR
        END IF
      NEXT j

'   Node corresponding to shear division may be a function of flow depth
'   and and therefore needs to be updated within this discharge convergence
'   loop (where flow depth is adjusted to attain convergence).

    CALL Stembending

    IF he < y THEN
      ysheardiv = he
    ELSE
      ysheardiv = y
    END IF

    jsheardiv = jbot

    IF ysheardiv < 0 THEN
      ysheardiv = 0
      jsheardiv = jbot
    ELSE
      FOR j = jtop TO 1 STEP -1
       IF yj(j) <= ysheardiv THEN
         jsheardiv = j
         EXIT FOR
       END IF
      NEXT j
    END IF

'     Initialise velocity values - assume linear distribution

      FOR j = jbot TO jtop
        vj(j) = 2 * (yj(j) / (y - yo)) * (q / (y - yo))
      NEXT j

'     Boundary condition at bed : no-slip condition

      vj(jbot - 1) = 0

'     Loop (3) for velocity convergence using previous estimates

      viter = 1

      DO

        CALL SolnMatrix
        CALL SolveMatrix
```

```
'       Convergence of velocity profile ?

        CALL Velconverg

        viter = viter + 1

      LOOP UNTIL vconverg = "yes"

      CALL Dischargecompute
      CALL Reeddragcoeff

'     Convergence of discharge ?

      CALL Dischargeconverg

      yiter = yiter + 1

      IF alphadet$ = "Auto" THEN
        alpha = (10 ^ 1.54 * y ^ .961 * ks ^ .525) / ((a / d) ^ 2.427 * So
^ .506)
      END IF

     LOOP UNTIL Qconverg = "yes" OR yiter > yitermax

    CALL Stembending

    CALL Stembendconverg

    heiter = heiter + 1

  LOOP UNTIL heconverg = "yes" OR heiter > heitermax

  CALL Shearstress

  Forceappl = gamma * y * So
  Forcebed = Tauj(jbot - 1)
  Forcebalerr = ABS(Forceappl - (Fstem + Forcebed)) / Forceappl * 100

  CALL Outputresults

  END

SUB Bedroughness

' Subprogramme to compute the velocity distribution for a bed of given
' roughness for uniform flow conditions.

'-------------------------------------------------------------------------
--

' Definition and dimensioning of local variables

' ydiff         - difference between velocity estimates (Q/A & Einstein's)
' yest          - flow depth estimates

  DIM ydiff, ydiff1, ydiff2
  DIM yest1, yest2

'-------------------------------------------------------------------------
--
```

```
' Inital flow depth estimate - bed roughness only
  ybedonly = 1

' Intialise variable values
  interpolatey = "no"

1 yroughiter = yroughiter + 1

' Hydraulic radius

  xsarea = flowidth * ybedonly
  P = 2 * ybedonly + flowidth
  r = xsarea / P

  vshear = (g * r * So) ^ .5
  v = (q * flowidth) / xsarea
  f = 8 * (vshear / v) ^ 2
  Re = 4 * v * r / eta
  Reshear = vshear * ks / eta

  IF sidewall = "yes" THEN
'   Side wall correction
    CALL Sidewallcorrection
  ELSE
'   friction factor for the bed is equivalent to the Darcy-Weisbach value
    fbed = f
  END IF

  Rbed = r * fbed / f
  vshearbed = (g * Rbed * So) ^ .5
  Rebed = 4 * v * Rbed / eta

' Einstein's velocity equation
  CALL Einsteinsvelocity

' Check average velocity according to Einstein for this flow depth

' This section of coding finds the value of the flow depth that gives
' equivalent average velocities computed using Einstens and the
' continuity equation.

  ydiff = q / (vEinstein - v)

  IF ydiff = 0 THEN
    GOTO 2
  ELSEIF ydiff * ydiff1 < 0 AND interpolatey = "no" THEN

'   Flow depths bound the actual solution - initiate interpolation

    ind1 = ydiff1
    ind2 = ydiff
    ind3 = 0
    dep1 = yest1
    dep2 = ybedonly

    CALL Linearinterp

    yest2 = ybedonly
    ydiff2 = ydiff
    ybedonly = dep3
```

```
    interpolatey = "yes"

    GOTO 1

  ELSEIF interpolatey = "yes" THEN

'   Disregard one of the flow depths

    IF ydiff * ydiff2 > 0 THEN

      ydiff2 = ydiff
      yest2 = ybedonly

      ind1 = ydiff1
      ind2 = ydiff2
      ind3 = 0
      dep1 = yest1
      dep2 = yest2

      IF (ABS(yest2 - yest1) / (yest1 + yest2) / 2) * 100 < .1 THEN GOTO 2

      CALL Linearinterp

      ybedonly = dep3

      GOTO 1

    ELSE

      ydiff1 = ydiff
      yest1 = ybedonly

      ind1 = ydiff1
      ind2 = ydiff2
      ind3 = 0
      dep1 = yest1
      dep2 = yest2

      IF (ABS(yest2 - yest1) / (yest1 + yest2) / 2) * 100 < .1 THEN GOTO 2

      CALL Linearinterp

      ybedonly = dep3

      GOTO 1

    END IF

  ELSEIF interpolatey = "no" THEN

    yest1 = ybedonly
    ydiff1 = ydiff

    IF vEinstein < v THEN
'     Increase flow depth by half
      ybedonly = 1.5 * ybedonly
    ELSE
'     Reduce flow depth by half
      ybedonly = .5 * ybedonly
    END IF
```

```
  END IF

  GOTO 1

2 END SUB

SUB Dischargecompute

' Subprogramme to compute the discharge through a reedbed based on the
' vertical velocity distribution.

'-------------------------------------------------------------------------
--

' Definition and dimensioning of local variables

' j  - counter for printing nodal values

  DIM j AS INTEGER

' Qreed - discharge through reeded zone of reedbed (m3/s/m)

  DIM Qreed

'-------------------------------------------------------------------------
--

' Compute discharge and average velocity for this flow depth

  qit = vj(jbot) * (dy + dybot) / 2

  FOR j = jbot + 1 TO jtop - 1
    qit = qit + vj(j) * dy
  NEXT j

  qit = qit + vj(jtop) * (dytop + dy / 2)

  vave = qit / y

' Compute average flow velocity in reed zone

  Qreed = vj(jbot) * (dy + dybot) / 2

  FOR j = jbot + 1 TO jtopveg
    Qreed = Qreed + vj(j) * dy
  NEXT j

  Qreed = Qreed + vj(jtopveg) * (he - yj(jtopveg) + dy / 2)

  vreed = Qreed / (he - yo)

END SUB

SUB Dischargeconverg

' Subprogramme to check if the discharge has converged.  If not, the flow
' depth is adjusted based on the previous flow depths used and resulting
' estimates of discharge.

'-------------------------------------------------------------------------
--
```

```
  Qbal3 = Qbal2
  y3 = y2
  Qbal2 = Qbal1
  y2 = y1
  Qbal1 = q - qit
  y1 = y


  IF ABS(q - qit) / q < .01 / 100 THEN
    Qconverg = "yes"
    EXIT SUB
  END IF

  IF Qbal1 = 0 THEN
    Qconverg = "yes"
    EXIT SUB
  END IF

  IF interpolatey = "yes" THEN
'   Keep positive and negative balance estimates
    IF Qbal1 * Qbal2 > 0 THEN
      Qbal2 = Qbal3
      y2 = y3
    END IF
'   Qbal3 is discarded by default
  END IF

  IF yiter = 1 OR Qbal1 * Qbal2 > 0 THEN
    IF Qbal1 > 0 THEN
      y = 1.5 * y
      Qconverg = "no"
    ELSE
      y = .5 * y
      Qconverg = "no"
    END IF
  ELSE
'   Interpolatey for new estimate of depth
    interpolatey = "yes"
    ind1 = Qbal1
    ind2 = Qbal2
    ind3 = 0
    dep1 = y1
    dep2 = y2
    CALL Linearinterp
    y = dep3
    Qconverg = "no"
  END IF

END SUB

  SUB Dragshape

' Subprogramme to detemine the drag coefficient for a given shape as a
' function of the Reynolds no.

'
-----------------------------------------------------------------------
-

' Definition and dimensioning of local variables
```

```
' pt - data point in interpolation

  DIM pt AS INTEGER

'
-------------------------------------------------------------------------
-

' Interpolate from tabulated data

  IF Rereed <= Rey(1) THEN
    PRINT "Reynolds no. below limit of tabulated data to interpolate for
Cd"
    END
  ELSEIF Rereed >= Rey(nCddatapts) THEN
    IF comp = "reedonly" THEN
      Rereed = Rey(nCddatapts)
    ELSE
      END
    END IF
  ELSE
    FOR pt = 2 TO nCddatapts
      IF Rereed >= Rey(pt - 1) AND Rereed < Rey(pt) THEN
        ind1 = Rey(pt - 1)
        ind2 = Rey(pt)
        ind3 = Rereed
        dep1 = dragcoeff(pt - 1)
        dep2 = dragcoeff(pt)
        CALL Linearinterp
        Cd = dep3
        EXIT FOR
        END IF
    NEXT pt
  END IF

  END SUB

SUB Effectres

' Subprogramme to compute the bed and effective resistances (using the
' hydrauic radius).

'-------------------------------------------------------------------------
--

' Note: fbed computed in subprogramme "Sidewallcorrection"
  feff = 8 * g * y * So / vave ^ 2

  nbed = Rbed ^ (1 / 6) * (fbed / (8 * g)) ^ .5
  neff = 1 / vave * y ^ (2 / 3) * So ^ .5

  Cbed = vavebedonly / (Rbed * So) ^ .5
  Ceff = vave / (y * So) ^ .5

END SUB

  SUB Einsteinscorrfac

' Subprogramme to compute Einstein'c corection factor for hydraulically
' smooth and transitional flows.
```

```
'
-----------------------------------------------------------------------
-
' Definition and dimensioning of local variables
' pt - data point in interpolation
  DIM pt AS INTEGER
'
-----------------------------------------------------------------------
-
' Interpolate from tabulated data
  IF ratioksdelta <= ksdelta(1) THEN
    PRINT "ks/delta below limit of tabulated data to interpolate for x"
    END
  ELSEIF ratioksdelta >= ksdelta(nxdatapts) THEN
    Einsx = Einsteinsx(nxdatapts)
  ELSE
    FOR pt = 2 TO nxdatapts
      IF ratioksdelta >= ksdelta(pt - 1) AND ratioksdelta < ksdelta(pt)
THEN
        ind1 = ksdelta(pt - 1)
        ind2 = ksdelta(pt)
        ind3 = ratioksdelta
        dep1 = Einsteinsx(pt - 1)
        dep2 = Einsteinsx(pt)
        CALL Linearinterp
        Einsx = dep3
        EXIT FOR
        END IF
    NEXT pt
  END IF

  END SUB

SUB Einsteinsvelocity
' Subprogramme to compute the average velocity according to Einstein's eqn.
'-----------------------------------------------------------------------
--
' Definition and dimensioning of local variables
' pt - data point no. in Einstein's tabulated x data
  DIM pt AS INTEGER
'
-----------------------------------------------------------------------
  IF yroughiter = 1 THEN
    OPEN Einsteinsxfile FOR INPUT AS #1
    INPUT #1, title, title
    INPUT #1, nxdatapts
```

```
    FOR pt = 1 TO nxdatapts
      INPUT #1, ksdelta(pt), Einsteinsx(pt)
    NEXT pt

    CLOSE #1

  END IF

' Height of the viscous sub-layer, delta
  delta = C * eta / vshearbed
  ratioksdelta = ks / delta

  CALL Einsteinscorrfac

  vEinstein = vshearbed * 5.75 * LOG(12.27 * Rbed * Einsx / ks) / lnfac

END SUB

SUB FDGrid

' Subprogramme to compute the finite-difference grid

'
-------------------------------------------------------------------------
-

' Definition and dimensioning of local variables

' j  - node in vertical (y) direction

  DIM j AS INTEGER

'
-------------------------------------------------------------------------
-

' height above datum (y = 0) where velocity = 0

  yo = (ks / 30.2) 'Note : this assumes rough turbulent bed

' Node elevations

  FOR j = 0 TO 5000
    yj(j) = j * dy
    IF yj(j) >= y THEN
      yj(j) = y
      jtop = j - 1
      EXIT FOR
    END IF
  NEXT j

' Node directly above yo

  FOR j = 1 TO jtop
    IF yj(j) > yo THEN
      jbot = j
      EXIT FOR
    END IF
  NEXT j

  dytop = y - yj(jtop)
```

```
  dybot = yj(jbot) - yo

END SUB

  SUB Forcebalance

' Subprogramme to compute the balance of applied and resisting forces
' and to interpolate for flow depth using any imbalance.

'-------------------------------------------------------------------------
--

' Definition and dimensioning of local variables

' keyin$ - any key input from the keyboard

  DIM keyin$

'-------------------------------------------------------------------------
--

  forceba13 = forceba12
  y3 = y2
  forceba12 = forceba11
  y2 = y1
  forceba11 = Forceappl - Forceres
  y1 = y

  IF ABS(Forceappl - Forceres) / Forceappl * 100 < .1 THEN
    forcebalan = "yes"
    EXIT SUB
  END IF

  IF yiter > yitermax THEN
    PRINT "flow depth convergence not acheived within 20 iterations - check
error"
    PRINT "press <ENTER> to continue"
    INPUT keyin$
    forcebalan = "yes"
    EXIT SUB
  END IF

  IF forceba11 = 0 THEN
    forcebalan = "yes"
    EXIT SUB
  END IF

  IF interpolatey = "yes" THEN
'   Keep positive and negative balance estimates
    IF forceba11 * forceba12 > 0 THEN
      forceba12 = forceba13
      y2 = y3
    END IF
'   Forceba13 is discarded by default
  END IF

  IF yiter = 1 OR forceba11 * forceba12 > 0 THEN
    IF forceba11 > 0 THEN
      y = .5 * y
      forcebalan = "no"
    ELSE
```

```
      y = 1.5 * y
      forcebalan = "no"
    END IF
  ELSE
'   Interpolatey for new estimate of depth
    interpolatey = "yes"
    ind1 = forceba11
    ind2 = forceba12
    ind3 = 0
    dep1 = y1
    dep2 = y2
    CALL Linearinterp
    y = dep3
    forcebalan = "no"
  END IF

  END SUB

SUB Linearinterp

' Subprogramme to interpolate linearly

'-------------------------------------------------------------------------
--

  dep3 = dep1 + (ind3 - ind1) / (ind2 - ind1) * (dep2 - dep1)

END SUB

SUB Outputresults

' Subprogramme to print results to monitor and ASCII data files

'-------------------------------------------------------------------------
--

' Definition and dimensioning of local variables

' j  - counter for printing nodal values

  DIM j AS INTEGER

'-------------------------------------------------------------------------
--

' Compute effective resistance of reeded system

  CALL Effectres

' Output results to monitor

  PRINT "Arrangement (S/P)      ", arrangement
  PRINT "Discharge (m3/s/m)     ", USING "#####.###"; q
  PRINT "Flow depth (m)         ", USING "#####.###"; y
  PRINT "Average velocity (m/s)", USING "#####.###"; vave
  PRINT "Slope                  ", USING "#####.###"; So
  PRINT "Reed dia. (m)          ", USING "#####.###"; d
  PRINT "Reed height (m)        ", USING "#####.###"; hv
  PRINT "Reed spacing (m)       ", USING "#####.###"; a
  PRINT "Flexural rigidity      ", USING "#####.#####"; EI
  PRINT "Effective reed height ", USING "#####.###"; he
```

```
  PRINT "Velocity in reeds(m/s)", USING "#####.###"; vreed
  PRINT "Re(d) & Fr(d)          ", USING "#####.###"; Rereed; Frd
  PRINT "Cd (single stem)       ", USING "#####.###"; Cd
  PRINT "Cd (using ave. vel)    ", USING "#####.###"; Cdreed
  PRINT "alpha                  ", USING "####.####"; alpha
  PRINT "Applied force (N/m2)   ", USING "#####.###"; Forceappl
  PRINT "Reed force  (N/m2)     ", USING "#####.###"; Fstem
  PRINT "Bed force (N/m2)       ", USING "#####.###"; Forcebed
  PRINT "Force bal error (%)    ", USING "#####.###"; Forcebalerr
  PRINT
  PRINT "fbed & feff            ", USING "#####.###"; fbed; feff
  PRINT "nbed & neff            ", USING "#####.###"; nbed; neff
  PRINT "Cbed & Ceff            ", USING "#####.###"; Cbed; Ceff

' Output data to file

  OPEN outputfile FOR OUTPUT AS #1

  PRINT #1, "Reedflo v3 April 1999"
  PRINT #1,

  PRINT #1, "Arrangement (S/P)      ,"; arrangement
  PRINT #1, "Discharge (m3/s/m)     ,", USING "#####.###"; q
  PRINT #1, "Flow depth (m)         ,", USING "#####.###"; y
  PRINT #1, "Average velocity (m/s),", USING "#####.###"; vave
  PRINT #1, "Slope                  ,", USING "#####.###"; So
  PRINT #1,
  PRINT #1, "Reed dia. (m)          ,", USING "#####.###"; d
  PRINT #1, "Reed height (m)        ,", USING "#####.###"; hv
  PRINT #1, "Reed spacing (m)       ,", USING "#####.###"; a
  PRINT #1, "Flexural rigidity      ,", USING "#####.#####"; EI
  PRINT #1, "Effective reed height ,", USING "#####.###"; he
  PRINT #1, "Velocity in reeds(m/s),", USING "#####.###"; vreed
  PRINT #1, "Re(d) & Fr(d)          ,", USING "#####.###"; Rereed;
  PRINT #1, ",";
  PRINT #1, USING "#####.###"; Frd
  PRINT #1, "Cd (single stem)       ,", USING "#####.###"; Cd
  PRINT #1, "Cd (using ave. vel)    ,", USING "#####.###"; Cdreed
  PRINT #1,
  PRINT #1, "Applied force (N/m2)   ,", USING "#####.###"; Forceappl
  PRINT #1, "Reed force  (N/m2)     ,", USING "#####.###"; Fstem
  PRINT #1, "Bed force (N/m2)       ,", USING "#####.###"; Forcebed
  PRINT #1, "Force bal error (%)    ,", USING "#####.#"; Forcebalerr
  PRINT #1,
  PRINT #1, "fbed & feff            ,", USING "#####.###"; fbed;
  PRINT #1, ",";
  PRINT #1, USING "#####.###"; feff
  PRINT #1, "nbed & neff            ,", USING "#####.###"; nbed;
  PRINT #1, ",";
  PRINT #1, USING "#####.###"; neff
  PRINT #1, "Cbed & Ceff            ,", USING "#####.###"; Cbed;
  PRINT #1, ",";
  PRINT #1, USING "#####.###"; Ceff
  PRINT #1,
  PRINT #1, "Finite difference grid height (m),", USING "##.###"; dy
  PRINT #1,
  PRINT #1, "Data for shear stress/velocity distribution calculations"
  PRINT #1,
  PRINT #1, "Mixing length at the top of the reeds (m),"; USING "##.###";
lo
  PRINT #1, "Height of the shear division (m),"; USING "##.###"; ysheardiv
```

```
  PRINT #1, "Height of the mixing length datum (m), "; USING "##.###";
ymldat
  PRINT #1,
  PRINT #1, "Shear stress and velocity distributions above bed"
  PRINT #1,
  PRINT #1, "Height above bed (m), velocity (m/s)"
  PRINT #1,
  FOR j = jbot TO jtop
    PRINT #1, USING "###.####"; yj(j);
    PRINT #1, ",";
    PRINT #1, USING "###.####"; vj(j)
  NEXT j

  PRINT #1,
  PRINT #1, "Height above bed (m), Shear stress (N/m2)"
  PRINT #1,

  PRINT #1, USING "###.####"; (yo + yj(jbot)) / 2;
  PRINT #1, ",,";
  PRINT #1, USING "###.####"; Tauj(jbot)
  FOR j = jbot TO jtop - 1
    PRINT #1, USING "###.####"; (yj(j) + yj(j + 1)) / 2;
    PRINT #1, ",,";
    PRINT #1, USING "###.####"; Tauj(j + 1)
  NEXT j
  PRINT #1, USING "###.####"; y;
  PRINT #1, ",,";
  PRINT #1, USING "###.####"; 0

END SUB

  SUB Reeddragcoeff

' Subprogramme to compute the effective drag coefficient on a reed in an
' infinitely large bed of reeds as a fuction of the average flow velocity
' through the reedbed.

'-------------------------------------------------------------------------
--

' Definition and dimensioning of local variables

' Cdest       - iteratie estimate of drag force coefficient
' i, ii       - counters for rows in the stream-wise (x) direction
' i3percent   - the row no. where vmax/vapproach <= 3% (boundary condition)
' j           - counter for rows in a lateral (z) direction
' nj          - no. elements in z-dir. that have an influence on element i
' integral    - area under velocity defect function (m2/s)
' slopefn     - function for the effect of bed slope on vmax
' sumvdefect  - sum of the velocity defects due to upstream influence (m/s)
' sumintegral - sum of integrals due to all upstream influences (m2/s)
' vappr(i)    - approach velocity to the ith row of reeds (m/s)
' vdefect     - velocity defect at a point in the wake region (m/s)
' vinf        - vel. at an infinite lateral distance from the influence
'               on the wake defect (m/s)
' vmax        - maximum velocity defect in the wake region (m/s)
' x           - distance in the stream-wise (longitudinal) direction (m)
' z           - distance in the lateral direction (m)
' zw          - half wake width (m)

  DIM i AS INTEGER, ii AS INTEGER, i3percent AS INTEGER
```

```
  DIM j AS INTEGER, nj AS INTEGER

  DIM Cdest
  DIM vappr(500) AS DOUBLE, vinf AS DOUBLE, vmax AS DOUBLE
  DIM vdefect AS DOUBLE, sumvdefect AS DOUBLE
  DIM x, z, zw
  DIM integral AS DOUBLE, sumintegral AS DOUBLE
  DIM slopefn

'-------------------------------------------------------------------------
--

  Cdreed = 0

  DO

    vappr(1) = vreed

    FOR i = 2 TO ni

'   Initialise variable values

      sumintegral = 0
      sumvdefect = 0

      FOR ii = 1 TO i - 1

        x = a * (i - ii)
        zw = Cd * d * .48 * (x / (Cd * d)) ^ .59
        slopefn = (1 / (1 + g * So * x / ((vappr(ii) ^ 2) / 2))) ^ 1.5
        vmax = vappr(ii) * -.9 * (x / (Cd * d)) ^ -.7 * slopefn

'       Integral : area under defect over full wake width (2zw)

        integral = -.5 * vmax * 2 * zw

'       Velocity defect at reed element i due to all elements in row ii

        IF arrangement = "H" THEN

          nj = INT(zw / b)
          vdefect = vmax

          IF nj > 0 THEN
            FOR j = 1 TO nj
              z = j * b
              vdefect = vdefect + 2 * .5 * vmax * (1 + COS(pi * z / zw))
            NEXT j
          END IF

        ELSE

          IF INT((i - ii) / 2) = (i - ii) / 2 THEN

'           Horizontal upstream elements

            nj = INT(zw / b)
            vdefect = vmax

            IF nj > 0 THEN
              FOR j = 1 TO nj
```

```
            z = j * b
            vdefect = vdefect + 2 * .5 * vmax * (1 + COS(pi * z / zw))
          NEXT j
        END IF

      ELSE

        Staggered upstream elements

        IF zw >= 1.5 * b THEN
          nj = INT((zw - b / 2) / b + 1)
        ELSEIF zw >= b / 2 THEN
          nj = 1
        ELSE
          nj = 0
        END IF

        IF nj = 0 THEN
          vdefect = 0
        ELSE
          vdefect = 2 * .5 * vmax * (1 + COS(pi * (b / 2) / zw))
          IF nj > 1 THEN
            FOR j = 2 TO nj
              z = b / 2 + (j - 1) * b
              vdefect = vdefect + 2 * .5 * vmax * (1 + COS(pi * z /
zw))
            NEXT j
          END IF
        END IF

      END IF

      sumintegral = sumintegral + integral
      sumvdefect = sumvdefect + vdefect

    NEXT ii

    vinf = vreed + sumintegral / b
    vappr(i) = vinf + sumvdefect

  NEXT i

'   Compute no. of rows for vmax to reduce to 3% of vreed

  FOR i = 1 TO 1000
    x = a * i
    zw = Cd * d * .48 * (x / (Cd * d)) ^ .59
    slopefn = (1 / (1 + g * So * x / ((vreed ^ 2) / 2))) ^ 1.5
    vmax = vreed * -.9 * (x / (Cd * d)) ^ -.7 * slopefn
    IF -vmax <= .03 * vreed THEN
      i3percent = i
      IF i3percent > ni THEN
        PRINT "3% vmax/vreed boundary not achieved - increase no. of
rows, ni"
        END
      END IF
      EXIT FOR
    END IF
  NEXT i
```

```
'   Compute cylinder Reynolds no.

    Rereed = vappr(ni) * d / eta

'   Check the drag force coefficient using Rereed

    Cdest = Cd

    CALL Dragshape

  LOOP UNTIL (Cd - Cdest) / Cd * 100 < .1

' Correction to the drag coefficient for a single rod in an arrangement
' and using the average velocity in the reed zone as opposed to the
' approach velocity

' Cdreed = Cd * (1 + 1.9 * d / b * Cd) * (vappr(ni) / vreed) ^ 2
  Cdreed = Cd * (vappr(ni) / vreed) ^ 2

' Froude number
  Frd = vappr(ni) / (9.81 * d) ^ .5


  END SUB

SUB Shearstress

' Subprogramme to compute the distribution of shear stress between the
' bed and water surface.

'-------------------------------------------------------------------------
--

' Definition and dimensioning of local variables

' j  - node in vertical (y) direction

  DIM j AS INTEGER

' elev - height at nodes in the vertical (y) direction (m).
' l    - mixing length (m)

  DIM elev, l

'-------------------------------------------------------------------------
--

  IF jsheardiv = jbot THEN
'   Log-law throughout the depth
    elev = .5 * (yj(jbot) + yo)
    l = kappa * (elev - ymldat)
    Tauj(jbot) = rho * l ^ 2 * (vj(jbot) - vj(jbot - 1)) * ABS(vj(jbot) -
vj(jbot - 1)) / dybot ^ 2
    FOR j = jbot + 1 TO jtop
      elev = .5 * (yj(j) + yj(j - 1))
      l = kappa * (elev - ymldat)
      Tauj(j) = rho * l ^ 2 * (vj(j) - vj(j - 1)) * ABS(vj(j) - vj(j - 1))
/ dy ^ 2
    NEXT j
  ELSE
```

```
'    Eddy-viscosity in vegetated zone
     Tauj(jbot) = rho * alpha * a * (vj(jbot) + vj(jbot - 1)) / 2 *
(vj(jbot) - vj(jbot - 1)) / dybot
     FOR j = jbot + 1 TO jsheardiv
       Tauj(j) = rho * alpha * a * (vj(j) + vj(j - 1)) / 2 * (vj(j) - vj(j -
1)) / dy
     NEXT j
     IF jsheardiv = jtop THEN
'      Eddy-viscosity to water surface
       Tauj(jtop) = rho * alpha * a * (vj(j) + vj(j - 1)) / 2 * (vj(j) -
vj(j - 1)) / dy
     ELSE
'      Mixing length to water surface
       FOR j = jsheardiv + 1 TO jtop
         elev = .5 * (yj(j) + yj(j - 1))
         l = kappa * (elev - ymldat)
         Tauj(j) = rho * l ^ 2 * (vj(j) - vj(j - 1)) * ABS(vj(j) - vj(j -
1)) / dy ^ 2
       NEXT j
     END IF
  END IF
  Tauj(jbot - 1) = Tauj(jbot) + (Tauj(jbot) - Tauj(jbot + 1)) / dyTau *
dybot / 2
END SUB

SUB Sidewallcorrection

' Subprogramme to compute the correction to f, R and Re for flow in a
' narrow flume

'-------------------------------------------------------------------------
--

' Definition and dimensioning of local variables

' fwall          - friction factor for the side walls
' Rewall         - Reynold's no. for the side walls
' ratioRewofwall - Rewall/fwall
' diffx          - difference between lhs and rhs of friction eqn.
' lhs            - left hand side of friction equation (smooth wall)
' rhs            - right hand side of friction equation (smooth wall)
' festx          - friction factor estimate x

  DIM fwall, Rewall, ratioRewtofw
  DIM diff1, diff2, diff3, lhs, rhs
  DIM fest1, fest2, fest3

'-------------------------------------------------------------------------
--

' Start of subprogramme

  ratioRewtofw = Re / f

' Assume Rewall < 100000 - Blasius equation

  Rewall = (.316 * ratioRewtofw) ^ (1 / 1.25)
  fwall = Rewall / ratioRewtofw

  IF Rewall > 100000 THEN
```

```
'    Recompute Rewall & fwall using equation for smooth wall.  For the
'    first estimate use fwall from Blasius equation

     fest1 = fwall

     DO

     lhs = 1 / fest1 ^ .5
     rhs = 2 * LOG((ratioRewtofw * fest1 ^ 1.5) / 2.51) / lnfac

     fest2 = fest1
     diff2 = diff1
     diff1 = lhs - rhs

     IF lhs1 = rhs1 THEN
       GOTO 3
     ELSEIF lhs1 > rhs1 THEN
       fest1 = fest2 * 1.1
     ELSEIF lhs1 < rhs1 THEN
       fest1 = fest2 * .9
     END IF

     LOOP UNTIL diff1 * diff2 < 0

'    Interpolate for next estimate of f
     fest1 = 1E+20

     DO

     fest3 = fest2
     diff3 = diff2
     fest2 = fest1
     diff2 = diff1

     festlast = fest1
     fest1 = (0 - diff2) / (diff3 - diff2) * (fest3 - fest2) + fest2

     lhs = 1 / fest1 ^ .5
     rhs = 2 * LOG((ratioRewtofw * fest1 ^ 1.5) / 2.51) / lnfac
     diff1 = lhs - rhs

     IF diff1 * diff2 > 0 THEN
       diff2 = diff3
       fest2 = fest3
     END IF

     LOOP UNTIL ABS(fest1 - festlast) / fest1 * 100 < .01

     fwall = fest1

   END IF

3  fbed = f + 2 * ybedonly / flowidth * (f - fwall)

END SUB

SUB SolnMatrix

' Subprogramme that sets up a system of simultaneous equations in velocity.
' The system is tridiagonal and thus three columns of coefficients are
stored,
```

```
' viz. MatA(j), MatB(j) and MatC(j), and a set of constants, viz. MatR(j).

'-------------------------------------------------------------------------
--

' Definition and dimensioning of local variables

' dytopveg - vert. dist. between effective top of reeds and node below the
'            top of the reeds where Tau is computed (m)
' elev     - elevation of computational node for shear stress (m)
' Fj       - force on reed stems per unit height, velocity and bed area
(Ns/m3)
' l        - mixing length (m)
' term1,2  - computational terms for matrix of coefficients
' yTau     - height above bed of 1st node where shear stress is computed
(m)

  DIM dytoveg, elev, Fj, term1, term2, yTau

'-------------------------------------------------------------------------
--

' Initialise arrays

  FOR j = 1 TO jtop
    MatA(j) = 0
    MatB(j) = 0
    MatC(j) = 0
    MatR(j) = 0
  NEXT j

  Fstem = 0

' Setup arrays for solution

' Three principle conditions may exist:

' (1) Eddy-vicosity and mixing length approximaions below and above the
reeds
'     respectively (submerged reeds).
' (2) Eddy-viscosity approximation from bed to water surface (immergent
reeds).
' (3) Mixing length approximation from bed to water surface for v. low reed
height

'     ... and the set of simultaneous equtions is set-up accordingly.

  IF jsheardiv > jbot THEN

'   jbot node

    yTau = (yj(jbot) + yo) / 2
    dyTau = (yj(jbot) - yo) / 2 + (yj(jbot + 1) - yj(jbot)) / 2

'   Apply eddy-viscosity relationship at bottom node (condition (1) & (2))

    term2 = rho * alpha * a * .5 * (vj(jbot) + vj(jbot - 1)) / (dybot *
dyTau)
    term1 = rho * alpha * a * .5 * (vj(jbot + 1) + vj(jbot)) / (dy * dyTau)

    Fj = asym * rho * .5 * Cdreed * 1 / (a * b) * (dy / 2 + dybot) * d *
```

```
vj(jbot)
    Fstem = Fj * vj(jbot)

    MatB(jbot) = -term1 - term2 - Fj / (dy / 2 + dybot)
    MatC(jbot) = term1

    MatR(jbot) = -gamma * So - term2 * vj(jbot - 1)

'   Intermediate nodes (condition (1) & (2))

    FOR j = jbot + 1 TO jsheardiv - 1

      term2 = rho * alpha * a * .5 * (vj(j) + vj(j - 1)) / dy ^ 2
      term1 = rho * alpha * a * .5 * (vj(j + 1) + vj(j)) / dy ^ 2

      Fj = asym * .5 * rho * Cdreed * 1 / (a * b) * dy * d * vj(j)
      Fstem = Fstem + Fj * vj(j)

      MatA(j) = term2
      MatB(j) = -term1 - term2 - Fj / dy
      MatC(j) = term1

      MatR(j) = -gamma * So

    NEXT j

    IF jsheardiv = jtop THEN

'   Eddy-viscosity approximation to water surface (condition (3))

      j = jtop

      term2 = rho * alpha * a * .5 * (vj(j) + vj(j - 1)) / ((dytop + dy /
2) * dy)

      Fj = asym * .5 * rho * Cdreed * 1 / (a * b) * (dytop + dy / 2) * d *
vj(j)
      Fstem = Fstem + Fj * vj(j)

      MatA(j) = term2
      MatB(j) = -term2 - Fj / (dytop + dy / 2)

      MatR(j) = -gamma * So

    ELSE

'     Mixing length approximation above shear division to water surface
'     (condition (1))

      j = jsheardiv

      term2 = rho * alpha * a * .5 * (vj(j) + vj(j - 1)) / dy ^ 2

      elev = .5 * (yj(j + 1) + yj(j))
      l = kappa * (elev - ymldat)

      IF l < 0 THEN
        PRINT "l1 < 0"
      END IF

      term1 = rho * l ^ 2 * ABS(vj(j + 1) - vj(j)) / dy ^ 3
```

```
      Fj = asym * .5 * rho * Cdreed * 1 / (a * b) * dy * d * vj(j)
      Fstem = Fstem + Fj * vj(j)

      MatA(j) = term2
      MatB(j) = -term1 - term2 - Fj / dy
      MatC(j) = term1

      MatR(j) = -gamma * So

      FOR j = jsheardiv + 1 TO jtop - 1

        elev = .5 * (yj(j + 1) + yj(j))
        l = kappa * (elev - ymldat)
        IF l < 0 THEN
          PRINT "l2 < 0"
        END IF
        term1 = rho * l ^ 2 * ABS(vj(j + 1) - vj(j)) / dy ^ 3

        elev = .5 * (yj(j) + yj(j - 1))
        l = kappa * (elev - ymldat)
        IF l < 0 THEN
          PRINT "l3 < 0"
        END IF
        term2 = rho * l ^ 2 * ABS(vj(j) - vj(j - 1)) / dy ^ 3

        IF j < jtopveg THEN
          Fj = asym * .5 * rho * Cdreed * l / (a * b) * dy * d * vj(j)
          Fstem = Fstem + Fj * vj(j)
        ELSEIF j = jtopveg THEN
          dytopveg = he - (yj(j) + yj(j - 1)) / 2
          Fj = asym * .5 * rho * Cdreed * l / (a * b) * dytopveg * d *
vj(j)
          Fstem = Fstem + Fj * vj(j)
        ELSE
          Fj = 0
        END IF

        MatA(j) = term2

        IF j < jtopveg THEN
          MatB(j) = -term1 - term2 - Fj / dy
        ELSEIF j = jtopveg THEN
          MatB(j) = -term1 - term2 - Fj / dytopveg
        ELSE
          MatB(j) = -term1 - term2
        END IF

        MatC(j) = term1

        MatR(j) = -gamma * So

      NEXT j

'     jtop'th node

      elev = .5 * (yj(jtop) + yj(jtop - 1))
      l = kappa * (elev - ymldat)
      IF l < 0 THEN
        PRINT "l4 < 0"
      END IF
      term2 = rho * l ^ 2 * ABS(vj(jtop) - vj(jtop - 1)) / (dy ^ 2 * (dy /
```

```
2 + dytop))

      MatA(jtop) = term2
      MatB(jtop) = -term2

      MatR(jtop) = -gamma * So

    END IF

  ELSE

'   Mixing length approximation throughout (condition (3))

'   jbot node

    yTau = (yj(jbot) + yo) / 2
    dyTau = (yj(jbot) - yo) / 2 + (yj(jbot + 1) - yj(jbot)) / 2

    elev = .5 * (yj(jbot + 1) + yj(jbot))
    l = kappa * (elev - ymldat)
    IF l < 0 THEN
      PRINT "15 < 0"
    END IF
    term1 = rho * l ^ 2 * ABS(vj(jbot + 1) - vj(jbot)) / (dy ^ 2 * dyTau)

    l = kappa * (yTau - ymldat)
    IF l < 0 THEN
      PRINT "16 < 0"
    END IF
    term2 = rho * l ^ 2 * ABS(vj(jbot) - vj(jbot - 1)) / (dybot ^ 2 *
dyTau)

    Fj = asym * rho * .5 * Cdreed * l / (a * b) * (dy / 2 + dybot) * d *
vj(jbot)
    Fstem = Fstem + Fj * vj(jbot)

    MatB(jbot) = -term1 - term2 - Fj / (dy / 2 + dybot)
    MatC(jbot) = term1

    MatR(jbot) = -gamma * So - term2 * vj(jbot - 1)

'   Intermediate nodes

    FOR j = jbot + 1 TO jtop - 1

      elev = .5 * (yj(j + 1) + yj(j))
      l = kappa * (elev - ymldat)
      IF l < 0 THEN
        PRINT "17 < 0"
      END IF
      term1 = rho * l ^ 2 * ABS(vj(j + 1) - vj(j)) / dy ^ 3

      elev = .5 * (yj(j) + yj(j - 1))
      l = kappa * (elev - ymldat)
      IF l < 0 THEN
        PRINT "18 < 0"
      END IF
      term2 = rho * l ^ 2 * ABS(vj(j) - vj(j - 1)) / dy ^ 3

      IF j < jtopveg THEN
        Fj = asym * .5 * rho * Cdreed * l / (a * b) * dy * d * vj(j)
```

```
        Fstem = Fstem + Fj * vj(j)
      ELSEIF j = jtopveg THEN
        dytopveg = he - (yj(j) + yj(j - 1)) / 2
        Fj = asym * .5 * rho * Cdreed * 1 / (a * b) * dytopveg * d * vj(j)
        Fstem = Fstem + Fj * vj(j)
      ELSE
        Fj = 0
      END IF

      MatA(j) = term2

      IF j < jtopveg THEN
        MatB(j) = -term1 - term2 - Fj / dy
      ELSEIF j = jtopveg THEN
        MatB(j) = -term1 - term2 - Fj / dytopveg
      ELSE
        MatB(j) = -term1 - term2
      END IF

      MatC(j) = term1

      MatR(j) = -gamma * So

    NEXT j

'   jtop'th node

    elev = .5 * (yj(jtop) + yj(jtop - 1))
    l = kappa * (elev - ymldat)
    IF l < 0 THEN
      PRINT "19 < 0"
    END IF
    term2 = rho * l ^ 2 * ABS(vj(jtop) - vj(jtop - 1)) / (dy ^ 2 * (dy / 2
+ dytop))

    IF j = jtopveg THEN
      Fj = asym * .5 * rho * Cdreed * 1 / (a * b) * (dy / 2 + dytop) * d *
vj(j)
      Fstem = Fstem + Fj * vj(j)
    END IF

    MatA(jtop) = term2

    IF j = jtopveg THEN
      MatB(jtop) = -term2 - Fj / (dy / 2 + dytop)
    ELSE
      MatB(jtop) = -term2
    END IF

    MatR(jtop) = -gamma * So

  END IF

END SUB

SUB SolveMatrix

' Subprogramme to solve for the velocities along the vertical.

'-------------------------------------------------------------------------
--
```

```
' Definition and dimensioning of local variables

' j  - node in vertical (y) direction

  DIM j AS INTEGER

' beta  - computational variable
' gam()  - computational variable

  DIM beta, gam(1000) AS DOUBLE

'-------------------------------------------------------------------------
--

  FOR j = jbot TO jtop
    gam(j) = 0
    uj(j) = 0
  NEXT j

  IF MatB(jbot) = 0 THEN
  PRINT j
    PRINT "zero pivot value"
    END
  END IF
  beta = MatB(jbot)
  uj(jbot) = MatR(jbot) / beta
  FOR j = jbot + 1 TO jtop
    gam(j) = MatC(j - 1) / beta
    beta = MatB(j) - MatA(j) * gam(j)
    IF beta = 0 THEN
      PRINT j
      PRINT "Zero pivot value"
      END
    END IF
    uj(j) = (MatR(j) - MatA(j) * uj(j - 1)) / beta
  NEXT j

  FOR j = jtop - 1 TO jbot STEP -1
    uj(j) = uj(j) - gam(j + 1) * uj(j + 1)
  NEXT j

END SUB

SUB Stembendconverg

' Subprogramme to check for convergence of the effective reed height and
' asign iterative flow depth and effectibe reed height values

'-------------------------------------------------------------------------
--

  IF ABS(he - hepr) / he < .1 / 100 AND ABS(y - ypr) / y < .1 / 100 THEN
    heconverg = "yes"
  ELSE
    heconverg = "no"
  END IF

  ypr = y
  hepr = he

END SUB
```

```
SUB Stembending

' Subprogramme to compute the effective height of the reed stand due to
' bending (flexural rigidity of the stem).

'-------------------------------------------------------------------------
--

' Definition and dimensioning of local variables

' deflec            horizontal deflection at the top of the reeds or water
surface (m)
' defleclast        deflect for previous iteration (m)
' dz                vertical increment
' he/hel/hest       equivalent (& estimate) height of reed stem
' hlimit            the max. physical allowable height of the reeds (y/he,
m)
' slope/intercept   slope and intercept of line for he computation
' stemlength        cumulative stem length (m)
' UDL               drag force applied as uniformly distributed load

  DIM dz
  DIM hel, hest, hest1, hlimit
  DIM stemlength, deflec, defleclast
  DIM slope, intercept
  DIM UDL

'-------------------------------------------------------------------------
--

' Equivalent uniformly distributed load (N/m)

  UDL = .5 * rho * d * Cdreed * vreed ^ 2

' Reduction in height due to flexure of stem - the difficulty with this
' section of coding is that the deflection (vertical) is a function of the
' loading length - or effective length of the stem... but this is
' precisely what is being computed.  A solution is therefore applied
' whereby the effective loading length is solved for in combination with
' the deflection calculation - to give the same result!

' Note:  Small deflection theory is applied here and its applicability may
'        be questionable.

  IF y > hv THEN
    hlimit = hv
  ELSE
    hlimit = y
  END IF

  dz = hlimit / 100

  FOR hest = dz TO hlimit STEP dz
    deflec = 0
    stemlength = 0
    FOR z = dz TO hlimit STEP dz
     defleclast = deflec
     deflec = UDL / (24 * EI) * (6 * hest ^ 2 * z ^ 2 - 4 * hest * z ^ 3 +
z ^ 4)
     stemlength = stemlength + ((deflec - defleclast) ^ 2 + dz ^ 2) ^ .5
     IF stemlength >= hv OR z > y THEN
```

```
        EXIT FOR
      END IF
    NEXT z
    IF z > hv THEN z = hv
    IF z > y THEN z = y
    he = z
    IF hest >= he AND he1 >= hest1 AND he1 <> he THEN
      slope = (hest1 - hest) / (he1 - he)
      intercept = hest - slope * he
      he = intercept / (1 - slope)
      GOTO 4
    END IF
    hest1 = hest
    he1 = he
  NEXT hest

4 END SUB

SUB Velconverg

' Subprogramme to check for convergence in vertical velocity distribution
and
' reasign new estimates based on recent calcs.

'
-----------------------------------------------------------------------------
-

' Definition and dimensioning of local variables

' j   - node in vertical (y) direction

  DIM j AS INTEGER

'
-----------------------------------------------------------------------------
-

  vconverg = "yes"

  FOR j = jbot TO jtop
    IF ABS(uj(j) - vj(j)) / ABS(uj(j)) > .01 / 100 THEN
      vconverg = "no"
    END IF
    vj(j) = (uj(j) + vj(j)) / 2
  NEXT j

END SUB
```

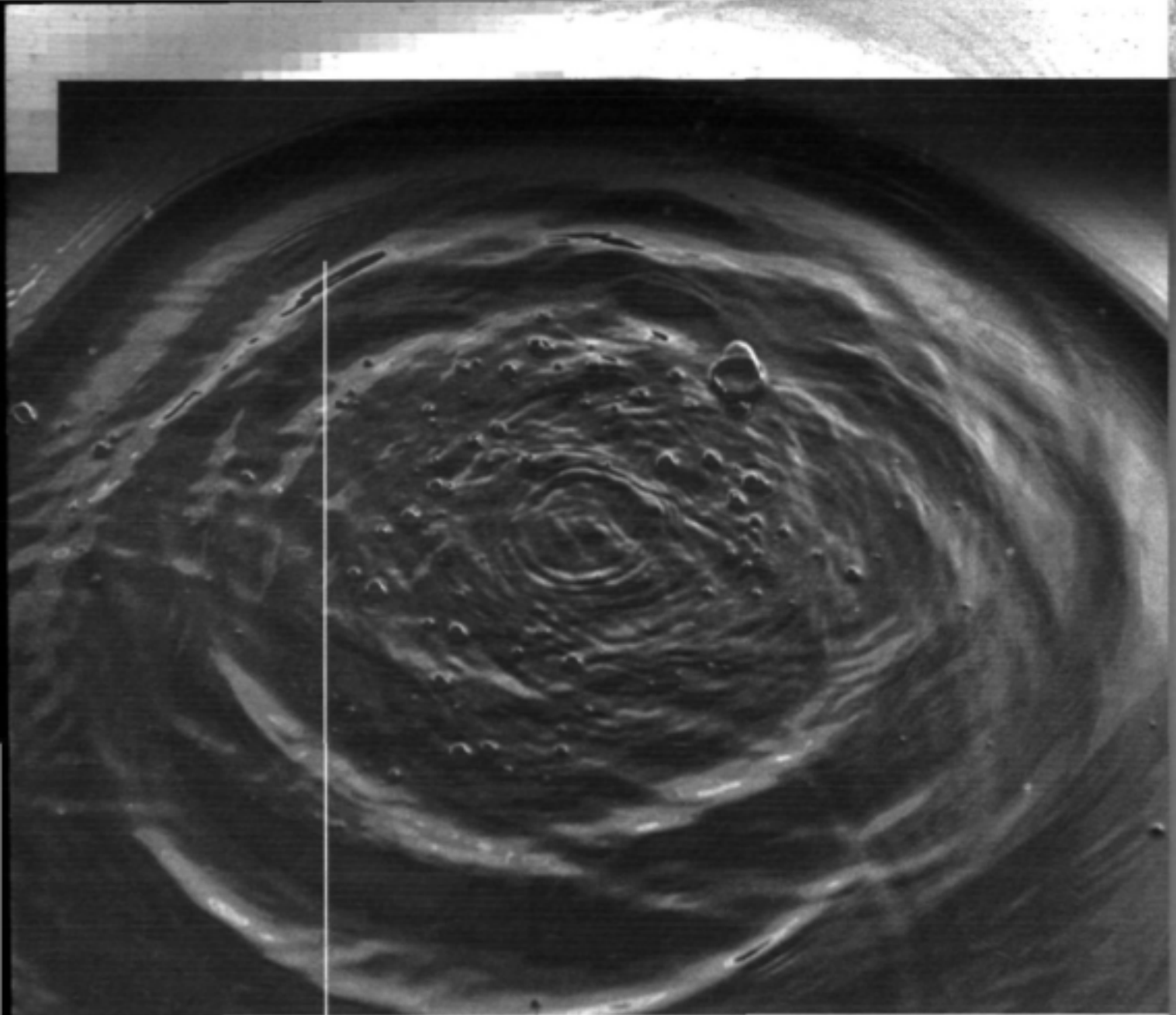

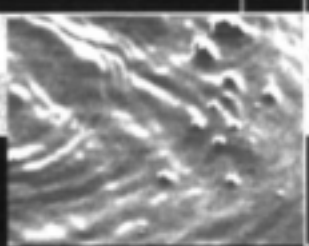

Water Research Commission
PO Box 824, Pretoria, 0001, South Africa
Tel: +27 12 330 0340, Fax: +27 12 331 2565
Web: http://www.wrc.org.za

1868457311